frontiers | Research Topics

Multi-limbed membrane guanylate cyclase cellular signaling pathways

Edited by
Rameshwar K. Sharma, Teresa Duda, Clint L. Makino and Kailash N. Pandey

Published in
Frontiers in Molecular Neuroscience

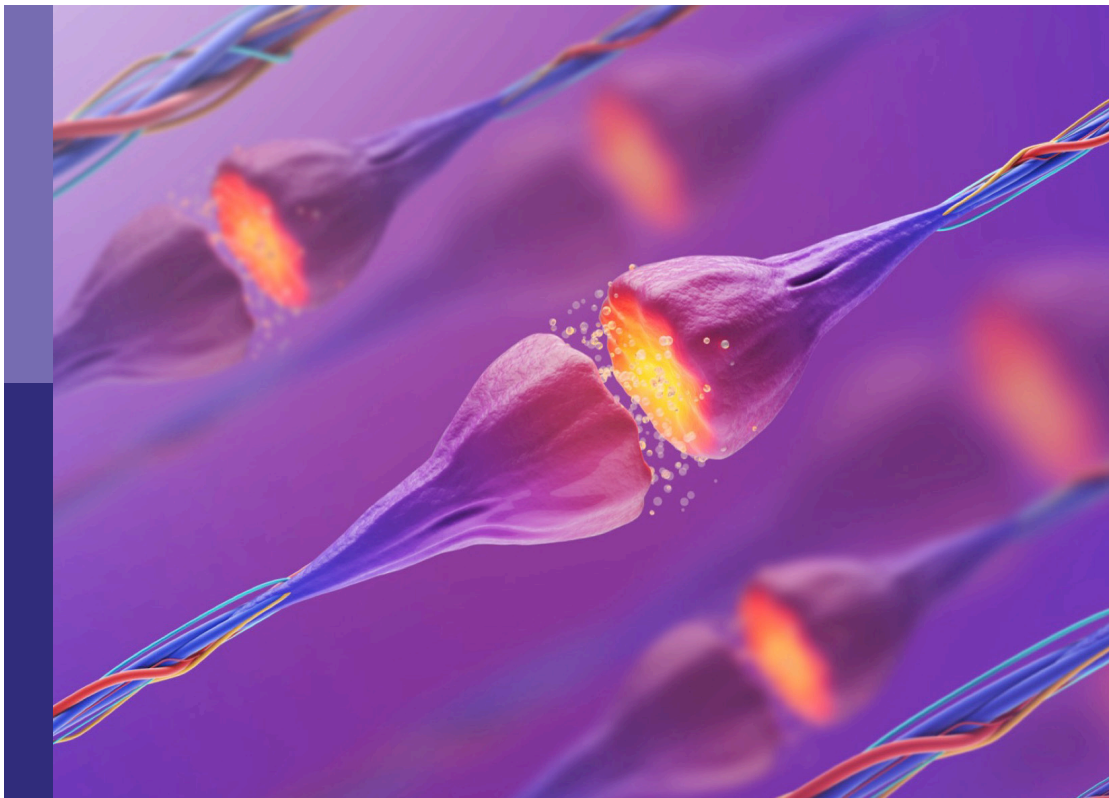

ISSN 1664-8714
ISBN 978-2-8325-2256-1
DOI 10.3389/978-2-8325-2256-1

About Frontiers

Frontiers is more than just an open access publisher of scholarly articles: it is a pioneering approach to the world of academia, radically improving the way scholarly research is managed. The grand vision of Frontiers is a world where all people have an equal opportunity to seek, share and generate knowledge. Frontiers provides immediate and permanent online open access to all its publications, but this alone is not enough to realize our grand goals.

Frontiers journal series

The Frontiers journal series is a multi-tier and interdisciplinary set of open-access, online journals, promising a paradigm shift from the current review, selection and dissemination processes in academic publishing. All Frontiers journals are driven by researchers for researchers; therefore, they constitute a service to the scholarly community. At the same time, the *Frontiers journal series* operates on a revolutionary invention, the tiered publishing system, initially addressing specific communities of scholars, and gradually climbing up to broader public understanding, thus serving the interests of the lay society, too.

Dedication to quality

Each Frontiers article is a landmark of the highest quality, thanks to genuinely collaborative interactions between authors and review editors, who include some of the world's best academicians. Research must be certified by peers before entering a stream of knowledge that may eventually reach the public - and shape society; therefore, Frontiers only applies the most rigorous and unbiased reviews. Frontiers revolutionizes research publishing by freely delivering the most outstanding research, evaluated with no bias from both the academic and social point of view. By applying the most advanced information technologies, Frontiers is catapulting scholarly publishing into a new generation.

What are Frontiers Research Topics?

Frontiers Research Topics are very popular trademarks of the *Frontiers journals series*: they are collections of at least ten articles, all centered on a particular subject. With their unique mix of varied contributions from Original Research to Review Articles, Frontiers Research Topics unify the most influential researchers, the latest key findings and historical advances in a hot research area.

Find out more on how to host your own Frontiers Research Topic or contribute to one as an author by contacting the Frontiers editorial office: frontiersin.org/about/contact

Multi-limbed membrane guanylate cyclase cellular signaling pathways

Topic editors
Rameshwar K. Sharma — Salus University, United States
Teresa Duda — Salus University, United States
Clint L. Makino — Boston University, United States
Kailash N. Pandey — Tulane University, United States

Citation
Sharma, R. K., Duda, T., Makino, C. L., Pandey, K. N., eds. (2023). *Multi-limbed membrane guanylate cyclase cellular signaling pathways*. Lausanne: Frontiers Media SA. doi: 10.3389/978-2-8325-2256-1

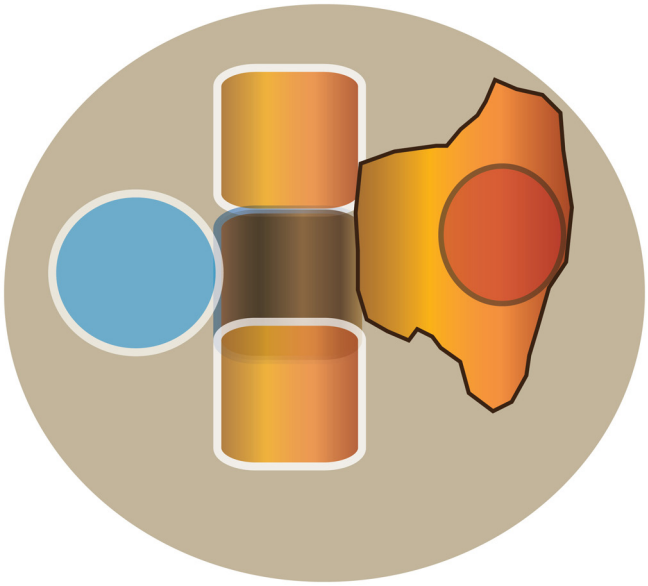

Cover image
Rameshwar K. Sharma

This figure shows a schematic representation of membrane guanylate cyclase.

Table of contents

frontiers | Frontiers in Molecular Neuroscience

TYPE Editorial
PUBLISHED 12 April 2023
DOI 10.3389/fnmol.2023.1185637

OPEN ACCESS

EDITED AND REVIEWED BY
Jean-Marc Taymans,
Institut National de la Santé et de la Recherche Médicale (INSERM), France

*CORRESPONDENCE
Clint L. Makino
cmakino@bu.edu

SPECIALTY SECTION
This article was submitted to Molecular Signalling and Pathways, a section of the journal Frontiers in Molecular Neuroscience

RECEIVED 13 March 2023
ACCEPTED 17 March 2023
PUBLISHED 12 April 2023

CITATION
Sharma RK, Pandey KN, Duda T and Makino CL (2023) Editorial: Multi-limbed membrane guanylate cyclase cellular signaling pathways. *Front. Mol. Neurosci.* 16:1185637. doi: 10.3389/fnmol.2023.1185637

Editorial: Multi-limbed membrane guanylate cyclase cellular signaling pathways

Rameshwar K. Sharma[1], Kailash N. Pandey[2], Teresa Duda[1] and Clint L. Makino [3]*

[1]The Unit of Regulatory and Molecular Biology, Research Divisions of Biochemistry and Molecular Biology, Salus University, Elkins Park, PA, United States, [2]Department of Physiology, Tulane University School of Medicine, New Orleans, LA, United States, [3]Department of Pharmacology, Physiology and Biophysics, Boston University Chobanian & Avedisian School of Medicine, Boston, MA, United States

KEYWORDS

receptor guanylate cyclase, cyclic GMP, ROS-GC, GC-A, GCAP, RD3, retina, mutant mouse

Editorial on the Research Topic
Multi-limbed membrane guanylate cyclase cellular signaling pathways

A single molecule was discovered that changed the existing field of cellular signal transduction (reviewed by Sharma and by Duda and Sharma in Chapters 1, 2). The membrane guanylate cyclase (MGC) *via* its seven-limbed structure controlled the entire physiological processes of cardiovasculature, endocrine and sensory neurons; and paved the way that indicated that it may be locked also with the perception of atmospheric conditions. This Research Topic narrates the saga of this molecule that is indispensable for all living beings, from silk pupae to Homo sapiens.

Unlike its predecessors, cyclic AMP and IP_3, MGC signaling systems consist of a single protein; yet their multi-limbs with diverse molecular structures control various physiological functions. Sharma and Duda and Sharma (Chapters 1, 2) narrate the history, from 1963 up-to-date, of the efforts involved in building on small projects, brick by brick, and its emergence from the chasm of disbelief, through continuous work. The foundational study was the establishment of the first ACTH-modulated limb. It became the structural-physiological template for the future ones. It demonstrated that a common evolutionary link exists between the generation of plant steroids, cardenolides, and the mammalian steroid hormones (see Figure 1 in Sharma, Chapter 1). In the evolutionary ladder, a change occurs. The mammals develop an extra adrenocorticotropic hormone (ACTH)-dependent branch locked with the primordial cholesterol formation. The branch is a sensor of the ACTH signal, generated in the tiniest gland of the brain, the pituitary. The signal is transmitted selectively to the adrenal fasciculata cells; these, from the stored cholesterol synthesized from mevalonic acid, generate the steroid hormone cortisol/corticosterone. In contrast, plants transform cholesterol into cardenolides. Outstandingly, in both cases, the targeted site of cholesterol is its side chain: cleavage in mammals and rearrangement in plants. Notably, the initial biosynthetic steps from mevalonic acid to cholesterol stay almost identical in both the cardenolides and in the rat adrenal mitochondria, only the last biosynthetic steps differ, transformation of the (the 20S)-20-hydroxycholesterol to pregnenolone and then to progesterone and to cortisol/corticosterone. In common, in both kingdoms, the cleavage of the cholesterol sidechain occurs between C-20 and C-22. Cyclic GMP and Ca^{2+} are the sole physiological co-messengers of ACTH.

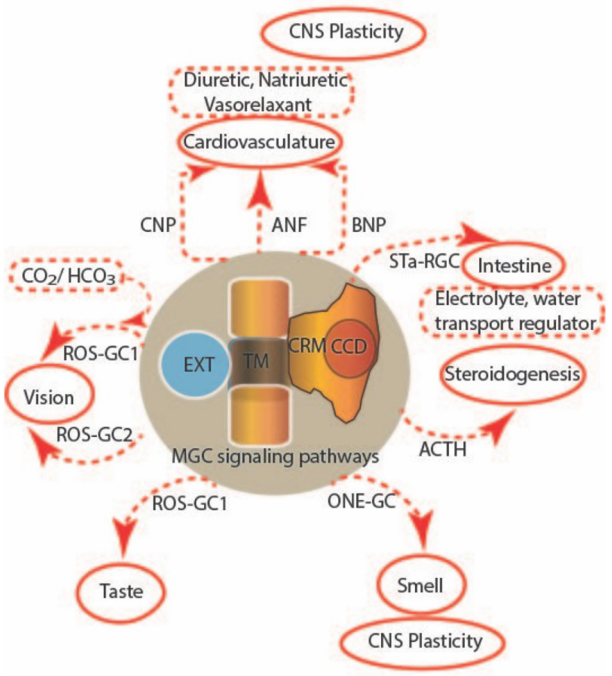

FIGURE 1
Multi-limbed membrane guanylate cyclase signaling. Seven subfamily forms of membrane guanylate cyclases, encoded by distinct genes, perform a multitude of functions. These uniquely designed surface receptors are all single-pass transmembrane proteins that detect hormones and other extracellular chemicals at an extracellular domain (EXT), translate the signal across a transmembrane domain (TM) to a catalytic regulatory module (CRM) and a catalytic core domain (CCD) to regulate cGMP synthesis. Together, they control steroidogenesis, cardiovasculature, sensory neurons in vision, taste and smell, the intestine, skeletal growth, and CNS plasticity.

More recent progress regarding the novel mechanisms of MGC activation, cellular signaling, molecular modeling of structural determinants, and physiological and pathophysiological functions (Figure 1) is presented in this Research Topic in the form of two additional reviews, two brief research reports, and seven original research articles. Chapters 3–6 and 13 are devoted to the MGC receptors for natriuretic factors, GC-A and GC-B, whereas chapters 7–12, to GC-E and GC-F in retinal photoreceptors.

Pandey (Chapter 3) reviews the generation and use of genetically engineered animals, including gene-targeted (gene-knockout and gene-duplication) and transgenic mutant mouse models to study the varied roles and pleiotropic functions of GC-A in intact animals. This chapter also provides a chronological development of the biochemical, molecular, physiological, and pathophysiological functions of this MGC, including signaling pathways, genomics, and gene regulation in both normal and diseased states. Egbert et al. (Chapter 4) describe the development of genetically modified mouse lines in which GC-A or GC-B were tagged with a hemagglutinin epitope for tissue localization of the MGCs or had putative phosphorylation sites substituted with glutamates, to mimic the negative charge of the phosphorylated forms so that their regulatory function could be explored. In Chapter 5, Otto and Potter show that vicinal glutamate substitutions mimic phosphorylation more closely than single glutamates in GC-A, and then identify the true regulatory phosphorylation sites. Calis et al. (Chapter 6) provide intriguing findings that GC-A may be linked to long term potentiation in the hippocampus and auditory neural gain through the balanced actions of MR/GR steroid receptors.

GC-E and GC-F in the retinal rods and cones are orphan receptors; no ligands are known to bind their extracellular domains. However, they interact intracellularly with neuronal calcium sensor proteins (e.g., GCAPs), RD3 and bicarbonate. Ames (Chapter 7) reviews control of GC-E activity and proposes a two-state concerted model in which the dimeric MGC allosterically switches between active (R-state) and inactive (T-state) conformational states with distinct quaternary structures. Binding of Ca^{2+}-free/Mg^{2+}-bound GCAP1 activates GC-E by shifting the balance to the R-state, whereas Ca^{2+}-bound GCAP1 and/or RD3 inhibit the cyclase by maintaining the T-state. Geva et al. (Chapter 8) describe how an axial gradient of bicarbonate within the rod outer segment creates spatial inhomogeneity in the rates of cGMP synthesis that affects variability in photon response amplitude and kinetics. Surprisingly, bicarbonate imposes markedly different effects in the rods of salamander and toad, increasing variability in the former while decreasing it in the latter. Bicarbonate appears to dampen the primary phototransduction cascade at one end of the toad rod outer segment by an unknown mechanism. This novel effect of bicarbonate solves a mystery as to how toad vision is able to function effectively in extremely dim light. Adhikari et al. (Chapter 9) describe how bicarbonate more profoundly affects flash response kinetics and maximal response amplitude in mouse rods, at a lower concentration, when compared to amphibian rods. In addition, bicarbonate expands the dynamic range over which rods respond to dimmer flashes in mouse, whereas the range is extended to brighter flashes in amphibians. Caruso et al. (Chapter 10) refined a previously developed, space-resolved biophysical model of rod phototransduction by incorporating several mechanisms that play significant roles in shaping the rod response under high illumination levels: the function of RGS9 in shutting off G protein, and Ca^{2+} dependences of: rhodopsin phosphorylation, cGMP binding to the light-regulated ion channel, and two MGC activities. The updated model explains how depletion of RGS9 complex with very bright flashes affects response saturation behavior and further predicts what would happen with flashes so bright that they activate all the available PDE. During a screening for murine models of human ocular disorders, Naggert et al. (Chapter 11) discovered a mutation in GC-E that leads to an early loss of cone photoreceptor function. Rods survive initially because they also express GC-F, but they eventually succumb to a progressive degeneration, which may be relevant to understanding disease pathology in LCA. During evolution, whole genome duplications resulted in as many as three MGCs in vertebrate visual photoreceptors, regulated by as many as eight GCAP Ca^{2+} sensors. Observing that most mammals retain two MGCs and up to three GCAPs, whereas reptiles and birds pair a single MGC with up to five GCAPs, Gesemann and Neuhauss (Chapter 12) hypothesized that evolutionary forces may drive diversity in GCAPs to offset the reduced number of MGCs.

Based on amino acid sequence homology, Chen et al. (Chapter 13), suspected that RD3 (retinal degeneration type 3), thought to suppress ROS-GC activity until it was localized properly

within the rod photoreceptor, might serve an analogous function on natriuretic peptide MGCs in other cells. Indeed, Chen et al. show RD3 expression in tissues expressing GC-A and GC-B: retina, cerebellum, hippocampus, neocortex and olfactory bulb, and inhibition of GC-A and GC-B activities by RD3 in biochemical assays.

Despite the ample progress that has been made, there is still much to discover regarding the molecular structures of MGCs, how they activate upon ligand binding or are controlled by regulatory proteins, and their expanding roles in cellular signaling, physiological and pathophysiological functions. Future investigations should also lead to exciting and innovative strategies toward the prevention, diagnosis, and treatment of a wide range of diseases.

Author contributions

RKS, TD, KNP, and CLM contributed to the writing and editing of the manuscript. Figure provided by RKS. All authors contributed to the article and approved the submitted version.

Conflict of interest

The authors declare that the research was conducted in the absence of any commercial or financial relationships that could be construed as a potential conflict of interest.

Publisher's note

All claims expressed in this article are solely those of the authors and do not necessarily represent those of their affiliated organizations, or those of the publisher, the editors and the reviewers. Any product that may be evaluated in this article, or claim that may be made by its manufacturer, is not guaranteed or endorsed by the publisher.

frontiers | Frontiers in Molecular Neuroscience

REVIEW
published: 09 August 2022
doi: 10.3389/fnmol.2022.929396

ACTH-Modulated Membrane Guanylate Cyclase Signaling System: Origin and Creation

*Rameshwar K. Sharma**

Unit of Regulatory and Molecular Biology, Salus University, Elkins Park, PA, United States

The membrane guanylate cyclase (MGC) cellular signaling pathway consists of seven signaling pathways and is critical for the survival of prokaryotes eukaryotes, and highly complex vertebrate organisms. A sequel to the author's earlier comprehensive reviews, covering the field of MGC from its origin to its establishment to the year 2014, this article exclusively deals with the history of its development from the year 1963 to 1987. It narrates the efforts involved in building on small projects, brick by brick, and its emergence from the chasm of disbelief, through steady, continuous work. To make the presentation simple and chronologically continuous, the subject matters of the earlier reviews and publication of these authors have been freely borrowed with appropriate citations.

OPEN ACCESS

Edited by:
Karl-Wilhelm Koch,
University of Oldenburg, Germany

Reviewed by:
Masahiro Kono,
Medical University of South Carolina, United States
James Ames,
University of California, Davis, United States

***Correspondence:**
Rameshwar K. Sharma
rsharma@salus.edu

Specialty section:
This article was submitted to Molecular Signalling and Pathways, a section of the journal Frontiers in Molecular Neuroscience

Received: *26 April 2022*
Accepted: *22 June 2022*
Published: *09 August 2022*

Citation:
Sharma RK (2022) ACTH-Modulated Membrane Guanylate Cyclase Signaling System: Origin and Creation. Front. Mol. Neurosci. 15:929396. doi: 10.3389/fnmol.2022.929396

Keywords: membrane guanylate cyclase, cyclic GMP signaling pathways, surface receptor, ACTH, transduction modes, signal transduction

INTRODUCTION

Pursuit

Ignited by the fervor of the author's early findings that a common evolutionary link exists between the generation of plant steroids, cardenolides, and the mammalian steroid hormones (Wickramsinghe et al., 1969; Sharma, 1970a,b,c; Kitabchi et al., 1971a,b), he decided to decode this link, and thus, entered the field of hormonal signal transduction. Because cholesterol in both generations was the central precursor molecule, it became the subject matter of the author's research for the next 18 years, from 1969 to 1987.

The basis of the concept was that in both plant and mammalian kingdoms, biosynthetic pathways of the cholesterol formation are identical; they start from the primordial mevalonic acid molecule (Wickramsinghe et al., 1969; Sharma, 1970b; Kitabchi et al., 1971b). In the evolutionary ladder, a change occurs, however. The mammals develop an extra adrenocorticotropic hormone (ACTH)-dependent branch locked with the primordial cholesterol formation. The locked branch now is a sensor of the ACTH signal, generated in the pituitary gland. Then, the signal is transmitted selectively to the isolated fasciculate cell of the adrenal gland; the cell using its stored cholesterol synthesized from mevalonic acid transforms it into the steroid hormone and cortisol/corticosterone (Kitabchi et al., 1971b). In the plant, in contrast, cholesterol is transformed into cardenolides (Wickramsinghe et al., 1969; Sharma, 1970a,b,c). Outstandingly, in both cases, the targeted site of cholesterol is its side chain: cleavage in mammals and rearrangement in plants. Notably, the initial biosynthetic steps from mevalonic acid to cholesterol stay almost identical in both the cardenolides and in the rat adrenal mitochondria (Wickramsinghe et al., 1969). Only the last biosynthetic steps differ, and solely operate in the fasciculate cell of the adrenal cortex, that is

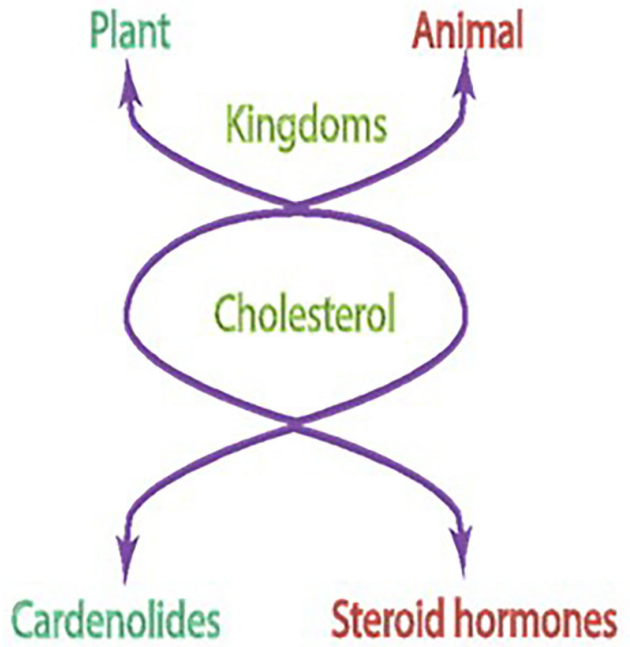

FIGURE 1 | Cholesterol is a common precursor molecule for steroids in animal and plant kingdoms.

transformation of the (the 20S)-20-hydroxycholesterol to pregnenolone and then to progesterone and to cortisol/corticosterone (Bhacca and Sharma, 1968; Sharma and Hebborn, 1968; Sawhney and Sharma, 1976). In common, in both kingdoms, the cleavage step of the cholesterol sidechain occurs between C-20 and C-22 (**Figure 1**).

A SPECIAL NOTE is deserved on the development and use of an extremely precise technology to arrive at the stated conclusions. The author picked it up during his tenure at the Worcester Foundation of Experimental Biology (Shrewsbury, Massachusetts, 1968–1969) when collaborating with Dr. E. Caspi's group (Wickramsinghe et al., 1969). Briefly, it involved the application of double isotope labels, 4R-4-^{3}H-2-C^{14}-mevalonic acid, or/and 7-^{3}H-(1,7,15,22,26)-C^{14}-cholesterol. In plants, they were fed through painting their leaves and in the fasciculate cells through their incubation in the reconstituted systems. The generated non-radioactive end product, steroid or cardenolide, was then mixed with the experimental product, crystallized, and the ^{3}H/C^{14} ratio was evaluated to trace the biosynthetic pathways.

With Caspi's group, the author used this technology for the *Digitalis Lanata* plant cardeneloids, digitoxigenin, tigogenin, and pseudotigogenin; and independently, with his group for the *Cammelia sinensis* plant cardenolides, α-spinasterol and aβ-amyrin (Wickramsinghe et al., 1969).

To attain the original aim, i.e., to decode the LINK between the two kingdoms, the pursuit began. The subject of study was the cholesterol molecule. The experimental models were the isolated fasciculate cell of the adrenal cortex and of the adrenocortical carcinoma 494 cells.

TASK 1. Decode the ACTH-modulated mechanism of the process of steroidogenesis. TASK 2. Apply this knowledge to understand deformities in the cancer cell.

TASK 1

It necessitated the development of a bioassay that detects the physiological concentration of ACTH in the human plasma (Kitabchi et al., 1971a). For this, the isolated system of the fasciculate cells of rats was constructed (Kitabchi et al., 1971a). The adrenal gland was treated with trypsin to selectively remove its zona glomerulosa and the zona reticularis, yielding the sole region of fasciculate. This, in turn, acted as a source of the pure isolated cells, used in the experiments. The cells were physiologically pure, solely synthesizing corticosterone, the counterpart of the human cortisol, detecting as little as 0.5 μunit of ACTH. Conspicuously, there was a small lag period in kicking on the response, demonstrating the auxiliary role of a labile factor. The factor was a protein because its inhibitor blocked the lag. Demonstrating specificity, these fasciculate cells did not respond to other polypeptide hormones, insulin, growth hormone, proinsulin, glucagon, and epinephrine.

In further affirmation, (1) there was a linear relationship between the number of cells, fifty to four hundred thousand, and steroidogenic response to ACTH; (2) in time-dependency, 0 to 180 min interval, the maximal physiological concentration of ACTH (50 μunits) generated corticosterone production in a linear fashion between 6 and 180 min; (3) a definite short lag period (6 min) occurred before the commencement of the linearity in steroidogenesis, a repeatable phenomenon with low (5 μunit) concentration of ACTH.

The physiological purity of the cells was matched with their morphological integrity. The light and electron microscopic analyses demonstrated that the cells embodied the typical fasciculate cell attributes, vascular mitochondria, the excessive cellular content of lipid globules, endoplasmocrine secretion of lipid globules together with the smooth-surfaced endoplasmic reticulum (Kitabchi and Sharma, 1971; Kitabchi et al., 1971a; Sharma et al., 1972).

The applicability of the isolated fasciculate cell assay system in a human study established that the plasma ACTH level in the fasting normal subjects is 2 μunits ± 0.1; the value increases about 6-fold when the generation of cortisol is blocked through the administration of metyrapone (Kitabchi et al., 1971a).

Thus, we had an extra sensitive tool in our possession. This could detect the physiological concentrations of ACTH and could be used in *in vitro* reconstitution studies for direct elucidation of the mechanism through which ACTH controls the steroid hormone cortisol. In turn, we were well-positioned to systematically define the ACTH-dependent physiological processes of stress, fighting infection, and maintaining blood pressure. In addition, we could apply this knowledge to understanding abnormalities in the 494 adrenocortical carcinoma cells.

Cognizant with the developing, at that time, a concept that all hormonal actions occur through the cyclic AMP second messenger system (reviewed in Sharma, 2002), this possibility was also considered in our studies. If applicable, the transformation of the ACTH signal into the production of the steroid hormones would be a three-component-system, consisting of the receptor, the G protein, and the adenylate cyclase. Structurally, the adenylate cyclase is composed of two cytoplasmic domains and two membrane-spanning domains, each of which contains 6 transmembrane spans. As will become clear, this was not the case. The ACTH hormonal signal transduction system was unique physiologically, biochemically, and molecularly.

This conclusion was arrived at through experiments that were conducted under conditions that were as close as possible to the physiological conditions. The five hundred thousand fasciculate cells representing one rat adrenal gland or its counterpart, the adrenocortical carcinoma 494, were used in the reconstitution studies.

The findings of these studies were as follows (reviewed in Sharma, 2002):

- ACTH stimulates the biosynthetic step of steroidogenesis from (the 20S)-20-hydroxycholesterol; this step is dependent on protein synthesis and is rate-limiting. Yet, the cyclic AMP does not mimic this stimulatory action of ACTH (Sharma, 1973, 1974; Sharma and Brush, 1974). Thus, cyclic AMP is not the physiological second messenger of ACTH challenging the prevailing universality of the "cyclic AMP second messenger concept".
- Accordingly, ACTH in the carcinoma cells inhibits steroidogenesis, yet cyclic AMP does not.
- In a bell-shaped curve, the physiological concentration of ACTH, 2.5–10 μunits, does not raise the level of cyclic AMP but does stimulate steroidogenesis. Yet, it stimulates the peak synthesis of cyclic GMP with a concomitant rise in corticosterone. Thus, cyclic GMP, not the cyclic AMP, is the physiological mediator of the ACTH hormone.
- A surprising finding was that supra-physiological concentrations, 10–100 μunits, of ACTH, indeed, stimulate cyclic AMP levels in a concentration-dependent manner with a concomitant rise of the corticosterone level. Notably, under these conditions, there was no rise in the cyclic GMP levels.

Taken together, these studies established that the physiological second messenger of ACTH is cyclic GMP thus, negating the concept that cyclic AMP is the universal second messenger of hormonal action and demonstrating that cyclic AMP is only a pharmacological transmitter of the ACTH response.

The above conclusions were in accord with the independent findings of other groups. They used different techniques and also reported that their data does not support the second messenger role of the cyclic AMP for the ACTH hormone (Davis and Garren, 1968; Montague and Howell, 1973; Richardson and Schulster, 1973; Sharma et al., 1976). Briefly, Moyle et al. (1973) in isolated adrenal cells found a lack of correlation between the ACTH–dependent steroidogenesis and cyclic AMP production. Using isolated adrenal cell column perfusion technology, Hudson and McMartin found that submaximal steroidogenic concentrations of ACTH do not release cyclic AMP into the perfuse (Hudson and McMartin, 1975). After ACTH stimulation of sheep adrenals *in vivo*, Espiner et al. (1974) did not detect cyclic AMP output at submaximal steroidogenic concentrations of ACTH. Honn and Chavin (1975) demonstrated that ACTH elevates cyclic GMP levels without a rise in cyclic AMP in the reptile adrenals.

Armed with the tools of the model isolated cell lines of the fasciculate and the adrenocortical carcinoma 494 cells, with the techniques of double-labeled $^{3}H/C^{14}$ radioisotopes, and with the information that ACTH control of steroidogenesis is indirect, occurring through the mediation of its second messengers, cyclic GMP, and cyclic AMP, we were in a good position to define the ACTH-dependent rate-limiting step of steroidogenesis (Wickramsinghe et al., 1969; Sharma, 1970a,b,c). Because none of the biosynthetic steps between cholesterol and (the 20S)-20-hydroxycholesterol were affected by ACTH, the transformation of (20S)-20-hydroxycholesterol to the final product corticosterone was investigated.

The results (Bhacca and Sharma, 1968; Sharma and Hebborn, 1968; Sawhney and Sharma, 1976) established that cleavage of the (the 20S)-20-hydroxycholesterol to corticosterone is the rate-limiting step and it is controlled by ACTH. The reaction occurs at the plasma membrane of the normal cells but does not occur in the malignant cells (Sawhney and Sharma, 1976). The cyclic GMP mimics the ACTH-dependent physiological effect and the cyclic AMP, the pharmacological effect. Notably, both cyclic nucleotides are unable to mimic the ACTH response in the carcinoma cells. These results were consistent with the conclusions that cyclic GMP and cyclic AMP are their respective physiological and pharmacological second messengers; they are generated inside the cell in response to the ACTH signal at the plasma membrane; the lesion/s in the carcinoma cell membrane terminates the ACTH, yet retains the second messenger activities.

To explain the bell-shaped configuration of the cyclic GMP curve in response to the ACTH concentration between one and 10 μunits, the following mathematical rate equation was derived from the ACTH-dependent membrane guanylate cyclase (Sharma, 1976). It has two sites with different affinities, $K_{1,}$ and K_2; the first molecule of ACTH activates the enzyme activity while the second molecule blocks it.

$$V = \frac{V_{max}SA}{K_1Km + (K_m + S)A + K_mA^2/K_2} \quad (1)$$

S and A represent the concentrations of GTP and ACTH, respectively, and K_1 and K_2 are equilibrium constants. Hence, the enzyme combines with the second molecule of ACTH with greater affinity than with the first one; the binding of the first ACTH molecule allosterically modifies the structure of the membrane guanylate cyclase.

The fact that the physiological concentrations of ACTH elevated cyclic GMP levels without affecting the level of cyclic

AMP indicated that cyclic GMP plays a critical role in mediating ACTH-stimulated steroidogenesis in the isolated fasciculate cell. Also, cyclic GMP may also be responsible for the formation of/or processing of specific mRNA that in turn may be translated into a process that is also cyclic GMP-dependent. However, at higher concentrations (more than 10 μunits) ACTH stimulates only the adenylate cyclase system. The latter stimulated system would be responsible for the synthesis of cyclic AMP, that in turn, through cyclic AMP-dependent protein kinase, may cause translation of the appropriate mRNA. Notably, at the time, the year 1976, cyclic GMP-dependent protein kinase was not known in the isolated fasciculate cell; however, at a later date, it was purified and characterized from the adrenal cortex (Ahrens and Sharma, 1979; Ahrens et al., 1982). Accordingly, the physiological concentration of ACTH generated cyclic GMP, activated cyclic GMP-dependent protein kinase, and finally produced the steroid hormone, corticosterone. Then, it was possible to prove that cyclic GMP-mediated steroidogenesis is mediated by cyclic GMP-dependent protein kinase.

In this manner, cyclic GMP originally detected in the rat urine by Ashman et al. (1963) was now qualified to be the second messenger of the polypeptide hormone ACTH. According to this concept, in sequential steps ACTH secreted from the pituitary through circulation was transported to the target fasciculate cell of the adrenal cortex; therein, it targeted the plasma membrane, generating intracellularly second messenger cyclic GMP; that in turn, through a chain of reactions produced corticosterone. The findings also demonstrated how this signaling was abnormal in the adrenocortical carcinoma 494 cells.

As stated, the second messenger role of cyclic GMP in the ACTH-modulated steroidogenesis was determined indirectly through the reconstituted *in vivo* cell studies, isolated fasciculate and carcinoma 494. To assess it in a direct and unequal fashion, the studies beyond the year 1976 were directed toward dissecting the components of these cells. Included in these studies was the component of the cyclic GMP-dependent protein kinase.

In the above-described studies, the level of cyclic GMP was measured through radioimmunoassay. To affirm these results, our group developed an alternate direct, yet equally sensitive assay (Perchellet et al., 1978). Based on the highly specific binding property of *E. coli* polypeptide chain elongation factor Tu (EF-Tu) with guanosine diphosphate (GDP), it included the conversion of cyclic GMP to 5′-GMP by phosphodiesterase (E.C.3.1.4.1) and the transfer of ^{32}P from [γ-^{32}P]adenosine triphosphate to GMP to yield [β-^{32}P]GDP by GMP kinase. There was no cross-reactivity with other cyclic nucleotides, including, cyclic AMP and cyclic IMP. The experiments where the cyclic GMP was measured through its radio-immunoassay were done side-by-side. The results were remarkably identical with both assay techniques.

They proved that, indeed, cyclic GMP was the physiological and cyclic AMP the pharmacological mediator of ACTH in the process of steroidogenesis. In the former case, there was the connected rise of cyclic GMP protein kinase, yet no rise of the cyclic AMP-dependent protein kinase. In the latter, the reverse was the case (Sharma and Sawhney, 1978).

The investigation moved on to define the physiological composition of the membrane guanylate cyclase transduction system (Perchellet and Sharma, 1979). Mimicking the natural cellular environment, the reconstitution study showed that the concentration of 2.5 mM Ca^{2+} was obligatory for the physiological levels of ACTH to generate the production of cyclic GMP and cause steroidogenesis in the isolated fasciculate cell. The Ca^{2+} alone did neither stimulate cyclic GMP production nor the process of steroidogenesis. Thus, Ca^{2+} and cyclic GMP are co-messengers in the ACTH-dependent steroidogenic process.

This fact taken together with the earlier one that cyclic GMP-dependent protein kinase activity concomitantly rises following the steroidogenic step, a model depicting the role of Ca^{2+} and cyclic GMP in ACTH-activated steroidogenesis was proposed (Figure 4 in Perchellet and Sharma, 1979).

MODEL

ACTH binds to its receptor located on the plasma membrane of the fasciculate adrenocortical cell. The Ca^{2+} regulates the transduction of information between hormone receptors and membrane guanylate cyclase. This leads to the increase in cyclic GMP which in turn, activates the cyclic GMP-dependent protein kinase activity, leading to the translation of a hypothetical preexistent mRNA. The synthesized protein controls the entry of cytoplasmic cholesterol into the mitochondrial precursor pool of cholesterol. The ACTH guided by these steps transforms this pool of cholesterol into the steroid hormone cortisol/corticosterone (**Figure 2**).

The validity of this model was supported by the purification of the adrenocortical cyclic GMP-dependent protein kinase from the bovine adrenal cortex (Sharma and Ahmed, 1976; Ahrens and Sharma, 1978; Ahrens et al., 1982). Notably, at that time, not only the identity of a cyclic GMP-dependent protein kinase was missing, but its existence was denied in the mammalian systems (Gill and McCune, 1979).

It was established that the Mr of the cyclic GMP-dependent protein kinase enzyme is 145,000; it is composed of two identical subunits each with Mr of 75,000. The enzyme self-phosphorylates; the stoichiometry of cyclic GMP binding is two molecules per holoenzyme, one to each of its subunits. The Ca^{2+}-modulated proteins, calmodulin or troponin C, markedly stimulate the maximal velocity of the enzyme. The steroidogenic potential of cyclic GMP and its analogs correlates closely with their ability to stimulate cyclic GMP-dependent protein kinase.

With the recognition of this puzzle piece, the ACTH signaling model was refined. Here, the two generated co-messengers of ACTH, Ca^{2+} and cyclic GMP activate the cyclic GMP-dependent protein kinase, this, in turn, accelerates the process. The mechanism of cyclic GMP activation of the protein kinase is that two molecules of cyclic GMP bind to the protein kinase holoenzyme, one to each of its subunits. Thus, the cyclic GMP-dependent protein kinase was no more a missing piece of the ACTH-modulated steroidogenic process, it was a part of it.

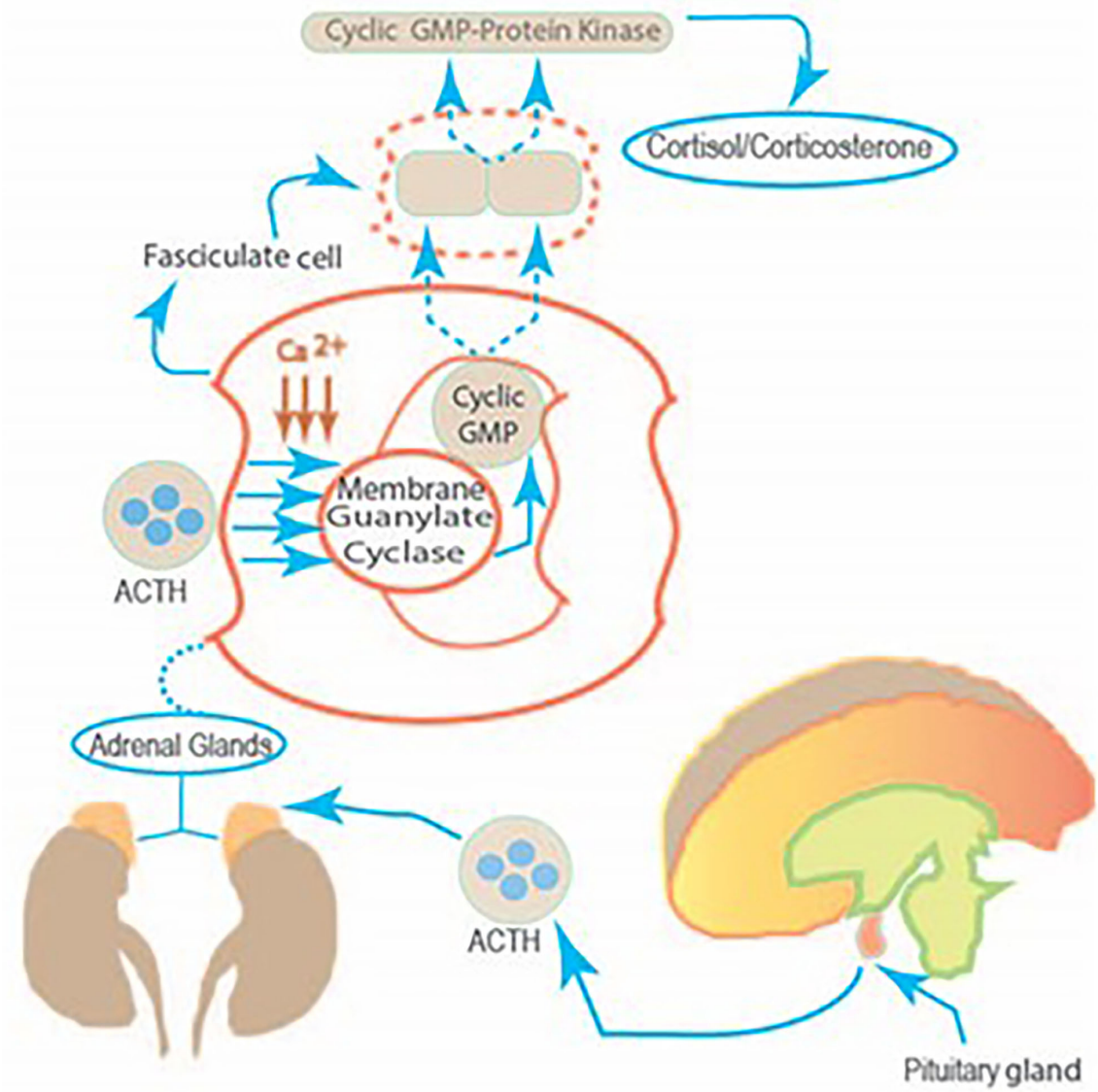

FIGURE 2 | The linkage between the pituitary gland and the fasciculate cell of the adrenal cortex. The molecular mechanism by which two ACTH co-messengers, Ca^{2+} and Cyclic GMP modulate steroidogenesis. The stimulus from the corticotropin-releasing factor, generated in the hypothalamus, produces corticotropin-releasing factor (CRF) in the anterior lobe of the pituitary. Therein, CRF controls ACTH release. This, in turn, targets the fasciculate cell of the adrenal cortex, causing a chain of molecular reactions and generating cortisol production.

It sub-served the activities of two complementary physiological second messengers of ACTH, cyclic GMP, and Ca^{2+}.

The discovery and molecular characterization of the cyclic GMP-dependent protein kinase powerfully impacted not only the field of hormonally-modulated membrane guanylate cyclase locked with the process of steroidogenesis but also corrected its molecular identity proposed by other laboratories as narrated below.

Originally, in 1971, Greengard's group discovered that the fat bodies of silk moth pupae and larvae contain exclusively cyclic GMP-dependent protein kinase activity (Kuo et al., 1971). Subsequently, the group identified this protein kinase in the mammalian cerebellum (Schlichter et al., 1980), expanding its presence from the MOTH kingdom to the mammalian. Its molecular identity from bovine lung and heart demonstrated that its Mr ranged from 145,000 to 165,000 (De Jonge and Rosen, 1977; Gill et al., 1977; Lincoln et al., 1977). The protein was composed of two equivalent subunits (Takai et al., 1975). Like the previously characterized cyclic AMP-dependent protein kinase holoenzyme, it was also a holoenzyme; each of its subunits was of a regulatory and a catalytic unit. Upon binding cyclic GMP, the holoenzyme underwent dissociation into regulatory and catalytic subunits (Miyamoto et al., 1973; Van Leemput-Coutrez et al., 1973; Kuo et al., 1974; Kuo, 1975; Kobayashi and Fang, 1976).

Ours and other groups, independently, showed that the assignment of the latter characteristic to the enzyme was flawed (Takai et al., 1976). The cyclic GMP-dependent protein kinase does not undergo dissociation upon binding into the stated subunits (Takai et al., 1976; Lincoln et al., 1977). It binds two molecules of cyclic GMP, one with each of its subunits (Sharma and Ahmed, 1976; Ahrens and Sharma, 1978; Kuroda and Sharma, 1982). Thus, the paradigms of signaling between the two systems, cyclic AMP and cyclic GMP are totally different.

Being confident now on the second messenger role of cyclic GMP in the ACTH-modulated process of steroidogenesis, our research advanced from the reconstituted isolated fasciculate cell to a cell-free system. Before the author recounts it, he describes its status in the cell signaling field at that time.

THE EXISTENCE OF THE HORMONALLY-DEPENDENT MEMBRANE GUANYLATE CYCLASE IN ANY MAMMALIAN SYSTEM WAS DENIED

The denial was aggressively driven by an elite group-linked network of investigators (Goldberg and Haddox, 1977; Murad et al., 1979). Their collective, yet diffused, reasoning was that the hormone-dependent membrane guanylate cyclase enzyme does not exist in nature; the rise of cyclic GMP observed in certain biological systems is artifactually caused by non-hormonal signals, like hydroxyl radical, hydrogen peroxide, lipids, and unsaturated fatty acids, oxidants, nitric oxide, and a variety of other nitric oxide generating compounds, such as nitrosoamines, including cigarette smoke (Wallach and Pastan, 1976; Arnold et al., 1977a,b; Katsuki et al., 1977a,b; Mittal and Murad, 1977a,b; Mittal et al., 1977; Murad et al., 1978a,b; Waldman et al., 1982). It was proposed that the underlying mechanism for the nitrite–generating compounds was the same, *via* nitric oxide gas (NO). Supporting this proposal, remarkably, the Murad's group published purification of a membrane guanylate cyclase from rat liver; yet it was not hormonally responsive. In contrast, NO targeted its catalytic site, its Mr was 80,000, and its substrate was Mn-GTP (Waldman et al., 1982); and, this membrane guanylate cyclase was present in all tissues ranging from peripheral to the central nervous system (Katsuki et al., 1977a,b). In 1981, Murad's group reported purification of the same enzyme from rat lungs but they revised its molecular weight to 150,000, a dimer consisting of two identical, Mr 72,000, subunits. The purified enzyme could be activated by nitric oxide, indicating that this compound interacts directly with the enzyme. Their later studies asserted that this guanylate cyclase could also be activated by other agents, hydroxyl radicals, and unsaturated fatty acids. In a subsequent 1986 publication, reporting similar results, yet, purified through immunoaffinity chromatography, the Murad's group again concluded that the rat lung enzyme inherits the pure soluble guanylate cyclase characteristics; its molecular weight is 150,000, it consists of two subunits with molecular weights of 82,000 and 70,000. Consequently, this group published similar characteristics of the purified rat liver, its molecular weight was 150,000; unreported was its subunit composition; yet the liver enzyme could be activated by nitroprusside, nitric oxide, arachidonate, linoleate, oleate, and superoxide dismutase (Braughler et al., 1979).

The conclusion of these erroneous claims was that the membrane guanylate cyclase was a non-specific enzyme that underwent regulation *via* the oxidation-reduction potential of the biochemical reactions (Murad et al., 1979). Also, at the time, the only known cyclic GMP-dependent cellular component was cyclic GMP-dependent protein kinase, yet not even one of its specific, distinct from that of the cyclic AMP-dependent protein kinase substrate was known. Hence, the revised consensus was that the cyclic GMP-dependent system lacked specificity and acted as a sub-servant to the cyclic AMP system. Therefore, no distinct hormonally dependent membrane guanylate cyclase or cyclic GMP-related specific signaling system existed in any of the biological systems and cyclic GMP had no second messenger role in cellular signaling (Gill and McCune, 1979).

Direct Membrane Guanylate Cyclase Studies in the Cell-Free System

To solve the confusion between the existence of the hormone (ACTH)-dependent membrane guanylate cyclase and its non-hormonal and non-specific soluble form, we used our model systems of the isolated fasciculate cell and the isolated adrenocortical carcinoma 494 cells. Their particulate fractions constituted the membranous and the soluble, the soluble form. The experiments were conducted side-by-side; and for the first time, it was possible to precisely compare their relative contents and their signaling properties from the same cells. The conclusions, summed below, settled that in the adrenal fasciculate and the adrenocortical carcinoma cells the membrane guanylate cyclase is solely coupled with the ACTH-dependent steroidogenesis, yet the soluble form is not (reviewed in Sharma, 2002).

1. The comparable cellular contents of the membrane vs. soluble forms of the guanylate cyclase are 80 vs. 20%.
2. Only the membrane form responds to the physiological concentrations of ACTH in the generation of cyclic GMP. The curve is bell-shaped; the 10^{-11} M brings it to the basal level.
3. The sodium nitroprusside or ascorbic acid only stimulates the soluble form.
4. The dithiol reagent inhibits the soluble form, yet has no effect on the membrane form.
5. Tuffstin, a four amino acid peptide, only stimulates the soluble form.
6. The dithiothreitol and N-ethylmaleimide, the sulfhydryl reagents, have very different types of effects on the membrane and soluble forms. The low concentrations of dithiothreitol (up to 2 mM), markedly stimulate the soluble, yet not the membrane form. N-ethylmaleimide inhibits the membrane but stimulates the soluble form.

After settlement that almost sole form in the intact isolated fasciculate cell is the membrane form of the guanylate cyclase and it is distinct from the soluble form, we endeavored to dissect the two co-messenger, Ca^{2+} and cyclic GMP, biochemical

components of the ACTH-modulated membrane guanylate cyclase system (Nambi et al., 1982c). For this task, we used the phenothiazone drug and chloropromazine. It selectively targets its Ca^{2+} site and blocks its interaction with the Ca^{2+}-receptor protein, calmodulin.

The conclusions were that chloropromazine, indeed, blocks the ACTH-modulated steroidogenesis; yet, it has no effect on the ACTH-binding step. Thus, in accordance with our previous conclusions, the guanylate cyclase functional system is composed of separate receptor and catalytic components; the Ca^{2+} *via* its Ca^{2+} binding protein, calmodulin, brings them together and makes the system biochemically active to catalyze the guanylate cyclase and generate its second messenger cyclic GMP. In this manner, Ca^{2+} and cyclic GMP serve as co-messengers of the ACTH-modulated membrane guanylate cyclase signaling system. Thereby, two independent forms of guanylate cyclase signaling systems were established in the fasciculate cell of the adrenal cortex and in the adrenocortical carcinoma 494 cell systems. One was membrane-bound and hormonally-modulated, the other was soluble and non-specifically activated. The ACTH-modulated signaling pathway originating from the tiniest gland in the brain, the pituitary, to the sole fasciculate cell in the adrenal cortex was established (**Figure 1**).

IN THIS MANNER, THE DOGMA THAT HORMONALLY-DEPENDENT MEMBRANE GUANYLATE CYCLASE DOES NOT EXIST IN NATURE WAS SHATTERED

A new cellular signal transduction field evolved. Ironically, in a lively scientific commentary the main group that consistently challenged its existence, later falsely claimed its foundation (Sharma, 1988). Besides being impure, consisting of at least 13 protein contaminants, the claim-based membrane guanylate cyclase was stimulated by hemin, a biochemical characteristic not inherited by the membrane guanylate cyclase, yet solely inherited by the soluble form of the membrane guanylate cyclase (Waldman et al., 1985).

The establishment of the ACTH-modulated membrane guanylate cyclase signaling pathway, originating in the pituitary gland of the brain and terminating at its target site in the isolated fasciculate cell of the adrenal cortex, at the morphological, physiological, and biochemical levels made it possible to compare it with its counterpart adrenocortical carcinoma 494 cells (Sharma, 1976, 1978, 1985; reviewed in Sharma and Criss, 1978). There were deformities at all levels, briefly summarized here; they were in accordance with the earliest concepts proposed by Claude Bernard and Charles Huggins. "... There must be controlling elements within the composition of fluids that bathe the cells of a multicellular organism". These thoughts were expanded in the book "Endocrine Control in Neoplasia" which the author edited together with Dr. Wayne E. Criss (Sharma and Criss, 1978), describing the lesions inflicted by carcinogenesis in a variety of cells.

Enlarging on these thoughts, the following sections demonstrate how these ACTH studies directly impacted the general cellular signal transduction pathways. They resulted in the discovery of a protein kinase, SPK 380 that controls the protein synthesis; a protein kinase, another AUT-PK 500 that only exists in the cancer cells, and $\alpha_{2\alpha D}$-adrenergic receptor that is linked with the epinephrine regulation.

THE ADRENOCORTICAL CARCINOMA 494

In 1971 our group established the rat colony bearing this cancer from the seed rats generously donated by Ney's group. This colony was maintained for 20 years (to the year 1989) in our laboratory; sadly the colony ceased to exist in the world when we were unable to sustain it for the lack of funds. Originally, this colony was developed by Snell and Stewart (1959) in sequential publications, both Ney's (Ney et al., 1969) and the Snell and Stewart's (Snell and Stewart, 1959) groups originally demonstrated that, in contrast to what occurs in the normal adrenal cortex, neither ACTH nor cyclic AMP stimulates the formation of corticosterone (reviewed in Sharma, 1976, 1978; Sharma and Criss, 1978).

In a systematic dissection, in contrast to the normal isolated fasciculate cell, our group found the following deformities in the adrenocortical carcinoma 494 cell system at the morphological, pharmacological, biochemical, and molecular levels.

Morphology

The ultrastructural characteristics of these cells were that they were round to oval and uniform in size; solidly packed and connected with inter-digitation of numerous villi projecting the cell membranes; no one cell was covered with a basal lamina; lipid granules were rare but when present, they were not surrounded by the smooth-surface endoplasmic reticulum (Sharma and Hashimoto, 1972).

Pharmacology

The cells had no physiological and pharmacological ACTH-responsive membrane guanylate cyclase and cyclic AMP second messenger signaling systems; yet, they contained an autonomous and powerful corticosterone generating system. Albeit, at the supra-pharmacological ACTH levels it contained a barely functional membrane guanylate cyclase transduction system (Perchellet and Sharma, 1977; Sharma et al., 1977).

Biochemistry

Direct studies demonstrated that the cells, not only lacked the second messenger cyclic AMP and cyclic GMP signaling networks, but they also were devoid of their next network components, cyclic GMP-dependent, and cyclic AMP-dependent protein kinases.

Thus, the biochemical conclusions were that the adrenocortical carcinoma 494 cells have generated an autonomic ACTH signaling machinery; it neither contains the normal second messenger signaling components of the membrane guanylate cyclase and cyclic AMP, nor of cyclic AMP-dependent protein kinase and cyclic GMP-dependent protein kinase, yet it generates huge amounts of ACTH with the concomitant production of an overabundance of corticosterone. Thus, this

autonomously controlled network functions to manifest the trophic activity of the steroid hormone, corticosterone. This activity is to sustain the survival of the cancer cell. Curiously, the normally sized adrenal gland weighs ∼30 mg, in contrast, one tumor nodule weighs 5–10 g; the bellies of the cancer-bearing rats are massively ballooned.

Ignited by these findings was a conscious awakening that the solution to this puzzle may reside in the cyclic nucleotide-independent protein kinase machinery present in the neoplastic cell. This defective tumor-evolved machinery will powerfully enhance the trophic effect of the steroid hormone corticosterone. It will be, however, absent in the normal cell. In addition, it was hypothesized that the normal fasciculate cell may contain its own unique protein kinase that keeps it non-malignant. The studies briefly narrated below, supported these concepts and exhilarated the mind. Two novel protein kinases with the following inquiries were discovered.

The inquiries were (1) Does the adrenal cortex contain a protein kinase that is locked with the initiation of the protein synthesis? (2) Does adrenocortical carcinoma 494 possess a unique protein kinase?

TASK 1

The self phosphorylating protein kinase 380 (SPK 380) was purified to homogeneity; biochemically and functionally characterized from the bovine adrenal cortex (Kuroda and Sharma, 1982, 1983; Kuroda et al., 1982a,b). The choice of the bovine species was based on the availability of a sufficient amount of the source material.

SPK 380 is a holoenzyme, consisting of three identical subunits of M_r 120,000. It is the self-phosphorylating protein kinase. It catalyzes the phosphorylation of its own histidine residue on τ-the amino group; this self-phosphorylation feature is reversible and unique to itself. In the presence of ADP and Mg^{2+}, the phosphate bound to the histidine residue is transferred to ADP, resulting in the formation of ATP. The SPK 380 specifically catalyzes the phosphorylation of serine residue of the α-subunit of eukaryotic initiation factor-2 (eIF-2α). Thus, inheriting a unique feature, a histidine protein kinase catalyzes the phosphorylation of the serine residue of another protein, eIF-2α. Functionally, in the reticulocyte lysate, SPK 380 by phosphorylating eIF-2α inhibits protein synthesis.

Significantly, focusing on the last property, SPK 380 is different from the two other cyclic nucleotide-independent eIF-2α protein kinases, hemin-controlled repressor (HCR) and double stranded-RNA activated inhibitor (dsRI) that also inhibit the initiation of protein synthesis. In contrast to these, its activity is independent of hemin and dsRI (discussed in Kuroda et al., 1982b).

Additional evidence for the SPK 380 (or its very close structurally-related protein kinase) role in protein synthesis was provided by its presence in the poly(A) mRNAs contained in the polysome fractions of the adrenal cortex (Moore and Sharma, 1980).

Thus, with the discovery of SPK 380, a new protein kinase feature arose. The protein kinase was no longer only a serine protein kinase that solely transmitted the signaling activities of cyclic AMP and cyclic GMP; or of eIF-2α regulating translational activities of HCR and dsRI. It also existed with a novel feature of being itself the Histidine Protein Kinase and eIF-2α-serine kinase that regulated the mammalian cell protein synthesis.

A model for the mechanism of translational control by SPK 380 is depicted below in the figure, reformatted and advanced from Sharma (1985) (**Figure 3**).

The elegance of this model was that the de-phosphorylation and the phosphorylation of eIF-2α represented the TURN "ON" and TURN "OFF" SWITCHES of the cellular protein synthesis. Thus, it solved the age-old puzzle of how polyamines, including tropic hormones—ACTH, Luteinizing, Thyroid Stimulating, Corticotropin-Releasing—are generated and secreted by the anterior pituitary; in turn, target and regulate their respective endocrine organs. Additionally, their eIF-2α-modulated "ON" and "OFF" switches are precisely tuned.

Any defect, affecting this switching mechanism will cause cellular abnormality, including cancer. Here, the endocrine cell embodies the unlimited protein-synthesizing machinery. The case in point is that the adrenocortical carcinoma 494 cells are the counterpart of the fasciculate cell of the adrenal cortex and it inherits the cancer deformities.

The validity of this hypothesis was attested by experimentation (Kuroda et al., 1982b).

The SPK 380 phosphorylated eIF-2α and polyamines—putrescine, spermidine, and spermine—inhibited phosphorylation of eIF-2α. The inhibition was concentration-dependent, with an order of potency: spermine > spermidine > putrescine. Since polyamine is basic, it was a possibility that the effect was artifactual. It, however, was not the case. Other basic peptides—polylysine and polyarginine—did not block SPK 380-dependent phosphorylation of eIF-2α.

Given the pieces of evidence that (i) the rate-limiting enzyme in the synthesis of putrescine, the precursor of the polyamines spermidine and spermine are, ornithine decarboxylase, (ii) its activity increases in parallel with the formation of putrescine and polyamines in rapidly growing tissues, (iii) in similarity with cases of the trophic hormone stimulation of the adrenal gland, thyroid, and gonads, it is possible that the activated SPK 380-dependent phosphorylation of eIF-2α is the determinant factor in the normal protein synthesis. Yet, it is broken down in their cancer counterpart organs.

Focusing on the adrenocortical carcinoma 494 cells, a brief description of the biochemistry of the Two Autonomously Controlled Systems is provided (Sharma et al., 1980; reviewed in Sharma, 1983; Ganguly et al., 1984; Majumdar et al., 1985, 1989).

ONE

Autophosphorylating Protein Kinase 500 (AUT-PK 500). Its purity and its self-phosphorylation characteristic were established by the criteria of (a) one- and two-dimensional polyacrylamide gel electrophoresis, (b) immuno-electrophoresis,

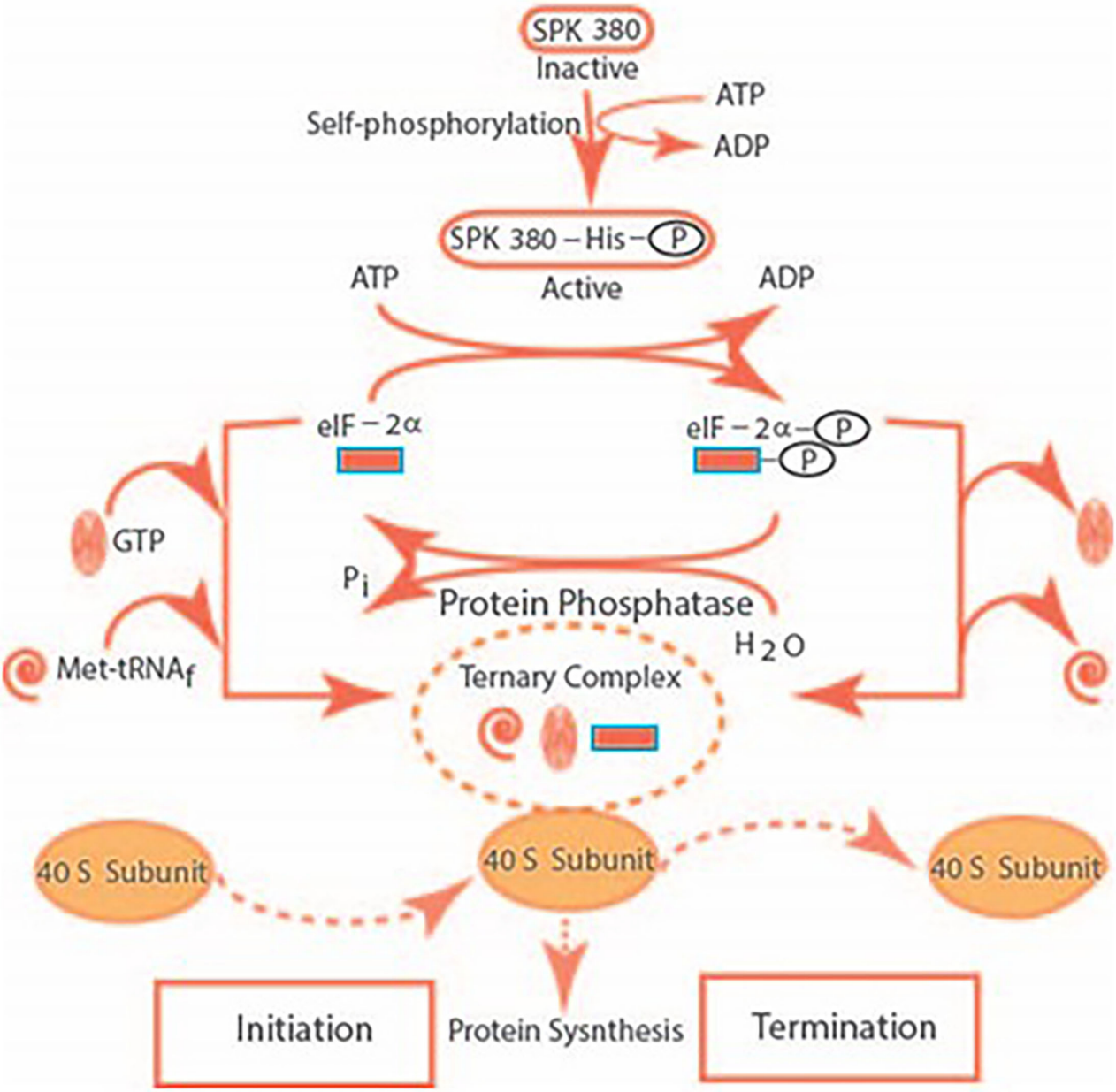

FIGURE 3 | The SPK self-phosphorylates its histidine residue and transforms itself from its inactive to the active form. It catalyzes the phosphorylation of the serine residue of eIF-2α. The eIF-2α-P dissociates the ternary complex of GTP, Met-tRNA$_f$, and the 40S ribosomal subunit. It results in the termination the of initiation of the protein synthesis. The ternary complex is restored after de-phosphorylation of eIF-2α, thus, restoring protein synthesis.

and crossed- immuno-electrophoresis with an immunoglobin produced against the enzyme, and (c) by the radioautography analysis of the phosphorylated and radio-iodinated enzyme.

Consisting of two identical subunits, 250,000-dalton, the AUT-PK 500 holoenzyme is a unique protein. Its activity or modulation is independent of the cyclic nucleotides, calcium, and also of another tumor-specific cyclic AMP-binding protein kinase, AUT-PK 85 (Shanker et al., 1979). It also is distinct from other cyclic nucleotide-independent protein kinases—the casein kinases I and II, the heme-controlled repressor, the double-stranded RNA-activated inhibitor, protease-activated kinases I and II and, the previously described SPK 380.

The AUT-PK 500 catalyzes the phosphorylation of its serine residue; the terminal phosphate of ATP is specifically used in this reaction. Anti-AUT-PK 500 blocks the self-phosphorylation reaction of the enzyme. Significantly, in contrast to SPK 380, polyarginine has no effect on the autophosphorylation of AUT-PK 500.

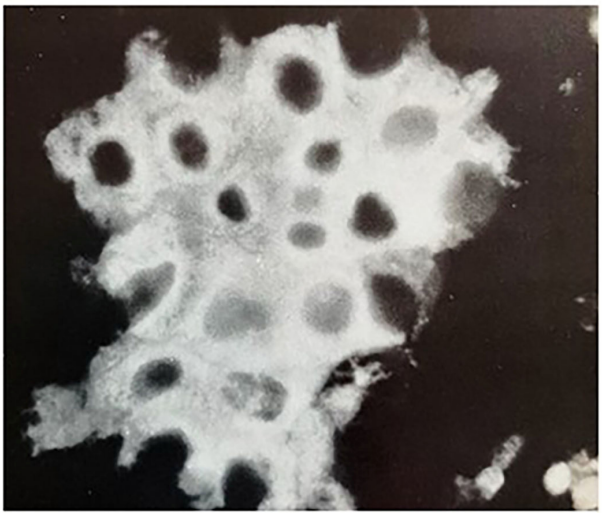

FIGURE 4 | Immunofluorescent localization of AUT-PK 500 in adrenocortical carcinoma 494 cells. Indirect immunofluorescence reaction of rabbit anti-AUT-PK 500 IgG with fixed cells that were freshly isolated from rat adrenocortical carcinoma demonstrated the perinuclear concentration of the enzyme as well as its homogenous cytoplasmic distribution. (Reproduced with permission, Ganguly et al., 1984).

Immunofluorescent search using rabbit anti-AUT-PK 500 IgG was made to detect the presence of AUT-PK 500 in the cultured colony of the adrenocortical carcinoma 494 cells. Its distribution was in vesicular cytoplasmic and perinuclear layers. The refined search demonstrated that the AUT-PK 500 resided exclusively in the membrane-bound ribosomal protein of Mr 31000, recognizing it to be its specific substrate; this finding was attested by screening through the use of its monoclonal antibody. Importantly, its level of presence was almost undetectable in the normal tissues—liver, spleen, testis, kidney, ovary, adrenal gland, pancreas, heart, lung, and pituitary. It became 100-fold elevated in the adrenocortical carcinoma 400, 50-fold in the four chemically-induced rapidly growing hepatomas, 30-fold in the chemically-induced mammary carcinoma, 20-fold in the cultured hepatoma cell line, and a 30-fold elevation in the pituitary tumor.

Its immunofluorescent localization in the adrenocortical carcinoma 494 cells is shown in the figure below (**Figure 4**).

Thus, the elevated expression of the AUT-PK 500 is reminiscent of neoplasia. It became a marker for its detection (United States Patent No. 4,594,319, Issued June 10, 1986, Protein Kinase Enzyme AUT-PK 500 and a Radioimmunoassay for Detection of Neoplasia).

TWO

Ectopic development of adrenergic receptors. Prior to the studies by our group that the adrenocortical carcinoma 494 embodies a novel ectopically-developed α_2-adrenergic receptor locked in with the membrane guanylate cyclase signal transduction system, it had been demonstrated that this tumor is linked with the ectopically developed epinephrine-dependent β-adrenergic receptor by the Lefkowitz's group (Williams et al., 1977; reviewed in Sharma, 1985). We proved that the α_2-adrenergic receptor-locked-in with the membrane guanylate cyclase signal transduction system is also modulated by epinephrine. Thus, by two independent signaling pathways, epinephrine modulates these autonomous pathways in the cancer cells. None of these pathways is present in the normal cells.

Below is recounted the establishment of the α_2-adrenergic receptor-locked membrane guanylate cyclase transduction system at the Pharmacological, Biochemical, and Molecular levels. Thus, the tumor contains two autonomously regulated signaling systems, both epinephrine-modulated, one mediated by the adenylate cyclase and the other by the membrane guanylate cyclase. Historically, it was the first demonstration that such a membrane guanylate signaling system exists in any mammalian cell. And, it still remains unknown in the normal cells. The task involved multiple steps. In all experiments, the isolated adrenocortical carcinoma 494 cells were the subject of investigation.

Step 1, Enzymatic and pharmacological characterization (Perchellet and Sharma, 1980; Shanker and Sharma, 1980). The epinephrine-modulated increase in cyclic GMP is blocked by the α-adrenergic antagonist phentolamine, yet not by the β-adrenergic antagonist propranolol. The rise of cyclic GMP level achieved is additive with that occurring with epinephrine. Thus, the cancer cell inherits two distinct cyclic GMP signaling pathways, one ACTH and the other epinephrine-dependent; yet, only the latter is coupled with the α-adrenergic receptor.

To jump to this critical decision, it needed the firm direct backup studies, as defined below (Perchellet and Sharma, 1980; Shanker and Sharma, 1980).

Mimicking epinephrine, the α-adrenergic agonist, phenylephrine, caused the concentration-dependent rise of cyclic GMP in the adrenocortical carcinoma 494 cells; the rise was blocked by its antagonist, phentolamine. Neither, acetylcholine, a cholinergic agonist, nor calcium caused any rise in cyclic GMP. Importantly, the rise maximally activated by ACTH was additive with that caused by the epinephrine. These results clearly dissected and showed that the adrenal cancer cell possesses ectopic α-adrenergic receptors and that epinephrine causes a rise in the cyclic GMP level through these receptors. They also affirmed the conclusion that the receptors for ACTH and epinephrine are distinct.

This was the first complete enzymatic and pharmacological analysis of the carcinoma cells and their bondage to the guanylate cyclase system.

Then, the studies with the non- and solubilized receptors moved on to settle that they were exclusive of the α_2-adrenergic receptor subtype; to that date, this subtype was not known. The experiments employed the use of a specific α_2-adrenergic agonist para-[^{3}H]aminoclonidine (PAC), and the α_2-adrenergic antagonist, yohimbine (Nambi et al., 1982a,b, 1983).

It was, thereby, established that the epinephrine-activated rise in cyclic GMP is mediated by the α_2-adrenergic receptors, it is coupled with the guanylate cyclase, and the transmembrane signal induced by the α_2-adrenergic agonist occurs by its

interaction with the α_2-adrenergic receptor, this, in turn, results in the rise of cyclic GMP. The conclusion was that it is one of the means of transmitting the catecholamine-sensitive biological response in the adrenocortical carcinoma 494 cells.

To elucidate the mechanism at the pharmacological, biochemical, and molecular levels by which adrenocortical carcinoma α_2-adrenergic receptor controls the membrane guanylate cyclase activity, it was critical to purify it and clone its mRNA.

PURIFICATION

It was achieved through an affinity chromatography step using a novel para-aminoclonidine-sepharose resin followed by a gel-permeation high-performance liquid chromatographic step. The radio-iodinated-receptor protein was homogeneous as evidenced by SDS-PAGE gel electrophoresis and by high-performance liquid chromatography. The protein was monomeric in nature with a M_r of 64,000 (Jaiswal and Sharma, 1985).

PHARMACOLOGY

It manifested the typical binding characteristics of α_2-adrenergic receptor, displacement of [^{3}H] para-amino-clonidine binding from the receptor by various adrenergic agonists and antagonists. Almost identical biochemical characteristics were then demonstrated in the human platelets (Jaiswal et al., 1989). Both the rat carcinoma and the human platelet forms were monomeric, 64,000-dalton proteins, with a pI of 4.2 and both showed typical α_2-adrenergic receptor binding characteristics. Nonetheless, the two-dimensional peptide maps of the trypsin-treated proteins showed minor, yet distinct, differences. It was possible that these were the species-specific, rodent vs. human differences. To assess this, the α_2-adrenergic receptor was cloned.

MOLECULAR CLONING AND EXPRESSION

It was achieved using the human platelet α_2-adrenergic receptor cDNA and rat genomic library. The major difference between the rat and the human forms resided in a stretch of 48-aminoacids within the third cytoplasmic loop. There, the identity was only 45%, demonstrating their differences in terms of their primary amino acid and the predicted secondary and tertiary structural features. The rat brain cDNA was expressed in a mammalian COS-2A cell line. It bound the α_2-adrenergic antagonist [^{3}H]-yohimbine. Based on the binding affinity for prazosin, the cloned receptor was closer pharmacologically and in molecular structure to its human form, α_{2A}-adrenergic receptor. Later studies demonstrated that these two forms were species-specific homologs, the one existing in the rodent rat was α_{2D}-adrenergic receptor subtype and the human form was α_{2A} subtype, settling that the α_{2D}-adrenergic receptor cA2-47 gene was nonexistent in the human genome. Furthermore, besides existing in the rat adrenocortical carcinoma, it existed in the rat tissues of the adrenal gland, brain, testes, and bovine retina. In the latter case crossing the evolutionary ladder (Chalberg et al., 1990).

There were several novel revelations brought forth with this study. One, this was the first cloned rodent α_2-adrenergic receptor. Two, it represented a new subtype, α_{2D}. Three, despite its very close structural identity with its human form, both being the seven-trans-membrane-spanning proteins, biochemically, it was uniquely linked with the membrane guanylate cyclase signaling system.

CONCLUSIONS IN RELEVANCE TO CANCER

This presentation demonstrates two important characteristics of a malignant cell. One, it grows without regulation by the cyclic GMP control signals present in the normal cells. Two, it possesses the property of metastasis. In addition, a typical characteristic of many adrenocortical carcinomas is their loss of regulation by ACTH in the synthesis of steroid hormones. Gaining an understanding of this loss requires precise knowledge of the ACTH-modulated machinery in its normal counterpart. The studies reviewed here have not addressed the question of whether the achievement of hormonal independence of adrenocortical cells is in any way related to malignancy. However, it can be speculated that the initial pre-neoplastic lesion in an adrenocortical cell results in the expression of a gene that is normally suppressed. This gene product, in turn, causes the transformation of the normal to the neoplastic cell. This speculation is in accordance with the multistep concept of neoplasia, in which the first event is immortalization, which subsequently leads to the neoplastic cell. The speculation is in accordance with the current notion that normal cells contain proto-oncogenes which under certain conditions can be activated to oncogenes, resulting in the initiation of/or sustaining carcinogenesis. It is then possible that (i) AUT-PK 500 is an adrenocortical cellular oncogene; (ii) the protein kinase is a cause for either immortalization or its subsequent steps in the adrenal cell; (iii) low-level expression of the enzyme is necessary for cellular growth with differentiation, but it is only when the gene expression is excessive that the cell acquires cancer phenotype (Reviewed in Sharma et al., 1988).

Broadening this concept to other cancers, it is in accordance with the original proposal that protein kinases complexed with the mRNAs, mRNP particles, play a key role in the translational processes of the liver and the hepatomas. The original observation demonstrated that the protein kinase of membranes of the endoplasmic reticulum of highly differentiated hepatomas has a different orientation within the membrane from that of the same enzyme found in the endoplasmic reticulum of the liver (Sharma et al., 1976). This difference may thus make it unavailable for phosphorylation of certain proteins in the tumor that are normally phosphorylated by this enzyme in the liver.

AUTHOR CONTRIBUTIONS

The author confirms being the sole contributor of this work and has approved it for publication.

ACKNOWLEDGMENTS

RS gratefully acknowledges the continuous financial support of the numerous USPHS awards from the National Institutes of Health, the beginning awards from the National Science Foundation, and the Damon Runyon Walter Winchell Cancer Fund; to the fellows in his group: Lynda Sutliff, Nahed K. Ahmed, Gouri Shanker, Rajinder Sawhney; Robert Moore, Jean-Pierre Perchellet, Elizabeth Perchellet, Yoshikazu Kuroda, Ponnal Nambi, Nambi Aiyar, Gypsy Majumdar, Helga Ahrens, Chhanda Ganguly, and Rama K. Jaiswal.

REFERENCES

Ahrens, H., Paul, A. K., Kuroda, Y., and Sharma, R. K. (1982). Adrenocortical cyclic GMP-dependent protein kinase: purification, characterization, and modification of its activity by calmodulin and its relationship with steroidogeneses. *Arch. Biochem. Biophys.* 215, 597–609. doi: 10.1016/0003-9861(82)90121-7

Ahrens, H., and Sharma, R. K. (1978). *Cyclic GMP-Dependent Protein Kinase in Bovine Adrenal Cortex*. (Abstract #3063) Am Soc Biol Chem, Atlanta, GA.

Ahrens, H., and Sharma, R. K. (1979). Guanosine 3′:5′-monophosphate-dependent protein kinase from bovine adrenal cortex: partial purification and characterization. *J. Steroid Biochem.* 11, 1099–1105. doi: 10.1016/0022-4731(79)90159-6

Arnold, W. P., Aldred, R., and Murad, F. (1977a). Cigarette smoke activates guanylate cyclase and increases cyclic GMP levels in tissues. *Science* 198, 934–936. doi: 10.1126/science.22126

Arnold, W. P., Mittal, C. K., Katsuki, S., and Murad, F. (1977b). Nitric oxide activates guanylate cyclase and increases guanosine 3′:5′-cyclic monophosphate levels in various tissue preparations. *Proc. Natl. Acad. Sci. U. S. A.* 74, 3203–3207. doi: 10.1073/pnas.74.8.3203

Ashman, D. F., Lipton, R., Melicow, M. M., and Price, T. D. (1963). Isolation of adenosine 3′, 5′-monophosphate and guanosine 3′, 5′-monophosphate from rat urine. *Biochem. Biophys. Res. Commun.* 11, 330–334. doi: 10.1016/0006-291X(63)90566-7

Bhacca, N. S., and Sharma, R. K. (1968). Mucronatinine, a new alkaloid from crotalaria mucronata Desv.-I. *Tetrahedron* 24, 6319–6326. doi: 10.1016/S0040-4020(01)96824-3

Braughler, J. M., Mittal, C. K., and Murad, F. (1979). Purification of soluble guanylate cyclase from rat liver. *Proc. Natl. Acad. Sci. U. S. A.* 76, 219–222. doi: 10.1073/pnas.76.1.219

Chalberg, S. C., Duda, T., Rhine, J. A., and Sharma, R. K. (1990). Molecular cloning, sequencing, and expression of an α2-adrenergic receptor complementary DNA from Rat brain. *Mol. Cell. Biochem.* 97, 161–172. doi: 10.1007/BF00221058

Davis, W. W., and Garren, L. D. (1968). On the mechanism of action of adrenocorticotropic hormone. *J. Biol. Chem.* 243, 5153–5157. doi: 10.1016/S0021-9258(18)92004-1

De Jonge, H. R., and Rosen, O. M. (1977). Self-phosphorylation of cyclic guanosine 3': 5'-monophosphate-dependent protein kinase from bovine lung. Effect of cyclic adenosine 3': 5'-monophosphate. *J. Biol. Chem.* 252, 2780–2783. doi: 10.1016/S0021-9258(17)40526-6

Espiner, E. A., Donald, R. A., Hart, D. S., Ross, J., and Jordan, R. B. (1974). Evidence for adrenocortical uptake of ACTH *in vivo*. *Am. J. Physiol.* 226, 96–104. doi: 10.1152/ajplegacy.1974.226.1.96

Ganguly, C., Roberts, A. N., Kuroda, Y., and Sharma, R. K. (1984). Rat adrenocortical carcinoma 494 autophosphorylating protein kinase, AUT-PK 500: purification, biochemical and immunological characterization and substrate specificity. *J. Biol. Chem.* 259, 5959–5969. doi: 10.1016/S0021-9258(18)91108-7

Gill, G. N., and McCune, R. W. (1979). Guanosine '3, 5'-monophosphate-dependent protein kinase. *Curr. Top. Cell. Regul.* 15, 1–45. doi: 10.1016/B978-0-12-152815-7.50005-3

Gill, G. N., Walton, G. M., and Sperry, P. J. (1977). Guanosine 3':5'-monophosphate-dependent protein kinase from bovine lung. Subunit structure and characterization of the purified enzyme. *J. Biol. Chem.* 252, 6443–6449. doi: 10.1016/S0021-9258(17)39979-9

Goldberg, N. D., and Haddox, M. K. (1977). Cyclic GMP metabolism and involvement in biological regulation. *Annu. Rev. Biochem.* 46, 823–896. doi: 10.1146/annurev.bi.46.070177.004135

Honn, K. V., and Chavin, W. (1975). ACTH control of adrenocortical c-GMP. *Gen. Comp. Endo.* 26, 374–381. doi: 10.1016/0016-6480(75)90091-X

Hudson, A. M., and McMartin, C. (1975). An investigation of the involvement of adenosine 3′:5′-cyclic monophosphate in steroidogenesis by using isolated adrenal cell column perfusion. *Biochem. J.* 148, 539–544. doi: 10.1042/bj1480539

Jaiswal, R. K., Marshak, D. R., and Sharma, R. K. (1989). Molecular comparison of α2-adrenergic receptors from rat adrenocortical carcinoma and human blood platelet. *Mol. Cell. Biochem.* 86, 41–53. doi: 10.1007/BF00231688

Jaiswal, R. K., and Sharma, R. K. (1985). Purification and characterization of α2-adrenergic receptors from the rat adrenocortical carcinoma. *Biochem. Biophys. Res. Commun.* 130, 58–64. doi: 10.1016/0006-291X(85)90381-X

Katsuki, S., Arnold, W., Mittal, C. K., and Murad, F. (1977b). Stimulation of guanylate cyclase by sodium nitroprusside, nitroglycerin and nitric oxide in various tissue preparations and comparison to the effects of sodium azide and hydroxylamine. *J. Cyclic Nucl. Res.* 3, 23–35.

Katsuki, S., Arnold, W. P., and Murad, F. (1977a). Effect of sodium nitroprusside, nitroglycerin and sodium azide on levels of cyclic nucleotides and mechanical activity of various tissues. *J. Cyclic Nucl. Res.* 3, 39–247.

Kitabchi, A. E., and Sharma, R. K. (1971). Corticosteroidogenesis in isolated adrenal cells of rats. I. effect of corticotropins and 3',5'-cyclic nucleotides on corticosterone production. *Endocrinology* 88, 1109–1116. doi: 10.1210/endo-88-5-1109

Kitabchi, A. E., Sharma, R. K., and West, W. H. (1971a). A sensitive bioassay method for ACTH using isolated rat adrenal cells. *Hormone Metab. Res.* 3, 133–134. doi: 10.1055/s-0028-1096767

Kitabchi, A. E., Wilson, D. B., and Sharma, R. K. (1971b). Steroidogenesis in isolated adrenal cells of rat. II. Effect of caffeine on ACTH and cyclic nucleotide-induced steroidogenesis and its relation to cyclic nucleotide phosphodiesterase (PDE). *Biochem. Biophys. Res. Commun.* 44, 898–904. doi: 10.1016/0006-291X(71)90796-0

Kobayashi, R., and Fang, V. S. (1976). Studies on cyclic GMP-dependent protein kinase properties by blue dextran-sepharose chromatography. *Biochem. Biopys. Res. Commun.* 69, 1080–1087. doi: 10.1016/0006-291X(76)90483-6

Kuo, J. F. (1975). Changes in relative levels of guanosine-3':5'-monophosphate-dependent and adenosine-3':5'-monophosphate-dependent protein kinases in lung, heart, and brain of developing guinea pigs. *Proc. Nat. Acad. Sci. U. S. A.* 72, 2256–2259. doi: 10.1073/pnas.72.6.2256

Kuo, J. F., Miyamoto, E., and Reyes, P. L. (1974). Activation and dissociation of adenosine 3′, 5′-monophosphate-dependent protein kinase by various cyclic nucleotide analogs. *Biochem. Pharmacol.* 23, 2011–2022. doi: 10.1016/0006-2952(74)90260-3

Kuo, J. F., Wyatt, G., and Greeengar, P. (1971). Cyclic Nucleotide-dependent Protein Kinases. IX. Partial purification and some properties of guanosine 3') 5'-monophosphatedependent and adenosine 3',5'-monophosphate-dependent protein kinases from various tissues and species of arthropoda. *J. Biol. Chem.* 246, 7159–7167. doi: 10.1016/S0021-9258(19)45868-7

Kuroda, Y., Merrick, W. C., and Sharma, R. K. (1982a). Specific phosphorylation of eukaryotic initiation factor 2α, eIF-2α, by bovine adrenocortical cyclic nucleotide-independent protein kinase, PK 380. *Arch. Biochem. Biophys.* 213, 271–275. doi: 10.1016/0003-9861(82)90462-3

Kuroda, Y., Merrick, W. C., and Sharma, R. K. (1982b). Polyamines inhibit the PK 380 catalyzed phosphorylation of eukaryotic initiation factor 2α. *Science* 215, 415–416. doi: 10.1126/science.7058326

Kuroda, Y., and Sharma, R. K. (1982). Bovine adrenocortical self-phosphorylating protein kinase, SPK 380: purification and characterization. *Arch. Biochem. Biophys.* 217, 588–596. doi: 10.1016/0003-9861(82)90541-0

Kuroda, Y., and Sharma, R. K. (1983). Reversibility of self-phosphorylation of a histidine residue of adrenocortical cyclic nucleotide-independent protein kinase, SPK 380. *Biochem. Biophys. Res. Commun*. 112, 884–890. doi: 10.1016/0006-291X(83)91700-X

Lincoln, T. M., Dills, W. L., Jr., and Corbin,. J. D. (1977). Purification and subunit composition of guanosine 3':5'-monophosphate-dependent protein kinase from bovine lung. *J. Biol. Chem*. 252, 4269–4275. doi: 10.1016/S0021-9258(17)40260-2

Majumdar, G., Cashel, M., and Sharma, R. K. (1985). Expression of autophosphorylating protein kinase (AUT-PK 500) in normal and neoplastic rat cells. *Proc. Natl. Acad. Sci. U. S. A*. 82, 5035–5039. doi: 10.1073/pnas.82.15.5035

Majumdar, G., Jefferson, W. E., and Sharma, R. K. (1989). A monoclonal antibody which identifies the autophosphorylation domain of autophosphorylating protein kinase 500. *Cancer Res*. 49, 1486–1491.

Mittal, C. K., Kimura, H., and Murad, F. (1977). Purification and properties of a protein required for sodium azide activation of guanylate cyclase. *J. Biol. Chem*. 252, 4384–4390. doi: 10.1016/S0021-9258(17)40276-6

Mittal, C. K., and Murad, F. (1977a). Properties and oxidative regulation of guanylate cyclase. *J. Cyclic Nucleotide Res*. 3, 381–391.

Mittal, C. K., and Murad, F. (1977b). Activation of guanylate cyclase by superoxide dismutase and hydroxyl radical: a physiological regulator of guanosine 3',5'-monophosphate formation. *Proc. Natl. Acad. Sci. U. S. A*. 74, 4360–4364. doi: 10.1073/pnas.74.10.4360

Miyamoto, E., Petzold, G. L., Kuo, J. F., and Greengard, P. (1973). Dissociation and activation of adenosine 3',5'-monophosphate-dependent and guanosine 3',5'-monophosphate-dependent protein kinases by cyclic nucleotides and by substrate proteins. *J. Biol. Chem*. 248, 179–189. doi: 10.1016/S0021-9258(19)44460-8

Montague, W., and Howell, S. L. (1973). The mode of action of adenosine 3′:5′-cyclic monophosphate in mammalian islets of Langerhans. Effects of insulin secretagogues on islet-cell protein kinase activity. *Biochem. J*. 134, 321–327. doi: 10.1042/bj1340321

Moore, R. E., and Sharma, R. K. (1980). The differential phosphorylation of free cytoplasmic and membrane-bound polysomal poly(A)mRNP particles in the adrenal cortex. *Endocrinology* 107, 1264–1265. doi: 10.1210/endo-107-4-1264

Moyle, W. R., Kong, Y. C., and Ramachandran, J. (1973). Steroidogenesis and cyclic adenosine 3′,5′-monophosphate accumulation in rat adrenal cells. Divergent effects of adrenocorticotropin and its o-nitryl sulfenyl derivative. *J. Biol. Chem*. 248, 2409–2417. doi: 10.1016/S0021-9258(19)44124-0

Murad, F., Arnold, W. P., Mittal, C. K., and Braughler, J. M. (1979). Properties and regulation of guanylate cyclase and some proposed functions for cyclic GMP. *Adv. Cyclic Nucleotide Res*. 11, 175–204.

Murad, F., Mittal, C. K., Arnold, W. P., Katsuki, S., and Kimura, H. (1978a). Guanylate cyclase: activation by azido, nitro compounds, nitric oxide, and hydroxyl radical and inhibition by hemoglobin and myoglobin. *Adv. Cyclic Nucleotide Res*. 9, 145–158.

Murad, F., Mittal, C., Arnold, W. P., Ichikara, K., Braughler, M., and El-Zayat, M. (1978b). "Properties and regulation of guanylate cyclase: activation by azide, nitro compounds, and hydroxyl radical and effects of heme containing proteins," in *Molecular Biology and Pharmacology of Cyclic Nucleotides*, eds G. Folco, and R. Paolettie (Elsevier, Amsterdam), 33–42.

Nambi, P., Aiyar, N. V., Roberts, A. N., and Sharma, R. K. (1982c). Relationship of calcium and membrane guanylate cyclase in adrenocorticotropin-induced steroidogenesis. *Endocrinology* 111, 196–200. doi: 10.1210/endo-111-1-196

Nambi, P., Aiyar, N. V., and Sharma, R. K. (1982a). Solubilization of epinephrine specific α2-adrenergic receptors from adrenocortical carcinoma. *FEBS Letters* 140, 98–102. doi: 10.1016/0014-5793(82)80529-2

Nambi, P., Aiyar, N. V., and Sharma, R. K. (1982b). Adrenocorticotropin-dependent particulate guanylate cyclase in rat adrenal and adrenocortical carcinoma: comparison of its properties with soluble guanylate cyclase and its relationship with ACTH-induced steroidogenesis. *Arch. Biochem. Biophys*. 217, 638–646. doi: 10.1016/0003-9861(82)90545-8

Nambi, P., Aiyar, N. V., and Sharma, R. K. (1983). Identification and characterization of ectopic α2-adrenergic receptors in adrenocortical carcinoma membranes. *J. Nutr. Growth Cancer* 1, 77–84.

Ney, R. L., Hochella, N. J., Grahame-Smith, D. G., Dexter, R. N., and Butcher, R. W. (1969). Abnormal regulation of adenosine 3',5'-monophosphate and corticosterone formation in an adrenocortical carcinoma. *J. Clin. Invest*. 48, 1733–1739. doi: 10.1172/JCI106139

Perchellet, J.-P., Shanker, G., and Sharma, R. K. (1978). Regulatory role of guanosine 3':5':-monophosphate in adrenocorticotropic hormone-induced steroidogenesis. *Science* 199, 311–312. doi: 10.1126/science.202028

Perchellet, J.-P., and Sharma, R. K. (1977). Metabolic regulation of steroidogenesis in isolated adrenocortical carcinoma cells. ACTH regulation of guanosine cyclic 3':5'-monophosphate levels. *Biochem. Biophys. Res. Commun*. 78, 676–683. doi: 10.1016/0006-291X(77)90232-7

Perchellet, J.-P., and Sharma, R. K. (1979). Mediatory role of calcium and guanosine 3',5'-monophosphate in adrenocorticotropin-induced steroidogenesis by adrenal cells. *Science* 203, 1259–1261. doi: 10.1126/science.34216

Perchellet, J.-P., and Sharma, R. K. (1980). Ectopic α-adrenergic accumulation of guanosine 3':5'-monophosphate in isolated adrenocortical carcinoma cells. *Endocrinology* 106, 1589–1593. doi: 10.1210/endo-106-5-1589

Richardson, M. C., and Schulster, D. (1973). The role of protein kinase activation in the control of steroidogenesis by adrenocorticotrophic hormone in the adrenal cortex. *Biochem. J*. 136, 993–998. doi: 10.1042/bj1360993

Sawhney, R. S., and Sharma, R. K. (1976). Different plasma membrane effects of adrenocorticotropic hormone and cyclic nucleotides in normal and malignant adrenal cells. *FEBS Letters* 70, 163–166. doi: 10.1016/0014-5793(76)80749-1

Schlichter, D. J., Detre, J. A., Aswad, D. W., Chehrazi, B., and Greengard, P. (1980). Localization of cyclic GMP-dependent protein kinase and substrate in mammalian cerebellum. *Proc. Natl. Acad. Sci. U. S. A*. 77, 5537–5541. doi: 10.1073/pnas.77.9.5537

Shanker, G., Ahrens, H., and Sharma, R. K. (1979). Novel protein kinase AUT-PK 85, isolated from adrenocortical carcinoma. Purification and characterization. *Proc. Natl. Acad. Sci. U. S. A*. 76, 66–70. doi: 10.1073/pnas.76.1.66

Shanker, G., and Sharma, R. K. (1980). Characterization of ectopic α-adrenergic binding receptors of adrenocortical carcinoma cells. *Endocrinology* 106, 1594–1598. doi: 10.1210/endo-106-5-1594

Sharma, R. K. (1970a). Biosynthesis of plant sterols and triterpenoids. The incorporation of (3RS)-2-14C, (4R)-43H1 mevaloate into α-spinasterol and β-amyrin, in Camellia sinensis. *Phytochemistry* 9, 565–568. doi: 10.1016/S0031-9422(00)85691-5

Sharma, R. K. (1970b). Biosynthesis of plant sterols: the stereochemistry of hydrogen elimination at C-7 in α-spinasterol. *Chem. Comm*. 117, 543. doi: 10.1039/C29700000543

Sharma, R. K. (1970c). Biosynthesis of plant sterols - the mechanism of the alkylation of α-spinasterol at C-24. *Curr. Sci*. 39, 466.

Sharma, R. K. (1973). Regulation of steroidogenesis by adrenocorticotropic hormone in isolated adrenal cells of rat. *J. Biol. Chem*. 248, 5473–5476. doi: 10.1016/S0021-9258(19)43627-2

Sharma, R. K. (1974). Metabolic regulation of steroidogenesis in isolated adrenal and adrenocortical carcinoma cells of rat. Effect of adrenocorticotropic hormone and adenosine cyclic 3',5'-monophosphate on the plasma membrane. *FEBS Letters* 38, 197–201. doi: 10.1016/0014-5793(74)80112-2

Sharma, R. K. (1976). "Regulation of steroidogenesis in adrenocortical carcinoma," in *Control Mechanisms in Cancer*, eds W. E. Criss, T. Ono, and J. R. Sabine (New York, NY: Raven Press; Honolulu: Tripartite Cancer Symposium Lecture), 109–124.

Sharma, R. K. (1978). "Abnormal adrenocorticotropic hormone control in adrenocortical carcinoma," in *Endocrine Control in Neoplasia*, eds R. K. Sharma and W. E. Criss (New York, NY: Raven Press), 13–52.

Sharma, R. K. (1983). "Regulation of adrenocortical protein synthesis - a new concept," in *CSIR Publications and Information Directorate, Council of Scientific and Industrial Research, India*, eds R. K. Sharma, U. K. Pandit, and P. D. Gupta (Jammu: Silver Jubilee Commemorative Lecture), 16–21.

Sharma, R. K. (1985). "Biochemical control in adrenocortical carcinoma," in *Hormonally Responsive Tumors*, eds V. P. Hollander (New York, NY: New York Academic Press), 185–217.

Sharma, R. K. (1988). Guanylate cyclase and the adrenal natriuretic factor receptor. *Science* 240, 805–806. doi: 10.1126/science.240.4853.805.b

Sharma, R. K. (2002). Evolution of the membrane guanylate cyclase transduction system. *Mol. Cell. Biochem*. 230, 3–30. doi: 10.1007/978-1-4615-0927-1_1

Sharma, R. K., and Ahmed, N. K. (1976). "Purification and characterization of adrenocortical carcinoma protein kinase enzyme," in *10th International Congress of Biochemistry, Hamburg, Germany, July 25–31*.

Sharma, R. K., Ahrens, H., Shanker, G., and Moore, R. E. (1980). Regulation of a novel autophosphorylating protein kinase by adrenocortical carcinoma. A review. *Cell. Mol. Biol*. 26, 65–76.

Sharma, R. K., and Brush, J. S. (1974). Metabolic regulation of steroidogenesis in adrenocortical carcinoma cells of rat. Effect of adrenocorticotropin and adenosine cyclic 3',5'-monophosphate on the incorporation of (20S)-20-hydroxy [7α-3H] cholesterol into deoxycorticosterone and corticosterone. *Biochem. Biophys. Res. Commun*. 56, 256–263. doi: 10.1016/S0006-291X(74)80342-6

Sharma, R. K., and Criss, W. E. (1978). *Endocrine Control in Neoplasia*. New York, NY: Raven Press.

Sharma, R. K., and Hashimoto, K. (1972). Ultrastructural studies and metabolic regulation of isolated adrenocortical carcinoma cells of rat. *Cancer Res*. 32, 666–674.

Sharma, R. K., Hashimoto, K., and Kitabchi, A. E. (1972). Steroidogenesis in isolated adrenal cells of rat. III. Morphological and biochemical correlation of cholesterol and cholesterol ester content in ACTH and N6-2'-0-dibutyryl-adenosine-3',5'-monophosphate activated adrenal cells. *Endocrinology* 91, 994–1003. doi: 10.1210/endo-91-4-994

Sharma, R. K., and Hebborn, P. (1968). Antitumor and antimicrobial screening of crosemperine, the otonecine ester occuring in crotalaria semperflorens vent. II. *J. Med. Chem*. 11, 620. doi: 10.1021/jm00309a053

Sharma, R. K., Marala, R. B., and Paul, A. K. (1988). "Mediatory role of cyclic GMP in receptor mediated signal transduction: membrane guanylate cyclase and its coupling with atrial natriuretic factor receptor," in: *Advances in Atrial Peptide Research, Vol II*, eds B. M. Brenner and J. H. Laragh (New York, NY: Raven Press; American Society of Hypertension Symposium Series), 61–77.

Sharma, R. K., and McLaughlin, C. A., and Pitot, H. C. (1976). Protein phosphorylation of the smooth and rough endoplasmic reticulum in normal and neoplastic liver of the rat. *Eur. J. Biochem*. 65, 577–586. doi: 10.1111/j.1432-1033.1976.tb10375.x

Sharma, R. K., and Sawhney, R. S. (1978). Metabolic regulation of steroidogenesis in isolated adrenal cell. investigation of the adrenocorticotropic hormone, guanosine 3':5'-monophosphate and adenosine 3':5'-monophosphate control step. *Biochemistry* 17, 316–321. doi: 10.1021/bi00595a019

Sharma, R. K., and Shanker, G., and Ahmed, N. K. (1977). Metabolic regulation and relationship of endogenous protein kinase activity and steroidogenesis in isolated adrenocortical carcinoma cells of the rat. *Cancer Res*. 37, 472–475.

Snell, K. C., and Stewart, H. L. (1959). Variations in histologic patterns and functional effects of a transplantable adrenal cortical carcinoma in intact, hypophysectomized, and newborn rats. *J. Nat. Cancer Inst*. 22, 1119–1132.

Takai, Y., Nakaya, S., Inoue, M., Kishimoto, A., Nishiyama, K., Yamamura, H., et al. (1976). Comparison of mode of activation of guanosine 3':5'-monophosphate-dependent and adenosine 3':5'-monophosphate-dependent protein kinases from silkworm. *J. Biol. Chem*. 251, 1481–1487. doi: 10.1016/S0021-9258(17)33765-1

Takai, Y., Nishiyama, K., Yamamura, H., and Nishizuka, Y. (1975). Guanosine 3':5'-monophosphate-dependent protein kinase from bovine cerebellum. Purification and characterization. *J. Biol. Chem*. 250, 4690–4695. doi: 10.1016/S0021-9258(19)41356-2

Van Leemput-Coutrez, M., Camus, J., and Christophe, J. (1973). Cyclic nucleotide-dependent protein kinases of the rat pancreas. *Biochem. Biophys. Res. Commun*. 54, 182–190. doi: 10.1016/0006-291X(73)90906-6

Waldman, S. A., Chang, L. Y., and Murad, F. (1985). A two-step procedure for obtaining highly purified particulate guanylate cyclase from rat lung. *Prep. Biochem*. 15, 103–106. doi: 10.1080/10826068508062265

Waldman, S. A., Lewicki, J. A., Brandwein, H. J., and Murad, F. (1982). Partial purification and characterization of particulate guanylate cyclase from rat liver after solubilization with trypsin. *J. Cyclic Nucleotide Res*. 8, 359–370.

Wallach, D., and Pastan, I. (1976). Stimulation of membranous guanylate cyclaseby concentrations of calcium that are in the physiological range. *Biochem. Biophys. Res. Commun*. 72, 859–865. doi: 10.1016/S0006-291X(76)80211-2

Wickramsinghe, J. A. F., Burrows, E. P., Sharma, R. K., Greig, J. B., and Caspi, E. (1969). The obligatory involvement of a C21 intermediate in the biosynthesis of cardenolides from cholesterol. *Phytochemistry* 8, 1433–1440. doi: 10.1016/S0031-9422(00)85911-7

Williams, L., T., Gore, T. B., and Lefkowitz, R.J. (1977). Ectopic beta-adrenergic receptor binding sites. Possible molecular basis of aberrant catecholamine responsiveness of an adrenocortical tumor adenylate cyclase. *J. Clin. Invest*. 59, 319–324. doi: 10.1172/JCI108643

Conflict of Interest: The author declares that the research was conducted in the absence of any commercial or financial relationships that could be construed as a potential conflict of interest.

Publisher's Note: All claims expressed in this article are solely those of the authors and do not necessarily represent those of their affiliated organizations, or those of the publisher, the editors and the reviewers. Any product that may be evaluated in this article, or claim that may be made by its manufacturer, is not guaranteed or endorsed by the publisher.

frontiers | Frontiers in Molecular Neuroscience

TYPE Review
PUBLISHED 05 January 2023
DOI 10.3389/fnmol.2022.1022771

OPEN ACCESS

EDITED BY
Robert A. Nichols,
University of Hawaii at Manoa,
United States

REVIEWED BY
Jean-Claude Desfontis,
Oniris, Ecole Nationale Vétérinaire Agroalimentaire et de l'Alimentation, France
Ana Méndez,
Institut d'Investigacio Biomedica de Bellvitge (IDIBELL), Spain

*CORRESPONDENCE
Teresa Duda
tduda@salus.edu

SPECIALTY SECTION
This article was submitted to Molecular Signalling and Pathways, a section of the journal Frontiers in Molecular Neuroscience

RECEIVED 18 August 2022
ACCEPTED 14 November 2022
PUBLISHED 05 January 2023

CITATION
Duda T and Sharma RK (2023) Multilimbed membrane guanylate cyclase signaling system, evolutionary ladder.
Front. Mol. Neurosci. 15:1022771.
doi: 10.3389/fnmol.2022.1022771

Multilimbed membrane guanylate cyclase signaling system, evolutionary ladder

Teresa Duda* and Rameshwar K. Sharma

The Unit of Regulatory and Molecular Biology, Research Divisions of Biochemistry and Molecular Biology, Salus University, Elkins Park, PA, United States

One monumental discovery in the field of cell biology is the establishment of the membrane guanylate cyclase signal transduction system. Decoding its fundamental, molecular, biochemical, and genetic features revolutionized the processes of developing therapies for diseases of endocrinology, cardiovasculature, and sensory neurons; lastly, it has started to leave its imprints with the atmospheric carbon dioxide. The membrane guanylate cyclase does so *via* its multi-limbed structure. The inter-netted limbs throughout the central, sympathetic, and parasympathetic systems perform these functions. They generate their common second messenger, cyclic GMP to affect the physiology. This review describes an historical account of their sequential evolutionary development, their structural components and their mechanisms of interaction. The foundational principles were laid down by the discovery of its first limb, the ACTH modulated signaling pathway (the companion monograph). It challenged two general existing dogmas at the time. First, there was the question of the existence of a membrane guanylate cyclase independent from a soluble form that was heme-regulated. Second, the sole known cyclic AMP three-component-transduction system was modulated by GTP-binding proteins, so there was the question of whether a one-component transduction system could exclusively modulate cyclic GMP in response to the polypeptide hormone, ACTH. The present review moves past the first question and narrates the evolution and complexity of the cyclic GMP signaling pathway. Besides ACTH, there are at least five additional limbs. Each embodies a unique modular design to perform a specific physiological function; exemplified by ATP binding and phosphorylation, Ca^{2+}-sensor proteins that either increase or decrease cyclic GMP synthesis, co-expression of antithetical Ca^{2+} sensors, GCAP1 and S100B, and modulation by atmospheric carbon dioxide and temperature. The complexity provided by these various manners of operation enables membrane guanylate cyclase to conduct diverse functions, exemplified by the control over cardiovasculature, sensory neurons and, endocrine systems.

KEYWORDS

membrane guanylate cyclase, cyclic GMP signaling pathways, surface receptors, calcium, sensory neurons, cardiovascular, carbon dioxide, transduction modes

Introduction

Existing initially in the shadows of cyclic AMP signaling, cyclic GMP has slowly rose to prominence as a critical signaling molecule controlled by the activities of soluble and membrane guanylate cyclases (MGCs) and phosphodiesterases. After a brief outline of the chronological development of the MGC field, we focus on the uniqueness of the modular design which adds layers of complexity and enables the enzyme to perform various physiological functions.

Some of the advancements made by the authors and their collaborators are featured. The narration is partially borrowed, with appropriate citations, from the authors' earlier reviews: (Sharma, 1978, 1985, 2002, 2010; Pugh et al., 1997; Sharma et al., 2004, 2014; Duda et al., 2005b, 2014; Sharma and Duda, 2012, 2014a,b).

Background

Beginning with the discovery of cyclic AMP in 1958, understanding of the molecular principles of hormonal signaling began to undergo a radical change. The new paradigm was that the hormone did not directly target its signaling site. Instead it did so through its second messenger, cyclic AMP (Sutherland and Rall, 1958; Sutherland and Rall, 1960; Ariëns and Simonis, 1966; Ariëns, 1967; Robison et al., 1967).

For constructing the building blocks of this "cyclic AMP second messenger" concept Sutherland in 1971 and Rodbell and Gilamn in 1994 were awarded Nobel prizes in physiology and medicine.

In Sutherland's original "second messenger" concept, hormone was the first messenger and its interacting cell surface receptor product, cyclic AMP, the second. Glycogen, catecholamines, and other polypeptide hormones manifested their biological activities within the cell in this manner. The principal features of this concept were envisioned to be applicable to all hormonal systems (Robison et al., 1967). The receptor was conceptualized as the critical component of a cell; there, the hormone interacted to produce a "stimulus." The term 'stimulus' was equivalent to the present term 'signal', which according to the "second messenger" concept, meant that adenylate cyclase was the means to convert the extracellular ligand-binding signal into the production of the intracellular cyclic AMP (Ariëns and Simonis, 1966; Ariëns, 1967). Implicit in this concept was the understanding that the events leading to the transformation of the binding signal to the production of the second messenger occurred in the cell's plasma membrane.

In the 1970's the term "transduction" was introduced by the Rodbell's group (Birnbaumer et al., 1970). It meant transformation of the hormonal signal into the generation of cyclic AMP. The critical molecule involved in transduction was GTP. It bound to its signaling component, termed G-protein that stimulated the next signaling component, the enzyme adenylate cyclase that catalyzed the production of cyclic AMP. The details of the last step were decoded by the groups of Gilman and Birnbaumer (reviewed in: Feder et al., 1986; Negishi et al., 1988; Hepler and Gilman, 1992; Birnbaumer and Birnbaumer, 1995).

The G proteins exist in two forms, stimulatory, G_s, and inhibitory, G_i; the former stimulates and the latter inhibits the transduction process. The molecular nature of the receptor specified the effect of the hormone. The cyclic AMP signaling system was thus a three-component system, composed of three distinct proteins – the receptor, the G protein, and the adenylate cyclase (Figure 1).

A similar G protein modulated pathway was discovered, subsequently. It was the phosphatidylinositol-signaling (reviewed in: Nishizuka, 1988; Berridge and Irvine, 1989; Bansal and Majerus, 1990; Harden, 1992; Strader et al., 1994). Here, the hormonal signal transformed phosphatidylinositol-4,5-bisphosphate (PIP_2), a lipid signaling molecule into two separate second messengers, diacylglycerol and inositol triphosphate (IP_3). IP_3 signal mobilized the intracellular Ca^{2+} pool that could open TRP channels, activate protein kinase C or act on other Ca^{2+} sensors. Diacylglycerol also activated protein kinase C and certain TRP channels.

The two G protein cellular signaling pathways had a common structural feature, the hormonal receptor transducer was G protein. The receptor was a seven transmembrane-spanning protein. The hormone bound the receptor and generated cyclic AMP or IP_3 *via* the amplifier component (Figure 1). The generated second messenger, cyclic AMP or IP_3, through a cascade of

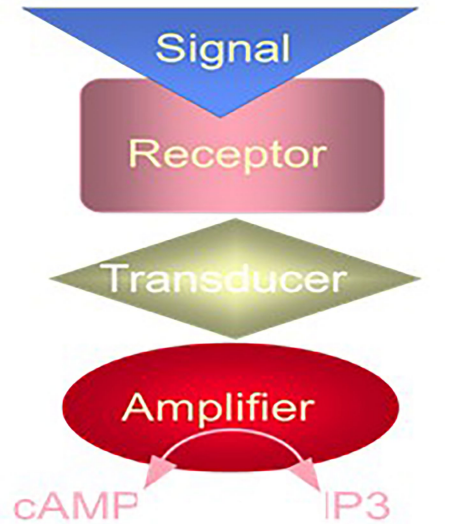

FIGURE 1
The cyclic AMP and IP3 signaling systems. The cyclic AMP and IP3 signaling systems consist of three separate components: hormone receptor, transducer (G protein) and amplifier adenylate cyclase (for cyclic AMP signaling) or phospholipase C (for IP3 signaling). (Modified from Sharma and Duda, 2014a).

biochemical reactions transduced the hormonal signal into a cell-specific physiological response.

Cyclic AMP signaling, modulated by the GTP-binding proteins, was the sole concept of cellular hormonal signaling from 1954 to 1970. Yet, relegated to its shadows, cyclic GMP had slowly begun to rise into prominence, and becoming an independent, third, hormonal signaling pathway. Its ascendance was, however, marked by un-surmounted hurdles by a few laboratories lead by Nobel laureates. Here, we briefly outline the sequential steps advancing the field of mammalian membrane guanylate cyclases, concentrating on their modular structures and complexity of their biochemistry and physiology. Note, that some contents are freely borrowed from earlier reviews (Sharma, 1978, 1985, 2002, 2010; Pugh et al., 1997; Sharma et al., 2004, 2014; Duda et al., 2005b, 2014; Sharma and Duda, 2012, 2014a,b).

Hormonally-modulated MGC signal-transduction pathway

Origin

Guanylate cyclase is an enzyme that catalyzes the transformation of GTP into cyclic GMP. Detection of cyclic GMP in rat urine (Ashman et al., 1963) and the observation that its concentration depended on the hormonal state (Hardman et al., 1969; Hardman and Sutherland, 1969) were the hints that it may be a hormonal second messenger. A model of membrane guanylate cyclase transduction system was first envisioned based on the cyclic AMP model. Finding of cyclic GMP and guanylate cyclase catalytic activity in the variety of tissues apparently supported this model (Goldberg et al., 1969, 1973; Ishikawa et al., 1969). It was short lived, however, with the superficial findings that the MGC activity was stimulated by various non-hormonal agents: polyunsaturated fatty acids, peroxides, hydroperoxides, free radicals, ascorbic acid, sodium nitroprusside, and even cigarette smoke (Goldberg and Haddox, 1977; Murad et al., 1979). Thus, the MGC lacked specificity and depended solely on cell's oxidation–reduction potential. In radical outlooks, no component of cyclic GMP turnover was viewed as linked to an intracellular signaling. A case in point, because the known cyclic GMP-dependent protein kinase exhibited cross-reactivity with cyclic AMP-dependent protein kinase, cyclic GMP was deemed only as an enhancer for cyclic AMP signaling (Gill and McCune, 1979; reviewed in: Goldberg and Haddox, 1977; Murad et al., 1979). Thus, cyclic GMP was a sub-servant of the cyclic AMP signaling.

Despite this, a few groups, including ours, moved on to explore and then established a role for cyclic GMP as a second messenger in hormonal signal transduction (reviewed in Sharma, 1978, 1985; Sharma et al., 1988a,b; Pugh et al., 1997; Sharma and Duda, 2012, 2014a,b; Sharma, 2002, 2010; Duda et al., 2005b, 2014; Sharma et al., 1997, 2016).

Two critical cell models were instrumental in achieving this goal. One, an ACTH-sensitive MGC transduction system that solely exists in the rat adrenocortical carcinoma 494 cells and also in the isolated adrenal fasciculata cells (Perchellet and Sharma, 1980; Shanker and Sharma, 1980; Jaiswal and Sharma, 1986; Jaiswal et al., 1986; reviewed in Sharma, 2002, 2010). Two, unlike adrenal homogenates, isolated adrenal fasciculata and adrenocortical carcinoma cells lacked cyclic AMP phosphodiesterase activity. These were therefore ideal for settling whether cyclic AMP is the sole hormonal second messenger or whether ACTH evokes MGC activity (Kitabchi et al., 1971; Sharma, 1972). This issue has extensively been discussed in the most recent review (Sharma, 2022).

The conclusions were:

(1) "The ACTH-modulated biosynthetic step is the cleavage of the (20S)-20-hydroxycholesterol to corticosterone. This step is dependent on the generation of cyclic GMP, yet, not on the cyclic AMP. Accordingly, the step requires the labile synthesis of protein and is rate limiting" (Sharma, 1973; Sharma, 1974; Sharma and Brush, 1974).
(2) In the model of the carcinoma cells, steroidogenesis gets out of ACTH control, yet not of cyclic GMP.
(3) The physiological concentrations of ACTH, 2.5 to 10 μunits, do not increase the synthesis of cyclic AMP but stimulate the peak synthesis of cyclic GMP with a simultaneous rise in corticosterone synthesis.
(4) Thus, "the hormone, ACTH, modulates the steroidogenic production was supported by purification from the bovine adrenal cortex of the cyclic GMP-dependent protein kinase, the enzyme directly locked in with cyclic GMP" (Sharma et al., 1976; Ahrens and Sharma, 1979; Ahrens et al., 1982).
(5) The Mr. of the cyclic GMP-dependent protein kinase is 145,000. Two identical subunits (75,000 Da each) form the functional enzyme. The enzyme binds two molecules of cyclic GMP per holoenzyme and self phosphorylates. Calmodulin and troponin C, markedly stimulate the enzyme. The ability of cyclic GMP and its analogs to stimulate steroidogenesis matches their ability to activate cyclic GMP-dependent protein kinase. Thus, this protein kinase is totally different from the cyclic AMP-dependent protein kinase which dissociates into its regulatory and catalytic subunits upon binding cyclic AMP.

These facts, and purification of the MGC from the rat adrenal cortex (Paul and Sharma, 1985), allowed us to propose the following model of MGC signaling (Figure 2).

While the studies on authenticity of the MGC signaling field were advancing, the investigators who originally doubted its existence took a turn around. Now, based on their new monoclonal antibody results with the lung soluble and MGC forms (Brandwein et al., 1981), they agreed on the independent existence of the MGC. Yet, they concluded, that biochemically and functionally the differences between both forms were only minor. Both forms were not the direct transducers of any hormonal signal. They responded only non-specifically to the common signals of

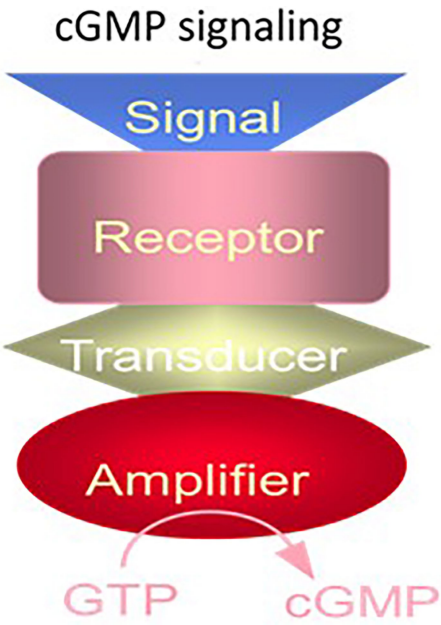

FIGURE 2
The cyclic GMP signaling system. The cyclic GMP signaling system consists of a single protein. The hormonal signal is recognized by the extracellular receptor domain; the signal is potentiated at the ATP-modulated ARM domain located next to the transmembrane domain in the intracellular portion of the protein (transducer) and the signal is amplified by the cyclase catalytic domain located at the C-terminus of the protein. (Modified from Sharma and Duda, 2014a).

hydroxyl radical, hydrogen peroxide, lipids and unsaturated fatty acids, oxidants, nitric oxide and a variety of other nitric oxide generating compounds such as nitrosoamines including cigarette smoke (Wallach and Pastan, 1976; Arnold et al., 1977; Mittal and Murad, 1977a; Murad et al., 1978a,b). This revised concept had two significant closings: (1) Underlying mechanism of action for all the nitrite-generating compounds is the same, *via* nitric oxide (NO) gas (Arnold et al., 1977; Katsuki et al., 1977; Mittal and Murad, 1977b; Waldman et al., 1982). (2) The NO activates the MGC at its catalytic site (Arnold et al., 1977).

They reinforced their concept by reporting the presence of NO-dependent MGC in almost all mammalian tissues, ranging from peripheral to the central nervous system. The response to NO varied, however; ranging from 3-fold stimulation in the liver to 14.7-fold in the rat cerebellum (Arnold et al., 1977).

The extraordinary conclusion was that both forms of guanylate cyclases are modulated by No; and none is hormonally modulated

This passionate pursuit on the physiological irrelevance of the hormone-dependent MGC was extended to the cyclic GMP-dependent protein kinase. The belief was that it did not phosphorylate any protein with higher specificity than cyclic AMP-dependent protein kinase did. The implication was that in the instances where a stimulus (signal) generated cyclic GMP in the intact cell, it acted through a cyclic AMP transduction component instead of the cyclic GMP. Again, reinforcing the concept that the cyclic GMP signaling pathway was a subservient to the cyclic AMP transduction system (Gill and McCune, 1979).

Remarkably, for the discovery of the NO, and NO-modulated cyclic GMP signaling system, Robert Furchgott, Louis Ignarro and Ferid Murad were awarded the 1998 Nobel Prize in Physiology or Medicine. The underlying mechanism for the NO action was cited as: the NO gas generated in the endothelial cell layer, signaled guanylyl cyclase activation, and the generated cyclic GMP caused relaxation of the blood vessels.

Also, notably, in this concept, the soluble guanylate cyclase was the sole cellular signaling pathway.

The details for these awards, none-the-less, are misleading for two reasons. (1) It totally ignored the historical evolution of the MGC signal transduction. Factually, in the beginning these laboratories not only denied its cellular existence, they aggressively negated the ongoing results of the other laboratories that had established the physiological, biochemical and structural integrity of the membrane guanylate cyclase signal transduction. Before 1998, the date of the award, other groups, including ours in 1982, had already demonstrated that the guanylate cyclase exists in two forms, soluble and the MGC (Nambi et al., 1982). Only, the membrane bound form is locked with the hormonal signal transduction. And, this transduction system is not sub-servient to the cyclic AMP signaling system. (2) The awarded recipients believed that "both forms, membrane and soluble, guanylate cyclases were modulated by NO."

The earliest documented facts, however, were that the membrane form is not NO-modulated and it is structurally and functionally different from the soluble form as summarized in Table 1 (according to Nambi et al., 1982).

The present understanding is that the soluble guanylate cyclase is modulated by NO, it is encoded by two genes (Denninger and Marletta, 1999), is heterodimeric and requires heme for its activity (Allerston et al., 2013). In contrast, the molecular structure of the membrane guanylate cyclase is totally different (Figure 3).

TABLE 1 Summary of the properties of particulate and soluble guanylate cyclase of rat adrenocortical tissue (from Sharma, 2002).

Conditions	Particulate	Soluble
Abundance	80%	20%
ACTH	Stimulation	No effect
Sodium nitroprusside	No effect	Stimulation
Sodium azide	No effect	Stimulation
Tuftsin	No effect	Stimulation
Cd^{2+}	Inhibition at high conc. (EC_{50}–400 μM)	Inhibition at low conc. (EC_{50}–2 μM)
Dithiothreitol	No effect	Strong stimulation
N-Ethylamide	Inhibition	Stimulation at low and inhibition at high conc.

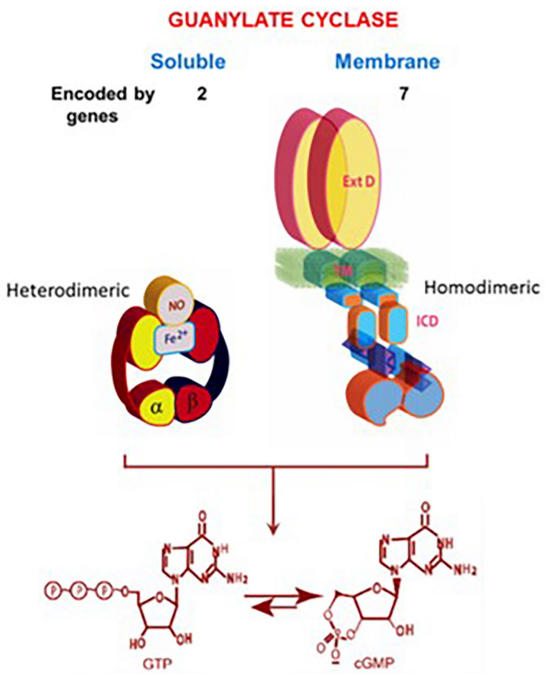

FIGURE 3
Soluble *vs.* membrane guanylate cyclase. Upper panel: Graphical representation of soluble and membrane guanylate cyclases. The soluble form is encoded by two genes; it is heterodimeric (subunits α and β) and requires heme for its activity. Both monomers contribute to the catalytic center, but their orientation is unknown yet (Allerston et al., 2013). The membrane guanylate cyclase is encoded by seven genes. It is a single transmembrane spanning protein. The extracellular domain (Ext) is located outside the cell; the transmembrane domain (TM) spans the plasma membrane; and the intracellular domain (ICD) is located inside the cell. The active form is homodimeric. The cyclase catalytic domain is located at the C-terminus of the protein. Both monomers in antiparallel orientation contribute to the catalytic center. Lower panel: Both cyclases are lyases (EC4.6.1.2) and catalyze synthesis of cyclic GMP from GTP. (From: (Sharma and Duda, 2014a).

Atrial natriuretic factor receptor guanylate cyclase (ANF-RGC) is the first purified and characterized MGC

The proposed structural model of the MGC purified from rat adrenocortical carcinoma (Paul and Sharma, 1985; Paul, 1986; Paul et al., 1987; Sharma et al., 1988a; Sharma and Duda, 2014b) and later from the rat adrenal cortex (Takayanagi et al., 1987a,b; Meloche et al., 1988) established that it is a receptor for atrial natriuretic factor (ANF); and, it is a three component transduction system, all components embodied in one protein. This MGC was named ANF-RGC, it specified the basis for ANF-stimulated cyclic GMP and corticosterone synthesis (Jaiswal et al., 1986). The narration in this original report is notable, "coexistence of the ANF receptor and guanylate cyclase activities on a single polypeptide chain indicates that the mechanism of transmembrane signal transduction involving mediation by second messenger, cyclic GMP, is different from the adenylate cyclase system. In hormone-dependent adenylate cyclase there is an assemblage of individual components – receptor, GTP binding protein, and catalytic moiety – for signal transduction (Figure 1). In contrast, the presence of dual activities – receptor binding and enzymatic – on a single polypeptide chain (Figure 2) indicates that this transmembrane protein contains both the information for signal recognition and its translation into a second messenger" (citation from Paul et al., 1987).

Thus, ANF-RGC was a multimodal signal transducer (Sharma et al., 1988a,b; Sharma, 2002). Its hallmark characteristics were that a hormone receptor domain projected extracellularly, a catalytic domain was inside the cell and a transmembrane domain linked the two. Its wide expression was shown through immunostaining by the antibody used to purify ANF-RGC to homogeneity from adrenocortical carcinoma and from adrenal cortex with neurons of the ventral horn region of rat spinal cord, cerebellar Purkinje cells, and renal glomerular cells (Ballermann et al., 1988; Marala and Sharma, 1988). A curious result of the early studies was that Ca^{2+} was needed for stimulation of steroidogenesis (Sayers et al., 1972; Haksar and Péron, 1973; Bowyer and Kitabchi, 1974), yet by itself, Ca^{2+} was ineffectual. Only with ACTH, did it become an effective steroidogenic factor (Perchellet and Sharma, 1979). Although the underlying mechanisms have not been known, Ca^{2+} would be, and was later found, to play a significant role in regulating MGC activity and multiplying its functionality.

In this manner the torturous debate questioning the independent existence of the hormone-dependent guanylate cyclase transduction system in mammalian systems ceased. Besides cyclic AMP and IP_3, it was recognized as the third cellular signaling system. Extraordinarily, being independent of heme and NO gas modulation, it shattered the dogma that membrane guanylate cyclase signal transduction is modulated by these agents. This point is historically critical as narrated below.

In 1988, shortly after the Paul et al. (1987) paper was published (Paul et al., 1987), the Murad's group, in a commentary in Science (Waldman et al., 1988) challenged our primacy in the discovery of ANF-RGC. The challenge was meritless, however (Sharma, 1988). By the authors' own statement (Kuno et al., 1986), the enzyme, they purified from the rat lung, was not homogeneous but only 95% pure, leaving the possibility that the 5% contaminant contained the separate ligand binding or the cyclase catalytic activity. Also, in contrast to the 1:1 stoichiometry, the lung enzyme bound only 14.5% of ANF theoretical value and was stimulated by hemin, a characteristic of the soluble guanylate cyclase.

Significantly, these issues were never countered by the Murad's group.

It was, thus, settled that ANF-RGC reported by our group was the first discovered surface receptor membrane guanylate cyclase. Particularly, it possesses two biological activities, a surface receptor and an enzyme. Subsequently, the ANF-RGC field grew logarithmically, with the new discoveries that (1) the source of ANF is the heart atria; (2) the heart is the endocrine gland; (3) ANF is the most potent hypotensive agent.

The studies initiated by the De Bold's group and followed by others' revolutionized the field of cardiovasculature and provided an opening for advancing the ANF research toward the development of drugs for hypertension (De Bold, 1982; Cantin and Genest, 1985; Schwartz et al., 1985; Atlas and Laragh, 1986; De Bold, 1986). It was shown that ANF regulates sodium excretion, water balance and blood pressure. And, significantly, ANF, a polypeptide hormone, besides ACTH, modulates the MGC activity. It, therefore, widened the mode of hormonal signal transduction providing clues for future explorations, basic and clinical.

With the knowledge that ANF-RGC is present in the adrenal gland, we asked two critical questions: (1) Does the heart-originated ANF signal modulate the steroidogenic machinery of the adrenal gland? And (2) how does ANF, *via* its surface receptor domain, activates the catalytic domain of ANF-RGC and generates cyclic GMP?

In reference to (1), ANF-RGC presence in the glandular tissues of the adrenal gland and testis supported the idea that the heart signals the metabolic processes of steroidogenesis in these endocrine tissues. Accordingly, studies from various groups showed that ANF raises the levels of cyclic GMP and down-regulates the aldosterone formation in the adrenal glomerulosa cells (Atarashi et al., 1984; Chartier et al., 1984; De Léan et al., 1984; Kudo and Baird, 1984). Noting that aldosterone is the most potent hypertensive steroid hormone and ANF, the most potent hypotensive agent, the presence of ANF-RGC in the glandular tissues indicated that ANF-RGC is a SWITCH that links heart and these glands (Figure 4).

It was now possible to elucidate the molecular principles of this SWITCH and conquer the diseases of hyper-and hypo-tension. Indeed, as the future holds, this was one of the game changer contribution in the field of cardiology.

In hindsight, additional investigations started to flood in. They ranged from the purification of ANF-RGC from other glandular tissues to its cloning and its' varied modes of steroidogenesis (reviewed in: Sharma, 2002).

Three years after the discovery of ANF-RC, its cDNA was cloned, and genetically tailored to probe the signaling site for ANF (Duda et al., 1991). Notably, purification of ANF-RGC expressed in COS cells using the antibody raised against the ANF-RGC purified from the rat adrenocortical carcinoma proved that the native and the cloned ANF-RGCs are immunologically identical.

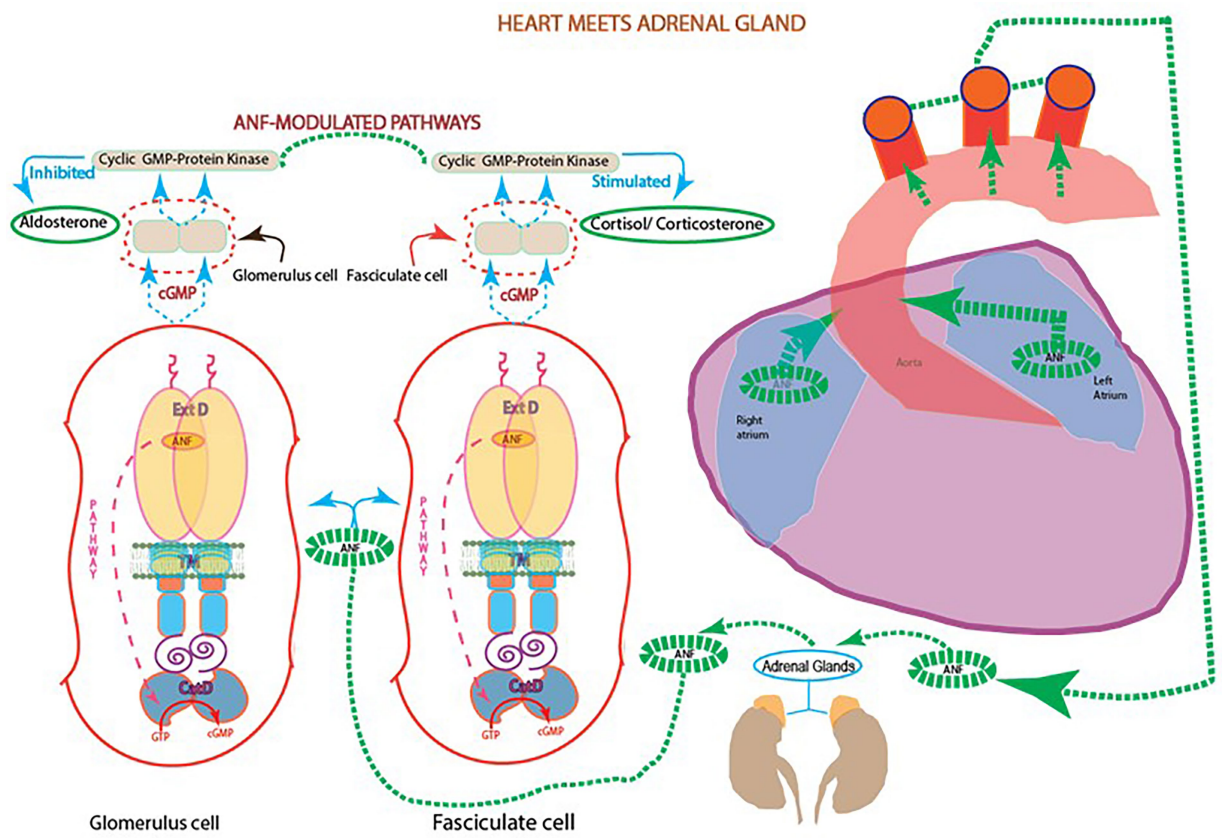

FIGURE 4
Heart meets adrenal gland: ANF reciprocal modulation of the two steroidogenic pathways. With every heartbeat, atria stretches and secretes ANF to the circulation. In the adrenal gland, ANF branches and initiates two signaling pathways involving cyclic GMP: one at the fasciculate cells to stimulate the production of cortisol/corticosterone; and the other at glomerular cells to inhibit the production of aldosterone and lower blood pressure.

Following the discovery of ANF-RGC, a very closely related MGC, type C natriuretic peptide receptor guanylate cyclase (CNP-RGC), was cloned first in a joint effort (Chinkers et al., 1989; Lowe et al., 1989) and then reported separately by the two laboratories (Chang et al., 1989; Schulz et al., 1989). The cloning of the mouse analog of ANF-RGC soon followed (Pandey and Singh, 1990). Another mRNA of a functionally defined form of MGC, STa-RGC, was cloned from the intestinal mucosa (Schulz et al., 1990; de Sauvage et al., 1991; Singh et al., 1991). This cyclase was a receptor for the bacterial enterotoxin and for the endogenous peptide hormones: guanylin and uroguanylin (Currie et al., 1992; Wiegand et al., 1992; Hamra et al., 1993; Khare et al., 1994).

Now, the identities of three forms of the MGCs were known. They, constituted a SURFACE RECEPTOR family. Two members, ANF-RGC and CNP-RGC were locked in with the physiology of cardiovasculature; third, STa-RGC, with the intestine. In a common theme, the family relaxed the vasculatures of their respective target organs and ANF-RGC also toned down the hypertensive activity.

The receptor MGC transduction system is also present in the central nervous system

Prior to 1993 the consensus was that the surface receptor MGC signaling system existed exclusively in the periphery (Needleman et al., 1989; Brenner et al., 1990; Rosenzweig and Seidman, 1991). Yet, there were clues, that this may not be true. Ours and two other groups had documented the presence of ANF-RGC in the retina, through immunology and molecular cloning studies (Cooper et al., 1989; Duda et al., 1992; Kutty et al., 1992; Ahmad and Barnstable, 1993). Similarly, *via* the Northern-blot analysis presence of the CNP-RGC was detected in the central nervous system and in the cells of the neural crest (Kojima et al., 1990; Sudoh et al., 1990). Molecular cloning studies had established presence of CNP-RGC in the brain (Cooper et al., 1989). Yet, the attempts to demonstrate CNP-RGC in the retina had failed (Ahmad and Barnstable, 1993).

In 1993, our group entered the field of sensory neurons in the retina. The goal was to explore the presence of CNP-RGC there, and if confirmed, define its transduction system.

Cloning and expression

CNP-RGC cDNA was cloned from a phage human retina cDNA library (Duda et al., 1993b). The cDNA was then inserted into the pSVL vector and expressed in COS-7 cells. With the prior availability of the cloned pSVL-ANF-RGC, it was possible to compare the properties of these two MGCs.

MGCs embody a modular design

Hydropathy analysis showed that ANF-RGC, CNP-RGC and STa-RGC, are modular, with matching topographies. The extracellular domain, the receptor domain, binds a hormone and has maximal structural diversity. The intracellular portion begins with a tyrosine protein kinase-like domain and extends to a catalytic domain (Duda et al., 1991; PNAS). Using the recombinant tools and guided by the ANF-RGC structural template, it was possible to map the domains, and propose the mechanism of the transmembrane migration of the hormonal signal (reviewed in Sharma et al., 2016).

The first goal was to verify that the extracellular domain (ExtD) of ANF-RGC indeed houses the hormone's (ANF) binding site. A GCα mutant of ANF-RGC, cloned from the adrenal cDNA library differed from ANF-RGC in two amino acid residues within the ExtD: position 338 was occupied by His instead of Gln and in position 364 Pro substituted for Leu (Duda et al., 1991). GCα exhibited cyclase catalytic activity but did not respond to ANF. Mutating the 338 and 364 residues of GCα to those of ANF-RGC restored ANF binding and ANF dependence in activation of the catalytic activity.

Thus, Gln^{338} and/or Leu^{364} are obligatory for ANF stimulation. Ensuing point mutation analyses singled out Leu^{364} as the key residue for both activities.

Thus, the following features of ANF-RGC were proven: (1) ExtD, (2) the Leu^{364} of this domain is critically necessary for ANF binding, (3) in the intracellular domain the catalytic domain follows the kinase-like domain, and (4) the catalytic domain possesses both the basal and the hormone-dependent activities. Binding of ANF to the ExtD controls the catalytic activity in the intracellular domain (Figure 5A).

From the historic perspective, GCα, that was decisive in determining the ANF binding site and was the first mutant of any MGC linked with hormonally-dependent catalytic activity (Duda et al., 1991).

In CNP-RGC, Val^{358} corresponds to Gln^{338} and Glu^{332} was found to be vital for CNP binding and CNP-dependent cyclase activity; similar to Leu^{364} of ANF-RGC it does not have any effect on the basal cyclase activity of CNP-RGC (Duda et al., 1994). Replacing Gln^{338} residue with Glu bestows ANF-RGC with significant CNP-dependent activity (Duda et al., 1995).Therefore, Leu^{364} and Glu^{332} in ANF-RGC and CNP-RGC, respectively are equivalent in controlling the ligand specificities of these MGCs. Later, crystallographic analyses of the ExtD of ANF-RGC provided validation for the above and showed that this domain forms head-to-head homodimers (He et al., 2001; Ogawa et al., 2004, 2009).

Hormonal signal transduction is ATP-regulated

A puzzling fact was that although purified ANF-RGC bound ANF stoichiometrically, its catalytic activity was unresponsive to ANF (Paul et al., 1987). This riddle was solved by two groups almost concomitantly, ours and Garbers's, demonstrating that ATP is obligatory for ANF-dependent ANF-RGC activity (Chinkers et al., 1991; Marala et al., 1991). Neither ANF nor ATP

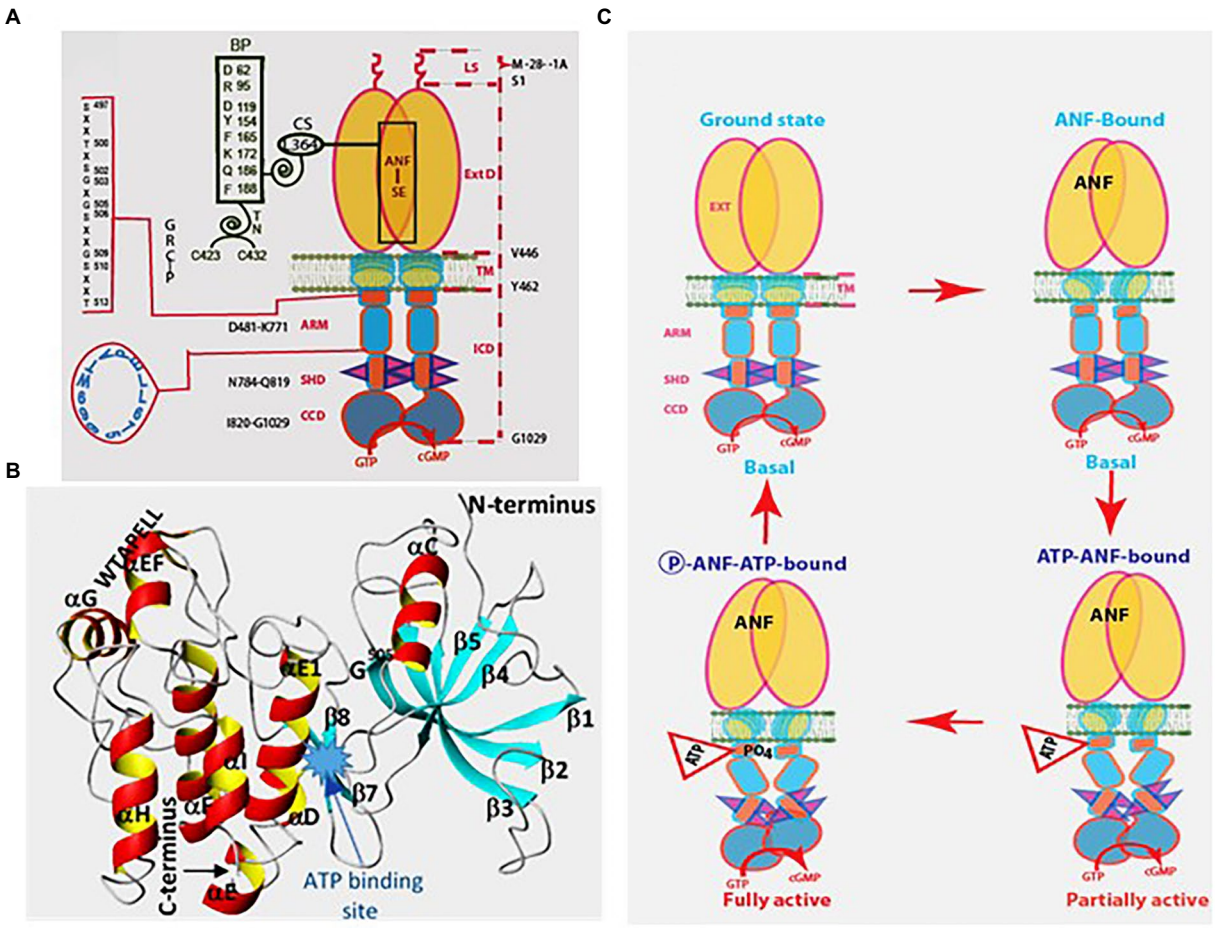

FIGURE 5
Model for signal transduction by atrial natriuretic factor-receptor guanylate cyclase (ANF-RGC). **(A)** Module segments involved in activation. An ANF-signaling element (ANF-SE) resides in the ExtD. A Central Switch (CS), L^{364}, controls the ANF binding site. A binding pocket (BP) is hinged with the CS (van den Akker et al., 2000; Ogawa et al., 2004, 2009). Two disulfide bridged cysteine residues act as a transduction node (TN) to guide the transmembrane migration of the ANF signal to an intracellular, ATP-Regulated Module (ARM; Duda et al., 2005b). Significantly, the TN is active only in the hormone receptor guanylate cyclases but not in the photoreceptor guanylate cyclases (Shahu et al., 2022). ATP amplifies the ANF signal by bringing two critical domains to the surface: a glycine rich cluster G-X-G^{505}-X-X-X-G, making surrounding serine and threonine available for phosphorylation (GRC-P) and a 7-aa residue W^{669}-TAPELL^{675} motif to activate the core catalytic domain (CCD). **(B)** Structure of the ARM in its apoform. Four antiparallel β strands and one helix constitute the small lobe. The large lobe is made up of eight α helices and two β strands. The positions of the key G^{505} residue of the GRC motif within the small lobe and of the W^{669}-TAPELL^{675} motif within the large lobe are indicated. ATP binding is sandwiched between the two lobes indicated by a star. **(C)** Activation model for ANF-RGC. Binding of an ANF molecule to the ExtDs of the dimer primes the ANF-SE, by rotating TN. The twisting motion propagates through TM to prepare ARM for ATP binding (Ogawa et al., 2004; Parat et al., 2010). ATP binding triggers a cascade of temporal and spatial changes (Duda et al., 2001c). With G^{505} in GRC-P acting as a pivot, the ATP binding site shifts its position and its floor rotates. There is movement of ARM's β4 and β5 strands and the loop between them and movement of the αE and F helices that exposes the hydrophobic WTAPELL motif for interaction with CCD (Duda et al., 2009). These structural rearrangements initiate 50% maximal catalytic activity. Full activation is attained after multiple serines and threonines in GRC-P become phosphorylated (Duda et al., 2011b). The conformational changes wrought by ATP binding reduce the affinity of ANF-RGC for ANF and phosphorylation lowers the affinity for ATP binding. Dissociation of ANF and ATP return ANF-RGC to its ground state. (Modified from Duda et al., 2011b; Sharma et al., 2016).

alone can stimulate ANF-RGC activity. Because ATPγS and AMP-PNP, the non-hydrolyzable analogs of ATP, mirror ATP effect with EC_{50s} between 0.3–0.5 mM (Duda et al., 1993a), ATP must function as an allosteric regulator (Chinkers et al., 1991; Marala et al., 1991). The Hill coefficient for ATP binding was near 1 (Duda et al., 2011b), making it impossible to determine whether ANF-RGC binds one or two ATPs per dimer. Importantly, the same was found to be true for recombinant CNP-RGC (Duda et al., 1993c).

Molecular mechanism by which ATP controls transmission of the hormonal signal was elucidated through studies involving multiple techniques, site directed mutation, deletion and expression (reviewed in Sharma, 2010). They showed that the so-called "kinase homology domain, KHD" of ANF-RGC extends from a juxta-membrane domain (JMD) to the catalytic domain (Chinkers and Garbers, 1989; Marala et al., 1992). Within it, a glycine rich cluster (GRC), Gly^{503}-Arg-Gly-Ser-Asn-Tyr-Gly^{509} confers ATP effect on ANF-dependent ANF-RGC

activity (Goraczniak et al., 1992). This motif was, therefore, more appropriately named ATP-regulatory module (ARM; Figure 5A). The ARM in CNP-RGC is Leu^{497}-Arg-Gly499-Ser-Ser-Tyr-Gly^{503}. Replacing ANF-RGC's ARM sequence with its counterpart in the CNP-RGC, has no effect on the ATP/ANF response (Duda et al., 1993a). These results were in agreement with an earlier finding that the KHDs of ANF-RGC and CNP-RGC are interchangeable (Koller et al., 1992) and that the transduction mechanisms of these two MGCs are identical. Mutational analyses of individual glycine residues in the ARM sequence pointed out to Gly^{505} and Gly^{499} in ANF-RGC and CNP-RGC, respectively, as essential for ATP binding and ANF signaling (Duda et al., 1993b). Thus, one residue controlled the both activities.

To determine the 3D-structure of the ANF-RGC ARM domain, homology-based modeling technique was used. The domain was modelled using the crystal structures of insulin receptor kinase and hematopoietic cell kinase as templates (Duda et al., 2000b; Sharma et al., 2001). Its functional determinants were deciphered and verified through point mutation/expression, time-resolved tryptophan fluorescence, Forster Resonance Energy Transfer, reconstitution and mass spectroscopic studies (reviewed in Sharma and Duda, 2014b).

The ARM consists of residues 481–771. It is composed of two lobes; a smaller, N-terminal of 91 residues (496–586) and larger of 185 residues C-terminal (587–771; Figure 5B; Duda et al., 2000b; Sharma et al., 2001). ATP binding results in repositioning of the W^{669}-TAPELL^{675} motif within the larger lobe. This repositioning is obligatory for hormone-dependent activation of ANF-RGC; deletion of the WTAPELL motif caused unresponsiveness to ANF and ATP in the recombinant system (Duda et al., 2009).

In a genetically modified mouse model in which the WTAPELL motif was deleted from the ANF-RGC gene, hypertension and cardiac hypertrophy were observed (Duda et al., 2013; United States Patent No. 8835711 issued on September 16, 2014; Patent Publication Number: 20130291132). Thus, the seven-residue motif – WTAPELL – of ANF-RGC controls the hormonal regulation of blood pressure.

Binding of ATP causes that six buried serine and threonine of the smaller lobe are moved to the surface, and become available for phosphorylation by a hypothetical kinase. Phosphorylation is necessary for full ANF signaling. The maximal activation of ANF-RGC ceases upon ATP binding causing loss of the affinity for ANF (Larose et al., 1991; Jewett et al., 1993; Duda and Sharma, 1995a,b) and phosphorylation causes loss of the affinity for ATP; the enzyme undergoes homologous desensitization and returns to its basal state (Potter and Garbers, 1992). Based on these facts we proposed a working model for ANF-RGC activation (Figure 5C).

The same model was applicable to CNP-RGC and STa-RGC (Potter and Hunter, 1998; Bhandari et al., 2001; Jaleel et al., 2006). Later studies established that ATP regulation through the ARM is a unique feature of the hormonally-modulated subfamily of the membrane guanylate cyclases.

Discovery of the Ca^{2+}-modulated MGC subfamily locked in with phototransduction

SEEING, the beautiful gift of nature, starts with phototransduction, the conversion of light into an electrical signal in the outer segments of rod and cone photoreceptors. The historical finding of Koch and Stryer (1988) established that the retinal MGC is inhibited by $[Ca^{2+}]_i$ *via* a Ca^{2+} binding protein. Yet, the molecular nature of the MGC was not known and following the cyclic AMP model MGC was suspected to be a three separate components system – receptor, GTP-binding protein and adenylate cyclase – (Stryer, 1986).

From 1988 to 1991, search for the molecular identity of the vision-linked MGC was actively pursued. Yet, the conclusions were confusing and often flawed (reviewed in Pugh and Cobbs, 1986; Pugh et al., 1997).

Finally, four independent laboratories reported purification of the retinal MGC. Its biochemical characteristics reported by three were similar (Hayashi and Yamazaki, 1991; Koch, 1991; Margulis et al., 1993). The molecular mass of MGC was 110–120 kDa and importantly, its catalytic activity was unresponsive to ANF and to the $[Ca^{2+}]_i$ alone.

In sharp contrast, the fourth laboratory reported its Mr. of 67 kDa. And, notably the MGC was nitric oxide-dependent (Horio and Murad, 1991a,b). Later results, including from our group, demonstrated that these conclusions were flawed. This MGC was neither a 67 kDa protein, nor its catalytic activity was NO-modulated.

For historical reasons these studies from our group are briefly narrated below. For the first time they provided unequivocal identity of the wild type MGC at the biochemical and the molecular level. Reconstitution studies showed that ROS-GC was $[Ca^{2+}]_i$ modulated with a pattern that mirrored the physiological conditions of phototransduction.

The MGC was purified from the ROD OUTER SEGMENTS of the bovine retina (Margulis et al., 1993). Hence named ROS-GC. Based on the protein sequence of it four fragments, its cDNA was cloned from the bovine retina cDNA library (Goraczniak et al., 1994). The cloned enzyme was unresponsive to ANF and CNP and showed an overall minimal, 27%–30%, sequence identity with the three hormone receptor guanylate cyclases – ANF-RGC, CNP-RGC and STa-RGC (Goraczniak et al., 1994).

Comparison of the biochemical estimates with those acquired from cloning/expression experiments led to the realization that ROS-GC aminoacid sequence includes an N-terminal leader sequence (LS) that gets deleted post-translationally. The calculated molecular mass of ROS-GC with the 56-amino acid LS is 120,361 Da; without it, it is 114,360 Da (Goraczniak et al., 1994). The 114,360 Da molecular mass was quite close to the previously determined bovine (Koch, 1991) and toad photoreceptor guanylate cyclases (Hayashi and Yamazaki, 1991). A second ROS-GC, ROS-GC2, was discovered in bovine retina (Goraczniak

et al., 1997) shortly thereafter and its human variety was termed Ret-GC2 (Lowe et al., 1995). Theoretically, ROS-GC1 and ROS-GC2 could organize into homodimers and heterodimers, but in reality only few, if any, heterodimers are formed in the retina despite the co-expression of both guanylate cyclases in rods (Yang and Garbers, 1997). As of today, no extracellular ligand has been identified for ROS-GC therefore, it remains an orphan receptor.

Proper identification of ROS-GC had an important historical impact. It corrected an earlier structural flaw.

In 1992 Shyjan et al. reported the molecular cloning of a membrane guanylate cyclase from the human retina (Shyjan et al., 1992) and named it retGC. Because retGC *via in situ hybridization* analysis was detected in the inner segments and outer nuclear layers of the monkey's retina and the cyclase was different from ANF-RGC and CNP-RGC, the authors suggested that it may be a part of the phototransduction machinery (Shyjan et al., 1992).

The cloning and identification of ROS-GC proved, however, that retGC was not ROS-GC. There were critical structural differences between them. Remarkably, in 1995, the structure of retGC was revised (Lowe DG, accession number M92432), yet not published, to show its complete identity with the structure of ROS-GC, published in the early part of 1994 (Goraczniak et al., 1994). Thus, ROS-GC structure helped to establish retGC as the human counter part of bovine ROS-GC.

The discovery of mutations in ROS-GC1 linked with retinal disorders made it possible to establish the critical role of ROS-GC1 in phototransduction and define its abnormalities in molecular terms (Duda et al., 1999a,b, 2000a; Tucker et al., 1999; Wilkie et al., 2000; Ramamurthy et al., 2001).

The modulation of ROS-GC occurs *via* Ca^{2+}-binding proteins

Long before the molecular identity of the first Ca^{2+}-modulated ROS-GC1 was known, Koch and Stryer provided the evidence that a calcium binding protein stimulates MGC activity in ROS in a $[Ca^{2+}]$-dependent fashion (Koch and Stryer, 1988). Subsequently, two Ca^{2+}-binding proteins were purified and cloned from the retina (Palczewski et al., 1994; Dizhoor et al., 1995; Frins et al., 1996). They were termed GCAP1 and GCAP2, and have been linked with phototransduction.

A third GCAP, GCAP3, was also cloned from the retina (Haeseleer et al., 1999). It appears to be cone-specific but the molecular mechanisms underlying its function remain largely unknown.

The phototransduction model presented in Figure 6 shows that ROS-GC in its native state is bound to GCAPs. Fluctuating levels of $[Ca^{2+}]_i$ change the conformation of GCAP/s. This, in turn, regulates the cyclase through specified modules in ROS-GC. These model features have been borrowed from (Sharma and Duda, 2014a) and they incorporate our and others conclusions (Pugh et al., 1999; Burns and Baylor, 2001; Koch et al., 2002; Sharma, 2002; Koch, 2006; Luo et al., 2008; Stephen et al., 2008; Wensel, 2008; Koch et al., 2010; reviewed in Koch et al., 2010; Sharma, 2010; Koch and Dell'Orco, 2013). Notably, the model also explains

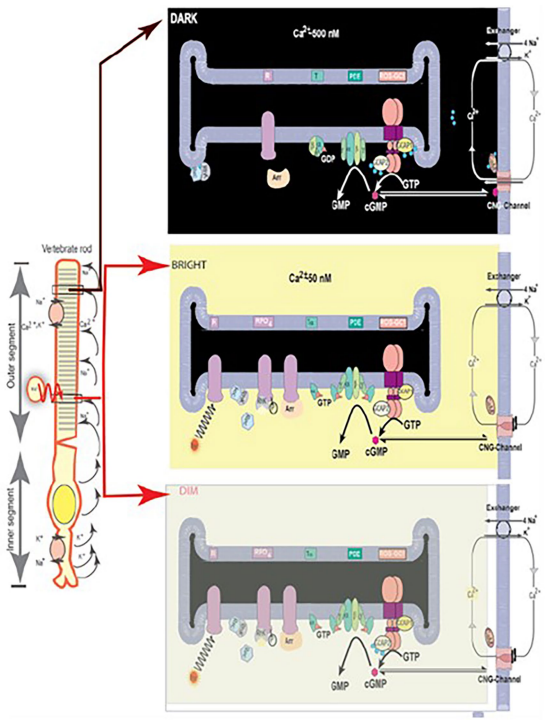

FIGURE 6
Schematic representation of the luminosity-dependent operation of the ROS-GC-GCAP transduction system. Left panel. An illustration of a typical vertebrate rod. In the DARK a circulating current (arrows) is present. It is outward in the inner segment and carried primarily by K^+; in the outer segment the net charge is inward, with about 90% of the inward flow carried by the Na^+ and 10% by Ca^{2+} ions. Na^+/K^+ exchange pumps in the inner segment membrane and Na^+/K^+-Ca^{2+} exchangers in the outer segment membrane (see also right panels) maintain the overall ionic gradients against the dark flows. The capture of a photon ($h\nu$) by a rhodopsin molecule in one of the disc membranes of the outer segment initiates the photo-transduction cascade. Right upper panel, DARK. The components of the Photo-Transduction cascade are shown in the dark/resting steady-state. Cytoplasmic cyclic GMP (red circle), generated by the basal catalytic activity of ROS-GC, keeps a fraction of CNG channels in the plasma membrane open. ROS-GC1 *via* its ^{415}M-L^{456} segment is GCAP1-and *via* ^{965}Y-N^{981} is GCAP2-bound. Ca^{2+} ions enter the cell *via* the CNG-channel and are extruded *via* the Na^+/K^+, Ca^{2+}-exchanger. Synthesis and hydrolysis of cyclic GMP by ROS-GC and PDE, respectively, occur at a low rate. The heterotrimeric G protein, transducin, is in its GDP-bound state and is inactive. The Ca^{2+} binding proteins calmodulin (CaM), recoverin (Rec) are bound to their target proteins, the CNG-channel, rhodopsin kinase (Rhk), respectively. Right middle panel. Absorption of BRIGHT LIGHT by the visual pigment rhodopsin leads to the activation of the transduction cascade: the GTP-bound α-subunit of transducing activates PDE that rapidly hydrolyzes cyclic GMP. Subsequently, the CNG-channels close and the Ca^{2+}-concentration falls. The fall in cytoplasmic $[Ca^{2+}]i$ is sensed by Ca^{2+}-binding proteins: CaM dissociates from the CNG-channel what leads to an increase in cyclic GMP sensitivity of the channel; recoverin stops inhibiting rhodopsin kinase; rhodopsin becomes phosphorylated. Both Ca^{2+}-free GCAPs in their changed configurations activate ROS-GC and synthesis of cyclic GMP increases. Arrestin (Arr) binds to phosphorylated rhodopsin and interferes with the binding and further activation of transducin. Enhancement of cyclic GMP synthesis brings it to its original DARK state level and termination of the cascade, which leads to reopening of CNG channels. Right bottom panel, DIM LIGHT. The initial fall of $[Ca^{2+}]_i$ is selectively detected only by GCAP1. In its Ca^{2+}-free state GCAP1attains the activated mode and stimulates ROS-GC activity. GCAP2 remains Ca^{2+}-bound and in its inhibitory mode. (Reproduced from Sharma and Duda, 2014a).

the results of the GCAPs null mice study that questioned the role of GCAP2 in phototransduction (Howes et al., 2002).

It was thereby established that (1) Vision begins with PHOTOTRANSDUCTION, i.e., the conversion of light (photon) into an electrical signal in the photoreceptors outer segments. (2) Ca^{2+} and cyclic GMP are essential components of the photoreceptors' response to a captured photon. (3) Significantly, cyclic GMP is the second messenger of phototransduction; it increases the conductance of ion channels (Fesenko et al., 1985). (4) ROS-GC (1 and 2) is the source of the cyclic GMP. (5) ROS-GC1 *in statu nascendi* contains N-terminal leader sequence (LS) that is deleted post-translationally; the calculated molecular mass of the protein with the LS is 120,361 Da; without it, 114,360 Da. (5) No extracellular modulator was found for ROS-GC. (6) Ca^{2+}-free GCAP1 activates ROS-GC1 but Ca^{2+}-bound (IC_{50} ~ 100 nM), becomes an inhibitor (Dizhoor and Hurley, 1996; Duda et al., 1996b). Thereby, at low and high Ca^{2+} levels, GCAP1 is a Ca^{2+}-sensing subunit of the ROS-GC1. (7) In recombinant system, GCAP2 is a more powerful stimulator of ROS-GC1 activity at low Ca^{2+} but with significantly higher than for GCAP1 EC_{50} (compare of 6–8 mM for GCAP2 and 0.8 mM for GCAP1; Duda et al., 1996b; Goraczniak et al., 1998; Krishnan et al., 1998). (8) Ca^{2+}-free GCAP2 with an EC_{50} of 1 mM stimulates ROS-GC2 activity by 12-fold whereas GCAP1 is unable to do so (Duda et al., 1996b; Goraczniak et al., 1998); thus, GCAP2 is the only modulator of ROS-GC2 activity. (9) ROS-GC1 binds the two GCAPs are different sites; GCAP1 at M^{445}-L^{456} and L^{503}-I^{522} (Lange et al., 1999); GCAP2 at Y^{965}-N^{981} (Duda et al., 2005a; Rehkamp et al., 2018; Figure 7).

In contrast, one group proposes that both GCAPs bind to the same site on ROS-GC1 (Peshenko et al., 2015a,b).

(10) Even though GCAPs bind to opposite sides of the ROS-GC1's CCD, they both use the W^{657}-TAPELL^{663} motif for stimulation of the cyclase catalytic activity at low Ca^{2+} (Duda et al., 2011a). Finally, (11) studies on double knockout mice demonstrated that without ROS-GC1/ROS-GC2, rods and cones do not respond to light. Expression of a third guanylate cyclase and a third GCAP linked with phototransduction is therefore excluded in mouse.

A third GCAP, GCAP3, is present in the human retina and in reconstitution system it stimulates ROS-GC1/ROS-GC2 in a Ca^{2+}-dependent manner similar to that of GCAP1. Its role in phototransduction is unclear, however (Haeseleer et al., 1999). Most recent study suggests that mutation in GCAP3 may lead to retinitis pigmentosa (Avesani et al., 2022). Apparently mammalian photoreceptors utilize a Ca^{2+}-modulated system composed of a pair of ROS-GCs and up to three GCAPs in their outer segments. Studies on mice deficient for either GCAP1 or GCAP2 support these conclusions (Makino et al., 2008, 2012; Koch and Dell'Orco, 2013). GCAP1 has lower affinity for Ca^{2+} and is the first to sense light-induced fall in intracellular Ca^{2+} and start activating ROS-GC. Over time after, when Ca^{2+} concentrations are further lowered the effect of GCAP1 saturates and GCAP2 takes over stimulation of ROS-GC activity. Together, the two GCAPs limit the growth of the photon response and accelerate the kinetics of the response recovery (Mendez et al., 2001 and Figures 4A,B in Sharma et al., 2016).

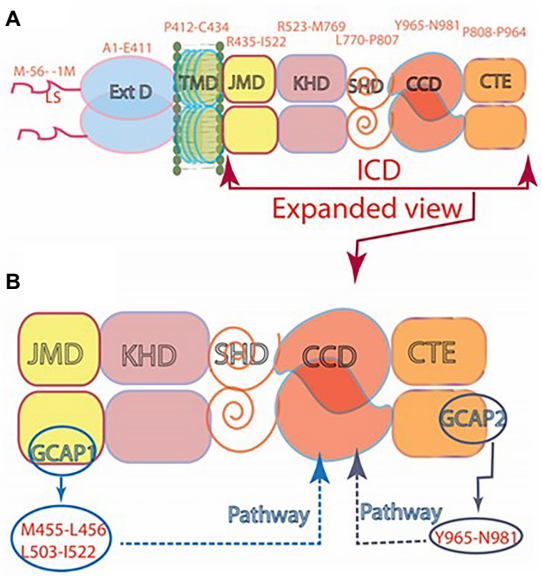

FIGURE 7
(A) Modular construction of the ROS-GC1 dimer. A 56 aminoacid leader sequence (LS) precedes the extracellular domain (ExtD) in the nascent, immature protein. All signaling events occur in the intracellular domain (ICD), which is composed of: JMD, juxtamembrane domain; KHD, kinase homology domain; SHD, signaling helix domain; CCD, catalytic core domain; and CTE, C-terminal extension. **(B)** Interaction with GCAP1 and GCAP2. Two specific switches for Ca^{2+} sensing subunits, one for GCAP1 in the JMD, and one for GCAP2 in the CTE, are located on opposing sides of the CCD. The MGC complex exists as a dimer of homodimers in which two ROS-GC1s combine either two GCAP1s or two GCAP2s.

Although ATP is not required, yet it raises the ROS-GC1 basal catalytic activity and GCAP1-stimulated activity at low Ca^{2+} (Gorczyca et al., 1994; Aparicio and Applebury, 1996). ROS-GC1 exhibits self-phosphorylating kinase activity. Four serine residues in its ARM are subject to phosphorylation due to this activity (Aparicio and Applebury, 1996; Bereta et al., 2010) yet, its purpose remains unknown; it does not affect the basal and GCAP1-stimulated activities. Additional accounts of properties of ROS-GCs in control of phototransduction can be found in (Sharma and Duda, 2014a; Wen et al., 2014; Koch and Dell'Orco, 2015).

The discovery that the synthesis of cyclic GMP in photoreceptor outer segments is Ca^{2+}-dependent added another dimension to the understanding of MGC signal transduction. It is not limited to the transduction of hormones and other extracellular signals but is able to sense intracellular signals as well.

Recoverin, a misplaced molecule that diverted the MGC research

In an enormous historical prospective, the progression of the phototransduction field will leave behind a huge voyage if the story of RECOVERIN is not narrated.

After the seminal observation that a soluble fraction of bovine ROS causes activation of the photoreceptor MGC in the absence of [Ca^{2+}] (Koch and Stryer, 1988), the structure of ROS-GC was believed to be composed of "separate regulatory and catalytic subunits" (Stryer, 1991). In hindsight, as indicated earlier, this belief was powered by the influence of the cyclic AMP signaling pathway involving three separate subcomponents – hormone surface receptor, GTP-binding protein and catalytic (adenylate cyclase; Figure 1). With the unknown structure of ROS-GC and its modulation, the groups from the United States and the former Soviet Union joined forces to decode the molecular principles of a protein that appeared to regulate guanylate cyclase activity (Dizhoor et al., 1991) and adhered to the functional description of the protein described by Koch and Stryer (1988). They named it RECOVERIN "because it promoted recovery of the dark state" of phototransduction. For 2 years this concept remained dominant.

However, the purer preparations of recoverin showed a disturbing decline in guanylate cyclase stimulation. It became evident that recoverin was not the sought after regulator of guanylate cyclase activity. Thus, the initial conclusion was withdrawn (Hurley et al., 1993).

Later findings demonstrated that recoverin had no role in the ROS-GC modulation. Rather it exerted Ca^{2+}-dependent control over the phosphorylation of photo-excited rhodopsin by rhodopsin kinase (Kawamura, 1993; Chen et al., 1995; Klenchin et al., 1995).

At almost the same time, GCAP1 and GCAP2 were discovered, and it became evident that they indeed stimulate ROS-GC catalytic activity (Palczewski et al., 1994; Subbaraya et al., 1994; Dizhoor et al., 1995; Gorczyca et al., 1995; Frins et al., 1996). Thereby, the saga of RECVERIN in the modulation of ROS-GC ended.

ROS-GC is a bimodal Ca^{2+} switch

With the discovery of GCAPs the dogma developed that they are the sole modulators of ROS-GC activity. The curious aspect was, however, that the GCAPs/$[Ca^{2+}]_i$ inhibited ROS-GC activity, yet, in surface receptor MGC family, the ligand, stimulated the MGC activity. The following questions were explored: (1) Do the vision linked retinal neurons embody an additional ROS-GC linked pathway where $[Ca^{2+}]_i$ stimulates it? (2) If, "yes," how does it operate?

The answer to the first question was, yes. To the second, that the ligand of ROS-GC1was S100B protein (*vide infra*).

When the studies on GCAPs regulation of ROS-GC activity were in full swing, our group purified another Ca^{2+}-dependent regulator of ROS-GC's activity from the retina; it was named Ca^{2+}-dependent GCAP (CD-GCAP; reviewed in Sharma et al., 2014). CD-GCAP turned out to be an isomer of the brain S100B (the only commercially available form; Pozdnyakov et al., 1995, 1997; Duda et al., 1996a, 2002; Margulis et al., 1996; Wen et al., 2012). The retinal form has Ca^{2+}-bound whereas the brain form is Zn^{2+}-bound. It is of importance because the cations bound result in opposite effects of S100B on ROS-GC activity; the Zn^{2+}-bound form inhibits while the Ca^{2+}-bound form stimulates ROS-GC1 (Pozdnyakov et al., 1997). Here, we focus on the retinal form.

The evidence that S100B directly interacts with ROS-GC1 came from cross-linking experiments. Biochemical parameters of this interaction were determined through surface plasmon resonance spectroscopy. S100B binds ROS-GC1 with a $K_{1/2}$ of 198–395 nM (Duda et al., 2002) and stimulates cyclic GMP synthesis with a $K_{1/2}$ for Ca^{2+} of ~400 nM (Duda et al., 1996a). Peptide competition experiments pointed out to two C-terminal segments: aa 962–981 and 1,030–1,042 on ROS-GC1 as the binding sites for S100B. This was confirmed by the deletion mutagenesis/expression experiments. They narrowed down to R^{966}-IHVNS^{972} motif as the binding site and the R^{1039}–RQK^{1042} flanking cluster as promoting maximal ROS-GC1 activation (Duda et al., 2002). S100B is a small protein with molecular weight of 10 kDa; it has only 2 EF Ca^{2+} binding hands, and organizes into a tetramer (Donaldson et al., 1995).

Since in the recombinant reconstituted systems ROS-GC1 has the ability to interact with the GCAPs and S100B, it could operate as a bimodal Ca^{2+} switch under the conditions that a cell expresses all three components. The possibility was tested using isolated photoreceptor-bipolar synaptic membranes of the bovine retina. This region was chosen because prior immunohistochemical studies had demonstrated the co-presence of ROS-GC1 with GCAP1 and S100B there (Liu et al., 1994; Cooper et al., 1995; Duda et al., 2002). Indeed, these membranes exhibited high ROS-GC1 activity at 10 nM $[Ca^{2+}]_i$, the activity decreased as $[Ca^{2+}]_i$ raised to a few hundred nM and then, when Ca^{2+} concentration was about 1 mM, it raised again (Figure 5 in Venkataraman et al., 2003).

The presence of ROS-GC1, GCAPs and S100B in the photoreceptor outer segments (Cuenca et al., 1998; Kachi et al., 1999; Rambotti et al., 1999) implicated a role for bimodal switching in phototransduction. The possibility was probed with mouse knockout models: S100B$^{-/-}$, GCAP1$^{-/-}$, GCAP2$^{-/-}$, GCAP1/GCAP2$^{-/-}$, ROS-GC1$^{-/-}$. Biochemical experiments demonstrated functional linkage of S100B with ROS-GC1 but not with ROS-GC2 at $[Ca^{2+}]_i > 200$ nM in the generation of cyclic GMP. Although these concentrations exceed the physiological range for Ca^{2+} in mouse ROS (Woodruff et al., 2002), they were appropriate for cones, which sustain higher levels of Ca^{2+} in darkness. It was therefore reasonable that the most recent immunocytochemistry co-localizes S100B and GCAP1 with ROS-GC1 in murine retinal cone outer segments but not ROS (Wen et al., 2012).

A new Ca^{2+} sensor neurocalcin δ (NCδ) is expressed in the retinal neurons and modulates ROS-GC activity

With the finding that ROS-GC signaling pathway in the retinal neurons is governed by the Ca^{2+}-sensor proteins, GCAPs,

and S100B, the possibility was explored for the existence of other similar pathway/s in these neurons. One such pathway was found. It was modulated by the Ca^{2+}-sensor NCδ (comprehensively reviewed in Sharma et al., 2016).

Found in the neurons of the inner retina, the sequence of NCδ is 35% identical with that of GCAPs. Purified from the bovine brain, Ca^{2+}-free NCδ has no effect on recombinant ROS-GC1 activity. Yet, when Ca^{2+}-bound, it stimulates the MGC catalytic activity with a $K_{1/2}$ for Ca^{2+} of 0.8 mM (Kumar et al., 1999; Krishnan et al., 2004). NCδ stimulates only ROS-GC1; it remains ineffective with ROS-GC2. Functionally, NCδ is comparable to S100B but not with the GCAPs. One molecule of NCδ has four EF Ca^{2+}-binding hands (as GCAPs have) while S100B has only two. Despite significant sequence differences between S100B and the C-terminal half of NCδ (GenBank accession numbers NP-001029727.1 and NP-776823.1, respectively), their Ca^{2+}-bound crystal structures are very similar with respect to helix-packing arrangements of their EF hands (Vijay-Kumar and Kumar, 1999). Thus, NCδ and S100B are structural and functional analogs.

NCδ is a homodimer of 20 kDa (Krishnan et al., 2004; Venkataraman et al., 2008). Similar to other NCSs, it exhibits a Ca^{2+}-dependent electrophoretic mobility shift (Ladant, 1995; Frins et al., 1996). Out of its four EF-hand motifs, only three – EF2, EF3, EF4 – are functional in binding Ca^{2+} (Okazaki et al., 1992; Terasawa et al., 1992; Vijay-Kumar and Kumar, 1999). Following the NCS family trait, NCδ is myristoylated at the N-terminus; the only known exception from the trait is the Kv-channel interacting protein subfamily (Braunewell and Gundelfinger, 1999; Burgoyne and Weiss, 2001). Ca^{2+} myristoyl switch determines NCδ activity. In the absence of Ca^{2+} myristoyl group is buried within NCδ hydrophobic pocket but becomes exposed upon Ca^{2+} binding enabling membrane binding of the protein (Lim et al., 2011). From the functional viewpoint, NCδ is a true subunit of ROS-GC1 transduction complex; because the resting intracellular Ca^{2+} concentration of 100–200 nM is sufficient to keep some of its molecules associated with ROS-GC1 thus, allowing very short response time. NCδ and ROS-GC1 are co-present together in the inner plexiform layer of the retina where addition of Ca^{2+} stimulates ROS-GC1 activity (Krishnan et al., 2004); the myristoylation of NCδ causes a 2-fold amplification of the ROS-GC1activity. Determined by surface plasmon resonance spectroscopy, Ca^{2+}-bound NCδ attaches ROS-GC1 with $K_A = 2.3 \times 10^6\,M^{-1}$ and $K_D = 4.6 \times 10^{-7}\,M$ (Krishnan et al., 2004).

Mapping studies defined that the NCδ binding site resides within the aa732–962 stretch of ROS-GC1 (Krishnan et al., 2004). The site does not overlap with the GCAP1, GCAP2-, or S100B-binding domains of ROS-GC1 (*vide supra*). Finer analyses pin pointed the modulated site to the V^{836}-L^{857} region located in the heart of the ROS-GC1 catalytic domain (Venkataraman et al., 2008; note: the numbering in this reference is offset by one aminoacid). Spatially, this segment of ROS-GC1 accommodates the V-shaped crevice of NCδ, and, it forms a distinct hydrophobic–hydrophilic patch, a characteristic feature of the Ca^{2+}-dependent signaling property of NCδ. It has a secondary structure of the helix–loop–helix. It is acidic with a pI of 3.37 (Venkataraman et al., 2008).

These findings challenged the existing concept that the CCD, located at the C-terminus of the MGC is devoid of any ligand binding ability and depended exclusively on the upstream binding modules to translate the ligand signals for generation of GMP.

Localization of the NCδ binding site within the core catalytic domain of ROS-GC1 created a new signaling model (Duda et al., 2012c). Now the Ca^{2+}-bound NCδ direct interaction with the ROS-GC1 catalytic domain was sufficient for the ROS-GC activation.

NC δ is also the Ca^{2+} sensor modulator of ANF-RGC

Because NCδ binds the catalytic module of ROS-GC and the sequence of this module is highly conserved in all members of the MGC family, it was natural to anticipate that the catalytic activity of all other members of the family is modulated by NCδ in a Ca^{2+}-dependent manner. It was first tested with the ANF-RGC where the V^{851}-L^{872} segment corresponding to the V^{836}-L^{857} site of ROS-GC1 with the sequence identity of 68.2%. Accordingly, the experiments demonstrated that Ca^{2+}-bound NCδ stimulated the catalytic activity of ANF-RGC in a dose-dependent fashion with an EC_{50} of 0.5 mM Ca^{2+} (Duda et al., 2012b). Neither ANF nor ATP were needed for the stimulation. Thus, the Ca^{2+}-dependent stimulation was sufficient and was independent of the hormonal, ANF/ATP-dependent stimulation.

These results directed a new paradigm of the ANF-RGC signal transduction. Now, in addition to the ANF signal transduction, ANF-RGC was locked in with the NCδ-modulated Ca^{2+} signal transduction.

Myristoylation of NCδ was essential for activation of ANF-RGC. This finding rationalized the earlier results where Ca^{2+}/non-myristoylated NCδ did not stimulate the ANF-GC activity (Kumar et al., 1999). Significantly, the myristoylation increased the ANF-RGC catalytic efficiency, *k*cat, from 6.5 ± 0.3 to 41.4 ± 0.5 pmol cyclic GMP/s. Myristoylated Ca^{2+}-bound NCδ dimer forms a functional unit with the ANF-RGC dimer.

To determine the relationship between the Ca^{2+}- and the ANF-modulated ANF-RGC signaling pathways, the ANF-RGC catalytic activity was monitored first in the presence of increasing concentrations of ANF (10^{-11}–10^{-6} M) and constant 0.8 mM ATP, followed with the added 1 mM Ca^{2+} and 2 mM myristoylated NCδ. ANF/ATP caused 3.5-and 4.5-fold increase in the catalytic activity, and adding Ca^{2+}-bound NCδ led to about 15-fold increase. Thus, the Ca^{2+}-modulated and the ANF hormone-modulated pathways function independently.

To determine, and understand, the linkage of the biochemistry of NCδ modulation of ANF-RGC activity with cardiovascular

physiology, a hemizygous NCδ knockout mouse, NCδ$^{+/}$, was generated (Duda et al., 2012b). Immunohistochemical analyses demonstrated the co-presence of ANF-RGC and NCδ in adrenocortical zona glomerulosa (Takayanagi et al., 1987b; Sharma et al., 1989; Duda et al., 1991; Nakano et al., 1993; Rondeau et al., 1995). The particulate fraction of the adrenal gland from NCδ$^{+/-}$ mice showed only 50% of the ANF-RGC activity of the NCδ$^{+/+}$ mice; addition of exogenous NCδ and Ca^{2+} restored the total ANF-RGC activity.

Conclusion

The adrenal glands of mice embody the Ca^{2+}/NCδ-modulated ANF-RGC signaling pathway. And, as anticipated, its functional activity is halved in the NCδ$^{+/-}$ mice.

Physiologically, in adrenal glands the ANF/ANF-RGC hypotensive activity counterbalances the renin-angiotensin-aldosterone hypertensive activity. This results in lowering blood pressure (Aoki et al., 2000; Shi et al., 2001). As anticipated, in plasma of the NCδ$^{+/-}$ mice the levels of aldosterone were about 27% higher than in the plasma of NCδ$^{+/+}$ mice. But, significantly, the levels of corticosterone were similar in the plasma of both mice strains (Duda et al., 2014). Because aldosterone is synthesized in the adrenal glomerulosa cells, while corticosterone in the fasciculata cells, these results together with immunohistochemical analyses established co-expression of NCδ and ANF-RGC in the mouse adrenal glomerulosa cells, the cells that are physiologically linked with the blood pressure regulation (Duda et al., 2012b). Indeed, the systolic blood pressure of the NCδ$^{+/-}$ mice was 38% higher than of the wild type mice, 127 vs. 92 mm Hg (Duda et al., 2012b).

Exposure of this novel Ca^{2+}-modulated ANF-RGC signaling pathway presented an alternate mechanism to the control of the endocrine systems that prevent hypertension.

It also pointed that the new ANF-RGC transduction pathway is bimodal. It exists in some selected cells. There, when appropriate it controls the extracellular surface receptor signals and the intracellular Ca^{2+}-modulated signals. This mechanism is illustrated in Figure 8.

Notably, following the same pattern, NCS and VILIP-1, two ANF-RGC Ca^{2+}-binding proteins, were shown to bind ANF-RGC (Braunewell et al., 2001). As yet, there is no information, however, if they modulate ANF-RGC activity.

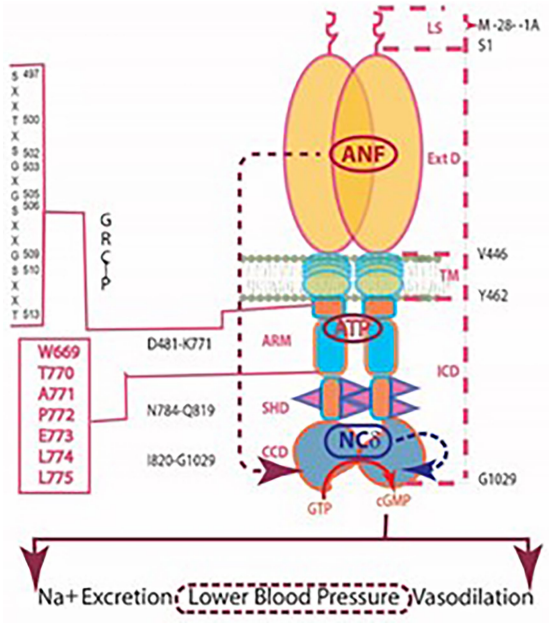

FIGURE 8
Independent signaling pathways of ANF/ATP and of NCδ. The trajectory of the ANF pathway (maroon dashed arrow) originates at the ExtD and passes through the TM, ARM and signaling helix domain (SHD) in its course to CCD. In contrast, the trajectory of the NCδ pathway (blue dashed arrow) lies within the CCD. The ANF-RGC dimer is thought to bind a dimer of NCδ, but only a single subunit is shown. Both pathways are the physiological regulators of the mouse blood pressure.

Interlaced with Ca^{2+}-sensing modulators, CO_2/bicarbonate modulates a novel ROS-GC signaling pathway

In trail blazing studies, the MGC (ONE-GC) in olfactory neuro-epithelium was shown to sense atmospheric carbon dioxide (CO_2; Hu et al., 2007; Guo et al., 2009). CO_2 is the source of bicarbonate that signals ONE-RGC activation. The follow up observations of these authors were that the action of bicarbonate was ONE-GC-specific, since it did not affect the catalytic activity of the other recombinant forms of MGCs – ANF-RGC, CNP-RGC, STa-RGC and ROS-GCs (Guo et al., 2009; Sun et al., 2009).

Our group revisited this issue and found that bicarbonate targets directly the ONE-GC's catalytic domain to stimulate it (Duda and Sharma, 2010). Since this structural domain is conserved, (85%) in all MGCs, we pursued the issue with recombinant ROS-GC1 with the following results.

The bicarbonate robustly stimulates the catalytic activity of recombinant bovine ROS-GC1 with an ED_{50} of 27 mM and a Hill coefficient of 2.8 and of ROS-GC2 with an ED_{50} of 39 mM and a Hill coefficient of 2.3 (Duda et al., 2015). The Hill coefficients >2 indicate that one or more bicarbonate molecules bind to each monomer. Similarly, bicarbonate stimulated the activities of ROS-GCs in the membranes of photoreceptor outer segments (Figure 9A).

To rule out the possibility that the observed increase in ROS-GC's catalytic activity was through a pH dependent mechanism, the activity was tested over a range of pH from 7 to 9, and it remained constant (Duda et al., 2015).

The bicarbonate signaling of ROS-GC1 is independent of $[Ca^{2+}]_i$. Yet, bicarbonate synergizes with the Ca^{2+}-sensors: GCAP1, GCAP2 and S100B to enhance Ca^{2+} modulation; the synergic effect is especially evident for GCAP2 (Duda et al., 2015, 2016;

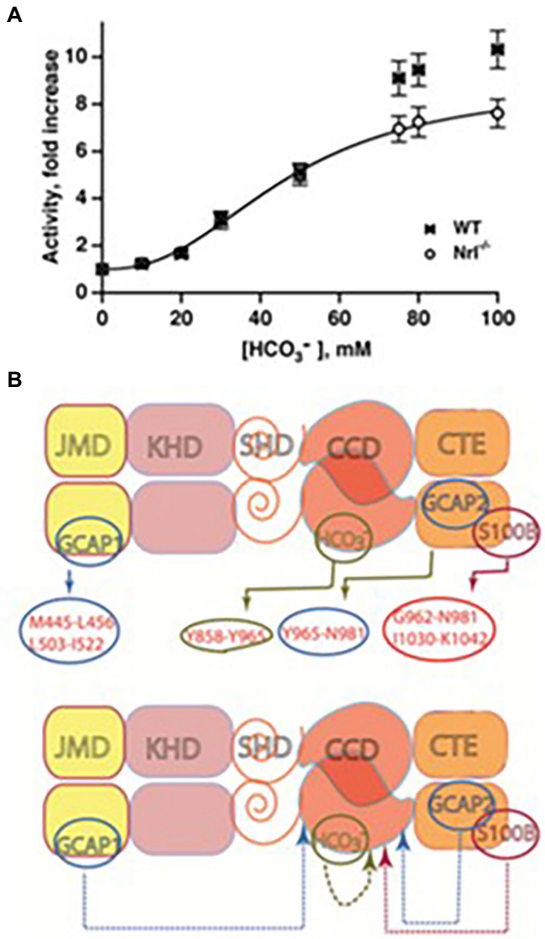

FIGURE 9
Bicarbonate modulation of ROS-GC activity. **(A)** Stimulation of ROS-GC in photoreceptor outer segment preparations from WT and neural retina leucine zipper transcription factor knock out (NRL−/−) mice. NRL−/− photoreceptors express ROS-GC1 and GCAP1 exclusively. The dependence of guanylate cyclase activity on bicarbonate is cooperative with an EC_{50} of 47 mM. The elevated activity at high bicarbonate concentration in WT outer segments is attributed to their additional expression of GCAP2. Error bars show SEM (Duda et al., 2015). **(B)** Ca^{2+}-dependent and-independent modulators of ROS-GC1 activity. Upper panel: three Ca^{2+} sensor proteins – GCAP1, GCAP2, and S100B – and one Ca^{2+}-independent modulator, bicarbonate, target individually the indicated domains within the intracellular portion of ROS-GC1. Lower panel: the targeted domains are specific switches all of which signal activation of the catalytic domain. The signaling pathways are indicated as dashed arrows.

Figure 9B). The purpose of ROS-GCs activation in photoreceptors is to elevate the circulating current, to decrease sensitivity to flashes and to accelerate flash response recovery. Bicarbonate is a charged molecule and as such cannot freely pass through cell membranes. To gain access to ROS-GC in ROS it enters through the inner segment/synapse of intact rods. In contrast, it accesses ROS-GC1 of red-sensitive cones from the inner and outer segments (Makino et al., 2019).

Thereby, the findings clarified a large body of apparently controversial results on bicarbonate and cyclic GMP synthesis in retinal photoreceptors. They also provided a clue that bicarbonate signaling would be characteristic of most, if not all MGCs.

Clinical implications

In human patients, a $F^{514}S$ mutation in ROS-GC1 was identified as the cause of Leber's congenital amaurosis type1 (Perrault et al., 1996, 1999; Rozet et al., 2001). The mutation resulted in a 10-fold decrease in ROS-GC1 catalytic activity (Duda et al., 1999a,b); it also made the cyclase almost totally unresponsive to GCAP1 although the binding of GCAP1 to ROS-GC was not affected (Duda et al., 2016). It implies that the loss in GCAP1 modulation occurs at the signal transduction level and possibly involves one or more of the core catalytic residues: D^{834}, E^{874}, D^{878}, R^{925}, C^{946}, and N^{953}. In contrast, Ca^{2+}-dependent modulations by GCAP2 and by S100B are unaffected by the $F^{514}S$ mutation (Duda et al., 1999a,b, 2016), even though the absolute achieved activities are reduced in all cases. The interaction of this disease-causing ROS-GC1 mutant with bicarbonate led to some insights into the intramolecular signaling pathways in ROS-GC1 catalytic activity.

Bicarbonate partially restores the basal as well as the GCAP2-and S100B-dependent activities of the $F^{514}S$ mutant but is ineffective for the deficit in GCAP1stimulation. The recuperative ability of bicarbonate indicates that it operates either downstream or independently of the $F^{514}S$ mutation. These findings support the earlier conclusion that the S100B-and GCAP2-targeted sites within ROS-GC1 overlap (Duda et al., 2002). Yet, both are distinct from the GCAP1-targeted site (Duda et al., 1996a, 2012c; Krishnan et al., 1998; Koch et al., 2010; Koch and Dell'Orco, 2013) although some indicate that GCAP2 binds to the same as GCAP1 site (Peshenko et al., 2015a,b).

At a clinical level, higher levels of bicarbonate could offer some relief for patients bearing the $F^{514}S$-mutation by reinstating some basal and GCAP2-modulated guanylate cyclase activities in rods and cones. The mice stricken with the mutation would not be so lucky, however, as their cones express GCAP1 but not GCAP2 (Xu et al., 2013).

ONE-GC senses odorants

Cloning of a MGC, GC-D, alternately termed ONE-GC from an olfactory cDNA library (Fulle et al., 1995) came at a time when G protein coupled receptors and the cyclic AMP signaling pathway were thought to be the sole components of the olfactory transduction (Buck, 1995; Belluscio et al., 1998; Breer, 2003; Lai et al., 2005). Even though an odorant for ONE-GC was not known, there were hints for a role of cyclic GMP in olfaction. *In situ* hybridization and immunocytochemistry results demonstrated that ONE-GC co-exists with PDE2, the phosphodiesterase, that hydrolyzes cyclic GMP as well as cyclic AMP and with a cyclic GMP gated ion channel (Fulle et al., 1995;

Juilfs et al., 1997; Meyer et al., 2000). They are expressed only in a small subpopulation of neuroepithelial neurons that do not express any of the "standard" components: G*olf*, ACIII, PDE1C2, and the a3 and b1b subunits of the cyclic nucleotide gated ion channel. The ONE-GC/PDE2 expressing neurons project to specific "necklace glomeruli" of the olfactory bulb. Significantly, various anti-ONE-GC antibodies show more extensive labeling of olfactory neuroepithelial cilia suggesting the possible expression of more than one type of MGC and/or a subsidiary role for cGMP in a majority of the olfactory cells (Juilfs et al., 1997; Duda et al., 2001a).

To assess the possibility that a novel Ca^{2+}-modulated MGC is present in the subpopulation of rat olfactory neuroepithelium cilia, our group cloned ONE-GC from the rat olfactory neuroepithelium cDNA library (Duda et al., 2001a). Sequence alignment revealed that the cloned cyclase is identical with the previously cloned GC-D (Juilfs et al., 1997), yet is only 47.9% and 47.6%, identical with, respectively, ROS-GC1 and ROS-GC2. A polyclonal antibody raised against its unique12 aminoacid C-terminal epitope recognizes neither ROS-GC1 nor ROS-GC2 indicating no immunological identity between these MGCs (Duda et al., 2001a). Thus, ONE-GC and GC-D are the same guanylate cyclase. Because ONE-GC resides in the olfactory neuroepithelium, the authors prefer the ONE-GC nomenclature over GC-D.

The ONE-GC system fulfils the requirements set forth to guarantee its role as a genuine, Ca^{2+}-modulated odorant transducer (Duda et al., 2001a, 2004; Duda and Sharma, 2008; Sharma and Duda, 2010).

(1) It responds to uroguanylin in its natural environment. Uroguanylin is a very potent stimulus for ONE-GC expressing neurons (Leinders-Zufall et al., 2007), it binds the ONE-GC ExtD with an EC_{50} of 20 pM reaching plateau at 500 pM (Duda and Sharma, 2008). Although STa-RGC is a receptor for both uroguanylin and guanylin, ONE-GC is more selective and does not recognize guanylin; (2) Uroguanylin promotes the acquisition of food preferences in mice (Arakawa et al., 2013); (3) It responds to the odorant relatively quickly for an amplifying system; (4) ONE-GC is located within the ciliary membrane; (5) it is modulated by free Ca^{2+} with a $K_{1/2}$ of 700 nM, generating responses similar to that of odorant; and (6) The Ca^{2+}-responsive system can be reconstituted with recombinant myr-NCδ and ONE-GC.

ONE-GC binds NCδ through its M^{880}-L^{921} segment that corresponds to the V^{836}-L^{857} NCδ binding site in ROS-GC1, allowing direct access to the catalytic domain (Duda and Sharma, 2008). *In vivo* studies demonstrate that in resting cells, the NCδ-ONE-GC complex is solely located at the plasma membrane (Duda et al., 2004). The kinetic parameters of the Ca^{2+}-bound NCδ binding to ONE-GC assessed by the surface plasmon resonance spectroscopy, are: K_D 2.8×10^{-7} M; *k*on = 5.7×10^{3} M^{-1} s^{-1}; *k*off = 1.56×10^{-3} s^{-1}.

Gene-knockout studies in mouse establish that in olfactory neuroepithelium another NCS, hippocalcin (Hpca) activates ONE-GC activity in the Ca^{2+} $K_{1/2}$ range of 0.5–0.7 mM (Krishnan et al., 2009). Besides neurocalcin and Hpca, ONE-GC interacts with yet one more Ca^{2+} sensor, GCAP1 (Pertzev et al., 2010). The interaction was missed initially, because it is antithetical to that with ROS-GC in phototransduction. Instead of stimulating ONE-GC at the low nM range of free Ca^{2+} (i.e., in the Ca^{2+}-free state), GCAP1 stimulates at the upper range of Ca^{2+} i.e., in the Ca^{2+} bound state (Duda et al., 2006, 2012a; Figure 10). To add to the trickery, stimulation of ONE-GC activity by GCAP1 occurs at an EC_{50} that is higher than the apparent IC_{50} for ROS-GC1 activity.

It was the first, and is to date, the only example of an NCS switching the directionality of its action with a change in binding partners. Biochemical assays with antibodies indicate that 35% of the total ONE-GC transduction activity is controlled by GCAP1, 27% by NCδ, and 38% by Hpca (Krishnan et al., 2009; reviewed in Sharma and Duda, 2010).

ONE-GC resembles the ANF-RGC in combining a surface hormone/odorant transduction with internal Ca^{2+} sensing. Yet, a primary sequence identity of only 28.1% with ANF-RGC but a sequence identity of 47.6% with ROS-GC makes it closer akin to the latter subfamily. Like photoreceptor ROS-GCs, ONE-GC is stimulated by bicarbonate (Guo et al., 2009; Sun et al., 2009). The target site of the bicarbonate signal resides within Y^{922}-P^{1028} segment of the catalytic domain (Hu et al., 2007; Sun et al., 2009; Duda and Sharma, 2010).

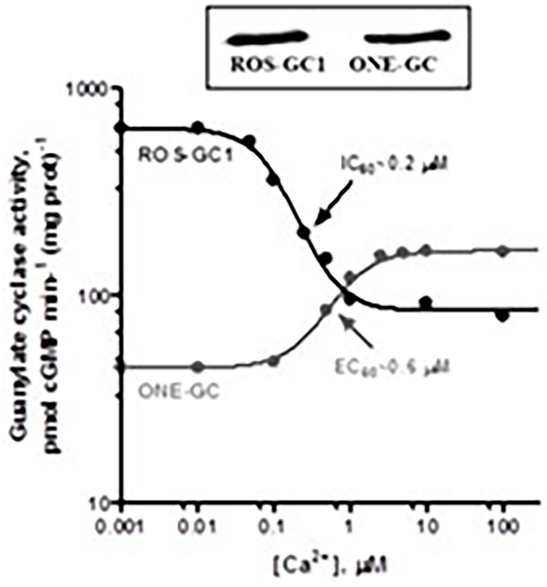

FIGURE 10
Antithetical Ca^{2+} modulation of ROS-GC1 and olfactory neuroepithelial guanylate cyclase (ONE-GC) activities by GCAP1. In the presence of GCAP1, the catalytic activity of recombinant ROS-GC1 decreases as Ca^{2+} is raised from 1 nM to100 mM, but the catalytic activity of recombinant ONE-GC increases. Western blots confirming ROS-GC1 and ONE-GC expression are shown above. Redrawn from Duda et al. (2012a).

Hippocampus embodies ONE-GC linked with memory

The information that ONE-GC neurons sense the odorant and its perception occurs in the hippocampal neurons, paved the way for an exploration as to whether these neurons embody the ONE-GC-modulated signaling pathway? The issue was not fully decoded, yet pointed in that direction.

Because the Ca^{2+} sensor frequenin (Frq) is evolutionary the most ancient member of the NCSs family with homologs already expressed in yeast, it became the subject matter. The question was: Is Frq the Ca^{2+}-sensor of ONE-GC?

Bovine Frq has a molecular mass of 22 kDa and shows a Ca^{2+}-dependent electrophoretic mobility shift typical of the NCS family (Ladant, 1995). Its sequence is highly conserved within the evolutionary ladder with the identities of 100% with chicken (Nef et al., 1995; Olafsson et al., 1997; McFerran et al., 1999) rat, and human (Jeromin et al., 1999; Bourne et al., 2001); 98% with frog (Olafsson et al., 1995), 75% with *C. elegans* (De Castro et al., 1995), 72% with *Drosophila* (Pongs et al., 1993), and 60% with the yeast form (Hendricks et al., 1999). In common with the NCS family trait, it contained four EF-hands, yet only three – 2, 3 and 4 – are functional in binding Ca^{2+}; and it is myristoylated.

Co-immunoprecipitation experiments determined that Frq and a ONE-GC-like MGC assemble in a complex in the neurons of bovine hippocampus (Fik-Rymarkiewicz et al., 2006). The complex lasts as long as Ca^{2+} is present and dissociates when Ca^{2+} is reduced or removed with EGTA. Remarkably, a very small fraction of Frq immunoprecipitates with the hippocampal MGC even in the presence of 5 mM EGTA. Hippocampal neurons respond to $[Ca^{2+}]_i$ with a five-fold increase in the MGC catalytic activity and a $K_{1/2}$ for Ca^{2+} of 0.7 mM. The EC_{50} of hippocampal MGC for recombinant myr-Frq is 0.7 mM, and at saturating levels of Ca^{2+}, the activity increases five-fold.

Recombinant myr-Frq stimulates the catalytic activity of recombinant ONE-GC 6-fold with an EC_{50} of 0.7 mM. It only marginally (1.5-fold) stimulates the rROS-GC1 activity, and fails to stimulate ROS-GC2.

The binding parameters between Frq and the M^{836}-C^{1110} segment of ONE-GC were measured through surface plasmon resonance spectroscopy. They are: $K_D = 0.43$ mM; *k*on (the association rate constant) $= 7.14 \times 10^3\ M^{-1}\ s^{-1}$; *k*off (dissociation rate constant) $= 3.04 \times 10^{-3}\ s^{-1}$; and *K*A (equilibrium association constant) $= 2.35 \times 10^6\ M^{-1}$.

Thus, Frq is a soluble modulator rather than a subunit of the hippocampal MGC. Functionally, the existence of Frq in two forms, permanently bound to the hippocampal MGC (a minor fraction) and free in the cytoplasm of resting neurons (a larger fraction) serves to efficiently increase the Ca^{2+} requirement, extend the Ca^{2+} range and prolong the duration of the Ca^{2+} rise essential for stimulation of the hippocampal MGC activity.

Modulation of an MGC by myr-Frq suggests that evolutionary, Ca^{2+}-sensors that stimulate MGCs at high Ca^{2+} probably preceded the GCAPs that stimulate at low Ca^{2+}.

Additional studies demonstrate that hippocalcin, is also present in the hippocampal neurons, couples with ONE-GC, and modulates its activity in the Ca^{2+}-dependent manner (Krishnan et al., 2009). Thus, it is potentially a second soluble Ca^{2+} modulator of the MGC.

Diverging from the interwoven concept of Ca^{2+}-modulated ONE-GC, it is important to point out that the CNP-RGC expressed in hippocampal neurons may be locked in with the memory (Langub et al., 1995; Herman et al., 1996). Rats expressing a dominant-negative mutant of CNP-RGC lacking the intracellular cyclase catalytic domain show disturbances in long term potentiation and long term depression (Barmashenko et al., 2014). The studies on hippocampus has begun to unravel a role for MGCs for synaptic information storage and learning.

Clued new frontiers of Ca^{2+}-interlocked MGCS

At present there is growing evidence that MGCs have taken on in cellular signaling pathways throughout the body. A few examples are listed below.

Pineal gland

The adrenergic receptor activity is linked to cyclic GMP synthesized by ROS-GC1 in a $[Ca^{2+}]_i$–dependent fashion (Venkataraman et al., 1998). Expression of both GCAP1 and the S100B in the pineal gland raises the possibility for the presence of two "Turn ON" Ca^{2+}-modulated switches in the two separate subtypes of the pinealocytes (Venkataraman et al., 2000). One is GCAP1-and the other is S100B-modulated.

Pinealocytes also express ANF, CNP and CNP-RGC (Olcese et al., 1994; Middendorff et al., 1996). How they embody their signal transduction pathways is not yet explored?

Gustatory epithelium

Expression of a Ca^{2+} modulated MGC transduction system in the anterior portion of the bovine gustatory epithelium, points out its role at the biochemical, molecular and functional levels in taste (Duda and Sharma, 2004). There are two components of the system: S100B, the Ca^{2+}-sensor, and ROS-GC1, the transducer. ROS-GC1 and S100B co-immunoprecipitate indicating their physical interaction.

Olfactory bulb

Biochemical and functional analyses of the rat olfactory bulb demonstrate the presence of GCAP1-modulated ROS-GC1

transduction system in its mitral cells. The system functions identically as in phototransduction model. GCAP1 senses lowering of free levels of Ca^{2+} and stimulates ROS-GC1 activity. The IC_{50} for Ca^{2+} is 70 nM. The bulb neurons do not express GCAP2, nor do they express ROS-GC2. The olfactory bulb receives neural input from the olfactory neurons and functions as a "processing unit" directing the information about odorants to the olfactory tract and to cortical centers of the brain for odorant perception (Duda et al., 2001b).

Testes

There is ample evidence for the second messenger role of the cyclic GMP and for the presence of ANF-dependent ANF-RGC transduction system in testes. There, it appears they are involved in the varying physiological processes: sperm motility, development of testicular germ cells, relaxation of peritubular lamina propia cells, testosterone synthesis in Leydig cells and dilation of testicular blood vessels (Marala and Sharma, 1988; Singh et al., 1988; Garbers, 1989; Pandey and Singh, 1990; Armstrong et al., 1994; Middendorff et al., 1997, 2000; Pandey et al., 1999; Mourdjeva et al., 2001).

Biochemical studies demonstrate the presence of also ROS-GC1 transduction systems modulated by GCAP1 and S100B in the plasma membrane of bovine testes (Jankowska et al., 2007, 2014). These transduction components co-localize in bovine and human sperms (Jankowska and Warchol, 2010). A combination of molecular genetics, biochemistry and immunohistochemistry tools reveal the presence of NCδ in male gonads (Jankowska et al., 2014). Accordingly, GCAP1, S100B, and NCδ, sense and transmit Ca^{2+} signals to ROS-GC1 in this tissue. The transduction unit is present in all germinal cells of the human testes: spermatogonias, spermatocytes, and spermatids. NCδ appears to be the major (75%) and S100B the minor (25%) contributor of Ca^{2+} signaling as determined through mouse-KO models. Although the contribution of GCAP1 has not been determined yet, there is an evidence for its function in bovine and human spermatozoa (Jankowska and Warchol, 2010). The bimodal operation of MGC activity is evidenced by the results that its activity is minimal at 800 nM, increases with a decline in Ca^{2+} with an IC_{50} of 200 nM and increases again as Ca^{2+} is raised with an EC_{50} of 2 mM.

A novel MGC (GC-G) is a thermosensor

Present in the certain temperature-sensitive neurons of the Grueneberg Ganglion in the mouse nasal cavity, GC-G is the latest discovered member of the MGC family (Schulz et al., 1998; Fleischer et al., 2009). At the time of this writing, its functional molecular mechanism is not defined. The limited information is provided below.

It has been cloned from rat and shown to be expressed in the selected Grueneberg Ganglion neurons. It is a thermosensor (Chao et al., 2015), reminiscent of MGCs encoded by gcy-8, gcy-18 and gcy-23 genes in *C. elegans* (Takeishi et al., 2016). It appears to have multiple functions such as sensing the predator odorant 2,4,5-trimethylthiazoline (Chao et al., 2015) and bicarbonate (Chao et al., 2010). Mild cooling of Grueneberg Ganglion neurons prompts ultrasound vocalization in pups, a behavior that is weakened in GC-G KO mice (Chao et al., 2015).

Conclusion

The 1967, more than 52 years ago, kindled by my earlier pursuit that a common evolutionary link exists between the generation of plant steroids and the mammalian steroid hormones, I (RKS) entered the field of hormonal signal transduction and continued with it till now. In the ensuing years, a powerful group, including Teresa Duda was developed. It was dedicated to explore, generate and establish the new avenues of the hormonal signal transduction pathways. In this pursuit a pivotal finding was made that changed the cellular signal transduction field. It was the discovery of the MGC signal transduction pathway/s.

The first foundational brick demonstrated that this system is embodied in the rat adrenocortical carcinoma 494 cells, and it is epinephrine-specific (Perchellet and Sharma, 1980; Shanker and Sharma, 1980). This monograph recounts its evolutionary tale. Its painstaking analysis, its growth from obscurity to its present position and its emergence as a dominant cellular signal transducer. Generating, its intracellular second messenger, cyclic GMP, it judiciously controls the, biochemistry and molecular biology of the innumerable physiological processes (Figures 11, 12).

What Are Its coded molecular features that make It achieve such complex tasks? (1) A modular structure. It makes the MGC enormously elastic and multimodal. Unlike its predecessor three component second messenger systems, adenylate cyclase and IP_3, the MGC is composed of a single unit. It is a trans-membrane-spanning protein. It functions both as surface receptor and the signal transducer. (2) All MGCs contain the ExtD. Except for ROS-GC1 and ROS-GC2, it is the binding domain of the hormones. Its role in ROS-GC1 and ROS-GC2 is unknown. (3) A few MGCs embody subunits. The subunits join to an intracellular domain (ICD) and bestow the MGC Ca^{2+} sensitivity. (4) The kinship between Ca^{2+} and MGC's catalytic activity is irregular. (5) ANF-RGC. High Ca^{2+} stimulates its catalytic activity without ligand binding. Yet, ROS-GC1 and ONE-GC can function as bimodal Ca^{2+} switches. Its catalytic activity fluctuates. It is maximal as Ca^{2+} levels lower, it wanes at midrange $[Ca^{2+}]_I$ and rises once again as $[Ca^{2+}]$ reaches its peak level. The reason for these different modes trace to the nature of the Ca^{2+} sensor involved – GCAPs, S100B, neurocalcin δ, hippocalcin, and frequenin. (6) In an amazing arrangement, the function of GCAP1 is its MGC partner-dependent; at low Ca^{2+}, it stimulates ROS-GCs and inhibits them at high Ca^{2+}. Yet, it stimulates ONE-GC at high Ca^{2+}. (7) ROS-GC1 has the ability to link with varied forms of Ca^{2+} sensors (Figure 11 of Sharma et al., 2016), in

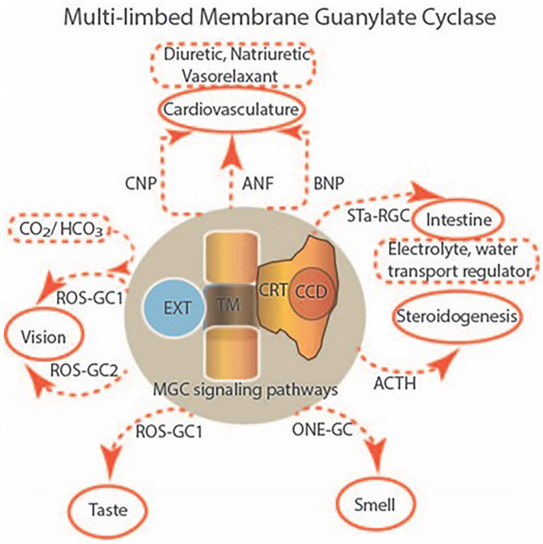

FIGURE 11
Multilimbed membrane guanylate cyclase. In mammals, membrane guanylate cyclase signaling is encoded by seven distinct genes. Through their expression in seven subfamily forms, they perform multi-limbed functions. The surface receptor subfamily, detects hormones and other extracellular chemicals, translate the signal across their plasma membrane domains and by way of their second messenger, cyclic GMP, regulate an intracellular pathway to impact physiology. Sequentially, other similar signaling networks, depicted in the figure, were discovered. Collectively, besides steroidogenesis, they control the physiology of the cardiovasculature, sensory neurons: vision, taste and smell, the intestine and skeletal growth. Uniquely designed, all forms are single-pass transmembrane proteins, embedded with an EXT, TM, CRM and CCD topography. Abbreviations: EXT, extracellular; TM, transmembrane; CRM, catalytic regulatory module; CCD, catalytic core domain.

part because of its CTE. (8) In contrast, ROS-GC2 is discriminatory, despite it possessing a CTE. Intriguingly, the CTE in STa-RGC points out additional functions this structure performs. (9) The conserved CCD dimer receives signals generated by both the C-terminal and N-terminal modules. (10) Extraordinarily, the CCD is also subject to direct tuning by Ca^{2+}/neurocalcin δ and bicarbonate. (11) With conservation, the CCD structure of every MGC responds to the bicarbonate signals. The response of ROS-GC to bicarbonate and Ca^{2+}-modulated GCAPs and S100B in combination exceeds the sum of the individual modulations. Thus, bicarbonate provides a means to amplify the transductions. (11) Probably, the bicarbonate signaling can amplify transduction of orthosteric ligand binding. (12) The modulation and regulation by phosphorylation plays a critical part in hormone receptor MGCs.

Author contributions

Both authors have made a substantial, direct, intellectual and equal contribution to the work and approved it for publication.

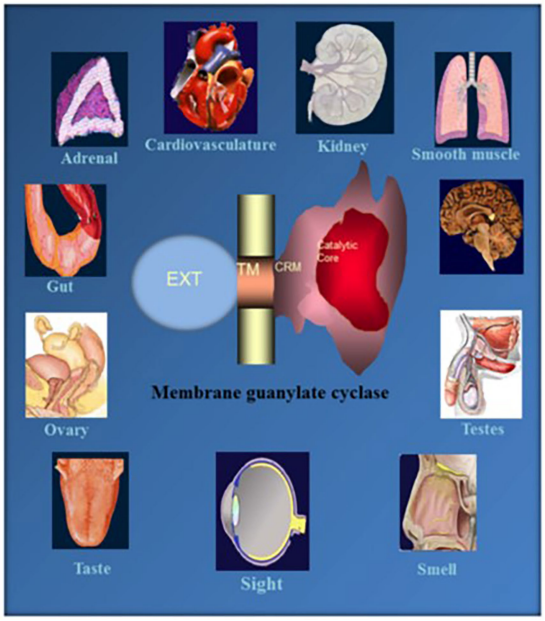

FIGURE 12
Ubiquitous expression of MGC signaling systems. MGCs is a multi-switching cyclic GMP generating machine linked with the physiology of cardio-vasculature, smooth muscle relaxation, sensory transduction, neuronal plasticity and memory in mammalian neurosensory, endocrine and peripheral tissues. (Reproduced from Sharma et al., 2015).

Acknowledgments

The authors gratefully acknowledge the continuous financial support of the numerous USPHS awards from the National Institutes of Health, awards from the National Science Foundation, the Damon Runyon Walter Winchell Cancer Fund, and PA Lions Club (PA Lions Sight Conservation and Eye Research Foundation). The authors appreciatively acknowledge the long-lasting and fruitful collaborations with Drs. Ari Sitaramayya (Oakland University), Karl-W. Koch (Oldenburg University) and Clint L. Makino (Boston University). Finally, this would have never be completed without the devotion of our other group members: Lynda Sutliff, Nahed K. Ahmed, Gouri Shanker, Rajinder Sawhney; Robert Moore, Jean-Pierre Perchellet, Elizabeth Perchellet, Yoshikazu Kuroda, Ponnal Nambi; Nambi Aiyar, Gypsy Majumdar; Helga Ahrens; Chhanda Ganguly, Rama K. Jaiswal, Ravi Marala, Rafal Goraczniak, Anna Jankowska, Venkat Venkataraman, Anurada Krishnan, Wolfgang Baehr, Sarangan Ravichandran and Alex Pertzev.

Conflict of interest

The authors declare that the research was conducted in the absence of any commercial or financial relationships that could be construed as a potential conflict of interest.

Publisher's note

References

Ahmad, I., and Barnstable, C. J. (1993). Differential laminar expression of particulate and soluble guanylate cyclase genes in rat retina. *Exp. Eye Res.* 56, 51–62. doi: 10.1006/exer.1993.1008

Ahrens, H., Paul, A. K., Kuroda, Y., and Sharma, R. K. (1982). Adrenocortical cyclic GMP-dependent protein kinase: purification, characterization, and modification of its activity by Calmodulin and its relationship with steroidogeneses. *Arch. Biochem. Biophys.* 215, 597–609. doi: 10.1016/0003-9861(82)90121-7

Ahrens, H., and Sharma, R. K. (1979). Guanosine 3′:5′-monophosphate-dependent protein kinase from bovine adrenal cortex: partial purification and characterization. *J. Steroid Biochem.* 11, 1099–1105. doi: 10.1016/0022-4731(79)90159-6

Allerston, C. K., von Delft, F., and Gileadi, O. (2013). Crystal structures of the catalytic domain of human soluble guanylate cyclase. *PLoS One* 8:e57644. doi: 10.1371/journal.pone.0057644

Aoki, H., Richmond, M., Izumo, S., and Sadoshima, J. (2000). Specific role of the extracellular signal-regulated kinase pathway in angiotensin II-induced cardiac hypertrophy in vitro. *Biochem J.* 347, 275–284.

Aparicio, J. G., and Applebury, M. L. (1996). The photoreceptor guanylate cyclase is an autophosphorylating protein kinase. *J. Biol. Chem.* 271, 27083–27089. doi: 10.1074/jbc.271.43.27083

Arakawa, H., Kelliher, K. R., Zufall, F., and Munger, S. D. (2013). The receptor guanylyl cyclase type D (GC-D) ligand uroguanylin Ppromotes the acquisition of food preferences in mice. *Chem. Senses* 38, 391–397. doi: 10.1093/chemse/bjt015

Ariëns, E. J. (1967). The structure-activity relationships of beta adrenergic drugs and beta adrenergic blocking drugs. *Review Ann. N. Y. Acad. Sci.* 139, 606–631. doi: 10.1111/j.1749-6632.1967.tb41232.x

Ariëns, E. J., and Simonis, A. M. (1966). Aspects of molecular pharmacology. II. Theories of receptors and structure-action relationships. *Farmaco. Sci.* 21, 581–608. PMID: 5338885

Armstrong, V. L., Clulow, J., Murdoch, R. N., and Jones, R. C. (1994). Intracellular signal transduction mechanisms of rat epididymal spermatozoa and their relationship to motility and metabolism. *Mol. Reprod. Dev.* 38, 77–84. doi: 10.1002/mrd.1080380113

Arnold, W. P., Mittal, C. K., Katsuki, S., and Murad, F. (1977). Nitric oxide activates guanylate cyclase and increases guanosine 3′:5′-cyclic monophosphate levels in various tissue preparations. *Proc. Natl. Acad. Sci. U. S. A.* 74, 3203–3207. doi: 10.1073/pnas.74.8.3203

Ashman, D. F., Lipton, R., Melicow, N. M., and Price, T. D. (1963). Isolation of adenosine 3′,5′-monophosphate and guanosine 3′,5′-monophosphate from rat urine. *Biochem. Biophys. Res. Commun.* 11, 330–334. doi: 10.1016/0006-291x(63)90566-7

Atarashi, K., Mulrow, P. J., Franco-Saenz, R., Snajdar, R., and Rapp, J. (1984). Inhibition of aldosterone production by an atrial extract. *Science* 224, 992–994. doi: 10.1126/science.6326267

Atlas, S. A., and Laragh, J. H. (1986). Atrial natriuretic peptide: a new factor in hormonal control of blood pressure and electrolyte homeostasis. *Annu. Rev. Med.* 37, 397–414. doi: 10.1146/annurev.me.37.020186.002145

Avesani, A., Bielefel, L., Weisschuh, N., Marino, V., Mazzola, P., Stingl, K., et al. (2022). Molecular properties of human guanylate cyclase-activating protein 3 (GCAP3) and its possible association with retinitis Pigmentosa. *Int. J. Mol. Sci.* 23:3240. doi: 10.3390/ijms23063240

Ballermann, B. J., Marala, R. B., and Sharma, R. K. (1988). Characterization and regulation by protein kinase C of renal glomerular atrial natriuretic peptide receptor-coupled guanylate cyclase. *Biochem. Biophys. Res. Commun.* 157, 755–761. doi: 10.1016/s0006-291x(88)80314-0

Bansal, V. S., and Majerus, P. W. (1990). Phosphatidylinositol-derived precursors and signals. *Annu. Rev. Cell Biol.* 6, 41–67. doi: 10.1146/annurev.cb.06.110190.000353

Barmashenko, G., Buttgereit, J., Herring, N., Bader, M., Ozcelik, C., Manahan-Vaughan, D., et al. (2014). Regulation of hippocampal synaptic plasticity thresholds and changes in exploratory and learning behavior in dominant negative NPR-B mutant rats. *Front. Mol. Neurosci.* 7:95. doi: 10.3389/fnmol.2014.00095

Belluscio, L., Gold, G. H., Nemes, A., and Axel, R. (1998). Mice deficient in G(olf) are anosmic. *Neuron* 20, 69–81. doi: 10.1016/s0896-6273(00)80435-3

Bereta, G., Wang, B., Kiser, P. D., Baehr, W., Jang, G. F., and Palczewski, K. (2010). A functional kinase homology domain is essential for the activity of photoreceptor guanylate cyclase1. *J. Biol. Chem.* 285, 1899–1908. doi: 10.1074/jbc.m109.061713

Berridge, M. J., and Irvine, R. F. (1989). Inositol phosphates and cell signalling. *Nature* 341, 197–205. doi: 10.1038/341197a0

Bhandari, R., Srinivasan, N., Mahaboobi, M., Ghanekar, Y., Suguna, K., and Visweswariah, S. S. (2001). Functional inactivation of the human guanylyl cyclase C receptor: modeling and mutation of the protein kinase-like domain. *Biochemistry* 40, 9196–9206. doi: 10.1021/bi002595g

Birnbaumer, L., and Birnbaumer, M. (1995). Signal transduction by G proteins: 1994 edition. *J. Recept. Signal Transduct. Res.* 15, 213–252. doi: 10.3109/10799899509045218

Birnbaumer, L., Pohl, S. L., Michiel, H., Krans, M. J., and Rodbell, M. (1970). The actions of hormones on the adenyl cyclase system. *Adv. Biochem. Psychopharmacol.* 3, 185–208. PMID: 4399634

Bourne, Y., Dannenberg, J., Pollmann, V., Marchot, P., and Pongs, O. (2001). Immunocytochemical localization and crystal structure of human frequenin (neuronal calcium sensor 1). *J. Biol.Chem.* 276, 11949–11955. doi: 10.1074/jbcM009373200

Bowyer, F., and Kitabchi, A. E. (1974). Dual role of calcium in steroidogenesis in the isolated adrenal cell of rat. *Biochem. Biophys. Res. Commun.* 57, 100–105. doi: 10.1016/S0006-291X(74)80362-1

Brandwein, H., Lewicki, J., and Murad, F. (1981). Production and characterization of monoclonal antibodies to soluble rat lung guanylate cyclase. *Proc. Natl. Acad. Sci. U. S. A.* 78, 4241–4245. doi: 10.1073/pnas.78.7.4241

Braunewell, K. H., Brackmann, M., Schaupp, M., Spilker, C., Anand, R., and Gundelfinger, E. D. (2001). Intracellular neuronal calcium sensor (NCS) protein VILIP-1 modulates cGMP signaling pathways in transfected neural cells and cerebellar granule neurones. *J. Neurochem.* 78, 1277–1286. doi: 10.1046/j.1471-4159.2001.00506.x

Braunewell, K. H., and Gundelfinger, E. D. (1999). Intracellular neuronal calcium sensor proteins: a family of EF-hand calcium-binding proteins in search of a function. *Cell Tissue Res.* 295, 1–12. doi: 10.1007/s0044100512079

Breer, H. (2003). Olfactory receptors: molecular basis for recognition and discrimination of odors. *Anal. Bioanal. Chem.* 377, 427–433. doi: 10.1007/s00216-003-2113-9

Brenner, B. M., Ballermann, B. J., Gunning, M. E., and Zeidel, M. L. (1990). Diverse biological actions of atrial natriuretic peptide. *Physiol. Rev.* 70, 665–699. doi: 10.1152/physrev.1990.70.3.665

Buck, L. B. (1995). Unraveling chemosensory diversity. *Cells* 83, 349–352. doi: 10.1016/0092-8674(95)90110-8

Burgoyne, R., and Weiss, J. L. (2001). The neuronal calcium sensor family of Ca2+−binding proteins. *Biochem. J.* 353, 1–12. doi: 10.1042/bj3530001

Burns, M. E., and Baylor, D. A. (2001). Activation, deactivation, and adaptation in vertebrate photoreceptor cells. *Annu. Rev. Neurosci.* 24, 779–805. doi: 10.1146/annurev.neuro.24.1.779

Cantin, M., and Genest, J. (1985). The heart, an endocrine gland. *Ann. Endocrinol. (Paris)* 46, 219–228.

Chang, M. S., Lowe, D. G., Lewis, M., Hellmiss, R., Chen, E., and Goeddel, D. V. (1989). Differential activation by atrial and brain natriuretic peptides of two different receptor guanylate cyclases. *Nature* 341, 68–72. doi: 10.1038/341068a0

Chao, Y. C., Chen, C. C., Lin, Y. C., Breer, H., Fleischer, J., and Yang, R. B. (2015). Receptor guanylyl cyclase-G is a novel thermosensory protein activated by cool temperatures. *EMBO J.* 34, 294–306. doi: 10.15252/embj.201489652

Chao, Y. C., Cheng, C. J., Hsieh, H. T., Lin, C. C., Chen, C. C., and Yang, R. B. (2010). Guanylate cyclase-G, expressed in the Grueneberg ganglion olfactory subsystem, is activated by bicarbonate. *Biochem. J.* 432, 267–273. doi: 10.1042/bj20100617

Chartier, L., Schiffrin, E., Thibault, G., and Garcia, R. (1984). Atrial natriuretic factor inhibits the stimulation of aldosterone secretion by angiotensin II, ACTH and potassium in vitro and angiotensin II-induced steroidogenesis in vivo. *Endocrinology* 115, 2026–2028. doi: 10.1210/endo-115-5-2026

Chen, C. K., Inglese, J., Lefkowitz, R. J., and Hurley, J. B. (1995). Ca(2+)-dependent interaction of recoverin with rhodopsin kinase. *J. Biol. Chem.* 270, 18060–18066. doi: 10.1074/jbc.270.30.18060

Chinkers, M., and Garbers, D. L. (1989). The protein kinase domain of the ANP receptor is required for signaling. *Science* 245, 1392–1394. doi: 10.1126/science.2571188

Chinkers, M., Garbers, D. L., Chang, M. S., Lowe, D. G., Chin, H. M., Goeddel, D. V., et al. (1989). A membrane form of guanylate cyclase is an atrial natriuretic peptide receptor. *Nature* 338, 78–83. doi: 10.1038/338078a0

Chinkers, M., Singh, S., and Garbers, D. L. (1991). Adenine nucleotides are required for activation of rat atrial natriuretic peptide receptor/guanylyl cyclase expressed in a baculovirus system. *J. Biol. Chem.* 266, 4088–4093. doi: 10.1016/S0021-9258(20)64289-2

Cooper, N. G. F., Fedinec, A. A., and Sharma, R. K. (1989). Immunocytochemistry of the 180 kD membrane guanylate cyclase in the retina. *Invest. Ophthalmol. Vis. Sci.* 30:129. Abstract #30

Cooper, N., Liu, L., Yoshida, A., Pozdnyakov, N., Margulis, A., and Sitaramayya, A. (1995). The bovine rod outer segment guanylate cyclase, ROS-GC, is present in both outer segment and synaptic layers of the retina. *J. Mol. Neurosci.* 6, 211–222. doi: 10.1007/bf02736766

Cuenca, N., Lopez, S., Howes, K., and Kolb, H. (1998). The localization of guanylyl cyclase-activating proteins in the mammalian retina. *Invest. Ophthalmol. Vis. Sci.* 39, 1243–1250.

Currie, M. G., Fok, K. F., Kato, J., Moore, R. J., Hamra, F. K., Duffin, K. L., et al. (1992). Guanylin: an endogenous activator of intestinal guanylate cyclase. *Proc. Natl. Acad. Sci. U. S. A.* 89, 947–951. doi: 10.1073/pnas.89.3.947

De Bold, A. J. (1982). Atrial natriuretic factor of the rat heart. Studies on isolation and properties. *Proc. Soc. Exp. Biol. Med.* 170, 133–138. doi: 10.3181/00379727-170-41408

De Bold, A. J. (1986). Atrial natriuretic factor; an overview. *Fed. Proc.* 45, 2081–2085. PMID: 2940116

De Castro, E., Nef, S., Fiumelli, H., Lenz, S. E., Kawamura, S., and Nef, P. (1995). Regulation of rhodopsin phosphorylation by a family of neuronal calcium sensors. *Biochem. Biophys. Res. Commun.* 216, 133–140. doi: 10.1006/bbrc.1995.2601

De Léan, A., Racz, K., Gutkowska, J., Nguyen, T.-T., Cantin, M., and Genest, J. (1984). Specific receptor-mediated inhibition by synthetic atrial natriuretic factor of hormone-stimulated steroidogenesis in cultured bovine adrenal cells. *Endocrinology* 115, 1636–1638. doi: 10.1210/endo-115-4-1636

de Sauvage, F. J., Camerato, T. R., and Goeddel, D. V. (1991). Primary structure and functional expression of the human receptor for *Escherichia coli* heat-stable enterotoxin. *J. Biol. Chem.* 266, 17912–17918. doi: 10.1016/S0021-9258(18)55214-5

Denninger, J. W., and Marletta, M. A. (1999). Guanylate cyclase and the NO/cGMP signaling pathway. *Review. Biochim. Biophys. Acta* 1411, 334–350. doi: 10.1016/s0005-2728(99)00024-9

Dizhoor, A. M., and Hurley, J. B. (1996). Inactivation of EF-hands makes GCAP-2 (p24) a constitutive activator of photoreceptor guanylyl cyclase by preventing a Ca^{2+}−induced "activator-to-inhibitor" transition. *J. Biol.Chem.* 271, 19346–19350. doi: 10.1074/jbc.271.32.19346

Dizhoor, A. M., Olshevskaya, E. V., Henzel, W. J., Wong, S. C., Stults, J. T., Ankoudinova, I., et al. (1995). Cloning, sequencing, and expression of a 24-kDa Ca(2+)-binding protein activating photoreceptor guanylyl cyclase. *J. Biol. Chem.* 270, 25200–25206. doi: 10.1074/jbc.270.42.25200

Dizhoor, A. M., Ray, S., Kumar, S., Niemi, G., Spencer, M., Brolley, D., et al. (1991). Recoverin: a calcium sensitive activator of retinal rod guanylate cyclase. *Science* 251, 915–918. doi: 10.1126/science.1672047

Donaldson, C., Barber, K. R., Kay, C. M., and Shaw, G. S. (1995). Human S100b protein: formation of a tetramer from synthetic calcium-binding site peptides. *Protein Sci.* 4, 765–772. doi: 10.1002/pro.5560040416

Duda, T., Bharill, S., Wojtas, I., Yadav, P., Gryczynski, I., Gryczynski, Z., et al. (2009). Atrial natriuretic factor receptor guanylate cyclase signaling: new ATP-regulated transduction motif. *Mol. Cell. Biochem.* 324, 39–53. doi: 10.1007/s11010-008-9983-2

Duda, T., Fik-Rymarkiewicz, E., Venkataraman, V., Krishnan, R., Koch, K. W., and Sharma, R. K. (2005a). The calcium-sensor guanylate cyclase activating protein type 2 specific site in rod outer segment membrane guanylate cyclase type1. *Biochemistry* 44, 7336–7345. doi: 10.1021/bi050068x

Duda, T., Fik-Rymarkiewicz, E., Venkataraman, V., Krishnan, A., and Sharma, R. K. (2004). Calcium-modulated ciliary membrane guanylate cyclase transduction machinery: constitution and operational principles. *Mol. Cell. Biochem.* 267, 107–122. doi: 10.1023/b:mcbi.0000049372.33965.4f

Duda, T., Goraczniak, R. M., and Sharma, R. K. (1991). Site-directed mutational analysis of a membrane guanylate cyclase cDNA reveals the atrial natriuretic factor signaling site. *Proc. Natl. Acad. Sci. U. S. A.* 88, 7882–7886. doi: 10.1073/pnas.88.17.7882

Duda, T., Goraczniak, R. M., and Sharma, R. K. (1993a). Core sequence of ATP regulatory module in receptor guanylate cyclases. *FEBS Lett.* 315, 143–148. doi: 10.1016/0014-5793(93)81151-o

Duda, T., Goraczniak, R. M., and Sharma, R. K. (1993c). The glycine residue of ATP regulatory module in receptor guanylate cyclases that is essential in natriuretic factor signaling. *FEBS Lett.* 335, 309–314. doi: 10.1016/0014-5793(93)80408-m

Duda, T., Goraczniak, R. M., and Sharma, R. K. (1994). Glutamic acid-332 residue of the type C natriuretic pepitde receptor guanylate cyclase is important for signaling. *Biochemistry* 33, 7430–7433. doi: 10.1021/bi00189a050

Duda, T., Goraczniak, R. M., and Sharma, R. K. (1995). Single amino acid residue-linked signaling shifts in the transduction activities of atrial and type C natriuretic factor receptor guanylate cyclases. *Biochem. Biophys. Res. Commun.* 212, 1046–1053. doi: 10.1006/bbrc.1995.2075

Duda, T., Goraczniak, R. M., and Sharma, R. K. (1996a). Molecular characterization of S100A1–S100B protein in retina and its activation mechanism of bovine photoreceptor guanylate cyclase. *Biochemistry* 35, 6263–6266. doi: 10.1021/bi960007m

Duda, T., Goraczniak, R. M., Sitaramayya, A., and Sharma, R. K. (1993b). Cloning and expression of an ATP-regulated human retina C-type natriuretic factor receptor guanylate cyclase. *Biochemistry* 32, 1391–1395. doi: 10.1021/bi00057a001

Duda, T., Goraczniak, R., Surgucheva, I., Rudnicka-Nawrot, M., Gorczyca, W. A., Palczewski, K., et al. (1996b). Calcium modulation of bovine photoreceptor guanylate cyclase. *Biochemistry* 35, 8478–8482. doi: 10.1021/bi960752z

Duda, T., Jankowska, A., Venkataraman, V., Nagele, R. G., and Sharma, R. K. (2001a). A novel calcium-regulated membrane guanylate cyclase transduction system in the olfactory neuroepithelium. *Biochemistry* 40, 12067–12077. doi: 10.1021/bi0108406

Duda, T., Koch, K. W., Venkataraman, V., Lange, C., Beyermann, M., and Sharma, R. K. (2002). Ca2+ sensor S100beta-modulated sites of membrane guanylate cyclase in the photoreceptor-bipolar synapse. *EMBO J.* 21, 2547–2556. doi: 10.1093/emboj/21.11.2547

Duda, T., Krishnan, R., and Sharma, R. K. (2006). GCAP1 Antithetical calcium censor of ROS-GC transduction machinery. *Calcium Bind. Proteins* 1, 102–107.

Duda, T., Krishnan, A., Venkataraman, V., Lange, C., Koch, K. W., and Sharma, R. K. (1999a). Mutations in the rod outer segment membrane guanylate cyclase (ROS-GC1) in a cone-rod dystrophy, cause defects in calcium signaling. *Biochemistry* 38, 13912–13919. doi: 10.1021/bi9915972

Duda, T., Pertzev, A., Koch, K. W., and Sharma, R. K. (2012a). Antithetical modes of and the Ca2+ sensors targeting in ANF-RGC and ROS-GC1 membrane guanylate cyclases. *Front. Mol. Neurosci.* 5: 544. doi: 10.3389/fnmol.2012.00044

Duda, T., Pertzev, A., Makino, C. L., and Sharma, R. K. (2016). Bicarbonate and Ca2+ sensing modulators activate photoreceptor ROS-GC1 synergistically. *Front. Mol. Neurosci.* 9:5. doi: 10.3389/fnmol.2016.00005

Duda, T., Pertzev, A., and Sharma, R. K. (2011a). 657WTAPELL663 motif of the photoreceptor ROS-GC1: a general phototransduction switch. *Biochem. Biophys. Res.Commun.* 408, 236–241. doi: 10.1016/j.bbrc.2011.03.134

Duda, T., Pertzev, A., and Sharma, R. K. (2012b). Ca2+ modulation of ANF-RGC: new signaling paradigm interlocked with blood pressure regulation. *Biochemistry* 51, 9394–9405. doi: 10.1021/bi301176c

Duda, T., Pertzev, A., and Sharma, R. K. (2012c). Differential Ca2+ sensor guanylate cyclase activating protein modes of photoreceptor rod outer segment membrane guanylate cyclase signaling. *Biochemistry* 51, 4650–4657. doi: 10.1021/bi300572w

Duda, T., Pertzev, A., and Sharma, R. K. (2013). The ANF-RGC gene motif (669) WTAPELL(675) is vital for bloodpressure regulation: biochemical mechanism. *Biochemistry* 52, 2337–2347. doi: 10.1021/bi400175d

Duda, T., Pertzev, A., and Sharma, R. K. (2014). Atrial natriuretic factor receptor guanylate cyclase, ANF-RGC, transduces two independent signals, ANF and Ca^{2+}. *Front. Mol. Neurosci.* 7:17. doi: 10.3389/fnmol.2014.00017

Duda, T., and Sharma, R. K. (1995a). ATP bimodal switch that regulates the ligand binding and signal transduction activities of the atrial natriuretic factor receptor guanylate cyclase. *Biochem. Biophys. Res. Commun.* 209, 286–292. doi: 10.1006/bbrc.1995.1501

Duda, T., and Sharma, R. K. (1995b). ATP modulation of the ligand binding and signal transduction activities of the type C natriuretic peptide receptor guanylate cyclase. *Mol. Cell. Biochem.* 152, 179–183. doi: 10.1007/bf01076081

Duda, T., and Sharma, R. K. (2004). S100B-modulated Ca2+−dependent ROS-GC1 transduction machinery in the gustatory epithelium: a new mechanism in gustatory transduction. *FEBS Lett.* 577, 393–398. doi: 10.1016/j.febslet.2004.09.089

Duda, T., and Sharma, R. K. (2008). ONE-GC membrane guanylate cyclase, a trimodal odorant signal transducer. *Biochem. Biophys. Res. Commun.* 367, 440–445. doi: 10.1016/j.bbrc.2007.12.153

Duda, T., and Sharma, R. K. (2010). Distinct ONE-GC transduction modes and motifs of the odorants: uroguanylin and CO2. *Biochem. Biophys. Res. Commun.* 391, 1379–1384. doi: 10.1016/j.bbrc.2009.12.068

Duda, T., Sitaramayya, A., and Sharma, R. K. (1992). Identification of ATP regulatory module and catalytic domain of ANF-activated guanylate cyclase in retina. *Invest. Ophthalmol. Vis. Sci.* 33:1400 Abstract #1890.

Duda, T., Venkataraman, V., Goraczniak, R., Lange, C., Koch, K. W., and Sharma, R. K. (1999b). Functional consequences of a rod outer segment membrane guanylate cyclase (ROS-GC1) gene mutation linked with Leber's congenital amaurosis. *Biochemistry* 38, 509–515. doi: 10.1021/bi9824137

Duda, T., Venkataraman, V., Jankowska, A., Lange, C., Koch, K. W., and Sharma, R. K. (2000a). Impairment of the rod outer segment membrane guanylate cyclase dimerization defective calcium signaling. *Biochemistry* 39, 12522–12533. doi: 10.1021/bi001514d

Duda, T., Venkataraman, V., Krishnan, A., Nagele, R. G., and Sharma, R. K. (2001b). Negatively calcium-modulated membrane guanylate cyclase signaling system in the rat olfactory bulb. *Biochemistry* 40, 4654–4662. doi: 10.1021/bi0027985

Duda, T., Venkataraman, V., Ravichandran, S., and Sharma, R. K. (2005b). ATP-regulated module (ARM) of the atrial natriuretic factor receptor guanylate cyclase. *Peptides* 26, 969–984. doi: 10.1016/j.peptides.2004.08.032

Duda, T., Wen, X. H., Isayama, T., Sharma, R. K., and Makino, C. L. (2015). Bicarbonate modulates photoreceptor guanylate cyclase (ROS-GC) catalytic activity. *J. Biol. Chem.* 290, 11052–11060. doi: 10.1074/jbc.m115.650408

Duda, T., Yadav, P., Jankowska, A., Venkataraman, V., and Sharma, R. K. (2000b). Three dimensional atomic model and experimental validation for the ATP-regulated module (ARM) of the atrial natriuretic factor receptor guanylate cyclase. *Mol. Cell. Biochem.* 214, 7–14. doi: 10.1023/A:1007144328682

Duda, T., Yadav, P., Jankowska, A., Venkataraman, V., and Sharma, R. K. (2001c). Three dimensional atomic model and experimental validation for the ATP-regulated module (ARM) of the atrial natriuretic factor receptor guanylate cyclase. *Mol. Cell. Biochem.* 217, 165–172. doi: 10.1023/A:1007236917061

Duda, T., Yadav, P., and Sharma, R. K. (2011b). Allosteric modification, the primary ATP activation mechanism of atrial natriuretic factor receptor guanylate cyclase. *Biochemistry* 50, 1213–1225. doi: 10.1021/bi1018978

Feder, D., Im, M. J., Klein, H. W., Hekman, M., Holzhofer, A., Dees, C., et al. (1986). Reconstitution of beta 1-adrenoceptor-dependent adenylate cyclase from purified components. *EMBO J.* 5, 1509–1514. Erratum in: EMBO J. 5: 3408. doi: 10.1002/j.1460-2075.1986.tb04390.x

Fesenko, E. E., Kolesnikov, S. S., and Lyubarsky, A. L. (1985). Induction by cyclic GMP of cationic conductance in plasma membrane of retinal rod outer segment. *Nature* 313, 310–313. doi: 10.1038/313310a0

Fik-Rymarkiewicz, E., Duda, T., and Sharma, R. K. (2006). Novel frequenin-modulated Ca2+−signaling membrane guanylate cyclase (ROS-GC) transduction pathway in bovine hippocampus. *Mol. Cell. Biochem.* 291, 187–204. doi: 10.1007/s11010-006-9215-6

Fleischer, J., Mamasuew, K., and Breer, H. (2009). Expression of cGMP signaling elements in the Grueneberg ganglion. *Histochem. Cell Biol.* 131, 75–88. doi: 10.1007/s00418-008-0514-8

Frins, S., Bönigk, W., Müller, F., Kellner, R., and Koch, K. W. (1996). Functional characterization of a guanylyl cyclase-activating protein from vertebrate rods. Cloning, heterologous expression and localization. *J. Biol. Chem.* 271, 8022–8027. doi: 10.1074/jbc.271.14.8022

Fulle, H. J., Vassar, R., Foster, D. C., Yang, R. B., Axel, R., and Garbers, D. L. (1995). A receptor guanylyl cyclase expressed specifically in olfactory sensory neurons. *Proc. Natl. Acad. Sci. U. S. A.* 92, 3571–3575. doi: 10.1073/pnas.92.8.3571

Garbers, D. L. (1989). Molecular basis of signaling in the spermatozoon. *J. Androl.* 10, 99–107. doi: 10.1002/j.1939-4640.1989.tb00068.x

Gill, G. N., and McCune, R. W. (1979). Guanosine 3′,5′-monophosphate-dependent protein kinase. *Curr. Top. Cell. Regul.* 15, 1–45. doi: 10.1016/b978-0-12-152815-7.50005-3

Goldberg, N. D., Dietz, S. B., and O'Toole, A. G. (1969). Cyclic guanosine 3′,5′-monophosphate in mammalian tissues and urine. *J. Biol. Chem.* 244, 4458–4466. doi: 10.1016/S0021-9258(18)94340-1

Goldberg, N. D., and Haddox, M. K. (1977). Cyclic GMP metabolism and involvement in biological regulation. *Annu. Rev. Biochem.* 46, 823–896. doi: 10.1146/annurev.bi.46.070177.004135

Goldberg, N. D., O'Dea, R. F., and Haddox, M. K. (1973). Cyclic GMP. *Adv. Cyclic Nucleotide Res.* 3, 155–223. PMID: 4150323

Goraczniak, R. M., Duda, T., and Sharma, R. K. (1992). A structural motif that defines the ATP-regulatory module of guanylate cyclase in atrial natriuretic factor signalling. *Biochem. J.* 282, 533–537. doi: 10.1042/bj2820533

Goraczniak, R., Duda, T., and Sharma, R. K. (1997). Structural and functional characterization of a second subfamily member of the calcium-modulated bovine rod outer segment membrane guanylate cyclase, ROS-GC2. *Biochem. Biophys. Res. Commun.* 234, 666–670. doi: 10.1006/bbrc.1997.6579

Goraczniak, R. M., Duda, T., and Sharma, R. K. (1998). Calcium modulated signaling site in type 2 rod outer segment membrane guanylate cyclase (ROS-GC2). *Biochem. Biophys. Res. Commun.* 245, 447–453. doi: 10.1006/bbrc.1998

Goraczniak, R. M., Duda, T., Sitaramayya, A., and Sharma, R. K. (1994). Structural and functional characterization of the rod outer segment membrane guanylate cyclase. *Biochem. J.* 302, 455–461. doi: 10.1042/bj3020455

Gorczyca, W. A., Polans, A. S., Surgucheva, I., Subbaraya, I., Baehr, W., and Palczewski, K. (1995). Guanylyl cyclase activating protein: a calcium-sensitive regulator of phototransduction. *J. Biol. Chem.* 270, 22029–22036. doi: 10.1074/jbc.270.37.22029

Gorczyca, W. A., Van Hooser, J. P., and Palczewski, K. (1994). Nucleotide inhibitors and activators of retinal guanylyl cyclase. *Biochemistry* 33, 3217–3222. doi: 10.1021/bi00177a011

Guo, D., Zhang, J. J., and Huang, X. Y. (2009). Stimulation of guanylyl cyclase-D by bicarbonate. *Biochemistry* 48, 4417–4422. doi: 10.1021/bi900441v

Haeseleer, F., Sokal, I., Li, N., Pettenati, M., Rao, N., Bronson, D., et al. (1999). Molecular characterization of a third member of the guanylyl cyclase-activating protein subfamily. *J. Biol. Chem.* 274, 6526–6535. doi: 10.1074/jbc.274.10.6526

Haksar, A., and Péron, F. G. (1973). The role of calcium in the steroidogenic response of rat adrenal cells to adrenocorticotropic hormone. *Biochim. Biophys. Acta* 313, 363–371. doi: 10.1016/0304-4165(73)90036-6

Hamra, F. K., Forte, L. R., Eber, S. L., Pidhorodeckyj, N. V., Krause, W. J., Freeman, R. H., et al. (1993). Uroguanylin: structure and activity of a second endogenous peptide that stimulates intestinal guanylate cyclase. *Proc. Natl. Acad. Sci. U. S. A.* 90, 10464–10468. doi: 10.1073/pnas.90.22.10464

Harden, T. K. (1992). G-protein-regulated phospholipase C. Identification of component proteins. *Adv. Sec. Mess. Phosphoprot. Res.* 26, 11–34.

Hardman, J. G., Davis, J. W., and Sutherland, E. W. (1969). Effects of some hormonal and other factors on the excretion of guanosine 3′,5′-monophosphate and adenosine 3′,5′-monophosphate in rat urine. *J. Biol. Chem.* 244, 6354–6362. doi: 10.1016/S0021-9258(18)63472-6

Hardman, J. G., and Sutherland, E. W. (1969). Guanyl cyclase, an enzyme catalyzing the formation of guanosine 3′,5′-monophosphate from guanosine triphosphate. *J. Biol. Chem.* 244, 6363–6370. doi: 10.1016/S0021-9258(18)63473-8

Hayashi, F., and Yamazaki, A. (1991). Polymorphism in purified guanylate cyclase from vertebrate rod photoreceptors. *Proc. Natl. Acad. Sci. U. S. A.* 88, 4746–4750. doi: 10.1073/pnas.88.11.4746

He, X.-L., Chow, D.-C., Martick, M. M., and Garcia, K. C. (2001). Allosteric activation of a spring-loaded natriuretic peptide receptor dimer by hormone. *Science* 293, 1657–1662. doi: 10.1126/science.1062246

Hendricks, K. B., Wang, B. Q., Schnieders, E. A., and Thorner, J. (1999). Yeast homologue of neuronal frequenin is a regulator of phosphatidylinositol-4-OH kinase. *Nat. Cell Biol.* 1, 234–241. doi: 10.1038/12058

Hepler, J. R., and Gilman, A. G. (1992). G proteins. *Trends Biochem. Sci.* 17, 383–387. doi: 10.1016/0968-0004(92)90005-T

Herman, J. P., Dolgas, C. M., Rucker, D., and Langub, M. C. Jr. (1996). Localization of natriuretic peptide-activated guanylate cyclase mRNAs in the rat brain. *J. Comp. Neurol.* 369, 165–187. doi: 10.1002/(SICI)1096-9861(19960527)369:2<165::AID-CNE1>3.0.CO;2-1

Horio, Y., and Murad, F. (1991a). Purification of guanylyl cyclase from rod outer segments. *Biochim. Biopys. Acta* 1133, 81–88. doi: 10.1016/0167-4889(91)90244-R

Horio, Y., and Murad, F. (1991b). Solubilization of guanylyl cyclase from bovine rod outer segments and effects of lowering Ca2+ and nitro compounds. *J. Biol. Chem.* 266, 3411–3415. doi: 10.1016/S0021-9258(19)67809-9

Howes, K. A., Pennesi, M. E., Sokal, I., Church-Kopish, J., Schmidt, B., Margolis, D., et al. (2002). GCAP1 rescues rod photoreceptor response in GCAP1/GCAP2 knockout mice. *EMBO J.* 21, 1545–1554. doi: 10.1093/emboj/21.7.1545

Hu, J., Zhong, C., Ding, C., Chi, Q., Walz, A., Mombaerts, P., et al. (2007). Detection of near-atmospheric concentrations of CO2 by an olfactory subsystem in the mouse. *Science* 317, 953–957. doi: 10.1126/science.1144233

Hurley, J. B., Dizhoor, A. M., Ray, S., and Stryer, L. (1993). Recoverin's role: conclusion withdrawn. *Science* 260:740. doi: 10.1126/science.8097896

Ishikawa, E., Ishikawa, S., Davis, J. W., and Sutherland, E. W. (1969). Determination of guanosine 3′,5′-monophosphate in tissues and of guanyl cyclase in rat intestine. *J. Biol. Chem.* 244, 6371–6376. doi: 10.1016/S0021-9258(18)63474-X

Jaiswal, N., Paul, A. K., Jaiswal, R. K., and Sharma, R. K. (1986). Atrial natriuretic factor regulation of cyclic GMP levels and steroidogenesis in isolated fasciculata cells of rat adrenal cortex. *FEBS Lett.* 199, 121–124. doi: 10.1016/0014-5793(86)81236-4

Jaiswal, N., and Sharma, R. K. (1986). Dual regulation of adenylate cyclase and guanylate cyclase: α2-adrenergic signal transduction in adrenocortical carcinoma cells. *Arch. Biochem. Biophys.* 249, 616–619. doi: 10.1016/0003-9861(86)90041-X

Jaleel, M., Saha, S., Shenoy, A. R., and Visweswariah, S. S. (2006). The kinase homology domain of receptor guanylyl cyclase C: ATP binding and identification of an adenine nucleotide sensitive site. *Biochemistry* 45, 1888–1898. doi: 10.1021/bi052089x

Jankowska, A., Burczynska, B., Duda, T., Warchol, J. B., and Sharma, R. K. (2007). Calcium-modulated rod outer segment membrane guanylate cyclase type1 transduction machinery in the testes. *J. Androl.* 28, 50–58. doi: 10.2164/jandrol.106.000182

Jankowska, A., Sharma, R. K., and Duda, T. (2014). Ca2+−modulated ROS-GC1 transduction system in testes and its presence in the spermatogenic cells. *Front. Mol. Neurosci.* 7:34. doi: 10.3389/fnmol.2014.00034

Jankowska, A., and Warchol, J. B. (2010). Ca2+−modulated membrane guanylate cyclase in the testes. *Mol. Cell. Biochem.* 334, 169–179. doi: 10.1007/s11010-009-0329-5

Jeromin, A., Shayan, A. J., Msghina, M., Roder, J., and Atwood, H. L. (1999). Crustacean frequenins: molecular cloning and differential localization at neuromuscular junctions. *J. Neurobiol.* 41, 165–175. doi: 10.1002/(SICI)1097-4695(19991105)41:2<165::AID-NEU1>3.0.CO;2-9

Jewett, J. R., Koller, K. J., Goeddel, D. V., and Lowe, D. G. (1993). Hormonal induction of low affinity receptor guanylyl cyclase. *EMBO J.* 12, 769–777. doi: 10.1002/j.1460-2075.1993.tb05711.x

Juilfs, D. M., Fulle, H. J., Zhao, A. Z., Houslay, M. D., Garbers, D. L., and Beavo, J. A. (1997). A subset of olfactory neurons that selectively express cGMP-stimulated phosphodiesterase (PDE2) and guanylyl cyclase-D define a unique olfactory signal transduction pathway. *Proc. Natl. Acad. Sci. U. S. A.* 94, 3388–3395. doi: 10.1073/pnas.94.7.3388

Kachi, S., Nishizawa, Y., Olshevskaya, E., Yamazaki, A., Miyake, Y., Wakabayashi, T., et al. (1999). Detailed localization of photoreceptor guanylate cyclase activating protein-1 and-2 in mammalian retinas using light and electronmicroscopy. *Exp. Eye Res.* 68, 465–473. doi: 10.1006/exer.1998.0629

Katsuki, S., Arnold, W., Mittal, C., and Murad, F. (1977). Stimulation of guanylate cyclase by sodium nitroprusside, nitroglycerin and nitric oxide in various tissue preparations and comparison to the effects of sodium azide and hydroxylamine. *J. Cyclic Nucleotide Res.* 3, 23–35. PMID: 14978

Kawamura, S. (1993). Rhodopsin phosphorylation as a mechanism of cyclic GMP phosphodiesterase regulation by S-modulin. *Nature* 362, 855–857. doi: 10.1038/362855a0

Khare, S., Wilson, D., Wali, R. K., Tien, X. Y., Bissonnette, M., Niedziela, S. M., et al. (1994). Guanylin activates rat colonic particulate guanylate cyclase. *Biochem. Biophys. Res. Commun.* 203, 1432–1437. doi: 10.1006/bbrc.1994.2345

Kitabchi, A. E., Wilson, D. B., and Sharma, R. K. (1971). Steroidogenesis in isolated adrenal cells of rat. II. Effect of caffeine on ACTH and cyclic nucleotide-induced Steroidogenesis and its relation to cyclic nucleotide Phosphodiesterase (PDE). *Biochem. Biophys. Res. Commun.* 44, 898–904. doi: 10.1016/0006-291x(71)90796-0

Klenchin, V. A., Calvert, P. D., and Bownds, M. D. (1995). Inhibition of rhodopsin kinase by recoverin. Further evidence for a negative feedback system in phototransduction. *J. Biol. Chem.* 270, 16147–16152. doi: 10.1074/jbc.270.27.16147

Koch, K. W. (1991). Purification and identification of photoreceptor guanylate cyclase. *J. Biol. Chem.* 266, 8634–8637. doi: 10.1016/S0021-9258(18)93021-8

Koch, K. W. (2006). GCAPs, the classical neuronal calcium sensors in the retina–a Ca2+−relay model of guanylate cyclase activation. *Calcium Binding Proteins* 1, 3–6.

Koch, K. W., and Dell'Orco, D. (2013). A calcium-relay mechanism in vertebrate phototransduction. *ACS Chem. Neurosci.* 4, 909–917. doi: 10.1021/cn400027z

Koch, K. W., and Dell'Orco, D. (2015). Protein and signaling networks in vertebrate photoreceptor cells. *Front. Mol. Neurosci.* 8:67. doi: 10.3389/fnmol.2015.00067

Koch, K. W., Duda, T., and Sharma, R. K. (2002). Photoreceptor specific guanylate cyclases in vertebrate phototransduction. *Mol. Cell. Biochem.* 230, 97–106. doi: 10.1023/A:1014209711793

Koch, K. W., Duda, T., and Sharma, R. K. (2010). Ca2+−modulated vision-linked ROS-GC guanylate cyclase transduction machinery. *Mol. Cell. Biochem.* 334, 105–115. doi: 10.1007/s11010-009-0330-z

Koch, K. W., and Stryer, L. (1988). Highly cooperative feedback control of retinal rod guanylate cyclase by calcium ions. *Nature* 334, 64–66. doi: 10.1038/334064a0

Kojima, M., Minamino, N., Kangawa, K., and Matsuo, H. (1990). Cloning and sequence analysis of a cDNA encoding a precursor for rat C-type natriuretic peptide (CNP). *FEBS Lett.* 276, 209–213. doi: 10.1016/0014-5793(90)80544-s

Koller, K. J., deSauvage, F. J., Lowe, D. G., and Goeddel, D. V. (1992). Conservation of the kinase like regulatory domain is essential for activation of the natriuretic peptide receptor guanylyl cyclases. *Mol. Cell. Biol.* 12, 2581–2590. doi: 10.1128/mcb.12.6.2581

Krishnan, A., Duda, T., Pertzev, A., Kobayashi, M., Takamatsu, K., and Sharma, R. K. (2009). Hippocalcin, new Ca2+ sensor of a ROS-GC subfamily member, ONE-GC, membrane guanylate cyclase transduction system. *Mol. Cell. Biochem.* 325, 1–14. doi: 10.1007/s11010-008-0015-z

Krishnan, A., Goraczniak, R. M., Duda, T., and Sharma, R. K. (1998). Third calcium-modulated rod outer segment membrane guanylate cyclase transduction mechanism. *Mol. Cell. Biochem.* 178, 251–259. doi: 10.1023/A:1006860018300

Krishnan, A., Venkataraman, V., Fik-Rymarkiewicz, E., Duda, T., and Sharma, R. K. (2004). Structural, biochemical and functional characterization of the calcium sensor neurocalcin delta in the innerretinal neurons and its linkage with the rod outers segment membrane guanylate cyclase transduction system. *Biochemistry* 43, 2708–2723. doi: 10.1021/bi035631v

Kudo, T., and Baird, A. (1984). Inhibition of aldosterone production in the adrenal glomerulosa by atrial natriuretic factor. *Nature* 312, 756–757. doi: 10.1038/312756a0

Kumar, V. D., Vijay-Kumar, S., Krishnan, A., Duda, T., and Sharma, R. K. (1999). A second calcium regulator of rod outer segment membrane guanylate cyclase, ROS-GC1: neurocalcin. *Biochemistry* 38, 12614–12620. doi: 10.1021/bi990851n

Kuno, T., Andresen, J. W., Kamisaki, Y., Waldman, S. A., Chang, L. Y., Saheki, S., et al. (1986). Co-purification of an atrial natriuretic factor receptor and particulate guanylate cyclase from rat lung. *J. Biol. Chem.* 261, 5817–5823. doi: 10.1016/S0021-9258(17)38456-9

Kutty, R. K., Fletcher, R. T., Chader, G. J., and Krishna, G. (1992). Expression of guanylate cyclase-A mRNA in the rat retina: detection using polymerase chain reaction. *Biochem. Biophys. Res. Commun.* 182, 851–857. doi: 10.1016/0006-291x(92)91810-d

Ladant, D. (1995). Calcium and membrane binding properties of bovine neurocalcin delta expressed in Escherichia coli. *J. Biol. Chem.* 270, 3179–3185. doi: 10.1016/S0021-9258(18)82908-8

Lai, P. C., Singer, M. S., and Crasto, C. J. (2005). Structural activation pathways from dynamic olfactory receptor-odorant interactions. *Chem. Senses* 30, 781–792. doi: 10.1093/chemse/bji070

Lange, C., Duda, T., Beyermann, M., Sharma, R. K., and Koch, K. W. (1999). Regions in vertebrate photoreceptor guanylyl cyclase ROS-GC1 involved in Ca2+−dependent regulation by guanylyl cyclase-activating protein GCAP-1. *FEBS Lett.* 460, 27–31. doi: 10.1016/s0014-5793(99)01312-5

Langub, M. C. Jr., Watson, R. E. Jr., and Herman, J. P. (1995). Distribution of natriuretic peptide precursor mRNAs in the rat brain. *J. Comp. Neurol.* 356, 183–199. doi: 10.1002/cne.903560205

Larose, L., McNicoll, N., Ong, H., and DeLéan, A. (1991). Allosteric modulation by ATP of the bovine adrenal natriureticfactor R1 receptor functions. *Biochemistry* 30, 8990–8995. doi: 10.1021/bi00101a012

Leinders-Zufall, T., Cockerham, R. E., Michalakis, S., Biel, M., Garbers, D. L., Reed, R. R., et al. (2007). Contribution of the receptor guanylyl cyclase GC-D to chemosensory function in the olfactory epithelium. *Proc. Natl. Acad. Sci. U. S. A.* 104, 14507–14512. doi: 10.1073/pnas.0704965104

Lim, S., Strahl, T., Thorner, J., and Ames, J. B. (2011). Structure of a Ca2+−myristoyl switch protein that controls activation of a phosphatidylinositol 4-kinase infissionyeast. *J. Biol. Chem.* 286, 12565–12577. doi: 10.1074/jbc.M110.208868

Liu, X., Seno, K., Nishizawa, Y., Hayashi, F., Yamazaki, A., Matsumoto, H., et al. (1994). Ultrastructural localization of retinal guanylate cyclase in human and monkey retinas. *Exp. Eye Res.* 59, 761–768. doi: 10.1006/exer.1994.1162

Lowe, D. G., Chang, M. S., Hellmiss, R., Chen, E., Singh, S., Garbers, D. L., et al. (1989). Human atrial natriuretic peptide receptor defines a new paradigm for second messenger signal transduction. *EMBO J.* 8, 1377–1384. doi: 10.1002/j.1460-2075.1989.tb03518.x

Lowe, D. G., Dizhoor, A. M., Liu, K., Gu, Q., Spencer, M., Laura, R., et al. (1995). Cloning and expression of a second photoreceptor-specific membrane retina guanylyl cyclase (RetGC), RetGC-2. *Proc. Natl. Acad. Sci. U. S. A.* 92, 5535–5539. doi: 10.1073/pnas.92.12.5535

Luo, D. G., Xue, T., and Yau, K. W. (2008). How vision begins: an odyssey. *Proc. Natl. Acad. Sci. U. S. A.* 105, 9855–9862. doi: 10.1073/pnas.0708405105

Makino, C. L., Duda, T., Pertzev, A., Isayama, T., Geva, P., Sandberg, M. A., et al. (2019). Modes of accessing bicarbonate for the regulation of membrane guanylate cyclase (ROS-GC) in retinal rods and cones. *eNeuro* 6:1. doi: 10.1523/ENEURO.0393-18.2019

Makino, C. L., Peshenko, I. V., Wen, X. H., Olshevskaya, E. V., Barrett, R., and Dizhoor, A. M. (2008). A role for GCAP2 in regulating the photoresponse. Guanylyl cyclase activation and rod electrophysiology in GUCA1B knock-out mice. *J. Biol. Chem.* 283, 29135–29143. doi: 10.1074/jbc.M804445200

Makino, C. L., Wen, X. H., Olshevskaya, E. V., Peshenko, I. V., Savchenko, A. B., and Dizhoor, A. M. (2012). Enzymatic relay mechanism stimulates cyclic GMP synthesis in rod photoresponse: biochemical and physiological study in guanylyl cyclase activating protein1 knock out mice. *PLoS One* 7:e47637. doi: 10.1371/journal.pone.0047637

Marala, R., Duda, T., Goraczniak, R. M., and Sharma, R. K. (1992). Genetically tailored atrial natriuretic factor-dependent guanylate cyclase. Immunological and functional identity with180kDa membrane guanylate cyclase and ATP signaling site. *FEBS Lett.* 296, 254–258. doi: 10.1016/0014-5793(92)80298-u

Marala, R. B., and Sharma, R. K. (1988). Characterization of atrial-natriuretic-factor-receptor-coupled membrane guanylate cyclase from rat and mouse testes. *Biochem. J.* 251, 301–304. doi: 10.1042/bj2510301

Marala, R. B., Sitaramayya, A., and Sharma, R. K. (1991). Dual regulation of atrial natriuretic factor-dependent guanylate cyclase activity by ATP. *FEBS Lett.* 281, 73–76. doi: 10.1016/0014-5793(91)80361-6

Margulis, A., Goraczniak, R. M., Duda, T., Sharma, R. K., and Sitaramayya, A. (1993). Structural and biochemical identity of retinal rod outer segment membrane guanylate cyclase. *Biochem. Biophys. Res. Commun.* 194, 855–861. doi: 10.1006/bbrc.1993.1900

Margulis, A., Pozdnyakov, N., and Sitaramayya, A. (1996). Activation of bovine photoreceptor guanylate cyclase by S100 proteins. *Biochem. Biophys. Res. Commun.* 218, 243–247. doi: 10.1006/bbrc.1996.0043

McFerran, B. W., Weiss, J. L., and Burgoyne, R. D. (1999). Neuronal Ca2+ sensor 1. Characterization of the myristoylated protein, its cellular effects in permeabilized adrenal chromaffin cells, Ca2+−independent membrane association and interaction with binding proteins, suggesting a role in rapid Ca2+ signal transduction. *J. Biol. Chem.* 274, 30258–30265. doi: 10.1074/jbc274.42.30258

Meloche, S., McNicoll, N., Liu, B., Ong, H., and De Lean, A. (1988). Atrial natriuretic factor R1 receptor from bovine adrenal zona glomerulosa: purification, characterization, and modulation by amiloride. *Biochemistry* 27, 8151–8158. doi: 10.1021/bi00421a025

Mendez, A., Burns, M. E., Sokal, I., Dizhoor, A. M., Baehr, W., Palczewski, K., et al. (2001). Role of guanylate cyclase-activating proteins (GCAPs) in setting the flash sensitivity of rod photoreceptors. *Proc. Natl. Acad. Sci. U. S. A.* 98, 9948–9953. doi: 10.1073/pnas.171308998

Meyer, M. R., Angele, A., Kremmer, E., Kaupp, U. B., and Muller, F. (2000). A cGMP-signaling pathway in a subset of olfactory sensory neurons. *Proc. Natl. Acad. Sci. U. S. A.* 97, 10595–10600. doi: 10.1073/pnas.97.19.10595

Middendorff, R., Davidoff, M. S., Behrends, S., Mewe, M., Miethens, A., and Müller, D. (2000). Multiple roles of the messenger molecule cGMP in testicular function. *Andrologia* 32, 55–59. PMID: 10702869

Middendorff, R., Maronde, E., Paust, H. J., Müller, D., Davidoff, M., and Olcese, J. (1996). Expression of C-type natriuretic peptide in the bovine pineal gland. *J. Neurochem.* 67, 517–524. doi: 10.1046/j.1471-4159.1996.67020517.x

Middendorff, R., Müller, D., Wichers, S., Holstein, A. F., and Davidoff, M. S. (1997). Evidence for production and functional activity of nitric oxide in seminiferous tubules and blood vessels of the human testis. *J. Clin. Endocrinol. Metab.* 82, 4154–4161. doi: 10.1210/jc.82.12.4154

Mittal, C. K., and Murad, F. (1977a). Properties and oxidative regulation of guanylate cyclase. *J. Cyclic Nucleotide Res.* 3, 381–391. PMID: 40407

Mittal, C. K., and Murad, F. (1977b). Activation of guanylate cyclase by superoxide dismutase and hydroxyl radical: A physiological regulator of guanosine 3′,5′-monophosphate formation. *Proc. Natl. Acad. Sci. U. S. A.* 74, 4360–4364. doi: 10.1073/pnas.74.10.4360

Mourdjeva, M., Russinova, A., Kyurkchiev, S., and Kehayov, I. (2001). Spatial and temporal distribution of atrial natriuretic factor in the rat testis. *Biol. Cell.* 93, 301–307. doi: 10.1016/s0248-4900(01)01119-4

Murad, F., Arnold, W. P., Mittal, C. K., and Braughler, J. M. (1979). Properties and regulation of guanylate cyclase and some proposed functions for cyclic GMP. *Adv. Cyclic Nucleotide Res.* 11, 175–204. PMID: 40407

Murad, F., Mittal, C., Arnold, W. P., Ichikara, K., Braughler, M., and El-Zayat, M. (1978a). "Properties and regulation of guanylate cyclase: activation by azide, nitro compounds, and hydroxyl radical and effects of heme containing proteins," in *Molecular Biology and Pharmacology of Cyclic Nucleotides*. eds. G. Folco and R. Paolottie (Netherlands: Elsevier), 33–42.

Murad, F., Mittal, C. K., Arnold, W. P., Katsuki, S., and Kimura, H. (1978b). Guanylate cyclase: activation by azide, nitro compounds, nitric oxide, and hydroxyl radical and inhibition by hemoglobin and myoglobin. *Adv. Cyclic Nucleotide Res.* 9, 145–158. PMID: 27076

Nakano, A., Terasawa, M., Watanabe, M., Okazaki, K., Inoue, S., Kato, M., et al. (1993). Distinct regional localization of neurocalcin, a Ca2+−binding protein, in the bovine adrenal gland. *J. Endocrinol.* 138, 283–2NP. doi: 10.1677/joe.0.1380283

Nambi, P., Aiyar, N. V., and Sharma, R. K. (1982). Adrenocorticotropin-dependent particulate guanylate cyclase in rat adrenal and adrenocortical carcinoma:comparison of its properties with soluble guanylate cyclase and its relationship with AC TH-induced steroidogenesis. *Arch. Biochem. Biophys.* 217, 638–646. doi: 10.1016/0003-9861(82)90545-8

Needleman, P., Blaine, E. H., Greenwald, J. E., Michener, M. L., Saper, C. B., Stockmann, P. T., et al. (1989). The biochemical pharmacology of atrial peptides. *Annu. Rev. Pharmacol. Toxicol.* 29, 23–54. doi: 10.1146/annurev.pa.29.040189.000323

Nef, S., Fiumelli, H., de Castro, E., Raes, M. B., and Nef, P. (1995). Identification of neuronal calcium sensor (NCS-1) possibly involved in the regulation of receptor phosphorylation. *J. Recept. Signal Transduct. Res.* 15, 365–378. doi: 10.3109/10799899509045227

Negishi, M., Ito, S., Yokohama, H., Hayashi, H., Katada, T., Ui, M., et al. (1988). Functional reconstitution of prostaglandin E receptor from bovine adrenal medulla with guanine nucleotide binding proteins. *J. Biol. Chem.* 263, 6893–6900. doi: 10.1016/S0021-9258(18)68728-9

Nishizuka, Y. (1988). The molecular heterogeneity of protein kinase C and its implications for cellular regulation. *Nature* 334, 661–665. doi: 10.1038/334661a0

Ogawa, H., Qiu, Y., Huang, L., Tam-Chang, S. W., Young, H. S., and Misono, K. S. (2009). Structure of the atrial natriuretic peptide receptor extracellular domain in the unbound and hormone-bound states by single-particle electron microscopy. *FEBS J.* 276, 1347–1355. doi: 10.1111/j.1742-4658.2009.06870.x

Ogawa, H., Qiu, Y., Ogata, C. M., and Misono, K. S. (2004). Crystal structure of hormone-bound atrial natriuretic peptide receptor extracellular domain: rotation mechanism for transmembrane signal transduction. *J. Biol. Chem.* 279, 28625–28631. doi: 10.1074/jbc.m313222200

Okazaki, K., Watanabe, M., Ando, Y., Hagiwara, M., Terasawa, M., and Hidaka, H. (1992). Full sequence of neurocalcin, a novel calcium-binding protein abundant in central nervous system. *Biochem. Biophys. Res. Commun.* 185, 147–153. doi: 10.1016/s0006-291x(05)80968-4

Olafsson, P., Soares, H. D., Herzog, K. H., Wang, T., Morgan, J. I., and Lu, B. (1997). TheCa2+ binding protein, frequenin is a nervous system-specific protein in mouse preferentially localized in neurites. *Brain Res. Mol. Brain Res.* 44, 73–82. doi: 10.1016/s0169-328x(96)00188-x

Olafsson, P., Wang, T., and Lu, B. (1995). Molecular cloning and functional characterization of the Xenopus Ca2+−binding protein frequenin. *Proc. Natl. Acad. Sci. U. S. A.* 92, 8001–8005. doi: 10.1073/pnas.92.17.8001

Olcese, J., Müller, D., Münker, M., and Schmidt, C. (1994). Natriuretic peptides elevate cyclic 3′,5′-guanosine monophosphate levels in cultured rat pinealocytes: evidence for guanylate cyclase-linked membrane receptors. *Mol. Cell. Endocrinol.* 103, 95–100. doi: 10.1016/0303-7207(94)90074-4

Palczewski, K., Subbaraya, I., Gorczyca, W. A., Helekar, B. S., Ruiz, C. C., Ohguro, H., et al. (1994). Molecular cloning and characterization of retinal photoreceptor guanylyl cyclase-activating protein. *Neuron* 13, 395–404. doi: 10.1016/0896-6273(94)90355-7

Pandey, K. N., Oliver, P. M., Maeda, N., and Smithies, O. (1999). Hypertension associated with decreased testosterone levels in natriuretic peptidereceptor-A gene-knockout and gene-duplicated mutant mouse models. *Endocrinology* 140, 5112–5119. doi: 10.1210/en.140.11.5112

Pandey, K. N., and Singh, S. (1990). Molecular cloning and expression of murine guanylate cyclase/atrial natriuretic factor receptor cDNA. *J. Biol. Chem.* 265, 12342–12348. doi: 10.1016/S0021-9258(19)38352-8

Parat, M., Blanchet, J., and DeLéan, A. (2010). Role of juxta membrane and transmembrane domains in the mechanism of natriuretic peptide receptor A activation. *Biochemistry* 49, 4601–4610. doi: 10.1021/bi901711w

Paul, A. K. (1986). *Particulate Guanylate Cyclase from Adrenocortical Carcinoma 494. Purification, Biochemical and Immunological Characterization. Doctoral thesis* University of Tennessee.

Paul, A. K., Marala, R. B., Jaiswal, R. K., and Sharma, R. K. (1987). Coexistence of guanylate cyclase and atrial natriuretic factor receptor in a 180-kD protein. *Science* 235, 1224–1226. doi: 10.1126/science.2881352

Paul, A. K., and Sharma, R. K. (1985). "Purification and characterization of rat adrenocortical particulate guanylate cyclase," Abstract #744 67th Annual Meeting of Endocrinology, Baltimore, MD.

Perchellet, J.-P., and Sharma, R. K. (1979). Mediatory role of calcium and guanosine 3′,5′-monophosphate in adrenocorticotropin-induced steroidogenesis by adrenal cells. *Science* 203, 1259–1261. doi: 10.1126/science.34216

Perchellet, J.-P., and Sharma, R. K. (1980). Ectopic α-adrenergic accumulation of guanosine 3′:5′-monophosphate in isolated adrenocortical carcinoma cells. *Endocrinology* 106, 1589–1593. doi: 10.1210/endo-106-5-1589

Perrault, I., Rozet, J. M., Calvas, P., Gerber, S., Camuzat, A., Dollfus, H., et al. (1996). Retinal-specific guanylate cyclase gene mutations in Leber's congenital amaurosis. *Nat. Genet.* 14, 461–464. doi: 10.1038/ng1296-461

Perrault, I., Rozet, J. M., Gerber, S., Ghazi, I., Leowski, C., Ducroq, D., et al. (1999). Leber congenital amaurosis. *Mol. Genet. Metab.* 68, 200–208. doi: 10.1006/mgme.1999.2906

Pertzev, A., Duda, T., and Sharma, R. K. (2010). Ca2+ sensor GCAP1: a constitutive element of the ONE-GC-modulated odorant signal transduction pathway. *Biochemistry* 49, 7303–7313. doi: 10.1021/bi101001v

Peshenko, I. V., Olshevskaya, E. V., and Dizhoor, A. M. (2015a). Evaluating the role of retinal membrane guanylyl cyclase 1 (RetGC1) domains in binding guanylyl cyclase-activating proteins (GCAPs). *J. Biol. Chem.* 290, 6913–6924. doi: 10.1074/jbc.M114.629642

Peshenko, I. V., Olshevskaya, E. V., and Dizhoor, A. M. (2015b). Dimerization domain of retinal membrane Guanylyl Cyclase 1 (RetGC1) is an essential part of Guanylyl Cyclase-activating protein (GCAP) binding Interface. *J. Biol. Chem.* 290, 19584–19596. doi: 10.1074/jbc.M115.661371

Pongs, O., Lindemeier, J., Zhu, X. R., Theil, T., Engelkamp, D., Krah-Jentgens, I., et al. (1993). Frequenin–a novel calcium-binding protein that modulates synaptic efficacy in the drosophila nervous system. *Neuron* 11, 15–28. doi: 10.1016/0896-6273(93)90267-u

Potter, L. R., and Garbers, D. L. (1992). Dephosphorylation of the guanylyl cyclase-A receptor causes desensitization. *J. Biol. Chem.* 267, 14531–14534. doi: 10.1016/S0021-9258(18)42069-8

Potter, L. R., and Hunter, T. (1998). Identification and characterization of the major phosphorylation sites of the B-type natriuretic peptide receptor. *J. Biol. Chem.* 273, 15533–15539. doi: 10.1074/jbc.273.25.15533

Pozdnyakov, N., Goraczniak, R., Margulis, A., Duda, T., Sharma, R. K., Yoshida, A., et al. (1997). Structural and functional characterization of retinal calcium-dependent guanylate cyclase activator protein (CD-GCAP): identity with S100b protein. *Biochemistry* 36, 14159–14166. doi: 10.1021/bi971792l

Pozdnyakov, N., Yoshida, A., Cooper, N. G., Margulis, A., Duda, T., Sharma, R. K., et al. (1995). A novel calcium-dependent activator of retinal rod outer segment membrane guanylate cyclase. *Biochemistry* 34, 14279–14283. doi: 10.1021/bi00044a002

Pugh, E. N. Jr., and Cobbs, W. H. (1986). Visual transduction in vertebrate rods and cones: a tale of two transmitters, calcium and cyclic GMP. *Vis. Res.* 26, 1613–1643. doi: 10.1016/0042-6989(86)90051-9

Pugh, E. N. Jr., Duda, T., Sitaramayya, A., and Sharma, R. K. (1997). Photoreceptor guanylate cyclases: a review. *Biosci. Rep.* 17, 429–473. doi: 10.1023/A:1027365520442

Pugh, E. N., Nikonov, S., and Lamb, T. D. (1999). Molecular mechanisms of vertebrate photoreceptor light adaptation. *Curr. Opin. Neurobiol.* 9, 410–418. doi: 10.1016/S0959-4388(99)80062-2

Ramamurthy, V., Tucker, C., Wilkie, S. E., Daggett, V., Hunt, D. M., and Hurley, J. B. (2001). Interactions within the coiled-coil domain of RetGC-1 guanylyl cyclase are optimized for regulation rather than for high affinity. *J. Biol. Chem.* 276, 26218–26229. doi: 10.1074/jbc.M010495200

Rambotti, M. G., Giambanco, I., Spreca, A., and Donato, R. (1999). S100B and S100A1 proteins in bovine retina: their calcium-dependent stimulation of a membrane-bound guanylate cyclase activity as investigated by ultracytochemistry. *Neuroscience* 92, 1089–1101. doi: 10.1016/s0306-4522(99)00074-3

Rehkamp, A., Tänzler, D., Claudio Iacobucci, C., Golbik, R. P., Ihling, C. H., and Sinz, A. (2018). Molecular details of retinal guanylyl cyclase 1/GCAP-2 interaction. *Front. Mol. Neurosci.* 11:330. doi: 10.3389/fnmol.2018.00330

Robison, G. A., Butcher, R. W., and Sutherland, E. W. (1967). Adenyl cyclase as an adrenergic receptor. *Review Ann. N. Y. Acad. Sci.* 139, 703–723. doi: 10.1111/j.1749-6632.1967.tb41239.x

Rondeau, J. J., McNicoll, N., Gagnon, J., Bouchard, N., Ong, H., and De Lean, A. (1995). Stoichiometry of the atrial natriuretic factor-R1 receptor complex in the bovine zona glomerulosa. *Biochemistry* 34, 2130–2136. doi: 10.1021/bi00007a005

Rosenzweig, A. C., and Seidman, E. (1991). Atrial natriuretic factor and related peptide hormones. *Annu. Rev. Biochem.* 60, 229–255. doi: 10.1146/annurev.bi.60.070191.001305

Rozet, J. M., Perrault, I., Gerber, S., Hanein, S., Barbet, F., Ducroq, D., et al. (2001). Complete abolition of the retinal-specific guanylylcyclase (retGC-1) catalytic ability consistently leads to leber congenital amaurosis (LCA). *Invest. Ophthalmol. Vis. Sci.* 42, 1190–1192. PMID: 11328726

Sayers, G., Bealland, R. J., and Seelig, S. (1972). Isolated adrenal cells: adrenocorticotropic hormone, calcium, steroidogenesis, and cyclic adenosine monophosphate. *Science* 175, 1131–1133. doi: 10.1126/science.175.4026.1131

Schulz, S., Green, C. K., Yuen, P. S., and Garbers, D. L. (1990). Guanylyl cyclase is a heat-stable enterotoxin receptor. *Cells* 63, 941–948. doi: 10.1016/0092-8674(90)90497-3

Schulz, S., Singh, R., Bellet, A., Singh, G., Tubb, D. J., Chin, H., et al. (1989). The primary structure of a plasma membrane guanylate cyclase demonstrates diversity within this new receptor family. *Cells* 58, 1155–1162. doi: 10.1016/0092-8674(89)90513-8

Schulz, S., Wedel, B. J., Matthews, A., and Garbers, D. L. (1998). The cloning and expression of a new guanylyl cyclase orphan receptor. *J. Biol. Chem.* 273, 1032–1037. doi: 10.1074/jbc.273.2.1032

Schwartz, D., Geller, D. M., Manning, P. T., Siegel, N. R., Fok, K. F., Smith, C., et al. (1985). Ser-Leu-Arg-Arg-atriopeptin III: the major circulating form of atrial peptide. *Science* 229, 397–400. doi: 10.1126/science.3160114

Shahu, M. K., Schuhmann, F., Scholten, A., Solov'yov, I. A., and Koch, K. W. (2022). The transition of photoreceptor Guanylate Cyclase type 1 to the active state. *Int. J. Mol. Sci.* 23:4030. doi: 10.3390/ijms23074030

Shanker, G., and Sharma, R. K. (1980). Characterization of ectopic α-adrenergic binding receptors of adrenocortical carcinoma cells. *Endocrinology* 106, 1594–1598. doi: 10.1210/endo-106-5-1594

Sharma, R. K. (1972). Studies on adrenocortical carcinoma of rat cyclic nucleotide phosphodiesterase activities. *Cancer Res.* 32, 1734–1736. PMID: 4339750

Sharma, R. K. (1973). Regulation of steroidogenesis by adrenocorticotropic hormone in isolated adrenal cells of rat. *J. Biol. Chem.* 248, 5473–5476. doi: 10.1016/S0021-9258(19)43627-2

Sharma, R. K. (1974). Metabolic regulation of steroidogenesis in isolated adrenal and adrenocortical carcinoma cells of rat. Effect of adrenocorticotropic hormone and adenosine cyclic 3′,5′-monophosphate on the plasma membrane. *FEBS Lett.* 38, 197–201. doi: 10.1016/s0006-291x(74)80342-6

Sharma, R. K. (1978). "Abnormal Adrenocorticotropic hormone control in adrenocortical carcinoma," in *Endocrine control in Neoplasia*. eds. R. K. Sharma and W. E. Criss (New York: Raven Press), 13–52.

Sharma, R. K. (1985). "Biochemical control in adrenocortical carcinoma," in *Hormonally Responsive Tumors*. ed. V. P. Hollander (New York: Academic Press), 185–217.

Sharma, R. K. (1988). Guanylate cyclase and the adrenal natriuretic factor receptor. *Science* 240, 805–806. doi: 10.1126/science.240.4853.805-b

Sharma, R. K. (2002). Evolution of the membrane guanylate cyclase transduction system. *Mol. Cell. Biochem.* 230, 3–30. doi: 10.1023/A:1014280410459

Sharma, R. K. (2010). Membrane guanylate cyclase is a beautiful signal transduction machine: overview. *Mol. Cell. Biochem.* 334, 3–36. doi: 10.1007/s11010-009-0336-6

Sharma, R. K. (2022). ACTH-modulated membrane guanylate cyclase signaling system: origin and creation. *Front. Mol. Neurosci.* 15:929396. doi: 10.3389/fnmol.2022.929396

Sharma, R. K., Ahmed, N. K., and Shanker, G. (1976). Metabolic regulation of steroidogenesis in isolated adrenal cells of rat. Relationship of adrenocorticotropin-, adenosine 3′:5′-monophosphate-and guanosine 3′:5′-monophosphate-stimulated steroidogenesis with the activation of protein kinase. *Europ. J. Biochem.* 70, 427–433. doi: 10.1111/j.1432-1033.1976.tb11033.x

Sharma, R. K., Baehr, W., Makino, C. L., and Duda, T. (2015). Ca2+ and Ca2+-interlocked membrane guanylate cyclase modulation of neuronal and cardiovascular signal transduction.. *Front. Mol. Neurosci.* 8.

Sharma, R. K., and Brush, J. S. (1974). Metabolic regulation of steroidogenesis in adrenocortical carcinoma cells of rat. Effect of adrenocorticotropin and adenosine cyclic 3′,5′-monophosphate on the incorporation of (20S)-20-hydroxy [7a-3H] cholesterol into deoxycorticosterone and corticosterone. *Biochem. Biophys. Res. Commun.* 56, 256–263. doi: 10.1016/s0006-291x(74)80342-6

Sharma, R. K., and Duda, T. (2010). Odorant-linked ROS-GC subfamily membrane guanylate cyclase transduction system. *Mol. Cell. Biochem.* 334, 181–189. doi: 10.1007/s11010-009-0333-9

Sharma, R. K., and Duda, T. (2012). Ca^{2+} sensors and ROS-GC: interlocked sensory transduction elements: a review. *Front. Mol. Neurosci.* 5:42. doi: 10.3389/fnmol.2012.00042

Sharma, R. K., and Duda, T. (2014a). Membrane guanylate cyclase, a multimodal transduction machine: history, present and future directions. *Front. Mol. Neurosci.* 7:56. doi: 10.3389/fnmol.2014.00056

Sharma, R. K., and Duda, T. (2014b). "Atrial natriuretic factor receptor guanylate cyclase. The journey," in *Natriuretic Peptides. Physiology, Molecular Biology and Clinical Applications*. ed. K. N. Pandey (New York, NY: NovaScience Publishers), 109–118.

Sharma, R. K., Duda, T., Goraczniak, R., and Sitaramayya, A. (1997). Membrane Guanylate Cyclase signal transduction system. *Indian J. Biochem. Biophys.* 34, 40–49. PMID: 9343927

Sharma, R. K., Duda, T., and Makino, C. L. (2016). Integrative signaling networks of membrane guanylate cyclases: biochemistry and physiology. *Front. Mol. Neurosci.* 9:83. doi: 10.3389/fnmol.2016.00083

Sharma, R. K., Duda, T., Venkataraman, V., and Koch, K.-W. (2004). Calcium-modulated mammalian membrane guanylate cyclase ROS-GC transduction machinery in sensory neurons: a universal concept. *Res. Trends Curr. Topics Biochem. Res.* 334, 3–36. doi: 10.1007/s11010-009-0336-6

Sharma, R. K., Jaiswal, R. K., and Duda, T. (1988b). Second messenger role of cyclic GMP in atrial natriuretic factor receptor mediated signal transduction: 180-kD membrane guanylate cyclase, its coupling with atrial natriuretic factor receptor and its regulation by protein kinase C. *Biol. Mol. Aspects Atrial Factors* 81, 77–96.

Sharma, R. K., Makino, C. L., Hicks, D., and Duda, T. (2014). ROS-GC interlocked Ca(2+)-sensor S100B protein signaling in cone photoreceptors: review. *Front. Mol. Neurosci.* 7:21. doi: 10.3389/fnmol.2014.0002

Sharma, R. K., Marala, R. B., and Duda, T. (1989). Purification and characterization of the180-kDa membrane guanylate cyclase containing atrial natriuretic factor receptor from rat adrenal gland its regulation by protein kinase C. *Steroids* 53, 437–460. doi: 10.1016/0039-128x(89)90024-x

Sharma, R. K., Marala, R. B., and Paul, A. K. (1988a). "Mediatory role of cyclic GMP in receptor mediated signal transduction: membrane guanylate cyclase and its coupling with atrial natriuretic factor receptor," in *Advances in Atrial Peptide Research*, vol. *II* (New York: Raven Press), 61–77.

Sharma, R. K., Yadav, P., and Duda, T. (2001). Allosteric regulatory step and configuration of the ATP-binding pocket in atrial natriuretic factor receptor guanylate cyclase transduction mechanism. *Can. J. Physiol. Pharmacol.* 79, 682–691. doi: 10.1139/y01-033

Shi, S. J.,, Nguyen, H. T., Sharma, G. D., Navar, L. G., and Pandey, K. M. (2001). Genetic disruption of atrial natriuretic peptide receptor-A alters renin and angiotensinII levels. *Am. J. Physiol. RenalPhysiol.* 281, F665–F673.

Shyjan, A. W., deSauvage, F. J., Gillett, N. A., Goeddel, D. V., and Lowe, D. G. (1992). Molecular cloning of a retina-specific membrane guanylyl cyclase. *Neuron* 9, 727–737. doi: 10.1016/0896-6273(92)90035-c

Singh, S., Lowe, D. G., Thorpe, D. S., Rodriguez, H., Kuang, W. J., Dangott, L. J., et al. (1988). Membrane guanylate cyclase is a cell-surface receptor with homology to protein kinases. *Nature* 334, 708–712. doi: 10.1038/334708a0

Singh, S., Singh, G., Heim, J.-M., and Gerzer, R. (1991). Isolation and expression of a guanylate cyclase-coupled heat stable enterotoxin receptor cDNA from a human colonic cell line. *Biochem. Biophys. Res. Commun.* 179, 1455–1463. doi: 10.1016/0006-291X(91)91736-V

Stephen, R., Filipek, S., Palczewski, K., and Sousa, M. C. (2008). Ca2+−dependent regulation of Phototransduction. *Photochem. Photobiol.* 84, 903–910. doi: 10.1111/j.1751-1097.2008.00323.x

Strader, C. D., Fong, T. M., Tota, M. R., Underwood, D., and Dixon, R. A. (1994). Structure and function of G-protein-coupled receptors. *Annu. Rev. Biochem.* 63, 101–132. doi: 10.1146/annurev.bi.63.070194.000533

Stryer, L. (1986). Cyclic GMP cascade of vision. *Annu. Rev. Neurosci.* 9, 87–119. doi: 10.1146/annurev.neuro.9.1.87

Stryer, L. (1991). Visual excitation and recovery. *J. Biol. Chem.* 266, 10711–10714. doi: 10.1016/S0021-9258(18)99072-1

Subbaraya, I., Ruiz, C. C., Helekar, B. S., Zhao, X., Gorczyca, W. A., Pettenati, M. J., et al. (1994). Molecular characterization of human and mouse photoreceptor guanylate cyclase activating protein (GCAP) and chromosomal localization of the human gene. *J. Biol. Chem.* 269, 31080–31089. doi: 10.1016/S0021-9258(18)47393-0

Sudoh, T., Minamino, N., Kangawa, K., and Matsuo, H. (1990). C-type natriuretic peptide (CNP): a new member of natriuretic peptide family identified in porcine brain. *Biochem. Biophys. Res. Commun.* 168, 863–870. doi: 10.1016/0006-291x(90)92401-k

Sun, L., Wang, H., Hu, J., Han, J., Matsunami, H., and Luo, M. (2009). Guanylyl cyclase-D in the olfactory CO2 neurons is activated by bicarbonate. *Proc. Natl. Acad. Sci. U. S. A.* 106, 2041–2046. doi: 10.1073/pnas.0812220106

Sutherland, E. W., and Rall, T. W. (1958). Fractionation and characterization of a cyclic adenine ribonucleotide formed by tissue particles. *J. Biol. Chem.* 232, 1077–1091. doi: 10.1016/S0021-9258(19)77423-7

Sutherland, E. W., and Rall, T. W. (1960). The relation of adenosine-3′,5′-phosphate and phosphorylase to the actions of catecholamines and other hormones. *Pharmacol. Rev.* 12, 265–299.

Takayanagi, R., Inagami, T., Snajdar, R. M., Imada, T., Tamura, M., and Misono, K. S. (1987a). Two distinct forms of receptors for atrial natriuretic factor in bovine adrenocortical cells. Purification, ligand binding, and peptide mapping. *J. Biol. Chem.* 262, 12104–12113. doi: 10.1016/S0021-9258(18)45322-7

Takayanagi, R., Snajdar, R. M., Imada, T., Tamura, M., Pandey, K. N., Misono, K. S., et al. (1987b). Purification and characterization of two types of atrial natriuretic factor receptors from bovine adrenal cortex: guanylate cyclase-linked and cyclase-free receptors. *Biochem. Biophys. Res. Commun.* 144, 244–250. doi: 10.1016/s0006-291x(87)80502-8

Takeishi, A., Yu, Y. V., Hapiak, V. M., Bell, H. W., O'Leary, T., and Sengupta, P. (2016). Receptor-type guanylyl cyclases confer thermosensory responses in *C. elegans*. *Neuron* 90, 235–244. doi: 10.1016/j.neuron.2016.03.002

Terasawa, M., Nakano, A., Kobayashi, R., and Hidaka, H. (1992). Neurocalcin: a nove calcium-binding protein from bovine brain. *J. Biol. Chem.* 267, 19596–19599. doi: 10.1016/S0021-9258(18)41816-9

Tucker, C. L., Woodcock, S. C., Kelsell, R. E., Ramamurthy, V., Hunt, D. M., and Hurley, J. B. (1999). Biochemical analysis of a dimerization domain mutation in RetGC-1 associated with dominant cone–rod dystrophy. *Proc. Natl. Acad. Sci. U. S. A.* 96, 9039–9044. doi: 10.1073/pnas.96.16.9039

van den Akker, F., Zhang, X., Miyagi, M., Huo, X., Misono, K. S., and Yee, V. C. (2000). Structure of the dimerized hormone-binding domain of a guanylyl-cyclase-coupled receptor. *Nature* 406, 101–104. doi: 10.1038/35017602

Venkataraman, V., Duda, T., Ravichandran, S., and Sharma, R. K. (2008). Neurocalcin delta modulation of ROS-GC1, a new model of Ca2+ signaling. *Biochemistry* 47, 6590–6601. doi: 10.1021/bi800394s

Venkataraman, V., Duda, T., and Sharma, R. K. (1998). The alpha (2D/A)-adrenergic receptor-linked membrane guanylate cyclase: a new signal transduction system in the pineal gland. *FEBS Lett.* 427, 69–73. doi: 10.1016/s0014-5793(98)00396-2

Venkataraman, V., Duda, T., Vardi, N., Koch, K. W., and Sharma, R. K. (2003). Calcium-modulated guanylate cyclase transduction machinery in the photoreceptor–bipolar synaptic region. *Biochemistry* 42, 5640–5648. doi: 10.1021/bi034025x

Venkataraman, V., Nagele, R., Duda, T., and Sharma, R. K. (2000). Rod outer segment membrane guanylate cyclase type1-linked stimulatory and inhibitory calcium signaling systems in the pineal gland: biochemical, molecular and immunohistochemical evidence. *Biochemistry* 39, 6042–6052. doi: 10.1021/bi9929960

Vijay-Kumar, S., and Kumar, V. D. (1999). Crystal structure of recombinant bovine neurocalcin. *Nat. Struct. Biol.* 6, 80–88. doi: 10.10.1038/4956

Waldman, S. A., Leitman, D. C., Andersen, J., and Murad, F. (1988). Guanylate cyclase and the adrenal natriuretic factor receptor. *Science* 240, 805–806. doi: 10.1126/science.2896389

Waldman, S. A., Lewicki, J. A., Brandwein, H. J., and Murad, F. (1982). Partial purification and characterization of particulate guanylate cyclase from rat liver after solubilization with trypsin. *J. Cyclic Nucleotide Res.* 8, 359–370.

Wallach, D., and Pastan, I. (1976). Stimulation of membranous guanylate cyclase by concentrations of calcium that are in the physiological range. *Biochem. Biophys. Res. Commun.* 72, 859–865. doi: 10.1016/s0006-291x(76)80211-2

Wen, X. H., Dizhoor, A. M., and Makino, C. L. (2014). Membrane guanylyl cyclase complexes shape the photoresponses of retinal rods and cones. *Front. Mol. Neurosci.* 7:45. doi: 10.3389/fnmol.2014.00045

Wen, X. H., Duda, T., Pertzev, A., Venkataraman, V., Makino, C. L., and Sharma, R. K. (2012). S100B serves as a Ca2+ sensor for ROS-GC1 guanylate cyclase in cones but not in rods of the murine retina. *Cell. Physiol. Biochem.* 29, 417–430. doi: 10.1159/000338496

Wensel, T. G. (2008). Signal transducing membrane complexes of photoreceptor outer segments. *Vis. Res.* 48, 2052–2061. doi: 10.1016/j.visres.2008.03.010

Wiegand, R. C., Kato, J., and Currie, M. G. (1992). Rat guanylin cDNA: characterization of the precursor of an endogenous activator of intestinal guanylate cyclase. *Biochem. Biophys. Res. Commun.* 185, 812–817. doi: 10.1016/0006-291X(92)91699-Q

Wilkie, S. E., Newbold, R. J., Deery, E., Walker, C. E., Stinton, I., Ramamurthy, V., et al. (2000). Functional characterization of missense mutations at codon 838 in retinal guanylate cyclase correlates with disease severity in patients with autosomal dominant cone–rod dystrophy. *Hum. Mol. Gen.* 9, 3065–3073. doi: 10.1093/hmg/9.20.3065

Woodruff, M. L., Sampath, A. P., Matthews, H. R., Krasnoperova, N. V., Lem, J., and Fain, G. L. (2002). Measurement of cytoplasmic calcium concentration in the rods of wild-type and transducing knock-out mice. *J. Physiol.* 542, 843–854. doi: 10.1113/jphysiol.2001.013987

Xu, J., Morris, L., Thapa, A., Ma, H., Michalakis, S., Biel, M., et al. (2013). cGMP accumulation causes photoreceptor degeneration in CNG channel deficiency: evidence of cGMP cytotoxicity independently of enhanced CNG channel function. *J. Neurosci.* 33, 14939–14948. doi: 10.1523/JNEUROSCI.0909-13

Yang, R. B., and Garbers, D. L. (1997). Two eye guanylyl cyclases are expressed in the same photoreceptor cells and form homomers in preference to heteromers. *J. Biol. Chem.* 272, 13738–13742. doi: 10.1074/jbc.272.21.13738

frontiers | Frontiers in Molecular Neuroscience

TYPE Review
PUBLISHED 04 January 2023
DOI 10.3389/fnmol.2022.1076799

OPEN ACCESS

EDITED BY
Arun Asok,
Alien Therapeutics Inc., United States

REVIEWED BY
Sandhya Srikant Visweswariah,
Indian Institute of Science (IISc), India
Stuart E. Dryer,
University of Houston,
United States

*CORRESPONDENCE
Kailash N. Pandey
✉ kpandey@tulane.edu

SPECIALTY SECTION
This article was submitted to Molecular Signalling and Pathways, a section of the journal Frontiers in Molecular Neuroscience

RECEIVED 22 October 2022
ACCEPTED 02 December 2022
PUBLISHED 04 January 2023

CITATION
Pandey KN (2023) Guanylyl cyclase/natriuretic peptide receptor-A: Identification, molecular characterization, and physiological genomics. *Front. Mol. Neurosci.* 15:1076799. doi: 10.3389/fnmol.2022.1076799

Guanylyl cyclase/natriuretic peptide receptor-A: Identification, molecular characterization, and physiological genomics

Kailash N. Pandey*

Department of Physiology, School of Medicine, Tulane University Health Sciences Center, New Orleans, LA, United States

The natriuretic peptides (NPs) hormone family, which consists mainly of atrial, brain, and C-type NPs (ANP, BNP, and CNP), play diverse roles in mammalian species, ranging from renal, cardiac, endocrine, neural, and vascular hemodynamics to metabolic regulations, immune responsiveness, and energy distributions. Over the last four decades, new data has transpired regarding the biochemical and molecular compositions, signaling mechanisms, and physiological and pathophysiological functions of NPs and their receptors. NPs are incremented mainly in eliciting natriuretic, diuretic, endocrine, vasodilatory, and neurological activities, along with antiproliferative, antimitogenic, antiinflammatory, and antifibrotic responses. The main locus responsible in the biological and physiological regulatory actions of NPs (ANP and BNP) is the plasma membrane guanylyl cyclase/natriuretic peptide receptor-A (GC-A/NPRA), a member of the growing multi-limbed GC family of receptors. Advances in this field have provided tremendous insights into the critical role of *Npr1* (encoding GC-A/NPRA) in the reduction of fluid volume and blood pressure homeostasis, protection against renal and cardiac remodeling, and moderation and mediation of neurological disorders. The generation and use of genetically engineered animals, including gene-targeted (gene-knockout and gene-duplication) and transgenic mutant mouse models has revealed and clarified the varied roles and pleiotropic functions of GC-A/NPRA *in vivo* in intact animals. This review provides a chronological development of the biochemical, molecular, physiological, and pathophysiological functions of GC-A/NPRA, including signaling pathways, genomics, and gene regulation in both normal and disease states.

KEYWORDS

natriuretic peptides, particulate guanylyl cyclase receptor-A, structure–function relationship, genomics, gene-targeting, cyclic-GMP signaling

Introduction

A pioneering and innovative discovery by de Bold and colleagues four decades ago, found natriuretic and diuretic activity in the heart atrium extract, leading to the purification and characterization of atrial natriuretic factor/peptide (ANF/ANP) (de Bold et al., 1981). This discovery revealed a new natriuretic peptide (NP) hormone family and established that the heart is an endocrine organ (de Bold et al., 1981; de Bold, 1985; Pandey, 2005; Goetze et al., 2020). ANF/ANP exhibits diuretic, natriuretic, vasorelaxant, neurotransmission, antimitogenic, and anti-inflammatory responses directed largely toward the reduction of blood pressure (BP) and protection against renal and cardiovascular disorders (Brenner et al., 1990; Levin et al., 1998; Pandey, 2005; Ellmers et al., 2007; Pandey, 2008). After the discovery of ANP, other members of this family were isolated and characterized, including brain natriuretic peptide (BNP), C-type natriuretic peptide (CNP), *Dendroaspis* natriuretic peptide or D-type NP (DNP), and urodilatin (URO) (Goetz, 1990; Stingo et al., 1992; Suga et al., 1992; Lisy et al., 1999). All NPs show similar biochemical, structural, and pharmacological characteristics, with a common 17-amino acid disulfide-bonded ring. Interestingly, each member of the NP hormone family seems to be derived from a separate gene (Rosenzweig and Seidman, 1991). These peptides bind to different cognate receptors, exhibit distinct biological functions, and have varying sites of synthesis (Koller et al., 1992; Levin et al., 1998; Venugopal, 2001; Sharma, 2002; Pandey, 2005; Lee and Burnett Jr., 2007). ANP and BNP are predominantly produced in the cardiac atrium and ventricle, released in the plasma, and exhibit a high variation in sequence structure, whereas CNP is mainly synthesized in the brain and endothelial cells and is highly preserved across the species. DNP is predominantly synthesized in the venom of the green mamba (*Dendroaspis angusticeps*), and URO is produced in the kidney and secreted in the urine (Goetz, 1990; Lisy et al., 1999).

ANP plays a much wider and more significant role, particularly in hypertension and cardiovascular diseases. Both pro-ANP and pro-BNP genes (*Nppa* and *Nppb*) are also expressed in extra-cardiac tissues and cells, which seem to act in endocrine, autocrine, paracrine, and/or neurocrine manners (Vollmer and Schulz, 1990; Pandey and Orgebin-Crist, 1991; Huang et al., 1992; Gutkowska et al., 1993; Pandey, 2005). ANP targets the inhibition of aldosterone secretion from the adrenal glands (Atarashi et al., 1984; DeLean et al., 1984; Goodfriend et al., 1984), release of renin from the kidney (Burnett et al., 1984; Shi et al., 2001), and vasopressin release from the posterior pituitary (Obana et al., 1985). ANP also stimulates the release of testosterone from normal Leydig cells (Mukhopadhyay et al., 1986; Pandey et al., 1986), luteinizing hormone from the anterior pituitary gland (Obana et al., 1985; Horvath et al., 1986; Samson, 2004), and progesterone from granulosa-luteal cells (Pandey et al., 1987). BNP displays functions similar to ANP, but BNP also acts as a neurohormone and is preserved in the transient receptor potential vanilloid-1 (TRPV-1) in response to itch-inducing factors (Mishra and Hoon, 2013). DNP consists of 38 amino acid residues, however, its function has not yet been clearly established (Schweitz et al., 1992; Lisy et al., 1999). URO is a 32-residues peptide hormone similar to the carboxyl-terminal sequence of pro-ANP, which was isolated and characterized from urine (Schulz-Knappe et al., 1988; Feller et al., 1990). It is believed that URO is largely synthesized in the kidneys but mostly absent in the circulation (Saxenhofer et al., 1990; Goetz, 1991). Interestingly, URO is very resistant to proteolysis by endopeptidases and has an important role in the regulation of kidney function; more specifically, it controls the excretion of sodium and water, much like ANP and BNP (Goetz, 1990; Emmeluth et al., 1992).

The pharmacological and physiological functions of NPs is elicited through the binding of cognate plasma membrane receptor proteins. Three distinct subtypes of NPs receptor proteins have been identified and characterized: guanylyl cyclase (GC)/NP receptor-A (GC-A/NPRA), GC/NP receptor-B (GC-B/NPRB), and NP receptor-C (NPRC), encoded by specific genes, including *Npr1*, *Npr2*, and *Npr3*, respectively (Pandey, 2008). Both ANP and BNP activate GC-A/NPRA, also known as GC-A receptor, which responds to hormone binding by producing intracellular second messenger cGMP to this receptor molecule. CNP specifically activates GC-B/NPRB, known as GC-B receptor, and also produces a second messenger, cGMP. All three NPs (ANP, BNP, and CNP) invariably bind to NPRC, which lacks an intracellular GC region (Koller et al., 1992; Pandey, 1992; Pandey, 1996; Levin et al., 1998; Pandey, 2005). The prevalence of structurally related NPs and their three distinct receptors suggests that their role in physiological and pathophysiological control of BP, body fluid homeostasis, and metabolic regulation is complex. At the minimum, three distinct subtypes of effector molecules are prevalent: cGMP-dependent protein kinases (PKGs), cGMP-dependent phosphodiesterases (PDs), and cyclic-nucleotide gated ion channels (CNGs), which catalyze and amplify the signaling cascade of NP-specific cognate receptors (Pandey, 2005; Sharma, 2010; Kishimoto et al., 2011; Pandey, 2011).

In essence, GC-A/NPRA acts as the main functional receptor protein for both ANP and BNP; and in a large part, the biological and physiological functions of hormones are discharged by the production of intracellular generation cGMP (Lucas et al., 2000; Sharma, 2002; Pandey, 2005; Pandey, 2008; Sharma, 2010; Pandey, 2011). In mice, the gene-targeting strategy of *Npr1* revealed the hallmark significance of GC-A/NPRA in the regulation of BP and protection against renal and cardiovascular dysfunction (Oliver et al., 1997, 1998; Shi et al., 2003; Vellaichamy et al., 2005; Ellmers et al., 2007; Kishimoto et al., 2011; Pandey, 2011; Das et al., 2012; Vellaichamy et al., 2014; Subramanian et al., 2022). CNP is produced in the endothelial cells, activates NPRB in the neighboring vascular smooth muscle cells (VSMCs), and has a pivotal function in the clinical hypotension of septic shock by decreasing venous return (Suga et al., 1992, 1993; Hama et al., 1994). The current review briefly summarizes previous studies and salient discoveries in the NPs hormone family and their receptors with a major emphasis on GC-A/NPRA, including signaling

mechanisms, structure–function composition, and roles in the physiology and pathology of health and disease.

Identification, characterization, and biochemical properties of NP receptors

Initially, to identify NP receptors, specific ^{125}I-ANP binding was performed using plasma membrane preparations of different tissues and intact cells (Misono et al., 1985; Pandey et al., 1986, 1988; Leitman et al., 1988). Initial cross-linking and photoaffinity studies showed that the molecular weight (M_r) of ANP receptors varies widely, ranging from 60-to 180-kDa. They were classified and characterized by sodium dodecyl sulfate polyacrylamide gel electrophoresis (SDS-PAGE) and autoradiography using various tissues and cells (Misono et al., 1985; Schenk et al., 1985; Vandlen et al., 1985; Yip et al., 1985; Meloche et al., 1986; Pandey et al., 1986, 1987, 1988). Later, photoaffinity and cross-linking methods showed a single protein band of ANP receptor with an apparent M_r of 135-to 140-kDa in plasma membrane preparations of various tissue and cell types (Pandey et al., 1987; Takayanagi et al., 1987; Leitman et al., 1988; Pandey et al., 1988; Pandey, 1993). An additional protein band of 70-kDa was also identified using affinity cross-linking and photoaffinity labeling techniques in the isolated plasma membranes and intact cells (Hirose et al., 1985; Schenk et al., 1985; Vandlen et al., 1985; Meloche et al., 1986; Leitman et al., 1988; Pandey et al., 1988). Concurrently, ^{125}I-ANP high-affinity binding sites of 130-to 180-kDa of ANP receptors were co-purified with GC activity (Paul et al., 1987; Takayanagi et al., 1987; Marala and Sharma, 1988; Meloche et al., 1988). A 70-kDa ANP receptor which did not display GC activity was also isolated and characterized (Schenk et al., 1987; Takayanagi et al., 1987; Pandey et al., 1988). Based on the biological activity of the different lengths of ANP molecules, NPs receptor are classified into 130-to 180-kDa proteins (biologically active) and 60 to 68-kDa protein molecule (clearance) receptor, which was unable to produce cGMP (Pandey, 2005).

Later, three distinct subtypes of ANP receptors were identified and characterized by using the criteria, including binding characteristics, cross-linking and photoaffinity labeling techniques, and capacity to generate intracellular cGMP, which were found to be specific to different cell and tissue types (Leitman et al., 1988; Pandey et al., 1988). Three distinct NP receptor subtypes were identified, characterized, and classified in multiple cells and tissues, including non-reducible 135-kDa, reducible 140-kDa, and non-reducible 70-kDa protein bands (Pandey et al., 1988). In VSMCs, two specific binding sites of the 70-kDa and 140-kDa bands were identified, while under reducing conditions, the 70-kDa receptor band persisted; however, the 140-kDa protein band was disappeared and reduced to 70-kDa. Non-iodinated or unlabeled 28-amino-acid full-length ANP abolished both 70-kDa and 140-kDa bands; however, truncated ANF (c-ANF or AP I) inhibited only the 70-kDa receptor band. The renal extracts and established Maiden-Darby canine kidney (MDCK) cells showed 70-kDa and 120-kDa receptor bands, but Leydig tumor (MA-10) cells and neuroblastoma glial cells yielded just a 135-kDa receptor band, which was eliminated with full-length ANP but not with truncated AP-1 (Pandey et al., 1986; Pandey and Inagami, 1988). VSMCs contained approximately 90% low M_r 66–70-kDa protein bands (Pandey et al., 1987; Leitman et al., 1988; Pandey et al., 1988). Interestingly, adrenal glomerulosa cells, MDCK, and MA-10 cells contained the non-reducible 125-to 180-kDa ANP receptor bands and showed similar characteristics both biochemically and pharmacologically. Biochemical, cellular, molecular, and immunohistochemical studies suggested that ANP receptors seem to be widely distributed in different cells and tissue types, with pleiotropic functional characteristics in the renal, cardiac, vascular, and neural systems (Brenner et al., 1990; Levin et al., 1998; Pandey, 2005; Pandey, 2018).

Molecular cloning and determination of primary structure of NP receptors

Molecular cloning of cDNAs from mouse, rat, and humans deduced the primary structure of three subtypes of NP receptors (NPRs), including: GC-A/NPRA, GC-B/NPRB, and NPRC, which constitute the NP receptor family (Fuller et al., 1988; Chang et al., 1989; Chinkers et al., 1989; Lowe et al., 1989; Pandey and Singh, 1990; Marala et al., 1992). The primary structural topology of the extracellular ligand-binding domain (LBD) of NPRA and NPRB exhibit almost 45% sequence homology. The protein kinase-like homology domain (protein-KHD) contains 280 amino acid residues that follow the transmembrane domain (TD) region of the receptors; however, the intracellular carboxyl-terminus portion of GC-A/NPRA and GC-B/NPRB contains 250 amino acids, constituting GC catalytic domain (GCCD) (Pandey and Singh, 1990; Drewett and Garbers, 1994; Zhang et al., 1997). The GCCD enzymatic region showed the greatest homology, with GC-A/NPRA and GC-B/NPRB sharing almost 80% sequence identify while protein-KHD had only 60% sequence identify among both GC-A/NPRA and GC-B/NPRB. Over 80% of the conserved amino acid residues present in all protein kinases seem to be found in the protein-KHD of GC-A/NPRA and GC-B/NPRB receptors (Hanks et al., 1988; Koller et al., 1992). But the functional significance of protein-KHD remains unclear. Based on amino acid sequence comparisons, there seems to be over 60% sequence identity among GC-A/NPRA and GC-B/NPRB receptor proteins. Sequence homology data have revealed that the intracellular regions of these two GC receptors appear to be highly conserved, reaching almost 80% sequence identity. However, the extracellular LBD of these two GC receptors seem to have only 43% sequence similarity.

Five of the six cysteine residues of both GC receptors (NPRA and NPRB), are found in extracellular domains in the same relative positions (Pandey and Singh, 1990). The intracellular

region of GC-B/NPRB does not contain any putative glycosylation sites, and out of the all seven N-like glycosylation sites present in the extracellular domain of both receptors, only two are conserved across species (Schulz et al., 1989; Pandey and Singh, 1990; Drewett and Garbers, 1994). The nucleotide sequence in the GCCD of GC-A/NPRA and GC-B/NPRB is more highly conserved than in the protein-KHD region, whereas NPRC comprises a large extracellular LBD region of 496-amino acid residues, a single TD region, and a short 37-amino acid intracellular cytoplasmic tail, which does not exhibit any sequence homology with other known membrane receptor proteins. Extracellular LBD of NPRC contains only 30% sequence homology to GC-A/NPRA and GC-B/NPRB. Characteristically, NPRC possesses a very low specificity for different lengths of ANP peptides compared to GC-A/NPRA and GC-B/NPRB receptors (Fuller et al., 1988; Bovy, 1990; Khurana and Pandey, 1993). The clearance nomenclature of NPRC was given only by the default hypothesis; however, NPRC is also thought to display some biological functions (Pandey, 1992; Matsukawa et al., 1999; Palaparti and Anand-Srivastava, 2000; Zhou and Murthy, 2003).

Topology and domain structure of GC-A/NPRA and other GC receptors

Among the members of GC family of membrane receptors, GC-A/NPRA represents a biologically active NP receptor molecule, largely prevalent in peripheral tissues and cells which elicits most of ANP and BNP's known actions (Drewett and Garbers, 1994; Levin et al., 1998; Sharma, 2002; Pandey, 2005). In contrast, GC-B/NPRB is largely localized in vascular tissues and in the central nervous system (CNS) and it mediates the action of CNP, which also generates the production of second messenger, cGMP (Schulz et al., 1989; Duda and Sharma, 1995; Lowe, 1997; Lucas et al., 2000). Both GC-A/NPRA and GC-B/NPRB constitute an overall domain organization and topology structure much like that of other GC receptors. Both GC-A/NPRA and GC-B/NPRB consist of generally five separate domains, including LBD, a single membrane spanning TD, intracellular cytoplasmic protein-KHD, dimerization domain (DD), and enzymatic GCCD (Schulz et al., 1989; Pandey and Singh, 1990; Drewett and Garbers, 1994; Sharma, 2002; Pandey, 2005). One polypeptide molecule of transmembrane GC receptors contains a single GC catalytic active site, while the structural predicted data indicated that two-polypeptide chains are required to functionally activate GC-A/NPRA (Wilson and Chinkers, 1995; Yang and Garbers, 1997; Labrecque et al., 1999; van den Akker et al., 2000). Modeling data also predicted that the dimerization domain of GC-A/NPRA is embedded between the GCCD and protein-KHD catalytic regions and forms an amphipathic alpha helix structure of the receptor molecule (Garbers and Lowe, 1994). The sequences of different domains of GC-A/NPRA are conserved among mammalian species, including mouse, rat, and human (Chinkers et al., 1989; Lowe et al., 1989; Pandey and Singh, 1990; Marala et al., 1992; Garg et al., 2002). Based on sequence comparison analysis data, the protein-KHD of GC-A/NPRA is related more closely to the receptor tyrosine kinases (RTKs) than the serine/threonine kinases. The protein-KHDs of GC-A/NPRA and GC-B/NPRA have been suspected of exhibiting an important role in transmitting the ligand-induced signals of these receptor proteins (Chinkers and Garbers, 1989; Duda et al., 1993a; Sharma, 2002, 2010; Pandey, 2008). An intervening step may be necessary to activate the catalytic process of GCCD involving protein-KHD of GC-A/NPRA (Goraczniak et al., 1992; Koller et al., 1993; Sharma, 2002); however, the activation of GC-A/NPRA and GC-B/NPRB receptors probably requires ATP, which serves as an intracellular allosteric regulator to protein-KHD (Kurose et al., 1987; Chinkers et al., 1991; Larose et al., 1991; Duda et al., 1993a; Wong et al., 1995). The deletion of C-terminal sequences of GC-A/NPRA resulted in a truncated protein product that showed binding specificity to ANP but did not exhibit the GC activity of the receptor molecule (Thorp and Morkin, 1990; Koller et al., 1992; Pandey and Kanungo, 1993; Pandey et al., 2000). Crystal structure modeling analysis of adenylyl cyclase II C2 (ACII C2) domain indicated that the catalytic enzymatic active sites of GC receptors and ACs seem to be poorly related to the structural topology of GC-coupled receptors (Liu et al., 1997; Zhang et al., 1997; Sunahara et al., 1998; Tucker et al., 1998). The GCCD enzymatic active site of GC-A/NPRA seems to include a region of 31-amino acid residue sequence at the carboxyl-terminus end (974–1,004 residues) of the receptor. In fact, the members of the GC family of receptor protein constitute a single GCCD enzymatic business end for each polypeptide chain and exhibit catalytic activity as homodimers, which generates the second messenger cGMP and activates physiological signaling cascades (Figure 1).

Guanylyl cyclase C (GC-C) is also a member of the GC receptor family, which contains topology of domain structure, including extracellular LBD, TD, protein-KHD, and GCCD similar to GC-NPRs. However, GC-C is predominantly expressed and largely found on the apical surface of intestinal cells and activated by gastrointestinal peptides guanylin and uroguanylin and by heat-stable enterotoxin (ST) produced by *Escherichia coli* (Schulz et al., 1990; Currie et al., 1992; Hamra et al., 1993; Arshad and Visweswariah, 2012; Cappelli et al., 2019; Bose et al., 2020). GC-C is also expressed in the kidney and enhances the excretion of Na^+ and water. Paradoxically GC-C KO mice seem to exhibit normal gastrointestinal function but were found to be defiant to ST-activated diarrhea (Schulz et al., 1997; Sindice et al., 2002). Both guanylin and uroguanylin are thought to function in an endocrine manner (Forte et al., 2000; Carrithers et al., 2002). Among the GC family of receptors, besides NPRs and GC-C, several other members have been identified, including GC-D, GC-E, GC-F, GC-G, and Ret-GC or ROS-GC. However, the details of these receptors will not be discussed in this review; nevertheless, all members of GC-family of receptors transmit the signal by generating the second messenger cGMP.

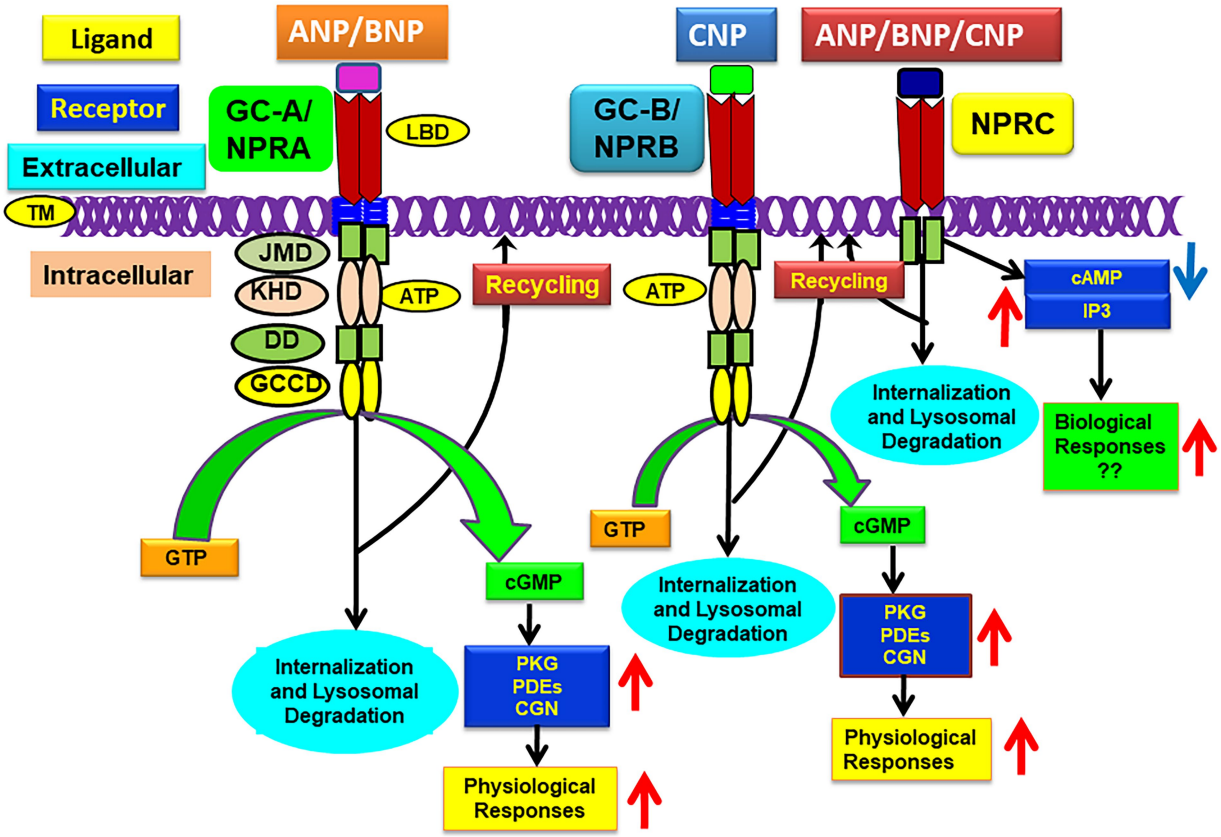

FIGURE 1
Schematic representation of ligand-dependent activation and physiological functions of GC-A/NPRA, GC-B/NPRB, and NPRC. ANP and BNP binding to amino-terminal domain activates GC-A/NPRA, which leads to enhanced production of intracellular second messenger cGMP with stimulation of PKG, PDFs, and CNG that activate ANP-dependent cellular and physiological responsiveness. CNP binds and activates GC-A/NPRB and also produces cGMP and physiological responsiveness. All three NPs activate NPRC that lead to some biological actions. ANP, atrial natriuretic peptide; BNP, brain natriuretic peptide; CNP, C-type natriuretic peptide; GC-A/NPRA, guanylyl cyclase-A/natriuretic peptide receptor-A; GC-B/NPRB, guanylyl cyclase-B/natriuretic peptide receptor-B; NPRC, natriuretic peptide clearance receptor; LBD, ligand binding domain; TM, transmembrane domain; KHD, protein-kinase like homology domain; DD, dimerization domain; GCCD, guanylyl cyclase catalytic domain; IP_3, inositol trisphosphate. Adopted with modification from reference Pandey, K. N. 2015, Membranes 5, 253–287.

Signal transduction mechanisms and intracellular signaling of GC-A/NPRA

ANP greatly increases the accumulation of intracellular cGMP levels and decreases the concentration of cAMP by stimulating the specific PDEs in target tissues and cells in a dose-and time-dependent manner (Waldman et al., 1984; Pandey et al., 1985; Tremblay et al., 1985; Pandey et al., 1986; Levin et al., 1998; Pandey, 2005). However, the inhibitory effects of ANP on cAMP levels seem to act indirectly, probably by involving cGMP-dependent PDEs (Pandey, 2005; Sharma, 2010). Earlier studies suggested that ANP binding to GC-A/NPRA alone might not be sufficient to stimulate the maximum levels of GC activity, but it may also require ATP (Kurose et al., 1987; Chinkers et al., 1991; Goraczniak et al., 1992). The nonhydrolyzable analogs of ATP mimics the effects of ANP, and ATP might act by allosteric regulation of GC activity of GC-A/NPRA. The deletion and/or point mutations in GC receptors lacking a protein-KHD region did not show responsiveness of either ANP or ATP to activate GC activity of these receptors (Chinkers and Garbers, 1989; Koller et al., 1992; Duda and Sharma, 1995; Sharma, 2002). The mutant receptor was thought to be independent of any ANP requirement; however, it showed the ability to bind the ligand and exhibited 100-fold excess GC activity compared with wild-type (WT) receptor protein (Chinkers and Garbers, 1989; Koller et al., 1992). ATP binding, possibly to protein-KHD, causes a structural conformational change to ease the protein-KHD autoinhibition of GC enzymatic catalytic region during the ligand-induced signaling cascade of GC-A/NPRA (Lowe, 1997; Foster and Garbers, 1998; Garbers, 1999). This model has been challenged by other investigators, who proposed that the deletion of the protein-KHD of GC-A/NPRA was unable to enhance the basal GC activity of the receptor (Goraczniak et al., 1992; Duda et al., 1993b; Sharma, 2002, 2010); however, those previous studies agreed that ATP is likely necessary for the hormone-dependent maximum activation of GC-coupled receptors. The authors

further suggested that the interactive action of ATP with protein-KHD enhances the effectiveness of the ligand-induced signaling mechanisms of GC-A/NPRA with enhanced accumulation of intracellular second messenger cGMP.

Earlier, it was predicted that after ligand binding, ATP interacts with protein-KHD, which increases the production of intracellular cGMP without affecting the affinity of the substrate to the receptor (Kurose et al., 1987; Chang et al., 1990; Duda et al., 1991; Gazzano et al., 1991; Wong et al., 1995; Sharma, 2002). Later studies suggested that ATP binding to protein-KHD seems to be critical for the effector-coupling of GC-coupled receptor proteins (Goraczniak et al., 1992; Duda et al., 1993a; Sharma, 2002, 2010). Those studies further indicated that the glycine-rich motif G-R-G-S-N-Y-G in the protein-KHD was important for ATP binding and activation of the ANP/NPRA signaling cascade (Duda et al., 1991, 1993a; Goraczniak et al., 1992). The consensus sequence of the glycine-rich motif was named the ATP-regulatory module (ARM) of the GC receptors (Goraczniak et al., 1992; Duda et al., 1993a; Sharma, 2002). Site-directed mutagenesis experiments suggested that the middle Gly residue in the glycine-rich consensus motif was crucial for the ATP-binding site and for the signal transduction cascade of GC-coupled receptors (Duda et al., 1993a; Sharma, 2002). Tight regulatory control of the receptor signal seems to be essential for the intracellular formation of the second messenger cGMP (Sharma et al., 1994; Sharma, 2002). ATP-binding to the protein-KHD has also been proposed to cause GC activation and induces a low-affinity shift that might release the bound ligand from the receptor molecule; however, this remains to be experimentally tested to whether modulates the signaling cascade of GC-coupled receptors (Jewett et al., 1993).

Crystallographic modeling data have shown that in the absence of ligand, LBD of GC-A/NPRA is self-associated to form a homodimer molecule (van den Akker et al., 2000). The binding of ligand to the receptor induces molecular conformational alterations and/or coordinated structural changes in the protein-KHD, which likely leads to ATP binding to enhance the signaling cascade (Huo et al., 1999; Misono et al., 2005). However, it is unclear whether native target cells also exhibit the dimeric nature of the receptor molecules. Evidence suggests two possible dimer pairs exist in the crystal packaging of the extracellular LBD of GC-A/NPRA; the tail-to-tail and head-to-head dimers seem to be associated with the membrane-distal and proximal subdomains of the receptor (Qiu et al., 2004), respectively. The tail-to-tail dimer of GC-A/NPRA may be required for ligand-induced signaling of this receptor protein (van den Akker et al., 2000; Misono et al., 2005). Moreover, the crystallographic structure of NPRC has also indicated that a dimerized form of this receptor seems to be essential in head-to-head configuration with bound ligand-receptor complex (He et al., 2001, 2005). The head-to-head dimer of NPRC seems to represent the inactive state of the receptor, whereas the tail-to-tail dimer may represent its hormone-activated state (He et al., 2001, 2005; van den Akker, 2001; Misono et al., 2005). The ligand-mediated activation of GC-A/NPRA may stabilize the membrane-distal dimer interface, indicating that ligand binding confers the GC-A/NPRA dimer interface interactive site of the receptor (DeLean et al., 2003). Chemical modifications and site-directed mutagenesis experiments have indicated that the head-to-head dimer structure confers with the physiological dimer of GC-A/NPRA (Qiu et al., 2004). The disruption of disulfide cysteine bonds in the juxtamembrane hinge region (JMHR) results in constitutive activation of the receptor, indicating that the JMHR might play a crucial role in the signal transduction and receptor activation mechanisms of GC receptors (Huo et al., 1999; Misono et al., 2005, 2011).

The heterogeneity and diverse cellular distribution of NP receptors indicates that different mechanisms might govern the activation of signaling and function of GC receptors in target cells (Pandey et al., 2000; Sharma, 2002; Pandey, 2005; Sharma, 2010; Kishimoto et al., 2011; Pandey, 2011). ANP stimulates the generation of inositol triphosphates (IP_3) at very low concentrations in cultured MA-10 cells and VSMCs (Resink et al., 1988; Hirata et al., 1989; Khurana and Pandey, 1994; Khurana and Pandey, 1995; Pandey, 2014); however, ANP stimulated the generation of IP_3 in the renal inner medullary collecting duct cells (RIMCDs) and MA-10 Leydig tumor cells at lower concentrations, while at higher hormone concentrations, it inhibited the formation of these metabolites, simultaneously increasing the accumulation of intracellular cGMP levels (Teitelbaum et al., 1990; Berl et al., 1991; Khurana and Pandey, 1995; Khurana and Pandey, 1996; Pandey, 2005; Pandey, 2014). Depending on cell type, ANP inhibits both the enzymatic activity and autophosphorylation of protein kinase C (PKC) (Pandey, 1989; Pandey, 1994; Kumar et al., 1997; Pandey, 2008). Furthermore, ANP stimulated potassium channels through the activation of PKGs, which requires ATP (White et al., 1993). Our studies have shown that GTPγS synergistically enhanced ANP's effect on the GC catalytic activity of GC-A/NPRA (Khurana and Pandey, 1995), but the antibodies against the subunits of G-proteins (Gsα and Giα) did not affect GC activity, although Goα antibodies blocked the agonist-stimulated GC catalytic activation of GC-A/NPRA (Khurana and Pandey, 1994; Pandey, 2005).

GC-A/NPRA seems to be present in the phosphorylated state. ANP causes a decrease in the phosphate content and thus dephosphorylation, in turn reducing ANP-dependent GC activity and desensitizing the receptor protein (Potter and Garbers, 1992; Potter and Garbers, 1994). Earlier findings have indicated that ANP seems to stimulate the phosphorylation of GC-A/NPRA (Ballerman et al., 1988; Pandey, 1989; Duda and Sharma, 1990; Larose et al., 1992). It was later suggested that ANP stimulates the phosphorylation of NPRA at serine and threonine residues in the protein-KHD region of the receptor that was considered essential for receptor activation (Foster and Garbers, 1998; Potter and Hunter, 1998). Those studies indicated that phosphorylation at serine and threonine sites induces the desensitization of GC-coupled receptors. In fact, the activation of GC-A/NPRA could also be attenuated by agents such as certain growth factor, including epidermal growth factor (EGF) and platelet-derived growth factor (PDGF) and pressure hormones, such as endothelin,

vasopressin, and ANG II, which decrease the responsiveness of GC-A/NPRA (Haneda et al., 1991; Yasunari et al., 1992; Potter and Garbers, 1994; Kumar et al., 1997; Pandey et al., 2000; Sharma et al., 2002; Garg and Pandey, 2003; Tripathi and Pandey, 2012; Alicic et al., 2018; Arise et al., 2020). The agonist-dependent activation of PKC by phorbol ester decreased GC catalytic activity of NPRA (Haneda et al., 1991; Yasunari et al., 1992; Potter and Garbers, 1994; Kumar et al., 1997; Pandey, 2005; Kumar et al., 2017). On the other hand, the desensitization of GC-A/NPRA may be correlated with mechanisms involving receptor phosphorylation (Duda and Sharma, 1990). The mechanism of desensitization of NPRA involving dephosphorylation does not seem to be consistent with G-protein-coupled receptor molecules, which also appear to be desensitized by protein phosphorylation (Zhang et al., 1997; Lefkowitz et al., 1998). Both protein kinases and protein phosphatases seem to be involved in the desensitization mechanisms of GC-A/NPRA, which remain poorly understood. But one study has suggested that PKG seems to phosphorylate the GC-A/NPRA *in vitro* system (Airhart et al., 2003). Previous studies further indicated that after ANP treatment, PKG is recruited to the plasma membrane and enhances the GC catalytic activity of the receptor. Interestingly, PKG seems to translocate in an ANP-mediated manner; however, not in the nitric oxide-mediated system. An ANP-mediated NPRA/PKG mechanism might initiate the cGMP-dependent signaling in the functional regulation of GC-A/NPRA in target cells.

Endocytosis, intracellular trafficking, and downregulation of GC-A/NPRA

Receptor internalization is a prominent mechanism underlying the concentrated uptake of ligand-receptor complexes for receptor-mediated intracellular signal transduction, neurotransmission, cellular activities, and physiological and pathophysiological functions. We have previously suggested that receptor endocytosis and intracellular signaling of GC-A/NPRA occur concurrently during internalization and subcellular trafficking. During endocytotic process the second-messenger cGMP signals are generated in intact cells (Mani et al., 2015, 2016; Mani and Pandey, 2019). Stoichiometric analyses of the endocytosed ANP/NPRA complexes and metabolic processing showed that the bound hormone-receptor complexes were endocytosed and intracellularly processed, and the metabolized degraded products were ultimately exocytosed and released into culture medium (Pandey et al., 1986; Rathinavelu and Isom, 1991; Pandey, 1993; Pandey et al., 2002; Mani et al., 2015). However, a small population of bound ligand-receptor complexes may escape the degradative lysosomal pathway and recycle back to the plasma membrane, leaving some intact ligands to be released in the cell exterior (Pandey et al., 2002, 2005; Saftig and Klumperman, 2009; Mani and Pandey, 2019). Using MA-10 cells (harboring the native receptor population) and HEK-293 cells (expressing the recombinant receptor molecules), we have shown that after ligand-binding, the bound hormone-receptor complexes of ANP-BNP/GC-A/NPRA are endocytosed, intracellularly processed, and metabolized inside the cell (Pandey et al., 1986, 2000, 2002; Pandey, 1993, 2001; Somanna et al., 2013; Mani et al., 2016). On the other hand, one study indicated that in renomedullary epithelial cells (RMECs), GC-A/NPRA with bound-ligand receptor complex was not processed intracellularly and rapid dissociation of ligand-receptor complexes occurred after ANP binding to GC-A/NPRA, and intact ligand was released into culture medium (Koh et al., 1992). However, since the ligand dissociation was performed using very high amount of cold (unlabeled) ANP, rebinding of the dissociated ligand to the receptor protein can be excluded, making these findings difficult to interpret (Koh et al., 1992). These findings also indicated that RMECs contained multiple receptor populations including GC-A/NPRA and NPRC (Koh et al., 1992). Studies of ligand binding and metabolic processing of ANP involving NPRCs have been reported using VSMCs, which predominantly contain 70-kDa NPRCs and only a small population of GC-A/NPRAs (Hirata et al., 1985; Napier et al., 1986; Pandey et al., 1988; Murthy et al., 1989; Cahill et al., 1990; Nussenzveig et al., 1990; Pandey, 1992, 2005; Cohen et al., 1996).

The antibody-tracking method has indicated that both GC-A/NPRA and GC-B/NPRB were found to be internalized in a ligand-independent manner (Dickey et al., 2011); however, this method only qualitatively determines the internalization kinetics of ligand-receptor complexes. Immunofluorescence confocal microscopy has revealed the visualization of the subcellular trafficking and ligand-dependent endocytosis of GC-A/NPRA tagged with eGFP- (eGFP-GC-A/NPRA) in HEK-293 and murine mesangial cells (MMCs) (Mani et al., 2015, 2016). The internalization of GC-A/NPRB was also demonstrated in hippocampal neurons and glioma cells (Brackmann et al., 2005). Endocytosis, sequestration, and metabolic processing of internalized hormone receptor complexes may all play roles in the downregulation of receptors (Pandey et al., 2002; Pandey, 2010; Pandey, 2015). GC-A/NPRA downregulation has been reported in PC-12 cells that contain endogenous receptors (Rathinavelu and Isom, 1991) and COS-7 and HEK-293 cells transfected with recombinant receptors (Pandey et al., 2000, 2002, 2005). The deletion of carboxyl-terminus regions of GC-A/NPRA suggested that the specific sequence in catalytic GCCD and protein-KHD played a pivotal role in the internalization, sequestration, and metabolic degradation of the receptor protein (Pandey et al., 2000; Pandey, 2015). Interestingly, several studies have indicated that micro-RNA (miR) plays critical roles in the regulatory mechanisms and function of ANP/NPRA system (Arora et al., 2013; Somanna et al., 2013; Wu et al., 2016; Vandenwijngaert et al., 2018; Khurana et al., 2022). Our recent findings have suggested that prolonged ANP treatments along with miR-128 and miR195 of cultured cells expressing high density of GC-A/NPRA caused downregulation of the receptor in a time-and dose-dependent manner (Khurana et al., 2022). Those findings showed that

miR-128 and miR-195 caused significant reduction in the protein levels of GC-A/NPRA. We implicated that ligand-mediated mechanisms involving miR-128 and miR-195 might instigate a prominent regulatory role in the regulation and activity of GC-coupled receptor proteins.

Using the confocal microscopy and ^{125}I-ANP binding assay, we delineated the significance of dynamin molecule in the trafficking and internalization of GC-A/NPRA utilizing the recombinant HEK-293 cells (Somanna et al., 2018). ANP treatment enhanced the internalization of NPRA in the cell interior, but the process was significantly impaired by the specific inhibitors of clathrin/dynamin, namely monodansylcadaverine (MDC) and chlorpromazine (CPZ) (Somanna et al., 2018). Mutant dynamin also specifically blocked the endocytic vesicle formation and internalization of NPRA (Somanna et al., 2018). Immunofluorescence visualization of GFP-tagged GC-A/NPRA in HEK-293 cells has revealed that endocytic vesicles are formed within 5 min after ANP treatment; however, the process was blocked by the inhibitors of clathrin (MDC and CPZ) and mutant dynamin (Somanna et al., 2018). We further showed that GC-A/NPRA undergoes internalization *via* clathrin-mediated endocytosis, including receptor internalization, signaling, and metabolic degradation. Our previous studies indicated that the internalization of GC-A/NPRA occurred *via* clathrin-dependent pathways following initial cluster formation of receptor-ligand cargo in clathrin-coated pits on the plasma membrane. The blockade of the endocytosis of ligand-receptor complexes by the clathrin inhibitors (MDC and CPZ), provided an efficient and valuable method to facilitate the mechanistic actions of the endocytosis of GCA/NPRA. *Via* confocal microscopy, the formation of endocytic vesicles during the internalization of receptor molecules was revealed. CPZ, MDC, and mutant dynamin all affected both the formation of clathrin-coated pits and the assembly of clathrin (Law et al., 2011; Schwartz et al., 2012; Smani et al., 2012). The role of this receptor in the physiology and pathophysiology of hypertension and cardiovascular homeostasis may be clarified by the fact that the clathrin-mediated endocytic pathway is considered a major route for the internalization of GC-A/NPRA.

Short signal-sequence motifs appear to be essential to the internalization and intracellular trafficking of plasma membrane receptors, which are thought to send the ligand-receptor cargo into trafficking endocytic vesicles (Pandey, 2009; Kozik et al., 2010; Pandey, 2010; Davey et al., 2012; Pandey, 2015). These small motifs comprise a linear array of a short sequence of amino acids containing 2–6 amino acid residues, however, only 2–3 amino acids of which are essential to receptor internalization and intracellular trafficking processes (Bonifacino and Traub, 2003; Davey et al., 2012; Mardones et al., 2013). The sequence motif Gly^{920}-Asp^{921}-Ala^{922}-Tyr^{923} (GDAY) in the C-terminal-region of GC-A/NPRA acts to promote the endocytosis and trafficking processes of NPRA (Pandey et al., 2005). Gly^{920} and Tyr^{923} residues in GDAY direct internalization of GC-A/NPRA, but Asp^{921} provides an acidic environment for GDAY signaling in the intracellular routing and subcellular trafficking processes. Site-directed mutagenesis of Gly^{920} and Tyr^{923} residues to Ala blocked the endocytosis of GC-A/NPRA by 50%; however, no effect on the recycling process was found. The site-directed mutation of Asp^{921} to Ala did not seem to affect receptor endocytosis, but it did potentially prevent the recycling of internalized receptors to the plasma membrane. We have demonstrated that FQQI short amino acid motif also plays a critical role in the endocytosis and subcellular trafficking of GC-A/NPRA (Mani et al., 2016; Mani and Pandey, 2019). Confocal immunofluorescence analyses showed that WT receptor (eGFP-GC-A/NPRA) was rapidly internalized and redistributed into cellular compartments, but the mutant FQQI/AAAA motif markedly inhibited endocytosis, signaling process, and subcellular trafficking of GC-A/NPRA (Mani et al., 2016; Mani and Pandey, 2019). FQQI short sequence motif plays a significant role in maintaining continuous receptor signaling. These findings expanded our knowledge of the cellular and molecular mechanisms of internalization, subcellular trafficking, and concurrent simultaneous signaling of GC-A/NPRA in intact cell.

GC-A/NPRA regulates renal hemodynamics, blood pressure, and cardiovascular events

The use of gene-targeting methods in mice has yielded novel approaches to decipher the biological and pathophysiological functions of the ablated gene products in intact animals *in vivo* (Takahashi and Smithies, 1999; Kim et al., 2002). Genetic strategies have generated mice carrying gene knockout (KO) or gene duplication, providing proof-of-concept for the physiological and pathophysiological roles of GC-A/NPRA in the regulation of renal and cardiovascular hemodynamic parameters (John et al., 1995; Lopez et al., 1995; Kishimoto et al., 1996; Oliver et al., 1997, 1998; Matsukawa et al., 1999; Pandey et al., 1999; Shi et al., 2003; Vellaichamy et al., 2005; Ellmers et al., 2007). Early studies demonstrated that the ablation of *Npr1* (encoding GC-A/NPRA) led to an increase in BP in *Npr1* KO mice (Oliver et al., 1997; Shi et al., 2001, 2003). Investigations in our laboratory have shown that at birth, loss of NPRA permitted increased synthesis and release of renin in KO mice compared with their WT counterparts; however, in adult mice, ANG II levels, along with circulating and kidney renin contents, were greatly reduced in *Npr1* null mutant KO mice compared to *Npr1* WT mice (Shi et al., 2001). Those studies showed that the reduced renin levels in the adult KO mice were largely due to a progressive increase in high BP, inhibiting renin synthesis and secretion from the juxtaglomerular (JG) cells of the kidneys (Shi et al., 2001; Pandey, 2008).

Studies from our laboratory further determined the quantitative contribution and mechanisms mediating the renal and cardiac hemodynamic responsiveness with decreasing or increasing numbers of *Npr1* gene copies (Shi et al., 2003; Vellaichamy et al., 2005, 2014; Das et al., 2010; Kumar et al., 2017;

Periyasamy et al., 2019). Pure blood volume expansion of *Npr1* KO and gene-duplicated mice was used to determine the effect on renal blood flow (RBF), urine flow, glomerular filtration rate (GFR), and release of Na^+ and K^+ *Npr1* KO (0-copy), WT (2-copy), and gene-duplicated (4-copy) mice (Shi et al., 2003). Interestingly, hemodilution did not occur in whole blood, and plasma protein levels were not affected. Significant functional responses in RBF, Na^+ excretion, and GFR were observed in *Npr1* WT (2-copy) and gene-duplicated (4-copy) mice but not in KO (0-copy) mice. Those previous studies indicated that mediating renal hemodynamic mechanisms and Na^+ excretion in genetically modified *Npr1* mutant mice are heavily influenced by the ANP/NPRA axis (Shi et al., 2003). Both RBF and GFR were significantly reduced in *Npr1* 0-copy KO mice but increased in 4-copy gene-duplicated mice compared with 2-copy WT mice after pure blood volume expansion in these animals (Shi et al., 2003).

The ablation of *Npr1* is known to increase BP of homozygous KO mice, which was not affected by either minimal or high-salt diets. This suggested that the major effect of GC-A/NPRA may occur at the level of the vasculature and is likely independent of salt concentrations (Lopez et al., 1995). In contrast, later studies showed chronic elevation of BP in mice fed with high-salt diets when *Npr1* was disrupted (Oliver et al., 1998; Zhao et al., 2007, 2013). Studies with *Nppa* KO mice have also shown that defects in ANP synthesis may cause salt-sensitive hypertension in these mutant animals (John et al., 1995; Melo et al., 1998). The physiological and pathophysiological roles of the ANP/NPRA system in the regulation of high BP and renal and cardiac dysfunction have been demonstrated in genetic mouse models of both *Nppa* and *Npr1* (John et al., 1995; Lopez et al., 1995; Oliver et al., 1997, 1998; Pandey et al., 1999; Shi et al., 2003; Vellaichamy et al., 2005; Ellmers et al., 2007; Das et al., 2020; Subramanian et al., 2022). Genetic defects that reduce the activity of GC receptors may contribute to hypertension, leading to renal and cardiac dysfunction and congestive heart failure (CHF) in mutant animals (Shi et al., 2003; Ellmers et al., 2007; Vellaichamy et al., 2007; Pandey, 2008; Das et al., 2012; Vellaichamy et al., 2014; Subramanian et al., 2016; Das et al., 2020). The consequences of the ablation of NPs and NPRs in mice and the resultant specific phenotypes are presented in Table 1. The ablation of GC-A/NPRA greatly increases high BP, altered levels of renin, ANG II, other components of RAAS, and lethal vascular and cardiac disorders, resembling untreated hypertensive heart disease patients (Vellaichamy et al., 2007; Sezai et al., 2010; Zhao et al., 2013; Vellaichamy et al., 2014; Kumar et al., 2017; Periyasamy et al., 2019; Das et al., 2020; Sangaralingham et al., 2022), although *Npr1* gene duplication in mice showed significantly increased levels of cGMP and reduced BP with increasing *Npr1* gene copy numbers in a gene-dose-dependent manner (Oliver et al., 1998; Pandey et al., 1999; Shi et al., 2003; Zhao et al., 2007; Vellaichamy et al., 2014; Periyasamy et al., 2019; Das et al., 2020). ANP and BNP expression is increased in patients with cardiac hypertrophy and CHF; whether the protective role of NPs and the GC-A/NPRA system are activated by reducing the harmful effects of high BP caused by retention of sodium and fluid volume; by inhibiting the RAAS; or as a result of the hypertrophic and/or fibrotic remodeling in the kidney, heart, and vasculature (Cannone et al., 2019; Rubattu et al., 2019). The GC-A/NPRA system is crucial to the regulation of systemic and intracellular components of RAAS (Shi et al., 2001; Pandey, 2008). ANP-BNP concentrations are usually found at much higher levels in the cardiac tissues and plasma of CHF patients (Wei et al., 1993a,b; Chen and Burnett, 1998). Both *Nppa* and *Nppb* are overexpressed in the hypertrophied heart and may act as endogenous protective mechanisms against maladaptive cardiac hypertrophy and cardiovascular disorders (Masciotra et al., 1999; Knowles et al., 2001; Volpe, 2014; Reginauld et al., 2019). GC-A/NPRA seems to be downregulated in the severe chronic CHF patients. Genetic disruption of *Npr1* in mice increases the cardiac mass, leading to hypertrophic growth and disorders (John et al., 1995; Oliver et al., 1997; Vellaichamy et al., 2005; Ellmers et al., 2007; Zhao et al., 2013; Subramanian et al., 2016). There is evidence of a significant inverse relationship between left ventricular cardiac hypertrophy and myocardial *Nppa* and *Nppb* expression, suggesting that ANP and BNP expression play a protective role in cardiovascular disorders and CHF (Wei et al., 1993b; Masciotra et al., 1999; Kobayashi et al., 2012; Sangaralingham et al., 2022). It has been recently suggested that CNP is synthesized in the cardiac myocytes and endothelial cells also preserves heart structure–function and coronary reactivity (Moyes et al., 2020).

GC-A/NPRA regulation of metabolic and immunogenic responses

Decreased plasma levels of ANP are known to be associated with obesity, insulin resistance, energy, and glucose metabolism in human patients (Wang et al., 2007; Birkenfeld et al., 2008; Coue and Moro, 2016; Cannone et al., 2019). Thus, ANP-BNP/GC-A/NPRA signaling has been suggested as playing a role in the regulation of whole-body metabolism and diabetic conditions (Moro, 2013; Coue et al., 2015). The GC-A/NPRA system has been shown to enhance lipid mobilization, mitochondrial oxidative pathway, and fat oxidation, maintaining energy expenditure and fatty acid supply to cardiac and skeletal muscle metabolic processes (Tsukamoto et al., 2009; Birkenfeld et al., 2012; Engeli et al., 2012; Schlueter et al., 2014). On the other hand, NPRC exhibits a lipolytic effect of NPs (ANP, BNP). Mice challenged with low temperature were shown to have increased release of ANP but reduced levels of NPRC in both white and brown adipocytes (Sengenes et al., 2002; Bordicchia et al., 2012). In fact, insulin enhanced the NPRC expression in adipocytes in a glucose-dependent manner (Bordicchia et al., 2016). Defective or absent NPs/GC-A/NPRA signaling may promote maladaptive metabolic disorders that lead in decreased mitochondrial function, hyperglycemia, insulin resistance, and lipid accumulation, in turn, leading to hypertension and CVD in humans. At balance, the

TABLE 1 Nomenclature, distribution, and gene-knockout phenotypes of natriuretic peptides and their specific receptors.

Peptide/Protein	Gene	Distribution	Gene-KO phenotype in mice	Literature cited
ANP	*Nppa*	Heart, kidney, brain,ovary, testis, and pituitary	Hypertension, hypertrophy, heart failure hypertension	John et al. (1995), Steinhelper et al. (1990), Lin et al. (1995), Melo et al. (1999), Tankersley et al. (2010)
BNP	*Nppb*	Brain and heart	Ventricular fibrosis, skeletal and vascular abnormalities	Tamura et al. (2000), Ogawa et al. (1994), Holditch et al. (2016)
CNP	*Nppc*	Vascular endothelium Brain, kidney, heart, and testis	Reduced long bone growth, dwarfism, abnormal chondrocyte growth	Chusho et al. (2001), Yasoda et al. (2004), Wang et al. (2007)
Guanylin		Intestine, kidney, brain, liver	Blockade of intestinal sodium and water excretion	Sangaralingham et al. (2022), Mattingly et al. (1994)
Uroguanylin		Intestine, kidney, Brain, liver	Disruption of intestinal fluid-ion balance, increase of BP	Sangaralingham et al. (2022), Mattingly et al. (1994)
GC-A/ NPRA	*Npr1*	Heart, kidney, adrenal glands, brain, lung, ovary, testis, thymus, vasculature, pituitary gland	Volume regulation, hypertension, cardiac hypertrophy and fibrosis, inflammation, cardiac overload, reduced testosterone, decreased estrogen	Ellmers et al. (2007), Oliver et al. (1997), Shi et al. (2003), Vellaichamy et al. (2005), Vellaichamy et al. (2014), Lopez et al. (1995), Das et al. (2010), Periyasamy et al. (2019), Zhao et al. (2007), Das et al. (2020), Subramanian et al. (2016), Reinhart et al. (2006), Nakanishi et al. (2005)
GC-B/NPRB	*Npr2*	Brain, heart, lung, ovary, pituitary gland, testis, cartilage, thymus, vasculature	Decreased adiposity, dwarfism, female sterility, seizures, vascular abnormalities	Tamura et al. (2004), Langenickel et al. (2006)
NPRC	*Npr3*	Kidney, brain, heart, intestine, liver, vasculature	Skeletal over-growth, bone deformation, long bone overgrowth	Jaubert et al. (1999), Matsukawa et al. (1999)
GC-C	*Gc-c*	Intestine, kidney, liver, brain	Resistance to exogenous *E. coli* heat-stable enterotoxin, disruption of intestinal fluid-ion homeostasis, unaffected BP	Schulz et al. (1997), Kuhn (2005)

ANP, atrial natriuretic peptide; BNP, brain natriuretic peptide; CNP, C-type natriuretic peptide; Nppa, coding for pro-atrial natriuretic peptide; Nppb, coding for pro-brain natriuretic peptide; Nppc, coding for pro-C-type natriuretic peptide. GC-A/NPRA, guanylyl cyclase/natriuretic peptide receptor-A; GC-B/NPRB, guanylyl cyclase/natriuretic peptide receptor-B; NPRC, natriuretic peptide receptor-C; Npr1, coding for GC-A/NPRA; Npr2, coding for GC-B/NPRB; Npr3, coding for NPRC; GC-C, guanylyl cyclase C.

circulating concentrations of ANP may serve as a protective mechanism; however, low circulating levels of ANP may be related to cardiometabolic syndrome and an increased risk of diabetes (Pereira et al., 2015; Ceddia and Collins, 2020).

Circulating levels of harmful proinflammatory cytokines, including interleukin-1β (IL-1β), interleukin-6 (IL-6), and tumor necrosis factor alpha (TNF-α) trigger to the development of hypertension and renal and cardiovascular disorders in humans (Testa et al., 1996; Vanderheyden et al., 2005). Studies from our laboratory have suggested that proinflammatory cytokines promote the onset of hypertension, kidney disorders, CHF, and cardiac hypertrophy in experimental animal models (Das et al., 2010; Vellaichamy et al., 2014; Subramanian et al., 2016; Kumar et al., 2017; Gogulamudi et al., 2019; Periyasamy et al., 2019; Das et al., 2020; Subramanian et al., 2022). Enhanced activation of IL-1β, IL-6, and TNF-α, induce phenotypic changes in myocardial apoptosis, deposition of matrix proteins, myocyte hypertrophy, and contractile dysfunction (Thaik et al., 1995; Sekiguchi et al., 2004; Vellaichamy et al., 2007, 2014; Subramanian et al., 2016). Furthermore, our previous findings have shown that the NPs/GC-A/NPRA cascade inhibits inflammation and immunogenic responses in the heart and kidneys (Vellaichamy et al., 2005; Das et al., 2010; Vellaichamy et al., 2014; Subramanian et al., 2016; Kumar et al., 2017; Das et al., 2020). In macrophages, ANP

blocked TNF-α production as well as TNF-α-induced adhesion molecule expression in endothelial cells (Tsukagoshi et al., 2001; Vollmer, 2005). We have found that genetically based differences in the expression levels of *Npr1* affect the contents of proinflammatory cytokine (Das et al., 2012; Zhao et al., 2013; Vellaichamy et al., 2014; Subramanian et al., 2016; Gogulamudi et al., 2019). Ablation of *Npr1* activates proinflammatory cytokine gene expression in addition to protein levels involved in cardiac hypertrophy and exaggerated ventricular remodeling, leading to cardiac dysfunction and CHF (Vellaichamy et al., 2014). However, in mice, cardiac proinflammatory cytokine expression and tissue remodeling were attenuated by *Npr1* gene duplication (Das et al., 2012; Vellaichamy et al., 2014; Subramanian et al., 2016; Kumar et al., 2017). *Npr1*$^{-/-}$ mutant mice expressed elevated levels of TNF-α, IL-6, interferon-gamma (IFN-γ), and transforming growth factor beta 1 (TGF-β1) mRNAs and proteins compared to *Npr1*$^{+/+}$ WT mice (Vellaichamy et al., 2014; Gogulamudi et al., 2019). In contrast, levels of IL-6, TNF-α, IFN-γ, and TGF-β1 were significantly reduced in *Npr1* gene-duplicated 3-copy and 4-copy mice compared to WT control mice.

The GC-A/NPRA-cGMP system exerts anti-inflammatory activity and inhibits the action of nuclear factor-kappa B (NF-κB) and proinflammatory cytokines (Tsukagoshi et al., 2001; Vollmer, 2005; Ellmers et al., 2007; Das et al., 2012; Pandey, 2018). Ablation of *Npr1* also enhances the expression of NF-kB, which seems to be involved in renal and cardiac disorders, fibrosis, hypertrophy, and extracellular matrix deposition (Vellaichamy et al., 2007, 2014; Kumar et al., 2017; Das et al., 2020). We speculated that activated NF-κB signaling triggers the production of proinflammatory cytokines, stimulating the development of tissue fibrosis and hypertrophy (Frantz et al., 2003; Purcell and Molkentin, 2003; Li et al., 2004; Vellaichamy et al., 2014; Subramanian et al., 2016; Das et al., 2020). Pathological forms of cardiac and renal remodeling, along with exacerbated disease conditions, are associated with the sustained activation of proinflammatory cytokines in experimental animals (Hirota et al., 1995; Baumgarten et al., 2002; Palmieri et al., 2002; Zhao et al., 2013; Vellaichamy et al., 2014; Pandey, 2021). We speculate that enhanced NPs and GC-A/NPRA signaling may have a protective effect on the heart and kidneys by inhibiting the expression of NF-κB, which is known to be a master regulator of proinflammatory cascade in health and disease.

NPs and sodium-glucose cotransporters inhibitors mediate renal homeostasis and hypertension

NPs (especially ANP and BNP) play critical and pleotropic roles in modulating the release of Na^+ and water from the kidneys thus decrease BP and prevent renal dysfunction (de Bold, 1985; Genest and Cantin, 1988; Brenner et al., 1990; Christensen, 1993; Levin et al., 1998; Pandey, 2005; Pandey, 2018). It was also reported that ANP restricted the intestinal absorption of water, Na^+, and glucose (Martinez Seeber et al., 1986; O'Grady, 1989; O'Grady et al., 1989; Gonzalez Bosc et al., 1997). Subsequently, ^{125}I-ANP binding studies demonstrated the presence of biologically active ANP receptor in the intestine jejunum (Bianchi et al., 1989). Further, it was suggested that the effect of ANP on the intestinal absorption of Na^+ could be due to the blockade of sodium-glucose cotransporter (SGLT-2) in the intestine (Gonzalez Bosc et al., 2000). In fact, the greedy organs such as kidney and intestine play critical roles in contributing toward hypertension and type-2 diabetes melitus (T2 DM) (Itoh and Tanaka, 2022). These authors suggested that a new type of therapeutic intervention might be necessary for the multigate-greedy organ dysfunction. In the retrospect, SGLT-2 inhibitors might provide expected outcome for the treatment and prevention of both hypertension and T2 DM conditions.

SGLT-2 inhibitors effectively lower the glucose and Na^+ levels, thus besides anti-diabetic effects, these agents may also exhibit renal and cardiac protective function (Maejima, 2019; Tsai et al., 2021). Major approved SGLT-2 inhibitors lower blood glucose, renal sodium, body weight and BP; however, improve adiposity and normalize serum uric acid and lipid levels (Alicic et al., 2018; Thomas and Cherney, 2018; Bailey, 2019; Tsai et al., 2021). It is stipulated that the renal-and cardio-protective mechanisms of SGLT-2 inhibitors include improved GFR, reduced inflammation, fibrosis, and sympathetic tone; as well as show enhanced mitochondrial biogenesis and function (Lee et al., 2019; Maejima, 2019; Zelniker and Braunwald, 2020; Margonato et al., 2021). It has been reported that SGLT-2 inhibitor treatment reduced the plasma ANP and BNP levels, thus reducing the cardiovascular risk in diabetic patients (Feng et al., 2020). However, N-terminal pro-BNP (NT-proBNP) is a better prognostic marker for prediction of heart failure in T2 DM (Cosson et al., 2009; Fraty et al., 2018).

Conclusion and perspectives

Over the past four decades, new insights have emerged regarding the structure–function relationship, signaling cascades, and physiological functions of NPs and their receptor systems. Cellular, molecular, and genetic investigations have revealed the complex molecular signaling systems of GC-A/NPRA and the significance of the intracellular cGMP in receptor biology, physiology/pathophysiology of hypertension, renal and cardiovascular disorders, and neurotransmission in CNS. Researchers have developed novel tools to delineate the domain structures, signaling mechanisms, internalization and cellular distribution, and downregulation and desensitization of GC-A/NPRA. Gene-targeting strategies (knockout and duplication) and transgenic approaches in mice have helped to clarify the role of NPs and GC-A/NPRA in creating and intervening in disease states using genetically modified mouse models. Molecular, cellular, and integrative approaches *in vitro*

and *in vivo* have provided revolutionary insights into the roles of NP/NPRA/cGMP signaling mechanisms in the regulation of hypertension and renal and cardiovascular diseases, paving the way toward discovery of effective therapeutics. The generation of the *Npr1*-deficient mouse model has contributed to advances in our understanding of the roles of GC-A/NPRA in the pathophysiology of hypertensive, endocrine, cardiovascular, and neurological dysfunction; however, the available models are still complex, partly due to the fact that the desired protein product is not present in the modified null animal models. As a result, the specific given phenotype may affect the degree of contribution of modifying gene products in disease conditions. In such situations, studies on haplotype or heterozygous mice might yield novel and useful information on disease states in animal models similar to those in genetic polymorphisms in human patients.

Despite the ample progress, there is still much to discover regarding the novel mechanisms of GC-coupled NP receptors and their ligands in relation to receptor activation mechanisms, cellular signaling, molecular modeling of structural determination, and physiological and pathophysiological functions. The mechanisms underlying ligand-dependent receptor activation and transmembrane signal transduction, which render the generation of second messenger cGMP, are not yet fully understood, nor are the molecular events that terminate the activated flow of receptor-mediated signal in the target cells. A more thorough understanding of the roles of NPs, GC-A/NPRA, and cGMP-specific signaling mechanisms in disease states is still needed. The identification and delineation of discrete switch points in signal transduction of GC-A/NPRA that elicit certain responses, such as renal function, cardioprotection, neurotransmission, and directional functions in reducing adverse BP and cardiovascular events, will provide new opportunities to intervene and deter renal, cardiac, endocrine, vascular, and neurological disorders. Future investigations should lead to exciting and innovative research strategies and new discoveries in the field of NPs and GC-A/NPRA/cGMP signaling mechanisms toward the prevention, diagnosis, and treatment of hypertension and renal and cardiovascular diseases.

Author contributions

KNP conceived and wrote the manuscript, and completed the composition and references.

Funding

The research in the author's laboratory is supported by the grants from the National Institutes of Health (HL062147 and DK133833).

Acknowledgments

I gratefully acknowledge the contributions of the previous and present members of my laboratory who have helped to advance our investigations. I sincerely acknowledge Ms. Loula Burton for reading the manuscript. I thank my wife Kamala Pandey for her help during the preparation of this manuscript. I sincerely acknowledge the work of numerous investigators that I could not include in this review.

Conflict of interest

The author declares that the research was conducted in the absence of any commercial or financial relationships that could be construed as a potential conflict of interest.

Publisher's note

All claims expressed in this article are solely those of the authors and do not necessarily represent those of their affiliated organizations, or those of the publisher, the editors and the reviewers. Any product that may be evaluated in this article, or claim that may be made by its manufacturer, is not guaranteed or endorsed by the publisher.

References

Airhart, N., Yang, Y. F., Roberts, C. T. Jr., and Silberbach, M. (2003). Atrial natriuretic peptide induces natriuretic peptide receptor-cGMP-dependent protein kinase interaction. *J. Biol. Chem.* 278, 38693–38698. doi: 10.1074/jbc.M304098200

Alicic, R. Z., Johnson, E. J., and Tuttle, K. R. (2018). SGLT2 inhibition for the prevention and treatment of diabetic kidney disease: a review. *Am. J. Kidney Dis.* 72, 267–277. doi: 10.1053/j.ajkd.2018.03.022

Arise, K. K., Kumar, P., Garg, R., Samivel, R., Zhao, H., Pandya, K., et al. (2020). Angiotensin II represses Npr1 expression and receptor function by recruitment of transcription factors CREB and HSF-4a and activation of HDACs. *Sci. Rep.* 10:4337. doi: 10.1038/s41598-020-61041-y

Arora, P., Wu, C., Khan, A. M., Bloch, D. B., Davis-Dusenbery, B. N., Ghorbani, A., et al. (2013). Atrial natriuretic peptide is negatively regulated by microRNA-425. *J. Clin. Invest.* 123, 3378–3382. doi: 10.1172/JCI67383

Arshad, N., and Visweswariah, S. S. (2012). The multiple and enigmatic roles of guanylyl cyclase C in intestinal homeostasis. *FEBS Lett.* 586, 2835–2840. doi: 10.1016/j.febslet.2012.07.028

Atarashi, K., Mulrow, P. J., Franco-Sanenz, R., Snajdar, R., and Rapp, J. (1984). Inhibition of aldosterone production by an atrial extract. *Science* 224, 992–994. doi: 10.1126/science.6326267

Bailey, C. J. (2019). Uric acid and the cardio-renal effects of SGLT2 inhibitors. *Diabetes Obes. Metab.* 21, 1291–1298. doi: 10.1111/dom.13670

Ballerman, B. J., Marala, R. B., and Sharma, R. K. (1988). Characterization and regulation by protein kinase C of renal glomerular atrial natriuretic peptide receptor-coupled guanylate cyclase. *Biochem. Biophys. Res. Commun.* 157, 755–761. doi: 10.1016/S0006-291X(88)80314-0

Baumgarten, G., Knuefermann, P., Kalra, D., Gao, F., Taffet, G. E., Michael, L., et al. (2002). Load-dependent and-independent regulation of proinflammatory

cytokine and cytokine receptor gene expression in the adult mammalian heart. *Circulation* 105, 2192–2197. doi: 10.1161/01.CIR.0000015608.37608.18

Berl, T., Mansour, J., and Teitelbaum, I. (1991). ANP stimulates phospholipase C in cultured RIMCT cells: roles of protein kinases and G proteins. *Am. J. Phys.* 260, F590–F595. PMID: 1849366

Bianchi, C., Thibault, G., De Lean, A., Genest, J., and Cantin, M. (1989). Atrial natriuretic factor binding sites in the jejunum. *Am. J. Phys.* 256, G436–G441. PMID: 2537581

Birkenfeld, A. L., Boschmann, M., Engeli, S., Moro, C., Arafat, A. M., Luft, F. C., et al. (2012). Atrial natriuretic peptide and adiponectin interactions in man. *PLoS One* 7:e43238. doi: 10.1371/journal.pone.0043238

Birkenfeld, A. L., Budziarek, P., Boschmann, M., Moro, C., Adams, F., Franke, G., et al. (2008). Atrial natriuretic peptide induces postprandial lipid oxidation in humans. *Diabetes* 57, 3199–3204. doi: 10.2337/db08-0649

Bonifacino, J. S., and Traub, L. M. (2003). Signals for sorting of transmembrane proteins to endosomes and lysosomes. *Annu. Rev. Biochem.* 72, 395–447. doi: 10.1146/annurev.biochem.72.121801.161800

Bordicchia, M., Ceresiani, M., Pavani, M., Minardi, D., Polito, M., Wabitsch, M., et al. (2016). Insulin/glucose induces natriuretic peptide clearance receptor in human adipocytes: a metabolic link with the cardiac natriuretic pathway. *Am. J. Physiol. Regul. Integr. Comp. Physiol.* 311, R104–R114. doi: 10.1152/ajpregu.00499.2015

Bordicchia, M., Liu, D., Amri, E. Z., Ailhaud, G., Dessi-Fulgheri, P., Zhang, C., et al. (2012). Cardiac natriuretic peptides act via p38 MAPK to induce the brown fat thermogenic program in mouse and human adipocytes. *J. Clin. Invest.* 122, 1022–1036. doi: 10.1172/JCI59701

Bose, A., Banerjee, S., and Visweswariah, S. S. (2020). Mutational landscape of receptor guanylyl cyclase C: functional analysis and disease-related mutations. *IUBMB Life* 72, 1145–1159. doi: 10.1002/iub.2283

Bovy, P. R. (1990). Structure activity in the atrial natriuretic peptide (ANP) family. *Med. Res. Rev.* 10, 115–142. doi: 10.1002/med.2610100105

Brackmann, M., Schuchmann, S., Anand, R., and Braunewell, K. H. (2005). Neuronal Ca2+ sensor protein VILIP-1 affects cGMP signalling of guanylyl cyclase B by regulating clathrin-dependent receptor recycling in hippocampal neurons. *J. Cell Sci.* 118, 2495–2505. doi: 10.1242/jcs.02376

Brenner, B. M., Ballerman, B. J., Gunning, M. E., and Zeidel, M. L. (1990). Diverse biological actions of atrial natriuretic peptide. *Physiol. Rev.* 70, 665–699.

Burnett, J. C. J., Granger, J. P., and Opgenorth, T. J. (1984). Effects of synthetic atrial natriuretic factor on renal function and renin release. *Am. J. Phys.* 247, F863–F866. PMID: 6238539

Cahill, P. A., Redmond, E. M., and Keenan, A. K. (1990). Vascular atrial natriuretic factor receptor subtypes are not independently regulated by atrial peptides. *J. Biol. Chem.* 265, 21896–21906. doi: 10.1016/S0021-9258(18)45823-1

Cannone, V., Cabassi, A., Volpi, R., and Burnett, J. C. (2019). Atrial natriuretic peptide: a molecular target of novel therapeutic approaches to cardio-metabolic disease. *Int. J. Mol. Sci.* 20:3265. doi: 10.3390/ijms20133265

Cappelli, K., Gialletti, R., Tesei, B., Bassotti, G., Fettucciari, K., Capomaccio, S., et al. (2019). Guanylin, Uroguanylin and Guanylate Cyclase-C are expressed in the gastrointestinal tract of horses. *Front. Physiol.* 10:1237. doi: 10.3389/fphys.2019.01237

Carrithers, S. L., Jackson, B. A., Cai, W. Y., Greenberg, R. N., and Ott, C. E. (2002). Site-specific effects of dietary salt intake on guanylin and uroguanylin mRNA expression in rat intestine. *Regul. Pept.* 107, 87–95. doi: 10.1016/S0167-0115(02)00069-1

Ceddia, R. P., and Collins, S. (2020). A compendium of G-protein-coupled receptors and cyclic nucleotide regulation of adipose tissue metabolism and energy expenditure. *Clin. Sci.* 134, 473–512. doi: 10.1042/CS20190579

Chang, C.-H., Kohse, K. P., Chang, B., Hirata, M., Jiang, B., Douglas, J. E., et al. (1990). Characterization of ATP-stimulated guanylyl cyclase activation in rat lung membranes. *Biochim. Biophys. Acta* 1052, 159–165. doi: 10.1016/0167-4889(90)90071-K

Chang, M. S., Lowe, D. G., Lewis, M., Hellmiss, R., Chen, E., and Goeddel, D. V. (1989). Differential activation by atrial and brain natriuretic peptides of two different receptor guanylate cyclases. *Nature* 341, 68–72. doi: 10.1038/341068a0

Chen, H. H., and Burnett, J. C. Jr. (1998). C-type natriuretic peptide the endothelial component of the natriuretic peptide system. *J. Cardiovasc. Pharmacol.* 32, S22–S28.

Chinkers, M., and Garbers, D. L. (1989). The protein kinase of the ANP receptor is required for signaling. *Science* 245, 1392–1394. doi: 10.1126/science.2571188

Chinkers, M., Garbers, D. L., Chang, M. S., Lowe, D. G., Chin, H., Goeddel, D. V., et al. (1989). A membrane form of guanylate cyclase is an atrial natriuretic peptide receptor. *Nature* 338, 78–83. doi: 10.1038/338078a0

Chinkers, M., Singh, S., and Garbers, D. L. (1991). Adenine nucleotides are required for activation of rat atrial natriuretic peptide receptor/guanylyl cyclase expressed in a baculovirus system. *J. Biol. Chem.* 266, 4088–4093. doi: 10.1016/S0021-9258(20)64289-2

Christensen, G. (1993). Cardiovascular and renal effects of atrial natriuretic factor. *Scand. J. Clin. Lab. Invest.* 53, 203–209. doi: 10.1080/00365519309088410

Chusho, H., Tamura, N., Ogawa, Y., Yasoda, A., Suda, M., Miyazawa, T., et al. (2001). Dwarfism and early death in mice lacking C-type natriuretic peptide. *Proc. Natl. Acad. Sci. U. S. A.* 98, 4016–4021. doi: 10.1073/pnas.071389098

Cohen, D., Koh, G. Y., Nikonova, L. N., Porter, J. G., and Maack, T. (1996). Molecular determinants of the clearance function of type-C receptor of natriuretic peptides. *J. Biol. Chem.* 271, 9863–9869. doi: 10.1074/jbc.271.16.9863

Cosson, E., Nguyen, M. T., Pham, I., Pontet, M., Nitenberg, A., and Valensi, P. (2009). N-terminal pro-B-type natriuretic peptide: an independent marker for coronary artery disease in asymptomatic diabetic patients. *Diabet. Med.* 26, 872–879. doi: 10.1111/j.1464-5491.2009.02788.x

Coue, M., Badin, P. M., Vila, I. K., Laurens, C., Louche, K., Marques, M. A., et al. (2015). Defective natriuretic peptide receptor signaling in skeletal muscle links obesity to type 2 diabetes. *Diabetes* 64, 4033–4045. doi: 10.2337/db15-0305

Coue, M., and Moro, C. (2016). Natriuretic peptide control of energy balance and glucose homeostasis. *Biochimie* 124, 84–91. doi: 10.1016/j.biochi.2015.05.017

Currie, M. G., Fok, K. F., Kato, J., Moore, R. J., Hamra, F. K., Duffin, K. L., et al. (1992). Guanylin: an endogenous activator of intestinal guanylate cyclase. *Proc. Natl. Acad. Sci. U. S. A.* 89, 947–951. doi: 10.1073/pnas.89.3.947

Das, S., Au, E., Krazit, S. T., and Pandey, K. N. (2010). Targeted disruption of guanylyl cyclase-A/natriuretic peptide receptor-A gene provokes renal fibrosis and remodeling in null mutant mice: role of proinflammatory cytokines. *Endocrinology* 151, 5841–5850. doi: 10.1210/en.2010-0655

Das, S., Neelamegam, K., Peters, W. N., Periyasamy, R., and Pandey, K. N. (2020). Depletion of cyclic-GMP levels and inhibition of cGMP-dependent protein kinase activate p21(Cip1) /p27(Kip1) pathways and lead to renal fibrosis and dysfunction. *FASEB J.* 34, 11925–11943. doi: 10.1096/fj.202000754R

Das, S., Periyasamy, R., and Pandey, K. N. (2012). Activation of IKK/NF-kappaB provokes renal inflammatory responses in guanylyl cyclase/natriuretic peptide receptor-A gene-knockout mice. *Physiol. Genomics* 44, 430–442. doi: 10.1152/physiolgenomics.00147.2011

Davey, N. E., Van Roey, K., Weatheritt, R. J., Toedt, G., Uyar, B., Altenberg, B., et al. (2012). Attributes of short linear motifs. *Mol. BioSyst.* 8, 268–281. doi: 10.1039/C1MB05231D

de Bold, A. J. (1985). Atrial natriuretic factor a hormone produced by the heart. *Science* 230, 767–770. doi: 10.1126/science.2932797

de Bold, A. J., Borenstein, H. B., Veress, A. T., and Sonnenberg, H. (1981). A rapid and potent natriuretic response to intravenous injection of atrial myocardial extract in rats. *Life Sci.* 28, 89–94. doi: 10.1016/0024-3205(81)90370-2

DeLean, A., McNicoll, N., and Labrecque, J. (2003). Natriuretic peptide receptor-A activation stabilizes a membrane distal dimer interface. *J. Biol. Chem.* 278, 11159–11166. doi: 10.1074/jbc.M212862200

DeLean, A., Racz, K., Gutkowska, J., Nguyen, T. T., Cantin, M., and Genest, J. (1984). Specific receptor-mediated inhibition by atrial natriuretic factor of hormone-stimulated steroidogenesis in cultured bovine adrenal cells. *Endocrinology* 115, 1636–1638.

Dickey, D. M., Flora, D. R., and Potter, L. R. (2011). Antibody tracking demonstrates cell type-specific and ligand-independent internalization of guanylyl cyclase A and natriuretic peptide receptor C. *Mol. Pharmacol.* 80, 155–162. doi: 10.1124/mol.110.070573

Drewett, J. G., and Garbers, D. L. (1994). The family of guanylyl cyclase receptors and their ligands. *Endocr. Rev.* 15, 135–162. doi: 10.1210/edrv-15-2-135

Duda, T., Goraczniak, R. M., and Sharma, R. K. (1991). Site-directed mutational analysis of a membrane guanylate cyclase cDNA reveals the atrial natriuretic factor signaling site. *Proc. Natl. Acad. Sci. U. S. A.* 88, 7882–7886. doi: 10.1073/pnas.88.17.7882

Duda, T., Goraczniak, R. M., and Sharma, R. K. (1993a). Core sequence of ATP regulatory module in receptor guanylate cyclases. *FEBS Lett.* 315, 143–148. PMID: 8093355

Duda, T., Goraczniak, R. M., and Sharma, R. K. (1993b). The glycine residue of ATP regulatory module in receptor guanylate cyclases that is essential in natriuretic factor signaling. *FEBS Lett.* 335, 309–314. doi: 10.1016/0014-5793(93)80408-M

Duda, T., and Sharma, R. K. (1990). Regulation of guanylate cyclase activity by atrial natriuretic factor and protein kinase C. *Mol. Cell. Biochem.* 93, 179–184.

Duda, T., and Sharma, R. K. (1995). ATP modulation of the ligand binding and signal transduction activities of the type C natriuretic peptide receptor guanylate cyclase Mol. *Cell Biochem.* 152, 179–183. doi: 10.1007/BF01076081

Ellmers, L. J., Scott, N. J., Piuhola, J., Maeda, N., Smithies, O., Frampton, C. M., et al. (2007). Npr1-regulated gene pathways contributing to cardiac hypertrophy and fibrosis. *J. Mol. Endocrinol.* 38, 245–257. doi: 10.1677/jme.1.02138

Emmeluth, C., Drummer, C., Gerzer, R., and Bie, P. (1992). Roles of cephalic Na^+ concentration and urodilatin in control of renal Na^+ excretion. *Am. J. Physiol.* 262, F513–F516.

Engeli, S., Birkenfeld, A. L., Badin, P. M., Bourlier, V., Louche, K., Viguerie, N., et al. (2012). Natriuretic peptides enhance the oxidative capacity of human skeletal muscle. *J. Clin. Invest.* 122, 4675–4679. doi: 10.1172/JCI64526

Feller, S. M., Mägert, H. J., Schulz-Knappe, P., and Forssmann, W. G. (1990). "Urodilatin (hANF 95-126)-Characteristics of a new atrial natriuretic factor peptide" in *Atrial Natriuretic Factor*. ed. A. D. Struthers (Oxford: UK Blackwell), 209–226.

Feng, X., Gu, Q., Gao, G., Yuan, L., Li, Q., and Zhang, Y. (2020). The plasma levels of atrial natriuretic peptide and brain natriuretic peptide in type 2 diabetes treated with sodium-glucose cotransporter-2 inhibitor. *Ann. Endocrinol.* 81, 476–481. doi: 10.1016/j.ando.2020.07.1113

Forte, L. R., London, R. M., Freeman, R. H., and Krause, W. J. (2000). Guanylin peptides: renal actions mediated by cyclic GMP. *Am. J. Physiol. Renal Physiol.* 278, F180–F191. doi: 10.1152/ajprenal.2000.278.2.F180

Foster, D. C., and Garbers, D. L. (1998). Dual role for adenine nucleotides in the regulation of the atrial natriuretic peptide receptor guanylyl cyclase-a. *J. Biol. Chem.* 273, 16311–16318. doi: 10.1074/jbc.273.26.16311

Frantz, S., Fraccarollo, D., Wagner, H., Behr, T. M., Jung, P., Angermann, C. E., et al. (2003). Sustained activation of nuclear factor kappa B and activator protein 1 in chronic heart failure. *Cardiovasc. Res.* 57, 749–756. doi: 10.1016/S0008-6363(02)00723-X

Fraty, M., Velho, G., Gand, E., Fumeron, F., Ragot, S., Sosner, P., et al. (2018). Prognostic value of plasma MR-proADM vs NT-proBNP for heart failure in people with type 2 diabetes: the SURDIAGENE prospective study. *Diabetologia* 61, 2643–2653. doi: 10.1007/s00125-018-4727-7

Fuller, F., Porter, J. G., Arfsten, A. E., Miller, J., Schilling, J. W., Scarborough, R. M., et al. (1988). Atrial natriuretic peptide clearance receptor. Complete sequence and functional expression of cDNA clones. *J. Biol. Chem.* 263, 9395–9401. doi: 10.1016/S0021-9258(19)76554-5

Garbers, D. L. (1999). The guanylyl cyclase receptors. *Methods* 19, 477–484. doi: 10.1006/meth.1999.0890

Garbers, D. L., and Lowe, D. G. (1994). Guanylyl cyclase receptors. *J. Biol. Chem.* 269, 30714–30744.

Garg, R., Oliver, P. M., Maeda, N., and Pandey, K. N. (2002). Genomic structure, organization, and promoter region analysis of murine guanylyl cyclase/atrial natriuretic peptide receptor-A gene. *Gene* 291, 123–133. doi: 10.1016/S0378-1119(02)00589-9

Garg, R., and Pandey, K. N. (2003). Angiotensin II-mediated negative regulation of Npr1 promoter activity and gene transcription. *Hypertension* 41, 730–736. doi: 10.1161/01.HYP.0000051890.68573.94

Gazzano, H., Wu, H. I., and Waldman, S. A. (1991). Adenine nucleotide regulation of particulate guanylate cyclase from rat lung. *Biochim. Biophys. Acta* 1077, 99–106. doi: 10.1016/0167-4838(91)90531-4

Genest, J., and Cantin, M. (1988). The atrial natriuretic factor: its physiology and biochemistry. *Rev. Physiol. Biochem. Pharmacol.* 110, 1–145. doi: 10.1007/BFb0027530

Goetz, K. L. (1990). Evidence that atriopeptin is not a physiological regulator of sodium excretion. *Hypertension* 15, 9–19. doi: 10.1161/01.HYP.15.1.9

Goetz, K. L. (1991). Renal natriuretic peptide (urodilatin?) and atriopeptin evolving concepts. *Am. J. Physiol.* 261, F921–F932.

Goetze, J. P., Bruneau, B. G., Ramos, H. R., Ogawa, T., de Bold, M. K., and de Bold, A. J. (2020). Cardiac natriuretic peptides. *Nat. Rev. Cardiol.* 17, 698–717. doi: 10.1038/s41569-020-0381-0

Gogulamudi, V. R., Mani, I., Subramanian, U., and Pandey, K. N. (2019). Genetic disruption of Npr1 depletes regulatory T cells and provokes high levels of proinflammatory cytokines and fibrosis in the kidneys of female mutant mice. *Am. J. Physiol. Renal Physiol.* 316, F1254–F1272. doi: 10.1152/ajprenal.00621.2018

Gonzalez Bosc, L. V., Elustondo, P. A., Ortiz, M. C., and Vidal, N. A. (1997). Effect of atrial natriuretic peptide on sodium-glucose cotransport in the rat small intestine. *Peptides* 18, 1491–1495. doi: 10.1016/S0196-9781(97)00240-4

Gonzalez Bosc, L. V., Majowicz, M. P., and Vidal, N. A. (2000). Effects of atrial natriuretic peptide in the gut. *Peptides* 21, 875–887. doi: 10.1016/S0196-9781(00)00222-9

Goodfriend, T. L., Elliott, M. E., and Atlas, S. A. (1984). Actions of synthetic atrial natriuretic factor on bovine adrenal glomerulosa. *Life Sci.* 35, 1675–1682. doi: 10.1016/0024-3205(84)90179-6

Goraczniak, R. M., Duda, T., and Sharma, R. K. (1992). A structural motif that defines the ATP-regulatory module of guanylate cyclase in atrial natriuretic factor signaling. *Biochem. J. Rev.* 282, 533–537. doi: 10.1042/bj2820533

Gutkowska, J., Tremblay, J., Antakly, T., Mayer, R., Mukaddam-Dahere, S., and Nemer, M. (1993). The atrial natriuretic peptide system in rat ovaries. *Endocrinology* 132, 693–700. doi: 10.1210/endo.132.2.8425488

Hama, N., Itoh, H., Shirakami, G., Sugga, S.-I., Komatsu, Y., Yoshimasa, T., et al. (1994). Detection of C-type natriuretic peptide in humban circulation and marked increase of plasma CNP level in septic shock patients. *Biochem. Biophys. Res. Commun.* 198, 1177–1182. doi: 10.1006/bbrc.1994.1166

Hamra, F. K., Forte, L. R., Eber, S. L., Pidhorodeckyj, N. V., Krause, W. J., Freeman, R. H., et al. (1993). Uroguanylin: structure and activity of a second endogenous peptide that stimulates intestinal guanylate cyclase. *Proc. Natl. Acad. Sci. U. S. A.* 90, 10464–10468. doi: 10.1073/pnas.90.22.10464

Haneda, M., Kikkawa, R., Maeda, S., Togawa, M., Koya, D., Horide, N., et al. (1991). Dual mechanism of angiotensin II inhibits ANP-induced mesangial cGMP accumulation. *Kidney Int.* 40, 188–194. doi: 10.1038/ki.1991.199

Hanks, S. K., Quinn, A. M., and Hunter, T. (1988). The protein kinase C family conserved features and deduced phylogeny of the catalytic domains. *Science* 241, 42–52. doi: 10.1126/science.3291115

He, X., Chow, D., Martick, M. M., and Garcia, K. C. (2001). Allosteric activation of a spring-loaded natriuretic peptide receptor dimer by hormone. *Science* 293, 1657–1662. doi: 10.1126/science.1062246

He, X. L., Dukkipati, A., Wang, X., and Garcia, K. C. (2005). A new paradigm for hormone recognition and allosteric receptor activation revealed from structural studies of NPR-C. *Peptides* 26, 1035–1043. doi: 10.1016/j.peptides.2004.08.035

Hirata, M., Chang, C. M., and Murad, F. (1989). Stimulatory effect of atrial natriuretic factor on phosphoinositide hydrolysis in cultured bovine aortic smooth muscle cells. *Biochim. Biophys. Acta Rev. Cancer* 1010, 346–351. doi: 10.1016/0167-4889(89)90060-8

Hirata, Y., Takata, S., Tomita, M., and Takaichi, S. (1985). Binding, internalization, and degradation of atrial natriuretic peptide in cultured vascular smooth muscle cells of rat. *Biochem. Biophys. Res. Commun.* 132, 976–984. doi: 10.1016/0006-291X(85)91903-5

Hirose, S., Akiyama, F., Shinjo, M., Ohno, H., and Murakami, K. (1985). Solubilization and molecular weight estimation of atrial natriuretic factor receptor from bovine adrenal cortex. *Biochem. Biophys. Res. Commun.* 130, 574–579. doi: 10.1016/0006-291X(85)90455-3

Hirota, H., Yoshida, K., Kishimoto, T., and Taga, T. (1995). Continuous activation of gp130, a signal-transducing receptor component for interleukin 6-related cytokines, causes myocardial hypertrophy in mice. *Proc. Natl. Acad. Sci. U. S. A.* 92, 4862–4866. doi: 10.1073/pnas.92.11.4862

Holditch, S. J., Schreiber, C. A., Burnett, J. C., and Ikeda, Y. (2016). Arterial remodeling in B-type natriuretic peptide knock-out females. *Sci. Rep.* 6:25623. doi: 10.1038/srep25623

Horvath, J., Ertl, T., and Schally, A. V. (1986). Effect of atrial natriuretic peptide on gonadotropin release in superfused rat pituitary cells. *Proc. Natl. Acad. Sci. U. S. A.* 83, 3444–3446. doi: 10.1073/pnas.83.10.3444

Huang, W., Lee, D., Yang, J., Carley, D. J., Trosby, M., Copolou, D. L., et al. (1992). Evidence for ANP production by rat placental cytotrophoblasts. *Endocrinology* 131, 919–924. PMID: 1386304

Huo, X., Abe, T., and Misono, K. S. (1999). Ligand binding-dependent limited proteolysis of the atrial natriuretic peptide juxtamembrane hinge structure essential for transmembrane signal transduction. *Biochemistry* 38, 16941–16951. doi: 10.1021/bi9919448

Itoh, H., and Tanaka, M. (2022). "Greedy Organs Hypothesis" for sugar and salt in the pathophysiology of non-communicable diseases in relation to sodium-glucose co-transporters in the intestines and the kidney. *Metabol. Open* 13:100169. doi: 10.1016/j.metop.2022.100169

Jaubert, J., Jaubert, F., Martin, N., Washburn, L. L., Lee, B. K., Eicher, E. M., et al. (1999). Three new allelic mouse mutations that cause skeletal overgrowth involve the natriuretic peptide receptor C gene (Npr3). *Proc. Natl. Acad. Sci. U. S. A.* 96, 10278–10283. doi: 10.1073/pnas.96.18.10278

Jewett, J. R., Koller, K. J., Goeddel, D. V., and Lowe, D. G. (1993). Hormonal induction of low affinity receptor guanylyl cyclase. *EMBO J.* 12, 769–777. doi: 10.1002/j.1460-2075.1993.tb05711.x

John, S. W., Krege, J. H., Oliver, P. M., Hagaman, J. R., Hodgin, J. B., Pang, S. C., et al. (1995). Genetic decreases in atrial natriuretic peptide and salt-sensitive hypertension. *Science* 267, 679–681. doi: 10.1126/science.7839143

Khurana, M. L., Mani, I., Kumar, P., Ramasamy, C., and Pandey, K. N. (2022). Ligand-dependent downregulation of guanylyl cyclase/natriuretic peptide receptor-A: role of miR-128 and miR-195. *Int. J. Mol. Sci.* 23:13381. doi: 10.3390/ijms232113381

Khurana, M. L., and Pandey, K. N. (1993). Receptor-mediated stimulatory effect of atrial natriuretic factor, brain natriuretic peptide, and C-type natriuretic peptide on testosterone production in purified mouse Leydig cells: activation of cholesterol side-chain cleavage enzyme. *Endocrinology* 133, 2141–2149. doi: 10.1210/endo.133.5.8404664

Khurana, M. L., and Pandey, K. N. (1994). Modulation of guanylate cyclase-coupled atrial natriuretic factor receptor activity by mastoparan and ANF in murine Leydig tumor cells: role of G-proteins. *Biochim. Biophys. Acta* 1224, 61–67. doi: 10.1016/0167-4889(94)90113-9

Khurana, M. L., and Pandey, K. N. (1995). Catalytic activation of guanylate cyclase/atrial natriuretic factor receptor by combined effects of ANF and GTP gamma S in plasma membranes of Leydig tumor cells: involvement of G-proteins. *Arch. Biochem. Biophys.* 316, 392–398. doi: 10.1006/abbi.1995.1052

Khurana, M. L., and Pandey, K. N. (1996). Atrial natriuretic peptide inhibits the phosphoinositide hydrolysis in murine Leydig tumor cells. *Mol. Cell. Biochem.* 158, 97–105. PMID: 8817470

Kim, H. S., Lu, G., John, S. W. M., Maeda, N., and Smithies, O. (2002). Molecular phenotyping for analyzing subtle genetic effects in mice application to an angiotensinogen gene titration. *Proc. Natl. Acad. Sci. U. S. A.* 99, 4602–4607. doi: 10.1073/pnas.072083799

Kishimoto, I., Dubois, S. K., and Garbers, D. L. (1996). The heart communicates with the kidney exclusively through the guanylyl cyclase-A receptor acute handling of sodium and water in response to volume expansion. *Proc. Natl. Acad. Sci. U. S. A.* 93, 6215–6219. doi: 10.1073/pnas.93.12.6215

Kishimoto, I., Tokudome, T., Nakao, K., and Kangawa, K. (2011). Natriuretic peptide system: an overview of studies using genetically engineered animal models. *FEBS J.* 278, 1830–1841. doi: 10.1111/j.1742-4658.2011.08116.x

Knowles, J. W., Esposito, G., Mao, L., Hagaman, J. R., Fox, J. E., Smithies, O., et al. (2001). Pressure-independent enhancement of cardiac hypertrophy in natriuretic peptide receptor A-deficient mice. *J. Clin. Invest.* 107, 975–984. doi: 10.1172/JCI11273

Kobayashi, D., Yamaguchi, N., Takahashi, O., Deshpande, G. A., and Fukui, T. (2012). Human atrial natriuretic peptide treatment for acute heart failure: a systematic review of efficacy and mortality. *Can. J. Cardiol.* 28, 102–109. doi: 10.1016/j.cjca.2011.04.011

Koh, G. Y., Nussenzweig, D. R., Okolicany, J., Price, D. A., and Maack, T. (1992). Dynamics of atrial natriuretic factor-guanylate cyclase recetpors and receptor-ligand complexes in cultured glomerular mesangial and renomedullary interstitial cells. *J. Biol. Chem.* 267, 11987–11994. doi: 10.1016/S0021-9258(19)49795-0

Koller, K. J., deSauvage, F. J., Lowe, D. G., and Goeddel, D. V. (1992). Conservation of the kinase-like regulatory domain is essential for activation of the natriuretic peptide receptor guanylyl cyclase. *Mol. Cell. Biol.* 12, 2581–2590. PMID: 1350322

Koller, K. J., Lipari, M. T., and Goeddel, D. V. (1993). Proper glycosylation and phosphorylation of the type a natriuretic peptide receptor are required for hormone-stimulated guanylyl cyclase activity. *J. Biol. Chem.* 268, 5997–6003. doi: 10.1016/S0021-9258(18)53418-9

Kozik, P., Francis, R. W., Seaman, M. N., and Robinson, M. S. (2010). A screen for endocytic motifs. *Traffic* 11, 843–855. doi: 10.1111/j.1600-0854.2010.01056.x

Kuhn, M. (2005). Cardiac and intestinal natriuretic peptides: insights from genetically modified mice. *Peptides* 26, 1078–1085. doi: 10.1016/j.peptides.2004.08.031

Kumar, R., Cartledge, W. A., Lincoln, T. M., and Pandey, K. N. (1997). Expression of guanylyl cyclase-A/atrial natriuretic peptide receptor blocks the activation of protein kinase C in vascular smooth muscle cells. Role of cGMP and cGMP-dependent protein kinase. *Hypertension* 29, 414–421. doi: 10.1161/01.HYP.29.1.414

Kumar, P., Gogulamudi, V. R., Periasamy, R., Raghavaraju, G., Subramanian, U., and Pandey, K. N. (2017). Inhibition of HDAC enhances STAT acetylation, blocks NF-kappaB, and suppresses the renal inflammation and fibrosis in Npr1 haplotype male mice. *Am. J. Physiol. Renal Physiol.* 313, F781–F795. doi: 10.1152/ajprenal.00166.2017

Kurose, H., Inagami, T., and Ui, M. (1987). Participation of adenosine 5′ triphosphate in the activation of membrane-bound guanylate cyclase by the atrial natriuretic factor. *FEBS Lett.* 219, 375–379. doi: 10.1016/0014-5793(87)80256-9

Labrecque, J., McNicoll, N., Marquis, M., and De Lean, A. (1999). A disulfide-bridged mutant of natriuretic peptide receptor-A displays constitutive activity. Role of receptor dimerization in signal transduction. *J. Biol. Chem.* 274, 9752–9759. doi: 10.1074/jbc.274.14.9752

Langenickel, T. H., Buttgereit, J., Pagel-Langenickel, I., Lindner, M., Monti, J., Beuerlein, K., et al. (2006). Cardiac hypertrophy in transgenic rats expressing a dominant-negative mutant of the natriuretic peptide receptor B. *Proc. Natl. Acad. Sci. U. S. A.* 103, 4735–4740. doi: 10.1073/pnas.0510019103

Larose, L., McNicoll, N., Ong, H., and De Lean, A. (1991). Allosteric modulation by ATP of the bovine adrenal natriuretic factor R1 receptor functions. *Biochemistry* 30, 8990–8995. doi: 10.1021/bi00101a012

Larose, L., Rondeau, J. J., Ong, H., and De Lean, A. (1992). Phosphorylation of atrial natriuretic factor R1 receptor by serine/threonine protein kinases. Evidence for receptor regulation. *Mol. Cell. Biochem.* 115, 203–211. doi: 10.1007/BF00230332

Law, H. T., Lin, A. E., Kim, Y., Quach, B., Nano, F. E., and Guttman, J. A. (2011). *Francisella tularensis* uses cholesterol and clathrin-based endocytic mechanisms to invade hepatocytes. *Sci. Rep.* 1:192. doi: 10.1038/srep00192

Lee, C. Y., and Burnett, J. C. Jr. (2007). Natriuretic peptides and therapeutic applications. *Heart Fail. Rev.* 12, 131–142. doi: 10.1007/s10741-007-9016-3

Lee, W. C., Chau, Y. Y., Ng, H. Y., Chen, C. H., Wang, P. W., Liou, C. W., et al. (2019). Empagliflozin protects HK-2 cells from high glucose-mediated injuries via a mitochondrial mechanism. *Cells* 8:1085. doi: 10.3390/cells8091085

Lefkowitz, R. J., Pitcher, J., Krueger, K., and Daaka, Y. (1998). Mechanisms of β-adrenergic receptor desensitization and resensitization. *Adv. Pharmacol.* 42, 416–420. PMID: 9327928

Leitman, D. C., Andresen, J. W., Catalano, R. M., Waldman, S. A., Tuan, J. J., and Murad, F. (1988). Atrial natriuretic peptide binding, cross-linking, and stimulation of cyclic GMP accumulation and particulate guanylate cyclase activity in cultured cells. *J. Biol. Chem.* 263, 3720–3728. doi: 10.1016/S0021-9258(18)68984-7

Levin, E. R., Gardner, D. G., and Samson, W. K. (1998). Natriuretic peptides. *N. Engl. J. Med.* 339, 321–328. doi: 10.1056/NEJM199807303390507

Li, Y., Ha, T., Gao, X., Kelley, J., Williams, D. L., Browder, I. W., et al. (2004). NF-kappaB activation is required for the development of cardiac hypertrophy in vivo. *Am. J. Physiol.* 287, H1712–H1720. doi: 10.1152/ajpheart.00124.2004

Lin, K. F., Chao, J., and Chao, L. (1995). Human atrial natriuretic peptide gene delivery reduces blood pressure in hypertensive rats. *Hypertension* 26, 847–853. doi: 10.1161/01.HYP.26.6.847

Lisy, O., Jougasaki, M., Heublein, D. M., Schirger, J. A., Chen, H. H., Wennberg, P. W., et al. (1999). Renal actions of synthetic Dendrocespis natriuretic peptide. *Kidney Int.* 56, 502–508.

Liu, Y., Ruoho, E. R., Rao, V. D., and Hurley, J. H. (1997). Catalytic mechanism of the adenylyl cyclase modeling and mutational analysis. *Proc. Natl. Acad. Sci. U. S. A.* 94, 13414–13419. doi: 10.1073/pnas.94.25.13414

Lopez, M. J., Wong, S. K.-F., Kishimoto, I., Dubois, S., Mach, V., Friesen, J., et al. (1995). Salt-resistant hypertension in mice lacking the guanylyl cyclase-A receptor for atrial natriuretic peptide. *Nature* 378, 65–68. doi: 10.1038/378065a0

Lowe, D. G. (1997). "The guanylyl cyclase-B receptor" in *Natriuretic peptides in health and disease*. eds. W. K. Samson and E. R. Levin (Totowa, NJ: Humana Press), 35–50.

Lowe, D. G., Chang, M.-S., Hellmis, R., Chen, E., Singh, S., Garbers, D. L., et al. (1989). Human atrial natriuretic peptide receptor defines a new paradigm for second messenger signal transduction. *EMBO J.* 8, 1377–1384. doi: 10.1002/j.1460-2075.1989.tb03518.x

Lucas, K. A., Pitari, G. M., Kazerousnian, S., Ruiz-Stewart, I., Park, J., Schulz, S., et al. (2000). Guanylyl cyclases and signaling by cGMP. *Pharmacol. Rev.* 52, 375–414. PMID: 10977868

Maejima, Y. (2019). SGLT2 inhibitors play a salutary role in heart failure via modulation of the mitochondrial function. *Front. Cardiovasc. Med.* 6:186.

Mani, I., Garg, R., and Pandey, K. N. (2016). Role of FQQI motif in the internalization, trafficking, and signaling of guanylyl-cyclase/natriuretic peptide receptor-A in cultured murine mesangial cells. *Am. J. Physiol. Renal Physiol.* 310, F68–F84. doi: 10.1152/ajprenal.00205.2015

Mani, I., Garg, R., Tripathi, S., and Pandey, K. N. (2015). Subcellular trafficking of guanylyl cyclase/natriuretic peptide receptor-A with concurrent generation of intracellular cGMP. *Biosci. Rep.* 35, 1–17. doi: 10.1042/BSR20150136

Mani, I., and Pandey, K. N. (2019). Emerging concepts of receptor endocytosis and concurrent intracellular signaling: mechanisms of guanylyl cyclase/natriuretic peptide receptor-A activation and trafficking. *Cell. Signal.* 60, 17–30. doi: 10.1016/j.cellsig.2019.03.022

Marala, R., Duda, T., Goraczniak, R. M., and Sharma, R. K. (1992). Genetically tailored atrial natriuretic factor-dependent guanylate cyclase. Immunological and functional identity with 180 kDa membrane guanylate cyclase and ATP signaling site. *FEBS Lett.* 296, 254–258. doi: 10.1016/0014-5793(92)80298-U

Marala, R. B., and Sharma, R. K. (1988). Characterization of atrial-natriuretic factor-coupled membrane guanylate cyclase from rat and mouse testes. *Biochem. J.* 251, 301–304. doi: 10.1042/bj2510301

Mardones, G. A., Burgos, P. V., Lin, Y., Kloer, D. P., Magadan, J. G., Hurley, J. H., et al. (2013). Structural basis for the recognition of tyrosine-based sorting signals by the mu3A subunit of the AP-3 adaptor complex. *J. Biol. Chem.* 288, 9563–9571. doi: 10.1074/jbc.M113.450775

Margonato, D., Galati, G., Mazzetti, S., Cannistraci, R., Perseghin, G., Margonato, A., et al. (2021). Renal protection: a leading mechanism for cardiovascular benefit in patients treated with SGLT2 inhibitors. *Heart Fail. Rev.* 26, 337–345. doi: 10.1007/s10741-020-10024-2

Martinez Seeber, A., Vidal, N. A., Carchio, S. M., and Karara, A. L. (1986). Inhibition of water-sodium intestinal absorption by an atrial extract. *Can. J. Physiol. Pharmacol.* 64, 244–247. doi: 10.1139/y86-039

Masciotra, S., Picard, S., and Deschepper, C. F. (1999). Cosegregation analysis in genetic crosses suggests a protective role for atrial natriuretic factor against ventricular hypertrophy. *Circ. Res.* 84, 1453–1458. doi: 10.1161/01.RES.84.12.1453

Matsukawa, N., Grzesik, W. J., Takahashi, N., Pandey, K. N., Pang, S., Yamauchi, M., et al. (1999). The natriuretic peptide clearance receptor locally modulates the physiological effects of the natriuretic peptide system. *Proc. Natl. Acad. Sci. U. S. A.* 96, 7403–7408. doi: 10.1073/pnas.96.13.7403

Mattingly, M. T., Brandt, R. R., Heublein, D. M., Wei, C. M., Nir, A., and Burnett, J. C. Jr. (1994). Presence of C-type natriuretic peptide in human kidney and urine. *Kidney Int.* 46, 744–747. doi: 10.1038/ki.1994.329

Melo, L. G., Veress, A. T., Ackermann, U., Steinhelper, M. E., Pang, S. C., Tse, Y., et al. (1999). Chronic regulation of arterial blood pressure in ANP transgenic and knockout mice: role of cardiovascular sympathetic tone. *Cardiovasc. Res.* 43, 437–444. doi: 10.1016/S0008-6363(99)00104-2

Melo, L. G., Veress, A. T., Chong, C. K., Pang, S. C., Flynn, T. G., and Sonnenberg, H. (1998). Salt-sensitive hypertension in ANP knockout mice: potential role of abnormal plasma renin activity. *Am. J. Phys.* 274, R255–R261. doi: 10.1152/ajpregu.1998.274.1.R255

Meloche, S., McNicoll, N., Liu, B., Ong, H., and DeLean, A. (1988). Atrial natriuretic factor R1 receptor from bovine adrenal glomerulosa: purification characterization and modulation by amiloride. *Biochemistry* 27, 8151–8158. doi: 10.1021/bi00421a025

Meloche, S., Ong, H., Cantin, M., and DeLean, A. (1986). Affinity cross-linking of atrial natriuretic factor to its receptor in bovine adrenal zona glomerulosa. *J. Biol. Chem.* 261, 1525–1528. doi: 10.1016/S0021-9258(17)35971-9

Mishra, S. K., and Hoon, M. A. (2013). The cells and circuitry for itch responses in mice. *Science* 340, 968–971. doi: 10.1126/science.1233765

Misono, K. S., Grammer, R. T., Rigby, J. W., and Inagami, T. (1985). Photoaffinity labeling of atrial natriuretic factor receptor in bovine and rat adrenal cortical membranes. *Biochem. Biophys. Res. Commun.* 130, 994–1001. doi: 10.1016/0006-291X(85)91713-9

Misono, K. S., Ogawa, H., Qiu, Y., and Ogata, C. M. (2005). Structural studies of the natriuretic peptide receptor: a novel hormone-induced rotation mechanism for transmembrane signal transduction. *Peptides* 26, 957–968. doi: 10.1016/j.peptides.2004.12.021

Misono, K. S., Philo, J. S., Arakawa, T., Ogata, C. M., Qiu, Y., Ogawa, H., et al. (2011). Structure, signaling mechanism and regulation of the natriuretic peptide receptor guanylate cyclase. *FEBS J.* 278, 1818–1829. doi: 10.1111/j.1742-4658.2011.08083.x

Moro, C. (2013). Natriuretic peptides and fat metabolism. *Curr. Opin. Clin. Nutr. Metab. Care* 16, 645–649. doi: 10.1097/MCO.0b013e32836510ed

Moyes, A. J., Chu, S. M., Aubdool, A. A., Dukinfield, M. S., Margulies, K. B., Bedi, K. C., et al. (2020). C-type natriuretic peptide co-ordinates cardiac structure and function. *Eur. Heart J.* 41, 1006–1020. doi: 10.1093/eurheartj/ehz093

Mukhopadhyay, A. K., Bohnet, H. G., and Leidenberger, F. A. (1986). Testosterone production by mouse Leydig cells is stimulated in vitro by atrial natriuretic factor. *FEBS Lett.* 202, 111–116. doi: 10.1016/0014-5793(86)80659-7

Murthy, K. K., Thibault, G., and Cantin, M. (1989). Binding and intracellular degradation of atrial natriuretic factor by cultured vascular smooth muscle cells. *Mol. Cell. Endocrinol.* 67, 195–206. doi: 10.1016/0303-7207(89)90210-4

Nakanishi, M., Saito, Y., Kishimoto, I., Harada, M., Kuwahara, K., Takahashi, N., et al. (2005). Role of natriuretic peptide receptor guanylyl cyclase-A in myocardial infarction evaluated using genetically engineered mice. *Hypertension* 46, 441–447. doi: 10.1161/01.HYP.0000173420.31354.ef

Napier, M., Arcuri, K., and Vandlen, R. (1986). Binding and internalization of atrial natriuretic factor by high-affinity receptors in A10 smooth muscle cells. *Arch. Biochem. Biophys.* 248, 516–522. doi: 10.1016/0003-9861(86)90504-7

Nussenzveig, D. R., Lewicki, J. A., and Maack, T. (1990). Cellular mechanisms of the clearance function of type-C receptors of atrial natriuretic factor. *J. Biol. Chem.* 265, 20952–20958. doi: 10.1016/S0021-9258(17)45309-9

O'Grady, S. M. (1989). Cyclic nucleotide-mediated effects of ANF and VIP on flounder intestinal ion transport. *Am. J. Phys.* 256, C142–C146. doi: 10.1152/ajpcell.1989.256.1.C142

Obana, K., Naruse, N., Inagami, T., Brown, A. B., Naruse, K., Kurimoto, F., et al. (1985). Atrial natriuretic factor inhibits vasopressin secretion from rat posterior pituitary. *Biochem. Biophys. Res. Commun.* 132, 1088–1094. doi: 10.1016/0006-291X(85)91918-7

Ogawa, Y., Itoh, H., Tamura, N., Suga, S., Yoshimasa, T., Uehira, M., et al. (1994). Molecular cloning of the complementary DNA and gene that encode mouse brain natriuretic peptide and generation of transgenic mice that overexpress the brain natriuretic peptide gene. *J. Clin. Invest.* 93, 1911–1921. doi: 10.1172/JCI117182

O'Grady, S. M., Wolters, P. J., Hildebrand, K., and Brown, D. R. (1989). Regulation of ion transport in porcine gallbladder: effects of VIP and norepinephrine. *Am. J. Phys.* 257, C52–C57. doi: 10.1152/ajpcell.1989.257.1.C52

Oliver, P. M., Fox, J. E., Kim, R., Rockman, H. A., Kim, H. S., Reddick, R. L., et al. (1997). Hypertension, cardiac hypertrophy, and sudden death in mice lacking natriuretic peptide receptor a. *Proc. Natl. Acad. Sci. U. S. A.* 94, 14730–14735. doi: 10.1073/pnas.94.26.14730

Oliver, P. M., John, S. W., Purdy, K. E., Kim, R., Maeda, N., Goy, M. F., et al. (1998). Natriuretic peptide receptor 1 expression influences blood pressures of mice in a dose-dependent manner. *Proc. Natl. Acad. Sci. U. S. A.* 95, 2547–2551. doi: 10.1073/pnas.95.5.2547

Palaparti, A. L. Y., and Anand-Srivastava, M. B. (2000). Inhibition of atrial natriuretic peptide (ANP) C receptor expression by antisense oligonucleotides in A10 vascular smooth muscle cells is associated with attenuation of ANP-C receptor mediated inhibition of adenylyl cyclase. *Biochem. J.* 346, 312–320.

Palmieri, E. A., Benincasa, G., Di Rella, F., Casaburi, C., Monti, M. G., De Simone, G., et al. (2002). Differential expression of TNF-alpha, IL-6, and IGF-1 by graded mechanical stress in normal rat myocardium. *Am. J. Physiol.* 282, H926–H934. PMID: 11834488

Pandey, K. N. (1989). Stimulation of protein phosphorylation by atrial natriuretic factor in plasma membranes of bovine adrenal cortical cells. *Biochem. Biophys. Res. Commun.* 163, 988–994. doi: 10.1016/0006-291X(89)92319-X

Pandey, K. N. (1992). Kinetic analysis of internalization, recycling and redistribution of atrial natriuretic factor-receptor complex in cultured vascular smooth-muscle cells. *Biochem. J. Rev.* 288, 55–61. PMID: 1445281

Pandey, K. N. (1993). Stoichiometric analysis of internalization, recycling, and redistribution of photoaffinity-labeled guanylate cyclase/atrial natriuretic factor receptors in cultured murine Leydig tumor cells. *J. Biol. Chem.* 268, 4382–4390. doi: 10.1016/S0021-9258(18)53621-8

Pandey, K. N. (1994). Atrial natriuretic factor inhibits autophosphorylation of protein kinase C and A 240-kDa protein in plasma membranes of bovine adrenal glomerulosa cells: involvement of cGMP-dependent and independent signal transduction mechanisms. *Mol. Cell. Biochem.* 141, 103–111. doi: 10.1007/BF00926173

Pandey, K. N. (1996). "Vascular action Natriuretic peptide receptor" in *Endocrinology of the Vasculature*. ed. J. R. Sowers (Totowa, NJ: Humana Press), 255–267.

Pandey, K. N. (2001). Dynamics of internalization and sequestration of guanylyl cyclase/atrial natriuretic peptide receptor-A. *Can. J. Physiol. Pharmacol.* 79, 631–639. doi: 10.1139/y01-035

Pandey, K. N. (2005). Biology of natriuretic peptides and their receptors. *Peptides* 26, 901–932. doi: 10.1016/j.peptides.2004.09.024

Pandey, K. N. (2008). Emerging roles of natriuretic peptides and their receptors in pathophysiology of hypertension and cardiovascular regulation. *J. Am. Soc. Hypertens.* 2, 210–226. doi: 10.1016/j.jash.2008.02.001

Pandey, K. N. (2009). Functional roles of short sequence motifs in the endocytosis of membrane receptors. *Front. Biosci.* 14, 5339–5360. doi: 10.2741/3599

Pandey, K. N. (2010). Small peptide recognition sequence for intracellular sorting. *Curr. Opin. Biotechnol.* 21, 611–620. doi: 10.1016/j.copbio.2010.08.007

Pandey, K. N. (2011). The functional genomics of guanylyl cyclase/natriuretic peptide receptor-A: perspectives and paradigms. *FEBS J.* 278, 1792–1807. doi: 10.1111/j.1742-4658.2011.08081.x

Pandey, K. N. (2014). Guanylyl cyclase/natriuretic peptide receptor-A signaling antagonizes phosphoinositide hydrolysis, Ca(2+) release, and activation of protein kinase C. *Front. Mol. Neurosci.* 7:75. doi: 10.3389/fnmol.2014.00075

Pandey, K. N. (2015). Endocytosis and trafficking of natriuretic peptide receptor-A: potential role of short sequence motifs. *Membranes* 5, 253–287. doi: 10.3390/membranes5030253

Pandey, K. N. (2018). Molecular and genetic aspects of guanylyl cyclase natriuretic peptide receptor-A in regulation of blood pressure and renal function. *Physiol. Genomics* 50, 913–928. doi: 10.1152/physiolgenomics.00083.2018

Pandey, K. N. (2021). Molecular signaling mechanisms and function of natriuretic peptide receptor-A in the pathophysiology of cardiovascular homeostasis. *Front. Physiol.* 12:693099. doi: 10.3389/fphys.2021.693099

Pandey, K. N., and Inagami, T. (1988). Kidney tubular epithelium cells and vascular smooth muscle cells contain different types of atrial natriuretic factor receptors. *J. Hypertens. Suppl.* 6, S292–S294. doi: 10.1097/00004872-198812040-00090

Pandey, K. N., Inagami, T., and Misono, K. S. (1986). Atrial natriuretic factor receptor on cultured Leydig tumor cells: ligand binding and photoaffinity labeling. *Biochemistry* 25, 8467–8472. doi: 10.1021/bi00374a022

Pandey, K. N., Inagami, T., and Misono, K. S. (1987). Three distinct forms of atrial natriuretic factor receptors: kidney tubular epithelium cells and vascular smooth

muscle cells contain different types of receptors. *Biochem. Biophys. Res. Commun.* 147, 1146–1152. doi: 10.1016/S0006-291X(87)80189-4

Pandey, K. N., and Kanungo, J. (1993). Expression of extracellular ligand-binding domain of murine guanylate cyclase/atrial natriuretic factor receptor cDNA in Escherichia coli. *Biochem. Biophys. Res. Commun.* 190, 724–731. doi: 10.1006/bbrc.1993.1109

Pandey, K. N., Kovacs, W. J., and Inagami, T. (1985). The inhibition of progesterone secretion and the regulation of cyclic nucleotides by atrial natriuretic factor in gonadotropin responsive murine Leydig tumor cells. *Biochem. Biophys. Res. Commun.* 133, 800–806. doi: 10.1016/0006-291X(85)90975-1

Pandey, K. N., Nguyen, H. T., Garg, R., Khurana, M. L., and Fink, J. (2005). Internalization and trafficking of guanylyl (guanylate) cyclase/natriuretic peptide receptor A is regulated by an acidic tyrosine-based cytoplasmic motif GDAY. *Biochem. J.* 388, 103–113. doi: 10.1042/BJ20041250

Pandey, K. N., Nguyen, H. T., Li, M., and Boyle, J. W. (2000). Natriuretic peptide receptor-A negatively regulates mitogen-activated protein kinase and proliferation of mesangial cells: role of cGMP-dependent protein kinase. *Biochem. Biophys. Res. Commun.* 271, 374–379. doi: 10.1006/bbrc.2000.2627

Pandey, K. N., Nguyen, H. T., Sharma, G. D., Shi, S. J., and Kriegel, A. M. (2002). Ligand-regulated internalization, trafficking, and down-regulation of guanylyl cyclase/atrial natriuretic peptide receptor-A in human embryonic kidney 293 cells. *J. Biol. Chem.* 277, 4618–4627. doi: 10.1074/jbc.M106436200

Pandey, K. N., Oliver, P. M., Maeda, N., and Smithies, O. (1999). Hypertension associated with decreased testosterone levels in natriuretic peptide receptor-A gene-knockout and gene-duplicated mutant mouse models. *Endocrinology* 140, 5112–5119. doi: 10.1210/endo.140.11.7121

Pandey, K. N., and Orgebin-Crist, M. C. (1991). Atrial natriuretic factor in mammalian testis: immunological detection in spermatozoa. *Biochem. Biophys. Res. Commun.* 180, 437–444. doi: 10.1016/S0006-291X(05)81312-9

Pandey, K. N., Pavlou, S. N., and Inagami, T. (1988). Identification and characterization of three distinct atrial natriuretic factor receptors. Evidence for tissue-specific heterogeneity of receptor subtypes in vascular smooth muscle, kidney tubular epithelium, and Leydig tumor cells by ligand binding, photoaffinity labeling, and tryptic proteolysis. *J. Biol. Chem.* 263, 13406–13413. doi: 10.1016/S0021-9258(18)37719-6

Pandey, K. N., and Singh, S. (1990). Molecular cloning and expression of murine guanylate cyclase/atrial natriuretic factor receptor cDNA. *J. Biol. Chem.* 265, 12342–12348. doi: 10.1016/S0021-9258(19)38352-8

Paul, A. K., Marala, R. B., Jaiswal, R. K., and Sharma, R. K. (1987). Co-existence of guanylate cyclase and atrial natriuretic factor receptor in 180 kDa protein. *Science* 235, 1224–1226. doi: 10.1126/science.2881352

Pereira, N. L., Tosakulwong, N., Scott, C. G., Jenkins, G. D., Prodduturi, N., Chai, Y., et al. (2015). Circulating atrial natriuretic peptide genetic association study identifies a novel gene cluster associated with stroke in whites. *Circ. Cardiovasc. Genet.* 8, 141–149. doi: 10.1161/CIRCGENETICS.114.000624

Periyasamy, R., Das, S., and Pandey, K. N. (2019). Genetic disruption of guanylyl cyclase/natriuretic peptide receptor-A upregulates renal (pro) renin receptor expression in Npr1 null mutant mice. *Peptides* 114, 17–28. doi: 10.1016/j.peptides.2019.03.001

Potter, L. R., and Garbers, D. L. (1992). Dephosphorylation of the guanylyl cyclase-A receptor causes desensitization. *J. Biol. Chem.* 267, 14531–14534. doi: 10.1016/S0021-9258(18)42069-8

Potter, L. R., and Garbers, D. L. (1994). Protein kinase C-dependent desensitization of the atrial natriuretic peptide receptor is mediated by dephosphorylation. *J. Biol. Chem.* 269, 14636–14642. doi: 10.1016/S0021-9258(17)36672-3

Potter, L. R., and Hunter, T. (1998). Phosphorylation of the kinase homology domain is essential for activation of the A-type natriuretic peptide receptor. *Mol. Cell. Biol.* 18, 2164–2172.

Purcell, N. H., and Molkentin, J. D. (2003). Is nuclear factor kappaB an attractive therapeutic target for treating cardiac hypertrophy? *Circulation* 108, 638–640. doi: 10.1161/01.CIR.0000085362.40608.DD

Qiu, Y., Ogawa, H., Miyagi, M., and Misono, K. S. (2004). Constitutive activation and uncoupling of the atrial natriuretic peptide receptor by mutations at the dimer interface: role of the dimer structure in signaling. *J. Biol. Chem.* 279, 6115–6123. doi: 10.1074/jbc.M310225200

Rathinavelu, A., and Isom, G. E. (1991). Differential internalization and processing of atrial natriuretic factor B and C receptors in PC-12 cells. *Biochem. J.* 276, 493–497.

Reginauld, S. H., Cannone, V., Iyer, S., Scott, C., Bailey, K., Schaefer, J., et al. (2019). Differential regulation of ANP and BNP in acute decompensated heart failure: deficiency of ANP. *JACC Heart Fail* 7, 891–898. doi: 10.1016/j.jchf.2019.05.012

Reinhart, K., Meisner, M., and Brunkhorst, F. M. (2006). Markers for sepsis diagnosis: what is useful? *Crit. Care Clin.* 22, 503–519. doi: 10.1016/j.ccc.2006.03.003

Resink, T. J., Scott-Burden, T., Baur, U., Jones, C. R., and Buhler, F. R. (1988). Atrial natriuretic peptide induces breakdown of phosphatidylinositol phosphates in cultured vascular smooth muscle cells Eur. *J. Biochem.* 172, 499–505.

Rosenzweig, A., and Seidman, C. E. (1991). Atrial natriuretic factor and related peptide hormones. *Annu. Rev. Biochem.* 60, 229–255. doi: 10.1146/annurev.bi.60.070191.001305

Rubattu, S., Forte, M., Marchitti, S., and Volpe, M. (2019). Molecular implications of natriuretic peptides in the protection from hypertension and target organ damage development. *Int. J. Mol. Sci.* 20:798. doi: 10.3390/ijms20040798

Saftig, P., and Klumperman, J. (2009). Lysosome biogenesis and lysosomal membrane proteins: trafficking meets function. *Nat. Rev. Mol. Cell Biol.* 10, 623–635. doi: 10.1038/nrm2745

Samson, W. K. (2004). Atrial natriuretic factor inhibits dehydration and hemorrhage-induced vasopressin release. *Neuroendocrinology* 40, 277–279. doi: 10.1159/000124085

Sangaralingham, S. J., Kuhn, M., Cannone, V., Chen, H. H., and Burnett, J. C. (2022). Natriuretic peptide pathways in heart failure: further therapeutic possibilities. *Cardiovasc. Res.* doi: 10.1093/cvr/cvac125

Saxenhofer, H., Roselli, A., Weidmann, P., Forssmann, W. G., Bub, A., Ferrari, P., et al. (1990). Urodilatin, a natriuretic factor from kidneys can modify renal and cardiovascular function in men. *Am. J. Physiol.* 259, F832–F838. doi: 10.1152/ajprenal.1990.259.5.F832

Schenk, D. B., Phelps, M. N., Porter, J. G., Fuller, F., Cordell, B., and Lewicki, J. A. (1987). Purification and subunit composition of atrial natriuretic peptide receptor. *Proc. Natl. Acad. Sci. U. S. A.* 84, 5121–5125.

Schenk, D. B., Phelps, M. N., Porter, J. G., Scarborough, R. M., McEnroe, G. A., and Lewicki, J. A. (1985). Identification of the receptor for atrial natriuretic factor on cultured vascular cells. *J. Biol. Chem.* 260, 14887–14890. doi: 10.1016/S0021-9258(18)95674-7

Schlueter, N., de Sterke, A., Willmes, D. M., Spranger, J., Jordan, J., and Birkenfeld, A. L. (2014). Metabolic actions of natriuretic peptides and therapeutic potential in the metabolic syndrome. *Pharmacol. Ther.* 144, 12–27. doi: 10.1016/j.pharmthera.2014.04.007

Schulz, S., Green, C. K., Yuen, P. S., and Garbers, D. L. (1990). Guanylyl cyclase is a heat-stable enterotoxin receptor. *Cells* 63, 941–948. doi: 10.1016/0092-8674(90)90497-3

Schulz, S., Lopez, M. J., Kuhn, M., and Garbers, D. L. (1997). Disruption of the guanylyl cyclase-C gene leads to a paradoxical phenotype of viable but heat-stable enterotoxin-resistant mice. *J. Clin. Invest.* 100, 1590–1595. doi: 10.1172/JCI119683

Schulz, S., Singh, S., Bellet, R. A., Singh, G., Tubb, D. J., Chin, H., et al. (1989). The primary structure of a plasma membrane guanylate cyclase demonstrates diversity within this new receptor family. *Cells* 58, 1155–1162. doi: 10.1016/0092-8674(89)90513-8

Schulz-Knappe, P., Forssmann, K., Herbst, F., Hock, D., Pipkorn, R., and Forssmann, W. D. (1988). Isolation and structural analysis of urodilatin, a new peptide of the cardiodilatin (ANP)-family extracted from human urine. *Klin. Wochenschr.* 66, 752–759. doi: 10.1007/BF01726570

Schwartz, V., Kruttgen, A., Weis, J., Weber, C., Ostendorf, T., Lue, H., et al. (2012). Role for CD74 and CXCR4 in clathrin-dependent endocytosis of the cytokine MIF. *Eur. J. Cell Biol.* 91, 435–449. doi: 10.1016/j.ejcb.2011.08.006

Schweitz, H., Vigne, P., Moinier, D., Frelin, C. H., and Lazdunski, M. (1992). A new member of the natriuretic peptide family is present in the venom of the green mamba (*Dendroaspis angusticeps*). *J. Biol. Chem.* 267, 13928–13932. doi: 10.1016/S0021-9258(19)49658-0

Sekiguchi, K., Li, X., Coker, M., Flesch, M., Barger, P. M., Sivasubramanian, N., et al. (2004). Cross-regulation between the renin-angiotensin system and inflammatory mediators in cardiac hypertrophy and failure. *Cardiovasc. Res.* 63, 433–442. doi: 10.1016/j.cardiores.2004.02.005

Sengenes, C., Zakaroff-Girard, A., Moulin, A., Berlan, M., Bouloumie, A., Lafontan, M., et al. (2002). Natriuretic peptide-dependent lipolysis in fat cells is a primate specificity. *Am. J. Physiol. Regul. Integr. Comp. Physiol.* 283, R257–R265. doi: 10.1152/ajpregu.00453.2001

Sezai, A., Hata, M., Niino, T., Yoshitake, I., Unosawa, S., Wakui, S., et al. (2010). Continuous low-dose infusion of human atrial natriuretic peptide in patients with left ventricular dysfunction undergoing coronary artery bypass grafting: the NU-HIT (Nihon University working group study of low-dose Human ANP Infusion Therapy during cardiac surgery) for left ventricular dysfunction. *J. Am. Coll. Cardiol.* 55, 1844–1851.

Sharma, R. K. (2002). Evolution of the membrane guanylate cyclase transduction system. *Mol. Cell. Biochem.* 230, 3–30. doi: 10.1023/A:1014280410459

Sharma, R. K. (2010). Membrane guanylate cyclase is a beautiful signal transduction machine: overview. *Mol. Cell. Biochem.* 334, 3–36. doi: 10.1007/s11010-009-0336-6

Sharma, R. K., Duda, T., and Sitaramayya, A. (1994). Plasma membrane guanylate cyclase is a multimodule transduction system. *Amino Acids* 7, 117–127. doi: 10.1007/BF00814155

Sharma, G. D., Nguyen, H. T., Antonov, A. S., Gerrity, R. G., von Geldern, T., and Pandey, K. N. (2002). Expression of atrial natriuretic peptide receptor-A antagonizes the mitogen-activated protein kinases (Erk2 and P38MAPK) in cultured human vascular smooth muscle cells. *Mol. Cell. Biochem.* 233, 165–173. doi: 10.1023/A:1015882302796

Shi, S. J., Nguyen, H. T., Sharma, G. D., Navar, L. G., and Pandey, K. N. (2001). Genetic disruption of atrial natriuretic peptide receptor-A alters renin and angiotensin II levels. *Am. J. Phys.* 281, F665–F673. doi: 10.1073/pnas.96.13.7403

Shi, S. J., Vellaichamy, E., Chin, S. Y., Smithies, O., Navar, L. G., and Pandey, K. N. (2003). Natriuretic peptide receptor A mediates renal sodium excretory responses to blood volume expansion. *Am. J. Phys.* 285, F694–F702. doi: 10.1152/ajprenal.00097.2003

Sindice, A., Basoglu, C., Cerci, A., Hirsch, J. R., Potthast, R., Kuhn, M., et al. (2002). Guanylin, uroguanylin, and heat-stable euterotoxin activate guanylate cyclase C and/or a pertussis toxin-sensitive G protein in human proximal tubule cells. *J. Biol. Chem.* 277, 17758–17764. doi: 10.1074/jbc.M110627200

Smani, Y., Docobo-Perez, F., Lopez-Rojas, R., Dominguez-Herrera, J., Ibanez-Martinez, J., and Pachon, J. (2012). Platelet-activating factor receptor initiates contact of *Acinetobacter baumannii* expressing phosphorylcholine with host cells. *J. Biol. Chem.* 287, 26901–26910. doi: 10.1074/jbc.M112.344556

Somanna, N. K., Mani, I., Tripathi, S., and Pandey, K. N. (2018). Clathrin-dependent internalization, signaling, and metabolic processing of guanylyl cyclase/natriuretic peptide receptor-A. *Mol. Cell. Biochem.* 441, 135–150. doi: 10.1007/s11010-017-3180-0

Somanna, N. K., Pandey, A. C., Arise, K. K., Nguyen, V., and Pandey, K. N. (2013). Functional silencing of guanylyl cyclase/natriuretic peptide receptor-A by microRNA interference: analysis of receptor endocytosis. *Int. J. Biochem. Mol. Biol.* 4, 41–53. PMID: 23638320

Steinhelper, M. E., Cochrane, K. L., and Field, L. J. (1990). Hypotension in transgenic mice expressing atrial natriuretic factor fusion genes. *Hypertension* 16, 301–307. doi: 10.1161/01.HYP.16.3.301

Stingo, A. J., Clavell, A. L., Heublein, D. M., Wei, C. M., Pittelkom, M. R., and Burnett, J. C. J. (1992). Presence of C-type natriuretic peptide in cultured human endothelial cells and plasma. *Am. J. Physiol.* 263, H1318–H1321.

Subramanian, U., Kumar, P., Mani, I., Chen, D., Kessler, I., Periyasamy, R., et al. (2016). Retinoic acid and sodium butyrate suppress the cardiac expression of hypertrophic markers and proinflammatory mediators in Npr1 gene-disrupted haplotype mice. *Physiol. Genomics* 48, 477–490. doi: 10.1152/physiolgenomics.00073.2015

Subramanian, U., Ramasamy, C., Ramachandran, S., Oakes, J. M., Gardner, J. D., and Pandey, K. N. (2022). Genetic disruption of guanylyl cyclase/natriuretic peptide receptor-A triggers differential cardiac fibrosis and disorders in male and female mutant mice: role of TGF-beta1/SMAD signaling pathway. *Int. J. Mol. Sci.* 23:11487. doi: 10.3390/ijms231911487

Suga, S., Itoh, H., Komatsu, Y., Ogawa, Y., Hama, N., Yoshimasa, T., et al. (1993). Cytokine-induced C-type natriuretic peptide (CNP) secretion from vascular endothelial cells-evidence for CNP as a novel autocrine/paracrine regulator from endothelial cells. *Endocrinology* 133, 3038–3041. doi: 10.1210/endo.133.6.8243333

Suga, S., Nakao, K., Hosoda, K., Mukoyama, M., Ogawa, Y., Shirakami, G., et al. (1992). Phenotype-related alteration in expression of natriuretic peptide receptors in aortic smooth muscle cells. *Circ. Res.* 71, 34–39.

Suga, S., Nakao, K., Itoh, H., Komatsu, Y., Ogawa, Y., Hama, N., et al. (1992). Endothelial production of C-type natriuretic peptide and its marked augmentation by transforming growth factor-beta possible existence of vascular natriuretic peptide system. *J. Clin. Invest.* 90, 1145–1149. doi: 10.1172/JCI115933

Sunahara, R. K., Beuve, A., Tesmer, J. J. G., Sprang, S. R., Garbers, D. L., and Gilman, A. G. (1998). Exchange of substrate and inhibitor specificities between adenylyl and guanylyl cyclase. *J. Biol. Chem.* 273, 16332–16338. doi: 10.1074/jbc.273.26.16332

Takahashi, N., and Smithies, O. (1999). Gene targeting approaches to analyzing hypertension. *J. Am. Soc. Nephrol.* 10, 1598–1605. doi: 10.1681/ASN.V1071598

Takayanagi, R., Snajdar, R. M., Imada, T., Tamura, M., Pandey, K. N., Misono, K. S., et al. (1987). Purification and characterization of two types of atrial natriuretic factor receptors from bovine adrenal cortex guanylate cyclase-linked and cyclase-free receptors. *Biochem. Mol. Cell Biol. Res. Commun.* 144, 244–250. doi: 10.1016/S0006-291X(87)80502-8

Tamura, N., Doolittle, L. K., Hammer, R. E., Shelton, J. M., Richardson, J. A., and Garbers, D. L. (2004). Critical roles of the guanylyl cyclase B receptor in endochondral ossification and development of female reproductive organs. *Proc. Natl. Acad. Sci. U. S. A.* 101, 17300–17305. doi: 10.1073/pnas.0407894101

Tamura, N., Ogawa, Y., Chusho, H., Nakamura, K., Nakao, K., Suda, M., et al. (2000). Cardiac fibrosis in mice lacking brain natriuretic peptide. *Proc. Natl. Acad. Sci. U. S. A.* 97, 4239–4244. doi: 10.1073/pnas.070371497

Tankersley, C. G., Peng, R. D., Bedga, D., Gabrielson, K., and Champion, H. C. (2010). Variation in echocardiographic and cardiac hemodynamic effects of PM and ozone inhalation exposure in strains related to Nppa and Npr1 gene knock-out mice. *Inhal. Toxicol.* 22, 695–707. doi: 10.3109/08958378.2010.487549

Teitelbaum, I., Strasheim, A., and Berl, T. (1990). Epidermal growth factor-stimulated phosphoinositide hydrolysis in cultured rat inner medullary collecting tubule cells. Regulation by G protein, calcium, and protein kinase C. *J. Clin. Invest.* 85, 1044–1050. doi: 10.1172/JCI114534

Testa, M., Yeh, M., Lee, P., Fanelli, R., Loperfido, F., Berman, J. W., et al. (1996). Circulating levels of cytokines and their endogenous modulators in patients with mild to severe congestive heart failure due to coronary artery disease or hypertension. *J. Am. Coll. Cardiol.* 28, 964–971. doi: 10.1016/S0735-1097(96)00268-9

Thaik, C. M., Calderone, A., Takahashi, N., and Colucci, W. S. (1995). Interleukin-1 beta modulates the growth and phenotype of neonatal rat cardiac myocytes. *J. Clin. Invest.* 96, 1093–1099. doi: 10.1172/JCI118095

Thomas, M. C., and Cherney, D. Z. I. (2018). The actions of SGLT2 inhibitors on metabolism, renal function and blood pressure. *Diabetologia* 61, 2098–2107. doi: 10.1007/s00125-018-4669-0

Thorp, D. S., and Morkin, E. (1990). The carboxyl region contains the catalytic domain of the membrane form of guanylate cyclase. *J. Biol. Chem.* 265, 14717–14720. doi: 10.1016/S0021-9258(18)77168-8

Tremblay, J., Gertzer, R., Vinay, P., Pang, S. C., Beliveau, R., and Hamet, P. (1985). The increase of cGMP by atrial natriuretic factor correlates with the distribution of particulate guanylate cyclase. *FEBS Lett.* 181, 17–22. PMID: 2857657

Tripathi, S., and Pandey, K. N. (2012). Guanylyl cyclase/natriuretic peptide receptor-A signaling antagonizes the vascular endothelial growth factor-stimulated MAPKs and downstream effectors AP-1 and CREB in mouse mesangial cells. *Mol. Cell. Biochem.* 368, 47–59. doi: 10.1007/s11010-012-1341-8

Tsai, K. F., Chen, Y. L., Chiou, T. T., Chu, T. H., Li, L. C., Ng, H. Y., et al. (2021). Emergence of SGLT2 inhibitors as powerful antioxidants in human diseases. *Antioxidants* 10, 1–26.

Tsukagoshi, H., Shimizu, Y., Kawata, T., Hisada, T., Shimizu, Y., Iwamae, S., et al. (2001). Atrial natriuretic peptide inhibits tumor necrosis factor-alpha production by interferon-gamma-activated macrophages via suppression of p38 mitogen-activated protein kinase and nuclear factor-kappa B activation. *Regul. Pept.* 99, 21–29. doi: 10.1016/S0167-0115(01)00218-X

Tsukamoto, O., Fujita, M., Kato, M., Yamazaki, S., Asano, Y., Ogai, A., et al. (2009). Natriuretic peptides enhance the production of adiponectin in human adipocytes and in patients with chronic heart failure. *J. Am. Coll. Cardiol.* 53, 2070–2077. doi: 10.1016/j.jacc.2009.02.038

Tucker, C. L., Hurley, J. H., Miller, T. R., and Hurley, J. B. (1998). Two amino acid substitutions convert a guanylyl cyclase, ret GC-1 into an adenylyl cyclase. *Proc. Natl. Acad. Sci. U. S. A.* 95, 5993–5997. doi: 10.1073/pnas.95.11.5993

van den Akker, F. (2001). Structural insights into the ligand binding domains of membrane bound guanylyl cyclases and natriuretic peptide receptors. *J. Mol. Biol.* 311, 923–937. doi: 10.1006/jmbi.2001.4922

van den Akker, F., Zang, X., Miyagi, H., Huo, X., Misono, K. S., and Yee, V. C. (2000). Structure of the dimerized hormone-binding domain of a guanylyl cyclase-coupled receptor. *Nature* 406, 101–104. doi: 10.1038/35017602

Vandenwijngaert, S., Ledsky, C. D., Agha, O., Wu, C., Hu, D., Bagchi, A., et al. (2018). MicroRNA-425 and microRNA-155 cooperatively regulate atrial natriuretic peptide expression and cGMP production. *PLoS One* 13:e0196697. doi: 10.1371/journal.pone.0196697

Vanderheyden, M., Paulus, W. J., Voss, M., Knuefermann, P., Sivasubramanian, N., Mann, D., et al. (2005). Myocardial cytokine gene expression is higher in aortic stenosis than in idiopathic dilated cardiomyopathy. *Heart* 91, 926–931. doi: 10.1136/hrt.2004.035733

Vandlen, R. L., Arcuri, K. E., and Napier, M. A. (1985). Identification of a receptor for atrial natriuretic factor in rabbit aorta membranes by affinity cross-linking. *J. Biol. Chem.* 260, 10889–10892. doi: 10.1016/S0021-9258(17)39114-7

Vellaichamy, E., Das, S., Subramanian, U., Maeda, N., and Pandey, K. N. (2014). Genetically altered mutant mouse models of guanylyl cyclase/natriuretic peptide receptor-A exhibit the cardiac expression of proinflammatory mediators in a gene-dose-dependent manner. *Endocrinology* 155, 1045–1056. doi: 10.1210/en.2013-1416

Vellaichamy, E., Kaur, K., and Pandey, K. N. (2007). Enhanced activation of pro-inflammatory cytokines in mice lacking natriuretic peptide receptor-A. *Peptides* 28, 893–899. doi: 10.1016/j.peptides.2006.12.009

Vellaichamy, E., Khurana, M. L., Fink, J., and Pandey, K. N. (2005). Involvement of the NF-kappa B/matrix metalloproteinase pathway in cardiac fibrosis of mice lacking guanylyl cyclase/natriuretic peptide receptor A. *J. Biol. Chem.* 280, 19230–19242. doi: 10.1074/jbc.M411373200

Vellaichamy, E., Sommana, N. K., and Pandey, K. N. (2005). Reduced cGMP signaling activates NF-kappaB in hypertrophied hearts of mice lacking natriuretic

peptide receptor-A. *Biochem. Biophys. Res. Commun.* 327, 106–111. doi: 10.1016/j.bbrc.2004.11.153

Vellaichamy, E., Zhao, D., Somanna, N., and Pandey, K. N. (2007). Genetic disruption of guanylyl cyclase/natriuretic peptide receptor-A upregulates ACE and AT1 receptor gene expression and signaling: role in cardiac hypertrophy. *Physiol. Genomics* 31, 193–202. doi: 10.1152/physiolgenomics.00079.2007

Venugopal, J. (2001). Cardiac natriuretic peptides-hope or hype? *J. Clin. Hosp. Pharm.* 26, 15–31. doi: 10.1046/j.1365-2710.2001.00322.x

Vollmer, A. M. (2005). The role of atrial natriuretic peptide in the immune system. *Peptides* 26, 1087–1094. doi: 10.1016/j.peptides.2004.08.034

Vollmer, A. M., and Schulz, R. (1990). Atrial natriuretic peptide is synthesized in the human thymus. *Endocrinology* 126, 2277–2280. doi: 10.1210/endo-126-5-2277

Volpe, M. (2014). Natriuretic peptides and cardio-renal disease. *Int. J. Cardiol.* 176, 630–639. doi: 10.1016/j.ijcard.2014.08.032

Waldman, S. A., Rappoport, R. M., and Murad, F. (1984). Atrial natriuretic factor selectively activates particulate guanylyl cyclase and elevates cyclic GMP in rat tissues. *J. Biol. Chem.* 259, 14332–14334. doi: 10.1016/S0021-9258(17)42597-X

Wang, Y., de Waard, M. C., Sterner-Kock, A., Stepan, H., Schultheiss, H. P., Duncker, D. J., et al. (2007). Cardiomyocyte-restricted over-expression of C-type natriuretic peptide prevents cardiac hypertrophy induced by myocardial infarction in mice. *Eur. J. Heart Fail.* 9, 548–557. doi: 10.1016/j.ejheart.2007.02.006

Wang, T. J., Larson, M. G., Keyes, M. J., Levy, D., Benjamin, E. J., and Vasan, R. S. (2007). Association of plasma natriuretic peptide levels with metabolic risk factors in ambulatory individuals. *Circulation* 115, 1345–1353. doi: 10.1161/CIRCULATIONAHA.106.655142

Wei, C. M., Aarhus, L. L., Miller, V. M., and Burnett, J. C. J. (1993a). Action of C-type natriuretic peptide in isolated canine arteries and veins. *Am. J. Phys.* 264, H71–H73. PMID: 8430863

Wei, C.-M., Heublein, D. M., Perrella, M. A., Lerman, A., Rodeheffer, R. J., McGregor, C. G. A., et al. (1993b). Natriuretic peptide system in human heart failure. *Circulation* 88, 1004–1009. doi: 10.1161/01.CIR.88.3.1004

White, R. E., Lee, A. B., Shcherbatko, A. D., Lincoln, T. M., Schonbrunn, A., and Armstrong, D. L. (1993). Potassium channel stimulation by natriuretic peptides through cGMP-dependent dephosphorylation. *Nature* 361, 263–266. doi: 10.1038/361263a0

Wilson, E. M., and Chinkers, M. (1995). Identification of sequences mediating guanylyl cyclase dimerization. *Biochemistry* 34, 4696–4701. doi: 10.1021/bi00014a025

Wong, S. K., Ma, C. P., Foster, D. C., Chen, A. Y., and Garbers, D. L. (1995). The guanylyl cyclase-a receptor transduces an atrial natriuretic peptide/ATP activation signal in the absence of other proteins. *J. Biol. Chem.* 270, 30818–30822. doi: 10.1074/jbc.270.51.30818

Wu, C., Arora, P., Agha, O., Hurst, L. A., Allen, K., Nathan, D. I., et al. (2016). Novel MicroRNA regulators of atrial natriuretic peptide production. *Mol. Cell. Biol.* 36, 1977–1987. doi: 10.1128/MCB.01114-15

Yang, R. B., and Garbers, D. L. (1997). Two eye guanylyl cyclase are expressed in the same photoreceptor cells and form homomers in preference to heteromers. *J. Biol. Chem.* 272, 13738–13742. doi: 10.1074/jbc.272.21.13738

Yasoda, A., Komatsu, Y., Chusho, H., Miyazawa, T., Ozasa, A., Miura, M., et al. (2004). Overexpression of CNP in chondrocytes rescues achondroplasia through a MAPK-dependent pathway. *Nat. Med.* 10, 80–86. doi: 10.1038/nm971

Yasunari, K., Kohno, M., Murakawa, K., Yokokawa, K., Horio, T., and Takeda, T. (1992). Phorbol ester and atrial natriuretic peptide receptor response on vascular smooth muscle. *Hypertension* 19, 314–319. doi: 10.1161/01.HYP.19.4.314

Yip, C. C., Laing, L. P., and Flynn, T. G. (1985). Photoaffinity labeling of atrial natriuretic factor receptors of rat kidney cortex plasma membranes. *J. Biol. Chem.* 260, 8229–8232. doi: 10.1016/S0021-9258(17)39458-9

Zelniker, T. A., and Braunwald, E. (2020). Mechanisms of cardiorenal effects of sodium-glucose cotransporter 2 inhibitors: JACC state-of-the-art review. *J. Am. Coll. Cardiol.* 75, 422–434. doi: 10.1016/j.jacc.2019.11.031

Zhang, G., Liu, Y., Arnold, E. R., and Hurley, J. H. (1997). Structure of the adenylyl cyclase catalytic core. *Nature* 386, 247–253. doi: 10.1038/386247a0

Zhao, D., Das, S., and Pandey, K. N. (2013). Interactive roles of Npr1 gene-dosage and salt diets on cardiac angiotensin II, aldosterone and pro-inflammatory cytokines levels in mutant mice. *J. Hypertens.* 31, 134–144. doi: 10.1097/HJH.0b013e32835ac15f

Zhao, D., Vellaichamy, E., Somanna, N. K., and Pandey, K. N. (2007). Guanylyl cyclase/natriuretic peptide receptor-A gene disruption causes increased adrenal angiotensin II and aldosterone levels. *Am. J. Physiol. Renal Physiol.* 293, F121–F127. doi: 10.1152/ajprenal.00478.2006

Zhou, H., and Murthy, K. S. (2003). Identification of the G-protein activation sequence of the single-transmembrane natriuretic peptide receptor C (NPR-C). *Cell Physiol.* 284, C1255–C1261. doi: 10.1152/ajpcell.00520.2002

Glossary

NPs	natriuretic peptides
ANF/ANP	atrial natriuretic factor/peptide
ANP, BNP, and CNP	atrial, brain, and C-type NPs
GC-A/NPRA	guanylyl cyclase/natriuretic peptide receptor-A
Npr1	Encoding GC-A/NPRA
BP	blood pressure
BNP	Brain natriuretic peptide
CNP	C-type natriuretic peptide
DNP	*Dendroaspis* natriuretic peptide or D-type NP
URO	urodilatin
GC-A/NPRA	Guanylyl cyclase NP receptor-A
GC-B/NPRB	GC/NP receptor-B
NPRC	NP receptor-C
PDs	phosphodiesterases
CNGs	cyclic-nucleotide gated ion channels
VSMCs	vascular smooth muscle cells
c-ANF or AP I	truncated ANF/ANP
MDCK	Maiden-Darby canine kidney
NPRs	NP receptors
CNS	central nervous system
LBD	ligand-binding domain
TD	transmembrane domain
protein-KHD	protein kinase-like homology domain
DD	dimerization domain
GCCD	guanylyl cyclase catalytic domain
RTKs	receptor tyrosine kinases
ACII C2	adenylyl cyclase II C2
WT	wild-type
JMHR	juxtamembrane hinge region
IP_3	inositol trisphosphates
RIMCDs	renal inner medullary collecting duct cells
RMECs	renal medullary epithelial cells
PKC	protein kinase C
EGF	epidermal growth factor
PDGF	platelet-derived growth factor
ST	heat-stable enterotoxin
MMCs	mouse mesangial cells
miR	micro-RNA
MDC	monodansylcadaverine
CPZ	chlorpromazine
KO	knockout
JG	juxtaglomerular cells
RBF	renal blood flow
GFR	glomerular filtration rate

CHF	congestive heart failure
IL-1β	interleukin-1β
IL-6	interleukin-6
TNF-α	tumor necrosis factor alpha
IFN-γ	interferon-gamma
TGF-β1	transforming growth factor beta 1
NT-proBNP	N-terminal pro-BNP

frontiers | Frontiers in Molecular Neuroscience

TYPE Brief Research Report
PUBLISHED 19 October 2022
DOI 10.3389/fnmol.2022.1007026

OPEN ACCESS

EDITED BY
Kailash N. Pandey,
Tulane University, United States

REVIEWED BY
Elangovan Vellaichamy,
University of Madras, India
Viacheslav Nikolaev,
University of Göttingen, Germany

*CORRESPONDENCE
Jeremy R. Egbert
egbert@uchc.edu
Lincoln R. Potter
potter@umn.edu
Laurinda A. Jaffe
ljaffe@uchc.edu
Siu-Pok Yee
syee@uchc.edu

SPECIALTY SECTION
This article was submitted to Molecular Signaling and Pathways, a section of the journal Frontiers in Molecular Neuroscience

RECEIVED 29 July 2022
ACCEPTED 28 September 2022
PUBLISHED 19 October 2022

CITATION
Egbert JR, Uliasz TF, Lowther KM, Kaback D, Wagner BM, Healy CL, O'Connell TD, Potter LR, Jaffe LA and Yee S-P (2022) Epitope-tagged and phosphomimetic mouse models for investigating natriuretic peptide-stimulated receptor guanylyl cyclases.
Front. Mol. Neurosci. 15:1007026.
doi: 10.3389/fnmol.2022.1007026

Epitope-tagged and phosphomimetic mouse models for investigating natriuretic peptide-stimulated receptor guanylyl cyclases

Jeremy R. Egbert[1]*, Tracy F. Uliasz[1], Katie M. Lowther[1,2], Deborah Kaback[1,2], Brandon M. Wagner[3], Chastity L. Healy[3], Timothy D. O'Connell[3], Lincoln R. Potter[3,4]*, Laurinda A. Jaffe[1]* and Siu-Pok Yee[1,2]*

[1]Department of Cell Biology, University of Connecticut Health Center, Farmington, CT, United States, [2]Center for Mouse Genome Modification, University of Connecticut Health Center, Farmington, CT, United States, [3]Department of Integrative Biology and Physiology, University of Minnesota, Minneapolis, MN, United States, [4]Department of Biochemistry, Molecular Biology, and Biophysics, University of Minnesota, Minneapolis, MN, United States

The natriuretic peptide receptors NPR1 and NPR2, also known as guanylyl cyclase A and guanylyl cyclase B, have critical functions in many signaling pathways, but much remains unknown about their localization and function *in vivo*. To facilitate studies of these proteins, we developed genetically modified mouse lines in which endogenous NPR1 and NPR2 were tagged with the HA epitope. To investigate the role of phosphorylation in regulating NPR1 and NPR2 guanylyl cyclase activity, we developed mouse lines in which regulatory serines and threonines were substituted with glutamates, to mimic the negative charge of the phosphorylated forms (NPR1-8E and NPR2-7E). Here we describe the generation and applications of these mice. We show that the HA-NPR1 and HA-NPR2 mice can be used to characterize the relative expression levels of these proteins in different tissues. We describe studies using the NPR2-7E mice that indicate that dephosphorylation of NPR2 transduces signaling pathways in ovary and bone, and studies using the NPR1-8E mice that indicate that the phosphorylation state of NPR1 is a regulator of heart, testis, and adrenal function.

KEYWORDS

natriuretic peptide receptor, guanylyl cyclase, phosphorylation, genetically modified mice, cyclic GMP

Introduction

Natriuretic peptide receptors 1 and 2 (NPR1 and NPR2) are membrane guanylyl cyclases, also known as guanylyl cyclase A and guanylyl cyclase B (Potter, 2011; Kuhn, 2016). Atrial natriuretic peptide (ANP) and brain natriuretic peptide (BNP) activate NPR1 to reduce blood pressure and cardiac hypertrophy and to regulate metabolism (Kuhn, 2016; Wagner et al., 2022a). C-type natriuretic peptide (CNP) activates NPR2 to regulate bone growth and oocyte meiosis (Kuhn, 2016; Jaffe and Egbert, 2017; see sections "Results and discussion"), as well as axon bifurcation (Schmidt et al., 2018, 2022) and cardiovascular remodeling and contractility (Kuhn, 2016; Subramanian et al., 2018).

NPR1 and NPR2 are structurally similar proteins, comprised of an extracellular ligand binding domain, a single plasma membrane-spanning region, and an intracellular domain composed of a juxtamembrane kinase homology domain, followed by a dimerization domain and a carboxy-terminal catalytic domain (**Figures 1A,B**). The kinase homology domain of these receptors does not appear to possess intrinsic kinase activity (Edmund et al., 2019) but is highly phosphorylated on multiple serines and threonines by unidentified kinases. Importantly, phosphorylation of the kinase homology domain is required to transduce the natriuretic peptide binding signal from the extracellular domain to the catalytic domain (Potter and Hunter, 1998a,b). Hence, dephosphorylation of these receptors provides a direct mechanism for inhibiting natriuretic peptide-dependent cellular cGMP generation, and thus opposing cGMP-dependent signaling pathways.

Tryptic phosphopeptide mapping and mass spectrometry studies identified the phosphorylation sites in NPR1 and NPR2 (Potter and Hunter, 1998a,b, 1999; Schröter et al., 2010; Yoder et al., 2010). Substitution of alanines to mimic dephosphorylated residues for known phosphorylated serine and threonine residues resulted in reduced natriuretic peptide-dependent guanylyl cyclase activity in transfected cells and genetically modified mice (Potter and Hunter, 1998a,b; Schmidt et al., 2018). Conversely, substitution of glutamates to constitutively mimic the negative charge of the phosphates resulted in the NPR1-8E and the NPR2-7E enzymes that are activated like the phosphorylated wild-type enzymes but cannot be inactivated by dephosphorylation (Yoder et al., 2012; Otto et al., 2017).

Much has been learned about the physiological functions of NPR1 and NPR2 from studies of natural mutations in humans and genetically modified mice in which these proteins are inactive or overactive (Oliver et al., 1997, 1998; Bartels et al., 2004; Tamura et al., 2004; Zhang et al., 2010; Miura et al., 2012; Pandey, 2019), and in mice expressing cyclic GMP biosensors (Götz et al., 2014; Subramanian et al., 2018; Feil et al., 2022). In this report, we describe several recently developed mouse models in which NPR1 and NPR2 are epitope-tagged or have phosphomimetic mutations. Because endogenous expression levels of natriuretic peptide-stimulated receptor guanylyl cyclases are relatively low, antibodies that work well for studies of NPR1 and NPR2 in overexpressing cells do not always have sufficient sensitivity and specificity to be useful for native tissues. To address this issue, we generated mice with influenza hemagluttinin (HA) epitope tags on NPR1 and NPR2 (Baena et al., 2020, and results to be described; **Figures 1A,B**).

To extend knowledge of how phosphorylation of these proteins regulates their activity in transfected cells to understanding of physiological functions *in vivo*, we generated mice in which the 7 serines and threonines of NPR1 and the 6 serines and threonines in NPR2 that are known to be phosphorylated were changed to glutamates (**Figures 1C,D**). We also converted to glutamate one additional serine that is highly conserved between guanylyl cyclases that are regulated by phosphorylation (Ser-473 in NPR1 and Ser-489 in NPR2). These modifications produced phosphomimetic forms of each receptor called NPR1-8E and NPR2-7E. These glutamate-substituted forms are activated by natriuretic peptides like the phosphorylated wild-type receptors but cannot be inactivated by dephosphorylation, resulting in consequences for multiple physiological systems (Shuhaibar et al., 2016, 2017; Egbert et al., 2018; Robinson et al., 2020; Wagner et al., 2021, 2022a,b).

This report describes how mice expressing HA-tagged and glutamate-substituted NPR1 and NPR2 were produced, and summarizes published studies using them. We also present new findings that have been obtained with these mice, which we hope will facilitate future studies.

Methods

Animal studies

Protocols covering the generation of mice, maintenance of mouse lines and subsequent use of the animals were approved by the Institutional Animal Care Committees at the University of Connecticut Health Center and the University of Minnesota. Mice were housed in ventilated cages and racks and kept under a 12/12 h or 14/10 h light/dark cycle. They were provided with standard mouse chow and water *ad libitum*.

Generation of mice with hemagluttinin tags on NPR1 and NPR2

To generate the HA-NPR1 and HA-NPR2 mouse lines, a 9-amino acid HA epitope tag (YPYDVPDYA) was added to the extracellular N-termini of the endogenous NPR1 and NPR2 proteins (**Figures 1A,B**), by CRISPR/Cas9 mediated genome editing of C57BL/6J embryos. Generation and validation

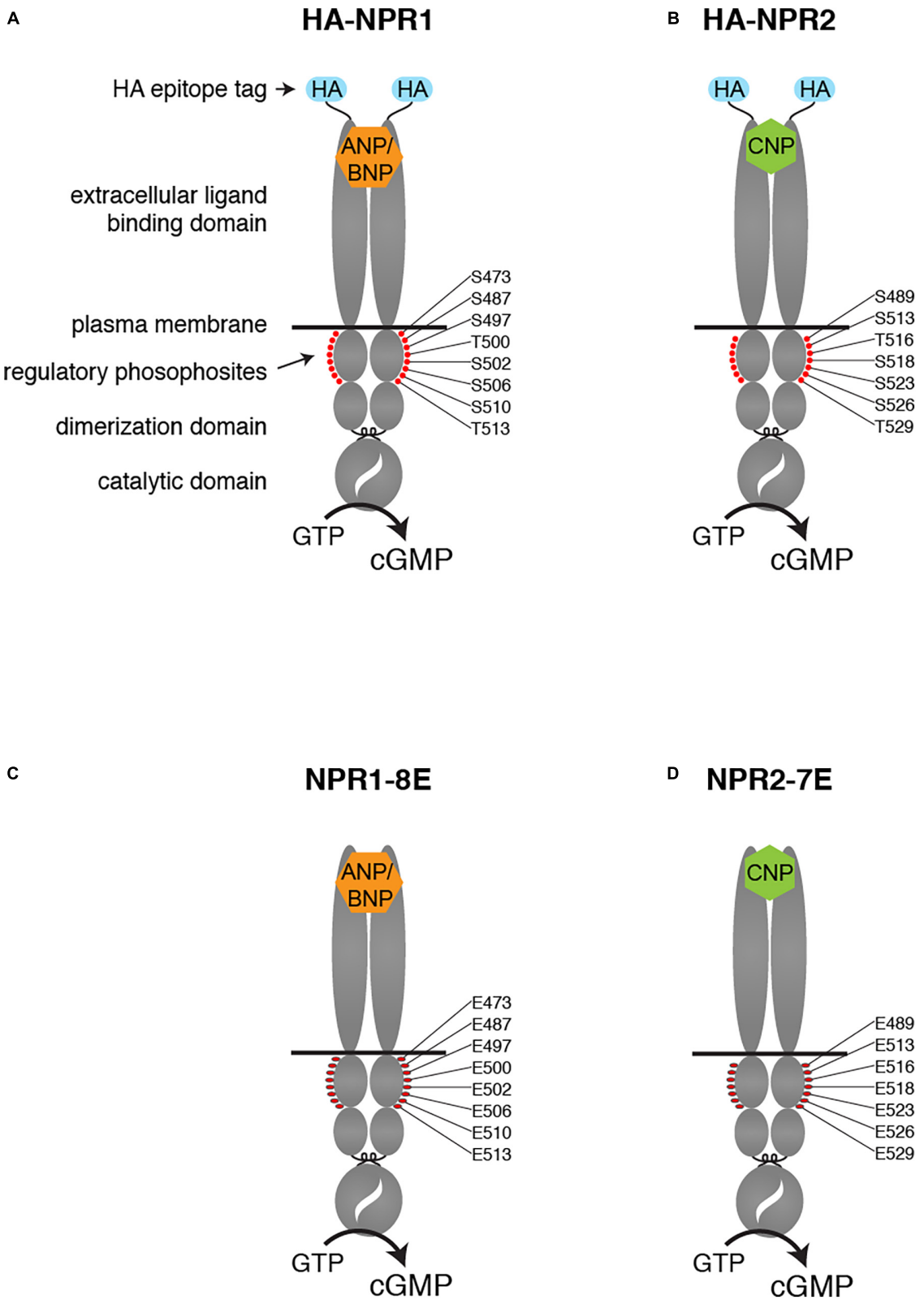

FIGURE 1
Modifications of the NPR1 and NPR2 proteins in HA-NPR1, HA-NPR2, NPR1-8E, and NPR2-7E mice. Diagrams show the domains of each protein, including the HA epitope tag at the N-terminus **(A,B)** and the glutamate substitutions for regulatory phosphosites within the kinase homology domain **(C,D)**.

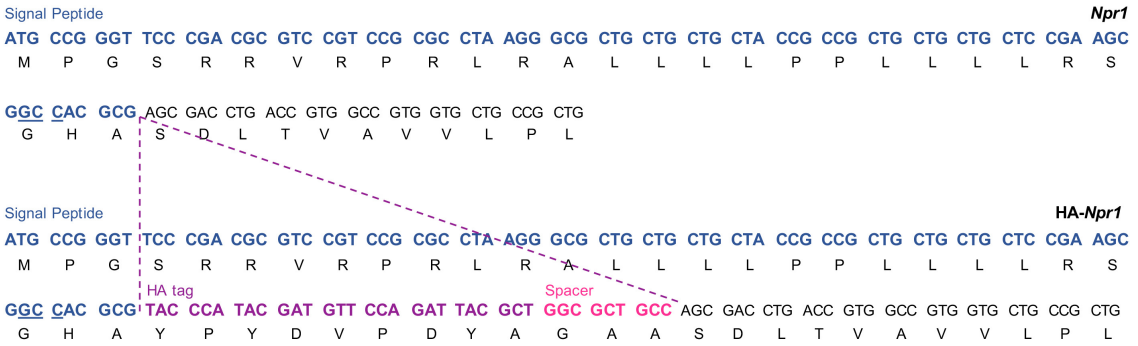

FIGURE 2
Generation of the HA-NPR1 mouse strain using CRISPR. The Npr1 signal peptide sequence is shown in blue with the PAM site for CRISPR underlined. The HA tag sequence is shown in purple, and the sequence of the 3 amino acid spacer is shown in pink. The Npr1 exon 1 coding sequence is shown in black.

of the HA-NPR2 mice have been previously described (Baena et al., 2020). We also made mice in which FLAG or PA epitope tags were used in place of the HA tag on NPR2, but these mice did not show specific labeling on western blots or immunofluorescence using available antibodies (Baena et al., 2020).

The HA-NPR1 mice were made similarly to the HA-NPR2 mice, except that the Cas9/sgRNA ribonucleoprotein (RNP) complex and ssDNA donor mixture were introduced directly into one-cell C57BL/6J embryos by electroporation rather than microinjection. The positions where the HA sequence and a 3 amino acid spacer were inserted are shown in **Figure 2**. The spacer is aimed to introduce structural flexibility to improve antibody binding efficiency as well as to minimize any interference of ligand binding. DNA sequences for generation and genotyping of these mice are listed in **Supplementary Table 1**.

The mice used for the studies to be described were homozygous for the indicated mutations, and the terms HA-NPR1 and HA-NPR2 refer to homozygotes. The mice used to generate them were obtained originally from The Jackson Laboratory (#000664).

Generation of mice in which the regulatory serines and threonines of NPR1 and NPR2 are substituted by glutamates

Generation and validation of the NPR1-8E and NPR2-7E mice have been previously described (Shuhaibar et al., 2016; Wagner et al., 2022a). In these lines, 8 serines and threonines of NPR1, and 7 serines and threonines in NPR2, were changed to glutamates (**Figures 1C,D**). The terms NPR1-8E and NPR2-7E refer to homozygotes that express the glutamate mutations globally.

In brief, the NPR1-8E mice were produced by CRISPR/Cas9 mediated genome editing of C57BL/6J one-cell embryos, to obtain a global knock-in line; they were initially named GC-A-8E (Wagner et al., 2022a). The mice were maintained on the C57BL/6J background.

The NPR2-7E mice were generated by homologous recombination in mouse ES cells derived from a F1 (C57BL/6Jx129sv) embryo, to obtain a conditional knock-in line (Shuhaibar et al., 2016). To remove the Neo cassette and obtain a globally expressing line, the conditional knock-in line was then bred with C57BL/6J *Hprt-Cre* mice (Tang et al., 2002). The *Hprt-Cre* mice had been previously backcrossed for >20 generations with C57BL/6J mice. The background of the resulting NPR2-7E global knock-in line was C57BL/6J (75%)/129sv (25%). The mice were maintained on this mixed background. Use of heterozygous breeding pairs to obtain homozygous mutants and wildtype controls ensured that background strain did not affect experimental results (Shuhaibar et al., 2016, 2017). In some studies, the NPR2-7E mice were further backcrossed with C57BL/6J mice (Egbert et al., 2018; Robinson et al., 2020; Wagner et al., 2021).

Western blotting

Tissues for western blots were collected from HA-NPR1 or HA-NPR2 homozygous mice, or wild-type controls. Ovaries were obtained from 24-day old female mice that had been injected ∼44 h prior to collection with 5 IU equine chorionic gonadotropin (ProSpec #HOR-272) to stimulate follicle growth. All other tissues were collected from adult male mice (16–20 weeks old). After removal, organs were rinsed in PBS, blotted on a laboratory wipe, and snap frozen in liquid N_2. Frozen organs were weighed and sonicated in an appropriate volume of 50 mM Tris HCl, 150 mM NaCl, 1% SDS; protein concentrations were determined by a BCA assay (Thermo Scientific #23227). Protein

samples were loaded on a 12% gel, and separated by SDS-PAGE, allowing the 45 kDa marker to run to the bottom of the gel. Loading of equal amounts of protein per lane was assured by performing BCA assays on all tissues, and confirmed by staining of blots for total protein, using Ponceau S (Sander et al., 2019) (Fisher Scientific #BP103-10) (**Supplementary Figure 1**). Blots were probed with a rabbit monoclonal antibody against the HA epitope (Cell Signaling Technology #3724).

Several commercially available HA tag antibodies were tested, and those from Cell Signaling resulted in the most specific signal. Depending on the application, either the mouse monoclonal (#2367) or rabbit monoclonal (#3724) antibody from Cell Signaling was found to be optimal (Baena et al., 2020; Egbert et al., 2021; Shuhaibar et al., 2021).

Measurement of ejection fraction and end systolic volume in hearts of aged NPR1-8E and wild-type mice

These parameters were measured as previously described (Wagner et al., 2022a). In brief, echocardiography was performed on isoflurane-anesthetized mice using the Vevo 2100 (FujiFilm VisualSonics Inc., Toronto, Canada) with a MS550 transducer. Echocardiographic images were captured as mice were recovering from anesthesia. At the time of imaging, heart rates for all groups were 400–500 bpm (**Supplementary Table 2**).

Results and discussion

Use of hemagluttinin-NPR1 and hemagluttinin-NPR2 mice to investigate tissue and cell expression patterns

To investigate the utility of the HA-tagged NPR1 and NPR2 mice for comparing expression levels of NPR1 and NPR2 proteins, lysates of several tissues were prepared from homozygous HA-tagged and wild-type mice, and an equal amount of protein from each tissue lysate was separated by SDS-PAGE. Western blots were probed with an HA antibody, and bands present at ∼120–130 kDa in HA-expressing tissues, but not in wild-type tissues, were identified as NPR1 or NPR2 (**Figure 3**). Doublet bands at ∼120 and 130 kDa represent differentially glycosylated and phosphorylated forms (Koller et al., 1993; Dickey et al., 2016; Shuhaibar et al., 2016).

Of the tissues tested, NPR1 was most highly expressed in the adrenal gland and testis (**Figure 3A**; 2 min exposure), whereas NPR2 was most highly expressed in ovary (**Figure 3B**; 3 min exposure). In addition to its presence in the adrenal gland and testis, NPR1 protein was detected at lower levels in kidney, lung, and ovary (**Figure 3A**; 2 and 10 min exposures). However, NPR1 was only detected in heart with more total protein loaded per lane and a longer exposure of the blot, indicating a relatively low expression level (**Figure 3A**; 40 μg protein, 20 min exposure). Consistently, although NPR1 activity is found in heart membranes, its activity in heart is only ∼10% of that in kidney (Wagner et al., 2022a). In addition to its presence in ovary, NPR2 was detected in adrenal gland, lung, heart, and epididymis (**Figure 3B**; 3 and 10 min exposures), and with a longer exposure of the blot, faint bands were seen in kidney and testis (**Figure 3B**; 30 min exposure). Previous western blot studies using HA-NPR2 mice have also demonstrated high NPR2 expression in primary chondrocytes (Shuhaibar et al., 2021).

Only a small subset of tissues was examined here, and previous studies indicate that many other tissues (including nerves, vasculature, and adipocytes) express these proteins as well (Kuhn, 2016; Schmidt et al., 2018, 2022). Because antibodies that are highly specific for NPR1 and NPR2 are not commercially available, mice expressing HA-tagged NPR1 and NPR2 will be useful for future studies evaluating protein expression levels in other tissues.

HA-NPR2 mice and HA antibodies have also been used to analyze the cellular localization of NPR2 within ovarian follicles, by immunofluorescence microscopy (Baena et al., 2020). These studies confirmed that NPR2 protein is present in granulosa cells, but not in the oocyte. Within the granulosa compartment, fluorescence measurements showed that the concentration of NPR2 is higher in the cumulus cells compared to the mural granulosa cells, and allowed a quantitative comparison of the amounts in each compartment (Baena et al., 2020). Immunofluorescence microscopy using HA-tagged NPR1 and NPR2 could also be useful for investigating the cellular distribution of these proteins in other complex tissues.

In addition to their use for examining protein expression levels in different tissues, HA-NPR2 mice and HA specific antibodies have been used together with Phostag gel western blots to show that fibroblast growth factor causes NPR2 dephosphorylation in chondrocytes (Shuhaibar et al., 2021). Similar methods using HA-NPR2 mice also showed that luteinizing hormone causes NPR2 dephosphorylation in ovarian follicles (Egbert et al., 2021), confirming previous studies using ovarian follicles from wild-type rats and an antibody made against an NPR2 peptide (Egbert et al., 2014).

Importantly, no obvious morphological or physiological defects have been noted with the HA-NPR1 and HA-NPR2 mice. A previous study demonstrated that addition of an epitope tag of similar size (FLAG, DYKDDDDK) to the N-terminus of NPR1 had no effect on the ANP concentration required to activate NPR1 guanylyl cyclase activity, or on the kinetics of the activation (Schröter et al., 2010). The N-terminal FLAG tag also had no effect on the expression level or subcellular

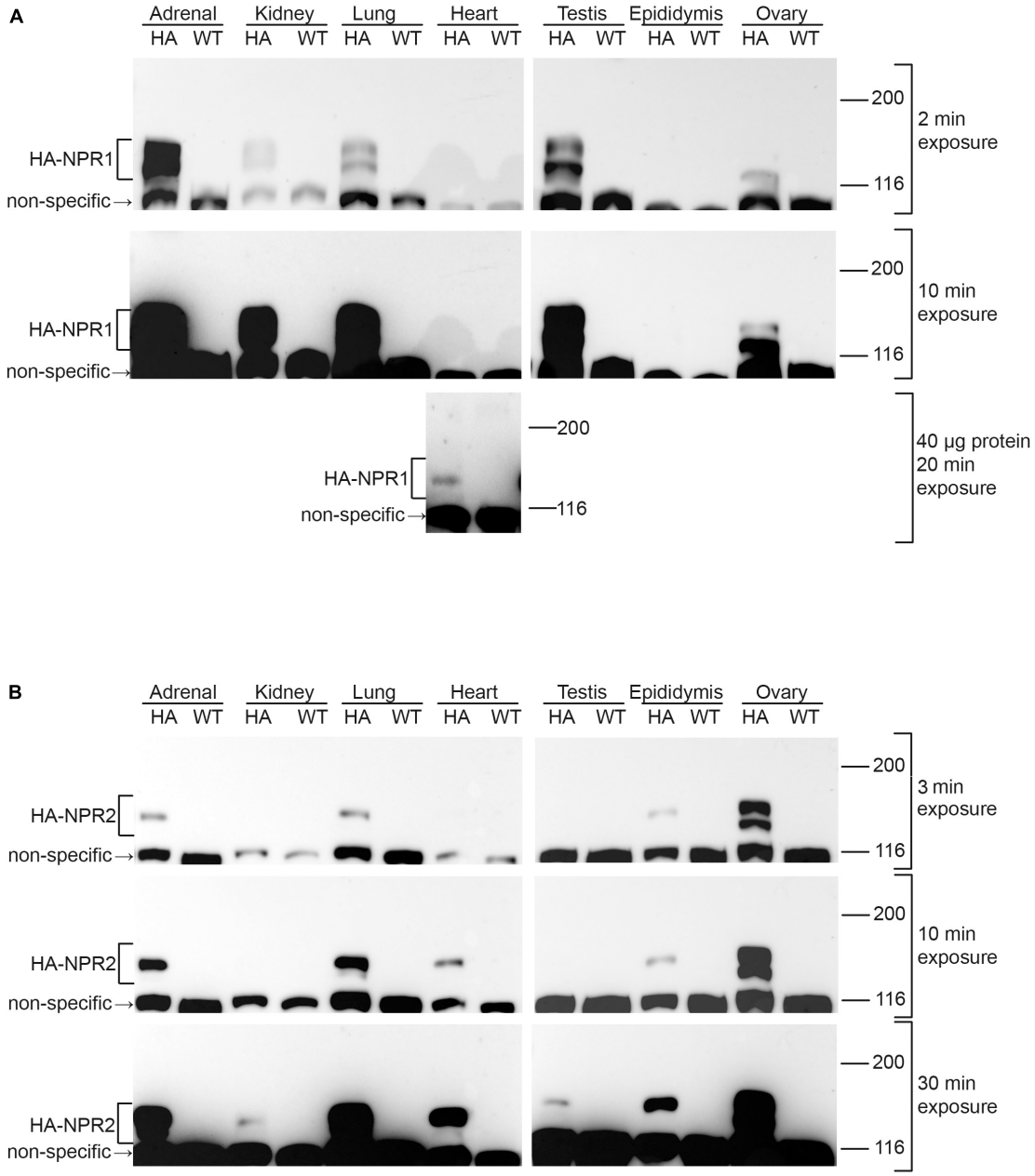

FIGURE 3
Western blots of NPR1 and NPR2 proteins in native tissues from mice expressing HA-NPR1 and HA-NPR2. Tissue samples from homozygous HA-NPR1 **(A)** and HA-NPR2 **(B)** mice were prepared similarly (see section "Methods"). Except as indicated, 20 µg of protein was loaded per lane (determined by a BCA assay). Three exposures of each blot are shown. Bands corresponding to NPR1 and NPR2 are seen only in the samples from the mice with the HA tags, not in those from wild-type mice. Doublet bands at ~120 and 130 kDa represent differentially glycosylated and phosphorylated forms (Koller et al., 1993; Dickey et al., 2016; Shuhaibar et al., 2016). A non-specific band is present at ~110 kDa. The figure shows only the top half of the blots, where NPR1 and NPR2 are located; the complete range of molecular weights for the blots in **(A)** is shown in **Supplementary Figure 1A**. **Supplementary Figures 1B,C** shows corresponding Ponceau stained blots and densitometry measurements, confirming that equal amounts of protein were loaded per lane.

localization of the NPR1 protein (Schröter et al., 2010). These findings for N-terminally FLAG-tagged NPR1, together with the evidence for the normal function of N-terminally HA-tagged NPR2 discussed below, support the conclusion that the HA-tag on NPR1 is unlikely to perturb its function.

A previous study demonstrated that addition of an HA tag to the N-terminus of NPR2 did not alter physiological processes that depend on NPR2 activity: regulation of meiotic arrest and resumption in ovarian follicles (Baena et al., 2020), and dephosphorylation of NPR2 in ovarian follicles and in

chondrocytes in response to hormone or growth factor signaling (Egbert et al., 2021; Shuhaibar et al., 2021). In addition, the cumulative numbers of pups weaned from both HA-NPR2 and HA-NPR1 homozygous breeding pairs were similar to the numbers of pups weaned from wild-type pairs (Baena et al., 2020 for HA-NPR2, and similar results for HA-NPR1). Thus the presence of the HA tags on NPR1 and NPR2 N-termini did not appear to impair the function of these proteins.

Use of NPR1-8E and NPR2-7E mice to investigate physiological functions of NPR1 and NPR2 phosphorylation

Analysis of the effects of substituting glutamates for the juxtamembrane phosphorylated serines and threonines of NPR1 and NPR2 in cells *in vitro* identified multiple phosphorylation sites in NPR1 and NPR2 that are important for regulation of enzyme activity (Potter and Hunter, 1998a,b, 1999; Schröter et al., 2010; Yoder et al., 2010, 2012; Otto et al., 2017). Subsequently, mice homozygous for these same mutations were generated, allowing determination of the functional consequences of the NPR2-7E mutations in ovarian follicles (Shuhaibar et al., 2016; Egbert et al., 2018), growing bones (Shuhaibar et al., 2017; Wagner et al., 2021), and adult bones (Robinson et al., 2020; Wagner et al., 2022b). Likewise, the NPR1-8E mutations were found to alter cardiac size and function, as well as plasma steroid and creatinine levels (Wagner et al., 2022a). Here we summarize what has been learned from these mice, and present new results about cardiac function in aging mice.

Importantly, previous studies have indicated that the NPR1-8E or NPR2-7E mutations have no effect on the ANP or CNP concentrations required to activate guanylyl cyclase activity (Shuhaibar et al., 2016; Otto et al., 2017) or on circulating plasma ANP, BNP, or CNP concentrations (Wagner et al., 2021, 2022b). The similar EC_{50} values for natriuretic peptide-dependent cyclic GMP generation indicate that the mutations do not affect ANP or CNP binding to their receptors. The 8E and 7E mutations also do not affect the amount of NPR1 and NPR2 protein in tissues from these mice (Shuhaibar et al., 2016, 2017; Wagner et al., 2022a).

Function of NPR2 phosphorylation state in control of meiotic progression in oocytes within ovarian follicles

In mammalian preovulatory ovarian follicles, cGMP produced by NPR2 in the somatic (granulosa) cells diffuses through gap junctions to the oocyte, where it prevents meiotic resumption (Norris et al., 2009; Zhang et al., 2010; Robinson et al., 2012; Geister et al., 2013; Shuhaibar et al., 2015). The mid-cycle surge of luteinizing hormone (LH) restarts oocyte meiosis largely through the rapid dephosphorylation and inactivation of NPR2, which lowers cGMP levels in the granulosa cells, and by way of gap junctions, lowers cGMP in the oocyte as well (Egbert et al., 2014, 2021; Shuhaibar et al., 2015). This model was conclusively tested with follicles from NPR2-7E/7E mice, which maintain elevated cGMP levels in the presence of LH (Shuhaibar et al., 2016; Egbert et al., 2018). In NPR2-7E/7E follicles, LH-induced oocyte meiotic resumption is delayed by 5 h, although it eventually occurs due to other parallel, but slower, signaling mechanisms (Shuhaibar et al., 2016).

Function of NPR2 phosphorylation state in control of bone length, mass, and strength

In chondrocytes of the growth plate in the bones of young mice, cGMP produced by CNP stimulation of NPR2 promotes bone elongation (Yasoda et al., 1998). Bones are shorter in mice and people with mutations that inactivate NPR2 (Bartels et al., 2004; Tamura et al., 2004; Tsuji and Kunieda, 2005; Khan et al., 2012; Geister et al., 2013; Nakao et al., 2015; Schmidt et al., 2018). Conversely bone length is increased by mutations that result in increased NPR2 activity in the absence of CNP (Miura et al., 2012, 2014; Hannema et al., 2013).

One pathway opposing bone elongation is fibroblast growth factor (FGF) signaling, which dephosphorylates and inactivates NPR2 in chondrocytes (Robinson et al., 2017; Shuhaibar et al., 2021), lowering cGMP levels in the growth plate (Shuhaibar et al., 2017, 2021). However, in growth plates from mice globally expressing NPR2-7E/7E, FGF has no effect on NPR2 activity, indicating that NPR2 dephosphorylation contributes to FGF signaling in chondrocytes (Shuhaibar et al., 2017). Correspondingly, NPR2-7E/7E mice have longer bones compared to wild-type mice (Shuhaibar et al., 2017; Wagner et al., 2021). Importantly, in mice with an activating mutation of the human FGF receptor 3 (FGFR3-G380R), which is a model of the congenital form of short stature known as achondroplasia (Lee et al., 2017), bone growth is rescued when the FGFR3-G380R mice are crossed with NPR2-7E/7E mice (Wagner et al., 2021). This suggests that a key part of the mechanisms that cause achondroplasia is the ability of FGFR3 activation to promote the dephosphorylation of NPR2. A phosphatase inhibitor that opposes this dephosphorylation increases bone elongation in a mouse model of achondroplasia (Shuhaibar et al., 2021).

In addition to these effects on bone elongation, the bones of NPR2-7E/7E mice have higher mineral density, a larger network of trabeculae, a thicker cortex, and larger diameter compared to wild type (Robinson et al., 2020). As a result of these features, NPR2-7E/7E tibias and femurs have elevated stiffness, toughness, and maximum load before fracture compared to wild type. Thus, NPR2-7E/7E mice not only have longer bones, but also increased bone mass and bone strength, as a result of increased osteoblasts as well as decreased osteoclasts (Robinson et al., 2020; Wagner et al., 2022b).

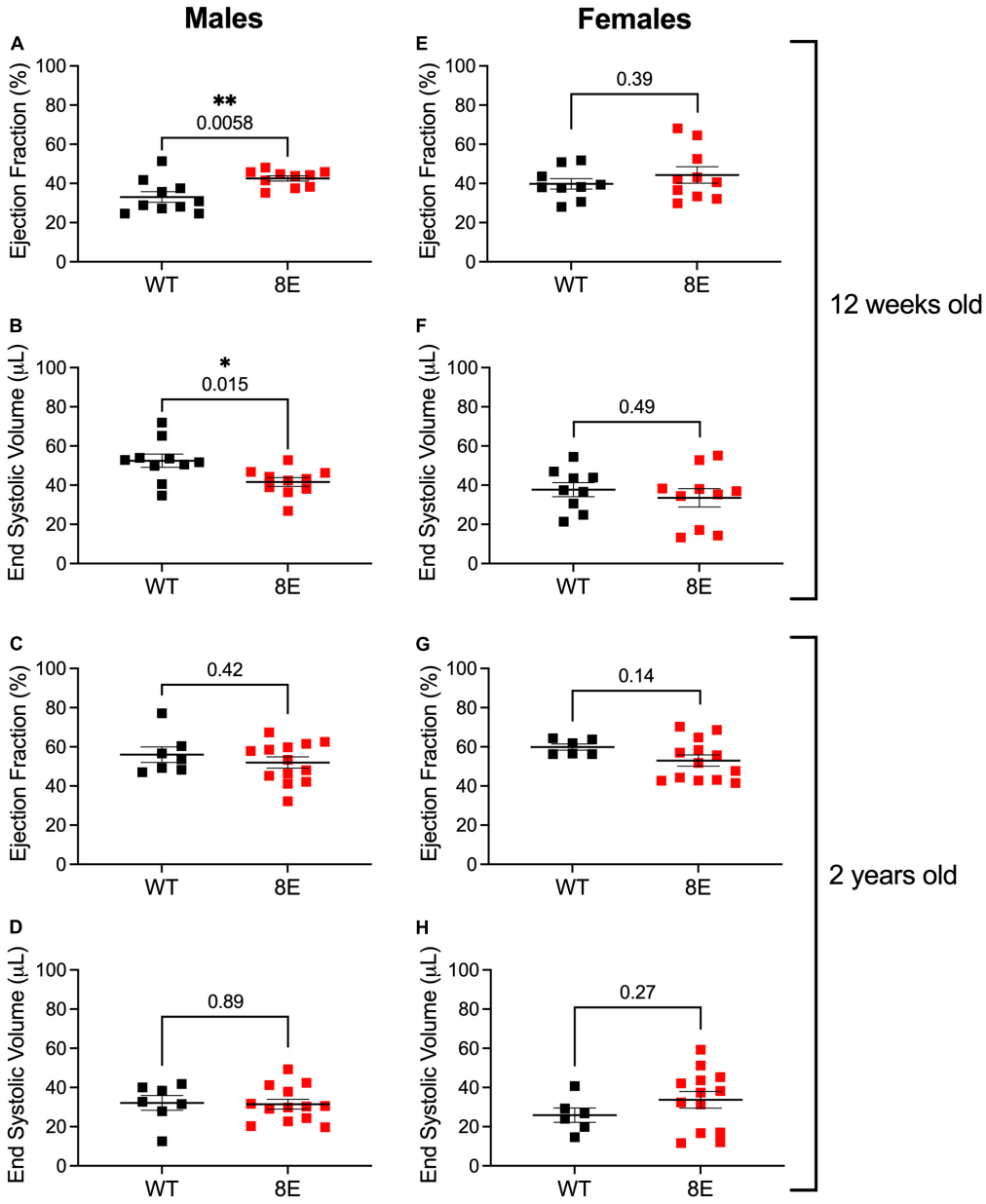

FIGURE 4
Unlike 12-week-old NPR1-8E male mice, 2-year-old NPR1-8E male mice do not have increased ejection fractions or decreased end systolic volumes. 12-week-old **(A,B,E,F)** and 2-year old **(C,D,G,H)** male and female mice were assessed by echocardiography for ejection fractions and end systolic volumes as described by Wagner et al. (2022a). Data for NPR1-WT and NPR1-8E mice are shown by black and red symbols, respectively. Long horizontal bars indicate the mean and vertical bars indicate SEM. Statistical differences were determined using a two-tailed student's *t*-test with associated *p*-values shown in each panel; asterisks indicate significant differences $*p < 0.05$ and $**p < 0.01$. Heart rates at the time of imaging were the same for all groups (**Supplementary Table 2**). **(A,B,E,F)** Reproduced, as permitted by the publisher, from Wagner et al. (2022a).

Function of NPR1 phosphorylation state in control of heart size and contractility

Twelve-week-old male NPR1-8E/8E mice have smaller hearts. This is due to smaller cardiomyocytes, resulting from diminished cardiac extracellular regulated kinase (ERK) activity (Wagner et al., 2022a). Importantly, the smaller hearts have improved systolic function, as indicated by increased ejection fraction and decreased end systolic volume (Wagner et al., 2022a; **Figures 4A,B**). These findings indicate that NPR1 phosphorylation is a regulator of heart size and contractility.

However, heart weight, ejection fraction, and end systolic volume in 12-week-old female mice were unaffected by the 8E mutations, despite similar levels of NPR1 protein in female and male mice (Wagner et al., 2022a; **Figures 4E,F**). Ejection fraction and end systolic volume were also unaffected by the 8E mutations in 2-year-old male or female mice (**Figures 4C,D,G,H**). Nevertheless, the hearts from the 2-year-old male NPR1-8E mice ($n = 9$) remained significantly smaller than hearts from age-matched wild-type male mice ($n = 5$) ($p = 0.0002$; two-tailed t-test).

Because NPR1 is expressed in multiple tissues, and at relatively low levels in the heart itself (**Figure 3A** and Wagner et al., 2022a), the effects of the 8E mutations on cardiac size and function, and their gender and age dependence, could have multiple causes. A direct effect of the phosphorylation state of NPR1 in the heart (Holtwick et al., 2003), which could be affected by adrenergic or other agonists, is one possible mechanism; systemic effects of elevated aldosterone and testosterone (Wagner et al., 2022a), could also contribute. Future studies of mice with tissue specific NPR1-8E mutations could help to identify the tissues in which NPR1 phosphorylation state acts to regulate cardiac function. Likewise, mice with HA-tagged NPR1 could be used to investigate the age dependence of NPR1 expression in the heart, which could contribute to understanding of why NPR1 phosphorylation state is a regulator of heart function only in young males. Similar studies of heart function in NPR2-7E mice would also be informative, and mice with HA-tagged NPR1 and NPR2 could be useful for analysis of the cellular and subcellular distribution of these proteins in the heart (Subramanian et al., 2018). Furthermore, these mice could be used to test whether inputs from the autonomic nervous system alter the phosphorylation state of NPR1 or NPR2 in the heart or other tissues (see below).

Function of NPR1 phosphorylation state in control of steroid generation in testis and adrenal gland

Correlating with the high levels of expression of NPR1 in testis and adrenal gland (**Figure 3**), plasma levels of steroids produced by these tissues, testosterone and aldosterone, respectively, are elevated in young male NPR1-8E/8E mice (Wagner et al., 2022a). Correspondingly, luteinizing hormone (LH) receptor agonists, and the NPR1 agonists ANP and BNP, elevate cGMP and stimulate production of testosterone in Leydig cells from rat testis (Andric et al., 2007). Thus the elevation of testosterone in NPR1-8E/8E mice suggests that LH stimulation of testosterone production could result in part from phosphorylation of NPR1. In future studies, HA-NPR1 mice and Phostag gel western blot analysis could be used to investigate if NPR1 phosphorylation in testis is increased in response to LH. In the adrenal gland, the stimulation of aldosterone production in zona glomerulosa cells by adrenocorticotropic hormone and by angiotensin II, is cGMP-dependent (Gambaryan et al., 2003), suggesting that NPR1 phosphorylation might also contribute to the action of these agonists. If LH, ACTH, and/or AngII do increase NPR1 phosphorylation, the phosphorylation state of NPR1 could be investigated as a possible mediator of hormone-stimulated testosterone and aldosterone synthesis. Similarly, autonomic inputs to these tissues could lead to changes in NPR1 phosphorylation, possibly revealing another facet of steroid regulation.

Summary and future directions

The discovery 25 years ago that the guanylyl cyclase activity of natriuretic peptide receptors requires receptor phosphorylation (Potter and Hunter, 1998a,b, 1999) raised the question of how this regulatory mechanism might function physiologically. Studies using the genetically modified mice described here have identified hormonal signaling pathways that act by decreasing phosphorylation of NPR2 in ovary and bone (Shuhaibar et al., 2016, 2017, 2021; Egbert et al., 2018, 2021; Robinson et al., 2020; Wagner et al., 2021, 2022b). Recent studies using these mice have suggested that related mechanisms may regulate physiological signaling in other organs such as the heart, testis and adrenal gland (Wagner et al., 2022a). Future studies using these and related mouse lines may help to elucidate these functions.

Data availability statement

Cryopreserved embryos for the mouse lines described here are freely available by request: HA-NPR1 (global), HA-NPR2 (global), PA-NPR2 (global), NPR1-8E (global), NPR2-7E (global), and NPR2-7E (conditional). Requests should be addressed to S-PY (syee@uchc.edu).

Ethics statement

This animal study was reviewed and approved by Institutional Animal Care and Use Committees at UCONN Health and University of Minnesota.

Author contributions

S-PY, KL, and DK designed, generated, and validated the genetically modified mice. JE, TU, and LJ designed, performed,

and analyzed the protein expression studies. BW, CH, TO'C, and LP designed, performed, and analyzed the heart measurements. JE, LP, S-PY, and LJ wrote the manuscript. All authors reviewed and approved it.

Funding

This study was supported by grants from the National Institutes of Health: R37 HD014939 from the *Eunice Kennedy Shriver* National Institute of Child Health and Human Development (LJ) and R01 HL130099 and R01 HL152215 from the National Heart, Lung, and Blood Institute (LP and TO'C). Additional funding was provided by grants from the Health Center Research Advisory Council (S-PY), the Fund for Science (LJ and LP), the Hormone Research Fund (LP), and by a University of Minnesota-Mayo Clinic Partnership Grant and a University of Minnesota Academic Health Center Faculty Research and Development Grant (LP).

Acknowledgments

We thank Leia Shuhaibar, Jerid Robinson, Valentina Baena, and Corie Owen for their contributions to the development of the mouse lines described here.

Conflict of interest

The authors declare that the research was conducted in the absence of any commercial or financial relationships that could be construed as a potential conflict of interest.

Publisher's note

Supplementary material

The Supplementary Material for this article can be found online at: https://www.frontiersin.org/articles/10.3389/fnmol.2022.1007026/full#supplementary-material

References

Andric, S. A., Janjic, M. M., Stojkov, N. J., and Kostic, T. S. (2007). Protein kinase G-mediated stimulation of basal Leydig cell steroidogenesis. *Am. J. Physiol. Endocrinol. Metab.* 293, E1399–E1408. doi: 10.1152/ajpendo.00482.2007

Baena, V., Owen, C. M., Uliasz, T. F., Lowther, K. M., Yee, S.-P., Terasaki, M., et al. (2020). Cellular heterogeneity of the LH receptor and its significance for cyclic GMP signaling in mouse preovulatory follicles. *Endocrinology* 161:bqaa074. doi: 10.1210/endocr/bqaa074

Bartels, C. F., Bükülmez, H., Padayatti, P., Rhee, D. K., van Ravenswaaij-Arts, C., Pauli, R. M., et al. (2004). Mutations in the transmembrane natriuretic peptide receptor NPR-B impair skeletal growth and cause acromesomelic dysplasia, type Maroteaux. *Am. J. Hum. Genet.* 75, 27–34. doi: 10.1086/422013

Dickey, D. M., Edmund, A. B., Otto, N. M., Chaffee, T. S., Robinson, J. W., and Potter, L. R. (2016). Catalytically active guanylyl cyclase B requires endoplasmic reticulum-mediated glycosylation, and mutations that inhibit this process cause dwarfism. *J. Biol. Chem.* 291, 11385–11393. doi: 10.1074/jbc.M115.704015

Edmund, A. B., Walseth, T. F., Levinson, N. M., and Potter, L. R. (2019). The pseudokinase domains of guanylyl cyclase-A and -B allosterically increase the affinity of their catalytic domains for substrate. *Sci. Signal.* 12:eaau5378. doi: 10.1126/scisignal.aau5378

Egbert, J. R., Robinson, J. W., Uliasz, T. F., Potter, L. R., and Jaffe, L. A. (2021). Cyclic AMP links luteinizing hormone signaling to dephosphorylation and inactivation of the NPR2 guanylyl cyclase in ovarian follicles. *Biol. Reprod.* 104, 939–941. doi: 10.1093/biolre/ioab029

Egbert, J. R., Shuhaibar, L. C., Edmund, A. B., Van Helden, D. A., Robinson, J. W., Uliasz, T. F., et al. (2014). Dephosphorylation and inactivation of the NPR2 guanylyl cyclase in the granulosa cells contributes to the LH-induced cGMP decrease that causes meiotic resumption in rat oocytes. *Development* 141:3594–3604. doi: 10.1242/dev.112219

Egbert, J. R., Yee, S.-P., and Jaffe, L. A. (2018). Luteinizing hormone signaling phosphorylates and activates the cyclic GMP phosphodiesterase PDE5 in mouse ovarian follicles, contributing an additional component to the hormonally induced decrease in cyclic GMP that reinitiates meiosis. *Dev. Biol.* 435, 6–14. doi: 10.1016/j.ydbio.2018.01.008

Feil, R., Lehners, M., Stehle, D., and Feil, S. (2022). Visualising and understanding cGMP signals in the cardiovascular system. *Br. J. Pharmacol.* 179, 2394–2412. doi: 10.1111/bph.15500

Gambaryan, S., Butt, E., Marcus, K., Glazova, M., Palmetshofer, A., Guillon, G., et al. (2003). cGMP-dependent protein kinase type II regulates basal level of aldosterone production by zona glomerulosa cells without increasing expression of the steroidogenic acute regulatory protein gene. *J. Biol. Chem.* 278, 29640–29648. doi: 10.1074/jbc.M302143200

Geister, K. A., Brinkmeier, M. L., Hsieh, M., Faust, S. M., Karolyi, I. J., Perosky, J. E., et al. (2013). A novel loss-of-function mutation in Npr2 clarifies primary role in female reproduction and reveals a potential therapy of acromesomelic dysplasia, Maroteaux type. *Hum. Mol. Genet.* 22, 345–357. doi: 10.1093/hmg/dds432

Götz, K. R., Sprenger, J. U., Perera, R. K., Steinbrecher, J. H., Lehnart, S. E., Kuhn, M., et al. (2014). Transgenic mice for real-time visualization of cGMP in intact adult cardiomyocytes. *Cir. Res.* 114, 1235–1245. doi: 10.1161/CIRCRESAHA.114.302437

Hannema, S. E., Duyvenvoorde, H. A., Premsler, T., Yang, R. B., Mueller, T. D., Gassner, B., et al. (2013). An activating mutation in the kinase homology domain of the natriuretic peptide receptor-2 causes extremely tall stature without skeletal deformities. *J. Clin. Endocrinol. Metab.* 98, E1988–E1998. doi: 10.1210/jc.2013-2358

Holtwick, R., van Eickels, M., Skryabin, B. V., Baba, H. A., Bubikat, A., Begrow, F., et al. (2003). Pressure-independent cardiac hypertrophy in mice with cardiomyocyte-restricted inactivation of the atrial natriuretic peptide receptor guanylyl cyclase-A. *J. Clin. Invest.* 111, 1399–1407. doi: 10.1172/JCI17061

Jaffe, L. A., and Egbert, J. R. (2017). Regulation of mammalian oocyte meiosis by intercellular communication within the ovarian follicle. *Ann. Rev. Physiol.* 79, 237–260. doi: 10.1146/annurev-physiol-022516-034102

Khan, S., Ali, R. H., Abbasi, S., Nawaz, M., Muhammed, N., and Ahmad, W. (2012). Novel mutations in natriuretic peptide receptor-2 gene underlie acromesomelic dysplasia, type maroteaux. *BMC Med. Genet.* 13:44. doi: 10.1186/1471-2350-13-44

Koller, K. J., Lipari, M. T., and Goeddel, D. V. (1993). Proper glycosylation and phosphorylation of the type A natriuretic peptide receptor are required for hormone-stimulated guanylyl cyclase activity. *J. Biol. Chem.* 268, 5997–6003.

Kuhn, M. (2016). Molecular physiology of membrane guanylyl cyclase receptors. *Physiol. Rev.* 96, 751–804. doi: 10.1152/physrev.00022.2015

Lee, Y. C., Song, I. W., Pai, Y. J., Chen, S. D., and Chen, Y. T. (2017). Knock-in human FGFR3 achondroplasia mutation as a mouse model for human skeletal dysplasia. *Sci. Rep.* 7:43220. doi: 10.1038/srep43220

Miura, K., Kim, O. H., Lee, H. R., Namba, N., Michigami, T., Yoo, W. J., et al. (2014). Overgrowth syndrome associated with a gain-of-function mutation of the natriuretic peptide receptor 2 (NPR2) gene. *Am. J. Med. Genet. A* 164A, 156–163. doi: 10.1002/ajmg.a.36218

Miura, K., Namba, N., Fujiwara, M., Ohata, Y., Ishida, H., Kitaoka, T., et al. (2012). An overgrowth disorder associated with excessive production of cGMP due to a gain-of-function mutation of the natriuretic peptide receptor 2 gene. *PLoS One* 7:e42180. doi: 10.1371/journal.pone.0042180

Nakao, K., Osawa, K., Yasoda, A., Yamanaka, S., Fujii, T., Kondo, E., et al. (2015). The local CNP/GC-B system in growth plate is responsible for physiological endochondral bone growth. *Sci. Rep.* 5:10554. doi: 10.1038/srep10554

Norris, R. P., Ratzan, W. J., Freudzon, M., Mehlmann, L. M., Krall, J., Movsesian, M. A., et al. (2009). Cyclic GMP from the surrounding somatic cells regulates cyclic AMP and meiosis in the mouse oocyte. *Development* 136, 1869–1878. doi: 10.1242/dev.035238

Oliver, P. M., Fox, J. E., Kim, R., Rockman, H. A., Kim, H.-S., Reddick, R. L., et al. (1997). Hypertension, cardiac hypertrophy, and sudden death in mice lacking natriuretic peptide receptor A. *Proc. Natl. Acad. Sci. U.S.A.* 94, 14730–14735. doi: 10.1073/pnas.94.26.14730

Oliver, P. M., John, S. W. M., Purdy, K. E., Kim, R., Maeda, N., Goy, M. F., et al. (1998). Natriuretic peptide receptor 1 expression influences blood pressures of mice in a dose-dependent manner. *Proc. Natl. Acad. Sci. U.S.A.* 95, 2547–2551. doi: 10.1073/pnas.95.5.2547

Otto, N. M., McDowell, W. G., Dickey, D. M., and Potter, L. R. (2017). A glutamate-substituted mutant mimics the phosphorylated and active form of guanylyl cyclase-A. *Mol. Pharmacol.* 92, 67–74. doi: 10.1124/mol.116.107995

Pandey, K. N. (2019). Genetic ablation and guanylyl cyclase/natriuretic peptide receptor-A: impact on the pathophysiology of cardiovascular dysfunction. *Int. J. Mol. Sci.* 20:3946. doi: 10.3390/ijms20163946

Potter, L. R. (2011). Regulation and therapeutic targeting of peptide-activated receptor guanylyl cyclases. *Pharmacol. Ther.* 130, 71–82. doi: 10.1016/j.pharmthera.2010.12.005

Potter, L. R., and Hunter, T. (1998a). Phosphorylation of the kinase homology domain is essential for activation of the A-type natriuretic peptide receptor. *Mol. Cell. Biol.* 18, 2164–2172. doi: 10.1128/MCB.18.4.2164

Potter, L. R., and Hunter, T. (1998b). Identification and characterization of the major phosphorylation sites of the B-type natriuretic peptide receptor. *J. Biol. Chem.* 273, 15533–15539. doi: 10.1074/jbc.273.25.15533

Potter, L. R., and Hunter, T. (1999). Identification and characterization of the phosphorylation sites of the guanylyl cyclase-linked natriuretic peptide receptors A and B. *Methods* 19, 506–520. doi: 10.1006/meth.199.0893

Robinson, J. W., Blixt, N. C., Norton, A., Mansky, K. C., Ye, Z., Aparicio, C., et al. (2020). Male mice with elevated C-type natriuretic peptide-dependent guanylyl cyclase-B activity have increased osteoblasts, bone mass and bone strength. *Bone* 135:115320. doi: 10.1016/j.bone.2020.115320

Robinson, J. W., Egbert, J. R., Davydova, J., Schmidt, H., Jaffe, L. A., and Potter, L. R. (2017). Dephosphorylation is the mechanism of fibroblast growth factor inhibiton of guanylyl cyclase-B. *Cell. Signal.* 40, 222–229. doi: 10.1016/j.cellsig.2017.09.021

Robinson, J. W., Zhang, M., Shuhaibar, L. C., Norris, R. P., Geerts, A., Wunder, F., et al. (2012). Luteinizing hormone reduces the activity of the NPR2 guanylyl cyclase in mouse ovarian follicles, contributing to the cGMP decrease that promotes resumption of meiosis in oocytes. *Dev. Biol.* 366, 308–316. doi: 10.1016/j.ydbio.2012.04.019

Sander, H., Wallace, S., Plouse, R., Tiwari, S., and Gomes, A. V. (2019). Ponceau S waste: Ponceau S staining for total protein normalization. *Anal. Biochem.* 575, 44–53. doi: 10.1016/j.ab.2019.03.010

Schmidt, H., Böttcher, A., Gross, T., and Schmidtko, A. (2022). cGMP signalling in dorsal root ganglia and the spinal cord: various functions in development and adulthood. *Br. J. Pharmacol.* 179, 2361–2377. doi: 10.1111/bph.15514

Schmidt, H., Dickey, D. M., Dumoulin, A., Octave, M., Robinson, J. W., Kühn, R., et al. (2018). Regulation of the natriuretic peptide receptor 2 (Npr2) by phosphorylation of juxtamembrane serine and threonine residues is essential for bifurcation of sensory axons. *J. Neurosci.* 38, 9768–9780. doi: 10.1523/JNEUROSCI.0495-18.2018

Schröter, J., Zahedi, R. P., Hartmann, M., Gassner, B., Gazinski, A., Waschke, J., et al. (2010). Homologous desensitization of guanylyl cyclase A, the receptor for atrial natriuretic peptide, is associated with a complex phosphorylation pattern. *FEBS J.* 277, 2440–2453. doi: 10.1111/j.1742-4658.2010.07658.x

Shuhaibar, L. C., Egbert, J. R., Edmund, A. B., Uliasz, T. F., Dickey, D. M., Yee, S.-P., et al. (2016). Dephosphorylation of juxtamembrane serines and threonines of the NPR2 guanylyl cyclase is required for rapid resumption of oocyte meiosis in response to luteinizing hormone. *Dev. Biol.* 409, 194–201. doi: 10.1016/j.ydbio.2015.10.025

Shuhaibar, L. C., Egbert, J. R., Norris, R. P., Lampe, P. D., Nikolaev, V. O., Thunemann, M., et al. (2015). Intercellular signaling *via* cyclic GMP diffusion through gap junctions restarts meiosis in mouse ovarian follicles. *Proc. Natl. Acad. Sci. U.S.A.* 112, 5527–5532. doi: 10.1073/pnas.1423598112

Shuhaibar, L. C., Kaci, N., Egbert, J. R., Horville, T., Loisay, L., Vigone, G., et al. (2021). Phosphatase inhibition by LB-100 enhances BMN-111 stimulation of bone growth. *JCI Insight* 6:e141426. doi: 10.1172/jci.insight.141426

Shuhaibar, L. C., Robinson, J. W., Vigone, G., Shuhaibar, N. P., Egbert, J. R., Baena, V., et al. (2017). Dephosphorylation of the NPR2 guanylyl cyclase contributes to inhibition of bone growth by fibroblast growth factor. *eLife* 6:e31343. doi: 10.7554/eLife.31343

Subramanian, H., Froese, A., Jönsson, P., Schmidt, H., Gorelik, J., and Nikolaev, V. O. (2018). Distinct submembrane localisation compartmentalises cardiac NPR1 and NPR2 signalling to cGMP. *Nat. Commun.* 9:2446. doi: 10.1038/s41467-018-04891-5

Tamura, N., Doolittle, L. K., Hammer, R. E., Shelton, J. M., Richardson, J. A., and Garbers, D. L. (2004). Critical roles of the guanylyl cyclase B receptor in endochondral ossification and development of female reproductive organs. *Proc. Natl. Acad. Sci. U.S.A.* 101, 17300–17305. doi: 10.1073/pnas.0407894101

Tang, S. H., Silva, F. J., Tsark, W. M., and Mann, J. R. (2002). A Cre/loxP-deleter transgenic line in mouse strain 129S1/SvImJ. *Genesis* 32, 199–202. doi: 10.1002/gene.10030

Tsuji, T., and Kunieda, T. (2005). A loss-of-function mutation in natriuretic peptide receptor 2 (Npr2) gene is responsible for disproportionate dwarfism in cn/cn mouse. *J. Biol. Chem.* 280, 14288–14292. doi: 10.1074/jbc.C500024200

Wagner, B. M., Robinson, J. R., Lin, Y.-W., Li, Y.-C., Kaci, N., Legeai-Mallet, L., et al. (2021). Prevention of guanylyl cyclase-B dephosphorylation rescues achondroplastic dwarfism. *JCI Insight* 6:e147832. doi: 10.1172/jci.insight.147832

Wagner, B. M., Robinson, J. W., Healy, C. L., Gauthier, M., Dickey, D. M., Yee, S.-P., et al. (2022a). Guanylyl cyclase-A phosphorylation decreases cardiac hypertrophy and improves systolic function in male, but not female, mice. *FASEB J.* 36:e22069. doi: 10.1096/fj.202100600RRR

Wagner, B. M., Robinson, J. W., Prickett, T. C. R., Espiner, E. A., Khosla, S., Gaddys, D., et al. (2022b). Guanylyl cyclase-B dependent bone formation in mice is associated with youth, increased osteoblasts, and decreased osteoclasts. *Calcified Tissue Int.* doi: 10.1007/s00223-022-01014-7 [Epub ahead of print].

Yasoda, A., Ogawa, Y., Suda, M., Tamura, N., Mori, K., Sakuma, Y., et al. (1998). Natriuretic peptide regulation of endochondral ossification. Evidence for possible roles of the C-type natriuretic peptide/guanylyl cyclase-B pathway. *J. Biol. Chem.* 273, 11695–11700. doi: 10.1074/jbc.273.19.11695

Yoder, A. R., Robinson, J. W., Dickey, D. M., Andersland, J., Rose, B. A., Stone, M. D., et al. (2012). A functional screen provides evidence for a conserved, regulatory juxtamembrane phosphorylation site in guanylyl cyclase A and B. *PLoS One* 7:e36747. doi: 10.1371/journal.pone.0036747

Yoder, A. R., Stone, M. D., Griffin, T. J., and Potter, L. R. (2010). Mass spectrometric identification of phosphorylation sites in guanylyl cyclase A and B. *Biochemistry* 49, 10137–10145. doi: 10.1021/bi101700e

Zhang, M., Su, Y.-Q., Sugiura, K., Xia, G., and Eppig, J. J. (2010). Granulosa cell ligand NPPC and its receptor NPR2 maintain meiotic arrest in mouse oocytes. *Science* 330, 366–369. doi: 10.1126/science.1193573

frontiers | Frontiers in Molecular Neuroscience

TYPE Original Research
PUBLISHED 04 November 2022
DOI 10.3389/fnmol.2022.1012784

OPEN ACCESS

EDITED BY
Clint L. Makino,
Boston University,
United States

REVIEWED BY
Sadaharu Miyazono,
Asahikawa Medical University,
Japan
Robert Lukowski,
University of Tübingen,
Germany

*CORRESPONDENCE
Lincoln R. Potter
potter@umn.edu

SPECIALTY SECTION
This article was submitted to Molecular Signalling and Pathways, a section of the journal Frontiers in Molecular Neuroscience

RECEIVED 05 August 2022
ACCEPTED 22 September 2022
PUBLISHED 04 November 2022

CITATION
Otto NM and Potter LR (2022) Vicinal glutamates are better phosphomimetics: Phosphorylation is required for allosteric activation of guanylyl cyclase-A. *Front. Mol. Neurosci.* 15:1012784. doi: 10.3389/fnmol.2022.1012784

Vicinal glutamates are better phosphomimetics: Phosphorylation is required for allosteric activation of guanylyl cyclase-A

Neil M. Otto and Lincoln R. Potter*

Department of Biochemistry, Molecular Biology and Biophysics at the University of Minnesota, Minneapolis, MN, United States

Multisite phosphorylation of guanylyl cyclase (GC)-A, also known as NPR-A or NPR1, is required for receptor activation by natriuretic peptides (NPs) because alanine substitutions for the first four GC-A phosphorylation sites produce an enzyme that cannot be stimulated by NPs. In contrast, single Glu substitutions for the first six chemically identified GC-A phosphorylation sites to mimic the negative charge of phosphate produced an enzyme that is activated by NPs but had an elevated Michaelis constant (Km), resulting in low activity. Here, we show that vicinal (double adjacent) Glu substitutions for the same sites to mimic the two negative charges of phosphate produced a near wild type (WT) enzyme with a low Km. Unlike the enzyme with single glutamate substitutions, the vicinally substituted enzyme did not require the functionally identified Ser-473-Glu substitution to achieve WT-like activity. Importantly, the negative charge associated with either phosphorylation or glutamate substitutions was required for allosteric activation of GC-A by ATP. We conclude that vicinal Glu substitutions are better phosphomimetics than single Glu substitutions and that phosphorylation is required for allosteric activation of GC-A in the absence and presence of NP. Finally, we suggest that the putative functionally identified phosphorylation sites, Ser-473 in GC-A and Ser-489 in GC-B, are not phosphorylation sites at all.

KEYWORDS

phosphorylation, cyclic GMP, guanylyl cyclase, hypertension, heart failure, natriuretic peptide

Introduction

Atrial natriuretic peptide (NP) and B-type NP reduce blood pressure, blood volume, heart size and metabolism by activating guanylyl cyclase (GC)-A (Potter et al., 2006; Bordicchia et al., 2012; Kuhn, 2016). C-type natriuretic peptide (CNP) activation of the homologous enzyme, GC-B, regulates female reproduction, long bone growth and density, neuron bifurcation and other processes (Potter, 2011a,b; Kuhn, 2016; Jaffe and Egbert,

2017). Both GC-A and GC-B are homo-dimeric, single membrane-spanning enzymes that contain a glycosylated, extracellular ligand binding domain, a single membrane-spanning region and multi-domain intracellular region consisting of a serine and threonine phosphorylated kinase homology domain, dimerization domain and C-terminal catalytic domain (Figure 1; Potter et al., 2009; Potter, 2011a; Kuhn, 2016). GC-A and GC-B are synthesized by the ribosome, glycosylated in the E. R. and glycosylated again in the Golgi apparatus (Dickey et al., 2016). At this point, the KHD can be phosphorylated, which is required for activation of the GC domain by natriuretic peptide binding (Koller et al., 1993; Dickey et al., 2016). As a result of the extensive post-translational processing, GC-A is often found in as many as three species when purified by immunoprecipitation followed by SDS-PAGE. Importantly, it is only the highest MW, fully glycosylated species that is phosphorylated in these gels (Koller et al., 1993).

The kinase homology domain of GC-A, as well as the same domains in GC-B, GC-C, and GC-E, bind to and are allosterically regulated by ATP (Jewett et al., 1993; Parkinson et al., 1994; Foster and Garbers, 1998; Jaleel et al., 2006; Bereta et al., 2010; Robinson and Potter, 2012; Edmund et al., 2019), which is consistent with known functions of other pseudokinase domain containing enzymes (Murphy et al., 2014; Eyers and Murphy, 2016). Both GC-A and GC-B are maximally phosphorylated and maximally responsive to NPs in serum-starved cells (Potter and Garbers, 1992; Koller et al., 1993; Potter, 1998; Joubert et al., 2001), but prolonged NP exposure or brief exposure to chemical activators of protein kinase C or hormones or growth factors that antagonize the actions of NPs cause the dephosphorylation and inactivation GC-A and GC-B in cell culture (Figure 1; Chrisman and Garbers, 1999; Muller et al., 2006; Egbert et al., 2014; Robinson et al., 2017).

Six phosphorylation sites were initially identified by tryptic phosphopeptide mapping of $^{32}PO_4$ labeled GC-A protein isolated from transfected 293 cells (Potter and Hunter, 1998b). Later, two groups identified the same six sites and one new site, Ser-487, by mass spectrometry (Schroter et al., 2010; Yoder et al., 2010). Mutation of four or more phosphorylation sites to Ala to mimic a dephosphorylated residue resulted in an enzyme that bound NP but could not transmit the NP binding signal to the catalytic domain (Potter and Hunter, 1998b). Conversely, single Glu substitutions for the same six sites resulted in an enzyme that was activated by NPs but to a much lower level than that of the phosphorylated WT enzyme (Potter and Hunter, 1999). Later, a functional screen identified a conserved juxta-membrane serine, Ser-473 in GC-A (Yoder et al., 2012), that when mutated to glutamate to make GC-A-8E resulted in a dephosphorylated enzyme with enzymatic characteristics like the phosphorylated WT enzyme (Otto et al., 2017). However, no physical evidence for the phosphorylation of Ser-473 in GC-A, or the corresponding residue, Ser-489, in GC-B (Yoder et al., 2012), has been found despite extensive attempts, which cast doubt on whether Ser-473 or Ser-489 are actually phosphorylated in a biological setting.

The first and most common phosphomimetic amino acid substitutions were single glutamates or single aspartates, both of which have a charge of −1 (Thorsness and Koshland, 1987). However, phosphorylated amino acids can have a charge between −1 and −2 depending on the surrounding pH, since phosphates have 3 pKas of 2.2, 7.2, and 12.4 (Hunter, 2012). The cytosolic pH of HEK 293T cells that were used for most of the phosphorylation studies on GC-A and GC-B is 7.4 (Matsuyama et al., 2000), so a charge close to −2 is expected for phosphorylated amino acids. Here, we replicated the −2 charge of phosphate by using vicinal Glu substitutions. We show that vicinal Glu substitutions for the seven definitive, chemically, identified sites produces a WT like enzyme that is no longer regulated by the Ser-473-Glu substitution. Finally, maximal activation of GC-A requires ANP binding to the extracellular domain and ATP binding to an allosteric site or sites in the intracellular domain (Joubert et al., 2005; Antos and Potter, 2007; Burczynska et al., 2007; Robinson and Potter, 2012; Edmund et al., 2019). Phosphorylation is required for ANP-dependent activation of GC-A, but previous studies failed to detect effects of phosphorylation on basal activity (Potter and Garbers, 1992; Potter and Hunter, 1998b). In contrast, phosphorylation is required for allosteric regulation of the homologous sea urchin GC receptor (Ramarao and Garbers, 1988). Here, we show that allosteric activation of GC-A under basal and NP-stimulated conditions requires phosphorylation of the chemically identified phosphorylation sites. Finally, our data indicate that the "functionally identified" phosphorylation sites in GC-A (S473) and GC-B (S489), are unlikely to phosphorylated under biologic conditions.

Experimental

Reagents

^{125}I-cGMP radioimmunoassay kits were from Perkin Elmer (Waltham, MA) and unlabeled NPs were from Sigma (St. Louis, MO). Protease inhibitor tablets were from Roche, Inc. (Baltimore, MD).

Mutagenesis

Ala or Glu substitutions for single or multiple phosphorylation sites were generated on the CMV3-GC-A plasmid as previously described (Potter and Hunter, 1998b).

Abbreviations: cGMP, cyclic guanosine monophosphate; GC, guanylyl cyclase; Km, Michaelis constant; NP, natriuretic peptide; Vmax, maximal velocity; WT, wild type.

Transient transfection

Human embryonic kidney 293T cells were transiently transfected with 5 µg of pCMV3-GC-A plasmids containing single or multiple phosphorylation site mutations by the HEPES-calcium-phosphate precipitation method as previously described (Yoder et al., 2012).

Plasma membrane preparation

Cells cultured on 10 cm plates were placed in serum-free media for 4 h before membranes were prepared. Membranes were harvested at 4°C by washing the plates twice with phosphate buffered saline, scraping the cells off the plates in 0.6 ml phosphatase inhibitor buffer (PIB; Antos et al., 2005). Cells were lysed by sonication and the lysates were centrifuged at 20,000*g* for 15 min at 4°C. The supernatant was aspirated and the membrane pellet was resuspended with 0.5 ml PIB and centrifuged again at 20,000*g* for 15 min at 4°C. The supernatant was aspirated, and the pellet was resuspended in PIB to yield a protein concentration between 1 and 3 mg/ml. Crude membranes were assayed for GC activity without freezing.

Guanylyl cyclase assays

Crude membranes were assayed for GC activity at 37°C in a buffer containing 0.5 mM isomethylxanthine to inhibit phosphodiesterases, 5 mM $MgCl_2$, and a nucleotide regenerating

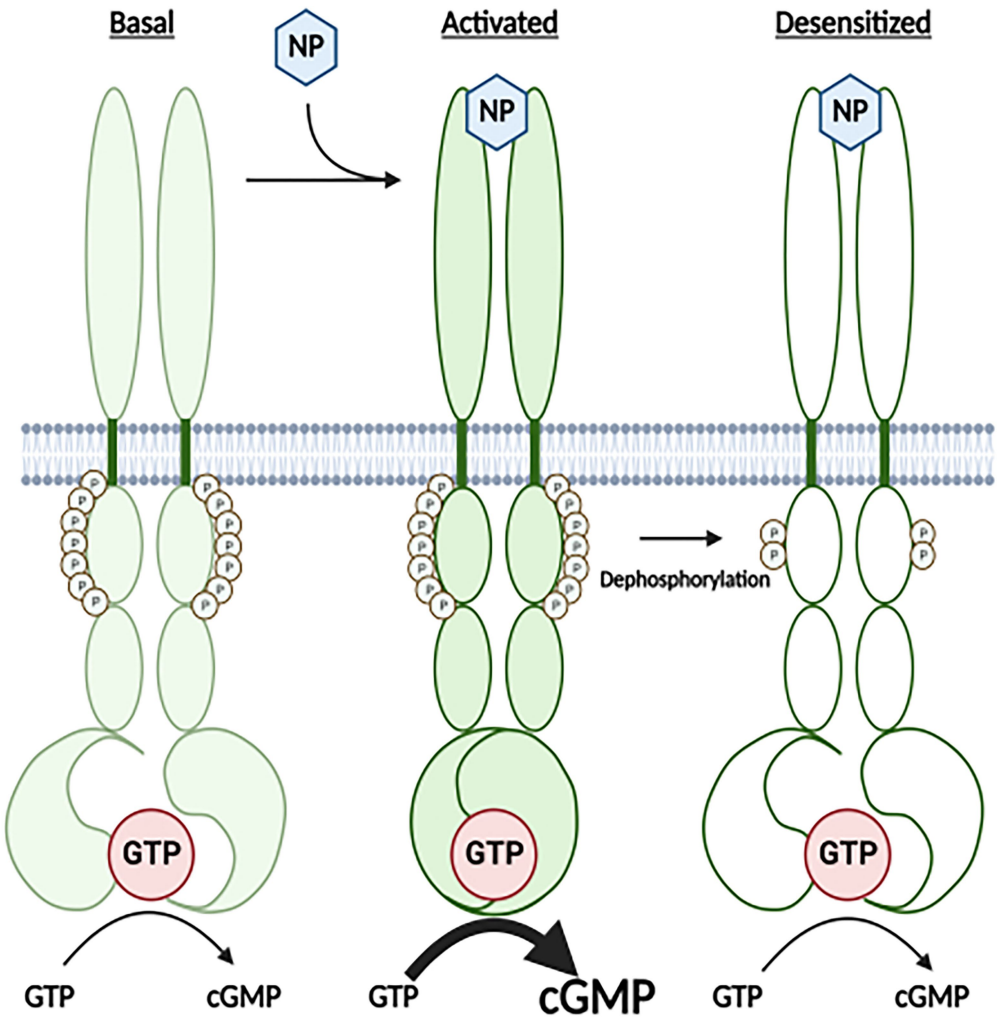

FIGURE 1
A Cartoon Model for how the highly phosphorylated version GC-A is activated by natriuretic peptide and how prolonged NP binding results in the dephosphorylation and inactivation of the receptor. Under basal conditions, GC-A is highly phosphorylated and has low GC activity. Once bound by natriuretic peptide (NP), affinity of the enzyme for GTP dramatically increases, which results in increased cGMP synthesis. With time the NP-bound receptor is dephosphorylated, which results in decreased affinity of the GC domain for GTP and reduced cGMP formation.

system as reported (Robinson and Potter, 2012). 0.02 ml of crude membranes were added per assay. A solution of 100 mM GTP and 100 mM $MgCl_2$ was diluted to the appropriate substrate concentrations used for each assay. For assays including NPs, assays were conducted for 5 min. For assays without NPs, assays were conducted for 10 min to allow enough cGMP generation to be detected by the radioimmunoassay. Because enzymatic activity was not completely linear with time, the kinetic parameters are considered "apparent." Since GC-A activity in these experiments was dependent on transfection efficiency as well as proper post-translational modification of the receptor by processes that can be overwhelmed by increased transfection efficiency, kinetic parameters can vary between individual experiments. Hence, comparisons between wild type and mutant enzymes were determined in the same assay that was repeated multiple times in order to achieve statistical significance.

SDS-PAGE and gel staining

Eight percent resolving gels were fixed in a 30 ml solution of 50% methanol and 10% acetic acid for 30 min with gentle rocking. The solution was changed two times for a total of three washes in the fixing solution. The gels were then washed twice in 100 ml of water for 10 min. Ten milliliters of Pro-Q Diamond phosphoprotein gel stain was added, and the gels were incubated with gentle rocking for 1.5 h in the dark. The gels were then destained with 80 ml of a solution of 20% acetonitrile and 50 mM sodium acetate (pH 4.0) for 15 min. This wash was repeated two times for a total of three washes. The gels were then rinsed in water, scanned with a 532 nm laser, and imaged with FUJI FLA 5000 software as previously described (Otto et al., 2017). After imaging, the same gels were stained with 50% Methanol, 7% Acetic Acid, and 0.1% Coomassie Brilliant Blue for 10 min and destained in a solution of 50% methanol and 7% acetic acid.

Statistical analysis

Substrate-velocity curves were analyzed by nonlinear regression with an allosteric sigmoidal model in Prism 7 to determine the Vmax, Km, and Hill coefficients. A Michaelis–Menten model was used to determine Vmax and Km in the presence of ATP. "Km is represented by K half in some figures." For each pair of enzymes and each model parameter, we compared the full model fit against a null model in which that parameter was set to be equal. Because of this, we used the extra sum of squares F test to generate *p*-values. Unpaired *t*-tests were used to analyze single substrate GC assays. A significant difference in all tests was where $p < 0.05$. Horizontal bars above and below individual data points represent the standard error of the mean. When no vertical bars are shown, they are within the symbol itself.

Results

Vicinal glutamates are better phosphomimetics

We created GC-A-8E with 8 individual single Glu substitutions that has similar ligand activation (EC_{50}) and enzymatic (Vmax and Km) characteristics to phosphorylated WT-GC-A (Otto et al., 2017). Importantly, we generated mice with these same substitutions for each GC-A allele that have smaller hearts but normal blood pressure compared to wild type mice (Wagner et al., 2022). However, the GC-A-8E mutant requires the Ser-473-Glu substitution, and there is no physical evidence that Ser-473 is phosphorylated in any living system (Yoder et al., 2012). One reason that the Ser-473-Glu substitution may be required is that the total negative charge for GC-A-8E is deficient since Glu with a charge of −1 was substituted for phosphoserines or phosphothreonines that have a charge closer to −2 in cells. If this hypothesis is true, then vicinal Glu substitutions that result in −2 charges for the chemically identified sites in GC-A should produce a WT-like enzyme without the need for the Glu substitution at Ser-473.

Initially, we made vicinal Glu substitutions at the first four N-terminal phosphorylation sites that were identified by tryptic phosphopeptide mapping (Potter and Hunter, 1998b). This mutant called GC-A-8E double amino-terminus, or GC-A-8ED-Nterm for short, contains Glu substitutions at Ser-497, Arg-498, Thr-500, Leu-501, Ser-502, Gly-503, Ser-506, and Asn-507. Substrate-velocity profiles for GC-A-8ED-Nterm, GC-A-8E and phosphorylated WT-GC-A revealed similar activities for all three enzymes, although the Km was significantly lower for GC-A-8ED-Nterm compared to the other two enzymes (Figure 2A).

We then examined if the Ser-473-Glu mutation was still required for maximum activation of GC-A-8ED-Nterm and found that neither Ala or Glu substitutions for Ser-473 significantly affected the activity of this vicinally-substituted enzyme (Figure 2B). These data suggest that if GC-A has sufficient negative charge at the chemically identified phosphorylation sites, then additional negative charge at Ser-473 is no longer required for normal ANP-dependent GC activity.

Since Ser-510 and Thr-513 could be phosphorylated in the GC-A-8ED-Nterm mutant, we blocked the ability of these two residues to be phosphorylated by converting them to alanine to produce GC-A-8ED-Nterm 510A 513A, which resulted in a 6.7-fold increase in the Km (Figure 2C). In contrast, substituting Glu for Ser-510 and Lys-511 in GC-A-8ED-Nterm to make GC-A-10E as well as at Thr-513 and Thr-514 to make GC-A-12E, progressively reduced the Km. These mutagenesis data suggest that Ser-510 and Thr-513 are phosphorylated in GC-A-8ED, and that the negative charge associated with phosphorylation at these residues reduces the Km of GC-A.

To directly determine if Ser-510 and Thr-513 are phosphorylated in GC-A-8ED-Nterm, Pro-Q Diamond phosphate staining of SDS gels was performed (Figure 2D) as previously

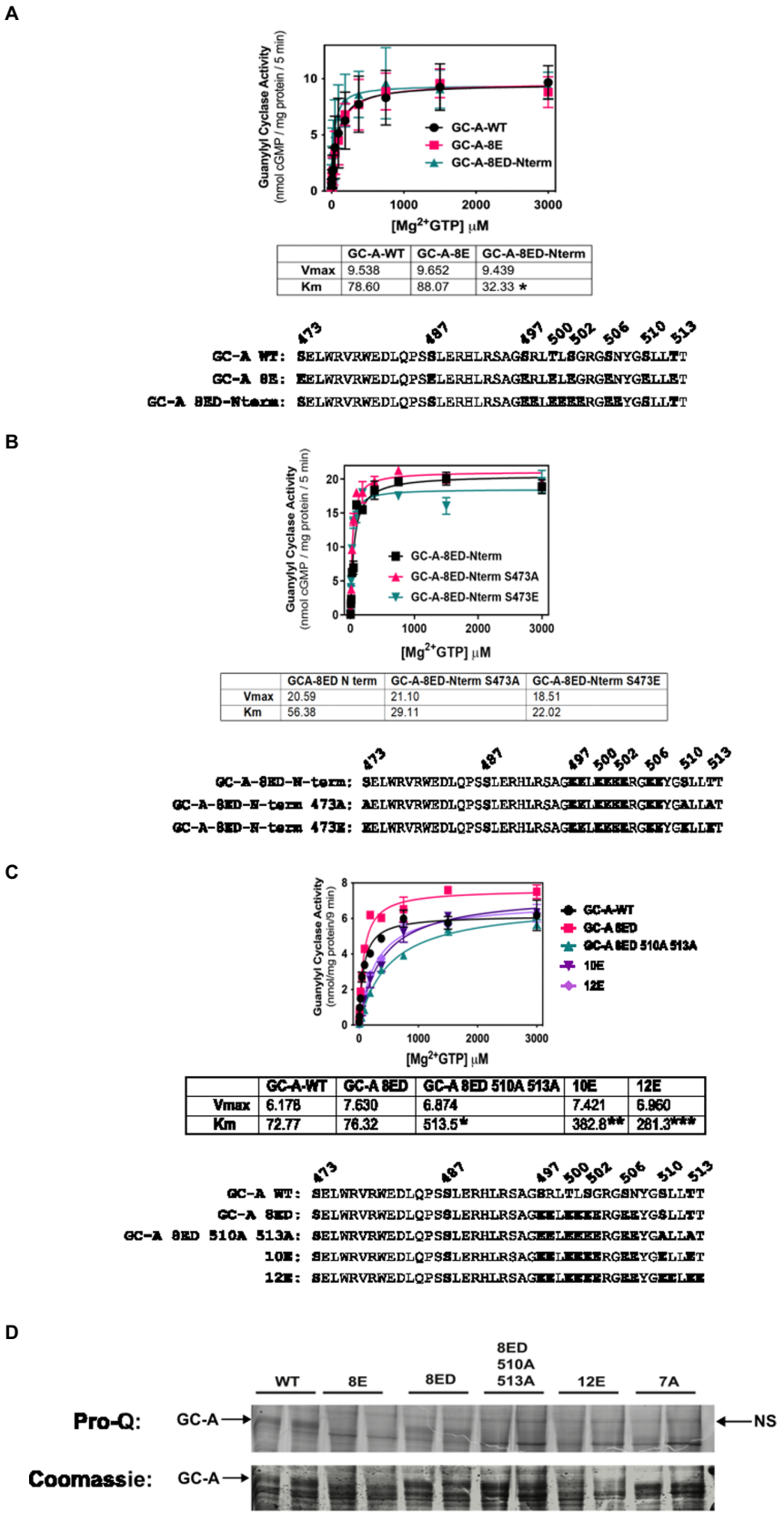

	GC-A-WT	GC-A-8E	GC-A-8ED-Nterm
Vmax	9.538	9.652	9.439
Km	78.60	88.07	32.33 *

	GCA-8ED N term	GC-A-8ED-Nterm S473A	GC-A-8ED-Nterm S473E
Vmax	20.59	21.10	18.51
Km	56.38	29.11	22.02

	GC-A-WT	GC-A 8ED	GC-A 8ED 510A 513A	10E	12E
Vmax	6.178	7.630	6.874	7.421	6.960
Km	72.77	76.32	513.5*	382.8**	281.3***

FIGURE 2
Vicinal Glu substitutions at Ser497, Thr-500, Ser-502 and Ser-506 produce a WT-like version of GC-A. 293T cells were transiently transfected with the indicated version of GC-A and membranes from these cells were assayed for GC activity for 5 min in the presence

(Continued)

Figure 2 (Continued)
of 1 uM ANP, 1 mM ATP, and increasing concentrations of GTP. The amino acid sequences of the individual constructs used in each experiment are shown below each panel. **(A)** Comparison between GC-A-WT, GC-A-8E, and GC-A-8ED-N term where n=4 from two experiments. * indicates that the Km of GC-A-8ED-Nterm is significantly lower than the Kms from the other two constructs. **(B)** Comparison between GC-A-8ED-Nterm, GC-A-8ED-Nterm-473E, GC-A-8ED-Nterm-473A, where n=3 from three transfections. **(C)** Comparison between, GC-A-WT, GC-A-8ED-Nterm, GC-A-8ED-Nterm-510A and 513A, GC-A-10E, and GC-A-12E where n=3 from three transfections. * indicates that the Km of GC-A-Nterm-510A and 513A is significantly different from those of both GC-A-WT and GC-A-8ED-Nterm. ** indicates that the Km of GC-A-10E is significantly different from the Km of GC-A-Nterm-510A and 513A. *** indicates that the Km of 12E is significantly different from GC-A-10E. All differences are at p<0.05 significance. **(D)** The indicated receptor constructs were transfected into 293T cells, then immunoprecipitated, fractionated by SDS-PAGE and stained with ProQ Diamond (top panel) to determine receptor phosphate content followed by Coomassie staining (bottom panel) to measure receptor protein levels. The arrows indicate the location of phosphorylated GC-A. NS next to the right-side arrow means non-specific band.

described (Bryan et al., 2006). This technique accurately measures the phosphate content of GC-A as indicated by dark, slightly diffuse band, that migrates around 130 KDa on an 8% SDS gel. We found that WT-GC-A was more phosphorylated than any mutant as expected. The mutant GC-A-8ED-Nterm, called 8ED in the figure, was also phosphorylated, although to a lesser extent than WT-GC-A, which was expected because it retains two sites that are obviously phosphorylated. Importantly, Ala substitutions at Ser-510 and Thr-513 reduced the phosphate signal of GC-A-8ED-Nterm, which indicates that Ser-510 and Thr-513 are phosphorylated in the 8ED mutant. As expected, GC-A-8E, GC-A-12E (a construct where vicinal Glu substitutions were incorporated for the first six sites identified), and GC-A-7A (a dephosphorylated mutant containing Ala substitutions for all 7 known chemically identified sites) stained poorly for ProQ Diamond but strongly for Coomassie blue, which indicates that these receptors are expressed but are not phosphorylated as expected. Together, data from all four panels of Figure 2 indicate that only the chemically identified phosphorylation sites are required to produce a hormonally responsive form of GC-A and that Ser-473 is not phosphorylated in a biological setting.

Glu substitutions at Ser-472 in GC-A or Ser-488 in GC-B increases GC activity

To further investigate the biological relevance of Ser-473 phosphorylation in GC-A as well as the corresponding residue, Ser-489 in GC-B, we tested whether negative charge at these exact residues is required for enzyme activation of 6E versions of GC-A and GC-B or whether introduction of negative charge at adjacent residues would also increase activity. We found that Glu substitutions at Val-472 dramatically reduced the Km of the GC-A-6E enzyme more than four-fold but the Glu substitution at Ser-473 reduced the Km to a greater extent for GC-A-6E, a construct containing single Glu substitutions for first six identified phosphorylation sites in GC-A (Figure 3A). Regarding GC-B, identical increases in activity were observed when Glu was substituted for either Ala-488 or Ser-489-Glu in GC-B-6E (Figure 3B). These data indicate that the introduction of negative charge in the general juxtamembrane region of the charge deficient, single Glu mutants of GC-A and GC-B, is sufficient to produce enzymes with WT like activity.

Vicinal Glu substitutions at Ser-487 and Leu-488 are inhibitory

The initial report describing the Ser-487 phosphorylation site in GC-A, suggested that phosphorylation at this residue is inhibitory (Schroter et al., 2010). However, our efforts to create a dephosphorylated mutant of GC-A that has WT-like activity required the conversion of Ser-487 to Glu in GC-A-7E to make the single Glu-substitution mutant GC-A-8E (Otto et al., 2017), which is consistent with this site increasing activity. To determine whether the Ser-487 increases or decreased activity, we tested whether Glu substitutions at both Ser-487 and Leu-488 would increase or decrease the activity of various forms of GC-A. First, we examined whether converting Ser-487 and Leu-488 in GC-A-12E to make GC-A-14E would affect the Km of the enzyme and found that the Km of GC-A-14E was higher than that of both WT-GC-A and GC-A-12E, which is consistent with this site inhibiting activity (Figure 4A). We also examined what effect substituting a Glu for Leu-488 in GC-A-8E to make GC-A-9E has on activity. Note that this construct has vicinal Glu substitutions at Ser-487 and Leu-488 but single Glu substitutions for the other seven chemically identified sites for a total of nine glutamates. Additionally, we converted Ser-487 and Leu-488 to Glu in WT-GC-A. We found that adding the vicinal Glu substitutions at Ser-487 and Leu-488 tended to increase the Km of GC-A regardless of whether the negative charge was from natural phosphorylation sites or from single Glu substitutions, although none of these differences were statistically significant (Figure 4B). Hence, our best interpretation of the data from the vicinal substitutions, like the single substitution, suggests that the Ser-487 site inhibits GC activity as originally reported by Schroter et al. (2010).

Phosphorylation is required for allosteric activation of GC-A

NPs decrease the Km of GC-A and GC-B by a process involving ATP binding to a pseudosymmetric allosteric site in the catalytic domains (Antos and Potter, 2007; Robinson and Potter, 2012) and possibly the kinase homology domains (Joubert et al., 2005;

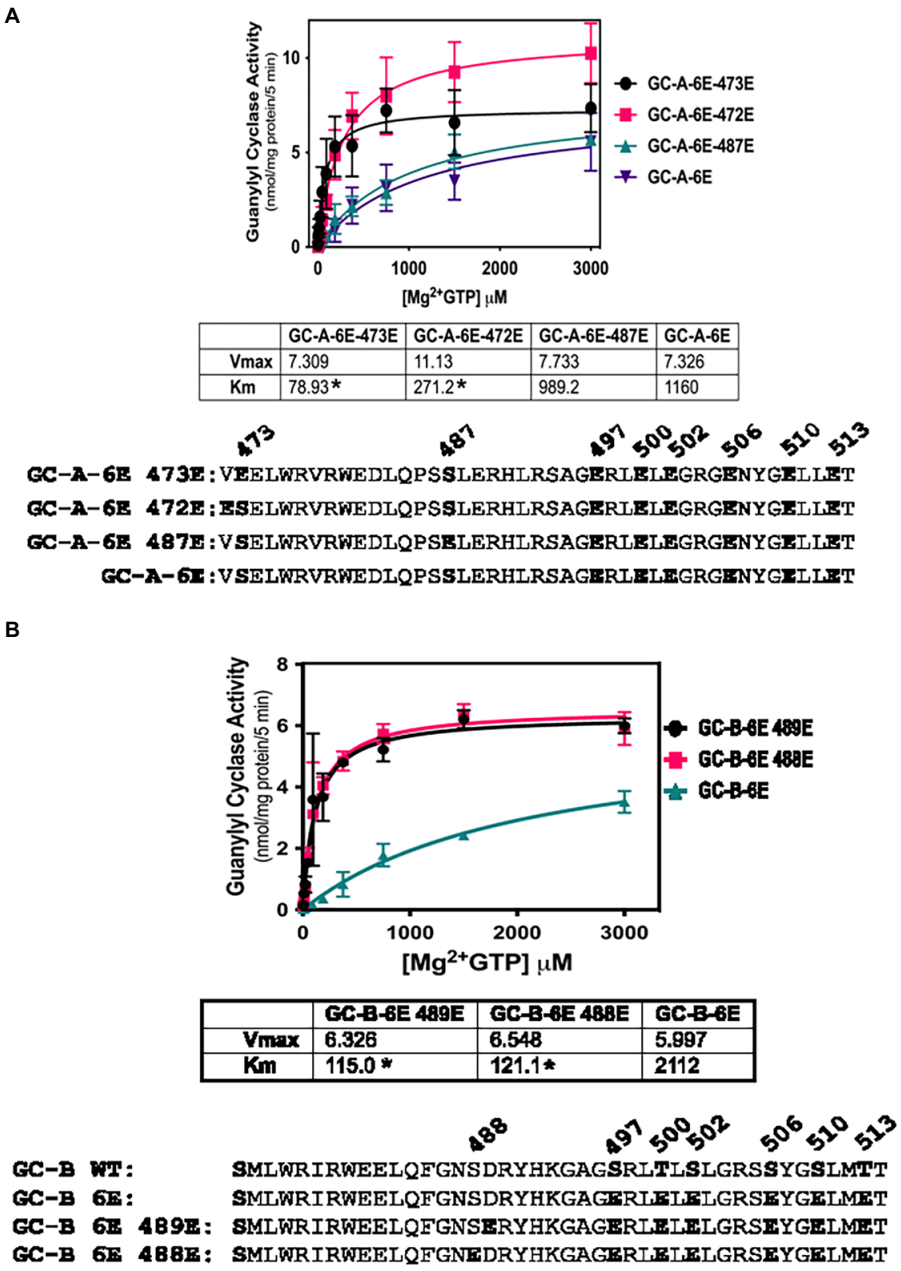

	GC-A-6E-473E	GC-A-6E-472E	GC-A-6E-487E	GC-A-6E
Vmax	7.309	11.13	7.733	7.326
Km	78.93*	271.2*	989.2	1160

	GC-B-6E 489E	GC-B-6E 488E	GC-B-6E
Vmax	6.326	6.548	5.997
Km	115.0 *	121.1*	2112

FIGURE 3
Activating Glu substitutions in juxta-membrane region of GC-A are not specific for Ser-473 in GC-A or Ser-489 in GC-B. 293T cells were transiently transfected with the indicated forms of GC-A or GC-B and membranes from these cells were assayed for GC activity for 5 min with 1 mM ATP, increasing concentrations of GTP and 1 uM ANP or CNP for GC-A and GC-B, respectively. **(A)** Comparison between GC-A-6E-473E, GC-A-6E-472E, and GC-A-6E, where $n=4$. * indicates significantly different from GC-A-6E for each construct, respectively at $p<0.05$. **(B)** Comparison between GC-B-6E-489E, GC-B-6E-488E, and GC-B-6E, where $n=4$. * indicates significantly different from GC-B-6E for each construct, respectively at $p<0.05$.

Burczynska et al., 2007; Edmund et al., 2019) of these enzymes. To determine whether phosphorylation is required for allosteric activation of GC-A, we compared the ability of ATP to reduce the Km of phosphorylated WT-GC-A, the original phosphomimetic mutant GC-A-8E (S473E, S487E, S497E, T500E, S502E, S506E, S510E, T513E) as initially described (Otto et al., 2017), and the dephosphorylated mutant, GC-A-7A (S487A, S497A, T500A, S502A, S506A, S510A, and T513A) in the presence (Figure 5B) and absence (Figure 5A) of ANP. Please note that the Km is represented by "K half" in Figure 5. With ANP, ATP reduced the Hill slope and Km of phosphorylated WT-GC-A and GC-A-8E but had no effect on GC-A-7A, consistent with phosphorylation being required for allosteric regulation of GC-A. In the absence of ANP, ATP allosterically shifted product formation from positive cooperative to

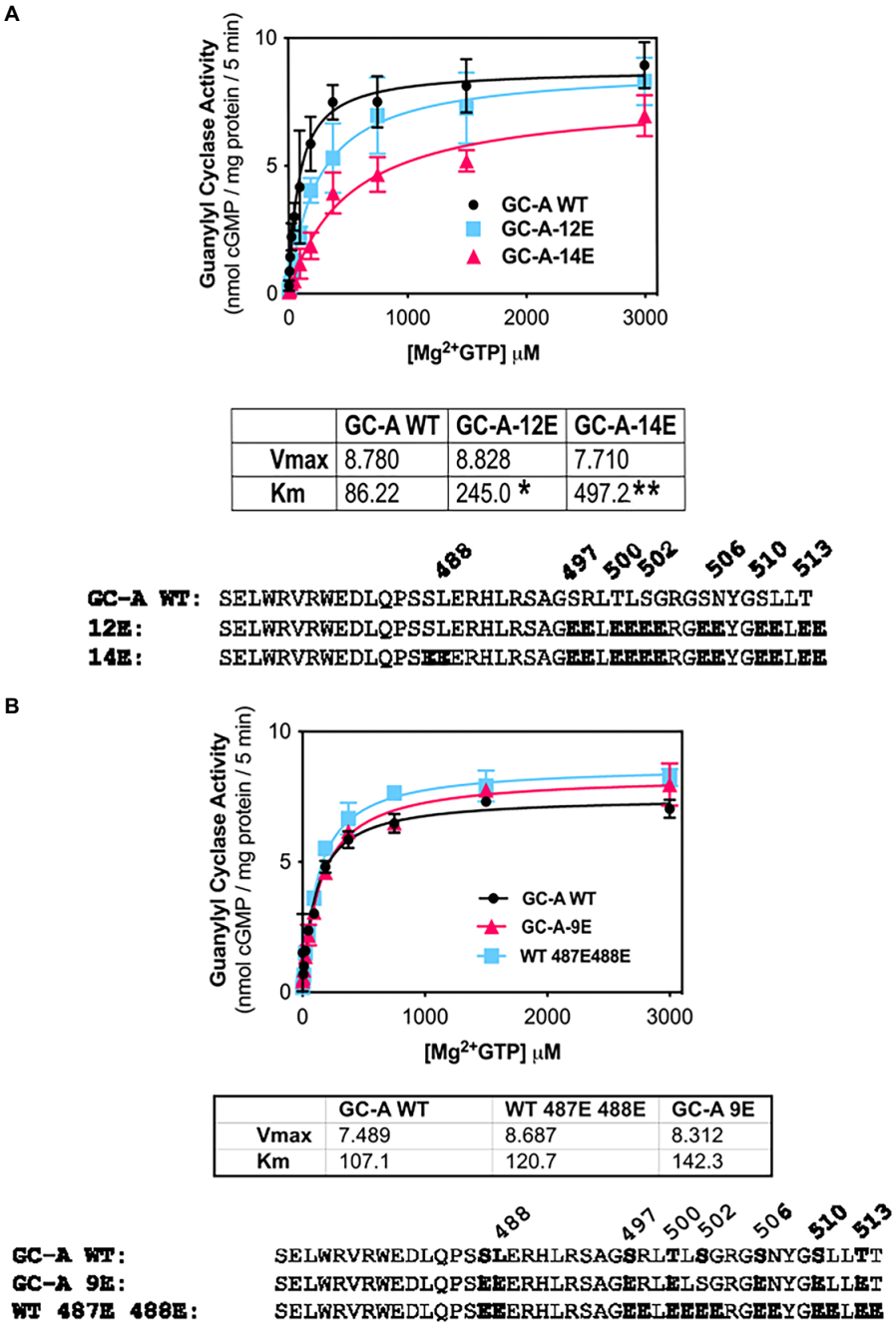

	GC-A WT	GC-A-12E	GC-A-14E
Vmax	8.780	8.828	7.710
Km	86.22	245.0 *	497.2**

	GC-A WT	WT 487E 488E	GC-A 9E
Vmax	7.489	8.687	8.312
Km	107.1	120.7	142.3

FIGURE 4
Vicinal Glu substitutions at Ser-487 and Leu-488 inhibit GC-A. **(A)** Comparison between, GC-A-WT, GC-A-12E, and GC-A-14E where n =4. * indicates that GC-A-14E is significantly different from GC-A-WT. ** indicates that GC-A-14E is significantly different from GC-A-12E. All differences are at p <0.05 significance. **(B)** Comparison between phosphorylated GC-A-WT, GC-A-9E, and GC-A-WT-487E-488E, where n =4.

linear for both WT-GC-A and GC-8E as evidenced by reductions in the Hill slope of the enzymes (Figure 5A). However, the Hill slope for GC-A-7A was approximately 1 and it did not change regardless of whether ATP was included in the reaction. These data indicate that phosphorylation, solely due to its ability to increase local negative charge, is required for allosteric regulation of GC-A.

Phosphorylation increases basal activity of GC-A in an ATP-dependent manner

Phosphorylation of GC-A and GC-B is essential for NP stimulation of their catalytic domains, but initial experiments measuring cGMP production by the insensitive ^{32}P-cGMP assay

A

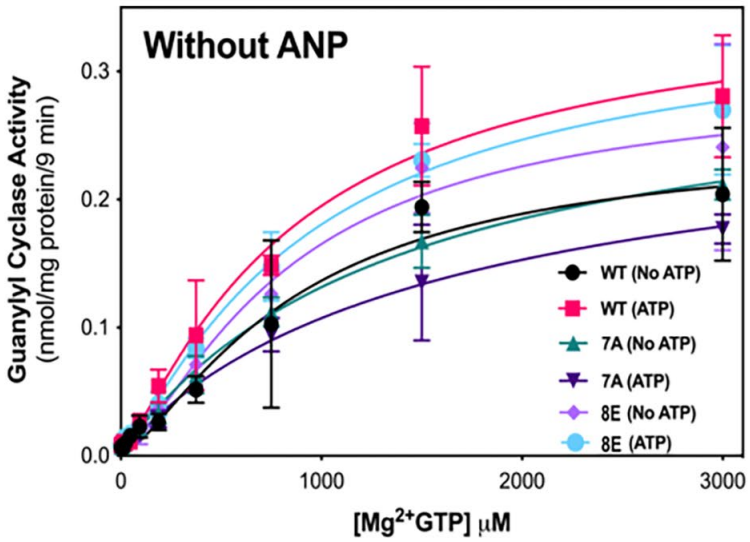

	WT (No ATP)	WT (ATP)	7A (No ATP)	7A (ATP)	8E (No ATP)	8E (ATP)
Vmax	0.2477	0.3588	0.3150	0.2829	0.2923	0.3452
h	1.381	1.186	0.9877	0.9438	1.387	1.190
Khalf	860.0	862.5	1399	1680	826.4	924.7

B

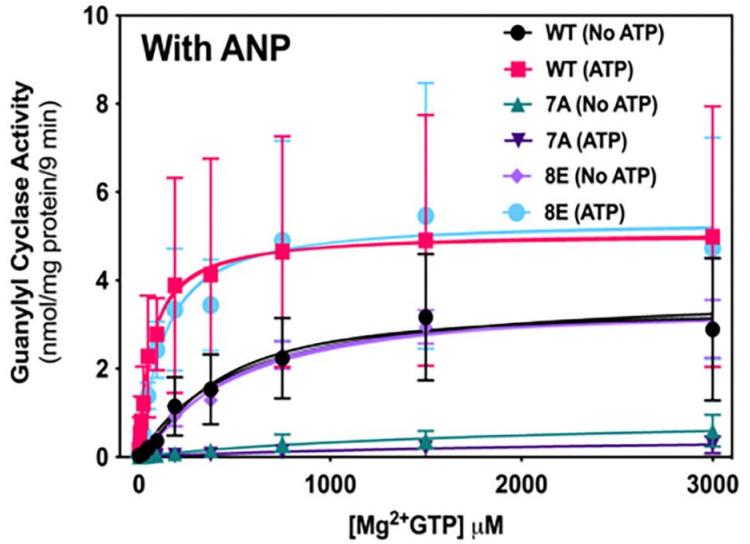

	WT (No ATP)	WT (ATP)	7A (No ATP)	7A (ATP)	8E (No ATP)	8E (ATP)
Vmax	3.358	5.132	1.108	0.5687	3.327	5.374
h	1.304	0.9472	0.9045	0.9485	1.309	1.090
Khalf	386.6	68.36*	2568	3017	428.2	128.8*

FIGURE 5
Phosphorylation is required for allosteric regulation of GC-A by NP and ATP. 293T cells were transiently transfected with the indicated GC-A constructs and membranes from these cells were assayed for GC activity for 9min in the absence **(A)** or presence **(B)** of 1 υM ANP with or without 1mM ATP with increasing concentrations of GTP. Comparison between WT-GC-A, GC-A-7A, and GC-A-8E in the presence or absence of 1mM ATP where $n=3$ from three transfections. * indicates significantly different from no ATP treatment for each receptor, respectively, at $p<0.05$ significance.

failed to detect effects of phosphorylation on basal GC activity (Potter, 1998; Potter and Hunter, 1998b). Experiments described here using a more sensitive radioimmunoassay to measure cGMP production indicated that phosphorylation increases basal GC activity for the first time. In the presence of ATP (cellular conditions), GC activity of phosphorylated WT-GC-A and the phosphomimetic mutant GC-A-8E did not differ (Figure 6A). However, incrementally decreasing the negative charge in GC-A-8E by converting single Glu to Ala, reduced the basal activity of the enzyme in a step-wise manner (Figure 6A). In contrast, without ATP the activities of all the GC-A mutants were the same regardless of the amount of negative charge from phosphate or glutamate (Figure 6B). These data indicate that increased negative charge resulting from phosphorylation increases basal activity of GC-A by an allosteric mechanism requiring ATP binding.

Discussion

Single glutamate substitutions at all six chemically identified phosphorylation sites in GC-A yielded an enzyme called GC-A-6E that had a Km 11-fold higher than the phosphorylated WT enzyme. A possible explanation for the inability of single Glu substitutions to completely mimic the effects of phosphorylation sites is that they only have a negative charge of −1, whereas phosphoserines and phosphothreonines can have a negative charge as high as negative as −2 in cells. As originally employed by Strickfaden et al. (2007) who were studying the effect of phosphorylation of Ste5 on cell cycle regulation in yeast, we used vicinal Glu mutations to mimic the −2 charge of a phosphoserine or a phosphothreonine. Vicinal Glu mutations at all six originally identified sites produced an enzyme called GC-A-12E with a Km only 2.8 higher than the WT enzyme, which is a large improvement over the activity observed for GC-A-6E with single Glu substitutions. However, the Km of GC-A-12E was still slightly higher than the Km of the phosphorylated WT enzyme. Only GC-A-8ED-Nterm, with vicinal Glu mutations for the first four N terminal phosphorylation sites and phosphates on the two remaining residues produced a Km lower than that of the phosphorylated WT enzyme. In GC-A-8ED-Nterm, Ser-510 and Ser-513 are phosphorylated, yet vicinal Glu mutations at these same residues to produce GC-A-12E does not produce an enzyme with WT activity. Why GC-A-12E had slightly less activity than the WT enzyme may be explained by the negative charge on each Glu being in different orientations since they are on different carbons, which would not be the case with the natural phospho-amino acids since the negative charges from the hydroxyl groups are on the same phosphate. It is also not known if having double negative charges at each phosphorylation site is the optimal configuration for GC activity or whether the double glutamate substitutions produce other unforeseen conformations.

Another question addressed by these studies is why the Ser-473-Glu and Ser-489-Glu substitutions in GC-A and GC-B, respectively, are required to produced dephosphorylated enzymes with WT-like activity when single Glu substitutions are introduce for the known phosphorylation sites. This is especially important to understand given that there is no evidence that these residues are phosphorylated *in vivo*. The current study demonstrates that Ala and Glu substitutions at Ser-473 do not affect the activity of GC-A-8ED-Nterm. Furthermore, substituting an Glu for the Val at 472 in GC-A or Glu for Ala at 488 in GC-B, also reduced the Km of enzymes, which indicates that increased charge in the general vicinity of these conserved serines is only important when there is a charge deficiency at the chemically identified phosphorylation sites. Given that the only evidence supporting phosphorylation of Ser-473 in GC-A or Ser-489 in GC-B is based solely on activity changes, our best estimate is that neither Ser-473 nor Ser-489 are phosphorylated *in vivo*. Why Glu substitutions at Ser-473 and Ser-489 have disproportional effects on activity is not known, but they are in a region known to have a great effect on activity, since the GC-B Ala-488-Pro activating mutation that increases long bone growth is only one residue away (Miura et al., 2014).

To date, phosphorylation has only been shown to affect NP-stimulation of GC-A and GC-B, although recently we have been able to demonstrate the physiological importance of this process by showing that GC-B dephosphorylation is the mechanism by which luteinizing hormone stimulates resumption of meiosis in the oocyte as well as the mechanism by which fibroblast growth factor receptor-3 activation causes achondroplasia (Shuhaibar et al., 2016, 2017; Robinson et al., 2017; Wagner et al., 2021). Here, we show that phosphorylation increases basal activity for the first time. With the loss of each negative charge, there is a stepwise decrease in activity in the presence of ATP. However, in the absence ATP, each GC-A construct has similar activity regardless of charge, consistent with the increased activity resulting from allosteric activation by ATP. Our previous reports suggest that phosphorylation does not affect basal activity (Potter and Hunter, 1998a,b). However, these studies measured cGMP formation with a less sensitive ^{32}P-GTP assay, which likely masked the differences in small amounts of cGMP produced in basal assays. Finally, the kinase or kinases that phosphorylate GC-A or GC-B have not been identified. However, LB-100, an inhibitor of PP2A and other similar phosphatases was recently shown to increased GC-B dependent long bone growth in mice (Shuhaibar et al., 2021), which suggest that phosphatase inhibitors may also increase GC-A activity *in vivo* as well.

In conclusion, we report that phosphorylation regulates basal activity and is required for allosteric regulation of GC-A by ATP, which is consistent with a report published more than 30 years earlier showing that phosphorylation is required for allosteric regulation of the homologous sea urchin GC receptor, the first member of the transmembrane GC family to be molecularly cloned (Ramarao and Garbers, 1988; Singh et al., 1988).

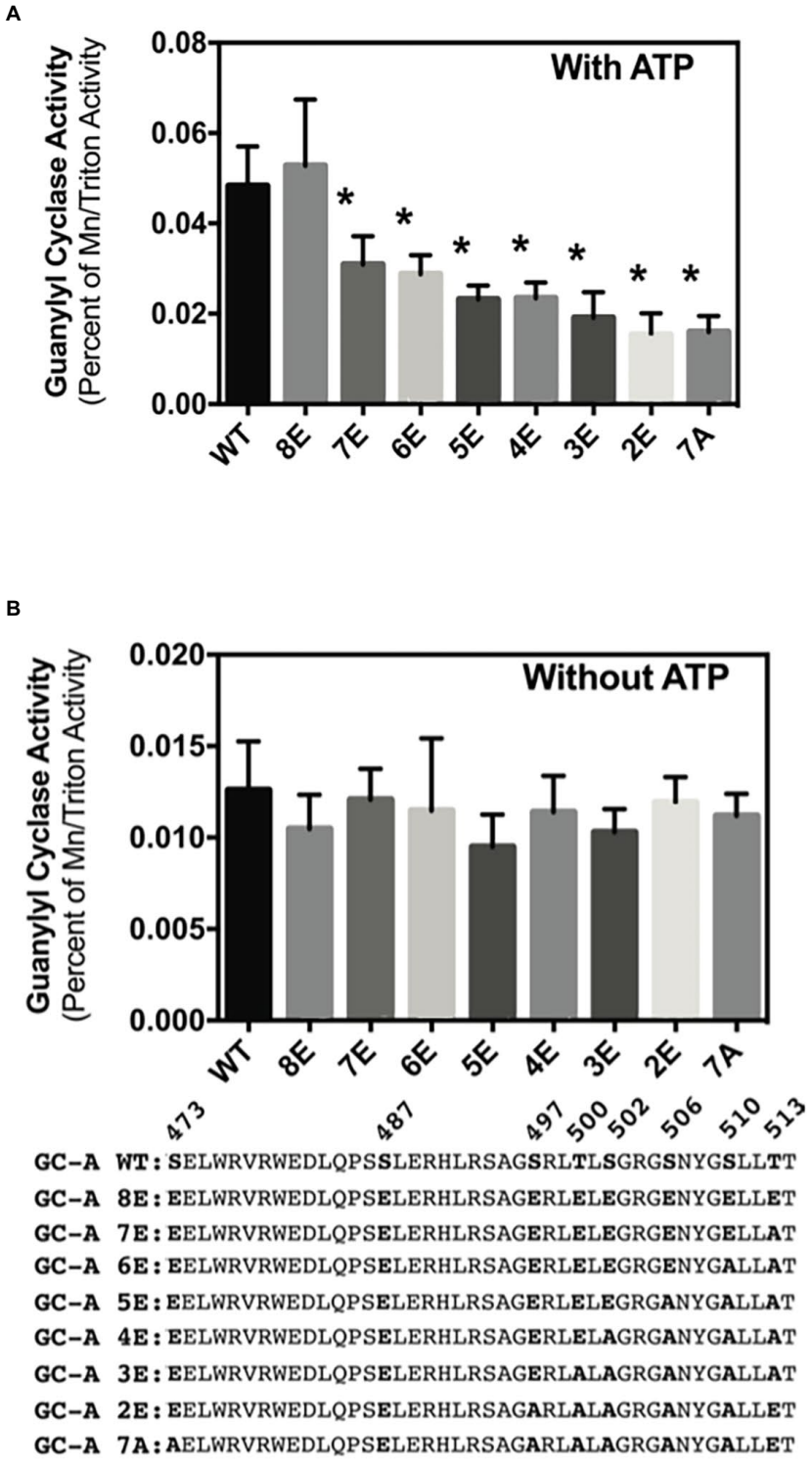

FIGURE 6
Phosphorylation increases ATP-dependent basal activity of GC-A. 293T cells were transiently transfected with the indicated GC-A constructs and membranes from these cells were assayed for GC activity for 5min in the presence **(A)** or absence **(B)** of 1mM ATP. All assays contained 0.1mM GTP. Comparison between the indicated versions of GC-A where $n=10$. * indicates significantly different from WT-GC-A at $p<0.05$.

Data availability statement

The original contributions presented in the study are included in the article/supplementary materials, further inquiries can be directed to the corresponding author.

Author contributions

NO conducted experiments, analyzed and interpreted experimental data, and wrote the paper. NO and LP conceived and coordinated the study, analyzed and interpreted data, and wrote the paper. All authors contributed to the article and approved the submitted version.

Funding

This work was supported by the National Institutes of Health grant R01GM098309 (to LP), The Fund for Science, and The Hormone Receptor Fund.

Acknowledgments

We thank Brandon M. Wagner for helpful comments on the manuscript and optimization of the figures.

Conflict of interest

The authors declare that the research was conducted in the absence of any commercial or financial relationships that could be construed as a potential conflict of interest.

Publisher's note

References

Antos, L. K., Abbey-Hosch, S. E., Flora, D. R., and Potter, L. R. (2005). ATP-independent activation of natriuretic peptide receptors. *J. Biol. Chem.* 280, 26928–26932. doi: 10.1074/jbc.M505648200

Antos, L. K., and Potter, L. R. (2007). Adenine nucleotides decrease the apparent km of endogenous natriuretic peptide receptors for GTP. *Am. J. Physiol. Endocrinol. Metab.* 293, E1756–E1763. doi: 10.1152/ajpendo.00321.2007

Bereta, G., Wang, B., Kiser, P. D., Baehr, W., Jang, G. F., and Palczewski, K. (2010). A functional kinase homology domain is essential for the activity of photoreceptor guanylate cyclase 1. *J. Biol. Chem.* 285, 1899–1908. doi: 10.1074/jbc.M109.061713

Bordicchia, M., Liu, D., Amri, E. Z., Ailhaud, G., Dessì-Fulgheri, P., Zhang, C., et al. (2012). Cardiac natriuretic peptides act via p38 MAPK to induce the brown fat thermogenic program in mouse and human adipocytes. *J. Clin. Invest.* 122, 1022–1036. doi: 10.1172/JCI59701

Bryan, P. M., Smirnov, D., Smolenski, A., Feil, S., Feil, R., Hofmann, F., et al. (2006). A sensitive method for determining the phosphorylation status of natriuretic peptide receptors: cGK-Ialpha does not regulate NPR-A. *Biochemistry* 45, 1295–1303. doi: 10.1021/bi051253d

Burczynska, B., Duda, T., and Sharma, R. K. (2007). ATP signaling site in the ARM domain of atrial natriuretic factor receptor guanylate cyclase. *Mol. Cell. Biochem.* 301, 93–107. doi: 10.1007/s11010-006-9400-7

Chrisman, T. D., and Garbers, D. L. (1999). Reciprocal antagonism coordinates C-type natriuretic peptide and mitogen-signaling pathways in fibroblasts. *J. Biol. Chem.* 274, 4293–4299. doi: 10.1074/jbc.274.7.4293

Dickey, D. M., Edmund, A. B., Otto, N. M., Chaffee, T. S., Robinson, J. W., and Potter, L. R. (2016). Catalytically active Guanylyl Cyclase B requires endoplasmic reticulum-mediated glycosylation, and mutations that inhibit this process cause dwarfism. *J. Biol. Chem.* 291, 11385–11393. doi: 10.1074/jbc.M115.704015

Edmund, A. B., Walseth, T. F., Levinson, N. M., and Potter, L. R. (2019). The pseudokinase domains of guanylyl cyclase-a and -B allosterically increase the affinity of their catalytic domains for substrate. *Sci. Signal.* 12, 1–14. doi: 10.1126/scisignal.aau5378

Egbert, J. R., Shuhaibar, L. C., Edmund, A. B., Van Helden, D. A., Robinson, J. W., Uliasz, T. F., et al. (2014). Dephosphorylation and inactivation of NPR2 guanylyl cyclase in granulosa cells contributes to the LH-induced decrease in cGMP that causes resumption of meiosis in rat oocytes. *Development* 141, 3594–3604. doi: 10.1242/dev.112219

Eyers, P. A., and Murphy, J. M. (2016). The evolving world of pseudoenzymes: proteins, prejudice and zombies. *BMC Biol.* 14:98. doi: 10.1186/s12915-016-0322-x

Foster, D. C., and Garbers, D. L. (1998). Dual role for adenine nucleotides in the regulation of the atrial natriuretic peptide receptor, guanylyl cyclase-a. *J. Biol. Chem.* 273, 16311–16318. doi: 10.1074/jbc.273.26.16311

Hunter, T. (2012). Why nature chose phosphate to modify proteins. *Philos. Trans. R. Soc. Lond. Ser. B Biol. Sci.* 367, 2513–2516. doi: 10.1098/rstb.2012.0013

Jaffe, L. A., and Egbert, J. R. (2017). Regulation of mammalian oocyte meiosis by intercellular communication within the ovarian follicle. *Annu. Rev. Physiol.* 79, 237–260. doi: 10.1146/annurev-physiol-022516-034102

Jaleel, M., Saha, S., Shenoy, A. R., and Visweswariah, S. S. (2006). The kinase homology domain of receptor guanylyl cyclase C: ATP binding and identification of an adenine nucleotide sensitive site. *Biochemistry* 45, 1888–1898. doi: 10.1021/bi052089x

Jewett, J. R., Koller, K. J., Goeddel, D. V., and Lowe, D. G. (1993). Hormonal induction of low affinity receptor guanylyl cyclase. *EMBO J.* 12, 769–777. doi: 10.1002/j.1460-2075.1993.tb05711.x

Joubert, S., Jossart, C., McNicoll, N., and De Lean, A. (2005). Atrial natriuretic peptide-dependent photolabeling of a regulatory ATP-binding site on the natriuretic peptide receptor-a. *FEBS J.* 272, 5572–5583. doi: 10.1111/j.1742-4658.2005.04952.x

Joubert, S., Labrecque, J., and De Lean, A. (2001). Reduced activity of the npr-a kinase triggers dephosphorylation and homologous desensitization of the receptor. *Biochemistry* 40, 11096–11105. doi: 10.1021/bi010580s

Koller, K. J., Lipari, M. T., and Goeddel, D. V. (1993). Proper glycosylation and phosphorylation of the type a natriuretic peptide receptor are required for hormone-stimulated guanylyl cyclase activity. *J. Biol. Chem.* 268, 5997–6003. doi: 10.1016/S0021-9258(18)53418-9

Kuhn, M. (2016). Molecular physiology of membrane Guanylyl Cyclase receptors. *Physiol. Rev.* 96, 751–804. doi: 10.1152/physrev.00022.2015

Matsuyama, S., Llopis, J., Deveraux, Q. L., Tsien, R. Y., and Reed, J. C. (2000). Changes in intramitochondrial and cytosolic pH: early events that modulate caspase activation during apoptosis. *Nat. Cell Biol.* 2, 318–325. doi: 10.1038/35014006

Miura, K., Kim, O. H., Lee, H. R., Namba, N., Michigami, T., Yoo, W. J., et al. (2014). Overgrowth syndrome associated with a gain-of-function mutation of the natriuretic peptide receptor 2 (NPR2) gene. *Am. J. Med. Genet. A* 164A, 156–163. doi: 10.1002/ajmg.a.36218

Muller, D., Cortes-Dericks, L., Budnik, L. T., Brunswig-Spickenheier, B., Pancratius, M., Speth, R. C., et al. (2006). Homologous and lysophosphatidic acid-

induced desensitization of the atrial natriuretic peptide receptor, guanylyl cyclase-a, in MA-10 leydig cells. *Endocrinology* 147, 2974–2985. doi: 10.1210/en.2006-0092

Murphy, J. M., Zhang, Q., Young, S. N., Reese, M. L., Bailey, F. P., Eyers, P. A., et al. (2014). A robust methodology to subclassify pseudokinases based on their nucleotide-binding properties. *Biochem. J.* 457, 323–334. doi: 10.1042/BJ20131174

Otto, N. M., McDowell, W. G., Dickey, D. M., and Potter, L. R. (2017). A glutamate-substituted mutant mimics the phosphorylated and active form of Guanylyl Cyclase-a. *Mol. Pharmacol.* 92, 67–74. doi: 10.1124/mol.116.107995

Parkinson, S. J., Carrithers, S. L., and Waldman, S. A. (1994). Opposing adenine nucleotide-dependent pathways regulate guanylyl cyclase C in rat intestine. *J. Biol. Chem.* 269, 22683–22690. doi: 10.1016/S0021-9258(17)31700-3

Potter, L. R. (1998). Phosphorylation-dependent regulation of the guanylyl cyclase-linked natriuretic peptide receptor B: dephosphorylation is a mechanism of desensitization. *Biochemistry* 37, 2422–2429. doi: 10.1021/bi972303k

Potter, L. R. (2011a). Guanylyl cyclase structure, function and regulation. *Cell. Signal.* 23, 1921–1926. doi: 10.1016/j.cellsig.2011.09.001

Potter, L. R. (2011b). Regulation and therapeutic targeting of peptide-activated receptor guanylyl cyclases. *Pharmacol. Ther.* 130, 71–82. doi: 10.1016/j.pharmthera.2010.12.005

Potter, L. R., Abbey-Hosch, S., and Dickey, D. M. (2006). Natriuretic peptides, their receptors, and cyclic guanosine monophosphate-dependent signaling functions. *Endocr. Rev.* 27, 47–72. doi: 10.1210/er.2005-0014

Potter, L. R., and Garbers, D. L. (1992). Dephosphorylation of the guanylyl cyclase-a receptor causes desensitization. *J. Biol. Chem.* 267, 14531–14534. doi: 10.1016/S0021-9258(18)42069-8

Potter, L. R., and Hunter, T. (1998a). Identification and characterization of the major phosphorylation sites of the B-type natriuretic peptide receptor. *J. Biol. Chem.* 273, 15533–15539. doi: 10.1074/jbc.273.25.15533

Potter, L. R., and Hunter, T. (1998b). Phosphorylation of the kinase homology domain is essential for activation of the A-type natriuretic peptide receptor. *Mol. Cell. Biol.* 18, 2164–2172. doi: 10.1128/MCB.18.4.2164

Potter, L. R., and Hunter, T. (1999). A constitutively "phosphorylated" guanylyl cyclase-linked atrial natriuretic peptide receptor mutant is resistant to desensitization. *Mol. Biol. Cell* 10, 1811–1820. doi: 10.1091/mbc.10.6.1811

Potter, L. R., Yoder, A. R., Flora, D. R., Antos, L. K., and Dickey, D. M. (2009). Natriuretic peptides: their structures, receptors, physiologic functions and therapeutic applications. *Handb. Exp. Pharmacol.* 191, 341–366. doi: 10.1007/978-3-540-68964-5_15

Ramarao, C. S., and Garbers, D. L. (1988). Purification and properties of the phosphorylated form of guanylate cyclase. *J. Biol. Chem.* 263, 1524–1529. doi: 10.1016/S0021-9258(19)57335-5

Robinson, J. W., Egbert, J. R., Davydova, J., Schmidt, H., Jaffe, L. A., and Potter, L. R. (2017). Dephosphorylation is the mechanism of fibroblast growth factor inhibition of guanylyl cyclase-B. *Cell. Signal.* 40, 222–229. doi: 10.1016/j.cellsig.2017.09.021

Robinson, J. W., and Potter, L. R. (2012). Guanylyl cyclases a and B are asymmetric dimers that are allosterically activated by ATP binding to the catalytic domain. *Sci. Signal.* 5:ra65. doi: 10.1126/scisignal.2003253

Schroter, J., Zahedi, R. P., Hartmann, M., Gassner, B., Gazinski, A., Waschke, J., et al. (2010). Homologous desensitization of guanylyl cyclase a, the receptor for atrial natriuretic peptide, is associated with a complex phosphorylation pattern. *FEBS J.* 277, 2440–2453. doi: 10.1111/j.1742-4658.2010.07658.x

Shuhaibar, L. C., Egbert, J. R., Edmund, A. B., Uliasz, T. F., Dickey, D. M., Yee, S. P., et al. (2016). Dephosphorylation of juxtamembrane serines and threonines of the NPR2 guanylyl cyclase is required for rapid resumption of oocyte meiosis in response to luteinizing hormone. *Dev. Biol.* 409, 194–201. doi: 10.1016/j.ydbio.2015.10.025

Shuhaibar, L. C., Kaci, N., Egbert, J. R., Horville, T., Loisay, L., Vigone, G., et al. (2021). Phosphatase inhibition by LB-100 enhances BMN-111 stimulation of bone growth. *JCI Insight* 6, 1–14. doi: 10.1172/jci.insight.141426

Shuhaibar, L. C., Robinson, J. W., Vigone, G., Shuhaibar, N. P., Egbert, J. R., Baena, V., et al. (2017). Dephosphorylation of the NPR2 guanylyl cyclase contributes to inhibition of bone growth by fibroblast growth factor. *elife* 6, 1–20. doi: 10.7554/eLife.31343

Singh, S., Lowe, D. G., Thorpe, D. S., Rodriguez, H., Kuang, W. J., Dangott, L. J., et al. (1988). Membrane guanylate cyclase is a cell-surface receptor with homology to protein kinases. *Nature* 334, 708–712. doi: 10.1038/334708a0

Strickfaden, S. C., Winters, M. J., Ben-Ari, G., Lamson, R. E., Tyers, M., and Pryciak, P. M. (2007). A mechanism for cell-cycle regulation of MAP kinase signaling in a yeast differentiation pathway. *Cells* 128, 519–531. doi: 10.1016/j.cell.2006.12.032

Thorsness, P. E., and Koshland, D. E. Jr. (1987). Inactivation of isocitrate dehydrogenase by phosphorylation is mediated by the negative charge of the phosphate. *J. Biol. Chem.* 262, 10422–10425. doi: 10.1016/S0021-9258(18)60975-5

Wagner, B. M., Robinson, J. W., Healy, C. L., Gauthier, M., Dickey, D. M., Yee, S. P., et al. (2022). Guanylyl cyclase-a phosphorylation decreases cardiac hypertrophy and improves systolic function in male, but not female, mice. *FASEB J.* 36:e22069. doi: 10.1096/fj.202100600RRR

Wagner, B. M., Robinson, J. W., Lin, Y. W., Lee, Y. C., Kaci, N., Legeai-Mallet, L., et al. (2021). Prevention of guanylyl cyclase-B dephosphorylation rescues achondroplastic dwarfism. *JCI Insight* 6, 1–14. doi: 10.1172/jci.insight.147832

Yoder, A. R., Robinson, J. W., Dickey, D. M., Andersland, J., Rose, B. A., Stone, M. D., et al. (2012). A functional screen provides evidence for a conserved, regulatory, Juxtamembrane phosphorylation site in Guanylyl Cyclase a and B. *PLoS One* 7:e36747. doi: 10.1371/journal.pone.0036747

Yoder, A. R., Stone, M. D., Griffin, T. J., and Potter, L. R. (2010). Mass spectrometric identification of phosphorylation sites in guanylyl cyclase a and B. *Biochemistry* 49, 10137–10145. doi: 10.1021/bi101700e

frontiers | Frontiers in Molecular Neuroscience

TYPE Original Research
PUBLISHED 17 February 2023
DOI 10.3389/fnmol.2023.1017761

OPEN ACCESS

EDITED BY
Clint L. Makino,
Boston University,
United States

REVIEWED BY
Clive R. Bramham,
University of Bergen,
Norway
Jenna Penney,
University of Guelph,
Canada

*CORRESPONDENCE
Marlies Knipper
✉ marlies.knipper@uni-tuebingen.de

†These authors have contributed equally to this work

SPECIALTY SECTION
This article was submitted to Molecular Signalling and Pathways, a section of the journal Frontiers in Molecular Neuroscience

RECEIVED 12 August 2022
ACCEPTED 18 January 2023
PUBLISHED 17 February 2023

CITATION
Calis D, Hess M, Marchetta P, Singer W, Modro J, Nelissen E, Prickaerts J, Sandner P, Lukowski R, Ruth P, Knipper M and Rüttiger L (2023) Acute deletion of the central MR/GR steroid receptor correlates with changes in LTP, auditory neural gain, and GC-A cGMP signaling.
Front. Mol. Neurosci. 16:1017761.
doi: 10.3389/fnmol.2023.1017761

Acute deletion of the central MR/GR steroid receptor correlates with changes in LTP, auditory neural gain, and GC-A cGMP signaling

Dila Calis[1†], Morgan Hess[1†], Philine Marchetta[1], Wibke Singer[1], Julian Modro[1], Ellis Nelissen[2], Jos Prickaerts[2], Peter Sandner[3], Robert Lukowski[4], Peter Ruth[4], Marlies Knipper[1*] and Lukas Rüttiger[1]

[1]Department of Otolaryngology, Head and Neck Surgery, Tübingen Hearing Research Centre, Molecular Physiology of Hearing, University of Tübingen, Tübingen, Germany, [2]Department of Psychiatry and Neuropsychology, School for Mental Health and Neuroscience (MHeNS), Maastricht University, Maastricht, Netherlands, [3]Bayer Health Care Pharmaceuticals, Global Drug Discovery Pharma Research Centre Wuppertal, Wuppertal, Germany, [4]Institute of Pharmacy, Pharmacology, Toxicology and Clinical Pharmacy, University of Tübingen, Tübingen, Germany

The complex mechanism by which stress can affect sensory processes such as hearing is still poorly understood. In a previous study, the mineralocorticoid (MR) and/or glucocorticoid receptor (GR) were deleted in frontal brain regions but not cochlear regions using a CaMKIIα-based tamoxifen-inducible *Cre*^{ERT2}/loxP approach. These mice exhibit either a diminished (MR^{TMX}cKO) or disinhibited (GR^{TMX}cKO) auditory nerve activity. In the present study, we observed that mice differentially were (MR^{TMX}cKO) or were not (GR^{TMX}cKO) able to compensate for altered auditory nerve activity in the central auditory pathway. As previous findings demonstrated a link between central auditory compensation and memory-dependent adaptation processes, we analyzed hippocampal paired-pulse facilitation (PPF) and long-term potentiation (LTP). To determine which molecular mechanisms may impact differences in synaptic plasticity, we analyzed Arc/Arg3.1, known to control AMPA receptor trafficking, as well as regulators of tissue perfusion and energy consumption (NO-GC and GC-A). We observed that the changes in PPF of MR^{TMX}cKOs mirrored the changes in their auditory nerve activity, whereas changes in the LTP of MR^{TMX}cKOs and GR^{TMX}cKOs mirrored instead the changes in their central compensation capacity. Enhanced GR expression levels in MR^{TMX}cKOs suggest that MRs typically suppress GR expression. We observed that hippocampal LTP, GC-A mRNA expression levels, and ABR wave IV/I ratio were all enhanced in animals with elevated GR (MR^{TMX}cKOs) but were all lower or not mobilized in animals with impaired GR expression levels (GR^{TMX}cKOs and MRGR^{TMX}cKOs). This suggests that GC-A may link LTP and auditory neural gain through GR-dependent processes. In addition, enhanced NO-GC expression levels in MR, GR, and MRGR^{TMX}cKOs suggest that both receptors suppress NO-GC; on the other hand, elevated Arc/Arg3.1 levels in MR^{TMX}cKOs and MRGR^{TMX}cKOs but not GR^{TMX}cKOs suggest that MR suppresses Arc/Arg3.1 expression levels. Conclusively, MR through GR inhibition may define the threshold for hemodynamic responses for LTP and auditory neural gain associated with GC-A.

KEYWORDS

glucocorticoid receptor, mineralocorticoid receptor, NO-GC, GC-A, cognition

Highlights

- Baseline MR suppresses GR levels.
- Enhanced GR suppresses presynaptic hippocampal excitability.
- Baseline MR and GR suppress hippocampal NO-GC.
- Baseline MR inhibits Arc/Arg3.1.
- Enhanced GR increases GC-A, LTP, and auditory neural gain.

Introduction

Hearing dysfunction in response to age, acoustic trauma, or posttraumatic stress has been linked with different stress responses possibly influencing cognitive functions (Meltser and Canlon, 2011; Canlon et al., 2013; Basner et al., 2014; Jafari et al., 2019; Mazurek et al., 2019; Wang and Puel, 2020; Nadhimi and Llano, 2021). During stress, the naturally occurring glucocorticoid hormones (corticosterone in rodents and cortisol in humans) activate two different receptors. Besides aldosterone, the mineralocorticoid receptor (MR) shows high affinity to glucocorticoids, while the glucocorticoid receptor (GR) gradually becomes occupied by stress-induced high glucocorticoid concentrations (see for a review de Kloet et al., 2018). Both MR and GR actions need to be in balance for maintenance of homeostasis and health (see for a review de Kloet et al., 2018). The expression of MR dominates in glutamatergic neurons of the hippocampus, while GR is more ubiquitously expressed in the CNS (Reul and de Kloet, 1985; Chao et al., 1989; de Kloet et al., 2005; McEwen et al., 2016). To better understand the thus far elusive relationship between balanced stress receptor activity, hearing, and cognition, we previously employed a Cre/loxP-based approach in which a tamoxifen (TMX)-inducible Cre is expressed in the forebrain and hippocampus *via* the CaMKIIα promoter (Dragatsis and Zeitlin, 2000; Wang et al., 2013). The resulting MRGR^{CaMKIIαCreERT2} double knockout (MRGR^{TMX}cKO) lacked MR and GR expression in frontal brain and in the hippocampal region, while cochlear MR and GR expression was unchanged (Marchetta et al., 2022). Remarkably, the examination of MR^{CaMKIIαCreERT2} single knockout (MR^{TMX}cKO), GR^{CaMKIIαCreERT2} single knockout (GR^{TMX}cKO), and MRGR^{TMX}cKO mice unraveled unfavorable effects of central MR deletion and favorable effects of central GR deletion on peripheral auditory nerve processing (Marchetta et al., 2022), suggesting a top-down effect of central MR and GR activities. We reconsidered that the coordinated function of central MR and GR are predominantly predicted to influence the extinction (MR) and consolidation (GR) of long-term potentiation (LTP; see for a review de Kloet et al., 2018). Any adaptive central auditory responses following sound enrichment or acoustic trauma were found to be accompanied by increased hippocampal LTP levels (Matt et al., 2018; Likhtik and Johansen, 2019; Knipper et al., 2020; Marchetta et al., 2020b; Knipper et al., 2022; Manohar et al., 2022; Savitska et al., 2022; Zhang et al., 2022). The association between adaptive central auditory responses following sound enrichment or auditory trauma and LTP changes is suggested to be triggered through corticothalamic feedforward and feedback circuits (Antunes and Malmierca, 2021; Knipper et al., 2022). This encouraged us to investigate the influence of changed peripheral auditory processing in MR^{TMX}cKO and GR^{TMX}cKO (Marchetta et al., 2022) on central auditory responses of these animals in relation to short- and long-term hippocampal plasticity responses. Since the stress-induced drop in central adaptive auditory responses is restorable by inhibition of 3′,5′-cyclic guanosine monophosphate (cGMP) hydrolyzing phosphodiesterase 9A (Savitska et al., 2022), we additionally asked to what extent cGMP-producing nitric oxide (NO)-sensitive (NO-GC), encoded by the mammalian *Gucy1a1*, *Gucy1a2,* and *Gucy1b1* genes, and membrane-bound (GC-A) guanylyl cyclase, encoded by the mammalian *Npr1* gene, may correlate with changes in auditory or hippocampal circuits acutely induced by MR and/or GR deletion. This is of particular interest because cGMP plays an important role in AMPA and NMDA receptor signaling, facilitating synaptic plasticity and memory formation (Giesen et al., 2022), specifically including functions of NO-GC (Koesling et al., 2016; Nelissen et al., 2021, 2022) and possibly also GC-A (Kroker et al., 2012). As AMPA receptor surface diffusion during LTP was shown to be changed by GR activation (Groc et al., 2008), the mRNA of activity-regulated cytoskeletal protein (Arc, also known as Arg3.1) that controls AMPA receptor trafficking during LTP/long-term depression (LTD; Guzowski et al., 1999; Plath et al., 2006; Kuipers et al., 2016) was analyzed.

Based on the herein presented findings, we conclude that balanced basal MR and GR activities play a critical role in setting the threshold for presynaptic reactivities in the hippocampus. Basal MR expression may suppress GR expression levels, which enables higher levels of LTP. This dynamic setting of MR and GR activity appears to keep the threshold for presynaptic excitability (PPF through GR), the NO-GC level (through MR and GR), and neuronal Arc/Arg3.1 level (through MR) low. The elevation of GR levels may lead to elevated hippocampal GC-A and Arc/Arg3.1, elevated LTP, and elevated central auditory neural gain. We conclusively suggest that GR-induced changes in GC-A activity are involved in auditory neural gain, and thus may provide a means for altering corticofugal top-down feedback.

Materials and methods

Animals

Animal care, use, and experimental protocols correspond to national and institutional guidelines and were reviewed and approved by University of Tübingen, Veterinary Care Unit, and the Animal Care and Ethics Committee of the regional board of the Federal State Government of Baden-Württemberg, Germany. All experiments were performed according to the European Union Directive 2010/63/EU for the protection of animals used for experimental and other scientific purposes. In-house bred mice were kept in a specified pathogen free

Abbreviations: Arc/Arg3.1, activity regulated cytoskeletal protein; ABR, auditory brainstem response; BW, body weight; cGMP, 3′,5′-cyclic guanosine monophosphate; FV, fiber volley; fEPSP, field excitatory postsynaptic potential; GC, glucocorticoids; GR, glucocorticoid receptor; GRE, glucocorticoid response element; GR^{TMX}cKO, GR^{CaMKIIαCreERT2} knockout; GC-A, guanylyl cyclase A; HFS, high-frequency stimulation; HPA, hypothalamus-pituitary–adrenal; ISI, interstimulus interval; LTD, long-term depression; LTP, long-term potentiation; MR, mineralocorticoid receptors; NO-GC, nitric oxide (NO)-sensitive (soluble) guanylyl cyclase; MR^{TMX}cKO, MR^{CaMKIIαCreERT2} knockout; MRGR^{TMX}cKO, MRGR^{CaMKIIαCreERT2} knockout; PPF, paired-pulse facilitation; SEM, standard error of the mean; TMX, tamoxifen.

facility at 25°C on a 12/12 h light/dark cycle with average noise levels of around 50–60 dB SPL. The weight of the animals was recorded on each experimental day.

In the present study, three TMX-inducible conditional knockout mouse lines were studied, in which MR and/or GR were deleted mainly in the forebrain. MRGR^{TMX}cKO, MR^{TMX}cKO, GR^{TMX}cKO and corresponding control animals were generated as previously described (Marchetta et al., 2022). In brief, homozygous floxed MR, GR (Berger et al., 2006; Erdmann et al., 2007), or MRGR lines, in which exon 3 of *Mr* and/or *Gr* is flanked by *loxP* sites, were crossed with a CaMKIIα CreERT2 line (kindly provided by Prof. Günther Schütz). After confirmation of normal hearing function, all mice received an intraperitoneal injection of 1 mg TMX in 100 µL TMX-solution (Sigma-Aldrich, T-5648, Munich) twice a day for five consecutive days at the lowest age of approximately eight weeks. 50 mg TMX were dissolved in 500 µL Ethanol abs. (Merck, Darmstadt) and 4.5 mL sunflower oil (Sigma-Aldrich, S-5007). After the last injection, animals were allowed to recover in their home cages for four weeks before experiments started. For the respective transgenic mouse line, homozygous floxed Cre-negative littermates, which also received TMX injections, were used as controls. For all lines, mice of both sexes ranging between 1.8 months (beginning of the experiment) and 7.9 months (end of the experiment) were used. The genetic status of all mouse lines was confirmed by genotyping using gene-specific PCR protocols.

Hearing measurements

Mice were anesthetized with an intraperitoneal injection of a mixture of Fentanyl (0.05 mg/kg bodyweight (BW), Fentanyl-Hameln, Hameln Pharma plus, Hameln, Germany), Midazolam (5.0 mg/kg BW, Midazolam-hameln®; Hameln Pharma plus), Medetomidin (0.5 mg/kg BW, Sedator®; Albrecht, Aulendorf, Germany) and atropine sulfate (0.2 mg/kg BW, B. Braun, Melsungen, Germany) diluted with water ad. inj. (Ampuwa, Fresenius KABI, Bad Homburg, Germany) to an injection volume of 10 mL/kg BW. Additional doses of anesthetics were administered if needed. The anesthesia was antagonized after the measurements by a subcutaneously administered mixture of Naloxon (1.2 mg/kg BW, Naloxon-hameln®; Hameln Pharma plus), Flumazenil (0.55 mg/kg BW, Flumazenil®; Fresenius KABI), and Atipazemol (2.5 mg/kg BW, Antisedan®; VETOQUINOL GmbH, Ravensburg, Germany) diluted with water ad. inj. (Ampuwa) to an injection volume of 10 mL/kg BW.

The anesthetized mice lay on a pre-warmed resting pad (37°C) in a soundproof chamber (IAC 400-A, Industrial Acoustics Company GmbH, Niederkrüchten, Germany). Auditory brainstem responses (ABRs) in anesthetized mice were evoked by short-duration sound stimuli with the same stimulus parameters for all groups. The ABRs represent the summed activity of neurons in distinct anatomical structures along the ascending auditory pathway recorded from subcutaneous cranial electrodes. A microphone (Bruel & Kjaer 4191, Naerum, Denmark) was used to calibrate and record the acoustic stimuli. ABR thresholds were elicited with click stimuli (100 µs duration with an FFT mean of 5.4 kHz). The stimulus level was increased stepwise from 10 to 100 dB SPL in 5 dB steps. Stimuli were generated with an I-O-card (PCI-6052E, PCI-6251, or PCIe-6259, National Instruments, Austin, Texas, United States) in an IBM compatible computer. The SPL of the stimuli was modulated by custom-made amplifier and attenuator systems (Wulf Elektronik, Frankfurt, Germany). The measured signals were band-pass filtered from 200 Hz to 5 kHz (F1, 6-pole Butterworth hardware Filter, Wulf Elektronik) and amplified by 100,000. The analog/digital (A/D) rate was 20 kHz. Each stimulus had a recording interval of 16 ms and was directly repeated and averaged up to 512 times.

Field excitatory postsynaptic potential recordings in hippocampal slices

Extracellular field excitatory postsynaptic potential (fEPSP) recordings were performed according to standard methods as previously described (Matt et al., 2011; Chenaux et al., 2016). In brief, 400 µm thick hippocampal brain slices were coronally sectioned on a vibratome (Leica VT 1000S, Wetzlar, Germany) in ice-cold dissection buffer (mM): 127 NaCl, 1.9 KCl, 1.2 KH2PO4, 26 NaHCO3, 10 D-glucose, 2 MgSO4, and 1.1 CaCl2, constantly saturated with 5% CO2 and 95% O2 (pH 7.4). Slices were incubated in carbogenated artificial cerebrospinal fluid (in mM: 127 NaCl, 1.9 KCl, 1.2 KH2PO4, 26 NaHCO3, 10 D-glucose, 1 MgSO4, 2.2 CaCl2; pH 7.4) for 1 h at 30°C and afterwards stored at room temperature. Recordings were performed in a submerged-type recording chamber (Warner Instruments, Holliston, MA, United States). Stimulation (TM53CCINS, WPI, Sarasota, FL, United States) and recording (artificial cerebrospinal fluid-filled glass pipettes, 2–3 MΩ) electrodes were positioned in the stratum radiatum to record Schaffer collateral fEPSPs. Signals were amplified with an Axopatch 200B (Molecular Devices, San Jose, CA, United States), digitized at 5 kHz with an ITC-16 (HEKA, Reutlingen, Germany) and recorded using WinWCP from the Strathclyde Electrophysiology Suite. Stimuli (100 µs) were delivered through the stimulus isolator (WPI). For each individual slice the strength of the stimulation (typically between 30 and125 µA) was chosen to evoke 40%–60% of the maximal response, defined by initial fEPSP slope. Only slices that showed stable fiber volley (FV) and fEPSP were used for further recording. The same stimulus intensity was applied during baseline recording (0.067 Hz, 20–30 min) and during induction of long-term potentiation (LTP) using 100 stimuli during 1 s (100 Hz). The baseline was determined by averaging fEPSP initial slopes from the period before the tetanic stimulation (at least 15 min of stable recording). The level of LTP was determined by averaging fEPSP slopes from the period between 50 and 60 min after the high-frequency stimulation (HFS). Before the tetanic stimulation, each slice was used to record paired-pulse facilitation [PPF, 10–20–50–100–200–500 ms interstimulus interval (ISI) at the same stimulation strength as LTP recordings]. The paired-pulse ratio of EPSP2/EPSP1 slope and amplitude at each ISI were defined per slice and mean values per group were plotted. EPSP1 was calculated as an average of EPSP1s from all ISIs for each single slice.

Four traces were averaged for each single data point analyzed.

Riboprobe synthesis

To amplify Arc/Arg3.1, we used the following primers: for: 5′-CGA AGT GTC CAA GCA GGT G-3′; and rev: 5′-TGA TGG CAT AGG GGC TAA CA-3′. To amplify NO-GC, we used the following primers: for: 5′-ATC CTC TTC AGC GGC ATT GTG-3′ and rev: 5′-TGC ATT

GGT TCC TTC TTG CCC-3′. To amplify GC-A, we used the following primers: for: 5′-TGT GAA ACG TGT GAA CCG GA-3′ and rev: 5′-AGG CGG ATC GTT GAA AGG G-3′. To amplify GR, we used the following primers: for: 5′-TCC CCC TGG TAG AGA CGA AG-3′ and rev: 5′-GGC TGG TCG ACC TAT TGA GG-3′. To amplify MR, we used the following primers: for: 5′-GAG ATG AGG CTT CTG GGT GT-3′ and rev: 5′-CAG GAT CAT GGA CGG GGA TG-3′. These fragments were cloned into the pCR II Topo vector (Invitrogen, Karlsruhe, Germany) and their nucleotide sequences were verified by an automated sequencer. Plasmids were isolated using QIAprep Spin Miniprep Kit from Qiagen (Hilden, Germany). Complementary strands for sense and antisense riboprobes were transcribed from either Sp6 or T7 RNA polymerases and labeled using rNTP mix containing digoxigenin labeled uridine triphosphates. All restriction enzymes, RNA polymerases and digoxigenin-labeled rNTP were purchased from Roche Diagnostics (Mannheim, Germany).

Co-localization of mRNA and protein in brain sections

A separate subset of mice from those used for *in vitro* electrophysiology measurements was deeply anesthetized with CO2 and then sacrificed by decapitation. Brain tissue was prepared and sectioned with a vibratome at 60 µm, as previously described (Singer et al., 2013a, 2016). mRNA and protein were co-localized on free-floating brain sections as previously described (Singer et al., 2013a). In brief, following prehybridization for 1 h at 37°C, sections were incubated overnight with NO-GC, GC-A, Arc/Arg3.1, MR, or GR riboprobes at 56°C, incubated with anti-digoxigenin antibody conjugated to alkaline phosphatase (anti-Dig-AP, Roche, 11093274910), and developed as previously described (Singer et al., 2013a). For protein detection, streptavidin–biotin was blocked according to the manufacturer's instructions (Streptavidin–Biotin Blocking Kit, Vector Laboratories, Newark, CA, United States) after blocking endogenous peroxidase. Sections were incubated overnight at 4°C with the primary antibody against parvalbumin (Abcam, Berlin, Germany, anti-rabbit, 1:500, ab11427) as a marker for inhibitory neurons, followed by incubation with the secondary antibody (biotinylated goat anti-rabbit, Vector Laboratories, BA-1000) and chromogenic detection (AEC, 3-amino-9-ethylcarbazole, Vector Laboratories, SK-4200). For microscopy (BX61 microscope, Olympus, Hamburg, Germany) evaluation photographs of the hippocampus and auditory cortex were taken at a bregma position between −1.58 and −2.18 with a bright-field camera (DP 71, Olympus) for detection of mRNA and protein, without adjusting the picture frame or the plane of focus.

Identification of GRE binding sites in NO-GC and GC-A upstream regions

To identify potential glucocorticoid-responsive elements (GRE) binding sites in NO-GC and GC-A upstream regions, Benchling was used to import and annotate the following genes: *Gucy1a1*, *Gucy1a2, Gucy1b1,* and *Npr1*. Subsequently, known sequences for GRE binding sites were aligned (see Supplementary Methods). These sequences were based on JASPAR and sequences previously identified by Meijsing et al. (2009), Polman et al. (2013), and van Weert et al. (2017).

Quantification and statistical analysis

All statistical information and *n*-numbers can be found in the results section and in Supplementary Table S1. Data was tested for a normal distribution (the Shapiro–Wilk normality test, $\alpha = 0.05$). Differences of the means were compared for statistical significance either by unpaired two-tailed Student's *t*-test (parametric)/Mann–Whitney *U*-test (non-parametric), repeated measurement (RM) 2-way ANOVA, 2-way ANOVA (parametric) with $\alpha = 0.05$ and correction for type 1 error using Sidak's and Bonferroni's multiple comparisons tests.

In figures, significance and a trend for significance is indicated by asterisks [(*) $p < 0.08$, * $p < 0.05$, ** $p < 0.01$, *** $p < 0.001$]. n.s. denotes non-significant results ($p \geq 0.08$). The *p*-values of the 2-way ANOVAs refer to the main effect of the genotype.

ABR analysis

For each individual ear, the peak input–output function for amplitude of the click-ABR measurements were averaged for intensities between 0 and 40 dB relative to threshold (re thr) and analyzed as previously described (Chumak et al., 2016).

Two peak classes were selected: (1) early peaks (at 1.2–1.8 ms, wave I), interpreted as the sum of the first stimulus-related action potential within the auditory nerve, and (2) delayed peaks (at 4.1–4.9 ms, wave IV), the response from the auditory midbrain.

Wave IV/I ratio was calculated by dividing the ABR wave IV amplitude by ABR wave I amplitude for individual animals at all intensities higher than 5 dB (re thr). For each individual ear, stimulus levels of 10–30 dB, 35–55 dB, and 60–80 dB re thr were averaged to yield three repeated measurements for fibers of different sensitivity and spontaneous rate [high-spontaneous rate (SR) low-threshold fibers, middle-SR, and low-SR high-threshold fibers; Bharadwaj et al., 2014]. Inter-peak latency growth functions were calculated by subtracting the ABR wave I latency from the ABR wave IV amplitudes for individual animals for increasing stimulus levels with reference to the ABR thresholds (from higher than 5 dB to a maximum of 80 dB re thr) and grouped into stimulus level ranges as described (10–30 dB, 35–55 dB, and 60–80 dB). For statistical analyses, single ears are used as sample size.

fEPSP recordings in hippocampal slices

Data was analyzed and processed using Clampfit 10 (Molecular Devices) and Excel (Microsoft). The data presented per experimental group/condition contained (in addition to mean ± SEM) single dots showing the fEPSP slope values for each individual brain slice. The *n* indicates the number of slices and animals (slices/animals) used in the analysis. Recordings which did not show stable baseline or shifting ±2% from the average in the baseline recording were not included in the statistical analysis. For statistical analyses, single slices are used as sample size.

Co-localization of mRNA and protein and immunohistochemistry in brain sections

Brain sections were quantified by integrating density values of color pixels for each single specimen using ImageJ software (NIH, Bethesda,

MD; United States). Quantification of the mRNA from the double method staining was performed by artificially separating the image into three defined color "channels," which were selected as the average signal from all groups of the background, the protein staining, and the mRNA staining. A detection threshold was then defined in the mRNA color "channel" which was consistent across all groups and genotypes. The integrated density was then calculated for each image and all images are averaged for one animal. The density values of all specimens stained within the same experiment were then normalized to the group mean (i.e., all hippocampal brain sections stained in the same experiment gave an average value of 1.0). This correction allowed for compensation of the high intertrial variation of staining intensity. All sections from one mouse were then averaged and entered the statistical evaluation as $n = 1$. When no quantifiable staining could be measured, the group was excluded from analysis.

Results

Acute deletion of MR in adult mice leads to elevated GR expression levels

Global and conditional MR deletion affected the expression profiles of GR in central neurons (Berger et al., 2006; Erdmann et al., 2007). We questioned if comparable effects are observed after TMX-induced acute deletion in MR and GR^{TMX}cKOs. Brain sections of MR and GR^{TMX}cKOs were exposed to GR- or MR-specific riboprobes. Data was evaluated quantitively as previously described (Singer et al., 2013a; Eckert et al., 2021). As exemplarily shown in Figure 1A, MR^{TMX}cKOs had a significantly higher expression of GR mRNA in the hippocampus in comparison to their WT controls [Figure 1A, unpaired two-tailed student's *t*-test, $t(6) = 3.530$, $p = 0.0124$, $n = 4$ mice each]. In contrast, conditional ablation of GR did not significantly affect the MR mRNA abundance in the hippocampus in comparison to WT controls [Figure 1B, unpaired two-tailed student's *t*-test, $t(8) = 1.993$, $p = 0.0814$, $n = 5$ mice each]. The finding confirms that the differential GR expression which was observed in global and conditional MR/GR double- and single-KOs (Berger et al., 2006; Erdmann et al., 2007) is also observed in TMX-induced MR^{TMX}cKOs. This proves the validity of the CaMKIIα-based TMX-inducible *Cre*^{ERT2}/*loxP* approach for central deletion of MR and GR.

This also means that the MR^{TMX}cKO phenotype should not only be interpreted with respect to the central MR deletion but also from the perspective of increased GR expression levels.

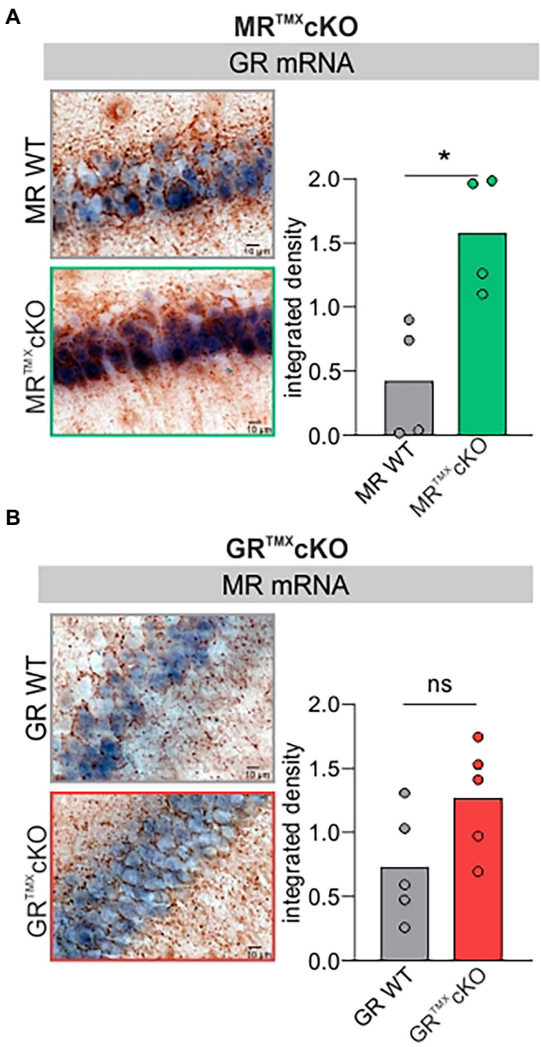

FIGURE 1
GR and MR mRNA expression level (blue) in the CA1 region of the hippocampus of MR and GR^{TMX}cKO mice. **(A)** MR^{TMX}cKO (green) mice showed significantly higher GR mRNA expression levels in comparison to their WT controls (gray). **(B)** GR^{TMX}cKO (red) mice showed no difference in MR mRNA expression levels in comparison to their WT controls (gray). Mean±SEM. ns=p>0.08, *=p<0.05.

Differential impact of central MR and/or GR deletion on central auditory neural gain, PPF, and LTP

We next analyzed the central auditory responses (ABR wave IV) relative to the altered cochlear auditory processing (ABR wave I) of MR^{TMX}cKOs, GR^{TMX}cKOs, and MRGR^{TMX}cKOs mice (Figure 2, left). Raw ABR wave amplitude and latency values were consistent with previously-reported data for all genotypes (data not shown; Marchetta et al., 2022). ABR wave IV/I ratio (input/output function) analysis for stimulus ranges corresponding to auditory fibers of different sensitivity and response range [10–30 dB, 35–55 dB, and 60–80 dB re thr for high-spontaneous rate (SR), middle-SR, and low-SR auditory fibers, respectively (Bharadwaj et al., 2014)] revealed that the reduced auditory nerve response of MR^{TMX}cKOs could be centrally compensated through neural gain [higher ABR wave IV/I ratio; Figure 2A, left, repeated measurement (RM) 2-way ANOVA, $F(1, 49) = 7.652$, $p = 0.008$, Sidak's multiple comparisons test, MR WT: $n = 30$ ears from 16 mice, MR^{TMX}cKO: $n = 21$ ears from 14 mice]. Accordingly, the inter-peak latency of MR^{TMX}cKO mice reached similar values in comparison to their WT controls (Supplementary Figure S2A). On the other hand, the TMX-mediated deletion of central GR resulted in slightly reduced ABR wave IV/I ratio indicating less neural gain, although this effect was not statistically significant (Figure 2B, left, RM 2-way ANOVA, $F(1, 28) = 3.284$, $p = 0.0807$, Sidak's multiple comparisons test, GR WT: $n = 14$ ears from 8 mice, GR^{TMX}cKO: $n = 16$ ears from 8 mice), despite the enhanced/disinhibited ABR wave amplitudes in these conditional mutants (Marchetta et al., 2022). The inter-peak latency of GR^{TMX}cKO mice was significantly shorter in comparison to their WT controls, particularly above 30 dB (Supplementary Figure S2B). Finally, the

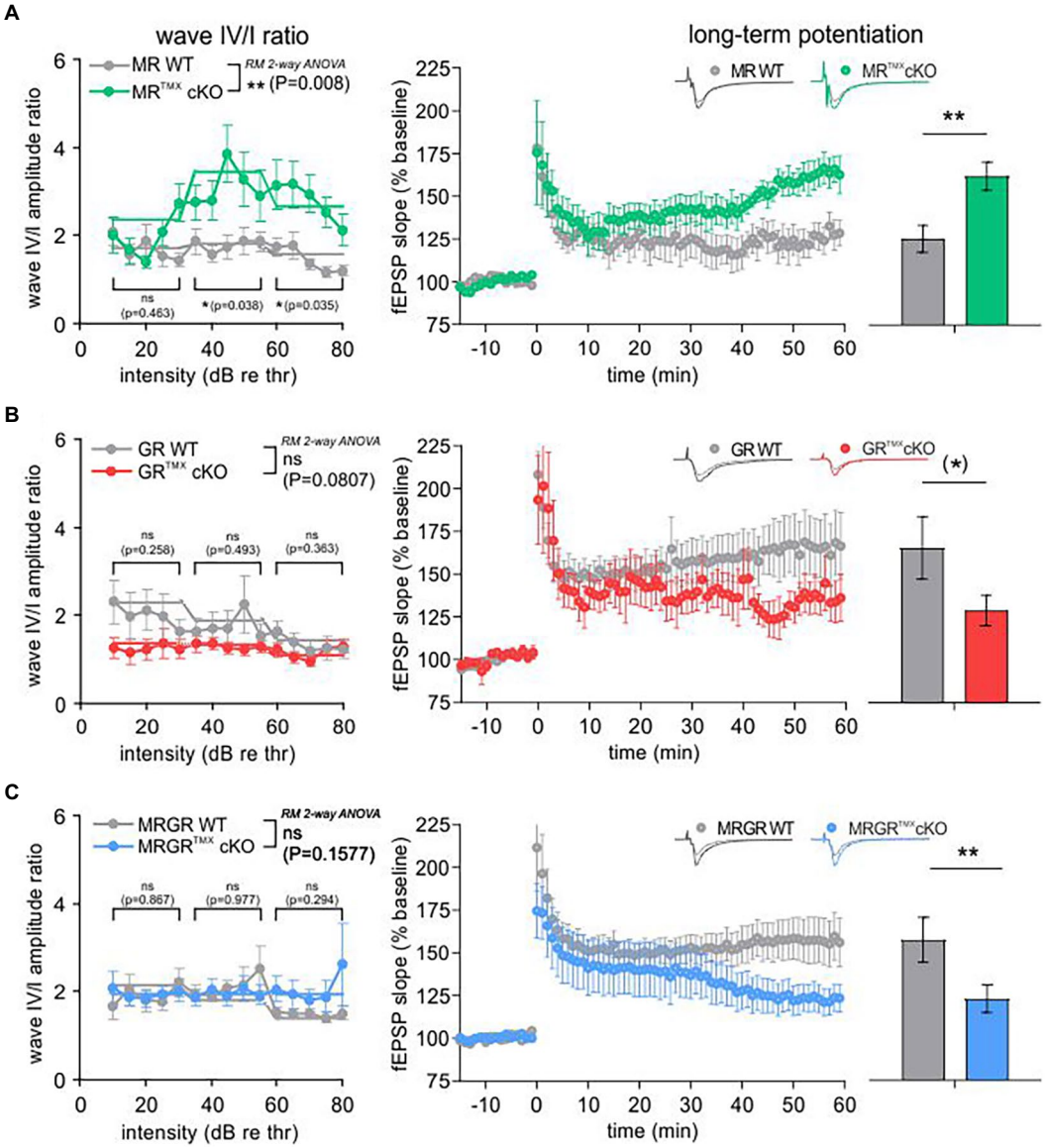

FIGURE 2
ABR wave IV/I amplitude ratio and LTP of MR^{TMX}cKO, GR^{TMX}cKO, and MRGR^{TMX}cKO in comparison to their WT controls. **(A)** MR^{TMX}cKOs (green) had a significantly higher wave IV/I ratio in comparison to their WT controls (gray). The MR^{TMX}cKOs had significantly higher LTP in comparison to their WT controls. **(B)** GR^{TMX}cKOs (red) had a slightly, non-significantly lower wave IV/I ratio compared to their WT controls (gray). GR^{TMX}cKOs had a trend toward lower LTP in comparison to their WT controls. **(C)** MRGR^{TMX}cKOs (blue) did not show a significant difference of wave IV/I ratio in comparison to their WT controls (gray). Contrary to this, MRGR^{TMX}cKOs had significantly lower LTP in comparison to their WT controls. Mean±SEM. ns=p>0.08, (*)=p<0.08, *=p<0.05, **=p<0.01.

conditional deletion of both MR and GR in the MRGR^{TMX}cKOs, resulted in an unchanged ABR wave IV/I ratio (Figure 2C, left, RM 2-way ANOVA, $F(1, 42) = 0.1546$, $p = 0.6962$, MRGR WT: $n = 19$ ears from 11 mice, MRGR^{TMX}cKO: $n = 25$ ears from 14 mice). We interpret this as an intermediate response resulting from counterbalancing effects of the individual cKOs. In addition, the inter-peak latency of MRGR^{TMX}cKO mice was equally long as for their WT controls (Supplementary Figure S2C). As we assume that in our mouse model MR and GR are not deleted in the ascending auditory pathway (cochlea, brainstem), the alterations observed in auditory neural gain are likely a top-down effect resulting from the forebrain deletion of MR and/or GR, as also described to be the case for blood pressure changes resulting from MR overexpression under the CamKIIα promoter (Lai et al., 2007).

The predicted influence of stress and hippocampal LTP on central auditory adaptive responses (Singer et al., 2013b; Jafari et al., 2018; Matt et al., 2018; Savitska et al., 2022; Zhang et al., 2022) motivated us to study hippocampal LTP on acute coronal brain slices in the individual and compound MR and GR^{TMX}cKO models (Figure 2, right). LTP was induced by tetanic stimulation (1 s, 100 Hz) of CA3 Schaffer's collateral axons, and fEPSPs were recorded from the dendrites of CA1 pyramidal cells that form synaptic contacts with CA3 neurons (Matt et al., 2018). LTP, determined by averaging fEPSP slopes from the period between 50 and 60 min after the high-frequency stimulation (HFS), was significantly higher after 50–60 min with changes seen from ~35 min onwards in MR^{TMX}cKOs (Figure 2A, right, green; 162.16% ± 8.25%, $n = 9$ slices from 5 animals) in comparison to WT controls [Figure 2A, right, gray;

125.44% ± 7.90%, $n = 7$ slices from 4 animals; Mann–Whitney U-test, $U(117.8, 167.9) = 6$, $p = 0.0093$], while the GR^{TMX}cKOs had a trend toward lower LTP in comparison to WT controls [Figure 2B, right, GR^{TMX}cKO, red, 128.96% ± 8.98%, $n = 9$ slices from 6 animals, WT, gray, 165.52% ± 18.27%, $n = 7$ slices from 5 animals; Mann–Whitney U-test, $U(151.0, 124.0) = 12$, $p = 0.0721$]. On the other hand, MRGR^{TMX}cKOs exhibited significantly lower LTP in comparison to their respective WT controls [Figure 2C, right, MRGR^{TMX}cKO, blue, 122.88% ± 8.12%, $n = 13$ slices from 7 animals, WT, gray, 157.30% ± 13.18%, $n = 12$ slices from 6 animals; Mann–Whitney U-test, $U(160.7, 121.3) = 45$, $p = 0.0076$].

To investigate to what extent the differences in central compensation or LTP are associated with differences in the presynaptic state of Schaffer's collaterals in the hippocampus, we studied paired-pulse facilitation (PPF), an indication of presynaptic activity underlying short-term plasticity. PPF, a transient increase in the probability of glutamate release (Zucker and Regehr, 2002), was studied in MR^{TMX}cKO, GR^{TMX}cKO, and MRGR^{TMX}cKO brain slices as described in methods and previous studies (Satake et al., 2012).

The PPF was investigated in each brain slice prior to LTP induction using varying ISIs of 10, 20, 50, 100, 200, and 500 ms and the same stimulation strength that was also used for LTP recordings (Figure 3). The MR^{TMX}cKO mice had a significantly lower PPF, seen in its slope ratio, in comparison to their WT controls [Figure 3A, green vs. gray circles, 2-way ANOVA, $F(1, 78) = 14.48$, $p = 0.0003$, Sidak's multiple comparisons test, MR^{TMX}cKO: $n = 8$ slices from 5 animals, WT: $n = 7$ slices from 4 animals]. In contrast, in GR^{TMX}cKO mice, the PPF slope ratio was not significantly different from their respective controls [Figure 3B, red vs. gray circles, 2-way ANOVA, $F(1, 78) = 2.172$, $p = 0.1446$, GR^{TMX}cKO: $n = 9$ slices from 6 animals, WT: $n = 7$ slices from 5 animals]. In MRGR^{TMX}cKO mice also, no difference in PPF slope ratio was observed in comparison to their WT controls [Figure 3C, blue vs. gray circles, 2-way ANOVA, $F(1, 138) = 2.217$, $p = 0.1388$, MRGR^{TMX}cKO: $n = 13$ slices from 7 animals, WT: $n = 12$ slices from 6 animals].

We further examined the fEPSP slopes and fiber volley (FV) amplitudes of individual cKOs, in order to ensure that the effects observed in the LTP and PPF were not due to a change in the basal synaptic transmission properties. fEPSP slope or FV amplitudes in MR^{TMX}cKOs (Supplementary Figure S3A), GR^{TMX}cKOs (Supplementary Figure S3B), and MRGR^{TMX}cKOs (Supplementary Figure S3C) were not different from their respective WT controls. Further, the increase in fEPSP slope remained proportional to FV amplitudes and did not differ between the different genotypes (Supplementary Figure S3A–C, bottom). Overall, the findings suggest that basal synaptic transmission properties were unchanged by cKO of MR and/or GR.

In conclusion, the reduced PPF in MR^{TMX}cKO implies that MR coordinates the release probability in the presynapse of hippocampal neurons, possibly through elevation of GR expression levels. We further conclude that the enhanced LTP and ABR wave IV/I ratio in MR^{TMX}cKOs are linked to the reduced suppression of GR expression levels in these mice. In that sense, GR expression levels regulate LTP and auditory neural gain. The lack of effect in GR^{TMX}cKOs and MRGR^{TMX}cKOs is consistent with this notion.

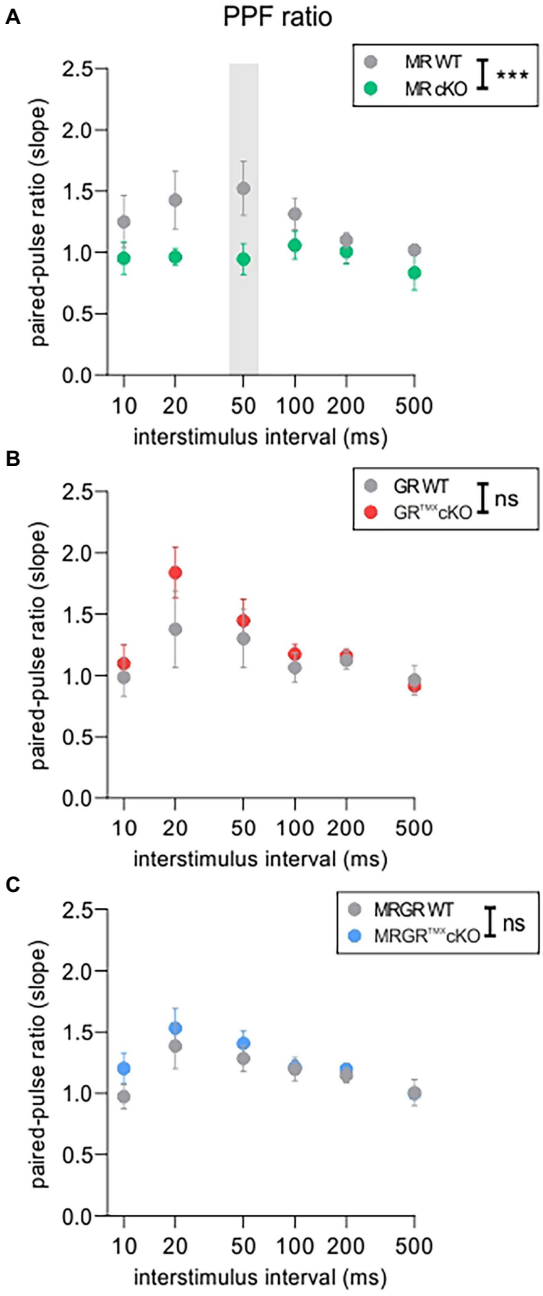

FIGURE 3
PPF as an indicator of short-term plasticity. **(A)** The analysis of PPF in MR^{TMX}cKOs (green) showed a significantly lower paired-pulse ratio of the EPSP2/EPSP1 slope in comparison to WT controls (gray) with a significant post-hoc test at 50ms ISI. **(B)** GR^{TMX}cKOs (red) showed no difference in paired-pulse ratio of the EPSP2/EPSP1 slope in comparison to WT controls (gray). **(C)** MRGR^{TMX}cKOs (blue) showed no difference in paired-pulse ratio of the EPSP2/EPSP1 slope in comparison to WT controls (gray). Mean±SEM. ns=p>0.08, ***=p<0.001.

Deletion of MR and/or GR in the hippocampus differentially affects NO-GC, GC-A, and Arc/Arg3.1 mRNA levels

To better understand the differential impact of acute deletion of MR and GR function on hippocampal LTP and auditory processing, we tested for altered cGMP generator expression profiles, previously hypothesized to provide the missing link between auditory processing and LTP. The mRNA expression profiles of a crucial NO-GC subunit and membrane-bound GC-A were analyzed in the CA1 region of the hippocampus. Two isoforms of NO-GC exist: the more widely expressed NO-GC1 and NO-GC2. Both isoforms build a heterodimer complex with the beta-1 subunit (Koesling et al., 2016), the changes of which parallel that of the alpha subunit (Mergia et al., 2006; Koesling et al.,

2016). Therefore, we targeted NO-GC β1 mRNA for analysis of expression profiles. The recently observed potentiating influence of altered cGMP generator activity on LTP and synaptic AMPA receptor transport activity (Nelissen et al., 2021, 2022) moreover motivated us to correlate levels of cGMP generators with changes of cytoplasmic Arc/Arg3.1, the mRNA of which is targeted to dendrites during LTP/LTD changes in response to neuronal activity (Korb and Finkbeiner, 2011; Goel et al., 2019). *In situ* hybridizations of NO-GC β1, GC-A, and Arc/Arg3.1 mRNA were analyzed in brain sections and quantified in the CA1 region of the hippocampus according to previously established protocols (Matt et al., 2018; Eckert et al., 2021; Figure 4). MR^{TMX}cKOs exhibited significantly higher levels of NO-GC, Arc/Arg3.1, and GC-A mRNA in comparison to their WT controls [Figure 4A, NO-GC left, unpaired two-tailed student's *t*-test, $t(10) = 3.651$, $p = 0.0045$, $n = 6$ mice each; Arc/Arg3.1 mRNA middle, unpaired two-tailed student's *t*-test, $t(6) = 53.63$, $p < 0.0001$, $n = 4$ mice each; GC-A mRNA right, unpaired two-tailed student's *t*-test, $t(8) = 6.874$, $p = 0.0001$, $n = 5$ mice each]. GR^{TMX}cKOs also had significantly higher levels of NO-GC mRNA [Figure 4B, left, unpaired two-tailed student's *t*-test, $t(8) = 3.924$, $p = 0.0044$, $n = 5$ mice each] but strikingly showed no significant differences in levels of Arc/Arg3.1 and GC-A mRNA in comparison to their WT controls [Figure 4B, Arc/Arg3.1 mRNA middle, unpaired two-tailed student's *t*-test, $t(6) = 0.4093$, $p = 0.6965$, $n = 4$ mice each; GC-A mRNA right, unpaired two-tailed student's *t*-test, $t(8) = 0.3671$, $p = 0.7231$, $n = 5$ mice each]. MRGR^{TMX}cKO displayed significantly higher levels of NO-GC mRNA and Arc/Arg3.1 mRNA, as also observed in MR^{TMX}cKOs [Figure 4C, NO-GC, left, unpaired two-tailed student's *t*-test, $t(4) = 11.17$, $p = 0.0004$, $n = 3$ mice each; Arc/Arg3.1 mRNA middle, unpaired two-tailed student's *t*-test, $t(4) = 2.883$, $p = 0.0449$, $n = 3$ mice each]. On the other hand, the GC-A expression levels in the MRGR^{TMX}cKO were significantly reduced [Figure 4C, right, unpaired two-tailed student's *t*-test, $t(4) = 5.941$, $p = 0.0040$, $n = 3$ mice each].

We additionally tested for altered cGMP generator expression levels in the auditory cortex of MR^{TMX}cKO and GR^{TMX}cKO mice in neurons of all cortical layers (layer I–VI). We found that GC-A expression levels in the auditory cortex for both MR^{TMX}cKO and GR^{TMX}cKO mice mirror the findings in the hippocampus (Supplementary Figure S4), hypothalamus, and amygdala (data not shown). NO-GC expression levels in MR^{TMX}cKO and GR^{TMX}cKO mice were also both significantly higher in the auditory cortex in comparison to their respective WT controls (Supplementary Figure S4), as also observed in the hippocampus; however, NO-GC levels throughout the rest of the brain were more variable (data not shown).

In order to test whether MR or GR directly influence NO-GC or GC-A *via* their classical transcriptional cis-activation GR element binding motifs, a search was carried out for MR/GR-specific binding

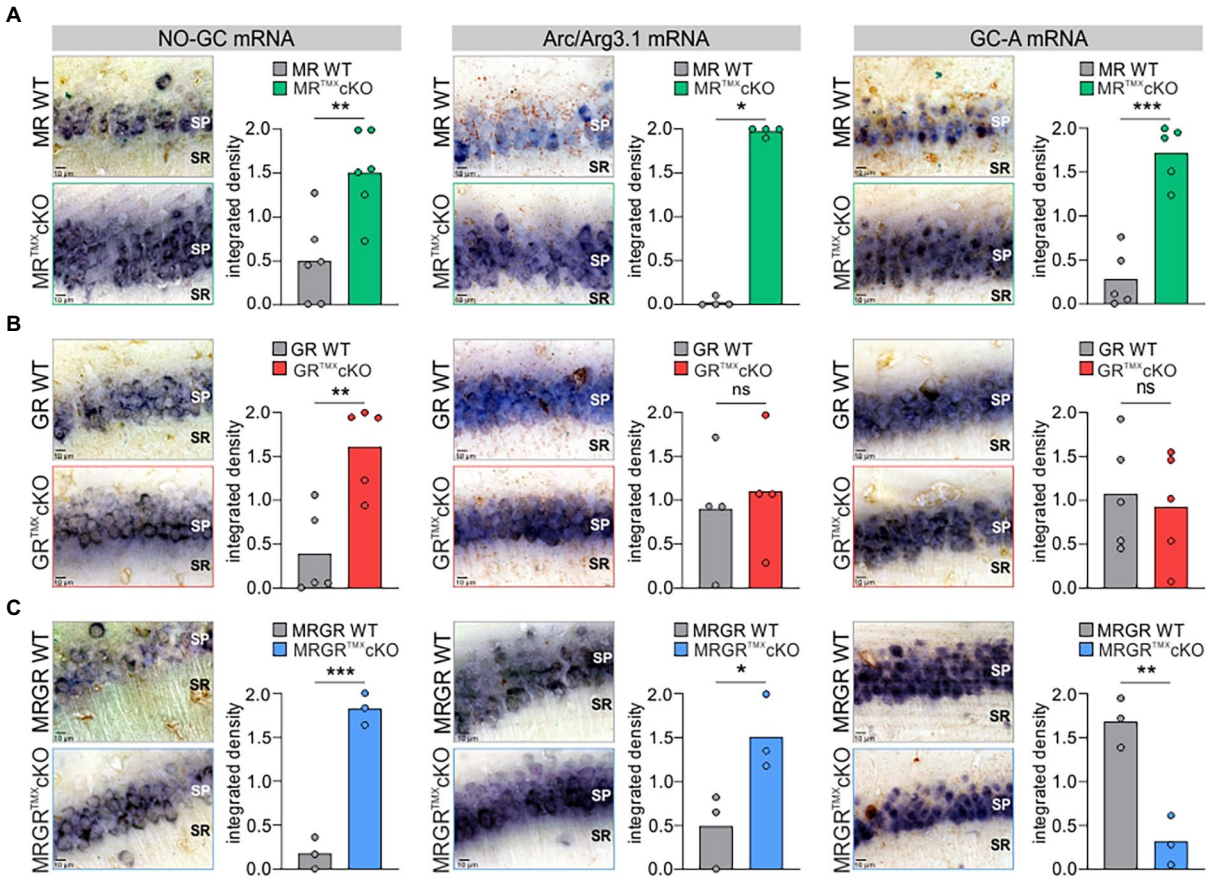

FIGURE 4
NO-GC, Arc/Arg3.1, and GC-A expression in the CA1 region of the hippocampus in MR, GR, and MRGR^{TMX}cKO mice. **(A)** MR^{TMX}cKO (green) mice showed significantly higher levels of NO-GC mRNA expression, Arc/Arg3.1 mRNA expression, and GC-A mRNA expression in comparison to their WT controls (gray). **(B)** GR^{TMX}cKO (red) mice showed significantly higher NO-GC mRNA expression levels, equal Arc/Arg3.1 mRNA expression levels, and equal GC-A mRNA expression levels in comparison to their WT controls (gray). **(C)** MRGR^{TMX}cKO (blue) mice showed significantly higher levels of NO-GC mRNA expression levels and Arc/Arg3.1 mRNA expression, but significantly lower GC-A mRNA expression levels in comparison to their WT controls (gray). Mean. ns=p>0.08, *=p<0.05, **=p<0.01, ***=p<0.001.

motifs (GRE sequences) in the genes encoding NO-GC (i.e., *Gucy1a1*, *Gucy1a2*, *Gucy1b1*) and GC-A (*Npr1*). No relevant GRE sequences could be detected in *Gucy1b1* or *Npr1*. For *Gucy1a1* and *Gucy1a2*, each gene was found to contain a conserved GRE sequence (Supplementary Figures S5, S6). Specifically, for *Gucy1a1*, this GRE sequence (5′-AGGAACACCATGTTCTG-3′) was found to span across the start codon of the transcribed part of the gene. This also included an Atoh sequence (5′-CAGAAGG-3′) 25 bp upstream of the GRE sequence. For *Gucy1a2*, the GRE sequence was a palindrome (5′-AGAACA AACTGTTCT-3′) located near multiple regulatory regions in the intron between exons 3 and 4.

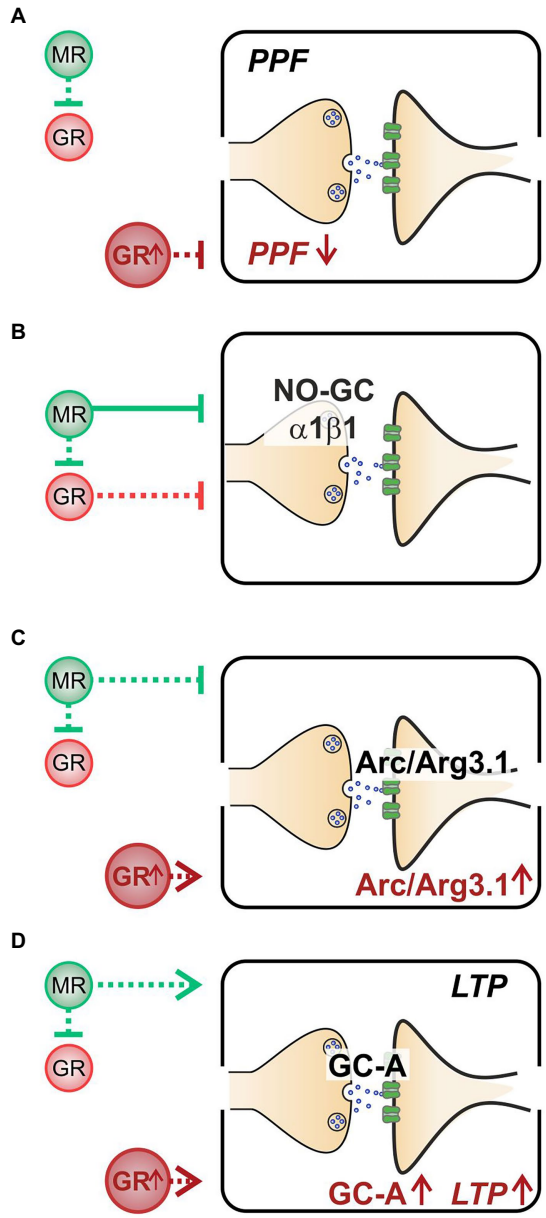

FIGURE 5
A summary of the hypothesized effects of MR and GR in a physiological state and stress state (GR↑). **(A)** When at a normal level, MR inhibits GR (green dashed line, upper half). However, neither MR nor GR affect PPF when at physiological levels. At elevated GR conditions (lower half), PPF is low. **(B)** Both stress receptors exhibit an inhibitory effect on NO-GC expression levels, though the inhibitory effect of MR (green solid line) is stronger than that of GR (red dashed line). **(C)** MR inhibits Arc/Arg3.1 expression levels (green dashed line, upper half); however, when GR is elevated, Arc/Arg3.1 is stimulated (lower half). **(D)** Basal MR stimulates GC-A expression levels and LTP (green dashed line, upper half). Elevated GR expression also leads to elevated GC-A and to elevated LTP (lower half).

Altogether, we here demonstrate that (i) decreased PPF in MR^{TMX}cKOs may be linked to elevated GR expression levels (Figure 5A). (ii) Enhanced NO-GC expression levels in MR, GR, and $MRGR^{TMX}$cKOs, imply that both receptors' activity is required to effectively suppress NO-GC in hippocampal neurons under physiological conditions, which may be supported by GRE elements responding to both MR and GR (Figure 5B). (iii) Increased Arc/Arg3.1 expression levels in MR^{TMX}cKOs and $MRGR^{TMX}$cKOs but not in GR^{TMX}cKOs (Figure 5C) do not correlate to LTP as simply. The changes of Arc/Arg3.1 in $MRGR^{TMX}$cKOs rather point to basal MR activity but not GR activity as being inhibitory to Arc/Arg3.1 levels (Figure 5C). Further, the gradient of Arc/Arg3.1 changes in MR^{TMX}cKOs and $MRGR^{TMX}$cKOs suggests that elevated GR expression may stimulate Arc/Arg3.1 (Figure 6B). (iv) MR^{TMX}cKOs exhibited an increased GR expression, suggesting that under physiological conditions MR suppresses GR expression. When this suppression is removed in MR^{TMX}cKOs, animals exhibit elevated LTP, GC-A, and ABR wave IV/I ratio. This is not seen in GR^{TMX}cKOs, suggesting that GR may contribute to the empowerment of central neural gain during auditory adaption by controlling the energization through GC-A (Figure 5D).

Discussion

By investigating TMX-induced conditional single or combined deletion of MR and GR in forebrain regions, we show for the first time that central MR and GR activity must be balanced in order to set thresholds for presynaptic activity and central auditory compensation (auditory neural gain). Changes in MR and GR activities result in significant alterations of cGMP generator expression levels in hippocampal neurons. In detail, we suggest (i) baseline hippocampal MR expression levels suppress GR expression. (ii) MR-induced control of GR may set a threshold for presynaptic plasticity. (iii) Basal MR may set a threshold for AMPA receptor trafficking by Arc/Arg3.1, while elevated GR levels may enhance Arc/Arg3.1 expression levels. (iv) Elevated GR may enhance LTP and GC-A expression levels and thereby contribute to LTP-dependent neural auditory gain.

Basal MR activities suppress GR expression

Until now, insights into the physiological function of stress receptors in the adult brain have been limited because global GR KOs (Cole et al., 1995) or early Cre-mediated deletion of GR (Erdmann et al., 2008) is lethal in mice. Also, a global lack of MR induces early postnatal death linked with bodily dehydration (exsiccosis) due to massive renal sodium and water loss (Berger et al., 1998). Early Cre-induced conditional MR deletion is expected to allow long-term adaptation processes to compensate for the absence of MR (Erdmann et al., 2008). Some of these limitations were avoided by the acute TMX-induced deletion of MR and GR studied here. Although in Marchetta et al., 2022, a TMX-induced deletion of MR and GR protein was only shown for the $MRGR^{TMX}$cKO and not for the single MR^{TMX}cKO and GR^{TMX}cKO, the observed higher GR expression levels in MR^{TMX}cKOs, also previously reported in global or conditional MR^{TMX}cKO mice (Berger et al., 2006; Erdmann et al., 2007), may point

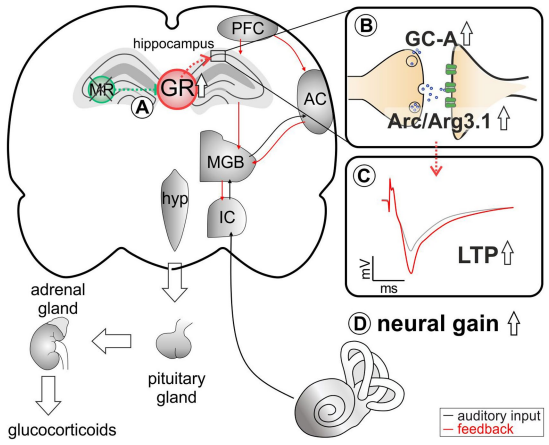

FIGURE 6
An abstract scheme of the pathways that can be concluded from the acute deletion of MR (green). **(A)** MR deletion leads to elevated GR expression levels. **(B)** As a result of elevated GR, an increase in GC-A and Arc/Arg3.1 expression levels in the hippocampus can be observed. **(C)** This change in expression pattern may be functionally related to higher hippocampal LTP. **(D)** Elevated GC-A and Arc/Arg3.1 expression levels and elevated LTP potentially provide a means for top-down mechanisms allowing for auditory neural gain.

to successful targeting of individual receptor expression. We however cannot entirely exclude that the receptor protein may not have been completely deleted (knocked out), at the time of the experiments. Nevertheless, it can be assumed that an upregulation of GR in MR^{TMX}cKOs reflects the previously-described balancing effect of MR on the hypothalamic-pituitary-adrenal (HPA) axis, which stems from central neurons (see for a review de Kloet et al., 2018). Thus, elevated corticosterone levels were reported in conditional GR but not MR mutants (Erdmann et al., 2007), and consistently higher corticosterone levels were measured in GR^{TMX}cKOs but not in MR^{TMX}cKOs (Marchetta et al., 2022). In line with this, normal corticosterone levels—occurring when HPA axis feedback regulation is balanced—are the result of physiologically lower GR levels when baseline MR activities prevent excessive GR expression (Harris et al., 2013), as also concluded from the findings of the present study. This tight control of the HPA axis was recently demonstrated in heterozygous GR mutants that had an enhanced HPA axis activity in response to restraint stress (Harris et al., 2013). Interestingly, the HPA axis overshoot in heterozygous GR mutants in response to stress was counterbalanced through an overexpression of MR in these heterozygous GR mutants (Harris et al., 2013). Apparently, MR exerts a tonic inhibitory influence on HPA axis activity, and thereby determines the threshold of reactivity during stress (see for a review de Kloet et al., 2018).

In conclusion, we suggest that the predicted tonic inhibitory influence of MR on the HPA axis is severely disturbed upon the acute MR or GR deletion.

GR may suppress plasticity in presynaptic hippocampal activity

The TMX-induced deletion of MR in hippocampal regions of MR^{TMX}cKOs resulted in reduced PPF (Figures 3, 5A). Because PPF results from a prior accumulation of residual Ca^{2+} at the synaptic terminal and a lingering effect of Ca^{2+} on the exocytotic Ca^{2+} sensor of releasable vesicles during the second stimulus (as reviewed in Thomson, 2000; Zucker and Regehr, 2002), we expect the probability of vesicular release to be transiently decreased in MR^{TMX}cKOs. This is likely due to increased GR expression in these mutants, as can be concluded from the absence of PPF effects in GR^{TMX}cKO and MRGR^{TMX}cKO (Figure 5A). We thus assume that baseline MR or GR activity alone do not strongly affect presynaptic excitability, but rather that increased GR activity, as occurs in the MR^{TMX}cKOs, suppresses PPF (Figures 1A, 3A, 5A). This finding may contrast findings in which corticosterone application in hippocampal CA1 neurons resulted in a brief increase in miniature excitatory postsynaptic current frequency, a feature described to occur through MR activities (Sarabdjitsingh et al., 2016; de Kloet et al., 2018; Joels, 2018). Further studies are required to clarify this controversy. It is noteworthy to consider the findings in our previous study, which implied a reduced activity at the inner hair cell synapse in the MR^{TMX}cKO (Marchetta et al., 2022). The peripheral depression of activity in MR^{TMX}cKOs is comparable to the here-observed more central changes of reduced release probability in the presynapse of hippocampal neurons (Figure 3; Marchetta et al., 2022). Overall, it gives credence to the hypothesis that balanced central MR and GR activities set the threshold for sensory activity centrally and peripherally by targeting presynaptic mechanisms, possibly through tuning reactivity of top-down auditory feedback loops, which would need to be examined in future studies.

Baseline MR and GR activity keeps NO-GC expression levels low in neurons

It was previously suggested that the complementary functions of MR and GR on presynaptic excitability in hippocampal brain neurons may be the result of distinct transcriptional networks activated by the glucocorticoid receptors (Reul and de Kloet, 1985; de Kloet et al., 2000; Obradovic et al., 2004; Mifsud and Reul, 2016; McCann et al., 2021).

Considering a possible MR/GR driven transcriptional control of pre- or post-synaptic activity by NO-GC, we searched for respective GREs that bind to MR and GR (Shimba and Ikuta, 2020) in the upstream regions of NO-GC subtypes (Shimba and Ikuta, 2020). GREs constitute a palindromic consensus sequence AGAACAnnnTGTTCT (Polman et al., 2013); however, several other GRE-like sequence motifs have been identified (Meijsing et al., 2009; van Weert et al., 2017). We found a GRE in the start codon region of *Gucy1a1* but not in the β1 subunit. In addition to a GRE sequence in *Gucy1a1,* the detection of a 25 bp Atoh sequence moreover suggests that this GRE binding motif is potentially used as a MR-specific recognition site, since GRE sequences that coincide with an Atoh consensus sequence within 400 bp of the GRE have been defined to be MR-specific (van Weert et al., 2017). Additionally, a GRE motif was found in *Gucy1a2* in an intron between exons 3 and 4, apparently completely outside of known regulatory regions, questioning the significance of this potential GRE motif. Regarding the observation of elevated *Gucy1b1* NO-GC expression levels both in single MR^{TMX}cKOs and GR^{TMX}cKOs as well as in double MRGR^{TMX}cKOs, we must question how a potential GRE in the start codon region of *Gucy1a1*, but not β1 subunit may be interpreted in the context of the findings in the present study. While it is necessary to confirm expression changes of *Gucy1a1* in MRGR^{TMX}cKOs in future studies, it is important to consider that changes in β1 subunits went along with changes in α1 expression (Mergia et al., 2006; Koesling et al., 2016). Further, expression levels of NO-GC1 and NO-GC2 in the brain mirror each other (Koesling et al., 2016). Thus, we hypothesize that

under physiological conditions, NO-GC1 (α1, β1) or NO-GC2 (α2, β1) is suppressed by MR and GR (Figure 5B). The elevation of NO-GC expression in MRGR^{TMX}cKOs in comparison to MR^{TMX}cKOs, which exhibit elevated GR expression levels. This may suggest that the inhibitory effect of MR on NO-GC may outweigh that of GR. Using NO-GC1 and NO-GC2 KO mice, the differential localization of NO-GC1 in hippocampal presynapses and NO-GC2 in postsynapses was shown to contribute to LTP through facilitation of presynaptic (NO-GC1) and postsynaptic (NO-GC2) excitability of hippocampal neurons (see for a review Koesling et al., 2016). Although more detailed studies are needed to validate the functionality of the GRE binding motifs, the data nevertheless suggest one possible pathway of how MR and GR could influence NO-GC1 (Figure 5B). This is in line with the observation that steroid hormone receptors exert positive or negative effects on the expression of target genes (Beato and Klug, 2000). Thereby, our findings suggest that baseline MR and GR activity could control the NO-GC abundance, which may be relevant for sensing NO released from eNOS- and nNOS-producing hippocampal cells to influence plasticity events (Son et al., 1996; Hopper and Garthwaite, 2006).

In conclusion, baseline MR and GR activity may keep NO-GC expression levels in neurons low. The target of a specific GRE element found in upstream regions of *Gucy1a1* NO-GC1, the dominant NO-GC isoform in hippocampal presynapses, may need further specification.

Baseline MR may keep Arc/Arg3.1 levels low in neurons

TMX-induced deletion of MR in frontal brain regions resulted in increased Arc/Arg3.1 expression levels in the hippocampus (Figure 4A). As Arc/Arg3.1 expression levels in the hippocampus are elevated in MRGR^{TMX}cKOs but not GR^{TMX}cKOs (Figure 4C), we hypothesize that basal activity of MR but not GR keeps Arc/Arg3.1 expression levels in hippocampal neurons low (Figure 5C). While we hypothesize that basal levels of GR have no effect on Arc/Arg3.1 expression levels, higher levels of GR (as seen in MR^{TMX}cKOs) enhance it (Figure 6B).

Arc/Arg3.1 expression changes have been shown to influence the strength of individual synapses, during both LTP (Rodriguez et al., 2005) and LTD (Guzowski et al., 1999; Plath et al., 2006; Tzingounis and Nicoll, 2006; Park et al., 2008; Waung et al., 2008; Bramham et al., 2010; Yilmaz-Rastoder et al., 2011; Wall and Correa, 2018; Zhang and Bramham, 2021). Moreover it is important to consider that neuronal stimuli induce the rapid transcription of the Arc/Arg3.1 gene (within 5 min; Ramirez-Amaya et al., 2005) and translocation of its mRNA from the nucleus to the cytoplasm (within 30 min; Guzowski et al., 1999). From the cytoplasm, Arc/Arg3.1 mRNA incorporates into a large ribonucleoprotein complex that is actively transported along the dendrite (Dynes and Steward, 2007). From the pre-existing Arc/Arg3.1 mRNA pool in dendrites, a selected pool is translated rapidly by acute neuronal activity, changing surface expression of AMPA receptors (Hedde et al., 2021). The present study may indicate that baseline MR levels influence the level of Arc/Arg3.1 mRNA in the cytoplasm of pyramidal neurons. In addition, when the control of GR expression by MR is lost (as in MR^{TMX}cKOs), Arc/Arg3.1 expression levels are enhanced more than in MRGR^{TMX}cKOs. This indicates that elevated GR levels may stimulate the level of Arc/Arg3.1 mRNA in the cytoplasm of pyramidal neurons. This makes sense considering that previous studies demonstrated that a selective activation of glucocorticoid receptors promotes lateral diffusion and enhanced surface expression of AMPA receptors in CA1 neurons (Karst and Joels, 2005; Groc et al., 2008; Martin et al., 2009), a feature linked with LTP (Groc et al., 2008). It is therefore feasible that MR—both at basal levels and through control of GR—sets the reactivity for Arc/Arg3.1 mobilization in dendrites and its rapid translation in spines through defining the cytoplasmatic Arc/Arg3.1 mRNA pool.

Elevated GR activity relates to elevated LTP, elevated GC-A, and elevated auditory neural gain

A strong association has been suggested between critical auditory nerve activity and central auditory neural gain, measured *via* enhanced ABR wave IV/I ratio, and plasticity changes in LTP, assessed both through *in vitro* electrophysiology (Marchetta et al., 2020b; Savitska et al., 2022) and through a hippocampus-dependent learning test in animal models (Matt et al., 2018). It has been speculated that a critical input of auditory activity is necessary for the recruitment of a reinforcement process that interacts between the auditory thalamus, prefrontal cortex (PFC), and the hippocampus. Thus, the dorsal aspect of the MGB, which receives input from the primary auditory cortex and projects to higher-order auditory regions (Antunes and Malmierca, 2021; Mease and Gonzalez, 2021), is likely part of the topographically complex connectivity pattern projecting between the medio-dorsal thalamus, the medial PFC, and the hippocampal formation (Bueno-Junior and Leite, 2018). These corticofugal projections from the PFC influence auditory processing at lower levels of the cortical sensory hierarchy and often include activation of mesolimbic areas, such as the basolateral amygdala, the activation of which is involved in top-down feedback reinforcement processes (Asilador and Llano, 2020; Suga, 2020).

The medio-dorsal thalamus/PFC/hippocampal connectivity (see Figure 6) is not only sensitive to stress responses (for review, see Jett et al., 2017), but is also part of the extra-hypothalamic pathways involved in stress-control, emotional states, attention, and vigilance influenced by glucocorticoids (de Kloet et al., 2000, 2019; Wingenfeld and Otte, 2019; Antunes and Malmierca, 2021; Knipper et al., 2022). Interestingly, the TMX-induced deletion of MR in frontal brain regions resulted in enhanced ABR wave IV/I ratio (neural gain) and LTP. If this response were due to increased GR expression resulting from the loss of MR, an acute deletion of GR should result in opposite changes of ABR wave IV/I ratio and LTP. In line, when GR is deleted (as in GR^{TMX}cKOs and MRGR^{TMX}cKOs), animals do not have higher wave IV/I ratio and their LTP is unchanged or lower, respectively, indicating that GR elevation – but not baseline GR levels – contributes to elevated neural gain and LTP. Interestingly, the higher wave IV/I ratio and LTP in MR^{TMX}cKO occurred with an elevation of GC-A expression levels. Also, lower LTP occurred with lower GC-A, as can be seen from MRGR^{TMX}cKOs (Figure 5D). Comparable changes in GC-A were detected not only in the hippocampus but also in the auditory cortex (Supplementary Figure S4) and amygdala. Differences in GC-A activity may thus provide a means for altering corticofugal top-down feedback facilitation processes (Asilador and Llano, 2020; Suga, 2020) and thereby contribute to auditory neural gain.

Oitzl and de Kloet were the first to demonstrate that MRs and GRs mediate the storage of spatial information in a coordinated manner (Oitzl and de Kloet, 1992). Their study suggested that MR promotes the extinction of information, while GR is essential for consolidation. Supporting this, memory storage was impaired when progesterone and

the glucocorticoid antagonist mifepristone was given immediately after the learning trial (Oitzl and de Kloet, 1992), while the MR antagonist spironolactone under the same condition did not affect consolidation but rather retrieval (Oitzl and de Kloet, 1992). Meanwhile, memory storage was shown to be impaired in numerous studies, e.g., when GRs are deleted in the amygdala or hippocampus or when GR antagonists are administered in the hippocampus immediately after learning, prior to consolidation (see for a review de Kloet et al., 1999; Rodrigues et al., 2009; Luksys and Sandi, 2011; Roozendaal and McGaugh, 2011; Schwabe et al., 2012; de Kloet et al., 2018).

Very recently, the treatment of WT mice with a phosphodiesterase 9A inhibitor restored a stress-induced drop of temporal auditory processing and hippocampal LTP (Savitska et al., 2022). This finding can now possibly be linked to elevated auditory neural gain, LTP, and GC-A expression levels. Increased GC-A expression levels here corresponded with elevated GR expression levels when the inhibition of GR was removed in MR^{TMX}cKOs, while expression levels were not elevated in GR^{TMX}cKOs (Figure 4). Indeed, the memory-enhancing phosphodiesterase 9A inhibitor (Kroker et al., 2012) has been suggested to regulate a pool of cGMP that is independent of nNOS (Harms et al., 2019). Other findings suggest that the phosphodiesterase 9A in the brain even preferentially regulates nuclear- and membrane-proximal pools of cGMP, which include the GC-A generated cGMP pools (Patel et al., 2018). Within this framework, the present study links for the first time the recognized function of the GR stress receptors in LTP (de Kloet et al., 2018; Joels, 2018) with the perfusion and blood supply driven metabolism-promoting function of the transmembrane GC-A. GC-A is activated through the atrial natriuretic peptide and brain natriuretic peptide (Potter, 2011) and has meanwhile emerged as a key regulator of energy consumption and metabolism counteracting vasoconstriction by inducing vasodilation (Kuhn, 2016). This role of GC-A has also been linked with neurogenesis (Muller et al., 2009) and angiogenesis (Kuhn et al., 2009), two processes which are essential for proper memory-dependent processes (Anacker and Hen, 2017). A critical role of GC-A for central auditory processing has been suggested through the use of global GC-A KO mice, which are unable to maintain proper central auditory processing following auditory trauma (Marchetta et al., 2020a).

Conclusion

Our data suggest that under physiological conditions, MR suppresses GR expression to keep the threshold for memory consolidation high (Figure 6A). The threshold of LTP is implemented *via* MR-induced control of postsynaptic Arc/Arg3.1 levels for optimized AMPA-receptor trafficking (Figure 6B), *via* MR- and GR-induced control of NO-GC (Figure 5B) and neuronal GC-A levels (Figure 6B) for optimized energy supply during hemodynamic responses.

Hemodynamic responses take place within a glutamatergic neural feedforward signaling, that includes a neuronal-derived nitric oxide (NO) release from the glutamatergic synapses as well as endothelial-derived NO from blood vessels (Sohal et al., 2009; Czeh et al., 2015; Lee et al., 2015; Chen et al., 2017; Csabai et al., 2018; Czeh et al., 2018; Han et al., 2019). This is followed by a metabolic feedback signal in the smooth muscle cells of parenchymal arterioles, which results in vasodilation (for a review see Attwell et al., 2010; Kisler et al., 2017; Ledo et al., 2021). cGMP signaling plays an integral role for the LTP results of the present study (Sanderson and Sher, 2013; Bradley and Steinert, 2016; Dorner-Ciossek et al., 2017; Borovac et al., 2018). We conclude that GR inhibition by MR may define the threshold for hemodynamic responses through the control of GC-A levels (Figure 6B). Through lowering GR expression levels *via* MR, the threshold for metabolically-demanding neuronal responses and vasodilation (possibly requiring GC-A) would be kept high. In future studies, it would be of particular interest to investigate how the suppression of NO-GC by MR and GR and the elevation of GC-A by increased GR levels contribute to LTP and related auditory neural gain (Figure 6).

Limitations of the study

The search for GRE- and MR-specific binding motifs requires experimental validation of the functionality of the binding sites. Moreover, the observation that the *in silico* prediction tools did not identify GRE motifs in the promoter regions of GC-A or Arc/Arg3.1 does not rule out their existence. Adequate validation of the function of GC-A for LTP-dependent auditory processing and its explicit relation to balanced stress levels is also pending and requires inducible deletion of GC-A under conditions comparable to those shown here for MR/GR deletion.

Data availability statement

The datasets generated and/or analyzed during the current study are available from the corresponding author upon reasonable request.

Ethics statement

The animal study was reviewed and approved by University of Tübingen, Veterinary Care Unit and the Animal Care and Ethics Committee of the regional board of the Federal State Government of Baden-Württemberg, Germany. Written informed consent was obtained from the owners for the participation of their animals in this study.

Author contributions

MK and LR conceived the study. DC, MH, PM, JM, and WS performed the experiments and analyzed the data. EN and JP performed data sequencing analysis. MK, LR, RL, PR, JP, and PS wrote the manuscript. MK, WS, and LR supervised the work. MK, LR, RL, PR, PS, EN, and JP reviewed and edited the manuscript. All authors contributed to the article and approved the submitted version.

Funding

This work was funded by the Deutsche Forschungsgemeinschaft (DFG, German Research Foundation) – DC, PM, MK, RL, and PR are members of the Research Training Group [grant number 335549539/GRK 2381]; FOR 2060 project RU 713/3-2, SPP 1608 RU 316/12-1, KN 316/12-1. JM was supported by the Interdisziplinäres Promotionskolleg Medizin of the University of Tübingen. EN and JP are supported by a restricted research grant from BAYER. Each source of funding provided a budget for personnel and material costs. We acknowledge support by Open Access Publishing Fund of University of Tübingen. BAYER was not

involved in the study design, collection, analysis, interpretation of data, the writing of this article, or the decision to submit it for publication.

Acknowledgments

We acknowledge support by Open Access Publishing Fund of University of Tübingen.

Conflict of interest

PS was employed by the company BAYER.

The remaining authors declare that the research was conducted in the absence of any commercial or financial relationships that could be construed as a potential conflict of interest.

Publisher's note

Supplementary material

The Supplementary material for this article can be found online at: https://www.frontiersin.org/articles/10.3389/fnmol.2023.1017761/full#supplementary-material

References

Anacker, C., and Hen, R. (2017). Adult hippocampal neurogenesis and cognitive flexibility—linking memory and mood. *Nat. Rev. Neurosci.* 18, 335–346. doi: 10.1038/nrn.2017.45

Antunes, F. M., and Malmierca, M. S. (2021). Corticothalamic pathways in auditory processing: recent advances and insights from other sensory systems. *Front. Neural Circuits* 15:721186. doi: 10.3389/fncir.2021.721186

Asilador, A., and Llano, D. A. (2020). Top-down inference in the auditory system: potential roles for Corticofugal projections. *Front. Neural Circuits* 14:615259. doi: 10.3389/fncir.2020.615259

Attwell, D., Buchan, A. M., Charpak, S., Lauritzen, M., Macvicar, B. A., and Newman, E. A. (2010). Glial and neuronal control of brain blood flow. *Nature* 468, 232–243. doi: 10.1038/nature09613

Basner, M., Babisch, W., Davis, A., Brink, M., Clark, C., Janssen, S., et al. (2014). Auditory and non-auditory effects of noise on health. *Lancet* 383, 1325–1332. doi: 10.1016/S0140-6736(13)61613-X

Beato, M., and Klug, J. (2000). Steroid hormone receptors: an update. *Hum. Reprod. Update* 6, 225–236. doi: 10.1093/humupd/6.3.225

Berger, S., Bleich, M., Schmid, W., Cole, T. J., Peters, J., Watanabe, H., et al. (1998). Mineralocorticoid receptor knockout mice: pathophysiology of Na+ metabolism. *Proc. Natl. Acad. Sci. U. S. A.* 95, 9424–9429. doi: 10.1073/pnas.95.16.9424

Berger, S., Wolfer, D. P., Selbach, O., Alter, H., Erdmann, G., Reichardt, H. M., et al. (2006). Loss of the limbic mineralocorticoid receptor impairs behavioral plasticity. *Proc. Natl. Acad. Sci. U. S. A.* 103, 195–200. doi: 10.1073/pnas.0503878102

Bharadwaj, H. M., Verhulst, S., Shaheen, L., Liberman, M. C., and Shinn-Cunningham, B. G. (2014). Cochlear neuropathy and the coding of supra-threshold sound. *Front. Syst. Neurosci.* 8:26. doi: 10.3389/fnsys.2014.00026

Borovac, J., Bosch, M., and Okamoto, K. (2018). Regulation of actin dynamics during structural plasticity of dendritic spines: signaling messengers and actin-binding proteins. *Mol. Cell. Neurosci.* 91, 122–130. doi: 10.1016/j.mcn.2018.07.001

Bradley, S. A., and Steinert, J. R. (2016). Nitric oxide-mediated posttranslational modifications: impacts at the synapse. *Oxid. Med. Cell. Longev.* 2016, 5681036–5681039. doi: 10.1155/2016/5681036

Bramham, C. R., Alme, M. N., Bittins, M., Kuipers, S. D., Nair, R. R., Pai, B., et al. (2010). The arc of synaptic memory. *Exp. Brain Res.* 200, 125–140. doi: 10.1007/s00221-009-1959-2

Bueno-Junior, L. S., and Leite, J. P. (2018). Input convergence, synaptic plasticity and functional coupling across hippocampal-prefrontal-thalamic circuits. *Front. Neural Circuits* 12:40. doi: 10.3389/fncir.2018.00040

Canlon, B., Theorell, T., and Hasson, D. (2013). Associations between stress and hearing problems in humans. *Hear. Res.* 295, 9–15. doi: 10.1016/j.heares.2012.08.015

Chao, H. M., Choo, P. H., and McEwen, B. S. (1989). Glucocorticoid and mineralocorticoid receptor mRNA expression in rat brain. *Neuroendocrinology* 50, 365–371. doi: 10.1159/000125250

Chen, G., Zhang, Y., Li, X., Zhao, X., Ye, Q., Lin, Y., et al. (2017). Distinct inhibitory circuits orchestrate cortical beta and gamma band oscillations. *Neuron* 96, 1403–1418.e6. doi: 10.1016/j.neuron.2017.11.033

Chenaux, G., Matt, L., Hill, T. C., Kaur, I., Liu, X.-B., Kirk, L. M., et al. (2016). Loss of SynDIG1 reduces excitatory synapse maturation but not formation *in vivo*. SynDIG1 regulates excitatory synapse maturation. *eNeuro* 3, ENEURO.0130–ENEU16.2016. doi: 10.1523/ENEURO.0130-16.2016

Chumak, T., Ruttiger, L., Lee, S. C., Campanelli, D., Zuccotti, A., Singer, W., et al. (2016). BDNF in lower brain parts modifies auditory fiber activity to gain Fidelity but increases the risk for generation of central noise after injury. *Mol. Neurobiol.* 53, 5607–5627. doi: 10.1007/s12035-015-9474-x

Cole, T. J., Blendy, J. A., Monaghan, A. P., Krieglstein, K., Schmid, W., Aguzzi, A., et al. (1995). Targeted disruption of the glucocorticoid receptor gene blocks adrenergic chromaffin cell development and severely retards lung maturation. *Genes Dev.* 9, 1608–1621. doi: 10.1101/gad.9.13.1608

Csabai, D., Wiborg, O., and Czeh, B. (2018). Reduced synapse and axon numbers in the prefrontal cortex of rats subjected to a chronic stress model for depression. *Front. Cell. Neurosci.* 12:24. doi: 10.3389/fncel.2018.00024

Czeh, B., Vardya, I., Varga, Z., Febbraro, F., Csabai, D., Martis, L. S., et al. (2018). Long-term stress disrupts the structural and functional integrity of GABAergic neuronal networks in the medial prefrontal cortex of rats. *Front. Cell. Neurosci.* 12:148. doi: 10.3389/fncel.2018.00148

Czeh, B., Varga, Z. K., Henningsen, K., Kovacs, G. L., Miseta, A., and Wiborg, O. (2015). Chronic stress reduces the number of GABAergic interneurons in the adult rat hippocampus, dorsal-ventral and region-specific differences. *Hippocampus* 25, 393–405. doi: 10.1002/hipo.22382

de Kloet, E. R., de Kloet, S. F., de Kloet, C. S., and de Kloet, A. D. (2019). Top-down and bottom-up control of stress-coping. *J. Neuroendocrinol.* 31:e12675. doi: 10.1111/jne.12675

de Kloet, E. R., Joels, M., and Holsboer, F. (2005). Stress and the brain: from adaptation to disease. *Nat. Rev. Neurosci.* 6, 463–475. doi: 10.1038/nrn1683

de Kloet, E. R., Meijer, O. C., de Nicola, A. F., de Rijk, R. H., and Joels, M. (2018). Importance of the brain corticosteroid receptor balance in metaplasticity, cognitive performance and neuro-inflammation. *Front. Neuroendocrinol.* 49, 124–145. doi: 10.1016/j.yfrne.2018.02.003

de Kloet, E. R., Oitzl, M. S., and Joels, M. (1999). Stress and cognition: are corticosteroids good or bad guys? *Trends Neurosci.* 22, 422–426. doi: 10.1016/s0166-2236(99)01438-1

de Kloet, E. R., Van Acker, S. A., Sibug, R. M., Oitzl, M. S., Meijer, O. C., Rahmouni, K., et al. (2000). Brain mineralocorticoid receptors and centrally regulated functions. *Kidney Int.* 57, 1329–1336. doi: 10.1046/j.1523-1755.2000.00971.x

Dorner-Ciossek, C., Kroker, K. S., and Rosenbrock, H. (2017). Role of PDE9 in cognition. *Adv. Neurobiol.* 17, 231–254. doi: 10.1007/978-3-319-58811-7_9

Dragatsis, I., and Zeitlin, S. (2000). CaMKIIalpha-Cre transgene expression and recombination patterns in the mouse brain. *Genesis* 26, 133–135. doi: 10.1002/(sici)1526-968x(200002)26:2<133::aid-gene10>3.0.co;2-v

Dynes, J. L., and Steward, O. (2007). Dynamics of bidirectional transport of arc mRNA in neuronal dendrites. *J. Comp. Neurol.* 500, 433–447. doi: 10.1002/cne.21189

Eckert, P., Marchetta, P., Manthey, M. K., Walter, M. H., Jovanovic, S., Savitska, D., et al. (2021). Deletion of BDNF in Pax2 lineage-derived interneuron precursors in the hindbrain hampers the proportion of excitation/inhibition, learning, and behavior. *Front. Mol. Neurosci.* 14:642679. doi: 10.3389/fnmol.2021.642679

Erdmann, G., Schutz, G., and Berger, S. (2007). Inducible gene inactivation in neurons of the adult mouse forebrain. *BMC Neurosci.* 8:63. doi: 10.1186/1471-2202-8-63

Erdmann, G., Schutz, G., and Berger, S. (2008). Loss of glucocorticoid receptor function in the pituitary results in early postnatal lethality. *Endocrinology* 149, 3446–3451. doi: 10.1210/en.2007-1786

Giesen, J., Mergia, E., Koesling, D., and Russwurm, M. (2022). Hippocampal AMPA- and NMDA-induced cGMP signals are mainly generated by NO-GC2 and are under tight control by PDEs 1 and 2. *Eur. J. Neurosci.* 55, 18–31. doi: 10.1111/ejn.15564

Goel, A., Cantu, D. A., Guilfoyle, J., Chaudhari, G. R., Newadkar, A., Todisco, B., et al. (2019). Author correction: impaired perceptual learning in a mouse model of fragile X

syndrome is mediated by parvalbumin neuron dysfunction and is reversible. *Nat. Neurosci.* 22:143. doi: 10.1038/s41593-018-0273-3

Groc, L., Choquet, D., and Chaouloff, F. (2008). The stress hormone corticosterone conditions AMPAR surface trafficking and synaptic potentiation. *Nat. Neurosci.* 11, 868–870. doi: 10.1038/nn.2150

Guzowski, J. F., McNaughton, B. L., Barnes, C. A., and Worley, P. F. (1999). Environment-specific expression of the immediate-early gene arc in hippocampal neuronal ensembles. *Nat. Neurosci.* 2, 1120–1124. doi: 10.1038/16046

Han, K., Min, J., Lee, M., Kang, B. M., Park, T., Hahn, J., et al. (2019). Neurovascular coupling under chronic stress is modified by altered GABAergic interneuron activity. *J. Neurosci.* 39, 10081–10095. doi: 10.1523/JNEUROSCI.1357-19.2019

Harms, J. F., Menniti, F. S., and Schmidt, C. J. (2019). Phosphodiesterase 9A in brain regulates cGMP signaling independent of nitric-oxide. *Front. Neurosci.* 13:837. doi: 10.3389/fnins.2019.00837

Harris, A. P., Holmes, M. C., de Kloet, E. R., Chapman, K. E., and Seckl, J. R. (2013). Mineralocorticoid and glucocorticoid receptor balance in control of HPA axis and behaviour. *Psychoneuroendocrinology* 38, 648–658. doi: 10.1016/j.psyneuen.2012.08.007

Hedde, P. N., Malacrida, L., Barylko, B., Binns, D. D., Albanesi, J. P., and Jameson, D. M. (2021). Membrane remodeling by arc/Arg3.1. *Front. Mol. Biosci.* 8:630625. doi: 10.3389/fmolb.2021.630625

Hopper, R. A., and Garthwaite, J. (2006). Tonic and phasic nitric oxide signals in hippocampal long-term potentiation. *J. Neurosci.* 26, 11513–11521. doi: 10.1523/JNEUROSCI.2259-06.2006

Jafari, Z., Kolb, B. E., and Mohajerani, M. H. (2018). Chronic traffic noise stress accelerates brain impairment and cognitive decline in mice. *Exp. Neurol.* 308, 1–12. doi: 10.1016/j.expneurol.2018.06.011

Jafari, Z., Kolb, B. E., and Mohajerani, M. H. (2019). Age-related hearing loss and tinnitus, dementia risk, and auditory amplification outcomes. *Ageing Res. Rev.* 56:100963. doi: 10.1016/j.arr.2019.100963

Jett, J. D., Bulin, S. E., Hatherall, L. C., McCartney, C. M., and Morilak, D. A. (2017). Deficits in cognitive flexibility induced by chronic unpredictable stress are associated with impaired glutamate neurotransmission in the rat medial prefrontal cortex. *Neuroscience* 346, 284–297. doi: 10.1016/j.neuroscience.2017.01.017

Joels, M. (2018). Corticosteroids and the brain. *J. Endocrinol.* 238, R121–R130. doi: 10.1530/JOE-18-0226

Karst, H., and Joels, M. (2005). Corticosterone slowly enhances miniature excitatory postsynaptic current amplitude in mice CA1 hippocampal cells. *J. Neurophysiol.* 94, 3479–3486. doi: 10.1152/jn.00143.2005

Kisler, K., Nelson, A. R., Montagne, A., and Zlokovic, B. V. (2017). Cerebral blood flow regulation and neurovascular dysfunction in Alzheimer disease. *Nat. Rev. Neurosci.* 18, 419–434. doi: 10.1038/nrn.2017.48

Knipper, M., Singer, W., Schwabe, K., Hagberg, G. E., Li Hegner, Y., Rüttiger, L., et al. (2022). Disturbed balance of inhibitory signaling links hearing loss and cognition. *Front. Neural Circuits* 15, 1–25. doi: 10.3389/fncir.2021.785603

Knipper, M., van Dijk, P., Schulze, H., Mazurek, B., Krauss, P., Scheper, V., et al. (2020). The neural bases of tinnitus: lessons from deafness and Cochlear implants. *J. Neurosci.* 40, 7190–7202. doi: 10.1523/JNEUROSCI.1314-19.2020

Koesling, D., Mergia, E., and Russwurm, M. (2016). Physiological functions of NO-sensitive Guanylyl Cyclase isoforms. *Curr. Med. Chem.* 23, 2653–2665. doi: 10.2174/0929867323666160812145050

Korb, E., and Finkbeiner, S. (2011). Arc in synaptic plasticity: from gene to behavior. *Trends Neurosci.* 34, 591–598. doi: 10.1016/j.tins.2011.08.007

Kroker, K. S., Rast, G., Giovannini, R., Marti, A., Dorner-Ciossek, C., and Rosenbrock, H. (2012). Inhibition of acetylcholinesterase and phosphodiesterase-9A has differential effects on hippocampal early and late LTP. *Neuropharmacology* 62, 1964–1974. doi: 10.1016/j.neuropharm.2011.12.021

Kuhn, M. (2016). Molecular physiology of membrane Guanylyl Cyclase receptors. *Physiol. Rev.* 96, 751–804. doi: 10.1152/physrev.00022.2015

Kuhn, M., Volker, K., Schwarz, K., Carbajo-Lozoya, J., Flogel, U., Jacoby, C., et al. (2009). The natriuretic peptide/guanylyl cyclase--a system functions as a stress-responsive regulator of angiogenesis in mice. *J. Clin. Invest.* 119, 2019–2030. doi: 10.1172/JCI37430

Kuipers, S. D., Trentani, A., Tiron, A., Mao, X., Kuhl, D., and Bramham, C. R. (2016). BDNF-induced LTP is associated with rapid arc/Arg3.1-dependent enhancement in adult hippocampal neurogenesis. *Sci. Rep.* 6:21222. doi: 10.1038/srep21222

Lai, M., Horsburgh, K., Bae, S. E., Carter, R. N., Stenvers, D. J., Fowler, J. H., et al. (2007). Forebrain mineralocorticoid receptor overexpression enhances memory, reduces anxiety and attenuates neuronal loss in cerebral ischaemia. *Eur. J. Neurosci.* 25, 1832–1842. doi: 10.1111/j.1460-9568.2007.05427.x

Ledo, A., Lourenco, C. F., Cadenas, E., Barbosa, R. M., and Laranjinha, J. (2021). The bioactivity of neuronal-derived nitric oxide in aging and neurodegeneration: switching signaling to degeneration. *Free Radic. Biol. Med.* 162, 500–513. doi: 10.1016/j.freeradbiomed.2020.11.005

Lee, S., Kang, B. M., Shin, M. K., Min, J., Heo, C., Lee, Y., et al. (2015). Chronic stress decreases cerebrovascular responses during rat Hindlimb electrical stimulation. *Front. Neurosci.* 9:462. doi: 10.3389/fnins.2015.00462

Likhtik, E., and Johansen, J. P. (2019). Neuromodulation in circuits of aversive emotional learning. *Nat. Neurosci.* 22, 1586–1597. doi: 10.1038/s41593-019-0503-3

Luksys, G., and Sandi, C. (2011). Neural mechanisms and computations underlying stress effects on learning and memory. *Curr. Opin. Neurobiol.* 21, 502–508. doi: 10.1016/j.conb.2011.03.003

Manohar, S., Chen, G. D., Ding, D., Liu, L., Wang, J., Chen, Y. C., et al. (2022). Unexpected consequences of noise-induced hearing loss: impaired hippocampal neurogenesis, memory, and stress. *Front. Integr. Neurosci.* 16:871223. doi: 10.3389/fnint.2022.871223

Marchetta, P., Eckert, P., Lukowski, R., Ruth, P., Singer, W., Ruttiger, L., et al. (2022). Loss of central mineralocorticoid or glucocorticoid receptors impacts auditory nerve processing in the cochlea. *iScience* 25:103981. doi: 10.1016/j.isci.2022.103981

Marchetta, P., Mohrle, D., Eckert, P., Reimann, K., Wolter, S., Tolone, A., et al. (2020a). Guanylyl Cyclase a/cGMP signaling slows hidden, age- and acoustic trauma-induced hearing loss. *Front. Aging Neurosci.* 12:83. doi: 10.3389/fnagi.2020.00083

Marchetta, P., Savitska, D., Kubler, A., Asola, G., Manthey, M., Mohrle, D., et al. (2020b). Age-dependent auditory processing deficits after Cochlear Synaptopathy depend on auditory nerve latency and the ability of the brain to recruit LTP/BDNF. *Brain Sci.* 10. doi: 10.3390/brainsci10100710

Martin, S., Henley, J. M., Holman, D., Zhou, M., Wiegert, O., van Spronsen, M., et al. (2009). Corticosterone alters AMPAR mobility and facilitates bidirectional synaptic plasticity. *PLoS One* 4:e4714. doi: 10.1371/journal.pone.0004714

Matt, L., Eckert, P., Panford-Walsh, R., Geisler, H. S., Bausch, A. E., Manthey, M., et al. (2018). Visualizing BDNF transcript usage during sound-induced memory linked plasticity. *Front. Mol. Neurosci.* 11:260. doi: 10.3389/fnmol.2018.00260

Matt, L., Michalakis, S., Hofmann, F., Hammelmann, V., Ludwig, A., Biel, M., et al. (2011). HCN2 channels in local inhibitory interneurons constrain LTP in the hippocampal direct perforant path. *Cell. Mol. Life Sci.* 68, 125–137. doi: 10.1007/s00018-010-0446-z

Mazurek, B., Boecking, B., and Brueggemann, P. (2019). Association between stress and tinnitus-new aspects. *Otol. Neurotol.* 40, e467–e473. doi: 10.1097/MAO.0000000000002180

McCann, K. E., Lustberg, D. J., Shaughnessy, E. K., Carstens, K. E., Farris, S., Alexander, G. M., et al. (2021). Novel role for mineralocorticoid receptors in control of a neuronal phenotype. *Mol. Psychiatry* 26, 350–364. doi: 10.1038/s41380-019-0598-7

McEwen, B. S., Nasca, C., and Gray, J. D. (2016). Stress effects on neuronal structure: hippocampus, amygdala, and prefrontal cortex. *Neuropsychopharmacology* 41, 3–23. doi: 10.1038/npp.2015.171

Mease, R. A., and Gonzalez, A. J. (2021). Corticothalamic pathways from layer 5: emerging roles in computation and pathology. *Front. Neural Circuits* 15:730211. doi: 10.3389/fncir.2021.730211

Meijsing, S. H., Pufall, M. A., So, A. Y., Bates, D. L., Chen, L., and Yamamoto, K. R. (2009). DNA binding site sequence directs glucocorticoid receptor structure and activity. *Science* 324, 407–410. doi: 10.1126/science.1164265

Meltser, I., and Canlon, B. (2011). Protecting the auditory system with glucocorticoids. *Hear. Res.* 281, 47–55. doi: 10.1016/j.heares.2011.06.003

Mergia, E., Friebe, A., Dangel, O., Russwurm, M., and Koesling, D. (2006). Spare guanylyl cyclase NO receptors ensure high NO sensitivity in the vascular system. *J. Clin. Invest.* 116, 1731–1737. doi: 10.1172/JCI27657

Mifsud, K. R., and Reul, J. M. (2016). Acute stress enhances heterodimerization and binding of corticosteroid receptors at glucocorticoid target genes in the hippocampus. *Proc. Natl. Acad. Sci. U. S. A.* 113, 11336–11341. doi: 10.1073/pnas.1605246113

Muller, D., Hida, B., Guidone, G., Speth, R. C., Michurina, T. V., Enikolopov, G., et al. (2009). Expression of guanylyl cyclase (GC)-a and GC-B during brain development: evidence for a role of GC-B in perinatal neurogenesis. *Endocrinology* 150, 5520–5529. doi: 10.1210/en.2009-0490

Nadhimi, Y., and Llano, D. A. (2021). Does hearing loss lead to dementia? A review of the literature. *Hear. Res.* 402:108038. doi: 10.1016/j.heares.2020.108038

Nelissen, E., Argyrousi, E. K., Van Goethem, N. P., Zhao, F., Hines, C. D. G., Swaminath, G., et al. (2021). Soluble Guanylate Cyclase stimulator Vericiguat enhances long-term memory in rats without altering cerebral blood volume. *Biomedicine* 9, 1–20. doi: 10.3390/biomedicines9081047

Nelissen, E., Possemis, N., Van Goethem, N. P., Schepers, M., Mulder-Jongen, D. A. J., Dietz, L., et al. (2022). The sGC stimulator BAY-747 and activator runcaciguat can enhance memory in vivo via differential hippocampal plasticity mechanisms. *Sci. Rep.* 12:3589. doi: 10.1038/s41598-022-07391-1

Obradovic, D., Tirard, M., Nemethy, Z., Hirsch, O., Gronemeyer, H., and Almeida, O. F. (2004). DAXX, FLASH, and FAF-1 modulate mineralocorticoid and glucocorticoid receptor-mediated transcription in hippocampal cells--toward a basis for the opposite actions elicited by two nuclear receptors? *Mol. Pharmacol.* 65, 761–769. doi: 10.1124/mol.65.3.761

Oitzl, M. S., and de Kloet, E. R. (1992). Selective corticosteroid antagonists modulate specific aspects of spatial orientation learning. *Behav. Neurosci.* 106, 62–71. doi: 10.1037//0735-7044.106.1.62

Park, S., Park, J. M., Kim, S., Kim, J. A., Shepherd, J. D., Smith-Hicks, C. L., et al. (2008). Elongation factor 2 and fragile X mental retardation protein control the dynamic translation of arc/Arg3.1 essential for mGluR-LTD. *Neuron* 59, 70–83. doi: 10.1016/j.neuron.2008.05.023

Patel, N. S., Klett, J., Pilarzyk, K., Lee, D. I., Kass, D., Menniti, F. S., et al. (2018). Identification of new PDE9A isoforms and how their expression and subcellular compartmentalization in the brain change across the life span. *Neurobiol. Aging* 65, 217–234. doi: 10.1016/j.neurobiolaging.2018.01.019

Plath, N., Ohana, O., Dammermann, B., Errington, M. L., Schmitz, D., Gross, C., et al. (2006). Arc/Arg3.1 is essential for the consolidation of synaptic plasticity and memories. *Neuron* 52, 437–444. doi: 10.1016/j.neuron.2006.08.024

Polman, J. A., de Kloet, E. R., and Datson, N. A. (2013). Two populations of glucocorticoid receptor-binding sites in the male rat hippocampal genome. *Endocrinology* 154, 1832–1844. doi: 10.1210/en.2012-2187

Potter, L. R. (2011). Regulation and therapeutic targeting of peptide-activated receptor guanylyl cyclases. *Pharmacol. Ther.* 130, 71–82. doi: 10.1016/j.pharmthera.2010.12.005

Ramirez-Amaya, V., Vazdarjanova, A., Mikhael, D., Rosi, S., Worley, P. F., and Barnes, C. A. (2005). Spatial exploration-induced arc mRNA and protein expression: evidence for selective, network-specific reactivation. *J. Neurosci.* 25, 1761–1768. doi: 10.1523/JNEUROSCI.4342-04.2005

Reul, J. M., and de Kloet, E. R. (1985). Two receptor systems for corticosterone in rat brain: microdistribution and differential occupation. *Endocrinology* 117, 2505–2511. doi: 10.1210/endo-117-6-2505

Rodrigues, S. M., LeDoux, J. E., and Sapolsky, R. M. (2009). The influence of stress hormones on fear circuitry. *Annu. Rev. Neurosci.* 32, 289–313. doi: 10.1146/annurev.neuro.051508.135620

Rodriguez, J. J., Davies, H. A., Silva, A. T., De Souza, I. E., Peddie, C. J., Colyer, F. M., et al. (2005). Long-term potentiation in the rat dentate gyrus is associated with enhanced arc/Arg3.1 protein expression in spines, dendrites and glia. *Eur. J. Neurosci.* 21, 2384–2396. doi: 10.1111/j.1460-9568.2005.04068.x

Roozendaal, B., and McGaugh, J. L. (2011). Memory modulation. *Behav. Neurosci.* 125, 797–824. doi: 10.1037/a0026187

Sanderson, T. M., and Sher, E. (2013). The role of phosphodiesterases in hippocampal synaptic plasticity. *Neuropharmacology* 74, 86–95. doi: 10.1016/j.neuropharm.2013.01.011

Sarabdjitsingh, R. A., Pasricha, N., Smeets, J. A., Kerkhofs, A., Mikasova, L., Karst, H., et al. (2016). Hippocampal fast Glutamatergic transmission is transiently regulated by Corticosterone Pulsatility. *PLoS One* 11:e0145858. doi: 10.1371/journal.pone.0145858

Satake, S., Inoue, T., and Imoto, K. (2012). Paired-pulse facilitation of multivesicular release and intersynaptic spillover of glutamate at rat cerebellar granule cell-interneurone synapses. *J. Physiol.* 590, 5653–5675. doi: 10.1113/jphysiol.2012.234070

Savitska, D., Hess, M., Calis, D., Marchetta, P., Harasztosi, C., Fink, S., et al. (2022). Stress affects central compensation of neural responses to Cochlear Synaptopathy in a cGMP-dependent way. *Front. Neurosci.* 16:864706. doi: 10.3389/fnins.2022.864706

Schwabe, L., Joels, M., Roozendaal, B., Wolf, O. T., and Oitzl, M. S. (2012). Stress effects on memory: an update and integration. *Neurosci. Biobehav. Rev.* 36, 1740–1749. doi: 10.1016/j.neubiorev.2011.07.002

Shimba, A., and Ikuta, K. (2020). Control of immunity by glucocorticoids in health and disease. *Semin. Immunopathol.* 42, 669–680. doi: 10.1007/s00281-020-00827-8

Singer, W., Geisler, H. S., and Knipper, M. (2013a). The Geisler method: tracing activity-dependent cGMP plasticity changes upon double detection of mRNA and protein on brain slices. *Methods Mol. Biol.* 1020, 223–233. doi: 10.1007/978-1-62703-459-3_15

Singer, W., Geisler, H. S., Panford-Walsh, R., and Knipper, M. (2016). Detection of excitatory and inhibitory synapses in the auditory system using fluorescence immunohistochemistry and high-resolution fluorescence microscopy. *Methods Mol. Biol.* 1427, 263–276. doi: 10.1007/978-1-4939-3615-1_15

Singer, W., Zuccotti, A., Jaumann, M., Lee, S. C., Panford-Walsh, R., Xiong, H., et al. (2013b). Noise-induced inner hair cell ribbon loss disturbs central arc mobilization: a novel molecular paradigm for understanding tinnitus. *Mol. Neurobiol.* 47, 261–279. doi: 10.1007/s12035-012-8372-8

Sohal, V. S., Zhang, F., Yizhar, O., and Deisseroth, K. (2009). Parvalbumin neurons and gamma rhythms enhance cortical circuit performance. *Nature* 459, 698–702. doi: 10.1038/nature07991

Son, H., Hawkins, R. D., Martin, K., Kiebler, M., Huang, P. L., Fishman, M. C., et al. (1996). Long-term potentiation is reduced in mice that are doubly mutant in endothelial and neuronal nitric oxide synthase. *Cells* 87, 1015–1023. doi: 10.1016/s0092-8674(00)81796-1

Suga, N. (2020). Plasticity of the adult auditory system based on corticocortical and corticofugal modulations. *Neurosci. Biobehav. Rev.* 113, 461–478. doi: 10.1016/j.neubiorev.2020.03.021

Thomson, A. M. (2000). Facilitation, augmentation and potentiation at central synapses. *Trends Neurosci.* 23, 305–312. doi: 10.1016/s0166-2236(00)01580-0

Tzingounis, A. V., and Nicoll, R. A. (2006). Arc/Arg3.1: linking gene expression to synaptic plasticity and memory. *Neuron* 52, 403–407. doi: 10.1016/j.neuron.2006.10.016

van Weert, L., Buurstede, J. C., Mahfouz, A., Braakhuis, P. S. M., Polman, J. A. E., Sips, H. C. M., et al. (2017). NeuroD factors discriminate mineralocorticoid from glucocorticoid receptor DNA binding in the male rat brain. *Endocrinology* 158, 1511–1522. doi: 10.1210/en.2016-1422

Wall, M. J., and Correa, S. A. L. (2018). The mechanistic link between arc/Arg3.1 expression and AMPA receptor endocytosis. *Semin. Cell Dev. Biol.* 77, 17–24. doi: 10.1016/j.semcdb.2017.09.005

Wang, J., and Puel, J. L. (2020). Presbycusis: an update on Cochlear mechanisms and therapies. *J. Clin. Med.* 9, 1–22. doi: 10.3390/jcm9010218

Wang, X., Zhang, C., Szabo, G., and Sun, Q. Q. (2013). Distribution of CaMKIIalpha expression in the brain in vivo, studied by CaMKIIalpha-GFP mice. *Brain Res.* 1518, 9–25. doi: 10.1016/j.brainres.2013.04.042

Waung, M. W., Pfeiffer, B. E., Nosyreva, E. D., Ronesi, J. A., and Huber, K. M. (2008). Rapid translation of arc/Arg3.1 selectively mediates mGluR-dependent LTD through persistent increases in AMPAR endocytosis rate. *Neuron* 59, 84–97. doi: 10.1016/j.neuron.2008.05.014

Wingenfeld, K., and Otte, C. (2019). Mineralocorticoid receptor function and cognition in health and disease. *Psychoneuroendocrinology* 105, 25–35. doi: 10.1016/j.psyneuen.2018.09.010

Yilmaz-Rastoder, E., Miyamae, T., Braun, A. E., and Thiels, E. (2011). LTP- and LTD-inducing stimulations cause opposite changes in arc/arg3.1 mRNA level in hippocampal area CA1 in vivo. *Hippocampus* 21, 1290–1301. doi: 10.1002/hipo.20838

Zhang, H., and Bramham, C. R. (2021). Arc/Arg3.1 function in long-term synaptic plasticity: emerging mechanisms and unresolved issues. *Eur. J. Neurosci.* 54, 6696–6712. doi: 10.1111/ejn.14958

Zhang, L., Wang, J., Sun, H., Feng, G., and Gao, Z. (2022). Interactions between the hippocampus and the auditory pathway. *Neurobiol. Learn. Mem.* 189:107589. doi: 10.1016/j.nlm.2022.107589

Zucker, R. S., and Regehr, W. G. (2002). Short-term synaptic plasticity. *Annu. Rev. Physiol.* 64, 355–405. doi: 10.1146/annurev.physiol.64.092501.114547

frontiers | Frontiers in Molecular Neuroscience

TYPE Review
PUBLISHED 08 September 2022
DOI 10.3389/fnmol.2022.988142

OPEN ACCESS

EDITED BY
Clint L. Makino,
Boston University, United States

REVIEWED BY
Ching-Kang Jason Chen,
Baylor College of Medicine,
United States
Tiansen Li,
National Institutes of Health (NIH),
United States

*CORRESPONDENCE
James B. Ames
jbames@ucdavis.edu

SPECIALTY SECTION
This article was submitted to Molecular Signaling and Pathways, a section of the journal Frontiers in Molecular Neuroscience

RECEIVED 07 July 2022
ACCEPTED 22 August 2022
PUBLISHED 08 September 2022

CITATION
Ames JB (2022) Structural basis of retinal membrane guanylate cyclase regulation by GCAP1 and RD3. *Front. Mol. Neurosci.* 15:988142. doi: 10.3389/fnmol.2022.988142

Structural basis of retinal membrane guanylate cyclase regulation by GCAP1 and RD3

James B. Ames*

Department of Chemistry, University of California, Davis, Davis, CA, United States

Retinal membrane guanylate cyclases (RetGC1 and RetGC2) are expressed in photoreceptor rod and cone cells, where they promote the onset of visual recovery during phototransduction. The catalytic activity of RetGCs is regulated by their binding to regulatory proteins, guanylate cyclase activating proteins (GCAP1-5) and the retinal degeneration 3 protein (RD3). RetGC1 is activated by its binding to Ca^{2+}-free/Mg^{2+}-bound GCAP1 at low cytosolic Ca^{2+} levels in light-activated photoreceptors. By contrast, RetGC1 is inactivated by its binding to Ca^{2+}-bound GCAP1 and/or RD3 at elevated Ca^{2+} levels in dark-adapted photoreceptors. The Ca^{2+} sensitive cyclase activation helps to replenish the cytosolic cGMP levels in photoreceptors during visual recovery. Mutations in RetGC1, GCAP1 or RD3 that disable the Ca^{2+}-dependent regulation of cyclase activity are genetically linked to rod/cone dystrophies and other inherited forms of blindness. Here I review the structural interaction of RetGC1 with GCAP1 and RD3. I propose a two-state concerted model in which the dimeric RetGC1 allosterically switches between active and inactive conformational states with distinct quaternary structures that are oppositely stabilized by the binding of GCAP1 and RD3. The binding of Ca^{2+}-free/Mg^{2+}-bound GCAP1 is proposed to activate the cyclase by stabilizing RetGC1 in an active conformation (R-state), whereas Ca^{2+}-bound GCAP1 and/or RD3 inhibit the cyclase by locking RetGC1 in an inactive conformation (T-state). Exposed hydrophobic residues in GCAP1 (residues H19, Y22, M26, F73, V77, W94) are essential for cyclase activation and could be targeted by rational drug design for the possible treatment of rod/cone dystrophies.

KEYWORDS

calcium, GCAP1, GCAP5, RD3 protein, guanylate cyclase (guanylyl cyclase), NMR

Introduction

Light activation of retinal rod and cone cells (called visual phototransduction) triggers a decrease in the cytosolic cGMP concentration that causes cyclic nucleotide gated (CNG) channels to close, which hyperpolarizes the plasma membrane to generate a neural signal (Stryer, 1991; Baylor, 1996; **Figure 1**). In dark-adapted photoreceptors, relatively high levels of cGMP keep CNG channels open, resulting in high cytosolic Ca^{2+} levels at or near 500 nM (Woodruff et al., 2002). By contrast, light-activation of the photoreceptor promotes the hydrolysis of cGMP and the light-induced lowering of cGMP causes CNG channels to close, resulting in a nearly 10-fold drop in the cytosolic Ca^{2+} level (Gray-Keller and Detwiler, 1994). The light-induced decrease in both cGMP and Ca^{2+} are important signals that promote the re-synthesis of cGMP by the enzyme retinal membrane guanylate cyclases (Dizhoor et al., 1994; Lowe et al., 1995). The re-synthesis of cGMP by the cyclase during visual recovery is highly regulated by the light-dependent cytosolic Ca^{2+} concentration (Koch and Stryer, 1988; Koutalos and Yau, 1996), and the Ca^{2+}-dependent regulation of the cyclase is mediated by guanylate cyclase activating proteins discussed below. Retinal membrane guanylate cyclase is also regulated by the retinal degeneration 3 (RD3) protein (Friedman et al., 2006). The binding of RD3 to the cyclase has been shown to inhibit the cyclase enzymatic activity (Peshenko et al., 2011). In addition, RD3 binding promotes trafficking of RetGC1 from the endoplasmic reticulum (ER) to the rod outer segment disk membrane (Azadi et al., 2010; Zulliger et al., 2015).

Retinal membrane guanylate cyclases (RetGC1 and RetGC2) (Dizhoor et al., 1994; Palczewski et al., 1994, 2004) are regulated by a family of guanylate cyclase activating proteins (GCAP1-5, see **Figure 2**). RetGC1 is known to interact with GCAP1 (Laura et al., 1996), whereas RetGC2 can interact with both GCAP1 and GCAP2 (Laura and Hurley, 1998). The functional differences between RetGC1 and RetGC2 are currently not well understood. RetGC1 knockout mice cause a loss of cone function but do not exhibit rod degeneration. By contrast, RetGC2 is important for rod function but the RetGC2 knockout has no effect on cones (Yang et al., 1999; Baehr et al., 2007; Boye et al., 2011, 2013). A related membrane guanylate cyclase (regulated by GCAP1) is also expressed in the olfactory bulb (Duda et al., 2001). RetGCs are regulated by up to 8 different vertebrate homologs of guanylate cyclase activating proteins (GCAP1-8) (Imanishi et al., 2004; Scholten and Koch, 2011). The binding of Ca^{2+}-free GCAP1 to RetGC1 activates the cyclase enzymatic activity at low Ca^{2+} levels in light activated photoreceptors (Peshenko and Dizhoor, 2006; Lim et al., 2009). By contrast, the binding of Ca^{2+}-bound GCAP1 to RetGC1 inhibits the cyclase activity at high Ca^{2+} levels in dark-adapted photoreceptors (Dizhoor and Hurley, 1996; Dizhoor et al., 1998). The Ca^{2+}-bound GCAP1 can also activate the odorant surface receptor ONE-GC (Duda et al., 2012), which raises the question about how Ca^{2+}-bound GCAP1 can oppositely regulate both RetGC1 and ONE-GC. The Ca^{2+}-dependent regulation of RetGCs by GCAPs in the retina coordinates the recovery phase of visual phototransduction (**Figure 1A**). Light-activation of the photoreceptor causes a reduction in both cGMP and Ca^{2+} levels (**Figure 1A**), which triggers a need for RetGC1 to become activated by Ca^{2+}-free GCAP1 when the cytosolic Ca^{2+} and cGMP levels are both low. This light-induced activation of RetGC1 is important for replenishing cGMP levels to recover the dark state during visual recovery (**Figure 1A**). The Ca^{2+}-dependent cyclase regulation is abolished in GCAP1 knockout mice (Burns et al., 2002; Howes et al., 2002; Mendez and Chen, 2002; Pennesi et al., 2003). Particular GCAP1 mutants that weaken Ca^{2+} binding to GCAP1 (Dell'orco et al., 2010) cause constitutive activation of RetGC1 that directly leads to retinal degenerative diseases known as rod-cone dystrophies (Semple-Rowland et al., 1996; Sokal et al., 1998; Baehr and Palczewski, 2007; Behnen et al., 2010; Bondarenko et al., 2010; Jiang and Baehr, 2010; Dell'orco et al., 2014).

RD3 is a 23-kDa retinal protein that is essential for proper photoreceptor function, and the deletion of RD3 causes retinal degeneration and blindness in human patients that possess recessive Leber Congenital Amaurosis 12 (LCA) (Friedman et al., 2006). The lack of RD3 expression in knockout mice leads to reduced levels of RetGC1 in the outer segment membrane of photoreceptors. This reduction of RetGC1 caused by a lack of RD3 is consistent with observations that RD3 promotes the trafficking of RetGC1 into the outer segment (Azadi et al., 2010; Zulliger et al., 2015; **Figure 1B**). The RetGC1 protein is first expressed inside the endoplasmic reticulum (ER), where it is processed and inserted into transport vesicles (**Figure 1B**). The RetGC1 containing transport vesicles in the inner segment then bind to RD3, which guides the trafficking of these vesicles into the outer segment. The binding of RD3 to RetGC1 facilitates the transfer of RetGC1 from transport vesicles into the outer segment disk membrane. RD3 binding to RetGC1 also inhibits the cyclase enzymatic activity, perhaps by obstructing the binding of GCAPs (Peshenko et al., 2011, 2016; **Figure 1A**). The RD3 binding site in RetGC1 involves multivalent contacts. Mutagenesis studies have suggested that RD3 contacts the RetGC1 dimerization domain (residues 800–851) that also interacts with GCAP1 (Peshenko et al., 2011, 2016). RD3 also interacts with a C-terminal region in RetGC1 that is downstream of the catalytic domain (Azadi et al., 2010). The RD3 binding to RetGC1 is important for keeping the cyclase enzymatic activity turned off during its vesicle trafficking to the disk membrane. The RetGC1 trafficking in the absence of RD3 causes elevated cGMP levels in the inner segment, which turns on apoptosis that leads to retinal degeneration (Dizhoor et al., 1998; Newbold et al., 2002). As a result, mutations in RD3 and/or RetGC1 that disable RD3 binding are believed to cause Lebering are belie amaurosis (Azadi et al., 2010; Zulliger et al., 2015) and various forms of retinal degeneration (Friedman et al., 2006;

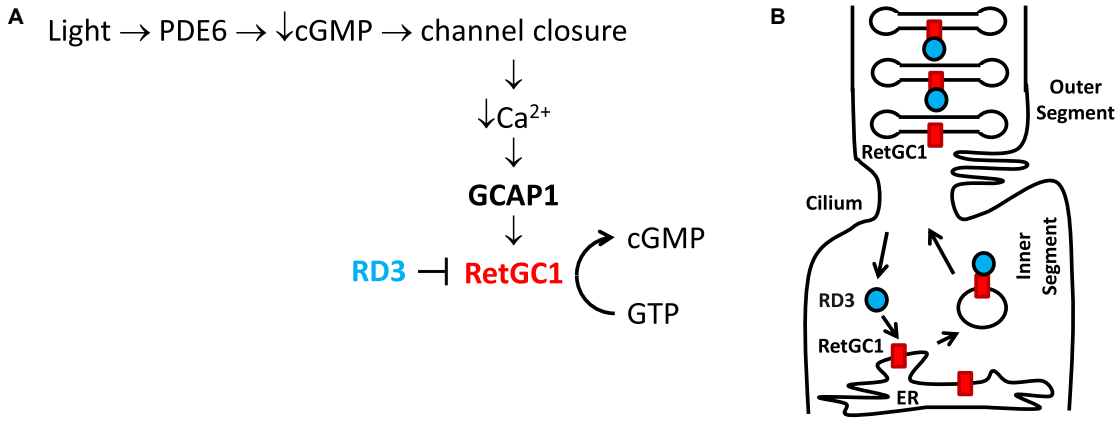

FIGURE 1
Physiological role of GCAP1 and RD3 in visual phototransduction. Adapted from Ames (2019). **(A)** Visual excitation pathway in retinal photoreceptor cells. Light-activated channel closure promotes a drop in cytosolic Ca^{2+} level that in turn causes Ca^{2+}-free/Mg^{2+}-bound GCAP1 to bind and activate RetGC1. RD3 binding to RetGC1 inhibits the cyclase activity. **(B)** RD3 (cyan) guides the trafficking of RetGC1 (red) to outer segment disk membranes.

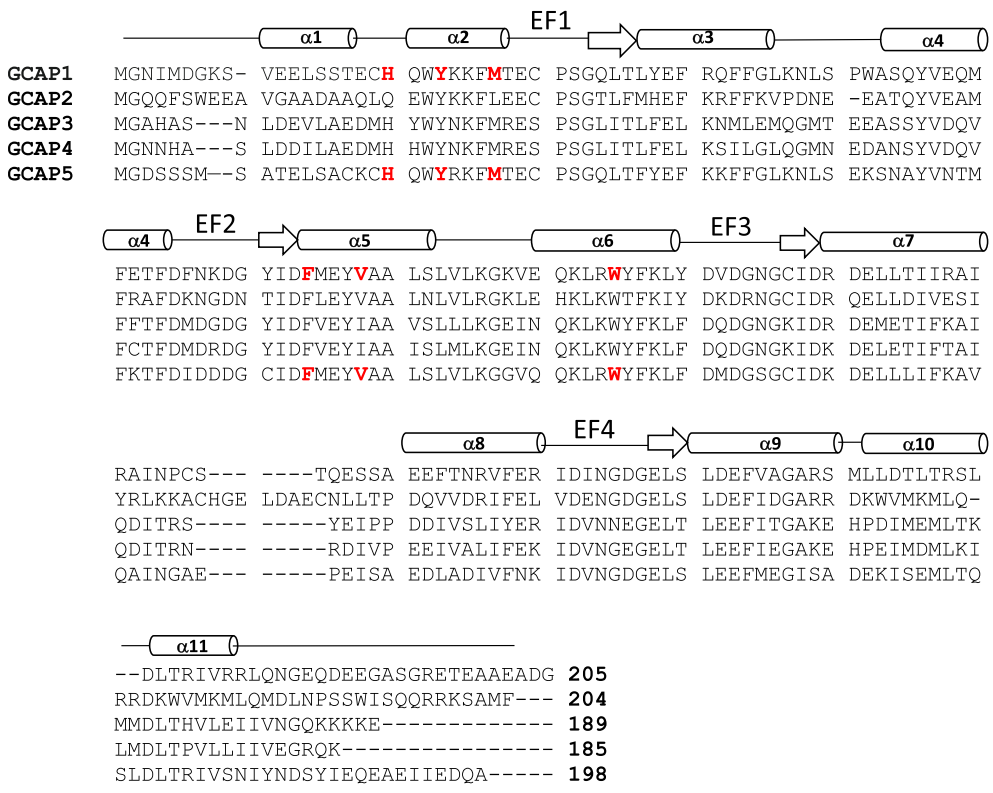

FIGURE 2
Amino acid sequence alignment of GCAP proteins. Swiss Protein Database accession numbers are P46065 (bovine GCAP1), P51177 (bovine GCAP2), O95843 (zebrafish GCAP3), Q6ZM98 (zebrafish GCAP4), and Q5MAC8 (zebrafish GCAP5). Exposed "hot spot" residues in GCAP1 and GCAP5 are highlighted red. Secondary structure (helices and strands) are shown above the sequence alignment depicted as cylinders and arrows.

Azadi et al., 2010; Molday et al., 2013, 2014). The ability of RD3 to prevent aberrant activation of RetGC1 by GCAPs is essential for the survival of photoreceptors (Peshenko et al., 2016). Lastly, RD3 may also interact with guanylate kinase to promote the synthesis of GDP to control the recycling of nucleotides in the inner segment (Wimberg et al., 2018). However, more

recent studies argue against any role for RD3 in GMP recycling (Dizhoor et al., 2021).

In this review, I provide an overview of previous atomic-resolution structures of GCAP1 (Stephen et al., 2007; Lim et al., 2016), GCAP5 (Cudia et al., 2021) and RD3 (Peshenko et al., 2019), and propose a molecular mechanism for how RetGC1 might be regulated by GCAP1 and RD3.

Molecular structure and function of guanylate cyclase activating proteins

Guanylate cyclase activating proteins are a family of retinal Ca^{2+} sensors

The GCAP proteins (GCAP1-5, see **Figure 2**) are a family of Ca^{2+} binding proteins expressed exclusively in vertebrate photoreceptors (Polans et al., 1996; Ames, 2021). GCAP1 (Palczewski et al., 1994) and GCAP2 (Dizhoor et al., 1995) were originally discovered in mammalian photoreceptors, but up to seven GCAP homologs were later discovered in zebrafish and other vertebrate species (Imanishi et al., 2004; Scholten and Koch, 2011). The GCAP proteins consist of about 200 amino acid residues that contain N-terminal myristoylation, four EF-hand Ca^{2+} binding sites (EF1, EF2, EF3, and EF4 in **Figure 2**), and non-conserved residues in the N-terminal and C-terminal helices (α1 and α11 in **Figure 2**). The EF-hands in GCAP1 can bind to both Ca^{2+} and Mg^{2+} (Peshenko and Dizhoor, 2006, 2007). Mg^{2+} can bind to the second EF-hand (magenta sphere in **Figure 3A**) in GCAP1 (Peshenko and Dizhoor, 2004, 2007; Lim et al., 2009), which stabilizes the Ca^{2+}-free/Mg^{2+}-bound protein conformation (**Figure 3A**) that activates RetGC1 in light-activated photoreceptors (Dizhoor et al., 1994; Peshenko and Dizhoor, 2004; Marino et al., 2015). In dark-adapted photoreceptors, Ca^{2+} binds to GCAP1 (in place of Mg^{2+}), which stabilizes the Ca^{2+}-bound structure (**Figure 3B**) that is important for the inhibition of RetGC1 (Dizhoor et al., 1998). Ca^{2+} binds to GCAP1 at the second, third and fourth EF-hands (orange spheres in **Figure 3B**; Ames et al., 1999; Stephen et al., 2007) with an apparent dissociation constant of 100 nM (Lim et al., 2009; Dizhoor et al., 2010). Dark-adapted photoreceptors maintain relatively high cytosolic Ca^{2+} levels (500 nM) (Woodruff et al., 2002), which promotes the formation of Ca^{2+}-bound GCAP1 (Dizhoor and Hurley, 1996; Dizhoor et al., 1998). Light-activation of the photoreceptor causes a 10-fold reduction in the cytosolic Ca^{2+} level (Gray-Keller and Detwiler, 1994; Woodruff et al., 2002) while the Mg^{2+} concentration remains fixed at ∼1 mM (Chen et al., 2003). Therefore, GCAP1 binds to Mg^{2+} instead of Ca^{2+} in light-activated photoreceptors, and the Ca^{2+}-free/Mg^{2+}-bound GCAP1 binds to RetGC1 to promote the synthesis of cGMP during visual recovery (Dizhoor et al., 1994, 1995; Gorczyca et al., 1995).

GCAP1 and GCAP5 form dimers in the absence of retinal membrane guanylate cyclases 1

GCAP1 and GCAP5 both form homodimers in solution in the absence of RetGC1 (**Figures 3C,D**). The dimerization of GCAP1 and GCAP5 are both Ca^{2+}-independent and have a dimerization dissociation constant in the micromolar range (Lim et al., 2018; Boni et al., 2020; Cudia et al., 2021). Structural models of GCAP1 and GCAP5 dimers were both determined previously by measuring intermolecular DEER distances that served as restraints for molecular docking (Lim et al., 2018; Cudia et al., 2021; **Figures 3C,D**). The overall structures of both dimers are fairly similar (RMSD = 2.4 Å) and residues at the dimer interface are highly conserved (see red residues in **Figure 3**). An important structural difference is that the GCAP5 dimer forms an intermolecular salt bridge between R22 and D71 that is not seen in the GCAP1 dimer, and the GCAP5 mutation R22A abolishes dimerization (Cudia et al., 2021). The dimer structures of GCAP1 and GCAP5 are both stabilized by hydrophobic contacts at the dimer interface (**Figures 3C,D**). The most prominent intermolecular contacts involve conserved hydrophobic residues, H19, Y22, M26, F73, V77, and W94 in GCAP1 (**Figure 3**). In particular, the methyl side-chain atoms of V77 (V76 in GCAP5) each contact one another at the dimer interface and therefore explain why the V77E (or V76E in GCAP5) mutation significantly weakens protein dimerization for both GCAP1 and GCAP5 (Lim et al., 2016; Cudia et al., 2021). Individual point mutations at the dimer interface in GCAP1 (H19A, Y22A, F73A, V77E, and W94A) or GCAP5 (H18A, Y21A, F72A, V76E, and W93E) each weaken the dimerization dissociation constant and completely abolish the activation of RetGC1 by GCAP1 (Lim et al., 2018) or GCAP5 (Cudia et al., 2021). Thus, the exposed hydrophobic residues at the dimer interface are essential for both GCAP dimerization and activation of RetGC1.

Mutational hotspot residues in GCAP1 and GCAP5

The structures of GCAP1 (**Figure 3B**; Stephen et al., 2007) and GCAP5 (**Figure 3A**; Cudia et al., 2021) reveal exposed hydrophobic residues (H19, Y22, M26, F73, V77, and W94 in GCAP1 or H18, Y21, F72, V76, and W93 in GCAP5) that I propose could be targeted by rational drug design (see exposed residues highlighted red in **Figure 3**). The exposed

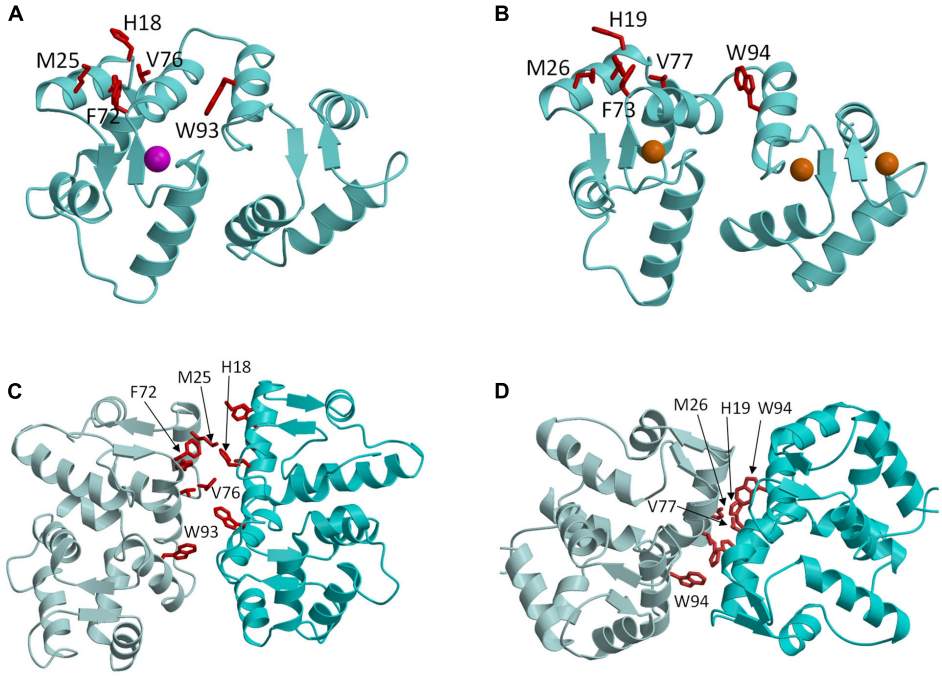

FIGURE 3
Molecular structures of GCAP1 and GCAP5. Main chain structures of Ca^{2+}-free/Mg^{2+}-bound GCAP5 (PDB ID: 7M2M) **(A)** and Ca^{2+}-bound GCAP1 (PDB ID: 2R2I) **(B)**. Bound Ca^{2+} and Mg^{2+} are orange and magenta. Dimeric structures of GCAP5 **(C)** and GCAP1 **(D)** determined by double electron electron resonance (DEER). Side chain atoms of exposed "hot spot" residues are shown as red sticks.

hydrophobic residues are located at the dimer interface for both GCAP1 and GCAP5 (**Figures 3C,D**). Mutating the exposed residues in GCAP1 (H19A, Y22A, M26A, F73A, V77E, and W94E) each weaken dimerization and abolish cyclase activation (Lim et al., 2018). The corresponding mutations in GCAP5 (H18E, Y21E, M25E, F72E, V76E, and W93E) also weaken dimerization and abolish cyclase activation (Cudia et al., 2021). These results initially suggested that the dimeric structures of GCAP1 (and GCAP5) might be essential for cyclase activation. However, the GCAP5 mutant (R22A) was recently shown to abolish GCAP5 dimerization but still caused a threefold activation of the cyclase, which suggests that formation of a GCAP5 dimer (as seen in **Figure 3C**) may not be required to activate the cyclase. The enhanced cyclase activation caused by the monomeric R22A mutant is consistent with a previous suggestion that the exposed hotspot residues in GCAP1 may interact directly with RetGC1 (Peshenko et al., 2014) rather than mediate GCAP dimerization. If the exposed hotspot were to bind to RetGC1 with higher affinity than it binds to itself, then the apparent dimerization of GCAP1 and GCAP5 that occurs in the absence of RetGC1 might be an artifact of not having the cyclase present. Future studies are needed to test whether RetGC1 binding to GCAP1 prevents GCAP1 dimerization to distinguish whether the GCAP1 hotspot binds to RetGC1. Regardless of whether the exposed hotspot facilitates GCAP1/GCAP5 dimerization (**Figure 3**) or binds to RetGC1 (**Figure 4**), this hotspot (highlighted red in **Figure 4**) could serve as a binding site for an inhibitor whose binding would increase the apparent K_m value of the cyclase activity. The binding of small molecules or peptides that selectively target the hotspot should prevent GCAP1 from activating RetGC1. In particular, small molecule inhibitors that selectively target the hot spot of constitutively active GCAP1 mutants [Y99C (Payne et al., 1998), D100G (Nong et al., 2014), E111V (Marino et al., 2018), and E155G (Wilkie et al., 2001)] should block the constitutive activation of RetGC1. Future studies are needed to screen for small molecule inhibitors that specifically target the exposed hotspot in GCAP1 mutants and test whether these drugs might slow the progression of cone-rod dystrophies.

Structural basis of rd3 binding to retinal membrane guanylate cyclases 1

Retinal degeneration 3 forms an elongated four-helix bundle

The NMR structure of RD3 (Peshenko et al., 2019) reveals an elongated overall structure (70 Å long by 30 Å wide)

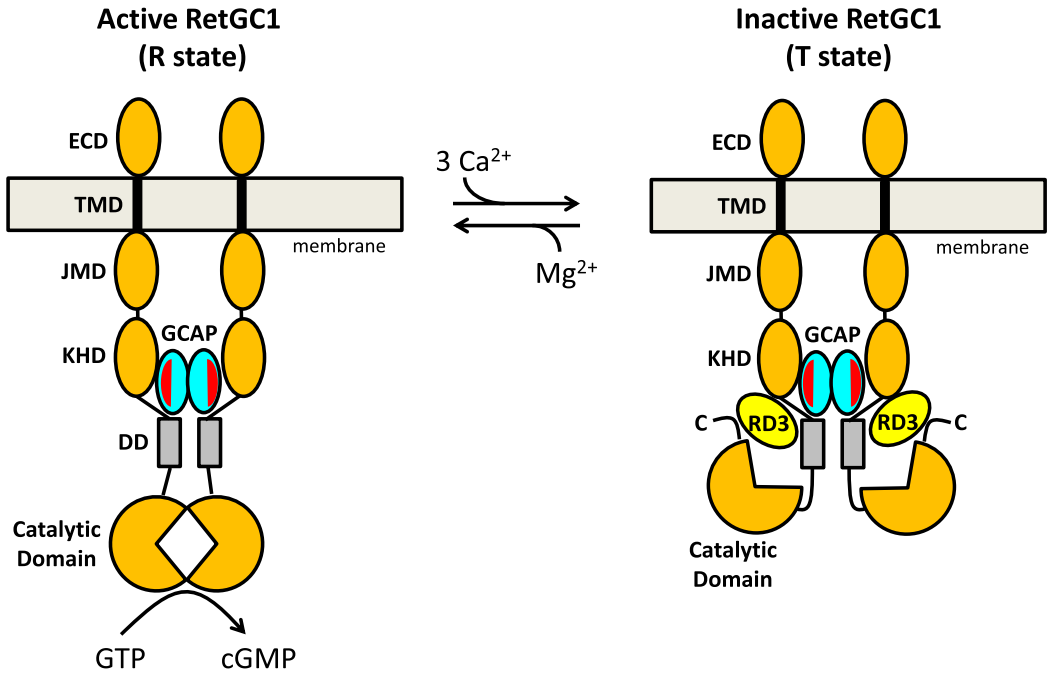

FIGURE 4
Schematic model of RetGC1 (orange) regulation by GCAP1 (cyan) and RD3 (yellow). Abbreviations of RetGC1 domains: ECD, extracellular domain; TMD, transmembrane domain; JMD, juxtamembrane domain; KHD, kinase homology domain; DD, dimerization domain (gray). The exposed hydrophobic patch in GCAP1 is red.

that adopts a four-helix bundle (helix α1: P21–V51; α2: P75–K87; α3: P90–Q107; α4: V111–T139) (**Figure 5A**). The four helices in RD3 are bundled together in an antiparallel fashion with interhelical contacts formed by hydrophobic residues on the inner surface of helices α1 (residues L29 and L33), α3 (F100), and α4 (V114, F118, L122) whose side chain atoms point inward toward the hydrophobic core. The N-terminal and C-terminal ends of helices α1 and α4 are solvent exposed and the ends of these helices are rigidified by a series of salt bridge interactions (see blue and red side chain atoms in **Figure 5A**), which generates a long end-to-end distance in the elongated structure. A map of the electrostatic surface potential of RD3 reveals a negatively charged protein surface on one side of the protein (**Figure 5B**), in which many negatively charged glutamate side chain atoms (from E106, E108, E110, E113, E127, E132, E134) are clustered together on the protein surface and are suggested to make electrostatic contacts with RetGC1. A separate set of exposed residues in RD3 (see H89, C93, P95, I97, R99, R101, Q102 in **Figure 5C**) are clustered on the opposite side of the protein surface located near the center of the structure (highlighted red in **Figure 5C**). Site-specific mutations of these solvent exposed residues (see H89, C93, P95, I97, R99, R101, Q102, S120 in **Figure 5C**) have been shown to abolish RetGC1 regulation (Peshenko et al., 2016), suggesting that these residues might make direct contact with RetGC1.

Retinal degeneration 3 binding to retinal membrane guanylate cyclases 1

The three-dimensional structure of RD3 (**Figure 5**) provides clues about how RD3 might bind to and regulate RetGC1. Previous studies suggested that RD3 and GCAP1 may competitively bind to RetGC1 (Peshenko et al., 2011, 2016). The RD3 binding site on RetGC1 was therefore initially suggested to overlap at least partially with the GCAP1 binding site in RetGC1. GCAP1 and GCAP2 have been shown to interact primarily with the kinase homology and dimerization domains within RetGC1 (Peshenko et al., 2015a,b). The W708R mutation within the kinase homology domain of RetGC1 was recently shown to abolish RetGC1 binding with both RD3 and GCAP1, which is consistent with a partial overlapping of the GCAP1 and RD3 binding sites (Peshenko et al., 2015b). However, RD3 binding to RetGC1 was also disrupted by the removal of a C-terminal fragment downstream of the cyclase catalytic domain (Azadi et al., 2010). This same C-terminal deletion does not affect RetGC1 binding to GCAP1 (Peshenko et al., 2015b). Furthermore, particular point mutations in the RetGC1 dimerization domain (R822A and M823A) that block RetGC1 binding to GCAP1 have no effect on RetGC1 binding to RD3 (Peshenko et al., 2015a). These different binding properties suggest that RD3 and GCAP1 may have non-overlapping binding regions or perhaps a non-localized and multivalent

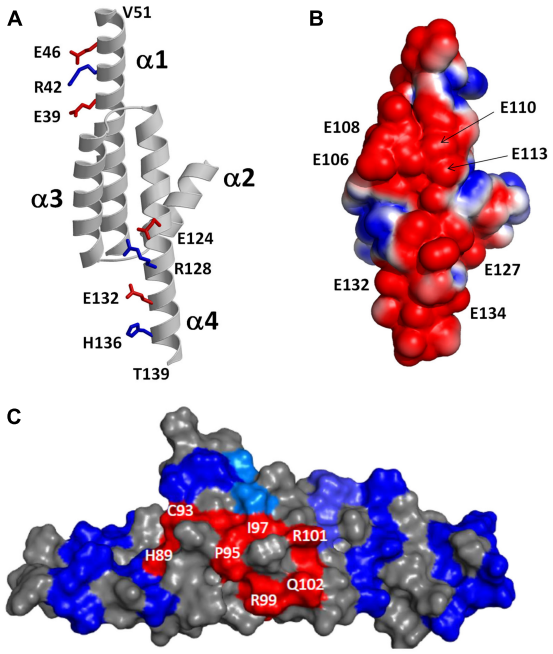

FIGURE 5
Structural analysis of RD3. Adapted from Peshenko et al. (2019). **(A)** Main chain structure of RD3. Salt bridges near the N-terminus (E39, R42, and E46) and C-terminus (E124, R128, E132, and H136) rigidify α1 and α4 to form an elongated 4-helix bundle. **(B)** Map of surface electrostatic potential of RD3 illustrates negatively charged protein surface (red). **(C)** Space-filling representation of RD3 shows residues on the protein surface (highlighted in red) that contact RetGC1.

binding site in each case. Future studies are needed to map the entire RD3 binding site in RetGC1.

Allosteric mechanism of retinal membrane guanylate cyclases 1 regulation by guanylate cyclase activating proteins 1 and retinal degeneration 3

A schematic model for the allosteric regulation of RetGC1 by GCAP1 and RD3 is presented in **Figure 4**. RetGC1 is known to form a dimer in the disk membrane (Liu et al., 1997; Olshevskaya et al., 1999; Yu et al., 1999). The dimeric RetGC1 is proposed to adopt two distinct quaternary structures: The R-state conformation places the two catalytic domains in close proximity to assemble the cyclase active site at the dimer interface in order to provide maximal enzymatic activity (**Figure 4**, left panel). The T-state conformation causes the catalytic domains to disassociate and disassemble the cyclase catalytic site, which should abolish the cyclase activity (**Figure 4**, right panel). The dimeric RetGC1 is believed to bind two molecules of GCAP1 to form a 2:2 complex (Peshenko et al., 2010). Previous studies have observed that GCAP1 may adopt a pre-formed dimer before binding to the RetGC1 dimer (Lim et al., 2018; Boni et al., 2020). However, more recent studies suggest that GCAP5 dimerization is not required for cyclase binding and activation (Cudia et al., 2021). Therefore, the exposed hydrophobic patch in GCAP1 (red residues in **Figure 3**) that facilitates GCAP1 dimerization in the absence of RetGC1 (**Figures 3C,D**) is proposed here to interact directly with RetGC1 as suggested previously (Peshenko et al., 2014) (see red patch in **Figure 4**). RetGC1 binding to Ca^{2+}-free/Mg^{2+}-bound GCAP1 at low Ca^{2+} levels (in light-activated photoreceptors) is proposed to stabilize the RetGC1 dimer in the active conformation (R), which shifts the equilibrium in favor of the active R state and turns on cyclase activity. The binding of Ca^{2+}-bound GCAP1 to RetGC1 at high Ca^{2+} levels (in dark-adapted photoreceptors) is proposed to stabilize the RetGC1 dimer in the inactive conformation (T). In essence, GCAP1 is suggested here to serve as both a positive and negative allosteric effector for RetGC1: Ca^{2+}-free GCAP1 shifts the allosteric equilibrium in favor of R, in contrast to Ca^{2+}-bound GCAP1 that shifts the equilibrium in favor of T. In the absence of GCAP1, the RetGC1 dimer can occupy both conformational states (T and R). However, the conformational equilibrium in the absence of GCAP1 is shifted toward the inactive T-state, because the basal cyclase activity (in the absence of GCAP1) is more than 100-fold lower than it is in the presence of GCAP1.

The structural model of the RetGC1 dimer also explains how RD3 (yellow in **Figure 4**) might inactivate the cyclase activity (**Figure 4**, right panel). RD3 is proposed to bind to the RetGC1 dimer by contacting the KHD/dimerization domains (Peshenko et al., 2011, 2016) and the C-terminal region downstream of the catalytic domain (Azadi et al., 2010). This multivalent interaction is proposed to lock the RetGC1 dimer in the inactive T-state conformation. The binding of RD3 to RetGC1 (without the binding of GCAP1) must be sufficient to stabilize the inactive T-state, because RD3 alone can bind to and inactivate RetGC1 in the inner segment, which lacks GCAP1. Therefore, the binding of RD3 to inactive T-state is suggest here to be independent of the binding of Ca2 + -bound GCAP1, which would imply that the binding of either RD3 or Ca^{2+}-bound GCAP1 are each sufficient to stabilize the inactive T-state. This hypothesis could be further tested by overexpressing RD3 (Peshenko et al., 2021) in the GCAP-/- double knockout strain (Pennesi et al., 2003) to verify whether the RD3 overexpression will cause lower basal RetGC1 activity and reduced dark current. Lastly, at low cytosolic Ca^{2+} levels, the binding of Ca^{2+}-free/Mg^{2+}-bound GCAP1 to the RetGC1 R-state (**Figure 4** left panel) should prevent RD3 from binding to RetGC1, because the structural model in **Figure 4** predicts that RD3 would not be able to form multivalent contacts with the active R-state. Therefore, an important prediction of this model is that Ca^{2+}-free/Mg^{2+}-bound GCAP1 should weaken RD3 binding to RetGC1 at low

Ca^{2+} levels, in contrast to Ca^{2+}-bound GCAP1 that can bind simultaneously with RD3 to the inactive T-state of RetGC1. Future studies are needed to test the predictions of the model and to determine atomic-resolution structures of RetGC1 bound to GCAP1 and RD3.

Conclusion

Retinal membrane guanylate cyclases (RetGC1 and RetGC2) are expressed in photoreceptor rod and cone cells where they promote the visual recovery phase of phototransduction. The cyclase enzymatic activity is oppositely regulated by GCAPs and RD3. Mutations in RetGC1, GCAP1 and RD3 that disable the Ca^{2+}-dependent cyclase regulation are genetically linked to retinal degenerative diseases and inherited forms of blindness. A molecular model (**Figure 4**) was presented that explains how a RetGC1 dimer is allosterically regulated by the binding of GCAP1 and RD3. The binding of Ca^{2+}-free/Mg^{2+}-bound GCAP1 is proposed to stimulate cyclase activity by stabilizing RetGC1 in an active conformational state (R), whereas RD3 binding is proposed to decrease cyclase activity by locking RetGC1 in the inactive conformational state (T). The model predicts that Ca^{2+}-free GCAP1 should inhibit RD3 binding to RetGC1, in contrast to Ca^{2+}-bound GCAP1 that should enhance RetGC1 binding to RD3. These predictions could be tested by overexpressing RD3 in a GCAP-/- double knockout photoreceptor and measuring its effect on dark current. Exposed hydrophobic residues in GCAP1 (residues H19, Y22, M26, F73, V77, W94) are essential for cyclase activation and could be targeted by rational drug design for the possible treatment of rod/cone dystrophies.

Author contributions

JA wrote and conceived the entire manuscript.

Funding

This work was supported by the NIH (EY012347) to JA.

Conflict of interest

The author declares that the research was conducted in the absence of any commercial or financial relationships that could be construed as a potential conflict of interest.

Publisher's note

All claims expressed in this article are solely those of the authors and do not necessarily represent those of their affiliated organizations, or those of the publisher, the editors and the reviewers. Any product that may be evaluated in this article, or claim that may be made by its manufacturer, is not guaranteed or endorsed by the publisher.

References

Ames, J. B. (2019). Retinal Degeneration-3 (RD3) Protein is a Molecular Linchpin for Retinal Disease. *EC Ophthalmol.* 10, 10–12.

Ames, J. B. (2021). Structural Insights into Retinal Guanylate Cyclase Activator Proteins (GCAPs). *Int. J. Mol. Sci.* 22:8731.

Ames, J. B., Dizhoor, A. M., Ikura, M., Palczewski, K., and Stryer, L. (1999). Three-dimensional structure of guanylyl cyclase activating protein-2, a calcium-sensitive modulator of photoreceptor guanylyl cyclases. *J. Biol. Chem.* 274, 19329–19337. doi: 10.1074/jbc.274.27.19329

Azadi, S., Molday, L. L., and Molday, R. S. (2010). RD3, the protein associated with Leber congenital amaurosis type 12, is required for guanylate cyclase trafficking in photoreceptor cells. *Proc. Natl. Acad. Sci. U.S.A.* 107, 21158–21163. doi: 10.1073/pnas.1010460107

Baehr, W., Karan, S., Maeda, T., Luo, D. G., Li, S., Bronson, J. D., et al. (2007). The function of guanylate cyclase 1 and guanylate cyclase 2 in rod and cone photoreceptors. *J. Biol. Chem.* 282, 8837–8847.

Baehr, W., and Palczewski, K. (2007). Guanylate cyclase-activating proteins and retina disease. *Subcell. Biochem.* 45, 71–91.

Baylor, D. (1996). How photons start vision. *Proc. Natl. Acad. Sci. U.S.A.* 93, 560–565.

Behnen, P., Dell' Orco, D., and Koch, K. W. (2010). Involvement of the calcium sensor GCAP1 in hereditary cone dystrophies. *Biol. Chem.* 391, 631–637.

Bondarenko, V. A., Hayashi, F., Usukura, J., and Yamazaki, A. (2010). Involvement of rhodopsin and ATP in the activation of membranous guanylate cyclase in retinal photoreceptor outer segments (ROS-GC) by GC-activating proteins (GCAPs): A new model for ROS-GC activation and its link to retinal diseases. *Mol. Cell Biochem.* 334, 125–139. doi: 10.1007/s11010-009-0323-y

Boni, F., Marino, V., Bidoia, C., Mastrangelo, E., Barbiroli, A., Dell'orco, D., et al. (2020). Modulation of Guanylate Cyclase Activating Protein 1 (GCAP1) Dimeric Assembly by Ca(2+) or Mg(2+): Hints to Understand Protein Activity. *Biomolecules* 10:1408. doi: 10.3390/biom10101408

Boye, S. L., Conlon, T., Erger, K., Ryals, R., Neeley, A., Cossette, T., et al. (2011). Long-term preservation of cone photoreceptors and restoration of cone function by gene therapy in the guanylate cyclase-1 knockout (GC1KO) mouse. *Invest. Ophthalmol. Vis. Sci.* 52, 7098–7108. doi: 10.1167/iovs.11-7867

Boye, S. L., Peshenko, I. V., Huang, W. C., Min, S. H., Mcdoom, I., Kay, C. N., et al. (2013). AAV-mediated gene therapy in the guanylate cyclase (RetGC1/RetGC2) double knockout mouse model of Leber congenital amaurosis. *Hum. Gene Ther.* 24, 189–202. doi: 10.1089/hum.2012.193

Burns, M. E., Mendez, A., Chen, J., and Baylor, D. A. (2002). Dynamics of Cyclic GMP Synthesis in Retinal Rods. *Neuron* 36, 81–91.

Chen, C., Nakatani, K., and Koutalos, Y. (2003). Free magnesium concentration in salamander photoreceptor outer segments. *J. Physiol.* 553, 125–135. doi: 10.1113/jphysiol.2003.053280

Cudia, D., Roseman, G. P., Assafa, T. E., Shahu, M. K., Scholten, A., Menke-Sell, S. K., et al. (2021). NMR and EPR-DEER Structure of a Dimeric Guanylate Cyclase Activator Protein-5 from Zebrafish Photoreceptors. *Biochemistry* 60, 3058–3070. doi: 10.1021/acs.biochem.1c00612

Dell'orco, D., Behnen, P., Linse, S., and Koch, K. W. (2010). Calcium binding, structural stability and guanylate cyclase activation in GCAP1 variants associated with human cone dystrophy. *Cell Mol. Life Sci.* 67, 973–984.

Dell'orco, D., Sulmann, S., Zagel, P., Marino, V., and Koch, K. W. (2014). Impact of cone dystrophy-related mutations in GCAP1 on a kinetic model of phototransduction. *Cell Mol. Life Sci.* 71, 3829–3840. doi: 10.1007/s00018-014-1593-4

Dizhoor, A. M., Boikov, S. G., and Olshevskaya, E. V. (1998). Constitutive activation of photoreceptor guanylate cyclase by Y99C mutant of GCAP-1. Possible role in causing human autosomal dominant cone degeneration. *J. Biol. Chem.* 273, 17311–17314. doi: 10.1074/jbc.273.28.17311

Dizhoor, A. M., and Hurley, J. B. (1996). Inactivation of EF-hands makes GCAP-2 (p24) a constitutive activator of photoreceptor guanylyl cyclase by preventing a Ca2+-induced "activator-to-inhibitor" transition. *J. Biol. Chem.* 271, 19346–19350. doi: 10.1074/jbc.271.32.19346

Dizhoor, A. M., Lowe, D. G., Olsevskaya, E. V., Laura, R. P., and Hurley, J. B. (1994). The human photoreceptor membrane guanylyl cyclase, RetGC, is present in outer segments and is regulated by calcium and a soluble activator. *Neuron* 12, 1345–1352. doi: 10.1016/0896-6273(94)90449-9

Dizhoor, A. M., Olshevskaya, E. V., Henzel, W. J., Wong, S. C., Stults, J. T., Ankoudinova, I., et al. (1995). Cloning, sequencing and expression of a 24-kDa Ca2+-binding protein activating photoreceptor guanylyl cyclase. *J. Biol. Chem.* 270, 25200–25206. doi: 10.1074/jbc.270.42.25200

Dizhoor, A. M., Olshevskaya, E. V., and Peshenko, I. V. (2010). Mg2+/Ca2+ cation binding cycle of guanylyl cyclase activating proteins (GCAPs): Role in regulation of photoreceptor guanylyl cyclase. *Mol. Cell Biochem.* 334, 117–124. doi: 10.1007/s11010-009-0328-6

Dizhoor, A. M., Olshevskaya, E. V., and Peshenko, I. V. (2021). Retinal degeneration-3 protein promotes photoreceptor survival by suppressing activation of guanylyl cyclase rather than accelerating GMP recycling. *J. Biol. Chem.* 296:100362. doi: 10.1016/j.jbc.2021.100362

Duda, T., Jankowska, A., Venkataraman, V., Nagele, R. G., and Sharma, R. K. (2001). A novel calcium-regulated membrane guanylate cyclase transduction system in the olfactory neuroepithelium. *Biochemistry* 40, 12067–12077. doi: 10.1021/bi0108406

Duda, T., Pertzev, A., Koch, K. W., and Sharma, R. K. (2012). Antithetical modes of and the Ca(2+) sensors targeting in ANF-RGC and ROS-GC1 membrane guanylate cyclases. *Front. Mol. Neurosci.* 5:44. doi: 10.3389/fnmol.2012.00044

Friedman, J. S., Chang, B., Kannabiran, C., Chakarova, C., Singh, H. P., Jalali, S., et al. (2006). Premature truncation of a novel protein, RD3, exhibiting subnuclear localization is associated with retinal degeneration. *Am. J. Hum. Genet.* 79, 1059–1070. doi: 10.1086/510021

Gorczyca, W., Polans, A., Surgucheva, I., Subbaraya, I., Baehr, W., and Palczewski, K. (1995). Guanylyl cyclase activating protein. A calcium-sensitive regulator of phototransduction. *J. Biol. Chem.* 270, 22029–22036. doi: 10.1074/jbc.270.37.22029

Gray-Keller, M. P., and Detwiler, P. B. (1994). The calcium feedback signal in the phototransduction cascade of vertebrate rods. *Neuron* 13, 849–861.

Howes, K. A., Pennesi, M. E., Sokal, I., Church-Kopish, J., Schmidt, B., Margolis, D., et al. (2002). GCAP1 rescues rod photoreceptor response in GCAP1/GCAP2 knockout mice. *EMBO J.* 21, 1545–1554.

Imanishi, Y., Yang, L., Sokal, I., Filipek, S., Palczewski, K., and Baehr, W. (2004). Diversity of guanylate cyclase-activating proteins (GCAPs) in teleost fish: Characterization of three novel GCAPs (GCAP4, GCAP5, GCAP7) from zebrafish (Danio rerio) and prediction of eight GCAPs (GCAP1-8) in pufferfish (Fugu rubripes). *J. Mol. Evol.* 59, 204–217. doi: 10.1007/s00239-004-2614-y

Jiang, L., and Baehr, W. (2010). GCAP1 Mutations Associated with Autosomal Dominant Cone Dystrophy. *Adv. Exp. Med. Biol.* 664, 273–282.

Koch, K. W., and Stryer, L. (1988). Highly cooperative feedback control of retinal rod guanylate cyclase by calcium ions. *Nature* 334, 64–66. doi: 10.1038/334064a0

Koutalos, Y., and Yau, K. W. (1996). Regulation of sensitivity in vertebrate rod photoreceptors by calcium. *Trends Neurosci.* 19, 73–81.

Laura, R. P., Dizhoor, A. M., and Hurley, J. B. (1996). The membrane guanylyl cyclase, retinal guanylyl cyclase-1, is activated through its intracellular domain. *J. Biol. Chem.* 271, 11646–11651.

Laura, R. P., and Hurley, J. B. (1998). The kinase homology domain of retinal guanylyl cyclases 1 and 2 specifies the affinity and cooperativity of interaction with guanylyl cyclase activating protein-2. *Biochemistry* 37, 11264–11271. doi: 10.1021/bi9809674

Lim, S., Peshenko, I. V., Dizhoor, A. M., and Ames, J. B. (2009). Effects of Ca2+, Mg2+, and myristoylation on guanylyl cyclase activating protein 1 structure and stability. *Biochemistry* 48, 850–862. doi: 10.1021/bi801897p

Lim, S., Peshenko, I. V., Olshevskaya, E. V., Dizhoor, A. M., and Ames, J. B. (2016). Structure of Guanylyl Cyclase Activator Protein 1 (GCAP1) Mutant V77E in a Ca2+-free/Mg2+-bound Activator State. *J. Biol. Chem.* 291, 4429–4441. doi: 10.1074/jbc.M115.696161

Lim, S., Roseman, G., Peshenko, I., Manchala, G., Cudia, D., Dizhoor, A., et al. (2018). Retinal Guanylyl Cyclase Activating Protein 1 Forms a Functional Dimer. *PLoS One* 13:e0193947. doi: 10.1371/journal.pone.0193947

Liu, Y., Ruoho, A. E., Rao, V. D., and Hurley, J. B. (1997). Catalytic mechanism of the adenylyl and guanylyl cyclases: Modeling and mutational analysis. *Proc. Natl. Acad. Sci. U.S A.* 94, 13414–13419. doi: 10.1073/pnas.94.25.13414

Lowe, D. G., Dizhoor, A. M., Liu, K., Gu, Q., Spencer, M., Laura, R., et al. (1995). Cloning and expression of a second photoreceptor-specific membrane retina guanylyl cyclase (RetGC), RetGC-2. *Proc. Natl. Acad. Sci. U.S.A.* 6, 5535–5539. doi: 10.1073/pnas.92.12.5535

Marino, V., Dal Cortivo, G., Oppici, E., Maltese, P. E., D'esposito, F., Manara, E., et al. (2018). A novel p.(Glu111Val) missense mutation in GUCA1A associated with cone-rod dystrophy leads to impaired calcium sensing and perturbed second messenger homeostasis in photoreceptors. *Hum. Mol. Genet.* 27, 4204–4217. doi: 10.1093/hmg/ddy311

Marino, V., Sulmann, S., Koch, K. W., and Dell'orco, D. (2015). Structural effects of Mg(2)(+) on the regulatory states of three neuronal calcium sensors operating in vertebrate phototransduction. *Biochim. Biophys. Acta.* 1853, 2055–2065. doi: 10.1016/j.bbamcr.2014.10.026

Mendez, A., and Chen, J. (2002). Mouse models to study GCAP functions in intact photoreceptors. *Adv. Exp. Med. Biol.* 514, 361–388.

Molday, L. L., Djajadi, H., Yan, P., Szczygiel, L., Boye, S. L., Chiodo, V. A., et al. (2013). RD3 gene delivery restores guanylate cyclase localization and rescues photoreceptors in the Rd3 mouse model of Leber congenital amaurosis 12. *Hum. Mol. Genet.* 22, 3894–3905. doi: 10.1093/hmg/ddt244

Molday, L. L., Jefferies, T., and Molday, R. S. (2014). Insights into the role of RD3 in guanylate cyclase trafficking, photoreceptor degeneration, and Leber congenital amaurosis. *Front. Mol. Neurosci.* 7:44. doi: 10.3389/fnmol.2014.00044

Newbold, R. J., Deery, E. C., Payne, A. M., Wilkie, S. E., Hunt, D. M., and Warren, M. J. (2002). Guanylate cyclase activating proteins, guanylate cyclase and disease. *Adv. Exp. Med. Biol.* 514, 411–438.

Nong, E., Lee, W., Merriam, J. E., Allikmets, R., and Tsang, S. H. (2014). Disease progression in autosomal dominant cone-rod dystrophy caused by a novel mutation (D100G) in the GUCA1A gene. *Doc. Ophthalmol.* 128, 59–67. doi: 10.1007/s10633-013-9420-z

Olshevskaya, E. V., Ermilov, A. N., and And Dizhoor, A. M. (1999). Dimerization of guanylyl cyclase-activating protein. *J. Biol. Chem.* 274, 25583–25587.

Palczewski, K., Sokal, I., and Baehr, W. (2004). Guanylate cyclase-activating proteins: Structure, function, and diversity. *Biochem. Biophys. Res. Commun.* 322, 1123–1130.

Palczewski, K., Subbaraya, I., Gorczyca, W. A., Helekar, B. S., Ruiz, C. C., Ohguro, H., et al. (1994). Molecular cloning and characterization of retinal photoreceptor guanylyl cyclase-activating protein. *Neuron* 13, 395–404.

Payne, A. M., Downes, S. M., Bessant, D. A., Taylor, R., Holder, G. E., Warren, M. J., et al. (1998). A mutation in guanylate cyclase activator 1A (GUCA1A) in an autosomal dominant cone dystrophy pedigree mapping to a new locus on chromosome 6p21.1. *Hum. Mol. Genet.* 7, 273–277. doi: 10.1093/hmg/7.2.273

Pennesi, M. E., Howes, K. A., Baehr, W., and Wu, S. M. (2003). Guanylate cyclase-activating protein (GCAP) 1 rescues cone recovery kinetics in GCAP1/GCAP2 knockout mice. *Proc. Natl. Acad. Sci. U.S.A.* 100, 6783–6788. doi: 10.1073/pnas.1130102100

Peshenko, I. V., and Dizhoor, A. M. (2004). Guanylyl cyclase-activating proteins (GCAPs) are Ca2+/Mg2+ sensors: Implications for photoreceptor guanylyl cyclase (RetGC) regulation in mammalian photoreceptors. *J. Biol. Chem.* 279, 16903–16906. doi: 10.1074/jbc.C400065200

Peshenko, I. V., and Dizhoor, A. M. (2006). Ca2+ and Mg2+ binding properties of GCAP-1. Evidence that Mg2+-bound form is the physiological activator of photoreceptor guanylyl cyclase. *J. Biol. Chem.* 281, 23830–23841. doi: 10.1074/jbc.M600257200

Peshenko, I. V., and Dizhoor, A. M. (2007). Activation and inhibition of photoreceptor guanylyl cyclase by guanylyl cyclase activating protein 1 (GCAP-1): The functional role of Mg2+/Ca2+ exchange in EF-hand domains. *J. Biol. Chem.* 282, 21645–21652. doi: 10.1074/jbc.M702368200

Peshenko, I. V., Olshevskaya, E. V., Azadi, S., Molday, L. L., Molday, R. S., and Dizhoor, A. M. (2011). Retinal degeneration 3 (RD3) protein inhibits catalytic activity of retinal membrane guanylyl cyclase (RetGC) and its stimulation by activating proteins. *Biochemistry* 50, 9511–9519.

Peshenko, I. V., Olshevskaya, E. V., and Dizhoor, A. M. (2015b). Evaluating the Role of Retinal Guanylyl Cyclase 1 (RetGC1) Domains In Binding Guanylyl Cyclase Activating Proteins (GCAP). *J. Biol. Chem.* 290, 6913–6924.

Peshenko, I. V., Olshevskaya, E. V., and Dizhoor, A. M. (2015a). Dimerization Domain of Retinal Membrane Guanylyl Cyclase 1 (RetGC1) Is an Essential Part of Guanylyl Cyclase-activating Protein (GCAP) Binding Interface. *J. Biol. Chem.* 290, 19584–19596. doi: 10.1074/jbc.M115.661371

Peshenko, I. V., Olshevskaya, E. V., and Dizhoor, A. M. (2016). Functional Study and Mapping Sites for Interaction with the Target Enzyme in Retinal Degeneration 3 (RD3) Protein. *J. Biol. Chem.* 291, 19713–19723. doi: 10.1074/jbc.M116.742288

Peshenko, I. V., Olshevskaya, E. V., and Dizhoor, A. M. (2021). Retinal degeneration-3 protein attenuates photoreceptor degeneration in transgenic mice expressing dominant mutation of human retinal guanylyl cyclase. *J. Biol. Chem.* 297:101201. doi: 10.1016/j.jbc.2021.101201

Peshenko, I. V., Olshevskaya, E. V., Lim, S., Ames, J. B., and Dizhoor, A. M. (2014). Identification of target binding site in photoreceptor guanylyl cyclase-activating protein 1 (GCAP1). *J. Biol. Chem.* 289, 10140–10154. doi: 10.1074/jbc.M113.540716

Peshenko, I. V., Olshevskaya, E. V., Yao, S., Ezzeldin, H. H., Pittler, S. J., and Dizhoor, A. M. (2010). Activation of retinal guanylyl cyclase RetGC1 by GCAP1: Stoichiometry of binding and effect of new LCA-related mutations. *Biochemistry* 49, 709–717. doi: 10.1021/bi901495y

Peshenko, I. V., Yu, Q., Lim, S., Cudia, D., Dizhoor, A. M., and Ames, J. B. (2019). Retinal degeneration 3 (RD3) protein, a retinal guanylyl cyclase regulator, forms a monomeric and elongated four-helix bundle. *J. Biol. Chem.* 294, 2318–2328. doi: 10.1074/jbc.RA118.006106

Polans, A., Baehr, W., and Palczewski, K. (1996). Turned on by Ca2+! The physiology and pathology of Ca(2+)-binding proteins in the retina. *Trends Neurosci.* 19, 547–554. doi: 10.1016/s0166-2236(96)10059-x

Scholten, A., and Koch, K. W. (2011). Differential calcium signaling by cone specific guanylate cyclase-activating proteins from the zebrafish retina. *PLoS One* 6:e23117. doi: 10.1371/journal.pone.0023117

Semple-Rowland, S. L., Gorczyca, W. A., Buczylko, J., Helekar, B. S., Ruiz, C. C., Subbaraya, I., et al. (1996). Expression of GCAP1 and GCAP2 in the retinal degeneration (rd) mutant chicken retina. *FEBS Lett.* 385, 47–52. doi: 10.1016/0014-5793(96)00345-6

Sokal, I., Li, N., Surgucheva, I., Warren, M. J., Payne, A. M., Bhattacharya, S. S., et al. (1998). GCAP1 (Y99C) mutant is constitutively active in autosomal dominant cone dystrophy. *Mol. Cell* 2, 129–133.

Stephen, R., Bereta, G., Golczak, M., Palczewski, K., and Sousa, M. C. (2007). Stabilizing function for myristoyl group revealed by the crystal structure of a neuronal calcium sensor, guanylate cyclase-activating protein 1. *Structure* 15, 1392–1402. doi: 10.1016/j.str.2007.09.013

Stryer, L. (1991). Visual excitation and recovery. *J. Biol. Chem.* 266, 10711–10714.

Wilkie, S. E., Li, Y., Deery, E. C., Newbold, R. J., Garibaldi, D., Bateman, J. B., et al. (2001). Identification and functional consequences of a new mutation (E155G) in the gene for GCAP1 that causes autosomal dominant cone dystrophy. *Am. J. Hum. Genet.* 69, 471–480. doi: 10.1086/323265

Wimberg, H., Janssen-Bienhold, U., and Koch, K. W. (2018). Control of the Nucleotide Cycle in Photoreceptor Cell Extracts by Retinal Degeneration Protein 3. *Front. Mol. Neurosci.* 11:52. doi: 10.3389/fnmol.2018.00052

Woodruff, M. L., Sampath, A. P., Mathews, H. R., Krasnoperova, N. V., Lem, J., and Fain, G. L. (2002). Measurement of cytoplasmic calcium concentration in the rods of wild-type and transducin knock-out mice. *J. Physiol.* 542, 843–854. doi: 10.1113/jphysiol.2001.013987

Yang, R.-B., Robinson, S. W., Xiong, W.-H., Yau, K. W., Birch, D. G., and Garbers, D. L. (1999). Disruption of a Retinal Guanylyl Cyclase Gene Leads to Cone-Specific Dystrophy and Paradoxical Rod Behavior. *J. Neurosci.* 19, 5889–5897. doi: 10.1523/JNEUROSCI.19-14-05889.1999

Yu, H., Olshevskaya, E., Duda, T., Seno, K., Hayashi, F., Sharma, R. K., et al. (1999). Activation of retinal guanylyl cyclase-1 by Ca2+-binding proteins involves its dimerization. *J. Biol. Chem.* 274, 15547–15555.

Zulliger, R., Naash, M. I., Rajala, R. V., Molday, R. S., and Azadi, S. (2015). Impaired association of retinal degeneration-3 with guanylate cyclase-1 and guanylate cyclase-activating protein-1 leads to leber congenital amaurosis-1. *J. Biol. Chem.* 290, 3488–3499. doi: 10.1074/jbc.M114.616656

frontiers | Frontiers in Molecular Neuroscience

TYPE Original Research
PUBLISHED 14 December 2022
DOI 10.3389/fnmol.2022.1050545

OPEN ACCESS

EDITED BY
Daniele Dell'Orco,
University of Verona, Italy

REVIEWED BY
Lorenzo Cangiano,
University of Pisa,
Italy
Gordon Fain,
University of California,
Los Angeles,
United States

*CORRESPONDENCE
Polina Geva
vpolina@walla.co.il

†Deceased

SPECIALTY SECTION
This article was submitted to Molecular Signalling and Pathways, a section of the journal Frontiers in Molecular Neuroscience

RECEIVED 21 September 2022
ACCEPTED 11 November 2022
PUBLISHED 14 December 2022

CITATION
Geva P, Caruso G, Klaus C, Hamm HE, Gurevich VV, DiBenedetto E and Makino CL (2022) Effects of cell size and bicarbonate on single photon response variability in retinal rods.
Front. Mol. Neurosci. 15:1050545.
doi: 10.3389/fnmol.2022.1050545

Effects of cell size and bicarbonate on single photon response variability in retinal rods

Polina Geva[1]*, Giovanni Caruso[2], Colin Klaus[3,4], Heidi E. Hamm[5], Vsevolod V. Gurevich[5], Emmanuele DiBenedetto[6†] and Clint L. Makino[1]

[1]Department of Physiology and Biophysics, Boston University Chobanian & Avedisian School of Medicine, Boston, MA, United States, [2]Italian National Research Council, Istituto di Scienze del Patrimonio Culturale, Roma, Italy, [3]Mathematical Biosciences Institute, Ohio State University, Columbus, OH, United States, [4]College of Public Health, Division of Biostatistics, Ohio State University, Columbus, OH, United States, [5]Department of Pharmacology, Vanderbilt University, Nashville, TN, United States, [6]Department of Mathematics, Vanderbilt University, Nashville, TN, United States

Accurate photon counting requires that rods generate highly amplified, reproducible single photon responses (SPRs). The SPR is generated within the rod outer segment (ROS), a multilayered structure built from membranous disks that house rhodopsin. Photoisomerization of rhodopsin at the disk rim causes a local depletion of cGMP that closes ion channels in the plasmalemma located nearby with relative rapidity. In contrast, a photoisomerization at the disk center, distant from the plasmalemma, has a delayed impact on the ion channels due to the time required for cGMP redistribution. Radial differences should be greatest in large diameter rods. By affecting membrane guanylate cyclase activity, bicarbonate could impact spatial inhomogeneity in cGMP content. It was previously known that in the absence of bicarbonate, SPRs are larger and faster at the base of a toad ROS (where the ROS attaches to the rest of the cell) than at the distal tip. Given that bicarbonate enters the ROS at the base and diffuses to the tip and that it expedites flash response recovery, there should be an axial concentration gradient for bicarbonate that would accentuate the base-to-tip SPR differences. Seeking to understand how ROS geometry and bicarbonate affect SPR variability, we used mathematical modeling and made electrophysiological recordings of single rods. Modeling predicted and our experiments confirmed minor radial SPR variability in large diameter, salamander rods that was essentially unchanged by bicarbonate. SPRs elicited at the base and tip of salamander rods were similar in the absence of bicarbonate, but when treated with 30mM bicarbonate, SPRs at the base became slightly faster than those at the tip, verifying the existence of an axial gradient for bicarbonate. The differences were small and unlikely to undermine visual signaling. However, in toad rods with longer ROSs, bicarbonate somehow suppressed the substantial, axial SPR variability that is naturally present in the absence of bicarbonate. Modeling suggested that the axial gradient of bicarbonate might dampen the primary phototransduction cascade at the base of the ROS. This novel effect of bicarbonate solves a

mystery as to how toad vision is able to function effectively in extremely dim light.

KEYWORDS

visual transduction, cyclic GMP, rod outer segment, retina, single cell recording, mathematical modeling, salamander, toad

Introduction

Rod photoreceptors in the vertebrate retina convert photons into electrical signals to provide for vision in dim light. The main cell body, or inner segment, extends a specialized cilium, called the rod outer segment (ROS), that is stacked with about a thousand disks whose membranes contain rhodopsin. In order for rods to accurately encode photons, they must generate highly amplified and reproducible single photon responses (SPRs). Wide fluctuations in SPR amplitude and shape would not allow for the overall response to increase linearly with the number of coincident photons and information about the timing of photon absorption would be degraded. Nevertheless, a cumulative body of evidence indicates numerous sources of variability affecting the peak and recovery phases of the SPR. One important source of variability arises from randomness in the timing of R* inactivation; slower shutoff of R* results in larger, more prolonged SPRs with a delayed time to peak (Rieke and Baylor, 1998; Whitlock and Lamb, 1999; Caruso et al., 2010). This source of variability does not appear to be prohibitive because rods manage to achieve a standard deviation for the SPR amplitude that is ~0.2 of the mean (Baylor et al., 1979b; Rieke and Baylor, 1998; Whitlock and Lamb, 1999).

A second source of variability arises from randomness in the location within the outer segment of the rhodopsin photoisomerization. Geometry and structural properties of the ROS affect the radial and longitudinal diffusion of the second messengers, cGMP and Ca^{2+}, that influences the kinetics and amplitude of the SPR (Caruso et al., 2006; Bisegna et al., 2008). Mathematical modeling indicates that the spatiotemporal pattern of cGMP depletion in the intradiskal space depends upon the radial location of photoisomerization on a disk (Caruso et al., 2020). No differences were discerned in toad rods (Lamb et al., 1981), but this source of variability should increase with ROS diameter and experimental determinations in rods with larger outer segment diameters have yet to be reported. Inhomogeneity in cGMP levels over time and space caused by random PDE activations adds further variability to the early, rising phase of the SPR. However, as the response to R* grows, the impact of this source of variability diminishes as more PDE*s are recruited across the disk surface and the depletion of cGMP spreads over a greater volume (Caruso et al., 2020).

Randomness in the axial position of the rhodopsin photoisomerization could also generate SPR variability. In frog (*Xenopus laevis*) and in toad (*Rhinella marina,* formerly named *Bufo marinus*), SPRs elicited at the base of the ROS (nearest the inner segment) are considerably larger and faster than those elicited at the tip in the absence of added bicarbonate (Baylor et al., 1979a; Lamb et al., 1981; Schnapf, 1983; Mazzolini et al., 2015). Although the basis of these differences is not understood, hindrance of axial diffusion within the ROS by the stacked disks (e.g., Olson and Pugh, 1993) make it likely that there are axial gradients of ions and cascade components that alter phototransduction as a function of distance from the inner segment. Novel findings indicate Ca^{2+} levels in a dark adapted ROS rise as a function of distance from the base (Li et al., 2020). Because Ca^{2+} is a secondary messenger of phototransduction, such a gradient should cause peak amplitude as well as kinetics of the SPR to differ at the base and tip.

Bicarbonate is abundant and ubiquitous in the body; it is essential for pH regulation and it provides a means for the disposal of CO_2, a metabolic waste product. In addition, bicarbonate increases dark current and accelerates flash response kinetics in vertebrate rods by enhancing the action of membrane guanylate cyclases that replenish cGMP after a photon response (Donner et al., 1990; Duda et al., 2015) and potentially, by altering intracellular pH (e.g., Liebman et al., 1984). Bicarbonate is taken up at the rod synapse, after which it moves to the ROS, where it is extruded by an anion exchanger (Koskelainen et al., 1994; Duda et al., 2016; Makino et al., 2019). If the movement is by passive diffusion, then there must be a higher concentration of bicarbonate at the ROS base than at the distal tip. The base vs. tip differences in the SPR of frogs and toads would already appear to be problematic for vision in dim light, and any substantive axial gradient of bicarbonate would accentuate those differences. A bicarbonate gradient might generate SPR variability in species that have shorter ROS length. In large diameter rods, there might even be a radial concentration gradient of bicarbonate. At the present time, nothing is known about the contribution of bicarbonate to SPR variability.

Here, we studied how SPR variability is affected by ROS dimensions and by an axial bicarbonate gradient, using a fully space-resolved, biophysical model of rod phototransduction and electrical recordings of single rods. The study revealed surprising differences in the effect of bicarbonate on SPR variability in the rods of two amphibian species: tiger salamanders (*Ambystoma tigrinum*) and toads (*Rhinella marina*).

Materials and methods

Animals

Larval tiger salamanders (*Ambystoma tigrinum,* Wadelco, Corpus Christi, TX), approximately 6–10 inches in length, were kept at 12°C and fed redworms twice a week. Cane toads (*Rhinella marina,* formerly named *Bufo marinus*, Backwater Reptiles, Rocklin, CA), 4–6 inches in length, were kept at 21–25°C and fed crickets twice a week. Similar numbers of male and female salamanders were used; sex of the toads was not determined. All animal care and use conformed to the Association for Research in Vision and Ophthalmology Statement for the Use of Animals in Ophthalmic and Vision Research and to a protocol approved by the Institutional Animal Care and Use Committee. For physiological experiments, retinas from animals that were dark adapted overnight were isolated under infrared illumination following euthanasia and stored in Ringer's or in MOPS-buffered Ringer's solution, on ice. Ringer's solution contained (mM): NaCl, 108; KCl, 2.5; $MgCl_2$, 1; $CaCl_2$, 1.5; HEPES, 10; EDTA, 0.02; glucose, 10; bovine serum albumin (Fraction V, A-3059, Sigma), 7.4e-4; pH 7.6. MOPS-buffered Ringer's contained (mM): NaCl, 58; KCl, 2.5; $MgCl_2$, 1; $CaCl_2$, 1.5; HEPES, 5; EDTA, 0.02, glucose, 10; bovine serum albumin, 7.4e-4; MOPS, 55; pH 7.6.

Electrical recordings

Shredded pieces of dark-adapted retina were placed in a recording chamber under infrared light and perfused continuously with Ringer's solution, MOPS-buffered Ringer's or Ringer's solution containing bicarbonate at room temperature, 19–22°C. Photocurrent responses to flashes were recorded from single rods using the suction electrode technique with outer segment inside (ROS-in) the pipette, except for a few preliminary salamander experiments in Ringer's, in which the inner segment was in the pipette (Baylor et al., 1979a; Makino et al., 2019). The pipette was filled with Ringer's or with MOPS-buffered Ringer's, pH 7.6, without albumin. Recordings were made with a current-to-voltage converter (Axopatch 200A, Axon Instruments, Foster City, CA), low-pass filtered at 20 Hz (−3 dB) with an 8-pole Bessel filter (Frequency Devices, Haverhill, MA) and digitized online at 400 Hz (Patchmaster v2x53, Heka, Holliston, MA). Traces were not adjusted for the delay introduced by low-pass filtering except in Figures 1C–F, where the recorded traces were offset by −21 ms. The recordings shown in the figures were subjected to additional digital filtering at 6.5 Hz (Igor Pro v7.02, Wavemetrics, Inc., Lake Oswego, OR). Flash duration for full field flashes was 21–22 ms. Salamander retinas contain two spectral types of rods, green-sensitive rods and blue-sensitive rods. Spectral type was determined by comparing the response amplitudes to flashes of similar intensity at 435 nm and 500 nm. All results were from green-sensitive rods.

To explore how location of the photoisomerization within the ROS affected the photon response, we passed flashes at 500 nm through one of two slit configurations. In one set of experiments, a slit that was 4 μm in length and less than 1 μm in width at the plane of the preparation was oriented parallel to the long axis of the ROS and located halfway between base and tip either at the edge of the ROS or at its center (Figure 1, inset). In a second set of experiments, the slit was positioned perpendicular to the ROS at various distances from the inner segment (Figure 2, inset; Figure 3, inset). Flash duration was 1–1.5 ms for both slit configurations. Flash response kinetics were determined for responses whose amplitudes were less than 0.25 of the maximum for full field flashes and less than 0.15 of the maximum for slit experiments.

Two concentrations of bicarbonate were tested. For the initial experiments with the 50 mM concentration, HCO_3^- replaced an equimolar amount of MOPS in the MOPS-buffered Ringer's. In later experiments with the 30 mM concentration, HCO_3^- replaced Cl^- in the Ringer's that did not contain MOPS. The solutions were not bubbled with O_2/CO_2 but were kept in covered reservoirs. Nevertheless, pH sometimes changed over a time scale of hours, so pH was measured after each recording session. A working range of 7.5 to 7.8 was deemed acceptable. Bath perfusion with Ringer's containing bicarbonate prompted dark current to change over the subsequent 10 to 15 min and responses were typically measured more than 20 min after the switch.

Biophysical space-resolved model

The fully space-resolved model of phototransduction along with the parameter values used to simulate the SPR in rods with incisures was described in (Bisegna et al., 2008; Caruso et al., 2010, 2020). Some parameters were adjusted in the present study for the effects of bicarbonate or for the structural differences in salamander and toad rods (see Supplementary Tables S1, S2). By rigorously incorporating the mathematical theories of homogenization and concentration of capacity, phototransduction in the ROS was modeled by a novel system of diffusion equations whose coefficients expressed the effects of the ROS's small scale geometries (e.g., interdiskal and diskal thicknesses) which enabled the domain geometry, itself, to become greatly simplified for numerical simulation: the ROS interior volume became a cylinder, the outer shell became a cylindrical boundary, the disk where photoisomerization occurred became a horizontal cross-section, and the incisures became vertical cross-sections (i.e., rectangles) with one for each incisure. A finite element formulation of the homogenized model was used for the numerical simulations. In particular, the activated disk was discretized into triangular elements (three nodes for each triangle), the interior volume into prismatic elements with triangular bases (six nodes for each prism) and the outer shell and the incisures into rectangular elements (four nodes for each rectangle), which coincided with the faces of the prisms in the interior volume lying on these surfaces. Bilinear shape functions for the rectangles and prisms and linear shape functions for the triangles were used for interpolating the nodal unknowns inside the discretization elements. The standard iso-parametric

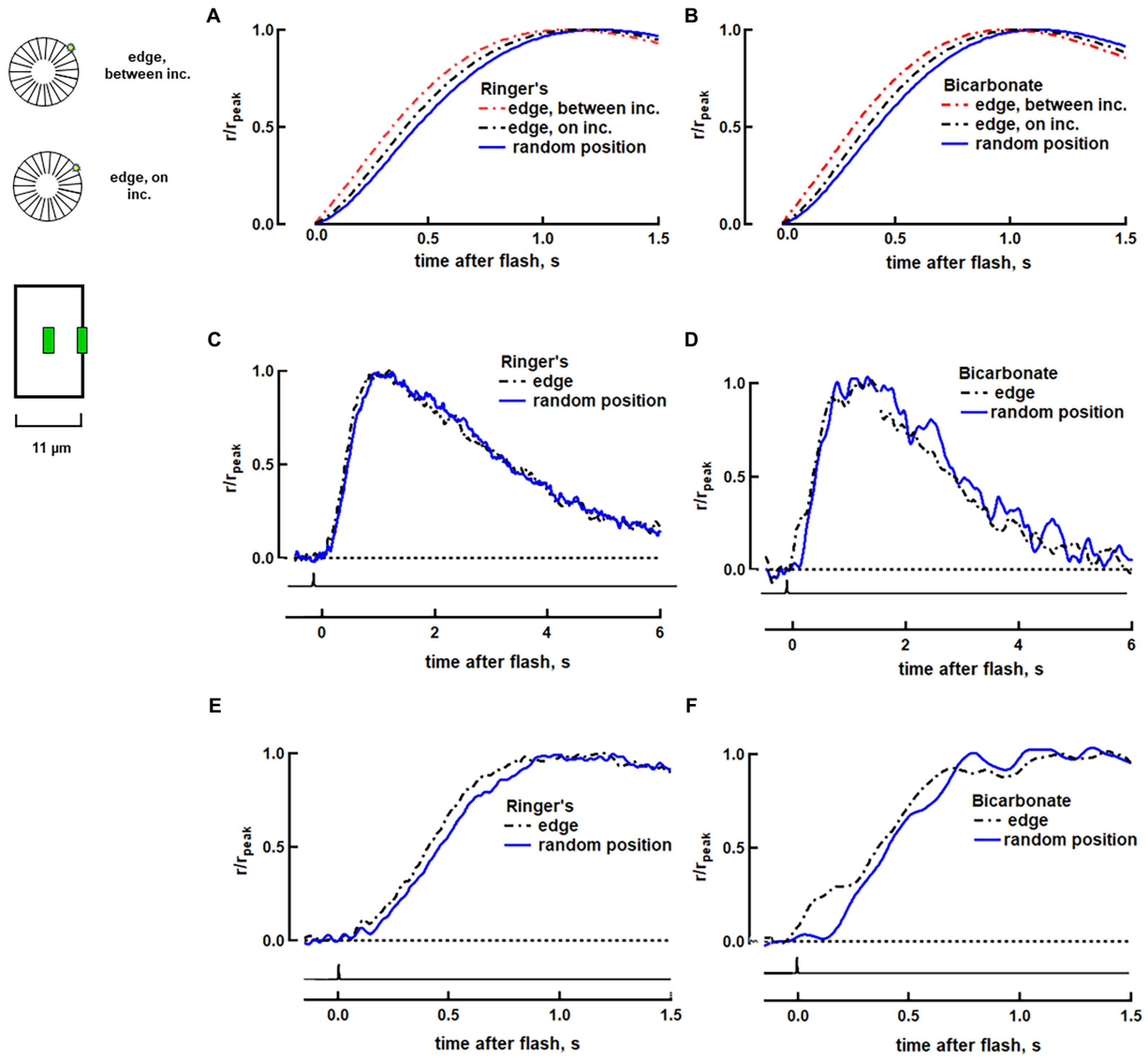

FIGURE 1
Faster rising phase with photoisomerization at the disk edge in a salamander rod. **(A)** Variability arising from R* position on a disk surface predicted by a biophysical model for rod phototransduction in Ringer's. The three traces show the response normalized to peak current for R* located: at random radial positions (averaged), at the disk rim between incisures or at the disk rim adjacent to an incisure. The simulations were deterministic with the spread of transducin/PDE activation across the disk following the diffusion of heat on a surface and with R* and transducin/PDE activities shutting off over exponential time courses. The simulations did not fully reproduce the effective time; although the model incorporated diffusional delays, it did not include processing times, e.g., for the creation of R*, T* and PDE* or for the CNG channel to respond to the fall in cGMP. **(B)** Simulations in bicarbonate. Guanylate cyclase activity at high Ca^{2+} was increased by 7% and activity at low Ca^{2+} was increased by 100% to produce the 13% increase in dark current and the 16.5% reduction of time constant, τ, that was observed experimentally with bicarbonate (See full list of parameters in Supplementary Table S1). Responses to 25 to 70 dim flash trials were averaged and the mean was then computed for 11 rods in Ringer's **(C,E)** and for 9 rods in 30mM bicarbonate **(D,F)**. Traces were corrected for the 21ms delay introduced by low pass filtering. Inset: Upper, visualization of photoisomerization position between and on incisures. OS represents in horizontal section. Lower, for single cell recordings, flashes were presented as a thin slit (green) centered along the length of the ROS and positioned either in the middle of the ROS or at an edge.

map was employed for computation and for evaluating the mass and stiffness matrices relevant to the discretized problem. Finally, the Wilson-theta method, a finite-difference scheme that requires an iterative procedure due to the presence of nonlinear forcing terms in the model, was adopted for the time integration.

The formulation was implemented in MATLAB in a very general manner, allowing for: deterministic or stochastic simulations, single or multiple activations, the presence of incisures of any number and size, and the testing of different hypotheses concerning activation biochemistry and cascade components. Disk diameter was set to 11 µm for salamander, the approximate size of the rods that were recorded. For bicarbonate simulations, the guanylate cyclase minimum rate of cGMP synthesis at high [Ca^{2+}] was raised by 13% and maximal rate at

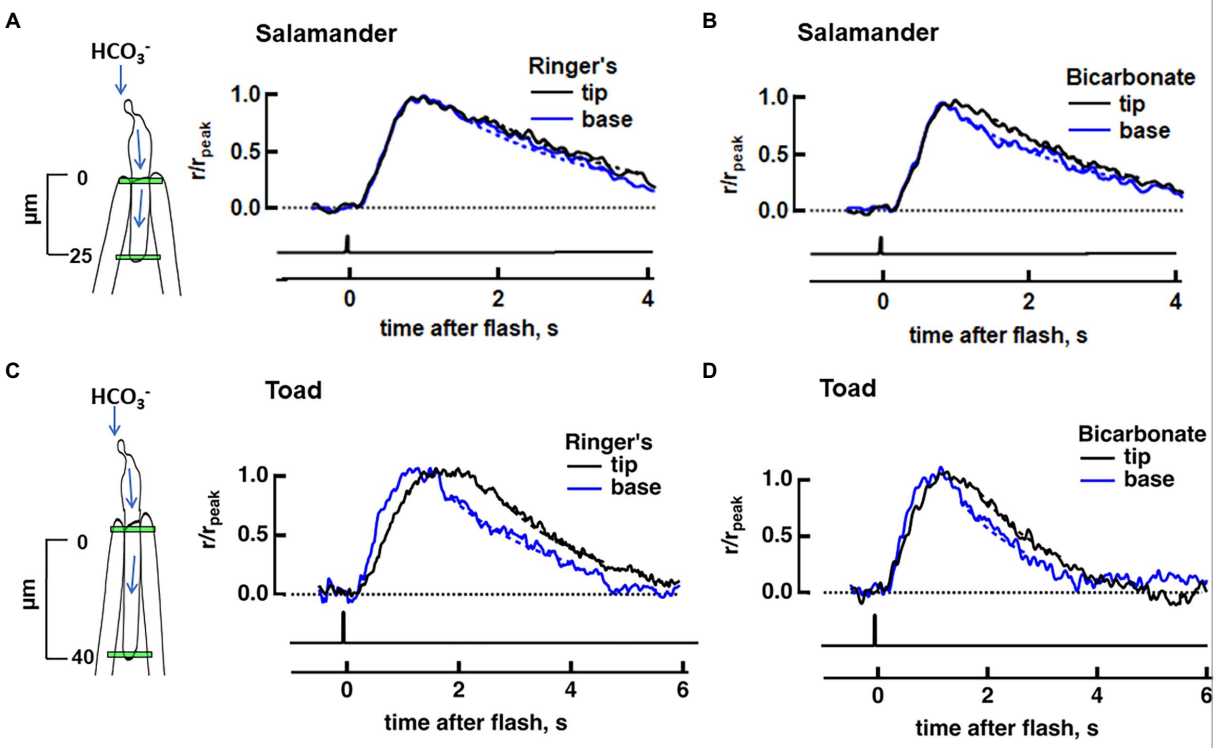

FIGURE 2
Effect of bicarbonate on the axial difference in SPR between base and tip in salamander and toad rods. Dim flash responses were normalized to their respective peak amplitudes. Dashed lines depict the exponential fits of the recovery phase. **(A)** No base vs. tip difference in the normalized, averaged dim flash responses in Ringer's for eight salamander rods (4 cells treated with 30mM bicarbonate and 4 cells treated with 50mM bicarbonate). **(B)** Dim flash response at the base was faster than that at the tip during perfusion with bicarbonate for the same cells as in **(A)**. **(C)** Faster average dim flash response at the base, compared to the tip, in 11 toad rods in Ringer's (9 cells treated with 30 mM bicarbonate and 2 cells treated with 50 mM bicarbonate). **(D)** Attenuated axial differences between base and tip photoresponse kinetics in bicarbonate for the same cells as in **(C)**. Inset: locations of slit illumination (green) during ROS-in recording. Blue arrows show the path for the intracellular diffusion of bicarbonate; it enters the rod at the synapse and moves to the outer segment, where it is extruded.

low [Ca^{2+}] was raised by 100% to increase dark current by 13.0% and to reduce the time constant for the exponential recovery of the photon response by 16.5%, to match observations from physiological recordings. To model experiments with the slit positioned at the edge of the ROS next to an incisure or halfway between two adjacent incisures, the simulations were deterministic in that the position of the photoisomerization was chosen and inactivation of R* was given by the solution of a continuous time Markov chain (Caruso et al., 2010). To model experiments with the slit in the middle of the ROS, 100 stochastic simulations were carried out, with the R* positioned randomly at different distances from the disk center, and an average of the obtained responses was then computed.

Experimental design and statistical analyses

Paired t-tests were used to assess whether a treatment or shift in slit position changed a flash response parameter (Excel version 2016, Microsoft, Redmond, WA). In cases for which there were few cells, statistical evaluations were made with a Wilcoxon signed-rank test for matched pairs performed by Social Science Statistics (n.d.).[1] For this test, if $5 \leq n \leq 10$, the *Z*-value was used to calculate the precise value for *p*.

Curve fittings were carried out using Igor Pro. Linear fits of the rising phases of dim flash responses were calculated from 20 to 60% r_{peak}, using cells for which $r_{Pearson}^2 > 0.8$, to characterize the rising phase trajectory. Dim flash response recovery was analyzed by fitting an exponential function, $r = A^*\exp(-t/\tau)$, to the falling phase from 80 to 20% r_{peak}. The per cent change was calculated for each cell individually as 100 x parameter for condition 1 divided by the parameter for condition 2, and then averaged across cells. For the effects of bicarbonate, bicarbonate treatment was condition 1 and the average of pretreatment with Ringer's and Ringer's wash was condition 2.

Single photon responses were stimulated with 30–100 dim flashes. Responses to single photoisomerizations were interspersed randomly amongst failures and multiple photoisomerizations.

1 https://www.socscistatistics.com/tests/signedranks/default.aspx

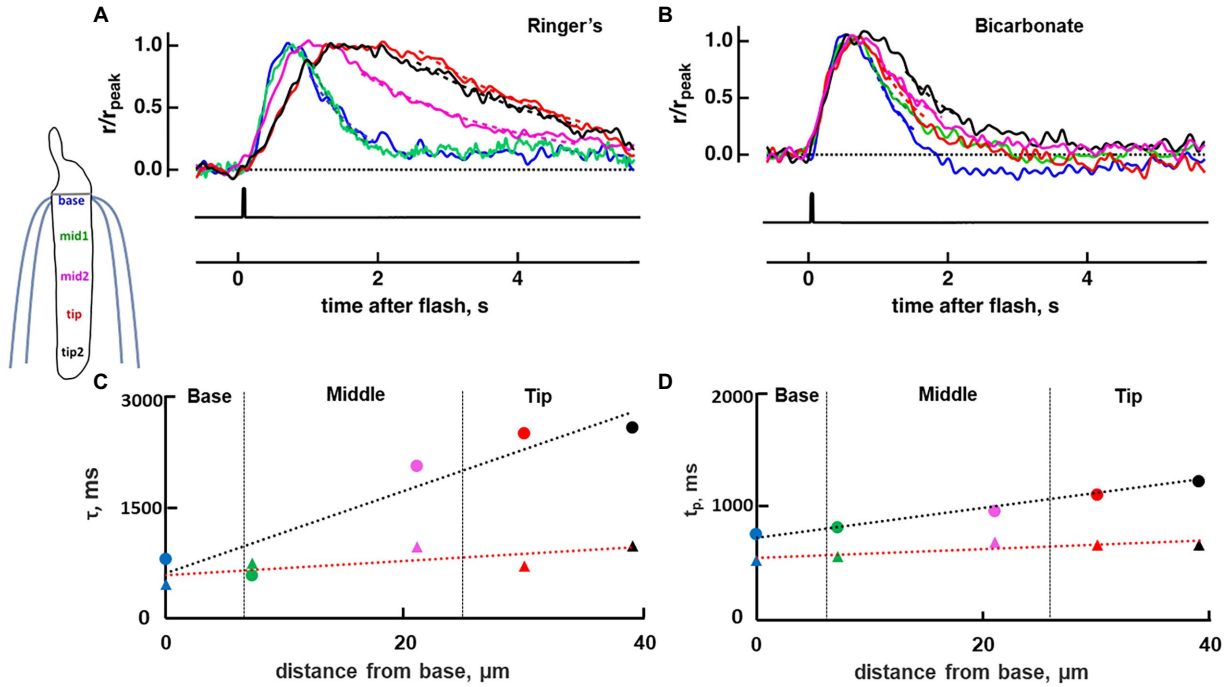

FIGURE 3
Diminished base to tip gradient in rising and recovery phase of a toad rod upon bath perfusion with 30mM bicarbonate. Normalized dim flash response recorded in Ringer's **(A)**, average of pretreatment and washed responses, or in bicarbonate **(B)** with a slit that was positioned at one of five locations along the ROS. Dashed lines show exponential fits to the recovery phases of the responses, from 80 to 20% r_{peak}. **(C)** The profile of the response recovery time constants (τ) from the cell in **(A,B)**. Ringer's (circles): slope=56.8ms/μm, $r_{Pearson}$ =0.94, p =0.016; bicarbonate (triangles): slope=9.858ms/μm, $r_{Pearson}n$ =0.74 not significant. Dashed lines represent the linear regression, black for Ringer's and red for bicarbonate. **(D)** The profile of the time to peak (t_p), same labeling as in **(C)**. Ringer's: slope=17.10ms/μm, $r_{Pearson}$ =0.99, p =0.002; bicarbonate: slope=8.66ms/μm, $r_{Pearson}$ =0.98, p =0.002; Colors in panels **(A–D)** correspond to positions shown in the inset. Inset: location of slit illumination during ROS-in recording.

Responses from individual trials were fitted with a seventh-degree polynomial equation constructed from the mean response of that rod and the obtained histogram (bin width = 0.1 pA) was fitted with the equation (Baylor et al., 1979b):

$$p(r|\sigma_0,m,\sigma_1,a)=\sum_{k=0}^{\infty}\frac{e^{-m}m^k}{k!}\frac{1}{\left(2\pi\left(\sigma_0^2+k\sigma_1^2\right)\right)^{0.5}}\exp\left(-\frac{(r-ka)^2}{2\left(\sigma_0^2+k\sigma_1^2\right)}\right) \quad (1)$$

where $p(r|\sigma_0,m,\sigma_1,a)$ is the probability density of the response with amplitude in the range r to r + dr when conditioned on fixed parameter values (σ_0, m, σ_1, and a), k is the specified number of photoisomerizations per trial, m is the mean number of photoisomerizations per trial, a is the mean SPR amplitude, σ_0 is variance of background noise and σ_1 is response variance. Responses for different trials were taken as independent. Goodness of fit was evaluated with a Kolmogorov–Smirnov (KS) test (DeGroot, 1986) on the observed, experimental data when response amplitudes were drawn from eq. 1 and the parameters σ_0, m, σ_1, a were fixed at the values obtained from Igor Pro. We note that to sample eq. 1, it was sufficient to sample the joint distribution for the number of detected photons and response amplitude, first drawing k according to its marginal Poisson distribution and then drawing a response amplitude conditional on k according to its corresponding normal distribution (Robert and Casella, 2004). Then the marginal value of the response amplitude could be taken. A $p < 0.05$ was considered to indicate a statistically significant disagreement between the data and the predicted distribution of eq. 1. Since 30–100 trials may have been too few for convergence of the KS statistic to its asymptotic distribution, p-values were estimated by a Monte-Carlo scheme: under each set of experimental conditions, the corresponding density from eq. 1 was independently sampled as many times as there were experimental data points. This resulted in a sample of the KS statistic by then computing the maximum absolute difference between the obtained sample distribution function and the theoretical distribution function fitted by Igor Pro when evaluated across the observed experimental data points. This process was independently repeated 100,000 times resulting in 100,000 Monte-Carlo KS samples. The value of p was estimated by the fraction of samples with KS values at or worse than the value presented by the data. This procedure was independently

performed 3 times to give 3 independent estimates of the *p*-values (see Supplementary Table S3). In computations, the infinite sum in eq. 1 was truncated to ensure an error term <1e-6.

Results

Faster SPR time to peak with photoisomerization at the disk edge

Our fully space-resolved biophysical model of rod phototransduction was used to predict how locality of rhodopsin photoisomerization on the surface of a salamander disk would affect SPR kinetics. SPRs were simulated in a rod that was 11 μm in diameter, with and without bicarbonate (see parameters in Supplementary Table S1). Twenty-three radial incisures were distributed evenly around the perimeter of each of its disks (Figure 1, upper inset). The middle position of the slit on the ROS was simulated with 100 stochastic trials, in which the photoisomerization was positioned at random distances from the disk rim. Positioning the slit on the ROS edge was simulated with two trials capturing the extreme possibilities, one for a photoisomerization bordering an incisure and one for a photoisomerization located halfway between neighboring incisures. It is emphasized that other than the location of the photoisomerization and changes associated with the presence of bicarbonate, all other parameters for ROS structure and for the cascade were invariant in these simulations. For both photoisomerization locations at the ROS edge, next to and between incisures, the responses were faster than the average response for random photoisomerization positions in terms of slope of the rising phase (by 10–14%) and time to peak of the response (by 60–70 ms) (Figure 1A). Given that bicarbonate raises cGMP levels in darkness and accelerates flash response kinetics by stimulating membrane guanylate cyclase activity (Duda et al., 2015), we wanted to explore how it would impact SPR differences due to radial position of the photoisomerization. As a first pass, bicarbonate concentration was assumed to be radially homogeneous. Simulations yielded SPR recovery time constants that were faster in bicarbonate than in Ringer's, but similar for edge and random positions. In addition, the differences in times to peak between edge and random positions were preserved in bicarbonate (Figure 1B).

Experimental determinations were made by recording from large salamander rods whose outer segments were 9.5–12 μm in diameter. In previous studies, 25 mM or 50 mM bicarbonate replaced equimolar amounts of MOPS and Cl^- concentrations were low (Duda et al., 2015; Makino et al., 2019). To more closely approximate physiological levels of Cl^- in this study, the Ringer's solution was prepared without MOPS, and bicarbonate when present, substituted for an equimolar amount of Cl^-. In control, ROS-in experiments carried out in the absence of bicarbonate, we observed no differences with full field flash stimulation in: dark current, sensitivity to flashes, or dim flash kinetics upon switching between Ringer's solution and "Ringer's" containing 50 mM MOPS in place of an equimolar amount of Cl^- ($n = 3$, results not shown). In 4 out of 4 rods attached to a piece of tissue, dark current increased from 25 ± 3 pA to 28 ± 3 pA, integration time of the dim flash response decreased from 2,230 ± 260 ms to 1,800 ± 110 ms indicative of a faster flash response recovery, and $i_{0.5}$ values increased from 10 ± 3 photons/μm^2 to 12 ± 4 photons/μm^2 indicating no change in relative sensitivity to flashes, upon treatment with 30 mM bicarbonate (MOPS was absent from both solutions). All bicarbonate-induced changes were reversible. Time to peak of the dim flash response was not altered. These effects were comparable to results obtained with 50 mM bicarbonate in experiments with MOPS-buffered Ringer's (Makino et al., 2019), suggesting that for salamander rods, bicarbonate exerted a more potent effect in normal Ringer's (Table 1). All subsequent recordings of salamander rods were made with Ringer's lacking MOPS.

A separate group of rods was then stimulated with slit illumination. The ROS, or in preliminary experiments, the inner segment, was pulled into a suction pipette and a tiny slit of light was presented side-on as a dim flash, the response to which had the same kinetics as the SPR. Placement of the slit near the edge of the ROS (Figure 1, lower inset) gave rise to photoisomerizations near the rim of the disk. With the slit in the middle of the ROS, photoisomerizations occurred at random radial distances from the disk rim. It was not possible to control proximity of the photoisomerization to an incisure at either slit location. Somewhat brighter flashes were often required with the slit at the edge, due to the reduced pathlength and because a portion of the slit was positioned past the boundary of the ROS to ensure that any photoisomerizations would be as close to the disk rim as possible. Responses peaked earlier for dim flashes at the disk edge (e.g., Figures 1C,E): t_p edge = 880 ± 80 ms, t_p middle = 1,010 ± 100 ms (mean ± SEM, $n = 11$, $p = 0.002$ from a paired t-test). No differences in response recovery time constant, τ, nor in integration time T_i, the integral of the response divided by its peak amplitude, were detected (Figure 1C), which meant that radial location of photoisomerization did not noticeably affect the later phase of response recovery. These results were consistent with our modeling that showed a slightly faster average SPR for a photoisomerization at the edge of the disk compared to that for random radial positions (Figure 1A) and a larger discrepancy with the SPR for a photoisomerization in the disk center (see Caruso et al., 2020).

The differences between the responses to photoisomerizations at the disk edge vs. random locations were preserved upon treatment with 30 mM bicarbonate. Time to peak remained 16 ± 2% faster at the edge: t_p edge = 870 ± 70 ms, t_p middle = 1,020 ± 100 ms ($p = 0.001$). Rising phase slope (e.g., Figures 1D,F) and integration time remained similar for both slit positions (Figure 1D); the main difference was in the shorter delay of onset for the responses at the edge. It was not possible to assess differences in SPR amplitude at the two slit positions in the presence or absence of bicarbonate, because of excessive drift in

TABLE 1 Changes in photoresponse parameters upon bath perfusion with bicarbonate.

Species, Ringer's vs. Bicarbonate	r_{max}	T_i	t_p	$i_{0.5}$	n
Salamander, Ringer's vs. 30 mM bicarbonate	1.12 ± 0.04, p = 0.001	0.79 ± 0.04, p = 0.043	1.0 ± 0.1, ns	1.3 ± 0.1, p = 0.005	4
Salamander, 55 mM MOPS -buffered Ringer's vs. 50 mM bicarbonate[a]	1.11 ± 0.02, p = 0.00013, n = 12	0.81 ± 0.06, p = 0.008, n = 12	1.00 ± 0.05, ns, n = 6	1.2 ± 0.1, p = 0.033, n = 10	–
Toad, Ringer's vs. 30 mM bicarbonate	1.08 ± 0.02, p = 0.049	0.81 ± 0.05, p = 0.014	1.01 ± 0.03, ns	1.1 ± 0.1, ns	7
Toad, 55 mM MOPS- buffered Ringer's vs. 50 mM bicarbonate	1.30 ± 0.06, p = 0.003	0.60 ± 0.08, p = 0.043	1.1 ± 0.1, ns	1.7 ± 0.2, p = 0.040	5

All cells were recorded with ROS-in and stimulated with full field flashes. Changes are expressed as ratios of the parameter in bicarbonate divided by that in Ringer's or MOPS-buffered Ringer's. r_{max}, saturated photoresponse amplitude which provided a measure of dark current; T_i, integration time of the dim flash response; t_p, time to peak of the dim flash response; $i_{0.5}$, flash strength at 500 nm producing a half-maximal flash response; n, number of cells. For the results of the present study, reversibility of bicarbonate treatment was not established for every parameter of every rod. Values given as mean ± SEM, value of p. P-values were from paired t-tests between parameter values given in the text (not ratios) in Ringer's and bicarbonate. ns, not significant. [a]from Makino et al. (2019).

the baseline that likely arose from noise in the phototransduction cascade (Baylor et al., 1980; Vu et al., 1997). Our modeling and experimental results were thus consistent. We conclude that radial position of the photoisomerization introduced some variability to the SPR in large salamander rods and that variability was unchanged by bicarbonate.

Axial SPR gradient generated by bicarbonate in salamander rods

In order to quantify the effect of an axial gradient of bicarbonate in the outer segment on SPR variability, we recorded flash responses from single salamander rods with ROS inside the pipette so that the synapse could access bicarbonate when it was added to the bath. First, we stimulated the rod in the absence of bicarbonate with dim flashes that passed through a tiny slit positioned either near the base or near the tip of the ROS in order to check for axial invariance of SPR kinetics. The distance between the two locations was ~25 μm. The average of each set of photoresponses was normalized to its respective peak, for comparison. Usually, a higher flash strength was required for the base, probably because a portion of the slit overlapped with inner segment and because some fraction of the light was scattered by the curvature at the end of the polished suction pipette. To check that the test flashes were dim enough and fell within the linear range, responses to at least two flash strengths were recorded at each position. Responses to the two weakest flash strengths varied only in amplitude, confirming linearity (e.g., Supplementary Figure S1) but as an extra precaution, further analysis was restricted to the responses to the dimmer of the two flashes. The largest mean ensemble response in any of the salamander rods for this dim slit stimulation was 0.8 pA.

No significant differences in kinetics were detected between dim flash responses at the two axial locations as assessed by time to peak or integration time in the absence of bicarbonate (Figure 2A). Rods were then perfused with bicarbonate for 20–30 min to allow conditions to reach a steady state, before we resumed the recording. An axial gradient of bicarbonate would accelerate responses at the base of the ROS more than at the tip. In fact, recovery did kick in sooner at the base with bicarbonate (Figure 2B) in every rod tested. For the analysis, we combined results from 4 cells treated with 30 mM bicarbonate and 4 cells treated with 50 mM bicarbonate, causing integration time to be 26 ± 5% shorter at the base: T_i base = 1,746 ± 275 ms, T_i tip = 2,241 ± 337 ms (p = 0.0058, Wilcoxon signed rank test for matched pairs). These experiments confirmed that there was an axial gradient of bicarbonate concentration in salamander ROSs with a higher concentration at the base, that gave rise to a faster SPR recovery at the base, compared to the tip.

Attenuated axial differences in the SPR with bicarbonate in toad rods

We expected to observe even more axial variability in a toad rod since its ROS is twice as long and should support a more pronounced base to tip difference in bicarbonate. To ensure bicarbonate uptake, rods were recorded from pieces of retina. We first carried out background experiments on 5 toad rods perfused with MOPS-Ringer's and stimulated with full field flashes to characterize the changes induced by bicarbonate under our recording conditions. Fifty mM bicarbonate increased dark current from 9.0 ± 0.4 pA before treatment to 11.0 ± 0.6 pA, reduced T_i from 2,620 ± 140 ms to 1,530 ± 80 ms, and lowered relative sensitivity with $i_{0.5}$ changing from 89 ± 8 photons/μm^2 to 163 ± 15 photons/μm^2. Our toad rod responses to bicarbonate were consistent with those of salamander rods above and in previous studies (Duda et al., 2015; Makino et al., 2019), making toad rods suitable for further investigation of the effect of bicarbonate on SPR variability. A previous study reported a twofold reduction in time to peak and a fourfold decrease in flash sensitivity in 22 mM bicarbonate compared to HEPES-buffered Ringer's (Lamb et al., 1981). Our results with higher concentrations of bicarbonate were less striking, perhaps due to differences in ion concentrations in the Ringer's and to our use of MOPS. Since

bicarbonate was more effective on salamander rods during perfusions with Ringer's lacking the MOPS, similar experiments without MOPS were carried out on an additional 7 toad rods stimulated with full field flashes. Thirty mM bicarbonate increased dark current from 10.1 ± 0.6 pA in Ringer's to 11.1 ± 0.7 pA and reduced the integration time of the dim flash response from 1,900 ± 70 ms in Ringer's to 1,570 ± 110 ms, but did not change time to peak (Figures 4A,B), similar to results in salamander. Relative sensitivity was not changed by bicarbonate (Figure 4C), nor was flash sensitivity, defined as dim flash response amplitude divided by flash strength. Collected results from all of the salamander and toad rods upon treatment with bicarbonate in Ringer's with and without MOPS, are summarized in Table 1.

For direct comparison to the results in salamander, slit experiments on toad rods were carried out in Ringer's lacking MOPS. In the absence of bicarbonate, toad rods exhibit a natural difference in photon responses elicited at the base of the ROS compared to those elicited at the tip (Baylor et al., 1979a; Lamb et al., 1981; Schnapf, 1983; Mazzolini et al., 2015) that is not present in salamander rods (Figures 2A,C). Upon flashing 11 toad rods with narrow slits at two axial locations separated by ~40 μm, we also observed faster response kinetics at the base. Time to peak was shorter: 1,230 ± 140 ms at the base, 1,540 ± 130 ms at the tip ($p = 0.005$), recovery time constant was faster: 1.4 ± 0.2 s at the base, 2.7 ± 0.3 s at the tip ($n = 10$, $p = 0.009$), and integration time was briefer: 2,130 ± 210 ms at the base, 2,730 ± 170 ms at the tip ($n = 10$, $p = 0.023$). Acceleration of the time to peak of the response upon perfusion with bicarbonate was significant at both base (1,230 ± 140 ms in Ringer's, 1070 ± 150 ms in bicarbonate, $n = 11$, $p = 0.043$) and tip (1,540 ± 130 ms in Ringer's, 1,180 ± 130 ms in bicarbonate, $n = 11$, $p = 0.003$), but in marked contrast to salamander rods, the acceleration in toad rods was greater at the tip ($n = 11$, $p = 0.019$) so that the times to peak and the response recoveries at the two axial positions were no longer different, $p = 0.116$ (Figures 2C,D). The disparity was investigated in greater depth by linear regression of the dim flash response from 20 to 60% r_{peak} to ascertain the slope of the rising phase. There was a steeper slope for the rising phase (1.0 ± 0.1 pA/ms in Ringer's, 1.3 ± 0.2 pA/ms in bicarbonate, $n = 7$, $p = 0.025$) at the tip of the toad ROS, upon perfusion with bicarbonate. At the base, the slope of the rising phase was not changed upon perfusion with bicarbonate (2.4 ± 0.4 pA/ms in Ringer's, 2.0 ± 0.3 pA/ms in bicarbonate, $n = 7$, $p = 0.296$).

To map the axial gradient in rising and recovery phases, dim flash responses were recorded at 5 ROS locations in 6 toad rods. Results from one of these cells are shown in Figures 3, 5. For the analysis of all 6 rods, we combined results from 3 cells treated with 30 mM bicarbonate and 3 cells treated with 50 mM bicarbonate, because the parameters did not differ between the two groups. The τ for response recovery increased linearly with distance from the base (slope = 53 ± 23 ms/μm), but bicarbonate appeared to flatten the relationship (slope = 15 ± 13 ms/μm, $p = 0.079$) (e.g., Figure 3C). Time to peak in Ringer's also increased linearly with distance from the base with a slope of 14.2 ± 0.9 ms/μm, but the slope was reduced 5.7-fold with bicarbonate, to 2.6 ± 2.1 ms/μm ($p = 0.002$) (e.g., Figure 3D). These results showed again that bicarbonate made the SPR more homogeneous by preferentially making responses at the tip faster (see Discussion).

Axial differences in SPR size in toad rods were assessed by plotting the amplitudes of dim flash responses in frequency histograms and fitting with a probability density function renormalized for frequency (see Materials and methods). In the absence of bicarbonate, the SPR at the base was 24 ± 7% larger than that from the tip (e.g., Figures 6A,B): base 0.88 ± 0.08 pA, tip 0.68 ± 0.08 pA ($n = 6$, $p = 0.042$), consistent with reports by others (Baylor et al., 1979a; Lamb et al., 1981; Schnapf, 1983; Mazzolini et al., 2015). With 30 mM bicarbonate, SPR amplitude between the base and tip of the ROS no longer differed (e.g., Figures 6C,D): base 0.61 ± 0.06 pA, tip 0.67 ± 0.06 pA ($n = 10$, $p = 0.175$). These bicarbonate-induced changes in toad rods contradicted our expectations for accentuated differences in the SPRs at the base and tip, due to an axial gradient for bicarbonate that would stimulate higher rates of cGMP synthesis at the base. Instead of making SPRs at the base and tip more disparate, bicarbonate functioned as a neuromodulator that *reduced* the axial variability of photon responses in toad rods.

Modeling the base versus tip differences in toad rod SPRs

The basis for the axial differences in SPR in toad rods in the absence of bicarbonate is not known. As a working hypothesis, we hypothesized that there might be higher transducin levels (Sokolov et al., 2002) and lower Ca^{2+} levels at the base (Li et al., 2020) than at the tip. We then used the fully space-resolved model to test whether SPRs at the base and tip would match more closely upon the addition of bicarbonate. Experimental determinations of axial concentration gradients of bicarbonate or cascade proteins in toad rods are not yet available, nor is there information on the axial diffusion of these substances. So, simulations were carried out in two theoretical rods for which second messengers and cascade proteins were homogeneously distributed throughout their ROSs (Figure 7). Rod-b was assigned concentrations of transducin, Ca^{2+} and bicarbonate that might be characteristic of the base and rod-t was assigned concentrations characteristic of the tip of a normal toad rod. Some other parameters for amphibian rods were adjusted within their reported ranges to obtain a closer fit to the traces in Figure 2C (Supplementary Table S2).

The effect of a lower transducin concentration at the tip was modeled in rod-t by decreasing the rate of transducin activation by R* by 48%. Higher Ca^{2+} at the tip could arise from Ca^{2+} release from disks, but we modeled it in rod-t as a 56% increase in the fraction of dark current carried by Ca^{2+}, resulting in a 60% increase in the total Ca^{2+} in darkness. These changes were made so that the response in rod-b would have a rising slope that was 36.3% steeper, a time to peak that was 39.5% shorter, and a recovery time constant, τ, that was 307 ms faster compared to the responses in rod-t, for consistency with the base vs. tip differences in our toad rod recordings.

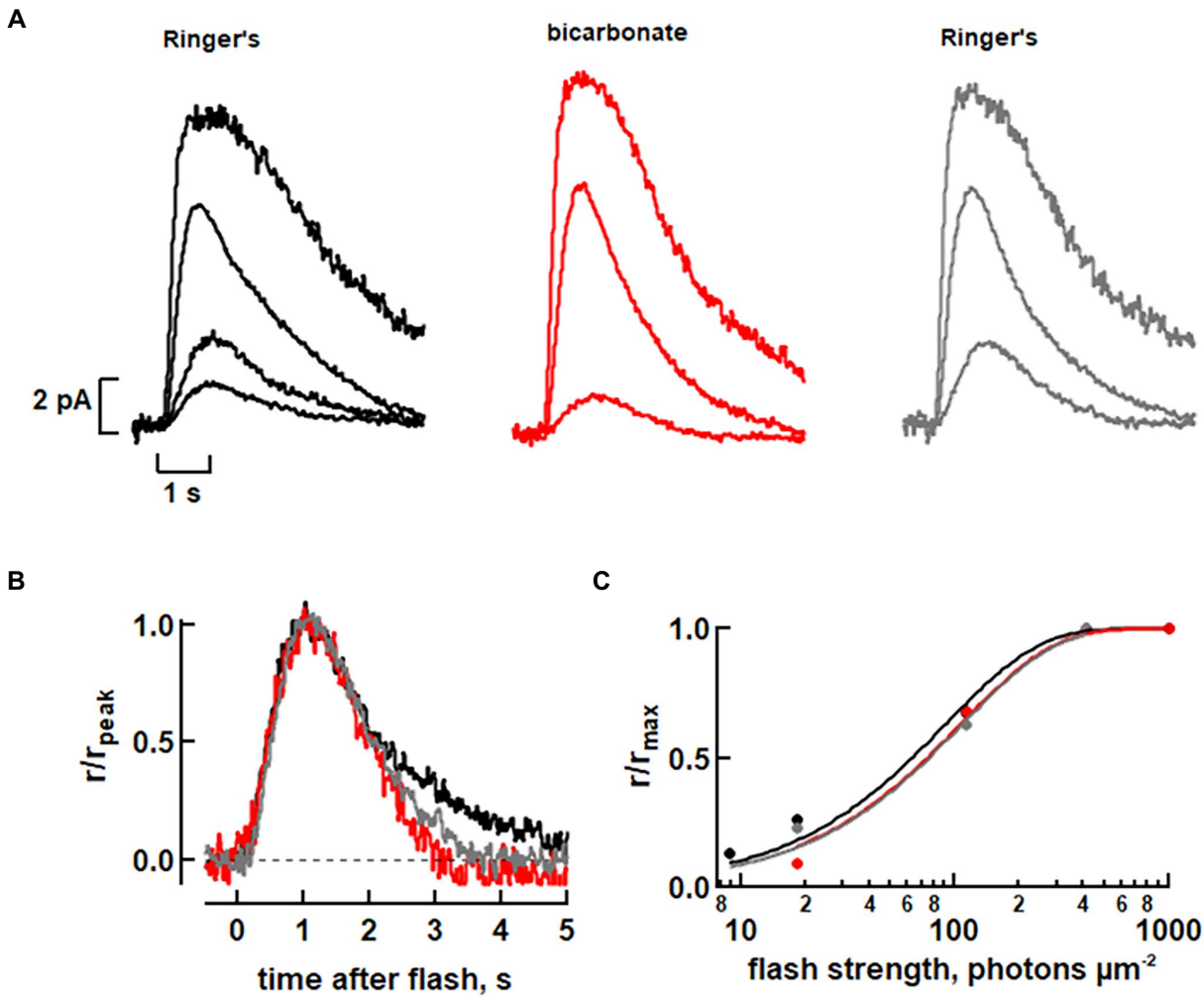

FIGURE 4
Faster flash response kinetics with 30mM bicarbonate in a toad rod. **(A)** Rod attached to a clump of retinal cells was recorded with its ROS inside the pipette and stimulated with full field flashes at 500nm. **(B)** Faster photon response recovery with bicarbonate. Dim flash responses from **A**, whose peak amplitudes were less than a fifth of the maximum, were scaled to their peak amplitudes. Integration time was ~19% less with bicarbonate. **(C)** Little change in relative sensitivity to flashes of the rod with bicarbonate. Results from **A** were fit with a saturating exponential function: $r/r_{max} = 1 - \exp(-ki)$ where k is a constant equal to $\ln(2)/i_{0.5}$ and $i_{0.5}$ is the flash strength eliciting a half-maximal response.

Taking into account that bicarbonate accelerates cGMP production and opens more channels, we increased the maximal rate of cGMP synthesis by 100% in rod-b. That change increased the dark current in rod-b by 8%. We assumed that the tip of a toad rod would have less bicarbonate than at the base, therefore we increased maximal rate of cGMP synthesis by 30% in rod-t. We also decreased by 25%, the fraction of dark current carried by Ca^{2+} with respect to Ringer's for rod-t on the grounds that Ca^{2+} release from disks would make a reduced relative contribution to the cytosolic Ca^{2+} levels. The net effect was to increase dark current in rod-t by 9%. Consistent with the effects of bicarbonate on flash responses at the base and tip of toad rods in our electrophysiological recordings, bicarbonate sped up the SPRs in both rod-b and in rod-t but in order to reduce the kinetic differences in the normalized responses between rod-b and rod-t that were observed experimentally, it was necessary to impose an additional change. In our modeling, we reduced the rate of transducin activation by R* in rod-b by 30% when bicarbonate was present. Then the difference in time to peak was half that in Ringer's and the difference in recovery time constant was reduced to 127 ms. The decrease in integration time with bicarbonate was 13% for rod-b and 16% for rod-t. Therefore, modeling suggested that bicarbonate could decrease SPR variability by attenuating the primary cascade at the base or by having the opposite effect at the tip in toad rods.

Discussion

Radial variability in the SPR of large diameter rods

Randomness in the site of rhodopsin photoisomerization on the disc surface could generate variability in the rising phase of the

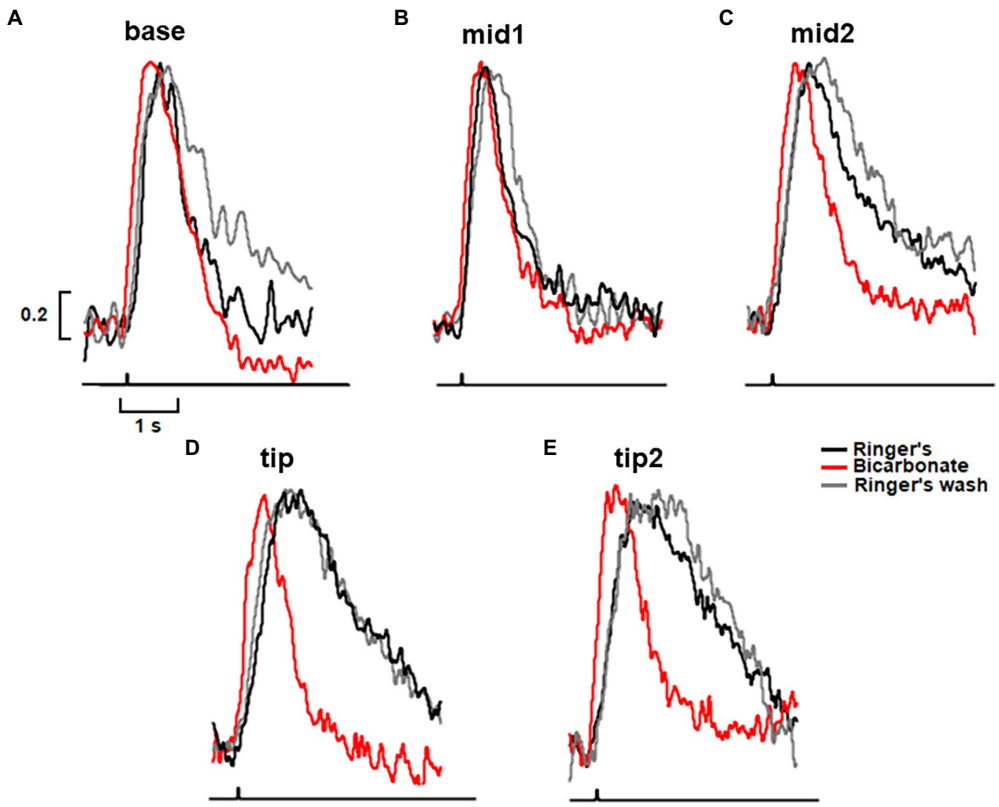

FIGURE 5
Greatest acceleration by bicarbonate of the rising and recovery phases of the dim flash response to flashes presented to the tip of the outer segment of a toad rod. **(A–E)** Traces from the same rod as in Figure 3. Dim flash responses were normalized to their peaks in Ringer's and in bicarbonate with the slit positioned along the ROS, as shown in the inset to Figure 3. For Ringer's: t_p(base)=740 ms, t_p(mid1)=750 ms, t_p(mid2)=820 ms, t_p(tip)=1130 ms, t_p(tip2)=1130 ms, τ(base)=-770 ms, τ(mid1)=848 ms, τ(mid2)=1670 ms, τ(tip)=2220 ms, τ(tip2)=2630 ms. For bicarbonate: t_p(base)=530ms, t_p(mid1)=560ms, t_p(mid2)=690ms, t_p(tip)=670ms, t_p(tip2)=670ms, τ(base)=460ms, τ(mid1)=750ms, τ(mid2)=960ms, τ(tip)=710ms, τ(tip2)=980ms. For Ringer's wash: t_p(base)=770ms, t_p(mid1)=880ms, t_p(mid2)=900ms, t_p(tip)=1,070ms, t_p(tip2)=1,430ms, τ(base)=1,270ms, τ(mid1)=820ms, τ(mid2)=1,720ms, τ(tip)=2,270ms, τ(tip2)=2,500ms. Each trace is an average of 30–50 trials.

SPR because photoisomerization at the edge of a disk initiates a local depletion of cGMP near the plasma membrane that closes CNG channels after a brief delay. In contrast, the local fall in cGMP following photoisomerization at the disk center takes more time to impact the CNG channels, because the fall in cGMP must spread radially before the disturbance reaches the channels in the plasma membrane. Moreover, the cGMP depletion dissipates axially and tends to spread around the circumference of the ROS, effecting a smaller change in cGMP levels in a more symmetric annulus at the plasma membrane. The CNG channel has a Hill coefficient > 1, so fewer channels close. In the present study, the fully space-resolved, mathematical model of rod phototransduction predicted that the SPR at the disk edge would manifest with a shorter delay and steeper rate of rise to a larger amplitude than the SPR in the middle of the disk (Figures 1A,B; see also Caruso et al., 2020). The disparity would be greatest for a photoisomerization at the disk edge occurring halfway between adjacent incisures.

Experimentally, no differences were detected in the dim flash responses elicited with slit illumination positioned either at the ROS edge or centered on the ROS of a toad rod (Lamb et al., 1981). However, disparities in SPR amplitude and kinetics arising from the radial position of the photoisomerization increase with ROS diameter (Caruso et al., 2020), so it was important to check whether variability might be present in salamander, for which ROS diameter can be twice as large as in toad. Another consideration was that previous modeling indicated that a radially symmetric array of incisures reduces SPR variability by promoting axial diffusion of cGMP and Ca^{2+} within the cytosol (Caruso et al., 2006, 2011, 2020; Bisegna et al., 2008), but in reality, the incisures in salamander rods follow tortuous paths, are of unequal lengths, and are not always evenly spaced around the ROS perimeter (Mariani, 1986). Asymmetric partitioning of the disk membrane surface would restrict lateral diffusion of membrane proteins and cause variability in the number of PDE activated. Here again, the effect could be more significant in larger diameter disks. In our experiments, we were able to elicit photoisomerizations at the disk edge, but we were not able to restrict photoisomerizations to the disk center. Therefore, we could only compare SPRs at the disk edge to the average SPR elicited at random distances from the disk center, a limitation that

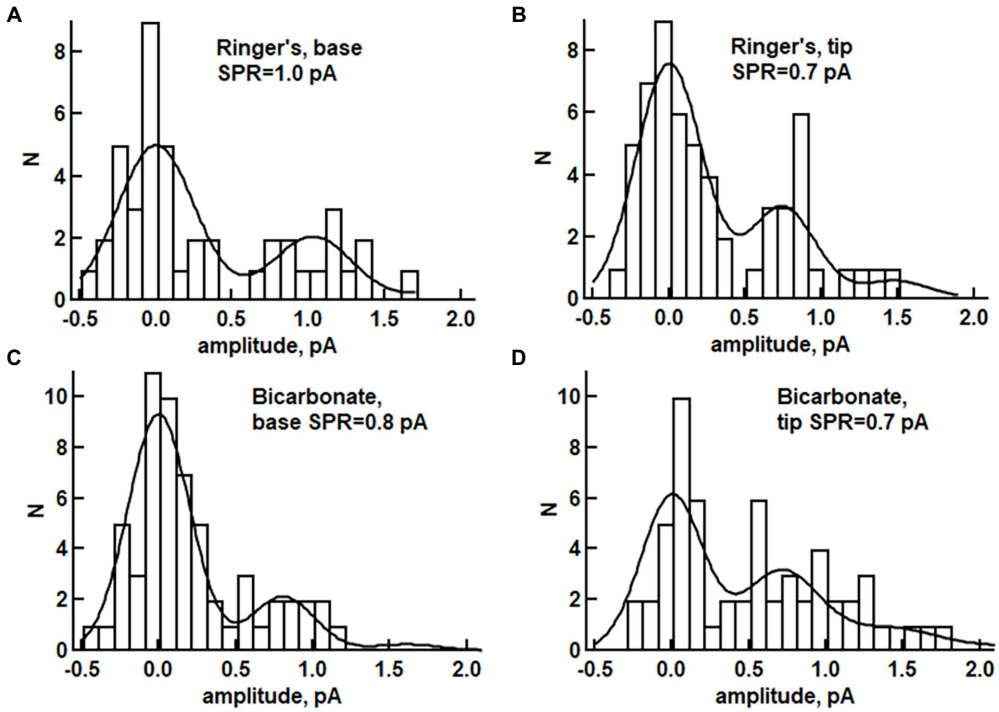

FIGURE 6
Histograms of response amplitudes for a toad rod exposed to dim flashes during perfusion without bicarbonate **(A,B)** or for a different rod perfused with 30mM bicarbonate **(C,D)**. Slit illumination was positioned either at the base of the ROS (n =48 for panel **A**, n =60 trials for panel **C**) or at the tip (n =61 for panel **B**, n =60 trials for panel **D**). The distributions were fitted with eq. 1 as described in Materials and methods, then assessed with a Kolmogorov–Smirnov significance test for goodness of fit (p-values for **A–D**: 0.097, 0.563, 0.917, 0.339). **(A)** p <0.05 was taken as evidence for statistically significant disagreement between the model prediction and the data, see, Supplementary Table S3; SPR is the mean response to a single photon.

would have diminished any differences. Nevertheless, SPRs at the disk edge were found to peak sooner than those elicited at other positions (Figure 1). Thus, locality of the photoisomerization on the disk surface does contribute to SPR variability in rods with large diameter ROSs. The magnitude of the difference conformed with predictions of our model, which incorporated radial incisures evenly spaced around the disk perimeter, suggesting that incisure asymmetry was not a major factor with regard to SPR variability.

Bicarbonate enters the ROS at the base and diffuses to the tip, but along the way, it is removed from the outer segment in exchange for chloride (Koskelainen et al., 1994; Duda et al., 2016; Makino et al., 2019) The location of the exchangers at the plasma membrane could affect SPR reproducibility by establishing a radial gradient of bicarbonate in the cytosol between the disks that affects the local rates of cGMP synthesis. As a starting point for modeling, bicarbonate levels were assumed to be radially homogeneous. The model predicted that axial differences in the SPR would still be present with bicarbonate and experimental observations were consistent, arguing against the existence of a large, radial bicarbonate gradient.

The "unreliable" rising phase of the SPR may be prohibitive soon after a very dim flash, but CV due to randomness in position of photoisomerization drops to very low levels after several hundred ms. Bicarbonate does not change this source of variability, but regardless, randomness in the radial location of the photoisomerization does not appear to constitute a major source of SPR variability, even in the large rods of salamander.

ROS-length dependent effects of bicarbonate on the axial variability of the SPR

Bicarbonate enters the ROS at the base, so immediately after switching the perfusion to bicarbonate, there must be a higher concentration of bicarbonate at the ROS base than at the distal tip. We wanted to find out whether the axial concentration gradient dissipates significantly with continued perfusion. Our experiments on salamander clearly indicated that the axial concentration gradient during long perfusions with bicarbonate was great enough to be detected; flash responses at the base and tip were the same in the absence of bicarbonate, but recovery was faster at the base than at the tip with bicarbonate (Figures 2A,B). Toad rods are longer than salamander rods, so the hypothesis was that the bicarbonate-induced base to tip differences in the SPR would be more pronounced than in salamander. Furthermore, there are

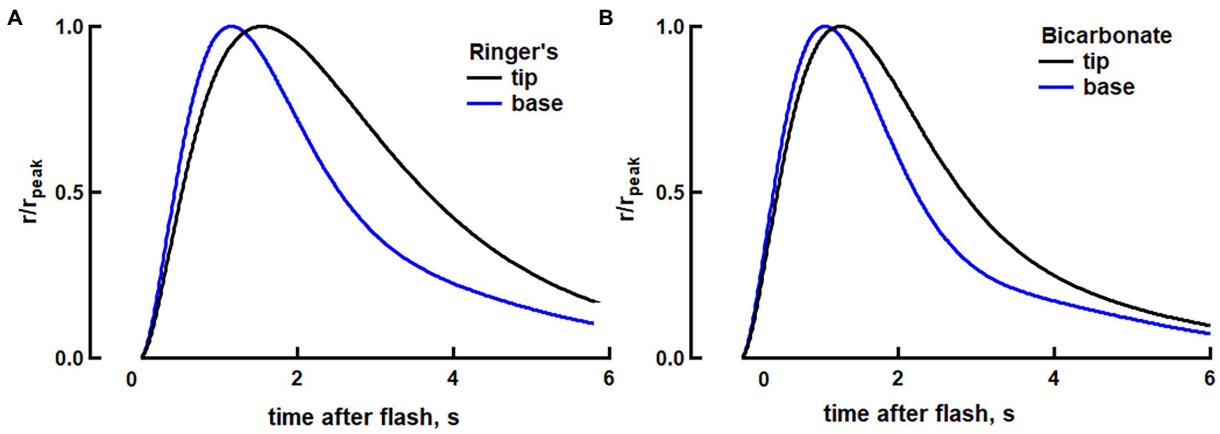

FIGURE 7
Modeling of the reduction in the kinetic differences between SPRs at the base vs. tip of a toad rod. **(A)** Modeling of faster dim flash response at the base, compared to the tip, in toad rods in Ringer's (see text for a description of our approach of using separate rods to simulate base and tip). The two traces show photon responses normalized to their peaks at base and at the tip of the ROS. For the response at the tip, ν_{RG} was 48% lower and f_{Ca} was 56% higher, compared to the values for the base. **(B)** Attenuated axial differences in photoresponse kinetics in bicarbonate between the base and tip. At the base, guanylate cyclase activity at low Ca^{2+} was increased by 100% to increase circulating dark current by 8% and reduce integration time by 14%. At the tip, guanylate cyclase activity at low Ca^{2+} was increased by 30% and the fraction of the dark current carried by Ca^{2+} was decreased by 25%, with respect to Ringer's, to produce a 9% increase in the circulating dark current and to reduce integration time by 16% to match the changes that were observed experimentally with bicarbonate. Finally, the rate of transducin activation by R* was decreased by 30% at the base in order for the rising phases at base and tip to more closely match (full list of parameters given in Supplementary Table S2).

already differences in SPR amplitude and kinetics at the base and tip of toad ROSs in the absence of bicarbonate, that were expected to be accentuated by bicarbonate. To our surprise, bicarbonate actually reduced the base to tip SPR differences (Figures 2C,D, 3, 5, 6).

The basis for the axial variability in SPR existing in the absence of bicarbonate is not yet known. However, the stack of membranous disks within the elongated ROS creates a barrier for the axial diffusion of substances within the cytoplasm. The occurrence of axial gradients of second messengers and cascade components in the absence of bicarbonate could cause SPRs from the tip of a frog or toad ROS to rise more slowly to a smaller amplitude and then take longer to recover, than those from the base (Baylor et al., 1979a; Lamb et al., 1981; Schnapf, 1983; Mazzolini et al., 2015). Our results on toad rods are consistent with these observations (Figures 2C, 3A,C,D, 5, 6A,B), whereas in salamander rods in Ringer's without bicarbonate, we did not detect this phenomenon (Figure 2A). A simple explanation is that salamander ROSs, being half as long as those of a toad or frog (Mariani, 1986; Nickell et al., 2007; Lu et al., 2018), did not support axial gradients of second messengers or cascade components that were steep enough to impact SPR kinetics, under fully dark-adapted conditions.

Regional differences in the rate of rise of the photon response in frog and toad could originate from an axial concentration gradient of transducin. A significant fraction of transducin exits the ROS for the inner segment following exposure to bright light, slowly returning only after a prolonged period in darkness (Sokolov et al., 2002). With as many as 2000 disks impeding axial diffusion within a toad ROS, transducin levels might not equilibrate fully even after dark adaptation overnight. Biochemical quantification of transducin showed that in dark adapted rats, for which ROS length is half that in toad, transducin levels at the tip of the ROS appear to be slightly lower than at the base (Sokolov et al., 2002). By reducing the rate of transducin activation by R*, a lower transducin concentration could account for the reduced photon response at the distal tip of the ROS and its slower rising phase.

The faster recovery of the dim flash response elicited at the base of the toad ROS compared to the tip in the absence of bicarbonate could also be attributed in part, to an increasingly higher concentration of bound or free Ca^{2+} along the ROS with distance from the base (Leibovic, 2001; Li et al., 2020). High Ca^{2+} would slow the recovery phase of the SPR by delaying the shutoff of photoexcited rhodopsin and by suppressing membrane guanylate cyclase activity (Gross and Wensel, 2011; Wen et al., 2014; Ingram et al., 2016). Higher Ca^{2+} at the tip could arise from preferential Ca^{2+} release from distal disks (Li et al., 2020). In addition, Na^+ is removed from the rod by Na^+K^+-ATPases in the inner segment (Stahl and Baskin, 1984; Ueno et al., 1984), so the tip may have a slightly higher concentration of Na^+ and be somewhat depolarized relative to the base. The $Na^+/Ca^{2+},K^+$ exchanger in the ROS is voltage-dependent and sensitive to the concentration of Na^+ inside (Lagnado et al., 1988), so the tip will have a lowered rate of Ca^{2+} extrusion. We captured the SPR base vs. tip differences in toad rods with our model by simulating base and tip as separate rods. Rod-t, for the tip, had a lower rate of transducin activation and an increased fraction of dark current carried by Ca^{2+} by 56%, which raised Ca^{2+} in darkness at the tip by 60% (see Supplementary Table S2).

Unexpectedly, bicarbonate greatly diminished the base to tip differences (Figures 2C,D, 3, 5, 6) and thus reduced SPR variability. The gradient reduction in the rising phase happened because of greater acceleration of the dim flash response by bicarbonate at the tip of the ROS, rather than a slowing at the base. Bicarbonate can alkalinize the ROS by combining spontaneously with a proton and subsequently releasing CO_2, which is membrane soluble and will diffuse away. Raising pH up to about 8.8 would have contributed to the increase in dark current with bicarbonate (Sampath and Baylor, 2002; Duda et al., 2015). Elevated pH would also have promoted Ca^{2+} extrusion by the Na^+/Ca^{2+}, K^+ exchanger (Hodgkin and Nunn, 1987) to a greater extent at the base, but such mechanisms cannot readily account for faster flash response kinetics at the tip. Acceleration at the tip must act on the initial steps of phototransduction involving the sequential activation of transducin and phosphodiesterase and subsequent CNG channel closure. Since bicarbonate and low Ca^{2+} stimulate guanylate cyclase to increase cGMP levels in darkness, as evidenced by the enhanced saturating response amplitude (Figure 4) and PDE activity is greatly dependent on substrate availability (Granovsky and Artemyev, 2000), a faster rate of cGMP hydrolysis should steepen the rising phase of the photon response and shorten its effective time. We tested this hypothesis utilizing our space-resolved biophysical model. The model predicted faster rising phases of flash responses at the base and tip but a selective reduction in cascade activity at the base (or an increase at the tip) was required in order to reduce the base to tip differences (see Supplementary Table S2; Figure 7). It is not clear why bicarbonate failed to influence the SPR rising phase in salamander rods using full field flashes (Figures 1C–F; see also Duda et al., 2015; Makino et al., 2019). Perhaps the effect was simply too small for detection (*cf.*, Figures 1A,B).

For toad rods, Baylor et al. (1979b) reported a CV at the peak of the SPR of ~0.2 in the absence of bicarbonate. However, they restricted photic stimulation to a central segment of the ROS, excluding the SPR variability arising from differences at the base and tip. Thus, the true CV for the SPR across the entire ROS would be considerably greater. Yet, behavioral tests of toads snapping towards moving dummy worms or preferring to jump toward dim green light indicate that their brains can interpret single photon signaling (Aho et al., 1993; Yovanovich et al., 2017). Our results provide an explanation; bicarbonate in the living eye plays an essential role in making photon counting possible by reducing the axial variability. In future studies, it will be interesting to unravel the basis for the axial SPR differences in the absence of bicarbonate in toad rods, to explain how bicarbonate improves SPR reproducibility, to explore whether additional species differences unrelated to ROS structure contribute to the different responses to bicarbonate in toad and salamander, and to examine whether bicarbonate contributes to or reduces axial SPR variance in mammalian rods with 3-5-fold thinner ROS (Nickell et al., 2007; Gilliam et al., 2012) and different incisure structures (Cohen, 1965).

Data availability statement

The raw data supporting the conclusions of this article will be made available by the authors, without undue reservation.

Ethics statement

The animal study was reviewed and approved by the Animal Care and Use Committee, Boston University.

Author contributions

CM and PG: conceptualization, performed electrophysiology recordings and wrote the original draft. CM: funding acquisition. GC: performed the simulations. PG, GC, and CK: performed formal analysis. All authors: revised and edited. All authors with the exception of ED have approved the final version of the manuscript and have agreed to be accountable for all aspects of the work, ensuring that questions related to the accuracy or integrity of any part of the work were appropriately investigated and resolved.

Funding

This work was supported by the National Science Foundation, DMS 1812601 and the National Eye Institute, EY011500, EY023980, and EY031702. The authors are solely responsible for the contents of this publication, which do not necessarily represent the official views of the National Institutes of Health or those of the National Science Foundation.

Conflict of interest

The authors declare that the research was conducted in the absence of any commercial or financial relationships that could be construed as a potential conflict of interest.

Publisher's note

Supplementary material

The Supplementary material for this article can be found online at: https://www.frontiersin.org/articles/10.3389/fnmol.2022.1050545/full#supplementary-material

SUPPLEMENTARY FIGURE S1

Test for linearity of responses to flashes through the slit. **(A)** Responses of a salamander rod in 30 mM bicarbonate to dim flashes at the base of its ROS. **(B)** Responses of the rod in **A** to flashes at its ROS tip. **(C)** Responses from **A** and from **B**, normalized to their respective peak amplitudes. **(D)** Responses of a toad rod in Ringer's to flashes at the ROS base. **(E)** Responses of the rod in **D** to flashes at the ROS tip. **(F)** Responses from **D** and from **E**, normalized to their respective peak amplitudes. For each panel, the two flash strengths at 500 nm varied by ~two-fold.

References

Aho, A. C., Donner, K., Helenius, S., Larsen, L. O., and Reuter, T. (1993). Visual performance of the toad *(Bufo bufo)* at low light levels: retinal ganglion cell responses and prey-catching accuracy. *J. Comp. Physiol. A* 172, 671–682. doi: 10.1007/BF00195393

Baylor, D. A., Lamb, T. D., and Yau, K. W. (1979a). The membrane current of single rod outer segments. *J. Physiol. Lond.* 288, 589–611. doi: 10.1113/jphysiol.1979.sp012715

Baylor, D. A., Lamb, T. D., and Yau, K. W. (1979b). Responses of retinal rods to single photons. *J. Physiol. Lond.* 288, 613–634. doi: 10.1113/jphysiol.1979.sp012716

Baylor, D. A., Matthews, G., and Yau, K. W. (1980). Two components of electrical dark noise in toad retinal rod outer segments. *J. Physiol. Lond.* 309, 591–621. doi: 10.1113/physiol.1980sp013529

Bisegna, P., Caruso, G., Andreucci, D., Shen, L., Gurevich, V. V., Hamm, H. E., et al. (2008). Diffusion of the second messengers in the cytoplasm acts as a variability suppressor of the single photon response in vertebrate phototransduction. *Biophys. J.* 94, 3363–3383. doi: 10.1529/biophysj.107.114058

Caruso, G., Bisegna, P., Andreucci, D., Lenoci, L., Gurevich, V., Hamm, H. E., et al. (2011). Identification of key factors that reduce the variability of the single photon response. *Proc. Natl. Acad. Sci. U. S. A.* 108, 7804–7807. doi: 10.1073/pnas.1018960108

Caruso, G., Bisegna, P., Lenoci, L., Andreucci, D., Gurevich, V. V., Hamm, H. E., et al. (2010). Kinetics of rhodopsin deactivation and its role in regulating recovery and reproducibility of rod photoresponse. *PLoS Comput. Biol.* 6:e1001031. doi: 10.1371/journal.pcbi.1001031

Caruso, G., Bisegna, P., Shen, L., Andreucci, D., Hamm, H. E., and DiBenedetto, E. (2006). Modeling the role of incisures in vertebrate phototransduction. *Biophys. J.* 91, 1192–1212. doi: 10.1529/biophysj.106.083618

Caruso, G., Klaus, C. J., Hamm, H. E., Gurevich, V. V., Makino, C. L., and DiBenedetto, E. (2020). Position of rhodopsin photoisomerization on the disk surface confers variability to the rising phase of the single photon response in vertebrate rod photoreceptors. *PLoS One* 15:e0240527. doi: 10.1371/journal.pone.0240527

Cohen, A. I. (1965). New details of the ultrastructure of the outer segments and ciliary connectives of the rods of human and macaque retinas. *Anat. Rec.* 152, 63–79. doi: 10.1002/ar.1091520108

DeGroot, M.H. (1986). *Probability and Statistics*, *2nd ed.* Reading, MA: Addison-Wesley, 723 pp.

Donner, K., Hemilä, S., Kalamkarov, G., Koskelainen, A., and Shevchenko, T. (1990). Rod phototransduction modulated by bicarbonate in the frog retina: roles of carbonic anhydrase and bicarbonate exchange. *J. Physiol. Lond.* 426, 297–316. doi: 10.1113/jphysiol.1990.sp018139

Duda, T., Pertzev, T., Makino, C. L., and Sharma, R. K. (2016). Bicarbonate and Ca^{2+} sensing modulators activate photoreceptor ROS-GC1 synergistically. *Front. Mol. Neurosci.* 9:5. doi: 10.3389/fnmol.2016.00005

Duda, T., Wen, X. H., Isayama, T., Sharma, R. K., and Makino, C. L. (2015). Bicarbonate modulates photoreceptor guanylate cyclase (ROS-GC) catalytic activity. *J. Biol. Chem.* 290, 11052–11060. doi: 10.1074/jbc.M115.650408

Gilliam, J. C., Chang, J. T., Sandoval, I. M., Zhang, Y., Li, T., Pittler, S. J., et al. (2012). Three-dimensional architecture of the rod sensory cilium and its disruption in retinal neurodegeneration. *Cells* 151, 1029–1041. doi: 10.1016/j.cell.2012.10.038

Granovsky, A. E., and Artemyev, N. O. (2000). Identification of the γ subunit-interacting residues on photoreceptor cGMP phosphodiesterase, PDE6α′. *J. Biol. Chem.* 275, 41258–41262. doi: 10.1074/jbc.M008094200

Gross, A.K., and Wensel, T.G. (2011). "Biochemical cascade of phototransduction". in: *Adler's Physiology of the Eye. 11th Edn.* eds. P. L. Kaufman, A. Alm, L. A. Levin, S. F. E. Nilsson, J. Ver Hoeve and S. Wu (Edinburgh: Saunders/Elsevier).

Hodgkin, A. L., and Nunn, B. J. (1987). The effect of ions on sodium-calcium exchange in salamander rods. *J. Physiol. Lond.* 391, 371–398. doi: 10.1113/jphysiol.1987.sp016743

Ingram, N. T., Sampath, A. P., and Fain, G. L. (2016). Why are rods more sensitive than cones? *J. Physiol. Lond.* 594, 5415–5426. doi: 10.1113/JP272556

Koskelainen, A., Donner, K., Kalamkarov, G., and Hemilä, S. (1994). Changes in the light-sensitive current of salamander rods upon manipulation of putative pH-regulating mechanisms in the inner and outer segment. *Vis. Res.* 34, 983–994. doi: 10.1016/0042-6989(94)90002-7

Lagnado, L., Cervetto, L., and McNaughton, P. A. (1988). Ion transport by the Na-Ca exchange in isolated rod outer segments. *Proc. Natl. Acad. Sci. U. S. A.* 85, 4548–4552. doi: 10.1073/pnas.85.12.4548

Lamb, T. D., McNaughton, P. A., and Yau, K. W. (1981). Spatial spread of activation and background desensitization in toad rod outer segments. *J. Physiol. Lond.* 319, 463–496. doi: 10.1113/jphysiol.1981.sp013921

Leibovic, K. N. (2001). The response gradient along the rod outer segment: cGMP, age and calcium. *Prog. Brain Res.* 131, 359–368. doi: 10.1016/s0079-6123(01)31029-4

Li, Y., Falleroni, F., Mortal, S., Bocchero, U., Cojoc, D., and Torre, V. (2020). Calcium flares and compartmentalization in rod photoreceptors. *Proc. Natl. Acad. Sci. U. S. A.* 117, 21701–21710. doi: 10.1073/pnas.2004909117

Liebman, P. A., Mueller, P., and Pugh, E. N. Jr. (1984). Protons suppress the dark current of frog retinal rods. *J. Physiol. Lond.* 347, 85–110. doi: 10.1113/jphysiol.1984.sp015055

Lu, Y., Benedetti, J., and Yao, X. (2018). Light-induced length shrinkage of rod photoreceptor outer segments. *Transl. Vis. Sci. Technol.* 7:29. doi: 10.1167/tvst.7.6.29

Makino, C. L., Duda, T., Pertzev, A., Isayama, T., Geva, P., Sandberg, M. A., et al. (2019). Modes of accessing bicarbonate for the regulation of membrane guanylate cyclase (ROS-GC) in retinal rods and cones. *eNeuro* 6, e0393–e0318. doi: 10.1523/ENEURO.0393-18.2019

Mariani, A. P. (1986). Photoreceptors of the larval tiger salamander retina. *Proc. R. Soc. Lond. B Biol. Sci.* 227, 483–492.

Mazzolini, M., Facchetti, G., Andolfi, L., Zaccaria, R. P., Tuccio, S., Treud, J., et al. (2015). The phototransduction machinery in the rod outer segment has a strong efficacy gradient. *Proc. Natl. Acad. Sci. U. S. A.* 112, e2715–e2724. doi: 10.1073/pnas.1423162112

Nickell, S., Park, P. S. H., Baumeister, W., and Palczewski, K. (2007). Three-dimensional architecture of murine rod outer segments determined by cryoelectron tomography. *J. Cell Biol.* 177, 917–925. doi: 10.1083/jcb.200612010

Olson, A., and Pugh, E. N. (1993). Diffusion coefficient of cyclic GMP in salamander rod outer segments estimated with two fluorescent probes. *Biophys. J.* 65, 1335–1352. doi: 10.1016/S0006-3495(93)81177-9

Rieke, F., and Baylor, D. A. (1998). Origin of reproducibility in the responses of retinal rods to single photons. *Biophys. J.* 75, 1836–1857. doi: 10.1016/S0006-3495(98)77625-8

Robert, C.P., and Casella, G.. (2004). *Monte Carlo Statistical Methods*, *2nd ed.* New York: Springer.

Sampath, A. P., and Baylor, D. A. (2002). Molecular mechanism of spontaneous pigment activation in retinal cones. *Biophys. J.* 83, 184–193. doi: 10.1016/S0006-3495(02)75160-6

Schnapf, J. L. (1983). Dependence of the single photon response on longitudinal position of absorption in toad rod outer segments. *J. Physiol. Lond.* 343, 147–159. doi: 10.1113/jphysiol.1983.sp014886

Social Science Statistics (n.d.). Available at: https://www.socscistatistics.com/tests/signedranks/default.aspx

Sokolov, M., Lyubarsky, A. L., Strissel, K. J., Savchenko, A. B., Govardovskii, V. I., Pugh, E.N. Jr., et al. (2002). Massive light-driven translocation of transducin between the two major compartments of rod cells: a novel mechanism of light adaptation. *Neuron* 34, 95–106. doi: 10.1016/s0896-6273(02)00636-0

Stahl, W. L., and Baskin, D. G. (1984). Immunocytochemical localization of Na^+, K^+ adenosine triphosphatase in the rat retina. *J. Histochem. Cytochem.* 32, 248–250. doi: 10.1177/32.2.6319483

Ueno, S., Bambauer, H. J., Umar, H., Ueck, M., and Ogawa, K. (1984). Ultracytochemical study of Ca^{++}-ATPase and K^+-NPPase activities in retinal photoreceptors of the Guinea pig. *Cell Tissue Res.* 237, 479–489. doi: 10.1007/BF00228432

Vu, T. Q., McCarthy, S. T., and Owen, W. G. (1997). Linear transformation of natural stimuli by dark-adapted and light-adapted rods of the salamander, *Ambystoma tigrinum*. *J. Physiol. Lond.* 505, 193–204. doi: 10.1111/j.1469-7793.1997.193bc.x

Wen, X. H., Dizhoor, A. M., and Makino, C. L. (2014). Membrane guanylyl cyclase complexes shape the photoresponses of retinal rods and cones. *Front. Mol. Neurosci.* 7:45. doi: 10.3389/fnmol.2014.00045

Whitlock, G. G., and Lamb, T. D. (1999). Variability in the time course of single photon responses from toad rods: termination of rhodopsin's activity. *Neuron* 23, 337–351. doi: 10.1016/S0896-6273(00)80784-9

Yovanovich, C. A. M., Koskela, S. M., Nevala, N., Kondrashev, S. L., Kelber, A., and Donner, K. (2017). The dual rod system of amphibians supports colour discrimination at the absolute visual threshold. *Philos. Trans. R. Soc. Lond. Ser. B Biol. Sci.* 372:20160066. doi: 10.1098/rstb.2016.0066

frontiers | Frontiers in Molecular Neuroscience

TYPE Brief Research Report
PUBLISHED 14 April 2023
DOI 10.3389/fnmol.2023.1125006

OPEN ACCESS

EDITED BY
Wolfgang Baehr,
The University of Utah,
United States

REVIEWED BY
Zuying Chai,
Johns Hopkins University,
United States
Nikolai O. Artemyev,
The University of Iowa,
United States
Karl-Wilhelm Koch,
University of Oldenburg,
Germany
Timothy W. Kraft,
University of Alabama at Birmingham,
United States

*CORRESPONDENCE
Rajan D. Adhikari
✉ rajanda@bu.edu

SPECIALTY SECTION
This article was submitted to Molecular Signalling and Pathways, a section of the journal Frontiers in Molecular Neuroscience

RECEIVED 15 December 2022
ACCEPTED 15 March 2023
PUBLISHED 14 April 2023

CITATION
Adhikari RD, Kossoff AM, Cornwall MC and Makino CL (2023) Bicarbonate boosts flash response amplitude to augment absolute sensitivity and extend dynamic range in murine retinal rods.
Front. Mol. Neurosci. 16:1125006.
doi: 10.3389/fnmol.2023.1125006

Bicarbonate boosts flash response amplitude to augment absolute sensitivity and extend dynamic range in murine retinal rods

Rajan D. Adhikari*, Amanda M. Kossoff, M. Carter Cornwall and Clint L. Makino

Department of Physiology and Biophysics, Boston University Chobanian and Avedisian School of Medicine, Boston, MA, United States

Rod photoreceptors in the retina adjust their responsiveness and sensitivity so that they can continue to provide meaningful information over a wide range of light intensities. By stimulating membrane guanylate cyclases in the outer segment to synthesize cGMP at a faster rate in a Ca^{2+}-dependent fashion, bicarbonate increases the circulating "dark" current and accelerates flash response kinetics in amphibian rods. Compared to amphibian rods, mammalian rods are smaller in size, operate at a higher temperature, and express visual cascade proteins with somewhat different biochemical properties. Here, we evaluated the role of bicarbonate in rods of *cpfl3* mice. These mice are deficient in their expression of functional cone transducin, Gnat2, making cones very insensitive to light, so the rod response to light could be observed in isolation in electroretinogram recordings. Bicarbonate increased the dark current and absolute sensitivity and quickened flash response recovery in mouse rods to a greater extent than in amphibian rods. In addition, bicarbonate enabled mouse rods to respond over a range that extended to dimmer flashes. Larger flash responses may have resulted in part from a bicarbonate-induced elevation in intracellular pH. However, high pH alone had little effect on flash response recovery kinetics and even suppressed the accelerating effect of bicarbonate, consistent with a direct, modulatory action of bicarbonate on Ca^{2+}- dependent, membrane guanylate cyclase activity.

KEYWORDS

cGMP, ERG, cpfl3, Gnat2, membrane guanylate cyclase, visual transduction, neuromodulation, mutant mouse

Introduction

Rod photoreceptors in the retina are highly specialized, unipolar neurons that provide for vision by producing an electrical signal in response to light (reviewed in Hofmann and Lamb, 2022; Kawamura and Tachibanaki, 2022; Lamb, 2022). In darkness, cGMP levels in the outer segment maintain a fraction of the cyclic nucleotide-gated (CNG) cation channels in the open state, allowing Na^+ and Ca^{2+} to enter. Photoactivated rhodopsin (R*) couples to the G protein transducin to activate PDE, that hydrolyzes cGMP, thereby closing CNG channels. Blockade of the circulating or "dark" current hyperpolarizes the rod and inhibits the vesicular release of the neurotransmitter glutamate.

The phototransduction cascade is regulated by Ca^{2+}-dependent feedback. In darkness, Ca^{2+} levels are relatively high. Ca^{2+}-bound recoverin sequesters rhodopsin kinase (RK), effectively

lowering the fraction available to phosphorylate R* in preparation for full quench of the R* by arrestin binding. Ca^{2+} bound to GCAPs suppresses the activity of membrane guanylate cyclases (ROS-GCs), restraining synthesis of cGMP and limiting the number of CNG channels in the open state. With Ca^{2+} bound, calmodulin decreases the affinity of CNG channel for cGMP, further reducing the number of open CNG channels. In response to light, Ca^{2+} entry is prevented by closure of CNG channels, but its extrusion by a Na^+/Ca^{2+}-K^+ exchanger continues, bringing about a light-induced fall in intracellular Ca^{2+}. Lowered Ca^{2+} accelerates R* phosphorylation, stimulates cGMP synthesis by ROS-GCs, and enhances the affinity of the CNG channel for cGMP. These regulatory mechanisms shape the responses to flashes in darkness and play important roles in light adaptation.

Bicarbonate provides additional cascade modulation; it stimulates ROS-GCs to synthesize cGMP at a faster rate (Mendez et al., 2001; Duda et al., 2015). As a result, the maximum response is larger. Because stimulation of ROS-GCs is greater when Ca^{2+} levels are low, bicarbonate also quickens flash response recovery. Systematic studies of the effects of bicarbonate on rods have been done exclusively on salamander and toads. Here, we wanted to see how bicarbonate impacts the physiology of mammalian rods, which are considerably smaller in size, operate at higher temperature, and generate faster photon responses.

Materials and methods

Gnat2$^{cpfl3/cpfl3}$ mice, hereafter referred to as *cpfl3* mice, were purchased from The Jackson Laboratory (Bar Harbor, ME, United States) and used to establish a colony at Boston University. Mice were housed, bred, and handled according to IACUC guidelines. In these mice, a missense mutation in the α-subunit of the cone transducin (*GNAT2*) gene leads to a poor cone-mediated response at 3 weeks that becomes undetectable by 9 months. Rod responses are initially normal but progressively decline with age (Chang et al., 2006; Chen et al., 2020). Mice were kept under a 12 h light/12 h dark cycle with free access to food and water. Both male and female mice were used at ages of 3–7 months. Mice were dark-adapted for 12 h before use. Retinas were isolated under infrared illumination. One retina was used immediately for recording while the other was incubated in Ames' bicarbonate at 35°C, bubbled with 95% O_2/5% CO_2 for up to 90 min prior to recording.

Ames' medium was prepared from powder obtained commercially (A1420, Sigma Aldrich, St. Louis, MO, United States). Such Ames' contained either 20 mM bicarbonate or equimolar Cl^- in place of bicarbonate. For other types of experiments, 200 μM acetazolamide (Sigma-Aldrich) was added to the Ames' medium that did not contain bicarbonate. For *ex vivo* electroretinographic recording, an isolated retina was mounted on a perfusion chamber with the photoreceptor side up (Vinberg et al., 2014) and perfused with Ames' solution at a constant rate of 4 mL/min at 35°C. 50 μM DL-AP4 (Tocris Bioscience, Bristol, United Kingdom) and 100 μM $BaCl_2$ (Sigma-Aldrich) were added to block post-photoreceptoral and glial responses, respectively. Solutions were equilibrated with 95% O_2/5% CO_2 at pH 7.4. In some experiments, the pH was raised to values between 8.4 and 9.2. Transretinal potentials were recorded with two Ag/AgCl electrodes (WPI, Sarasota, FL, United States), one located on the photoreceptor side of the retina and the other on the ganglion cell side, connected to a differential amplifier (Warner Instruments LLC, Hamden, CT, United States) and an integrated patch amplifier (IPA, Sutter Instruments, Novato, CA, United States). The recordings were low pass filtered at 300 Hz (−3 dB, 8 pole Bessel), and digitized at 5 kHz using Igor Pro (v.9.0.0 64 Bit, Wavemetrics, Portland, OR, United States).

Light from a halogen lamp passing through a 500 nm interference filter (20 nm full bandwidth at half-maximal transmission) was used to stimulate the retina. Intensity was attenuated using neutral density filters. Light intensity was calibrated with a photodiode amplifier (PDA200C, ThorLabs, NJ, United States) and a 200 μm pinhole (Edmund Optics, NJ, United States). Flashes at 500 nm that were nominally 20 ms in duration varied in strength from 0.29 to 127,746 photons μm^{-2}.

Figures show averages obtained from as many as six retinas in bicarbonate experiments and from as many as seven retinas in pH experiments, but analyses and statistical tests were carried out on the results of individual retinas. Paired *t*-test for matched pairs or ANOVA followed by a *post hoc* Tukey's test (Excel 2022) was used to assess whether treatment with bicarbonate and/or higher pH changed the responses. Curve fitting was carried out using Igor Pro.

Results

Figure 1 shows averaged responses from isolated, *cpfl3* mouse retinas to a series of flashes of increasing strength from electroretinogram (ERG) recordings. The ERG is a massed field potential that summates the electrical responses of retinal neurons to light. Here, the responses were generated almost entirely by rods; cones in this retina were several log units less sensitive than normal (Chen et al., 2020) and at the highest flash strengths, were unlikely to have contributed more than 6% to the flash responses. Glial responses and synaptic transmission were blocked pharmacologically (Coleman et al., 1987; Green and Kapousta-Bruneau, 2007). Bicarbonate produced an intensity-dependent increase in flash response amplitude (Figure 1A) that was reversed upon washing with Ames' medium not containing bicarbonate. During the wash, maximal responses were sometimes smaller than during pre-treatment due to rundown. Results from experiments in which the maximal response during the wash differed from the pre-treatment value by more than 20% were not included.

The absence of added bicarbonate to the perfusate did not necessarily mean that bicarbonate was absent, because at least some types of cones (Musser and Rosen, 1973) and Muller glia (Ochrietor et al., 2005) express carbonic anhydrase in the mammalian retina. Rods do not, but they take up bicarbonate at their synapses (Makino et al., 2019) *via* transport systems (Bok et al., 2003; Kao et al., 2011), by passage through Cl^- channels (Qu and Hartzell, 2000) and possibly through gap junctions. To assess whether rod photoresponses were modulated by bicarbonate from endogenous sources under our experimental conditions, retinas were perfused with 200 μM acetazolamide, a carbonic anhydrase inhibitor. No differences in flash response amplitude or kinetics were observed ($n = 4$, Supplementary Figure S1), confirming the lack of carbonic anhydrase activity in mouse rods and ruling out any significant basal uptake of endogenous bicarbonate.

10.3389/fnmol.2023.1125006

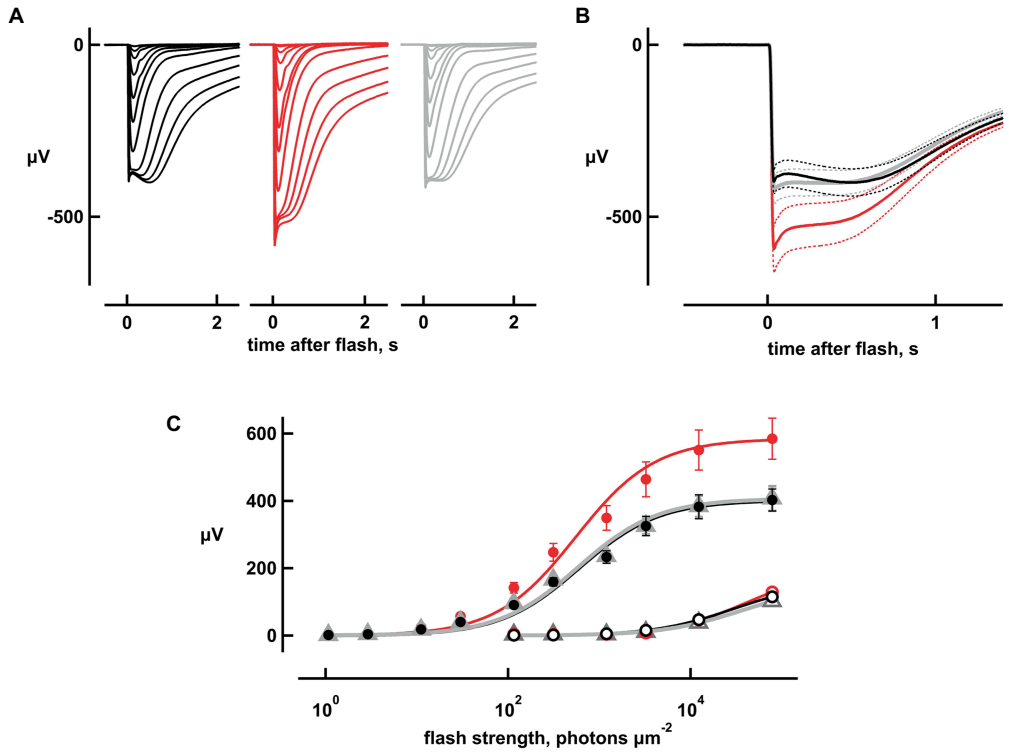

FIGURE 1
Increases in flash response amplitude and dynamic range with 20 mM bicarbonate. Traces are averaged responses of rods from *cpfl3* mouse retinas exposed to flashes of increasing strength during pre-treatment with Ames' medium that did not contain any added bicarbonate (black traces), during exposure to bicarbonate (red traces), and during wash with the Ames' medium lacking bicarbonate (gray traces). **(A)** Flash response families. Traces are averaged responses of six retinas for which there were up to five trials per flash. Flash strengths ranged from 1 to 127,746 photons μm^{-2} at 500 nm. **(B)** Averaged responses to the brightest flash, redrawn from **(A)**. Maximum response amplitude increased from 400 to 600 μV with bicarbonate and subsided to 420 μV upon washout. Dotted lines delineate ± SEM. **(C)** Stimulus–response relation. Response amplitudes from **(A)** were plotted against flash strength for perfusions with (red) or without bicarbonate (black, gray) at their peaks (filled symbols) and at 2 s after the flash (open symbols). For the latter, values for the dimmer flashes were omitted for clarity. Error bars plot SEM, which was exceedingly small for open symbols. Results were fit with the Michaelis–Menten function: $r=r_{max}i/(i+i_{1/2})$ where $i_{1/2}$ is the flash strength eliciting a half-maximal response.

The maximal, saturating rod response to a bright flash (r_{max}) provided an indirect measurement for the magnitude of the dark current, which was proportional to the number of CNG channels in the open state. However, there was a "nose" in the response that arose from changes in the activities of voltage-dependent ion channels in the inner segment (Bader et al., 1982; Vinberg et al., 2009). The nose was more prominent with bicarbonate (Figures 1A,B), because the larger dark current maintained the resting membrane potential at a more depolarized level in darkness and supported a larger current through voltage-gated K^+ channels. The delayed closure of a larger population of these channels during the flash response then caused a greater reduction in K^+ efflux at the peak of the response, causing a larger drop in amplitude to a plateau. Closure of these voltage-gated K^+ channels, as well as opening of cation channels activated by hyperpolarization meant that it was only possible to estimate a lower limit for the dark current in each retina. Maximum response amplitudes were increased by 46 ± 5% (mean ± sem, $n = 5$, $p = 0.0044$; Figures 1A,B), with 20 mM bicarbonate.

Although r_{max} was larger with bicarbonate, rod saturation occurred at approximately the same flash strength (Figure 1C). The $i_{1/2}$ value, which is the flash strength giving rise to a half-maximal response and is inversely proportional to relative sensitivity, decreased slightly, by 3.6 ± 1% ($n = 6$, $p = 0.0174$) with bicarbonate. The slowly rising "tail," that was especially notable in the recovery phase of the responses to the brighter flashes, appeared to be largely unchanged by bicarbonate (Figures 1A,B). The tail summates aberrant single photon responses that are thought to arise from the rare failure of some photoactivated rhodopsins to be phosphorylated and shut off properly (Baylor et al., 1984; Chen et al., 1995, 1999; Kraft and Schnapf, 1998). Preservation of the dependence of tail amplitude on flash strength upon treatment with bicarbonate (Figure 1C) may suggest that bicarbonate had little or no influence over the incidence, amplitude, and duration of aberrant responses.

The four dimmest flash response amplitudes (which were less than 15% of maximum, and hence were within the linear range) increased by 44, 28, 38, and 43% with bicarbonate. Figure 2A depicts the results for one flash strength. Overall, absolute sensitivity, assessed by the responses to dim flashes, increased with bicarbonate by 38 ± 7% ($n = 6$, $p = 0.0018$; Figure 2A). Therefore, dynamic range was extended to dimmer flashes by bicarbonate.

As is evident in Figure 2, bicarbonate quickened flash response kinetics. To quantify changes in the single photon response, we measured integration time, given by the response integral (area under the curve) of the response normalized to its peak, for dim flash responses that were less than 15% of the maximal. Integration time

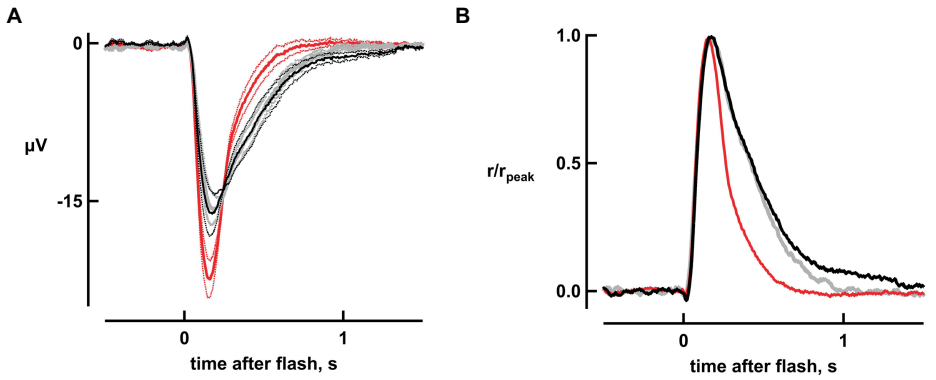

FIGURE 2
Improved absolute sensitivity and faster flash response recovery with bicarbonate. **(A)** Averaged responses to a flash of 11 photons μm^{-2}, replotted from Figure 1A. Black and gray traces represent pre-treatment and wash respectively, while the red trace represents the response during exposure to bicarbonate. Dotted lines delineate ± SEM. **(B)** Acceleration of response recovery with bicarbonate. Averaged responses to the four dimmest flash strengths were divided by their peak amplitudes and then averaged for each retina. Averages were then taken for six retinas to compare the response kinetics in the presence of bicarbonate (red trace) to those during pretreatment (black trace) and those taken during washout of bicarbonate (gray trace).

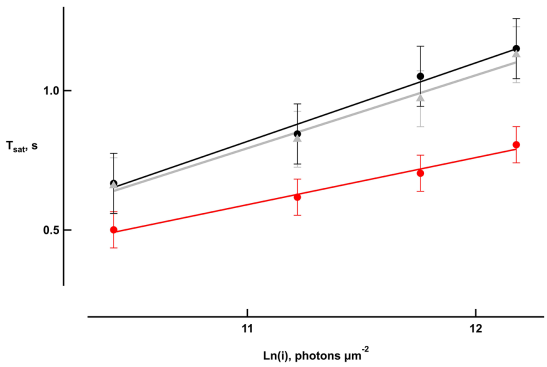

FIGURE 3
Reduced saturation time of bright flash responses with bicarbonate. Saturation time, T_{sat}, was measured from mid-flash to 25% recovery of the response peak in six retinas. Slopes of the saturation functions from linear regressions were: 282 ms pretreatment (black), 169 ms with bicarbonate (red), and 261 ms after washing (gray).

shortened by 65 ± 2% (n = 6, p = 0.000005) in bicarbonate (Figure 2B) without any change in time to peak.

Bicarbonate also shortened the time that bright flash responses remained in saturation, as shown in "Pepperberg plots" that graph response saturation time (T_{sat}) as a function of the natural logarithm of flash strength (Figure 3). Linear regressions yielded an average slope of 271 ± 21 ms (n = 6) during pretreatment that dropped to 165 ± 11 ms upon exposure to bicarbonate. The slope recovered to 250 ± 24 ms after washing for a duration exceeding 30 min. The change in slope induced by bicarbonate, when compared to the averages of pretreatment and wash for each retina, was significant (p = 0.0006).

To understand if the changes brought by bicarbonate were due to it causing a rise in intracellular pH or to a direct influence on the phototransduction cascade, retinas were perfused with Ames' at pH values ranging from 8.4 to 9.2. At pH 8.4, flash response amplitudes were increased (Figures 4A,B); the response to the dimmest flash increased by 31 ± 5% (n = 6, ANOVA p = 0.006057) and the maximal, saturating response increased by 37 ± 5% (n = 7, p = 0.00048) with an enlarged nose (Figure 4B). Response saturation was reached at a similar flash strength and the $i_{1/2}$ at pH 7.4 did not change at pH 8.4 (Figure 4D). All of these effects were similar to those produced by 20 mM bicarbonate, but a marked difference was that raising pH to 8.4 did not reduce integration time of the dim flash response nor did it reduce $i_{1/2}$. One retina was subjected to a series of pH elevations from 7.4 to 8.4, 8.8, 9.2, 8.8, and 8.4, before returning to 7.4. The pH was raised from 7.4 to 9.0 in two other retinas. In general, the maximal response was greater than normal at all elevated pH settings (p = 0.018, n = 10), as was integration time for the dim flash response (p = 0.0001; Supplementary Figure 2). The magnitude of the change did not appear to vary systematically over the pH range 8.4 to 9.2 for either parameter.

Application of 20 mM bicarbonate accentuated the effects of pH elevation. When bicarbonate was applied at pH 8.4, the increases in maximal response of 64 ± 6% (n = 6, p = 0.000003) and sensitivity to flashes of 76 ± 10% (n = 6, p = 0.0008619) were significant and were greater than those produced by raising pH alone for absolute sensitivity (p = 0.000051) and maximum response (p = 0.007609). Moreover, bicarbonate at pH 8.4 slowed dim flash response recovery by 16 ± 5% (n = 6; p = 0.01317), and lowered $i_{1/2}$, increasing the relative sensitivity on average by 5.6 ± 1% (n = 6, p = 0.02335; Figure 4D). The effects of bicarbonate at pH 9.0 also appeared to be greater than high pH alone in two retinas. The effect of bicarbonate at high pH on saturation time of responses to bright flashes was the same as that at high pH alone.

Discussion

Amphibian rods readily take up bicarbonate at their synapse, whereupon it diffuses throughout the cytosol, finally exiting from the outer segment by the action of a bicarbonate/chloride exchange (Koskelainen et al., 1994; Makino et al., 2019). Within the rod, bicarbonate opens a greater fraction of CNG channels and increases the dark current. In ERG recordings of amphibian rods, 6 mM bicarbonate replacing either phosphate or HEPES increased the dark current by 1.35–1.4-fold (Donner et al., 1990). In that study, there was no effect in single cell recordings of salamander rods, likely because

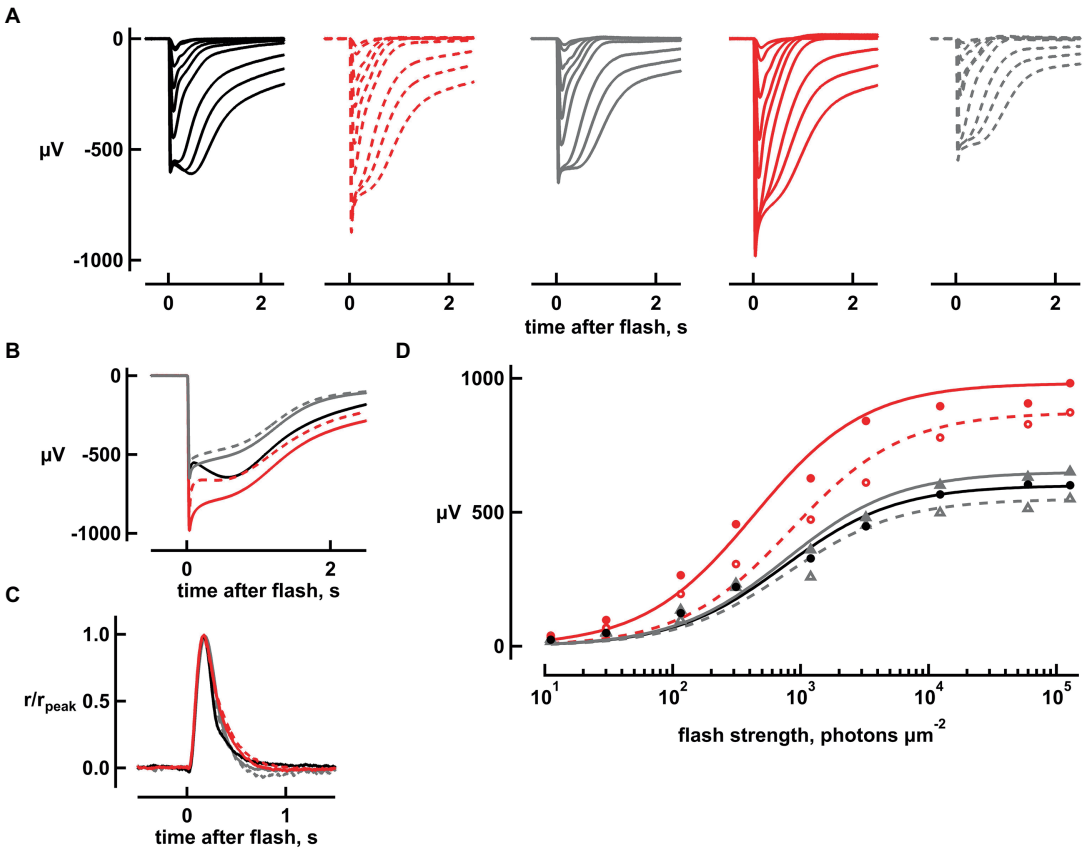

FIGURE 4
Increases in flash response amplitude and dynamic range but little change in flash response kinetics, upon raising pH to 8.4. **(A)** Flash response families. Traces are averaged responses of rods from seven retinas for which there were up to five trials per flash during pretreatment with Ames' medium at pH 7.4 that did not contain any added bicarbonate (black traces), during exposure to high pH without bicarbonate (red dashed traces), during first wash (gray traces), during exposure to 20 mM bicarbonate at high pH (red continuous traces), and during second wash (gray dashed traces). Flash strengths ranged from 1 to 127,746 photons μm^{-2} at 500 nm. **(B)** Averaged responses to the brightest flash, redrawn from **(A)**. Maximum response amplitude increased from 650 to 850 μV with high pH and returned to 640 μV upon washout. In the presence of bicarbonate and high pH, amplitude increased to 900 μV which subsided to 510 μV upon final washout. **(C)** Little change in dim flash response kinetics with high pH or with bicarbonate plus high pH. Averaged responses to the two dimmest flash strengths were divided by their peak amplitudes and then averaged for each retina. Averages were then taken for five retinas. **(D)** Stimulus–response relation. Response amplitudes from **(A)** were plotted against flash strength for perfusions at pH 7.4 without bicarbonate (black, gray filled, gray open symbols), at high pH (red open symbols) and at high pH with 20 mM bicarbonate (red filled symbols). Results were fit with the Michaelis–Menten function.

the synapse was lost during tissue preparation, precluding bicarbonate uptake. In subsequent single cell recordings of salamander rods with an intact synapse, there were increases in dark current by 1.2-fold with 30 mM bicarbonate and by 1.6-fold with 50 mM bicarbonate (Duda et al., 2015). These studies substituted bicarbonate for phosphate. Smaller, 1.1–1.2-fold increases in dark current were observed for single rods when 25–50 mM bicarbonate was substituted for MOPS (Duda et al., 2015; Makino et al., 2019). In the present study of mouse rods, bicarbonate was substituted for equimolar Cl^-. The maximal rod response as measured by the electroretinogram, which is proportional to the dark current, increased by more than 1.4-fold with bicarbonate (Figure 1). Variability in the efficacy of bicarbonate in enhancing dark current is therefore affected by the composition of the perfusion medium and perhaps, by species differences.

Lamb et al. (1981) found that responses to dim flashes in toad rods were diminished by 22 mM bicarbonate, but their bicarbonate solution also raised extracellular Ca^{2+} concentration by two-fold, which would have suppressed ROS-GC activity. With extracellular Ca^{2+} levels held constant, dim flash responses were approximately 2-fold larger for frog rods when 6 mM bicarbonate replaced phosphate (Donner et al., 1990), but there was no change for salamander rods when 30 mM bicarbonate replaced MOPS (Duda et al., 2015) or Cl^- (Makino et al., 2019). Flash sensitivity was approximately 1.4-fold higher in monkey rods when 20 mM bicarbonate replaced Cl^-, based on a comparison of 18 rods in bicarbonate to four other rods in the absence of bicarbonate (Baylor et al., 1984). In the present study of mouse rods, the response to dim flashes also increased 1.4-fold with bicarbonate (Figure 2). Enlargement of the dim flash response by bicarbonate improved flash sensitivity, and in doing so, it expanded the dynamic range of rod responsivity to dimmer flashes. In support of a role for bicarbonate in rods of the intact eye in the living animal, knockout of carbonic anhydrase XIV in mice led to a 0.4-fold decline in bright flash ERG a-wave amplitude and a 0.3-fold decline in b-wave amplitude. Lacking any significant changes in the number of rods in the retina or in rod outer segment length (Ogilvie et al., 2007), the diminished ERG was presumably due to a reduction in dark current in the rods.

In primate and amphibian rods, time to peak is faster and integration time is shorter for dim flash responses when bicarbonate is present (Baylor et al., 1984; Duda et al., 2015), but only the latter was true for mouse rods in the present study. The briefer integration time would improve temporal resolution but would diminish sensitivity to steady illumination.

Bicarbonate binds the core catalytic domain of ROS-GCs to stimulate cGMP synthesis at a faster rate. Stimulation is even more powerful at low Ca^{2+} levels (Duda et al., 2015; Makino et al., 2019). The ensuing rise in cGMP concentration supports the opening of a greater fraction of CNG channels to increase the dark current. Alkalinization of amphibian rods (Kalamkarov et al., 1996), due to bicarbonate combining with a proton to eventually form CO_2, also enhances the dark current (Liebman et al., 1984; Duda et al., 2015). To explore the mechanism of action of bicarbonate on the flash response in murine rods, retinas were perfused with Ames' medium at high pH, to raise intracellular pH (Saarikoski et al., 1997), with and without bicarbonate. Elevating pH above 8.4 reproduced the effects of 20 mM bicarbonate at pH 7.4 by increasing dark current and sensitivity to flashes, but differed from bicarbonate in that it failed to accelerate dim flash response kinetics (Figures 1, 4; Supplementary Figure S2). Raising extracellular pH to 8.4 even caused bicarbonate to slow dim flash recovery. ROS-GC activity is not pH dependent over the range 7.4–9 (Fleischman and Denisevich, 1979; Duda et al., 2015), therefore, direct stimulation of ROS-GC activity by bicarbonate is critical for its physiological effects on the flash response.

Increasing flash strength beyond that required for a maximum response caused responses to remain in saturation progressively longer before recovering. Bicarbonate shortened saturation time (Figure 3), because it accelerated cGMP synthesis and exerted a pH effect that supported CNG channel opening (Liebman et al., 1984; Duda et al., 2015). In Pepperberg plots, the slope of the relation, τ_D, estimates the time constant of the rate-limiting step in the flash response recovery (Pepperberg et al., 1992), namely the hydrolysis of GTP by transducin bound to PDE (Krispel et al., 2006). Interestingly, the τ_D of ~270 ms in the absence of bicarbonate shortened to 160 ms with bicarbonate. A value of ~200 ms was reported previously for mouse rods perfused with bicarbonate by many other groups (e.g., Calvert et al., 2000; Chen et al., 1999) although shorter values have sometimes been observed (e.g., Chen et al., 2010, 2012; Woodruff et al., 2014). We attribute the slower τ_D in the present study and the apparent slowing of τ_D in the absence of bicarbonate to the intrusion of aberrant single photon responses. Aberrant responses produced the tail, slowed the time course of the early recovery phase, and extended the time in saturation of the bright flash response (Figures 1A, B). Since their number and hence the overall magnitude of their effects increased with flash strength, aberrant responses inflated the slope of the Pepperberg relation. Constancy of aberrant response size (Figure 1B) meant that there was a relatively weaker prolongation of the T_{sat} of the responses enlarged by bicarbonate, when measured at a criterion level of response recovery. Another possibility was that bicarbonate raised pH (Kalamkarov et al., 1996) to a level that slowed the rate of Ca^{2+} extrusion (Hodgkin and Nunn, 1987; Schnetkamp, 1995) and delayed Ca^{2+} feedback onto ROS-GC activity. The extension of saturation time would have had a greater relative impact on the responses at the lower end of the flash strength range. Other mechanisms that cannot yet be ruled out include an acceleration of GTP hydrolysis by transducin as a direct effect of bicarbonate or by the bicarbonate-induced alkalinization.

Data availability statement

The raw data supporting the conclusions of this article will be made available by the authors, without undue reservation.

Ethics statement

The animal study was reviewed and approved by Boston University's Institutional Animal Care and Use Committee (IACUC).

Author contributions

RA and CM designed the study. RA carried out the experiments, collected data, and analyzed results. AK participated in some experiments and helped with analysis. RA wrote the first draft of the report. RA, CM, and MC edited and approved the final report. All authors contributed to the article and approved the submitted version.

Funding

This work was supported by National Eye Institute (EY01157, EY031702).

Acknowledgments

The content is solely the responsibility of the authors and does not necessarily represent the official views of the National Institutes of Health.

Conflict of interest

The authors declare that the research was conducted in the absence of any commercial or financial relationships that could be construed as a potential conflict of interest.

Publisher's note

Supplementary material

The Supplementary material for this article can be found online at: https://www.frontiersin.org/articles/10.3389/fnmol.2023.1125006/full#supplementary-material

References

Bader, C. R., Bertrand, D., and Schwartz, E. A. (1982). Voltage-activated and calcium-activated currents studied in solitary rod inner segments from the salamander retina. *J. Physiol. (Lond.)* 331, 253–284. doi: 10.1113/jphysiol.1982.sp014372

Baylor, D. A., Nunn, B. J., and Schnapf, J. L. (1984). The photocurrent, noise and spectral sensitivity of rods of the monkey *Macaca fascicularis*. *J. Physiol. (Lond.)* 357, 575–607. doi: 10.1113/jphysiol.1984.sp015518

Bok, D., Galbraith, G., Lopez, I., Woodruff, M., Nusinowitz, S., BeltrandelRio, H., et al. (2003). Blindness and auditory impairment caused by loss of the sodium bicarbonate cotransporter NBC3. *Nat. Genet.* 34, 313–319. doi: 10.1038/ng1176

Calvert, P. D., Krasnoperova, N. V., Lyubarsky, A. L., Isayama, T., Nicoló, M., Kosaras, B., et al. (2000). Phototransduction in transgenic mice after targeted deletion of the rod transducin α-subunit. *Proc. Natl. Acad. Sci. U. S. A.* 97, 13913–13918. doi: 10.1073/pnas.250478897

Chang, B., Dacey, M. S., Hawes, N. L., Hitchcock, P. F., Milam, A. H., Atmaca-Sonmez, P., et al. (2006). Cone photoreceptor function loss-3, a novel mouse model of achromatopsia due to a mutation in *Gnat2*. *Invest. Ophthalmol. Vis. Sci.* 47, 5017–5021. doi: 10.1167/iovs.05-1468

Chen, C. K., Burns, M. E., Spencer, M., Niemi, G. A., Chen, J., Hurley, J. B., et al. (1999). Abnormal photoresponses and light-induced apoptosis in rods lacking rhodopsin kinase. *Proc. Natl. Acad. Sci. U. S. A.* 96, 3718–3722. doi: 10.1073/pnas.96.7.3718

Chen, N. S., Ingram, N. T., Frederiksen, R., Sampath, A. P., Chen, J., and Fain, G. L. (2020). Diminished cone sensitivity in *cpfl3* mice is caused by defective transducin signaling. *Vis. Neurosci.* 61:26. doi: 10.1167/iovs.61.4.26

Chen, J., Makino, C. L., Peachey, N. S., Baylor, D. A., and Simon, M. I. (1995). Mechanisms of rhodopsin inactivation in vivo as revealed by a COOH-terminal truncation mutant. *Science* 267, 374–377. doi: 10.1126/science.7824934

Chen, C. K., Woodruff, M. L., Chen, F. S., Chen, Y., Cilluffo, M. C., Tranchina, D., et al. (2012). Modulation of mouse rod response decay by rhodopsin kinase and recoverin. *J. Neurosci.* 32, 15998–16006. doi: 10.1523/JNEUROSCI.1639-12.2012

Chen, J., Woodruff, M. L., Wang, T., Concepcion, F. A., Tranchina, D., and Fain, G. L. (2010). Channel modulation and the mechanism of light adaptation in mouse rods. *J. Neurosci.* 30, 16232–16240. doi: 10.1523/JNEUROSCI.2868-10.2010

Coleman, P. A., Carras, P. L., and Miller, R. F. (1987). Barium reverses the transretinal potassium gradient of the amphibian retina. *Neurosci. Lett.* 80, 61–65. doi: 10.1016/0304-3940(87)90495-2

Donner, K., Hemila, S., Kalamkarov, G., Koskelainen, A., and Shevchenko, T. (1990). Rod phototransduction modulated by bicarbonate in the frog retina: roles of carbonic anhydrase and bicarbonate exchange. *J. Physiol. (Lond.)* 426, 297–316. doi: 10.1113/jphysiol.1990.sp018139

Duda, T., Wen, X. H., Isayama, T., Sharma, R. K., and Makino, C. L. (2015). Bicarbonate modulates photoreceptor guanylate cyclase (ROS-GC) catalytic activity. *J. Biol. Chem.* 290, 11052–11060. doi: 10.1074/jbc.M115.650408

Fleischman, D., and Denisevich, M. (1979). Guanylate cyclase of isolated bovine retinal rod axonemes. *Biochemistry* 18, 5060–5066. doi: 10.1021/bi00590a006

Green, D. G., and Kapousta-Bruneau, N. V. (2007). Evidence that L-AP5 and D, L-AP4 can preferentially block cone signals in the rat retina. *Vis. Neurosci.* 24, 9–15. doi: 10.1017/S0952523807230123

Hodgkin, A. L., and Nunn, B. J. (1987). The effect of ions on sodium-calcium exchange in salamander rods. *J. Physiol. (Lond.)* 391, 371–398. doi: 10.1113/jphysiol.1987.sp016743

Hofmann, K. P., and Lamb, T. D. (2022). Rhodopsin, light-sensor of vision. *Prog. Retin. Eye Res.* 93:101116. doi: 10.1016/j.preteyeres.2022.101116

Kalamkarov, G., Pogozheva, I., Shevchenko, T., Koskelainen, A., Hemilä, S., and Donner, K. (1996). pH changes in frog rods upon manipulation of putative pH-regulating transport mechanisms. *Vis. Res.* 36, 3029–3036. doi: 10.1016/0042-6989(96)00052-1

Kao, L., Kurtz, L. M., Shao, X., Papadopoulos, M. C., Liu, L., Bok, D., et al. (2011). Severe neurologic impairment in mice with targeted disruption of the electrogenic sodium bicarbonate cotransporter NBCe2 (*Slc4a5* gene). *J. Biol. Chem.* 286, 32563–32574. doi: 10.1074/jbc.M111.249961

Kawamura, S., and Tachibanaki, S. (2022). Molecular bases of rod and cone differences. *Prog. Retin. Eye Res.* 90:101040. doi: 10.1016/j.preteyeres.2021.101040

Koskelainen, A., Donner, K., Kalamkarov, G., and Hemilä, S. (1994). Changes in the light-sensitive current of salamander rods upon manipulation of putative pH-regulating mechanisms in the inner and outer segment. *Vis. Res.* 34, 983–994. doi: 10.1016/0042-6989(94)90002-7

Kraft, T. W., and Schnapf, J. L. (1998). Aberrant photon responses in rods of the macaque monkey. *Vis. Neurosci.* 15, 153–159. doi: 10.1017/S0952523898151131

Krispel, C. M., Chen, D., Melling, N., Chen, Y. J., Martemyanov, K. A., Quillinan, N., et al. (2006). RGS expression rate-limits recovery of rod photoresponses. *Neuron* 51, 409–416. doi: 10.1016/j.neuron.2006.07.010

Lamb, T. D. (2022). Photoreceptor physiology and evolution: cellular and molecular basis of rod and cone phototransduction. *J. Physiol. Lond.* 600, 4585–4601. doi: 10.1113/JP282058

Lamb, T. D., McNaughton, P. A., and Yau, K. W. (1981). Spatial spread of activation and background desensitization in toad rod outer segments. *J. Physiol. (Lond.)* 319, 463–496. doi: 10.1113/jphysiol.1981.sp013921

Liebman, P. A., Mueller, P., and Pugh, E. N. Jr. (1984). Protons suppress the dark current of frog retinal rods. *J. Physiol. Lond.* 347, 85–110. doi: 10.1113/jphysiol.1984.sp015055

Makino, C. L., Duda, T., Pertzev, A., Isayama, T., Geva, P., Sandberg, M. A., et al. (2019). Modes of accessing bicarbonate for the regulation of membrane guanylate cyclase (ROS-GC) in retinal rods and cones. *eNeuro* 6, 0393–0318. doi: 10.1523/ENEURO.0393-18.2019

Mendez, A., Burns, M. E., Sokal, I., Dizhoor, A. M., Baehr, W., Palczewski, K., et al. (2001). Role of guanylate cyclase-activating proteins (GCAPs) in setting the flash sensitivity of rod photoreceptors. *Proc. Natl. Acad. Sci. U. S. A.* 98, 9948–9953. doi: 10.1073/pnas.171308998

Musser, G. L., and Rosen, S. (1973). Localization of carbonic anhydrase activity in the vertebrate retina. *Exp. Eye Res.* 15, 105–119. doi: 10.1016/0014-4835(73)90195-4

Ochrietor, J. D., Clamp, M. F., Moroz, T. P., Grubb, J. H., Shah, G. N., Waheed, A., et al. (2005). Carbonic anhydrase XIV identified as the membrane CA in mouse retina: strong expression in Müller cells and the RPE. *Exp. Eye Res.* 81, 492–500. doi: 10.1016/j.exer.2005.03.010

Ogilvie, J. M., Ohlemiller, K. K., Shah, G. N., Ulmasov, B., Becker, T. A., Waheed, A., et al. (2007). Carbonic anhydrase XIV deficiency produces a functional defect in the retinal light response. *Proc. Natl. Acad. Sci. U. S. A.* 104, 8514–8519. doi: 10.1073/pnas.0702899104

Pepperberg, D. R., Cornwall, M. C., Kahlert, M., Hofmann, K. P., Jin, J., Jones, G. J., et al. (1992). Light-dependent delay in the falling phase of the retinal rod photoresponse. *Vis. Neurosci.* 8, 9–18. doi: 10.1017/S0952523800006441

Qu, Z., and Hartzell, H. C. (2000). Anion permeation in Ca^{2+}-activated Cl^- channels. *J. Gen. Physiol.* 116, 825–844. doi: 10.1085/jgp.116.6.825

Saarikoski, J., Ruusuvuori, E., Koskelainen, A., and Donner, K. (1997). Regulation of intracellular pH in salamander retinal rods. *J. Physiol. Lond.* 498, 61–72. doi: 10.1113/jphysiol.1997.sp021841

Schnetkamp, P. P. (1995). How does the retinal rod Na-Ca+K exchanger regulate cytosolic free Ca^{2+}? *J. Biol. Chem.* 270, 13231–13239. doi: 10.1074/jbc.270.22.13231

Vinberg, F., Kolesnikov, A. V., and Kefalov, V. J. (2014). Ex vivo ERG analysis of photoreceptors using an in vivo ERG system. *Vis. Res.* 101, 108–117. doi: 10.1016/j.visres.2014.06.003

Vinberg, F. J., Strandman, S., and Koskelainen, A. (2009). Origin of the fast negative ERG component from isolated aspartate-treated mouse retina. *J. Vis.* 9, 1–17. doi: 10.1167/9.12.9

Woodruff, M. L., Rajala, A., Fain, G. L., and Rajala, R. V. (2014). Modulation of mouse rod photoreceptor responses by Grb14 protein. *J. Biol. Chem.* 289, 358–364. doi: 10.1074/jbc.M113.517045

frontiers | Frontiers in Molecular Neuroscience

TYPE Original Research
PUBLISHED 13 January 2023
DOI 10.3389/fnmol.2022.1054449

OPEN ACCESS

EDITED BY
Daniele Dell'Orco,
University of Verona,
Italy

REVIEWED BY
Takeshi Yoshimatsu,
University of Sussex,
United Kingdom
Michael L. Firsov,
Institute of Evolutionary Physiology and Biochemistry (RAS), Russia
Giorgio Rispoli,
Università degli Studi di Ferrara, Italy

*CORRESPONDENCE
Clint L. Makino
cmakino@bu.edu

†Deceased

SPECIALTY SECTION
This article was submitted to Molecular Signalling and Pathways, a section of the Journal Frontiers in Molecular Neuroscience

RECEIVED 26 September 2022
ACCEPTED 09 November 2022
PUBLISHED 13 January 2023

CITATION
Caruso G, Klaus C, Hamm HE, Gurevich VV, Bisegna P, Andreucci D, DiBenedetto E and Makino CL (2023) Pepperberg plot: Modeling flash response saturation in retinal rods of mouse.
Front. Mol. Neurosci. 15:1054449.
doi: 10.3389/fnmol.2022.1054449

Pepperberg plot: Modeling flash response saturation in retinal rods of mouse

Giovanni Caruso[1], Colin Klaus[2], Heidi E. Hamm[3], Vsevolod V. Gurevich[3], Paolo Bisegna[4], Daniele Andreucci[5], Emmanuele DiBenedetto[6†] and Clint L. Makino[7*]

[1]Italian National Research Council, Istituto di Scienze del Patrimonio Culturale, Rome, Italy, [2]The College of Public Health Division of Biostatistics and The Mathematical Biosciences Institute, The Ohio State University, Columbus, OH, United States, [3]Department of Pharmacology, Vanderbilt University Medical Center, Nashville, TN, United States, [4]Department of Civil Engineering and Computer Science, University of Rome Tor Vergata, Rome, Italy, [5]Department of Basic and Applied Sciences for Engineering, Sapienza University of Rome, Rome, Italy, [6]Department of Mathematics, Vanderbilt University, Nashville, TN, United States, [7]Department of Physiology & Biophysics, Boston University Chobanian & Avedisian School of Medicine, Boston, MA, United States

Retinal rods evolved to be able to detect single photons. Despite their exquisite sensitivity, rods operate over many log units of light intensity. Several processes inside photoreceptor cells make this incredible light adaptation possible. Here, we added to our previously developed, fully space resolved biophysical model of rod phototransduction, some of the mechanisms that play significant roles in shaping the rod response under high illumination levels: the function of RGS9 in shutting off G protein transducin, and calcium dependences of the phosphorylation rates of activated rhodopsin, of the binding of cGMP to the light-regulated ion channel, and of two membrane guanylate cyclase activities. A well stirred version of this model captured the responses to bright, saturating flashes in WT and mutant mouse rods and was used to explain "Pepperberg plots," that graph the time during which the response is saturated against the natural logarithm of flash strength for bright flashes. At the lower end of the range, saturation time increases linearly with the natural logarithm of flash strength. The slope of the relation (τ_D) is dictated by the time constant of the rate-limiting (slowest) step in the shutoff of the phototransduction cascade, which is the hydrolysis of GTP by transducin. We characterized mathematically the X-intercept (Φo) which is the number of photoisomerizations that just saturates the rod response. It has been observed that for flash strengths exceeding a few thousand photoisomerizations, the curves depart from linearity. Modeling showed that the "upward bend" for very bright flash intensities could be explained by the dynamics of RGS9 complex and further predicted that there would be a plateau at flash strengths giving rise to more than ~10^7 photoisomerizations due to activation of all available PDE. The model accurately described alterations in saturation behavior of mutant murine rods resulting from transgenic perturbations of the cascade targeting membrane guanylate cyclase activity, and expression levels of GRK, RGS9, and PDE. Experimental results from rods expressing a mutant light-regulated

channel purported to lack calmodulin regulation deviated from model predictions, suggesting that there were other factors at play.

KEYWORDS

visual transduction, RGS9, PDE, CNG channel, membrane guanylate cyclase, cyclic GMP, GRK, G protein

Introduction

Vision in dim light is mediated by rod photoreceptors in the retina that capture single photons and convert them into electrical signals *via* a biochemical cascade (reviewed in Zang and Neuhauss, 2021; Kawamura and Tachibanaki, 2022; Wensel, 2024). Briefly, photoexcited rhodopsin (R^*) catalyzes activation of the rod-specific G protein transducin (T in the inactive state, T^* in the active state), that stimulates a cGMP phosphodiesterase, PDE. The ensuing drop in cGMP levels closes cyclic-nucleotide-gated (CNG) cation channels in the plasma membrane, suppressing an inward current carried by Na^+ and to a lesser extent, by Ca^{2+}. Absorption of a single photon closes 5–10% of the open channels. The response terminates following phosphorylation of R^* by rhodopsin kinase (GRK1 or RK) and subsequent arrestin-1 binding and by GTP hydrolysis by T^*. Membrane guanylate cyclases (ROS-GCs) restore the cGMP levels enabling the CNG channels to reopen.

There is a light-induced fall in intracellular Ca^{2+} because upon closure of CNG channels, the extrusion of Ca^{2+} by a sodium/potassium/calcium exchanger exceeds its influx. The lowered Ca^{2+} stimulates cGMP synthesis by ROS-GCs to quicken the restoration of cGMP and reopen CNG channels, accelerates R^* shutoff by causing recoverin to release RK, and increases the affinity of CNG channels for cGMP.

The photocurrent response saturates with a flash that is sufficiently bright to close all CNG channels. Further increases in flash strength prolong the duration of the response. Although rods no longer convey meaningful visual information under bright illumination, studies of the saturation behavior yield important insights into the molecular mechanisms of the phototransduction cascade. David Pepperberg discovered that over a limited range, the time in saturation of a bright flash response increases linearly with the log of the flash strength (Pepperberg et al., 1992). The rationale is that with powerful cascade activation, the cGMP levels drop far below that required to hold open CNG channels. As phototransduction cascade activity declines and cGMP levels recover, the channels reopen along an exponential time course (Pepperberg et al., 1992; Nikonov et al., 2000). The slope of the relation between natural logarithm of the flash strength and time in saturation gives the time constant τ_D for the slower of the two steps, rhodopsin quench and shutoff of transducin-activated PDE. The latter was identified as rate-limiting (Krispel et al., 2006). For very bright flashes, the relation curves upward, indicating slowing of cascade shutoff. Here we used mathematical modeling to explain the saturation behavior of WT rods as well as the behaviors of rods of a number of mutant mice that were genetically engineered to modify their phototransduction cascades. To simplify calculations and reduce computation time, we implemented a globally well-stirred (GWS) version of our fully space resolved (FSR) model as described in (Andreucci et al., 2003; Bisegna et al., 2008; Caruso et al., 2011, 2019), because with hundreds of activated rhodopsins randomly distributed among rod discs and with random positions of active rhodopsin within each disc, the two models were equivalent. Modeling efforts were directed to mouse rods, for which many transgenic variants have been described.

Materials and methods

Simulations of the ordinary differential equation systems in this paper were performed in Matlab. The routines have been made available at https://github.com/klauscj68/Pepperberg. Symbols for the parameters used for mouse rods and their values are given in Supplementary Table S1. Minor adjustments were made within published ranges to optimize the fitting. Pepperberg curves for various mutant mice were taken from studies previously reported in the literature. A collecting area of 0.45 μm^2 was used to convert flash strength to photoisomerizations (Φ), based on measurements of rod outer segment dimensions (Burns and Pugh, 2009).

Results and discussion

Model of phototransduction

Intracellular Ca^{2+} drops significantly in the ROS during saturating responses, impacting a number of cascade reactions. Our FSR model was therefore further developed to include two different calcium-dependent membrane guanylate cyclase activities, calcium-dependent modulation of the CNG channel, and calcium-dependent phosphorylation of R^*, as described below. In addition, the GWS version of the FSR model incorporated regulation of the shutoff of T^*-activated PDE activity by RGS9.

Second messengers of the phototransduction cascade

The rate equations for cGMP and Ca^{2+} are:

$$\frac{d}{dt}\left[cGMP\right] = \alpha_{\min} + \left(\alpha_{\max} - \alpha_{\min}\right) \left[\frac{\beta}{1+\left(\left[Ca^{2+}\right]/K_{cyc1}\right)^{m_{cyc1}}} + \frac{1-\beta}{1+\left(\left[Ca^{2+}\right]/K_{cyc2}\right)^{m_{cyc2}}}\right] - k_{hyd}\left(E_{tot} - E^{*}\right)\left[cGMP\right] - k_{\sigma;hyd}E^{*}\left[cGMP\right], \quad (1a)$$

$$\frac{d}{dt}\left[Ca^{2+}\right] = \eta\left(\frac{1}{2}f_{Ca}J_{cG} - J_{ex}\right) \quad (1b)$$

where $\beta \in [0,1]$,

$$J_{cG} = \frac{j_{cG}^{\max}}{V_{cyt}} \frac{\left[cGMP\right]^{m_{cG}}}{K_{cG}{}^{m_{cG}} + \left[cGMP\right]^{m_{cG}}}, \quad (2a)$$

$$J_{ex} = \frac{j_{ex}^{sat}}{V_{cyt}} \frac{\left[Ca^{2+}\right]}{K_{ex} + \left[Ca^{2+}\right]}. \quad (2b)$$

In mouse rod outer segments, cGMP is synthesized by two membrane guanylate cyclases, ROS-GC1 and ROS-GC2, that are regulated by two neuronal Ca^{2+} sensors, GCAP1 and GCAP2, with different affinities for Ca^{2+} (reviewed in Wen et al., 2014). Their activities are described by the terms in brackets on the right-hand side of eq. (1a). The constants $\alpha_{\min} < \alpha_{\max}$, in $\mu M\, s^{-1}$ are given by the production rates of cGMP at maximum and minimum Ca^{2+} concentration (theoretically as $\left[Ca^{2+}\right] \to \infty$ and $\left[Ca^{2+}\right] \to 0$, respectively). K_{cyc} in μM is the Ca^{2+} concentration for which the rate of production of cGMP by a ROS-GC is half-maximal. The number m_{cyc} is the dimensionless Hill's exponent. ROS-GC2 pairs primarily with GCAP2 while ROS-GC1 pairs with either GCAP, but for modeling purposes, it is only important to distinguish the overall Ca^{2+} dependent activities. In the last two terms, k_{hyd} and $k_{\sigma;hyd}$ in $\mu m^3\ s^{-1}$ are the catalytic rates of hydrolysis of cGMP by basal and activated PDE subunits, respectively.

The term J_{cG} is the current carried by the CNG channels. The multiplying constant f_{Ca} is the dimensionless fraction of cGMP-activated current carried by Ca^{2+}. The constant $j_{cG}^{\max}$, in pA, is the current for maximal $\left[cGMP\right]$ (theoretically as $\left[cGMP\right] \to \infty$), whereas K_{cG}, in μM is the cGMP concentration corresponding to half-maximal channel opening, and m_{cG} is the dimensionless Hill's exponent. The parameter K_{cG} is itself a function of Ca^{2+} due to the presence of calmodulin as described by the equation:

$$K_{cG}\left(\left[Ca^{2+}\right]\right) = K_{cG,\max} + \left(K_{cG,\min} - K_{cG,\max}\right) \frac{K_{CaM}^{m_{CaM}}}{K_{CaM}^{m_{CaM}} + \left[Ca^{2+}\right]^{m_{CaM}}} \quad (3)$$

where m_{CaM} is the Hill's exponent for calmodulin activation by Ca^{2+}, the constant K_{CaM} is the Ca^{2+} concentration for a half-maximal calmodulin effect and $K_{cG,\min}$ and $K_{cG,\max}$ are the minimum and maximum binding affinities of each of the cGMP binding sites on the channel, occurring for $\left[Ca^{2+}\right] \to 0$ and $\left[Ca^{2+}\right] \to \infty$ respectively.

The term J_{ex} is the current due to Na^{+}/Ca^{2+}, K^{+} exchange, j_{ex}^{sat} in pA is the saturated exchange current occurring at maximum $\left[Ca^{2+}\right]$ (theoretically for $\left[Ca^{2+}\right] \to \infty$) and K_{ex} in μM is the $[Ca^{2+}]$ at which the exchange current is half-maximal. The constant η is of the form $\left(B_{Ca}\mathcal{F}\right)^{-1}$, where B_{Ca} is a dimensionless constant that takes into account the Ca^{2+}-buffering effects in the cytosol and $\mathcal{F} = 96{,}500$ C mol^{-1} is the Faraday constant. With these specifications, the units in eq. (1b) are self-consistent.

Dynamics of R* shutoff

Photon absorption converts R to R^{*}, which is a substrate for phosphorylation by RK. Phosphorylation decreases the ability of R^{*} to activate transducin, but complete quench only occurs after the binding of arrestin-1 (Arr). Denote by $\left[R_j^{*}\right]$ the concentrations of activated rhodopsins in their j^{th} phosphorylated state, identified with the number $j-1$ phosphates attached to R^{*} up to a maximum of six phosphorylations (for mouse). Newly activated R^{*} molecules have no attached phosphates, so they are in the state $j=1$. Rhodopsins in the state j transition either to the state $j+1$ at a rate of λ_j or they bind to Arr at a rate μ_j, thereby being quenched. Removal of phosphates from R^{*} occurs on a much slower time scale (Berry et al., 2016) and is disregarded in the model. The quantities λ_j and μ_j measure, in s^{-1}, the binding rates of R_j^{*} to RK and Arr, respectively. The numbers $\left(\lambda_j + \mu_j\right)^{-1}$ measure the statistical average of the sojourn time of an activated rhodopsin in the j^{th} state. It is assumed that μ_j of Arr to R_j^{*} depends only on the j^{th} phosphorylated state. For example, μ_j is zero if all phosphorylated states are removed or prevented, e.g., by knockout of RK. For the model, all μ_j values were set to zero for $j<4$ and set to the maximal rate of arrestin binding, $\mu_{\max}$, for $j \geq 4$. Similarly, $\lambda_{n+1} = 0$ after R_{n+1}^{*} binds Arr (is quenched). The quantities λ_j are functions of any biochemical process that either increases or decreases the probability of R_j^{*} binding RK. For example, a $[Ca^{2+}]$ drop releases RK from its complex with recoverin, thereby increasing the probability of R^{*} binding RK and thus shortening the sojourn times before the next phosphorylation. While other dependencies might be present, we assume that $\lambda_j = \lambda_j\left(\left[Ca^{2+}\right]\right)$ where the form of this function has to be specified. For $j \geq 2$, the $\left[R_j^{*}\right]$ is augmented by $\lambda_{j-1}\left[R_{j-1}^{*}\right]$, that is the $[R_j^{*}]$ imported from the previous state,

and is depleted by $(\lambda_j+\mu_j)\left[R_j^*\right]$, that is by the $\left[R_j^*\right]$ that transitions to the next state or is quenched. Thus, flashes produce only new $[R_1^*]$, which is depleted by $(\lambda_1+\mu_1)\left[R_1^*\right]$, and localized at times of flashes by the Dirac mass δ_t. The rate equations for $[R_j^*]$ are:

$$\frac{d}{dt}\left[R_1^*\right]=\Phi\delta_t-(\lambda_1+\mu_1)\left[R_1^*\right], \tag{4a}$$

$$\frac{d}{dt}\left[R_j^*\right]=\lambda_{j-1}\left[R_{j-1}^*\right]-(\lambda_j+\mu_j)\left[R_j^*\right] \quad \text{for } j=2,\ldots,n. \tag{4b}$$

The $[RK]$ and hence, the phosphorylation rates of the activated rhodopsin are a function of the $\left[Ca^{2+}\right]$ that changes over the course of a flash response. A description for the case of single step rhodopsin quenching and well stirred conditions will be adopted here for sequential, multiple phosphorylations and final quenching. Only the phosphorylation rates are influenced by the calcium concentration drop, whereas Arr binding rate is assumed to be calcium-independent. By extending equation (A12) of Nikonov et al. (2000):

$$\frac{\lambda_i\left(\left[Ca^{2+}\right]\right)}{\lambda_{i,\max}}=\frac{[RK]}{[RK]_{tot}}. \tag{5}$$

This equation holds true for a single-step deactivation, for which $k_R=\lambda$ and $k_{R,\max}=\lambda_{\max}$. Thus, it is assumed that the same biochemical relationship holds at each state of R^*. From equation (C1) of Nikonov et al. (2000):

$$\frac{[RK]}{[RK]_{tot}}=\left(1+C_1\frac{[Rec]}{[Rec]_{tot}}\right)^{-1}. \tag{6}$$

According to equations (C2) and (C4) of Nikonov et al. (2000):

$$C_1=\left(\frac{\left[Ca^{2+}\right]}{K_1}\right)^2\left[\frac{1}{K_3}+\frac{1}{K_4}\frac{M}{K_2}\right][Rec]_{tot}, \tag{7a}$$

$$C_2=1+\left(\frac{\left[Ca^{2+}\right]}{K_1}\right)^2\left(1+\frac{M}{K_2}\right). \tag{7b}$$

Then the dependence on $\left[Ca^{2+}\right]$ comes from the algebraic second order equation (C3) of Nikonov et al. (2000):

$$C_1C_2\left(\frac{[Rec]}{[Rec]_{tot}}\right)^2+\left[C_1\left(\frac{[RK]_{tot}}{[Rec]_{tot}}-1\right)+C_2\right]\frac{[Rec]}{[Rec]_{tot}}-1=0. \tag{8}$$

Here K_i for $i=1,\ldots,4$ and M are biochemical parameters defined in Nikonov et al. (2000).

Activation/deactivation of transducin and PDE

During its average lifetime τ_{R^*}, photoexcited rhodopsin R^* activates many transducins ($T\rightarrow T^*$) by catalyzing GTP exchange for the GDP bound to their α-subunits. Each molecule of T^* associates, one-to-one, with a catalytic subunit of the effector forming a T^*——E complex. Full activation of the catalytic subunit is assumed, denoted by E^*. A single molecule of E^*, during its average lifetime τ_{E^*}, hydrolyzes over 50 molecules of the second messenger cGMP which, dissociating from the cationic channels they keep open, causes channel closure and thereby suppression of the inward current J_{cG} (Pugh and Lamb, 1993, 2000). T^* possesses an intrinsic GTPase activity that terminates T^*——E activity. The synthesis of cGMP overtakes hydrolysis and as the levels rise, CNG channels reopen, ending the time in saturation, T_{sat}.

Let $[T]_0$ and $[T^*]$denote the initial, basal concentration of transducin in the rod outer segment (ROS) and the concentration of activated transducin, respectively. Also, let $[E]_0$ and $[E^*]$ denote the concentrations of subunits of the effector PDE in darkness and of subunits of activated effector PDE^*, respectively. Assuming independent activation of each PDE subunit, $[PDE]_0=\frac{1}{2}[E]_0$ and $\left[PDE^*\right]=\frac{1}{2}\left[E^*\right]$, the rate equations for $[T^*]$ and $[E^*]$, for a well-stirred activation/deactivation model are:

$$\frac{d}{dt}\left[T^*\right]=\left(\frac{[T]_0-\left[T^*\right]}{[T]_0}\right)\sum_{j=1}^{n}\nu_j\left[R_j^*\right]-k_{T^*E}\left([E]_0-\left[E^*\right]\right)\left[T^*\right] \tag{9a}$$

$$\frac{d}{dt}\left[E^*\right]=k_{T^*E}\left([E]_0-\left[E^*\right]\right)\left[T^*\right]-k_E\left[E^*\right]. \tag{9b}$$

The constant k_{T^*E} in $\mu m^2\ s^{-1}$, is the rate of formation of the complex T^*——E. It is assumed that activation of a molecule of transducin occurs upon encounter with a molecule of activated rhodopsin. Thus, the first term on the right-hand side of eq. (9a) measures the increase of $[T^*]$ due to activated rhodopsin $[R^*]$. The second term measures its depletion due to its binding to PDE. The constant $k_{E^*}=1/\tau_E$, where τ_E is the average E^* lifetime dictated by the deactivation rate of the T^*——E complex. It is remarked that eqs. (9a, b) represent a simplified model of the disc cascade widely used in the literature. In order to study the behavior of rod cells under a high saturating illumination, a more detailed model is proposed and used for the numerical simulations, as reported in eqs. (21a-f), explicitly accounting for the RGS9 dynamics.

Derivation of the Pepperberg equation

Suppose that a bright flash Φ (in instantaneous number of isomerizations) applied at time $t=0$ causes cGMP levels to fall below the minimum required for CNG channel opening. Then the output current drop saturates for a time, T_{sat} (Figure 1). In practice, there are technical difficulties in measuring T_{sat}; bright flash responses do not have sharp transitions into or out of

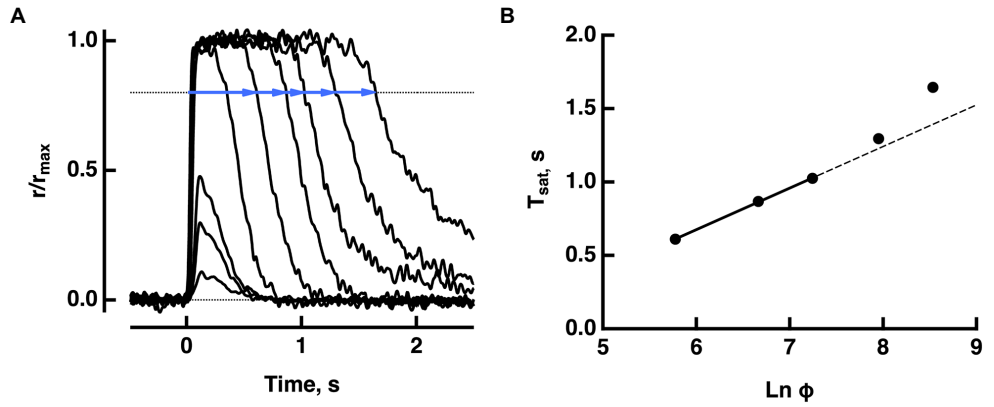

FIGURE 1
Pepperberg plot for a WT mouse rod. **(A)** Photocurrent responses of a rod to flashes of increasing strength, presented at time zero. For the brightest 5 flashes, saturation time (T_{sat}) was measured from mid-flash to a criterion recovery of 20% (blue lines). **(B)** Pepperberg plot. Flash strength was converted to photoisomerizations (Φ), using a collecting area of 0.45μm^2. The three shortest saturation times were fitted with a line; longer saturation times deviated from the line. The slope of the line τ_D=283ms, provided an estimate of τ_{E^*}, the time constant for the shutoff of T*——E. Adapted from Makino et al. (2008).

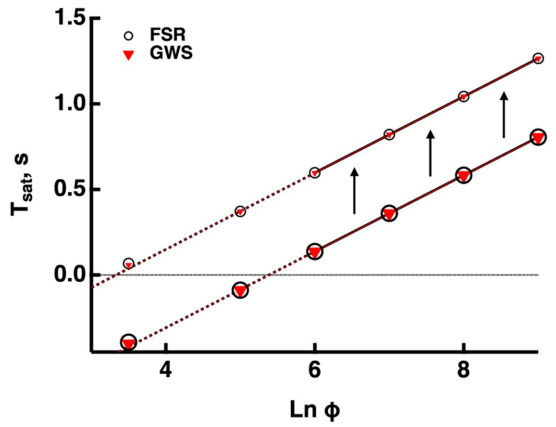

FIGURE 2
Validation of the GWS version of the model. GWS (red triangles) and FSR (open circles) models yielded nearly identical responses to bright flashes in a mouse rod. Only the four brightest flashes were saturating. The lines passing through the associated saturation times was extended to the left with dashed lines. Saturation time, T_{sat}, was measured from mid-flash to 2% recovery (larger symbols). For the purposes of illustration, T_{sat} was measured in the same way for the subsaturated responses to the two weakest flashes. For comparative purposes, T_{sat} was also measured from mid-flash to 20% recovery (smaller symbols). The slope of the Pepperberg relation was unaffected by the change in criterion recovery, but there was an upward translation equivalent to a lateral shift to a lower X-intercept.

saturation on the rising and recovery phases. Although J_{cG} terminates abruptly, the decline in J_{ex} carried by the sodium/potassium/calcium exchanger follows a slower time course and there is noise that is omnipresent in electrical recordings. To circumvent these difficulties, saturation time is typically measured from mid-flash or from flash onset to a criterion recovery of the response. Such a practice inflates T_{sat}, but the upward shift does not alter the slope of the linear portion of the Pepperberg curve (e.g., Figure 2). Various publications have adopted different criterion recovery levels, so care must be taken in comparing the X-intercepts across studies.

T_{sat} increases linearly with $Ln(\Phi)$, with slope τ_D that is determined by the shutoffs of R* and/or T*——E (Pepperberg et al., 1992, 1994). It was shown that the shutoff of T*——E was slower than that of R* (Krispel et al., 2006), so assuming that $\tau_{R^*} << \tau_{E^*}$, the value of τ_{E^*} can be determined from the slope of the Pepperberg curve. Hence,

$$T_{sat} = \tau_{E^*} Ln(\Phi) + C \tag{10}$$

for a constant $C > 0$ that has not been described previously and will be discussed in further detail below.

In deriving the Pepperberg curve equation, a well stirred condition was assumed, i.e., all concentrations were taken to be uniform inside the ROS. Moreover, it was assumed that the rhodopsins were all of one species denoted by R*. With this stipulation only eq. (4a) was in force and

$$\frac{1}{(\lambda_1 + \mu_1)} = \frac{1}{\lambda} = \tau_{R^*} \tag{11}$$

the average lifetime of R*. For a saturating flash Φ applied to the system at time $t = 0$,

$$\left[R^*\right] = \Phi e^{-t/\tau_{R^*}} \text{ for } t > 0. \tag{12}$$

It was further assumed that the effects of the intermediate activation of transducin can be lumped into a direct activation of E^* by R^*, then by a modified form of eq. (9b):

$$\frac{d}{dt}\left[E^*\right] = \nu_{RE}\left[R^*\right] - k_E\left[E^*\right] \text{ with } \left[E^*\right](0) = 0. \quad (13)$$

Integrating over $(0, T_{sat})$ where T_{sat} is a positive number to be defined:

$$\begin{aligned}[E^*](T_{sat}) &= \nu_{RE}\Phi\frac{\tau_{R^*}\tau_{E^*}}{\tau_{E^*}-\tau_{R^*}}\left(e^{-T_{sat}/\tau_{E^*}} - e^{-T_{sat}/\tau_{R^*}}\right) \\ &\approx \Phi\,\nu_{RE}\tau_{R^*}e^{-T_{sat}/\tau_{E^*}}\end{aligned} \quad (14)$$

for $\tau_{R^*} << \tau_{E^*}$. From this:

$$T_{sat} \approx \tau_{E^*}Ln(\Phi) + \tau_{E^*}Ln\left(\frac{\nu_{RE}\tau_{R^*}}{\left[E^*\right](T_{sat})}\right). \quad (15)$$

We notate $E^*_{char} = [E^*](T_{sat})$. It is a fundamental quantity that characterizes an essential feature of the system. To define T_{sat} and compute E^*_{char}, refer back to eq. (1a), viewed at times of saturation, originating from the dark-adapted state. Stipulate that the interval (0, T_{sat}) lies within the saturation regime, and that in such a regime, [*cGMP*] and [Ca^{2+}] are in quasi steady state. Thus, we may set approximately to zero the time-derivative in eqs. (1a) and (1b). Since $k_{hyd} << k_{\sigma,hyd}$, the term $k_{hyd}E^*[cGMP]$ can be neglected. It then follows from eqs. (1a) and (1b):

$$\alpha_{\max} - k_{hyd}E_{tot}[cGMP] - k_{\sigma;hyd}E^*_{char}[cGMP] = 0, \quad (16a)$$

$$\frac{1}{2}f_{Ca}J_{cG} - J_{ex} = 0. \quad (16b)$$

This relation holds for all times during which saturation is in force. For the same times, eq. (16b) yields $J_{ex} = \frac{1}{2}f_{Ca}J_{cG}$. Therefore, the total photocurrent is

$$J = J_{cG} + J_{ex} = \left(1 + \frac{1}{2}f_{Ca}\right)J_{cG}. \quad (17)$$

Let $J_{\max}$ be the maximum current that the ROS can output (typically, $J_{\max} = J_{dark}$). Then define T_{sat} as the time for which

$$J(T_{sat}) = \varepsilon J_{\max}, \text{ for a fixed small } \varepsilon \in (0,1). \quad (18)$$

Eqs. (16b) and (18) can be solved for the unknowns [*cGMP*] and [Ca^{2+}] at time T_{sat}. This permits the determination of E^*_{char} by eq. (16a). Inserting it in eq. (15) gives a linear relation between T_{sat} and $Ln(\Phi)$, with slope τ_{E^*}, of the form

$$\begin{aligned}T_{sat} &= \tau_{E^*}Ln(\Phi) - \tau_{E^*}Ln(\Phi o) \\ \text{where } \quad \Phi o &= \frac{E^*_{char}}{\nu_{RE}\tau_{R^*}}.\end{aligned} \quad (19)$$

The quantity Φo can be identified as the flash strength for which $T_{sat} = 0$. Measurement of Φo could permit the determination of E^*_{char}.

The constant *C* in eq. (10), is mathematically derived above as

$$C = -\tau_{E^*}Ln(\Phi o). \quad (20)$$

It is emphasized that *C* is proportional to τ_{E^*} and independent of Φ. This form of *C* implies that the straight lines described by eq. (19) corresponding to different values of τ_{E^*} have a common point (i.e., $\Phi = \Phi o$ and $T_{sat} = 0$) regardless of their slope. This feature actually occurs in the experimental curves of Krispel et al. (2006), reported in (Burns and Pugh, 2009) and is discussed below.

Modeling the Pepperberg plots of mutant mouse rods

Testing the validity of the GWS model

Outputs from the FSR model and the GWS version converge at very bright flashes. Since usage of the GWS version greatly facilitates numerical simulations, we ascertained whether it would be adequate for responses even to the weakest saturating flashes by computing bright flash responses for mouse rods using both models with the parameter set for mouse in the Supplementary Table S1. Figure 2 compares the Pepperberg curves; the close match of the curves verifies that even for two flash strengths that do not quite saturate the response, any spatial inhomogeneity of cascade activity was not distinguished by the two versions of the model. Hereafter, all simulations were made using the GWS model.

Since experimentally determined values for T_{sat} are always measured after some arbitrary criterion recovery, they are inflated relative to the true saturation times and the X-intercept is shifted to the left, underestimating the true values for Φo and E^*_{char} that describe the minimal conditions for saturation (see above). For modeled responses in Figure 2, we calculated that the T_{sat} values determined at 20% recovery were increased by 0.46 ms, compared to those determined at 2% recovery and that this had the effect of translating the X-intercept along the abscissa from a $Ln(\Phi)$ of 3.3 to 5.3, i.e., by a factor of 7.4-fold. Such a correction could be applied to the Pepperberg plots in the figures below for which T_{sat} was measured from mid-flash to 20% recovery, to improve the estimates of Φo and E^*_{char}. The magnitude of the translation

would have to be adjusted for determinations of T_{sat} made at different criterion levels of response recovery.

Upward bend in the Pepperberg curve due to depletion of the RGS9 complex

Once activated, T relieves an autoinhibition of PDE, allowing it to hydrolyze cGMP. The GTPase activity of T^* terminates the interaction between T^* and PDE. The intrinsic GTPase activity is slow, but is greatly enhanced by the encounter with an RGS9 complex. By showing that an increase in the expression level of the RGS9 complex accelerated flash response recovery and reduced the slope of the Pepperberg relations in rods, Krispel et al. (2006) validated the idea that the collisional delay of RGS9 complex with T^*——E was the major determinant of T^* lifetime and identified the shutoff of T^*——E as the rate-limiting step in the response recovery. Attempts to accelerate R^* shutoff by overexpression of RK did not alter the slope of the Pepperberg plot. Our model captured the Pepperberg relations for the four types of rods described in Burns and Pugh (2009), each expressing a different level of RGS9 (Figure 3). The values for τ_{E^*} from our model were: 792 ms for rods expressing 0.2x the normal amount of RGS9 complex, 381 ms for WT, 209 ms for 2-fold overexpression, and 191 ms for 4-fold overexpression. The values differ somewhat from the population averages of: 246 ms for WT, 108 ms for 2-fold overexpression, 80 ms for 4-fold overexpression obtained from linear fits over the lower range of flash strengths (Krispel et al., 2006) but conserve the overall trend.

Since the timing of T^* shutoff (i.e., τ_{E^*}) is too slow to affect the rising phase of the bright flash response, rods of each expression level should have reached saturation at a similar flash strength and all Pepperberg curves should have converged at the same X-intercept, Φo. The curves nearly converged, although the intersection fell slightly below $T_{sat} = 0$. We attribute the deviations of the experimental results from the model to biological variation and to technical issues associated with achieving the same collecting area for every rod during recording.

Burns and Pugh (2009) proposed a model for the experimentally obtained Pepperberg results of rods expressing various levels of RGS9 complex that consists essentially of eq. (9b), where k_E is replaced by $k_f[RGS9]$ for a suitable constant k_f to be computed by fitting. Since τ_{E^*} is the reciprocal of k_E, the larger [*RGS9*] the smaller τ_{E^*} and vice versa. A key assumption of that model is that [*RGS9*] remains *constant* over the range of light intensities that they analyzed. While the fit is good for lower saturating flash intensities (less than ~3,000 photoisomerizations), saturation times depart from the curves at higher flash intensities, becoming non-linear and exhibiting an upward, convex, super-linear bending (Figure 3). It would appear that a new mechanism dominates the response recovery at these flash strengths.

Because the convexity became more prominent in rods underexpressing the RGS9 complex, and was absent from rods overexpressing it, we propose that [*RGS9*] does not remain constant throughout the process. While the total mass $[RGS9]_0$ is constant, it dynamically subdivides into a portion [$RGS9$——T^*——E] bound to the complex T^*——E and a portion [$RGS9_0$] − [$RGS9$——T^*——E] available for binding to T^*——E according to the rate equations:

$$\frac{d}{dt}[T] = -\nu_{RT}[R^*]\frac{[T]}{[T]_0} + k_{cat}[RGS9--T^*--E], \quad (21a)$$

$$\frac{d}{dt}[T^*] = \nu_{RT}[R^*]\frac{[T]}{[T]_0} - k_{T^*E}[E][T^*], \quad (21b)$$

$$\frac{d}{dt}[E] = -k_{T^*E}[E][T^*] + k_{cat}[RGS9--T^*--E], \quad (21c)$$

$$\frac{d}{dt}[T^*--E] = k_{T^*E}[E][T^*] - k_f[RGS9][T^*--E] + k_b[RGS9--T^*--E], \quad (21d)$$

$$\frac{d}{dt}[RGS9] = k_{cat}[RGS9--T^*--E] + k_b[RGS9--T^*--E] - k_f[RGS9][T^*--E], \quad (21e)$$

$$\frac{d}{dt}[RGS9--T^*--E] = k_f[RGS9][T^*--E] - k_b[RGS9--T^*--E] - k_{cat}[RGS9--T^*--E], \quad (21f)$$

with initial conditions

$$[T](0) = [T]_0, [E](0) = [E]_0, [RGS9](0) = [RGS9]_0,$$

$$[T^*](0) = [T^*--E](0) = [RGS9--T^*--E](0) = 0$$

where $[T]_0$, $[E]_0$, and $[RGS9]_0$ are the initial, basal concentrations of the transducer G protein, the effector PDE and GTPase-activating protein RGS9. Here ν_{RT} is the catalytic activity of R^* to T^*, and k_{T^*E} is the coupling coefficient between T^* and E^*. Also k_f (forward) is the rate of association of the complex T^*--E per unit mass with available RGS9, and k_b (backward) is the rate of dissociation of RGS9 from the complex T^*——E. Finally, k_{cat} is the rate of deactivation of the RGS9——T^*——E complex by the hydrolysis of GTP by T^*.

The dynamics of RGS9 along its time evolution after the flash was traced from its basal values and was observed to lag slightly, the dynamics of T^*——E for flash strengths $Ln(\Phi) < 8$ (Figure 4).

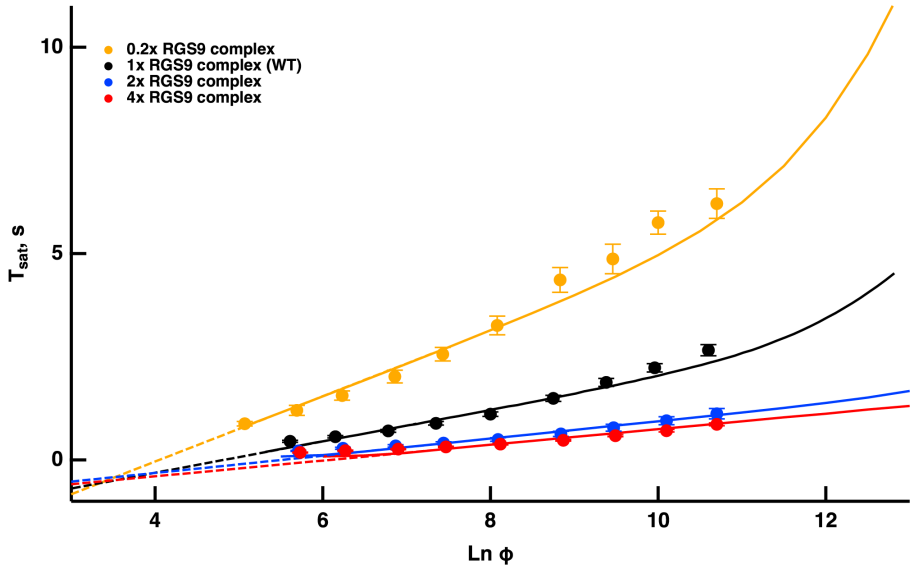

FIGURE 3
Fits of the model to experimental results of mouse rods with different expression levels of the RGS9 complex. For modeling, levels of RGS9 complex in the mutant rods were changed to 0.2x, 2x and 4x that of WT. Experimental results for R9AP+/–, R9AP75 and R9AP138 lines of mice were from Burns and Pugh (2009). T_{sat} was measured from mid-flash to 10% recovery. Continuous lines show the fits with the model, where the linear portions of the relations were extended with dashed lines to show that they intersect near T_{sat} = 0.

However, for brighter flashes there is an upward, convex, superlinear bending of the Pepperberg relations that the model attributed to a reduction in RGS9 complex availability. According to the model, T* shutoff was delayed by the extra time needed for an RGS9 complex to collide with T*——E under these conditions and in the extreme case, would theoretically approach a regime in which shutoff relied on transducin's intrinsic GTPase activity, unassisted by RGS9.

Reducing k_b slows the dissociation of RGS9 from the complex RGS9——T*——E and hence, for flashes of equal intensity, the time in saturation T_{sat} was shorter. Increasing k_f sped up the formation of the complex RGS9——T*——E, accelerating the shutoff of T*——E, and hence, for flashes of equal intensity, T_{sat} was shorter. Opposite effects occurred by increasing k_b or by decreasing k_f. In all cases, for $Ln(\Phi)<8$, their behavior is essentially that of a straight line, and in all cases, one observes a convex, superlinear bending with brighter flashes. To provide further evidence that such a pattern is due to RGS9 depletion, the red curve in Figure 3 was obtained by artificially augmenting the basal value $[RGS9]_0$ by a factor of 4 and at the same time by reducing the "forward" parameter k_f by the same factor. This way, at incipient phases of the process ($t \approx 0$), when only a negligible fraction of $[RGS9]_0$ has been turned into $[RGS9{-}{-}T^*{-}{-}E]$, the product

$$0.25\,k_f\left(4\left[RGS9\right]_0-\left[RGS9{-}{-}T^*{-}{-}E\right]\right)\approx k_f\left[RGS9\right]_0$$

remains essentially unchanged. Therefore, for low values of $[RGS9{-}{-}T^*{-}{-}E]$ the complex [T*——E] dissociates and the complex $[RGS9{-}{-}T^*{-}{-}E]$ is generated at the same rates as in the blue curve in Figure 3. A departure occurs at later times as $[RGS9]_0$ is depleted, by increasing $[RGS9{-}{-}T^*{-}{-}E]$.

Plateau in the Pepperberg curve upon exhaustion of PDE

For even brighter flashes, $Ln(\Phi)>15$, , the model predicted an asymptotic flattening in the Pepperberg curve caused by activation of all available PDE (Figure 5). Full activation of PDE achieves the greatest reduction of cGMP, hence it sets an upward limit on T_{sat}. To further explore the role of PDE expression, theoretical changes in PDE level were imposed on the model. A tenfold decrement in PDE content actually prolonged T_{sat} at all flash strengths, because there was a reduction in basal PDE activity that elevated cGMP level in darkness, extending the time required for E* activity to return to the dark level after a bright flash (gold trace, Figure 5, explained further in Nikonov et al., 2000 and commentary by Govardovskii et al., 2000). Interestingly, the upward bending from linearity in the Pepperberg curve appeared at a reduced flash strength and rose more steeply. The basis was that elevated cGMP supported a greater fraction of open CNG channels and a greater influx of Ca^{2+}. As a result, the content of Ca^{2+}-bound recoverin was higher and a greater proportion of RK was not available to initiate shutoff of R* until there was a sufficient light-induced fall in Ca^{2+}. Thus, even though PDE levels were reduced,

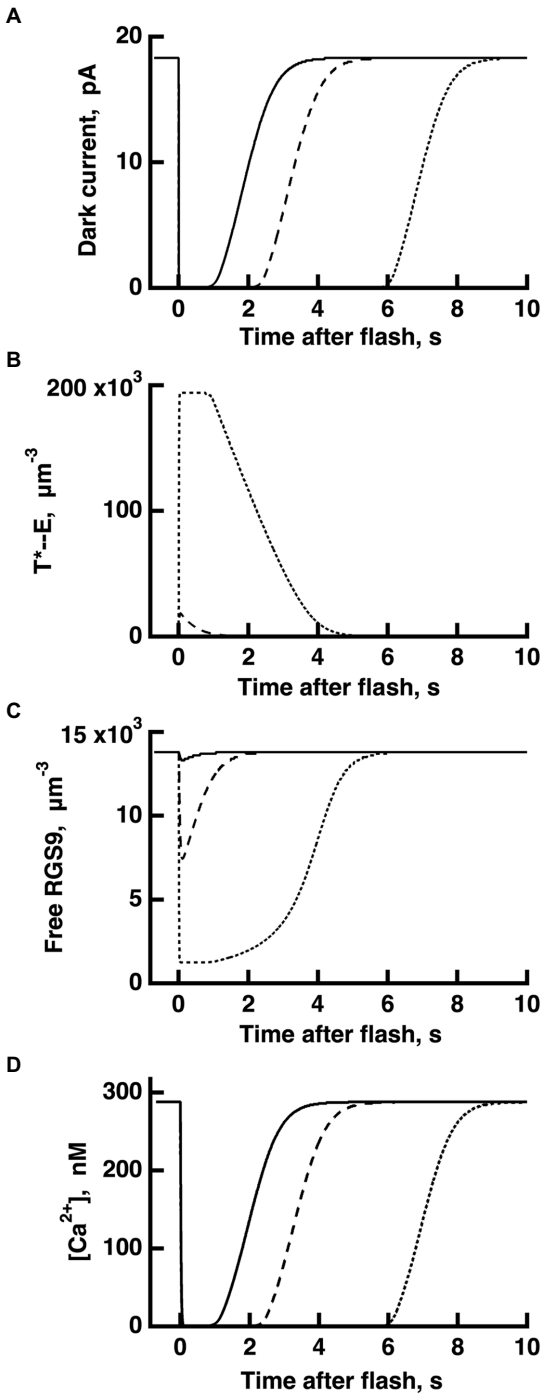

FIGURE 4
WT rod simulations for three flash responses **(A)**, and the associated dynamics for T*——E **(B)**, free RGS9 **(C)** and Ca^{2+} **(D)**. The flash was given at time zero. The three flashes elicited responses with T_{sat} values in the initial, linear segment of the Pepperberg plot, near the transition to the upward bend, and well within the upward bend, respectively (*cf.* Figure 3): *Ln* (Φ)=8 (continuous lines), *Ln* (Φ)=11 (dashed lines), *Ln* (Φ)=14 (dotted lines). Dynamics of free RGS9 deviated markedly from that of T*——E, and greatly prolonged T_{sat} for the response to the brightest flash.

each R* was able to generate more T*——E than normal. Reduced expression of PDE along with an increased number of PDE* per R* caused the Pepperberg curve to fully activate all PDE and approach the plateau with less intense flashes than for WT rods. Consistent with this explanation, the upward bending occurred with more intense flashes in mutant mice lacking recoverin (Makino et al., 2004) and occurred with less intense flashes in mutant mice expressing lower levels of RK (see below).

Under these conditions, the model was used to interrogate whether the upward bend reached its maximal rate of rise of 9–10 s, the time taken for the response recovery in the absence of RGS9 complex (Chen et al., 2000; Krispel et al., 2003a; Keresztes et al., 2004). The maximal slope within the range of the upward bend (convexity) was nearly 4 s, indicating that the maximal rate of rise was not achieved. Since the upward curvature rises less steeply for WT rods, we predict that the ratio of expression of RGS9 to PDE is adequate to ensure that T*——E shutoff would never rely on the T* GTPase activity free from RGS9 acceleration at any flash strength.

A theoretical, tenfold increment in PDE levels had minor effects in the opposite direction (red trace, Figure 5): T_{sat} was somewhat shorter at every flash strength, the upward bending and the plateau occurred at slightly greater $Ln(\Phi)$ values.

Experiments addressing the plateau in the Pepperberg plot are not yet available. Challenging technical issues and slower mechanisms of light adaptation arise with the recording of responses that remain in saturation for such extended periods to extremely bright flashes, but in principle, it could be done. An exciting recent development is that a mutant mouse has been generated with greatly reduced expression of PDE (Morshedian et al., 2022), that could be useful for testing the model predictions.

Effects of changing the rate of R* phosphorylation

A reduction in RK expression slowed R* shutoff, indicating that in large part, collision time between R* and its kinase dominates the process. Hemizygous knockout of RK reduced RK levels by 70%, increased saturation times and shifted the X-intercept to lower flash strengths, however, it did not change the slope of the Pepperberg significantly (Figure 6, see also Sakurai et al., 2011; Gross et al., 2012). Upward bending in the RK+/− Pepperberg curve occurred at a lower flash strength than in WT rods (Sakurai et al., 2011), because slower R* shutoff resulted in activation of more transducins, and a greater amount of T*——E that depleted more RGS9 at each flash strength.

Overexpression of RK by two-fold or even four-fold had little effect on saturation behavior (Krispel et al., 2006; Sakurai et al., 2011). However, expression of a mutant S561L RK on a WT background reduced saturation time without a change in slope (Figure 6, see also Gross et al., 2012). The total level of both types of RK was 8.7-fold higher than normal and the mutant form

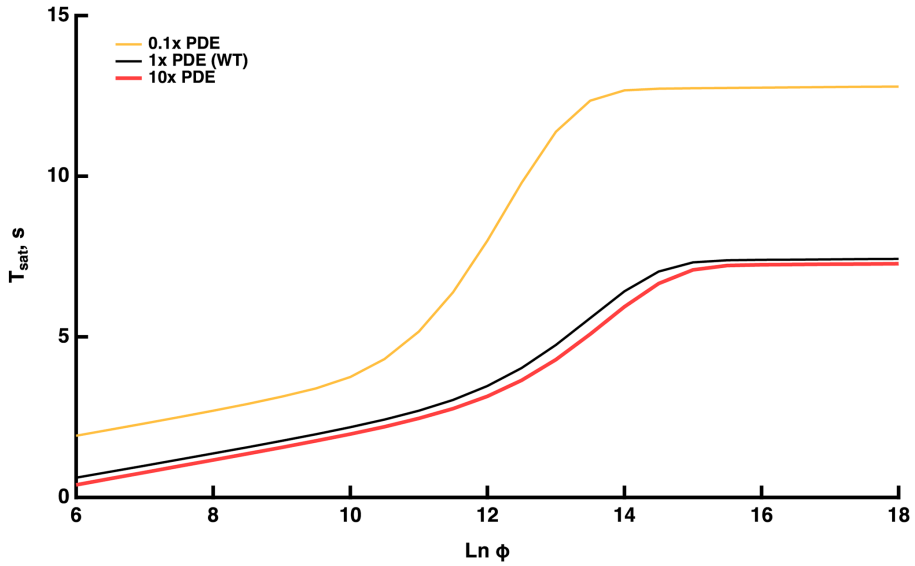

FIGURE 5
Model prediction that the Pepperberg relations will plateau with flash strengths that fully activate PDE. Predictions are also shown for theoretical variations in the level of PDE expression: 0.1x (10-fold lower level of PDE present than in WT), WT, 10x (10-fold higher level of PDE present than in WT).

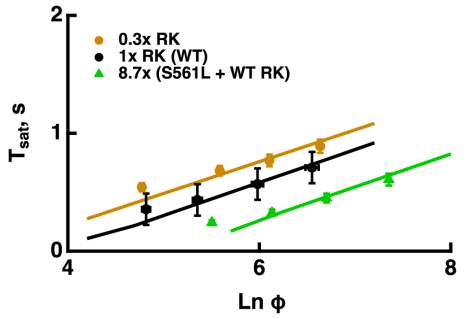

FIGURE 6
Changes in the rate of R* shutoff affected T_{sat} without a change in τ_D. Pepperberg plots for RK+/– rods with lower than normal levels of RK (0.3x RK), WT (1x RK) and rods expressing an excess of mutant, S561L RK as well as WT RK yielding a total RK content that was 8.7-fold higher than normal (S561L RK+WT). For modeling, the phosphorylation rate of R* was decreased 3-fold for RK+/– rods and increased 3-fold for S561L rods. T_{sat} was measured from mid-flash to 10% recovery. Adapted from Gross et al. (2012).

contained a sequence that specified geranylgeranylation instead of farnesylation to enhance membrane affinity and quicken R* phosphorylation. The constancy in slope in the face of changes in the rate of R* shutoff helped to advance the argument that the rate-limiting step in flash response recovery was the shutoff of T*——E.

Effects of reducing Ca^{2+}-dependent ROS-GC activity

Mouse rods normally express two GCAPs that differ in their $K_{1/2}$ for Ca^{2+}: 46–47 nM for GCAP1 and 133 nM for GCAP2 (Makino et al., 2008, 2012). According to the model, E^*_{char} changes with ROS-GC activity because the balance between cGMP synthesis and hydrolysis by E* sets the cGMP levels and thereby affects response saturation. Knockout of both GCAPs removes Ca^{2+} feedback onto ROS-GC and increases the size of the single photon response five-to six-fold by allowing for a greater drop in cGMP after the photoisomerizations (Mendez et al., 2001; Burns et al., 2002; Chen et al., 2010; Makino et al., 2012). The model captured the increases in saturation times without a change in slope in the Pepperberg relation, because τ_{E^*} remained the same (Figure 7B). Because the effect of T*——E was opposed by a lower ROS-GC activity, Φo shifts to less intense flashes. Similarly, knockout of both GCAPs from mice expressing varying levels of RK had the same effect of increasing saturation time without a change in slope (Figure 7C). Importantly, the proportional increase in saturation time was similar for all three types of rods (*cf.* Figure 6).

Knockout of GCAP2 has a less dramatic effect as the maximal rate of cGMP synthesis at low Ca^{2+} drops to 40% and the overall $K_{1/2}$ for Ca^{2+} shifts from 133 nM to ~47 nM (Makino et al., 2008). The slope of the Pepperberg is unchanged, but the X-intercept shifts to a lower value because of the response prolongation due to the reduction in Ca^{2+}-dependent ROS-GC activity (Figure 7A).

Effects of removing CNG channel modulation by calmodulin

Mutant mouse rods expressing a mutant CNG channel that lacks the calmodulin binding site have reduced saturation times and a subtle but significant decrease in slope, τ_D, with no change in dark current, sensitivity or dim flash response kinetics

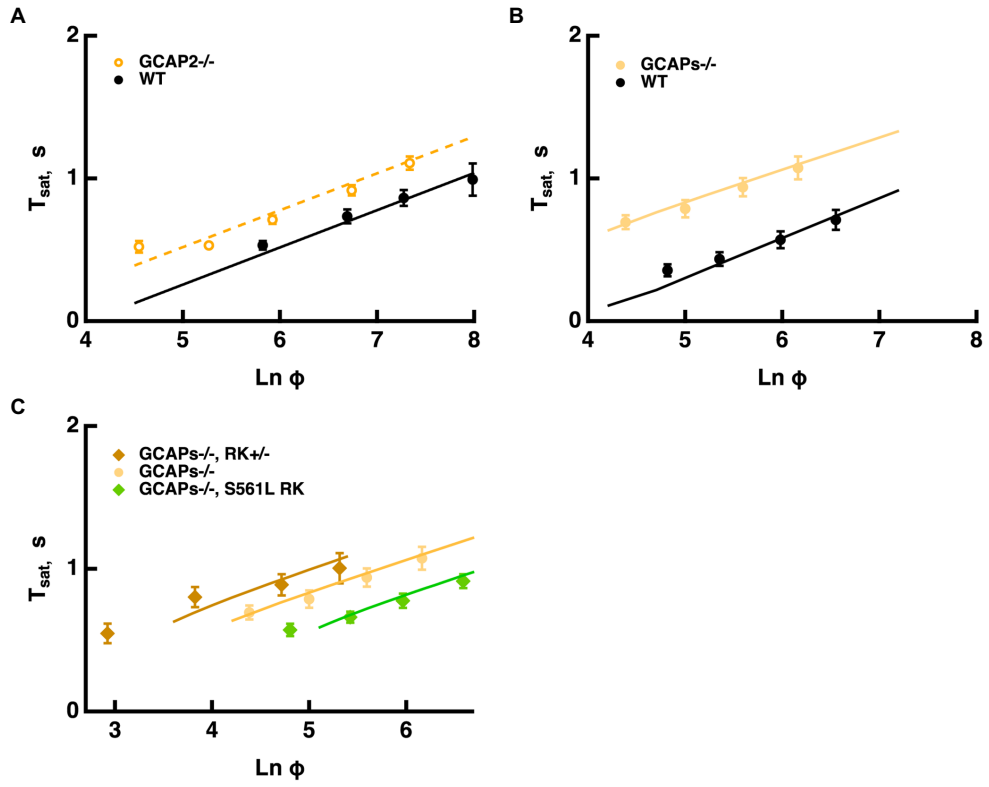

FIGURE 7
Longer T_{sat} without a change in slope of the Pepperberg relation upon reduction of Ca^{2+}-dependent ROS-GC activity. **(A)** Pepperberg plots for GCAP2 knockout and wild type rods. Results were from Makino et al. (2008); T_{sat} was measured from mid-flash to 20% recovery. **(B)** Pepperberg plots for GCAPs knockout and wild type rods. Results were from Gross et al. (2012); T_{sat} was measured from mid-flash to 10% recovery. **(C)** Pepperberg plots for mutant RK rods from Figure 6 but on a GCAPs knockout background. For the parameter set used, the model did not yield saturating responses for the double mutants at the lowest *Ln* (Φ) values used experimentally. Results were from Gross et al. (2012); T_{sat} was measured from mid-flash to 10% recovery.

(Chen et al., 2010). These experimental findings were not predicted by the model (Figure 8). Ca^{2+}/calmodulin lowers CNG channel affinity for cGMP in darkness so in the absence of calmodulin modulation, channel affinity for cGMP increases and dark current increases somewhat. During the response to a saturating flash, Ca^{2+} drops to a minimum so calmodulin no longer reduces the apparent affinity of the channel for cGMP, hence WT and mutant channels would reopen at the same concentration of cGMP. As cGMP levels recover and outer segment levels of Ca^{2+} rise, fewer WT channels will open compared to mutant channels. The steeper trajectory of the mutant rod response recovery would tend to shorten T_{sat} , but because the saturating response amplitude is larger in mutant rods, measurement of T_{sat} to 20% recovery would be made after a longer delay. The net result in simulations was a slight extension of T_{sat} at all flash strengths with the loss of CNG channel regulation by calmodulin, leaving the slope of the Pepperberg relation unchanged. The discrepancy between the experimental results and the predictions of the model indicate that other factors must come into play. The absence of calmodulin binding might indirectly affect regulation of the CNG channel in other ways, such as by affecting its phosphorylation state or by altering its interaction with Grb14. Knockout of Grb14 has the effect of reducing T_{sat} and τ_D (Woodruff et al., 2014). Another possibility is that levels of free calmodulin in the outer segment might be changed and impact other targets such as CaM kinase.

Summary and conclusion

After refining our mathematical model for phototransduction to incorporate: two Ca^{2+}-dependent ROS-GC activities to reflect the expression of GCAP1 and GCAP2 in mouse rods, Ca^{2+}-dependent shutoff of R^*, Ca^{2+}-dependence of the CNG channel affinity for cGMP, and regulation of T^*——E shutoff by RGS9, it was applied to the analysis of Pepperberg plots of mutant and WT mouse rods. Our model differed somewhat in the treatment of disk surface cascade reactions and Ca^{2+}-dependent regulations and in parameter choices, from other GWS models (e.g., Burns and Pugh, 2009; Chen et al., 2012; Invergo et al., 2014; Reingruber et al., 2020), so there were some minor quantitative differences, but all were in general agreement over their descriptions of the flash responses of WT mouse rods and those of mutant mice with various expression levels of GRK and RGS9. A distinct feature of

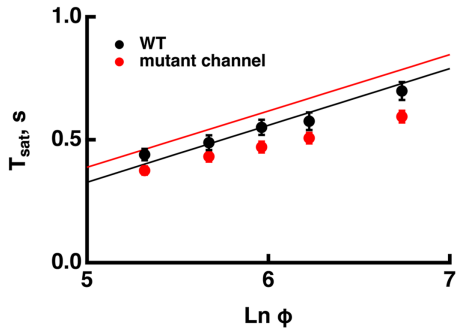

FIGURE 8
Increased CNG channel affinity for cGMP reduces saturation time with little change in Pepperberg slope in conflict with the model. T_{sat} was measured from flash onset to 25% recovery. The mutant CNG channel lacked calmodulin binding so for modeling, the K_{cG} was fixed at the minimum value at low Ca^{2+} of 13μM. For the WT, the maximum value of 32μM was used for high Ca^{2+}. The Pepperberg relation predicted by the model for rods expressing the mutant channel was shifted to longer saturation times, in comparison to that of wild type rods. Adapted from Chen et al. (2010).

our model is the inclusion of formalism describing RGS9 and PDE dynamics, that enabled us to explain three domains of Pepperberg plots: a linear segment, a segment with upward curvature, and a plateau. Other adjustments were made to explain the Pepperberg plots of various types of mutant mouse rods.

For flashes that send the response into saturation for brief periods, the time in saturation increases linearly with the natural logarithm of the flash strength. The slope of this linear domain gives the time constant of the cascade reaction that is rate-limiting to the flash response recovery. In WT rods, that reaction is the shutoff of T^*——E (Krispel et al., 2006). Changes in the expression level of RGS9 complex affect the rate of T^*——E shutoff by changing the delay before a diffusional encounter of T^*——E with an RGS9 complex. In contrast, the shutoff of R^* is faster and changes in expression level of RK over a wide range, do not change the slope. After setting up our mathematical model to incorporate these features, the model explained many features of Pepperberg plots of various mutant rods and made some predictions of how response saturation would be affected by certain conditions.

The Pepperberg relation for nearly every mutant rod that has been studied deviates from linearity at higher flash strengths, transitioning to an upward curvature, indicating that some condition has changed (e.g., Figures 1, 3). We successfully modeled the upward curvature as a flash-dependent decrease in the availability of RGS9 complex for accelerating T^*——E shutoff (summarized in Figure 9A). As the number of photoisomerizations reaches critical levels, a stoichiometric depletion of RGS9 complex by an excess of PDE activation would force some T^*——E to either wait their turn for RGS9 availability or to shut off without RGS9 complex. The flash strength at which the linear region transitions to upward curvature would then depend on how many transducins get activated per R^* and on the level of expression of RGS9 complex. Experimental observations verify both conditions (Figure 3). The model predicted that upward curvature would never asymptote to ~9s, the time required for T^*——E shutoff in the absence of RGS9 complex (Chen et al., 2000; Krispel et al., 2003a; Keresztes et al., 2004), because at extreme flash strengths, the Pepperberg relation would plateau upon activation of every PDE (Figures 5, 9A). It might at first seem paradoxical that the transition to upward bending would shift to fewer photoisomerizations with a drop in the expression level of PDE (Figures 5, 9A). However, the lower basal PDE activity permits higher cGMP levels at rest, more CNG channels open and higher internal Ca^{2+}. Recoverin then binds a greater fraction of RK, slowing R^* shutoff and allowing activation of a greater number of T^*. In addition, the greater dark current has a consequence that measurement of T_{sat} after a criterion recovery would be made at a later time after the flash, an effect that would artifactually inflate T_{sat}.

The Pepperberg relation also deviates from linearity for very short T_{sat} values because a finite time is required for Ca^{2+} levels to drop low enough to maximally accelerate ROS-GC activity. However, extrapolating the linear domain to the X-intercept yields Φo, the number of isomerizations that would just saturate the rod response with maximal ROS-GC activity and therefore stands as a gauge of sensitivity. Since flash sensitivity was unchanged by the level of RGS9 complex expression in mutant rods over a range varying from 0.3-fold to four-fold, the model predicted convergence of the Pepperberg relations of these rods, in rough agreement with our analyses of the experimental results (Figure 3). On the other hand, factors that influence flash sensitivity: Ca^{2+}-dependent ROS-GC activity (Figure 7), the affinity and the cooperativity (Hill coefficient) of the channel for cGMP (Figure 8) do alter T_{sat} and shift Φo without a change in slope of the Pepperberg relation (summarized in Figure 9B). Although moderate changes in the rate of R^* shutoff do not greatly affect flash sensitivity because of compensatory changes in Ca^{2+}-dependent ROS-GC activity (Krispel et al., 2006; Sakurai et al., 2011; Gross et al., 2012), they nonetheless shift the X-intercept because bright flash responses operate in a regime where the Ca^{2+}-dependent ROS-GC activity has reached a constant, maximal level (Figure 6). When Ca^{2+}-dependent ROS-GC activity is absent, then changes in flash sensitivity do accompany the shifts in X-intercept (Gross et al., 2012).

For practical reasons, T_{sat} is measured in experimental studies after some criterion recovery of the saturating response. This procedure inflates T_{sat} values at each flash strength (Figure 2). Although it does not affect the slope of the Pepperberg relation, it introduces a left-shift in the X-intercept, thereby underestimating the true Φo. For a criterion recovery of 20%, a correction factor of 7.4-fold would improve the estimate of Φo. A larger correction factor would be needed for use of a criterion recovery >20%.

Increases in the circulating current, for example by a theoretical increase in the density of channels in the plasma membrane or by increasing single channel conductance, were predicted to have relatively minor effects on the Pepperberg relation (summarized in Figure 9B). Mutant mice with a change in CNG channel Hill exponent or channel density in the membrane are not yet available for comparison to model predictions.

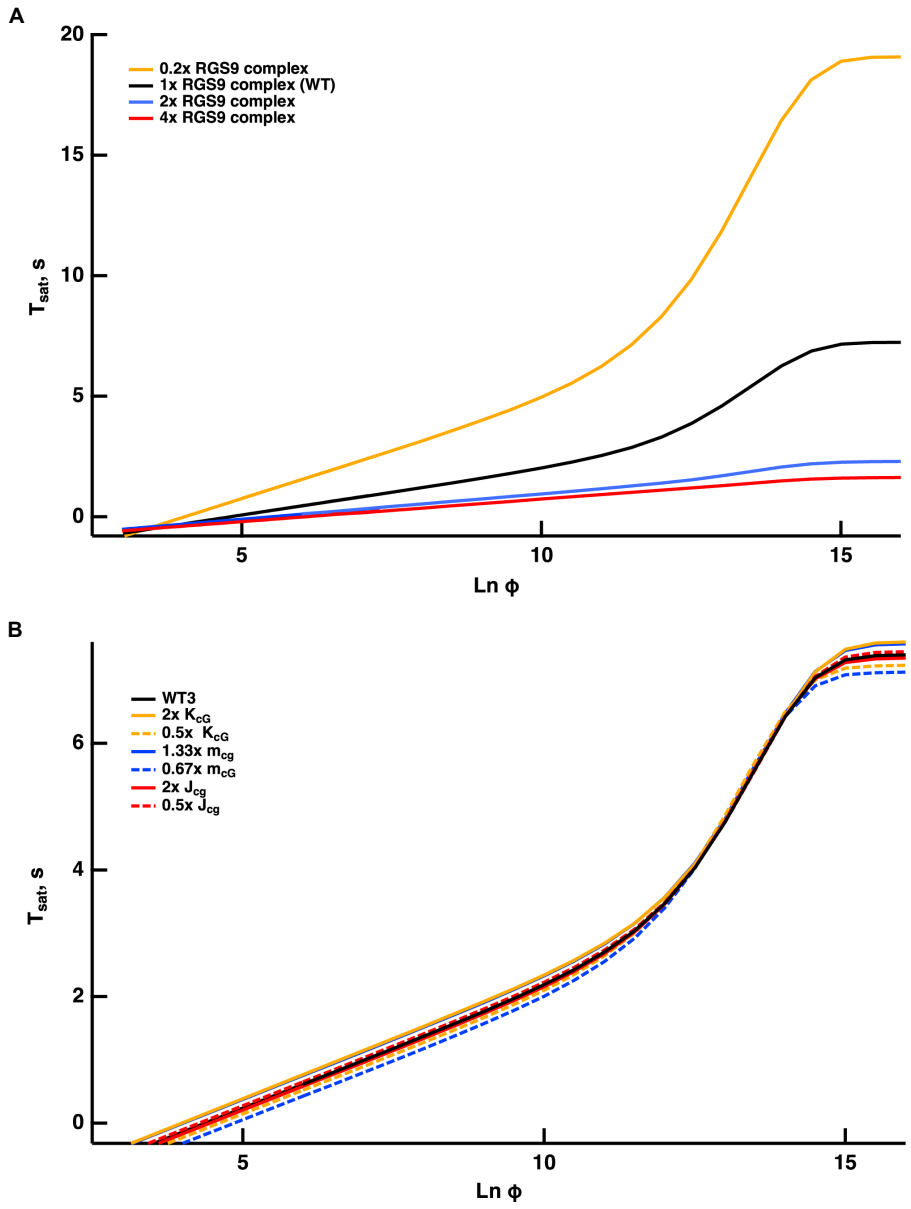

FIGURE 9
Model predictions for Pepperberg relations upon changing T*——E shutoff **(A)** or changing rod sensitivity **(B)**. Curves were generated for T_{sat} measured from mid-flash to 20% recovery. **(A)** Flash strength dependent deviations from linearity given by the model for various levels of RGS9 complex. **(B)** Shifts in the X-intercept predicted by the model for changes in sensitivity arising from alterations in the affinity of the CNG channel for cGMP or its cooperativity, or a change in dark current.

In the current version of our model, T_{sat} values reached a maximum with $Ln(\Phi) > 15$, i.e., with flashes that activate every PDE (Figure 9). But larger T_{sat} values are expected, based on the behavior of frog rods stimulated with exceedingly high flash strengths, because various phosphorylated states of R^*, late stage photointermediates and opsin continue to activate the cascade until rhodopsin is regenerated to complete dark adaptation (Firsov et al., 2005). These factors were not incorporated into our model, and new experimental results are needed for mouse rods to fully understand the how the form of the Pepperberg plot changes as this flash regime is approached.

Modeling efforts by others (e.g., Chen et al., 2010; Invergo et al., 2014) have made it clear that not all features of light adaptation can be explained by known, Ca^{2+}-dependent mechanisms regulating R^* lifetime, ROS-GC activity, and the affinity of the CNG channel for cGMP. Furthermore, additional mechanisms develop over more prolonged time courses (e.g., Calvert and Makino, 2002; Calvert et al., 2002; Krispel et al., 2003b). A future goal will be to incorporate additional modules for new mechanisms regulating the cascade into our model in order to understand the full extent of light adaptation.

Data availability statement

Publicly available datasets were analyzed in this study.

Author contributions

GC, PB, DA, and ED: conceptualization. GC, CK, HH, VG, PB, DA, ED, and CM: investigation. GC, PB, DA, ED, and CM: writing - original draft. GC, CK, HH, VG, PB, DA, and CM: review and editing. All authors contributed to the article and with the exception of ED, all approved the submitted version.

Funding

This research was funded by NEI EY031702 (CM), EY011500 (VG), and NSF DMS1812601 (ED and HH). The contents are solely those of the authors and do not necessarily express the official views of the National Science Foundation nor those of the National Institutes of Health.

Acknowledgments

We grateful to Prof. Burns for sharing Pepperberg results on mutant rods expressing different levels of RGS9 complex, expressing different RK activities, lacking GCAPs, or expressing mutant RK activities on the GCAPs knockout background, as well as for useful discussions. We also thank Prof. Fain for providing Pepperberg results on rods expressing mutant CNG channels.

Conflict of interest

The authors declare that the research was conducted in the absence of any commercial or financial relationships that could be construed as a potential conflict of interest.

Publisher's note

All claims expressed in this article are solely those of the authors and do not necessarily represent those of their affiliated organizations, or those of the publisher, the editors and the reviewers. Any product that may be evaluated in this article, or claim that may be made by its manufacturer, is not guaranteed or endorsed by the publisher.

Supplementary material

The Supplementary material for this article can be found online at: https://www.frontiersin.org/articles/10.3389/fnmol.2022.1054449/full#supplementary-material

References

Andreucci, D., Bisegna, P., Caruso, G., Hamm, H. E., and DiBenedetto, E. (2003). Mathematical model of the spatio-temporal dynamics of second messengers in visual transduction. *Biophys. J.* 85, 1358–1376. doi: 10.1016/S0006-3495(03)74570-6

Berry, J., Frederiksen, R., Yao, Y., Nymark, S., Chen, J., and Cornwall, C. (2016). Effect of rhodopsin phosphorylation on dark adaptation in mouse rods. *J. Neurosci.* 36, 6973–6987. doi: 10.1523/JNEUROSCI.3544-15.2016

Bisegna, P., Caruso, G., Andreucci, D., Shen, L., Gurevich, V. V., Hamm, H. E., et al. (2008). Diffusion of the second messengers in the cytoplasm acts as a variability suppressor of the single photon response in vertebrate phototransduction. *Biophys. J.* 94, 3363–3383. doi: 10.1529/biophysj.107.114058

Burns, M. E., Mendez, A., Chen, J., and Baylor, D. A. (2002). Dynamics of cyclic GMP synthesis in retinal rods. *Neuron* 36, 81–91. doi: 10.1016/S0896-6273(02)00911-X

Burns, M. E., and Pugh, E. N. Jr. (2009). RGS9 concentration matters in rod phototransduction. *Biophys. J.* 97, 1538–1547. doi: 10.1016/j.bpj.2009.06.037

Calvert, P. D., Govardovskii, V. I., Arshavsky, V. Y., and Makino, C. L. (2002). Two temporal phases of light adaptation in retinal rods. *J. Gen. Physiol.* 119, 129–146. doi: 10.1085/jgp.119.2.129

Calvert, P. D., and Makino, C. L. (2002). "The time course of light adaptation in vertebrate retinal rods," in *Photoreceptors and calcium*. eds. W. Baehr and K. Palczewski (New York, NY: Kluwer Academic/Plenum Publishers and Landes Bioscience), 37–60.

Caruso, G., Bisegna, P., Andreucci, D., Lenoci, L., Gurevich, V. V., Hamm, H. E., et al. (2011). Identification of key factors that reduce the variability of the single photon response. *Proc. Natl. Acad. Sci. U. S. A.* 108, 7804–7807. doi: 10.1073/pnas.1018960108

Caruso, G., Gurevich, V. V., Klaus, C., Hamm, H., Makino, C. L., and DiBenedetto, E. (2019). Local, nonlinear effects of cGMP and Ca^{2+} reduce single photon response variability in retinal rods. *PLoS One* 14:e0225948. doi: 10.1371/journal.pone.0225948

Chen, C. K., Burns, M. E., He, W., Wensel, T. G., Baylor, D. A., and Simon, M. I. (2000). Slowed recovery of rod photoresponse in mice lacking the GTPase accelerating protein RGS9-1. *Nature* 403, 557–560. doi: 10.1038/35000601

Chen, C.-K., Woodruff, M. L., Chen, F. S., Chen, Y., Cilluffo, M. C., Tranchina, D., et al. (2012). Modulation of mouse rod response decay by rhodopsin kinase and recoverin. *J. Neurosci.* 32, 15998–16006. doi: 10.1523/JNEUROSCI.1639-12.2012

Chen, J., Woodruff, M. L., Wang, T., Concepcion, F. A., Tranchina, D., and Fain, G. L. (2010). Channel modulation and the mechanism of light adaptation in mouse rods. *J. Neurosci.* 30, 16232–16240. doi: 10.1523/JNEUROSCI.2868-10.2010

Firsov, M. L., Kolesnikov, A. V., Golobokova, E. Y., and Govardovskii, V. I. (2005). Two realms of dark adaptation. *Vis. Res.* 45, 147–151. doi: 10.1016/j.visres.2004.08.005

Govardovskii, V. I., Calvert, P. D., and Arshavsky, V. Y. (2000). Photoreceptor light adaptation: untangling desensitization and sensitization. *J. Gen. Physiol.* 116, 791–794. doi: 10.1085/jgp.116.6.791

Gross, O. P., Pugh, E. N. Jr., and Burns, M. E. (2012). Calcium feedback to cGMP synthesis strongly attenuates single-photon responses driven by long rhodopsin lifetimes. *Neuron* 76, 370–382. doi: 10.1016/j.neuron.2012.07.029

Invergo, B. M., Dell'Orco, D., Montanucci, L., Koch, K.-W., and Bertranpetit, J. (2014). A comprehensive model of the phototransduction cascade in mouse rod cells. *Mol. BioSyst.* 10, 1481–1489. doi: 10.1039/C3MB70584F

Kawamura, S., and Tachibanaki, S. (2022). Molecular bases of rod and cone differences. *Prog. Ret. Eye Res.* 90:101040. doi: 10.1016/j.preteyeres.2021.101040

Keresztes, G., Martemyanov, K. A., Krispel, C. M., Mutai, H., Yoo, P. J., Maison, S. F., et al. (2004). Absence of the RGS9·Gβ5 GTPase-activating complex in photoreceptors of the R9AP knockout mouse. *J. Biol. Chem.* 279, 1581–1584. doi: 10.1074/jbc.C300456200

Krispel, C. M., Chen, C.-K., Simon, M. I., and Burns, M. E. (2003a). Prolonged photoresponses and defective adaptation in rods of $G\beta5^{-/-}$ mice. *J. Neurosci.* 23, 6965–6971. doi: 10.1523/JNEUROSCI.23-18-06965.2003

Krispel, C. M., Chen, C.-K., Simon, M. I., and Burns, M. E. (2003b). Novel form of adaptation in mouse retinal rods speeds recovery of phototransduction. *J. Gen. Physiol.* 122, 703–712. doi: 10.1085/jgp.200308938

Krispel, C. M., Chen, D., Melling, N., Chen, Y.-J., Martemyanov, K. A., Quillinan, N., et al. (2006). RGS expression rate-limits recovery of rod photoresponses. *Neuron* 51, 409–416. doi: 10.1016/j.neuron.2006.07.010

Makino, C. L., Dodd, R. L., Chen, J., Burns, M. E., Roca, A., Simon, M. I., et al. (2004). Recoverin regulates light-dependent phosphodiesterase activity in retinal rods. *J. Gen. Physiol.* 123, 729–741. doi: 10.1085/jgp.200308994

Makino, C. L., Peshenko, I. V., Wen, X.-H., Olshevskaya, E. V., Barrett, R., and Dizhoor, A. M. (2008). A role for GCAP2 in regulating the photoresponse. Guanylyl cyclase activation and rod electrophysiology in GUCA1B knock-out mice. *J. Biol. Chem.* 283, 29135–29143. doi: 10.1074/jbc.M804445200

Makino, C. L., Wen, X.-H., Olshevskaya, E. V., Peshenko, I. V., Savchenko, A. B., and Dizhoor, A. M. (2012). Enzymatic relay mechanism stimulates cyclic GMP synthesis in rod photoresponse: biochemical and physiological study of guanylyl cyclase activating protein 1 knockout mice. *PLoS One* 7:e47637. doi: 10.1371/journal.pone.0047637

Mendez, A., Burns, M. E., Sokal, I., Dizhoor, A. M., Baehr, W., Palczewski, K., et al. (2001). Role of guanylate-cyclase-activating proteins (GCAPs) in setting the flash sensitivity of rod photoreceptors. *Proc. Natl. Acad. Sci. U. S. A.* 98, 9948–9953. doi: 10.1073/pnas.171308998

Morshedian, A., Sendek, G., Ng, S. Y., Boyd, K., Radu, R. A., Liu, M., et al. (2022). Reproducibility of the rod photoreceptor response depends critically on the concentration of the phosphodiesterase enzyme. *J. Neurosci.* 42, 2180–2189. doi: 10.1523/JNEUROSCI.2119-21.2021

Nikonov, S., Lamb, T. D., and Pugh, E. N. Jr. (2000). The role of steady phosphodiesterase activity in the kinetics and sensitivity of the light-adapted salamander rod photoresponse. *J. Gen. Physiol.* 116, 795–824. doi: 10.1085/jgp.116.6.795

Pepperberg, D. R., Cornwall, M. C., Kahlert, M., Hofmann, K. P., Jin, J., Jones, G. J., et al. (1992). Light-dependent delay in the falling phase of the retinal rod photoresponse. *Vis. Neurosci.* 8, 9–18. doi: 10.1017/S0952523800006441

Pepperberg, D. R., Jin, J., and Jones, G. J. (1994). Modulation of transduction gain in light adaptation of retinal rods. *Vis. Neurosci.* 11, 53–62. doi: 10.1017/S095252380001110X

Pugh, E. N. Jr., and Lamb, T. D. (1993). Amplification and kinetics of the activation steps in phototransduction. *Biochim. Biophys. Acta* 1141, 111–149. doi: 10.1016/0005-2728(93)90038-H

Pugh, E. N. Jr., and Lamb, T. D. (2000). "Phototransduction in vertebrate rods and cones: molecular mechanisms of amplification, recovery and light adaptation," in *Handbook of biological physics Vol. 3 molecular mechanisms in visual transduction*. eds. D. G. Stavenga, W. J. DeGrip and E. N. Pugh Jr. (New York, NY: Elsevier), 183–255.

Reingruber, J., Ingram, N. T., Griffis, K. G., and Fain, G. L. (2020). A kinetic analysis of mouse rod and cone photoreceptor responses. *J. Physiol. Lond.* 598, 3747–3763. doi: 10.1113/JP279524

Sakurai, K., Young, J. E., Kefalov, V. J., and Khani, S. C. (2011). Variation in rhodopsin kinase expression alters the dim flash response shut off and the light adaptation in rod photoreceptors. *Invest. Ophthalmol. Vis. Sci.* 52, 6793–6800. doi: 10.1167/iovs.11-7158

Wen, X.-H., Dizhoor, A. M., and Makino, C. L. (2014). Membrane guanylyl cyclase complexes shape the photoresponses of retinal rods and cones. *Front. Mol. Neurosci.* 7:45. doi: 10.3389/fnmol.2014.00045

Wensel, T. G. (2024). "Biochemical cascade of phototransduction," in *Adler's physiology of the eye. 12th Edn.* eds. L. A. Levin, P. L. Kaufman, M. E. Hartnett, J. V. Busik, M. K. Duncan, D. M. Levi, et al (New York, NY: Elsevier).

Woodruff, M. L., Rajala, A., Fain, G. L., and Rajala, R. V. S. (2014). Modulation of mouse rod photoreceptor responses by Grb14 protein. *J. Biol. Chem.* 289, 358–364. doi: 10.1074/jbc.M113.517045

Zang, J., and Neuhauss, S. C. F. (2021). Biochemistry and physiology of zebrafish photoreceptors. *Pflugers Arch. Eur. J. Physiol.* 473, 1569–1585. doi: 10.1007/s00424-021-02528-z

frontiers | Frontiers in Molecular Neuroscience

TYPE Original Research
PUBLISHED 09 January 2023
DOI 10.3389/fnmol.2022.1080136

OPEN ACCESS

EDITED BY
Clint L. Makino,
Boston University,
United States

REVIEWED BY
Wolfgang Baehr,
The University of Utah, United States
Alecia K. Gross,
University of Alabama at Birmingham,
United States

*CORRESPONDENCE
Bo Chang
✉ bo.chang@jax.org

†These authors have contributed equally to this work

‡These authors share senior authorship

SPECIALTY SECTION
This article was submitted to Molecular Signaling and Pathways, a section of the journal Frontiers in Molecular Neuroscience

RECEIVED 25 October 2022
ACCEPTED 15 December 2022
PUBLISHED 09 January 2023

CITATION
Naggert ASEN, Collin GB, Wang J, Krebs MP and Chang B (2023) A mouse model of cone photoreceptor function loss *(cpfl9)* with degeneration due to a mutation in *Gucy2e*. *Front. Mol. Neurosci.* 15:1080136. doi: 10.3389/fnmol.2022.1080136

A mouse model of cone photoreceptor function loss *(cpfl9)* with degeneration due to a mutation in *Gucy2e*

Anna S. E. N. Naggert†, Gayle B. Collin†, Jieping Wang, Mark P. Krebs‡ and Bo Chang*‡

The Jackson Laboratory, Bar Harbor, ME, United States

During routine screening of mouse strains and stocks by the Eye Mutant Resource at The Jackson Laboratory for genetic mouse models of human ocular disorders, we identified *cpfl9*, a mouse model with cone photoreceptor function loss. The mice exhibited an early-onset phenotype that was easily recognized by the absence of a cone-mediated b-wave electroretinography response and by a reduction in rod-mediated photoresponses at four weeks of age. By genetic mapping and high-throughput sequencing of a whole exome capture library of *cpfl9*, a homozygous 25bp deletion within exon 11 of the *Gucy2e* gene was identified, which is predicted to result in a frame shift leading to premature termination. The corresponding protein in human, retinal guanylate cyclase 1 (GUCY2D), plays an important role in rod and cone photoreceptor cell function. Loss-of-function mutations in human *GUCY2D* cause LCA1, one of the most common forms of Leber congenital amaurosis, which results in blindness at birth or in early childhood. The early loss of cone and reduced rod photoreceptor cell function in the *cpfl9* mutant is accompanied by a later, progressive loss of cone and rod photoreceptor cells, which may be relevant to understanding disease pathology in a subset of LCA1 patients and in individuals with cone-rod dystrophy caused by recessive *GUCY2D* variants. *cpfl9* mice will be useful for studying the role of *Gucy2e* in the retina.

KEYWORDS

retinal membrane guanylate cyclase, leber congenital amaurosis, cone-rod dystrophy, mouse models, S opsin, M opsin

1. Introduction

The Eye Mutant Resource (EMR) has screened for and established robust genetic models of ocular diseases since 1988. Currently, retired mouse breeders from the production colony at The Jackson Laboratory (JAX) are screened by electroretinography (ERG), indirect ophthalmoscopy, and optical coherence tomography (OCT). Through the EMR screening program at JAX, the cone photoreceptor function loss 9 (*cpfl9*)

mutant was discovered as displaying abnormal ERG responses. The mutation was determined to cause an autosomal recessive disease, mapping to Chromosome 11, and through whole-exome sequencing was identified as a 25 bp deletion in the *Gucy2e* gene.

GUCY2E (also known as GUCY2D in humans and rats, and alternatively referred to as GC1, RGC-1, RetGC1, and PGCE) is one of two retina-specific membrane guanylate cyclases that catalyze the synthesis of cGMP in the phototransduction cascade (Pugh et al., 1997; Baehr and Palczewski, 2007). cGMP, a second messenger, affects phototransduction, calcium homeostasis, neurotransmission, and vessel dilation (Kuhn, 2016; Tolone et al., 2019) and in the retina, altered levels have been associated with photoreceptor degeneration (Yang et al., 1999; Baehr et al., 2007).

In humans, over 100 reported pathogenic mutations in *GUCY2D* (ClinVar) have been associated with an array of retinal diseases. These include autosomal recessive Leber congenital amaurosis (LCA1; MIM#204000), autosomal dominant or recessive cone-rod dystrophy 6 (CORD6; MIM#601777), choroidal dystrophy, central areolar (CACD1; MIM#215500) and night blindness, congenital stationary, Type1I (CSNB1I; MIM#618555). In mice, 27 strains with mutations in *Gucy2e* are listed in the Mouse Genome Informatics database (Blake et al., 2009), but only a few studies with mice carrying the same targeted knockout allele have characterized the disease phenotype in detail (Yang et al., 1999; Coleman et al., 2004; Baehr et al., 2007). The *cpfl9* mutation was previously reported, in a brief meeting abstract and further characterization is provided here. Extinguished cone responses and an abnormal distribution of cone photopigments and GNAT2 are early phenotypes that are similar to those previously reported (Yang et al., 1999; Coleman et al., 2004; Baehr et al., 2007). However, unique observations of the *cpfl9* model include: (1) similar cone nuclei counts compared to wild-type (WT) control mice, but a reduced number of cone matrix sheaths at 12 weeks of age, (2) prominent differences in the cellular distribution of OPN1MW (M opsin) across the retina of mutants, and (3) a partial rod and cone photoreceptor cell loss by 9–12 months of age.

2. Materials and methods

2.1. Mice

The mice utilized in this study were bred and maintained in standardized conditions of the Production or Research Animal Facilities at The Jackson Laboratory (JAX, Bar Harbor, Maine, United States). Mice provided with an NIH31 6% fat chow diet and acidified water, were housed in a pathogen-free vivarium environment with a 14-h light/10-h dark cycle. All experiments were approved by the Institutional Animal Care and Use Committee (active ACUC Protocol #99089) and conducted in accordance with the ARVO Statement for the Use of Animals in Ophthalmic and Vision Research.

2.2. Origin of *cpfl9*

The *cpfl9* abnormality was discovered in a male knock-in mouse, B6;129P2-*Foxl2*$^{tm1(GFP/cre/ERT2)Pzg}$/J (JAX stock #015854) through an ocular screen in the Eye Mutant Resource (EMR). The mouse presented with no cone ERG response at 5 weeks of age. Mice bearing the wild-type *Foxl2* allele were selected for breeding and phenotypic characterization to ensure that the ERG effects and associated disease phenotypes were not due to the *Foxl2* knock-in allele. The mutation was named *cpfl9* for cone photoreceptor function loss, further backcrossed to C57BL/6 (B6; JAX stock #000664) for two or three generations and has subsequently been maintained by repeated intercrossing to make a nearly fully inbred strain (Ne_4F_{19}), B6;129P2-*Gucy2e*^{cpfl9}/Boc (JAX stock #033197). For simplicity, we retain the original mutation designation *cpfl9*, respectively, for the remainder of the paper, and unless otherwise indicated the genotype is homozygous for the mutant allele.

2.3. Gene mapping and identification

To determine the heritability and the chromosomal location of the *cpfl9* mutation, we mated homozygous *cpfl9* mice to DBA/2 J mice. The F_1 mice, which did not exhibit retinal cone functional loss, were backcrossed to homozygous *cpfl9* mice to produce N_2 mice. Tail DNA from N_2 progeny was isolated as previously reported (Truett et al., 2000). A genome-wide scan using DNA pools from 12 affected (low cone amplitude) and 12 unaffected (normal cone amplitude) mice was carried out using 48 microsatellite markers evenly spaced throughout the genome. *cpfl9* co-segregated with markers on Chromosome 11. Subsequently, DNAs from 37 N_2 offspring were genotyped individually using microsatellite markers to develop a refined structure map of the Chromosome 11 region encompassing the recessive mutation.

The causative mutation was discovered by comparing the whole exome sequences from a homozygous *cpfl9* mutant to reference *Mus musculus* sequences (GRCm38; Fairfield et al., 2011). There was a 25 bp deletion in exon 11 of the *Gucy2e* gene in the homozygous *cpfl9* mouse. To confirm the 25 bp deletion in *cpfl9*, we chose a pair of PCR primers (Forward: TTAGATCAGCTATGGACACC, Reverse: TAGTTCCAGCATG GCATAAG) to cover the 25 bp deletion for Sanger sequencing and genotyping. PCR was carried out using tail DNA from *cpfl9* homozygous, heterozygous and wild-type mice in a 20 µl PCR reaction containing 1 × PCR buffer (10 mM Tris–HCl pH 8.3, 50 mM KCl), 250 µM of dATP, dCTP, dGTP, and dTTP, 0.2 µM of the forward and the reverse primer, 1.5 mM $MgCl_2$, and 0.6 U Taq polymerase. The following PCR program was used: 94°C for 90 s, followed by 35 cycles of 94°C for 30 s, 55°C for 45 s, and 72°C for 45 s with a final extension of 72°C for 2 min. For Sanger sequencing, PCR products were purified using HighPrep PCR magnetic beads (MagBIO, Gaithersburg, MD, United States,

catalog #AC-60050). Sequencing reactions composed of 5 µl of purified PCR product and 1 µl of primer at 10 µmol/µl. Cycle sequencing of DNA samples was performed using Edge Biosystem's BrilliantDye Terminator reaction kit Version 3.1. Sequencing reactions were purified using HighPrep DTR (MagBIO, catalog #DT-70050). Purified reactions were run on an Applied Biosystems 3730xl. Sequence data were analyzed using MacVector (v.18.2.5). For genotyping, PCR products were separated by electrophoresis on 3% MetaPhor (FMC, Rockland, ME, catalog #50184) agarose gels and visualized under UV light after staining with ethidium bromide. The sizes of the PCR products are 144 bp in wildtype and 119 bp in *cpfl9* mice.

2.4. Clinical evaluation and electroretinography

Eyes of mice used in linkage crosses and for characterization were dilated with 1% atropine ophthalmic drops (Bausch and Lomb Pharmaceuticals, Inc., Tampa, FL, United States) and evaluated by indirect ophthalmoscopy using a 78-diopter lens. Fundus photographs were taken with a Micron III *in vivo* bright-field retinal imaging microscope equipped with image-guided optical coherence tomography (OCT) capabilities (Phoenix Laboratories, Inc., Pleasanton, CA, United States).

For ERG evaluation of mutants, following an overnight dark adaptation, mice were anesthetized with an intraperitoneal injection of xylazine (80 mg/kg) and ketamine (16 mg/kg) in normal saline. Additional anesthetic was given if akinesia was inadequate. The equipment and protocol used here is as previously described (Chang et al., 2007). Briefly, dark-adapted, rod-mediated ERGs were recorded with responses to short-wavelength flashes over 4.0log units to the maximum intensity by the photopic stimulator. Cone-mediated ERGs were recorded with white flashes after 10 min of complete light adaptation. The signals were sampled at 1-ms intervals and averaged.

2.5. Histologic and immunohistochemical analysis

Mice were asphyxiated by carbon dioxide inhalation. Eyes were enucleated and immediately oriented to establish dorsal/ventral axes using a transilluminating dissecting microscope and marked at the nasal posterior artery using a tissue marking dye (Cancer Diagnostics Inc., catalog # 0762-S) prior to fixation. Tissue specimens were fixed overnight in cold methanol:glacial acetic acid:phosphate-buffered saline (3:1:4 by volume). Globes were paraffin-embedded and cut into 6-µm sections at the optic nerve and stained with hematoxylin and eosin. Stained eye sections were imaged on a NanoZoomer 2.0 digital scanner (Hamamatsu, Bridgewater, NJ). For immunohistochemical analysis, sections were deparaffinated in xylene, rehydrated through an alcohol gradient, and antigen retrieval was performed by microwave treatment in 10 mM citrate buffer. Sections were then blocked and permeabilized for 1 h at RT in blocking solution (2% normal donkey serum, 0.5% Triton X-100 in PBS), followed by primary antibody incubation at 4°C overnight. Fluorescent detection was performed with Alexa Fluor 488–conjugated goat anti-rabbit (#A21206) and Alexa Fluor 647-conjugated donkey anti-goat (#A32849TR) secondary antibodies (Invitrogen, Waltham, MA, United States). For detection of cone matrix sheaths, sections were co-stained with rhodamine-PNA (#RL-1072, Vector Laboratories, Burlingame, CA, United States) for 2 h at room temperature. For fresh cyrosections, enucleated eyes were oriented in a cryomold filled with optimal cutting temperature compound and snap-frozen in a 2-methyl butane in a lined metal box containing liquid nitrogen. Eyes were sectioned in 10-µm sections. Cryosections were fixed with 4% PFA in PBS for 10 min, incubated in blocking solution at RT for 30 min and incubated with primary antibody overnight. After washing in PBS, tissues were incubated in secondary antibodies/DAPI for 2 h at room temperature. After washing in PBS, samples were mounted in Vectashield and fluorescent signals visualized using a Zeiss Axio Observer with ApoTome 2.0 (Carl Zeiss, Germany).

Anti-guanyl cyclase E (GUCY2E; AB14788, Abcam), an antibody selected against the C-terminal end of murine retinal guanylyl cyclase 1 protein (AAC42081; according to the manufacturer), was tested on mutant and B6 control retinas. Other antibodies used were anti-rhodopsin (MAB5356; Millipore, Billerica, MA, United States), anti-blue opsin (OPN1SW; AB5407; Santa Cruz), anti-red/green opsin (OPN1MW; AB5405; Millipore, Billerica, MA, United States), anti-cone transducin (GNAT2; PA5-22340, Thermo Fisher), and anti-cone arrestin (ARR3, AB15282; Millipore, Billerica, MA, United States).

2.6. Retinal flatmounts

Following carbon dioxide inhalation, enucleated eyes were dissected mid-limbus in ice-cold 4% PFA. Eye cups were placed in 4% PFA for 2 h at 4°C, cut into petals, and retinas gently peeled from the retinal pigment epithelium (RPE)-choroid-sclera using a nitrocellulose membrane. After fixation, tissues were incubated in blocking solution for 2 h at RT followed by primary antibody for 3 days at 4°C with constant shaking. After washing in PBS, retinal flatmounts were immersed in a solution containing Alexa Fluor 488–conjugated goat anti-rabbit (#A21206) and Alexa Fluor 647-conjugated donkey anti-goat (#A32849TR) secondary antibodies (Invitrogen, Waltham, MA, United States). For cone staining, retinas were co-stained with rhodamine-PNA (#RL-1072, Vector Laboratories, Burlingame, CA, United States) for 2 days at 4°C with constant shaking. DAPI (#D1306, Invitrogen) was used as a nuclear stain. After several washes in PBS, tissues were post-fixed in 4% PFA for 10 min. Samples were rinsed through a glycerol gradient and then cover slipped in Vectashield mounting medium (H1000, Vector Laboratories). Samples were imaged at 10× using a Zeiss Axio Observer (Carl Zeiss). For cone counts, image stacks

through the outer retina were acquired at dorsal and ventral regions using a Stellaris confocal microscope. To quantify cone matrix sheaths stained with PNA in these regions, the Find Maxima tool of Fiji was adjusted manually to optimize the identification of individual sheaths, with additional manual review of the image stack to identify sheaths that were not detected by the Find Maxima operation or to resolve overlapping sheaths where needed. For high-resolution imaging, image stacks were acquired on a Leica SP8 confocal microscope using a 63× glycerol objective and 1.5x digital zoom, 1.0 µm z-step. Image stacks were analyzed in Imaris 9.7.4 (Bitplane, South Windsor, CT, United States).

2.7. qRT-PCR analysis

Total RNA was isolated from postnatal day 18 (P18) retinas of B6 ($n = 6$) and homozygous *cpfl9* mice ($n = 6$) using TRIzol (Life Technologies)/chloroform treatment as previously described (Weatherly et al., 2022). RNA clean-up and DNase digestion was performed on an RNeasy spin column (Qiagen, Germantown, MD). Total RNA was eluted in RNase-free water and quantified using a Nanodrop ND1000 spectrophotometer (Thermo Fisher) and cDNA was generated using the Superscript IV First Strand Synthesis System (Thermo Fisher) according to manufacturer's protocol.

Quantitative RT–PCR was performed in a 20 µl PCR reaction using the iTaq Universal SYBR Green SuperMix (Bio-Rad) and *Gucy2e*-specific primers positioned upstream (ex3F, CAGGGCTCAAGAACACCAGG; ex4R, GACCCCACAAAAGCCAGAGA) and downstream (ex12F, CTCAGCCACAGATGGAGGC; ex14R, CTTCGGATGCTGGAGCAGTA) of the *cpfl9* mutation and G*nat2*-specific primers (ex7F, TGTTTGATGTGGGAGGGCAG; ex8R, GATGGACGTAGCCGCAAAGA) on a CFX96 Real-Time PCR Detection System (Bio-Rad). The comparative CT method ($\Delta\Delta C_T$) was used to calculate a relative fold change in gene transcripts. Quantification was performed using $2^{-\Delta\Delta CT}$ with *Actb* (F, CCAGTTCGCCATGGATGACGATAT; R, GTCAGGATACCTCTCTTGCTCTG) as an internal control calibrator. Correct amplification of the target genes was verified by sequence and melting curve analyzes.

2.8. Western analysis

Enucleated eyes of four- and 12-week-old *cpfl9* and B6 mice were placed in ice-cold Dulbecco's phosphate-buffered saline (Invitrogen) containing a proteinase inhibitor (EDTA-free; Roche, Indianapolis, IN, United States). Extraneous tissue adhering to the eye globe was trimmed away, and anterior segments were removed. The neural retina was separated from the RPE-choroid-sclera, and immediately frozen in liquid nitrogen. For retina lysate preparation, the retinal tissue from a single eye was gently homogenized using a motorized pestle (Thermo Fisher) in 80 µl ice-cold RIPA lysis buffer (0.5% sodium deoxycholate, 0.1% SDS, 1% NP-40, 1× PBS), supplemented with complete EDTA-free, proteinase inhibitor, Roche, Indianapolis, IN, United States. The retinal lysates were then centrifuged at 12,000×*g* for 5 min at 4°C, and the supernatants were collected. To determine protein concentration, a Bio-Rad Protein Assay (Bio-Rad) was performed according to manufacturer's protocol and absorbance values recorded at 595 nm using a DU-530 spectrophotometer (Beckman Coulter, Indianapolis, IN). Equal amounts (20 µg) of lysate protein were fractionated by SDS-PAGE (10% Tris-glycine acrylamide gel) and transferred to a polyvinylidene difluoride membrane using standard protocols (Transblot Turbo system, Bio-Rad, Hercules, CA, United States). After blocking with 5% nonfat milk in TBST (137 mM sodium chloride, 20 mM Tris, and 0.05% Tween-20, pH 7.5), the blots were incubated with the indicated primary antibodies diluted in in TBST overnight and detected with either an anti-rabbit (#7074S, Cell Signaling) or anti-goat (#HAF017, R&D Systems) HRP-conjugated secondary antibody diluted 1:2000 in 5% nonfat milk (TBST). Signals were detected using Clarity Western ECL substrate (#1705060, Bio-Rad). Western blot bands were quantified by densitometry using Fiji (Schindelin et al., 2012) and the signals of the target protein were normalized to that of GAPDH. Images of immunoblots were acquired using the Syngene GeneFlash gel documentation system (Synoptics Ltd., Cambridge, United Kingdom) and immune-positive bands were digitally inverted in Fiji (Schindelin et al., 2012). Brightness and contrast were adjusted in Fiji.

Antibodies used for the studies included anti-arrestin (ARR3, 11100-2-AP, Proteintech, Rosemount, Illinois), anti-guanylate cyclase E (GUCY2E; AB14788, Abcam, Cambridge, UK), anti-cone transducin (GNAT2; PA5-22340; Thermo Fisher), anti-blue opsin (OPN1SW; AB5407; Santa Cruz), anti-red/green opsin (OPN1MW; AB5405; Millipore, Billerica, MA, United States) and anti-GAPDH (#2118, Cell Signaling, Danvers, MA).

2.9. Transmission electron microscopy

For ultrastructural analysis, enucleated eyes from six-week-old B6 and homozygous *cpfl9* mice were placed in 2.5% glutaraldehyde/2% paraformaldehyde fixative solution in phosphate buffer. Anterior segments were removed by incising along the limbus with Vannas scissors and discarded. The resulting eyecups were incubated in fixative for 2 h. The posterior segment was cut into four quadrants. Additional fixation with 0.25% glutaraldehyde/0.2% paraformaldehyde fixative was performed for 8 h followed by post-fixation with 1% osmium tetroxide. The dehydrated blocks were embedded in plastic. Posterior eyes were cut into ultra-thin sections, stained with uranyl acetate and lead citrate and examined with a JEM-1230 transmission electron microscope (JEOL, Ltd., Peabody, MA).

2.10. Variant analysis

Published missense and truncating alleles of the human *GUCY2D* gene were ascertained through UniProt (UniProt Consortium, 2021; Q02846) and ClinVar (Landrum et al., 2018), respectively.

2.11. Statistics

Results are represented as mean ± SEM except where noted. Statistical significance was determined in GraphPad Prism (Dotmatics, Boston, MA, United States) using unpaired two-tailed Student's *t*-tests, two-way repeated measures ANOVA, and mixed effect ANOVA for data in which values were missing. Values of $p < 0.05$ were considered statistically significant.

3. Results

3.1. Discovery of cone photoreceptor function loss 9 (*cpfl9*) mice

The spontaneous mutation, *cpfl9* was discovered during an ERG screen in the Eye Mutant Resource (EMR) at The Jackson Laboratory. The proband, which presented with no cone ERG response at 5 weeks of age, was mated to a B6 female mouse with normal cone function. The resultant F_1 progeny had normal cone ERG responses and were subsequently intercrossed. The intercrossed (F_2) offspring (3 female and 4 male mice) were tested for cone function by ERG, and 29% (2/7) showed no cone ERG responses. These findings indicated that the *cpfl9* was an autosomal recessive mutation.

Detailed characterization of ERG responses indicated defects in both rod and cone photoreceptor cell function of homozygous *cpfl9* mice. B6 mice at 4 weeks of age produce robust ERG responses under scotopic and photopic conditions (Figures 1A,B). Scotopic responses of 4-week-old homozygous *cpfl9* mice, although reduced compared to B6 control mice, were still observable (Figure 1A). By contrast, photopic b-wave responses recorded in the presence of background light were undetectable in homozygous *cpfl9* mutants even at the highest stimulus intensities (Figure 1B). Analysis of response amplitudes as a function of light stimulus intensity indicated that the scotopic responses in homozygous *cpfl9* mice were roughly a third of those in B6 control mice (Figure 1C). Statistically significant differences in the scotopic a- and b-wave amplitudes of *cpfl9* and B6 mice were observed at the highest stimulus intensities and in the photopic b-wave amplitude at all intensities (Figure 1C). These results indicate that homozygous *cpfl9* mice have phototransduction pathway deficits.

3.2. Genetic and molecular basis of the *cpfl9* mutation

Pooled DNA for linkage analysis of *cpfl9* showed the mutation co-segregated with markers on Chromosome 11. Subsequently, genotyping of individual DNAs of 37 N_2 offspring using microsatellite repeat markers was used to refine the critical region encompassing the mutation to a 9 cM interval between markers *D11Mit349* and *D11Mit4* (Supplementary Figure S1A).

To identify the causative mutation of *cpfl9*, whole exome sequences from a homozygous *cpfl9* mutant were compared with reference *Mus musculus* exome sequences (GRCm38). A 25 bp deletion in exon 11 (c.2209_2233del; Figure 2A) of the *Gucy2e* gene was discovered and subsequently confirmed to be specific to *cpfl9* by standard PCR and Sanger sequencing. PCR amplification of the region flanking the mutation revealed the expected 25 bp size difference between the mutant (119 bp) and wild-type (144 bp) alleles (Figure 2B). Chromatograms spanning the deletion are shown in Supplementary Figure S1B. This spontaneous deletion in exon 11 is predicted to result in a frame shift and premature termination at codon 746.

To determine whether the *cpfl9* deletion affects cone signaling early in phototransduction, we examined the expression of the gene encoding the alpha subunit of the cone-specific heterotrimeric G-protein, cone transducin (*Gnat2*) at postnatal day 18 (P18). Comparison of quantitative RT–PCR levels of *cpfl9* and B6 control mRNA revealed a significant reduction of *Gnat2* mRNA in *cpfl9* retinas compared to B6 retinas (relative normalized expression; two tailed Student's t-test; $p < 0.0001$; Figure 2C).

To examine the effects of the 25 bp deletion on *Gucy2e* transcript levels, we performed quantitative RT-PCR on *cpfl9* and B6 control retinal lysates. We observed a significant reduction in *Gucy2e* transcripts upstream (exon 3–4) and downstream (exon 12–14) of the *cpfl9* deletion (Figure 2C; relative normalized expression; two tailed t-test; $p < 0.00005$ for both). The use of an antibody directed against a carboxy terminal peptide of GUCY2E did not detect GUCY2E in isolated *cpfl9* retinal lysates by western analysis (Figure 2D), or in the mutant photoreceptor outer segment (OS) by immunohistochemistry from 4-week-old mice (Figure 2E), indicating that *cpfl9* mutants fail to make a full length GUCY2E protein.

3.3. Age-dependent clinical, histological, and functional features of *cpfl9* mutants

Fundus and OCT images at 4 and 12 weeks of age (Supplementary Figure S2) did not differ between homozygous *cpfl9* mutants and B6 controls. However, at 9 months of age some mutants showed small discrete white spots that were not observed in control mice. Interestingly, in other mouse eye disease models (Kameya et al., 2002; Fogerty and Besharse, 2011; Kim et al., 2014; Rice et al., 2015; Zhu et al., 2019) these white spots have been found to correspond to activated immune cells (macrophages and/or microglia) in the subretinal space.

To assess whether morphological changes to the retina occurred in homozygous *cpfl9* mice, representative histological sections were examined in mice at 4 and 12 weeks and at

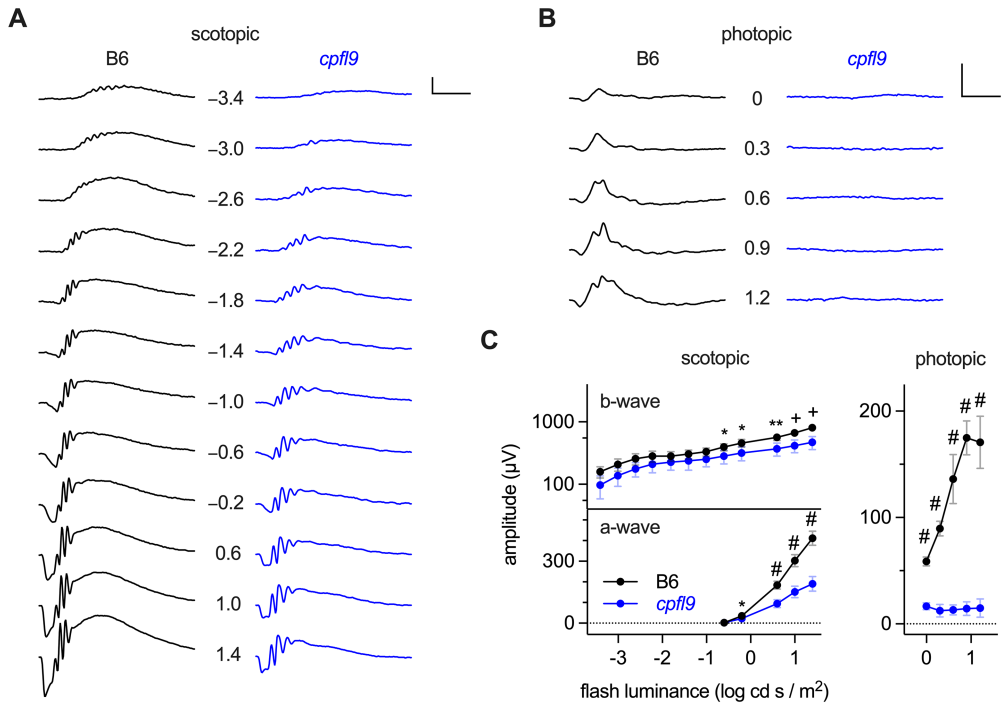

FIGURE 1
ERG responses of B6 and homozygous *cpfl9* mice at four weeks of age. **(A)** Representative scotopic ERG responses to light stimuli of increasing intensity as measured in a single eye of B6 (black traces) and homozygous *cpfl9* (blue traces) mice. Traces show the mean response recorded from two flashes. The flash illuminance in log cd s/m^2 is indicated. **(B)** Photopic responses of the same eyes. Vertical scale bars in **A** and **B**, 200µV; horizontal, 50ms. **(C)** Light dose–response analysis showing scotopic b-wave and a-wave and photopic b-wave amplitudes of B6 (black circles, n=7) and *cpfl9* (blue circles, n=8). Values indicate mean±SD. Two-way repeated-measures ANOVA indicated a statistically significant effect of strain on each response (scotopic b-wave, $F(1, 13)=16.5$, $p=0.0013$; scotopic a-wave, $F(1, 13)=131.6$, $p<0.0001$; photopic b-wave, $F(1, 13)=509.3$, $p<0.0001$). *Post hoc* multiple-comparison testing (Šídák) revealed statistically significant differences in response amplitude between strains as indicated by symbols (*, $p< 0.05$; **, $p<0.01$; +, $p< 0.001$; #, $p<0.0001$).

9–12 months of age (Figure 3A). At 4 weeks of age the rows of ONL nuclei counted at intervals throughout the retina were comparable between *cpfl9* and B6 age- and sex-matched controls (Figure 3B). A decrease in row count was observed in *cpfl9* at 12 weeks of age, but a statistically significant effect of strain on row count was not observed. By 9–12 months of age, a statistically significant effect of strain was apparent (two-way mixed effect ANOVA, $F(1,6)=28.8$, $p=0.0017$). At this age, *post hoc* multiple comparison testing (Šídák) indicated a statistically significant loss of rows in the central retina of *cpfl9* compared to B6 mice (Figure 3B). The number of cone nuclei, identified based on nuclear morphology, was also assessed at intervals throughout the retina (Figure 3C). At 4 and 12 weeks of age, no effect of strain on cone nuclei counts was evident. However, at 9–12 months of age, a statistically significant effect of strain was apparent (two-way mixed effect ANOVA, $F(1,13)=27.6$, $p=0.00016$; B6, n = 7, *cpfl9*, $n=8$). It should also be noted, that at 9–12 months of age the cone nuclei were morphologically abnormal and difficult to discern by this approach, even in B6 mice. As a further test of the loss of ONL nuclei, the rows of nuclei and cone counts at all locations were summed in samples for which the full retina was assessed (Figure 3D). A statistically significant decrease in rows was observed at 12 weeks of age (B6, 163 ± 9 rows; *cpfl9*, 144 ± 5 rows; t-test, $p=0.021$; B6, $n=5$, *cpfl9*, $n=3$) and 9–12 months of age (B6, 157 ± 13 rows; *cpfl9*, 115 ± 10 rows, or 73% of the B6 value; Student's t-test, $p=0.0020$; B6, $n=4$, *cpfl9*, $n=4$; values represent mean ± SD). The sum of the cone count at all locations (Figure 3D) showed no significant difference at 4 and 12 weeks but a statistically significant decrease at 9–12 months of age (B6, 65 ± 10 cone nuclei; *cpfl9*, 44 ± 6 cone nuclei, or 68% of the B6 value; Student's t-test, $p=0.00028$; B6, $n=7$, *cpfl9*, $n=8$). Together, these results reveal a progressive degenerative loss of rod and cone photoreceptor cells with age in homozygous *cpfl9* mice.

To assess whether photoreceptor cell loss was accompanied by functional decline, we analyzed ERG response amplitudes in older mice. As photopic responses were extinguished at 4 weeks of age (Figure 1), the analysis was limited to scotopic responses. Statistically significant differences in both a- and b-wave scotopic response amplitudes of homozygous *cpfl9* and B6 mice were observed at 12 weeks and 9–12 months of age (Supplementary Figure S3A), and a progressive decrease in ERG response in homozygous *cpfl9* mice over this period was apparent (Supplementary Figure S3B). However, the ERG response of B6 mice also declined (Supplementary Figure S3B), despite a negligible change in ONL nuclei count (Figure 3D). A similar age-dependent decrease in the scotopic ERG response without photoreceptor loss has been

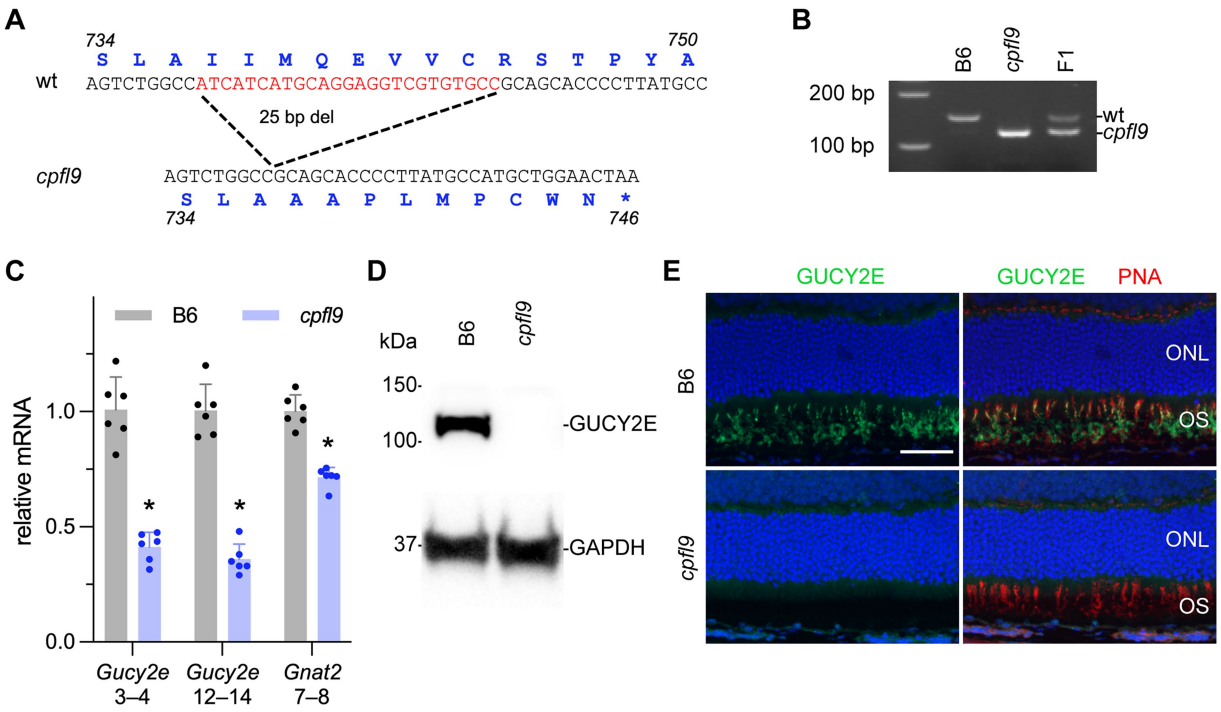

FIGURE 2
Molecular characterization of the *cpfl9* mutation. **(A)** Comparison of wild-type reference (Ensembl, ENSMUSG00000020890, GRCm39) and *cpfl9* genomic sequences of *Gucy2e* exon 11. A 25-bp deletion was observed in *cpfl9* mutant (shown in red). Corresponding amino acid sequences from *Gucy2e*-201 transcript are shown in blue. **(B)** Genotyping of homozygous *cpfl9*, B6 and F1 DNA by standard PCR/gel electrophoresis detects the WT allele at 144bp and the mutant allele at 119bp. F_1 mice are heterozygous carrying one copy of each WT and mutant allele. **(C)** Quantitative RT-PCR of retinal lysates at P18 was performed using primers specific for *Gucy2e* (exons 3–4 and exons 12–14) and *Gnat2* (exons 7–8). The mean fold-change value ± standard error is shown. B6 (n=6), gray; *cpfl9* (n=6), blue; circles represent the values from individual mice. Asterisks indicate p<0.0005, two-tailed Student's t-test. **(D)** Representative lanes of an immunoblot with anti-GUCY2E in 4-week-old B6 and *cpfl9* retinal lysates. The predicted 120kDa band was observed in B6 while absent in *cpfl9* retinas. The GAPDH loading control was observed at similar levels in both samples. Lysates from n=5 *cpfl9* and n=5 B6 mice were analyzed in separate lanes of the same blot. **(E)** Immunohistochemical staining with anti-GUCY2E (green) and PNA (red) shows absence of GUCY2E expression in photoreceptor OS of *cpfl9* retinas compared to B6. Images are representative of n=5 *cpfl9* and n=5 B6 mice. Scale bar, 50µm.

reported in previous studies of B6 mice (Li et al., 2001; Ferdous et al., 2021). Thus, to determine whether ERG responses decline more rapidly in *cpfl9* mice, response amplitudes as a function of age were fit to a mono-exponential decay with lag (Supplementary Figure S3B), which has been used previously to model progressive photoreceptor degeneration in mice (Clarke et al., 2000; Collin et al., 2020). A statistically significant increase in the rate constant of the a-wave response amplitude decay curve was observed in homozygous *cpfl9* mice, indicating a more rapid loss of rod photoreceptor function than in B6 mice (Supplementary Figure S3B). This finding supports our histological evidence for progressive rod photoreceptor cell loss in homozygous *cpfl9* mice.

As indicated by ERG, the photopic b-wave amplitude was absent in homozygous *cpfl9* mice at 4 weeks of age (Figure 1). However, cone nuclei counting indicated the number of cone photoreceptor cells at 4 and 12 weeks of age was comparable in B6 and *cpfl9* mice (Figure 3D). To assess whether the loss of cone function was due to changes in the expression of cone proteins, we performed western analysis on retinal lysates from *cpfl9* mutant and B6 control mice at 12 weeks of age (Figure 3E). While similar levels of cone arrestin (ARR3) were detected in retinas from *cpfl9* and B6 mice, immunoblotting with anti-GNAT2 showed a 43% reduction of protein in *cpfl9* mutants compared to the B6 control (two-tailed Student's t-test, $p < 0.005$). Moreover, protein levels of the cone opsins OPN1SW (blue or S opsin) and OPN1MW (green or M opsin) were decreased, while not significantly, in *cpfl9* compared to B6 retinas. These results indicate an effect of the *cpfl9* allele on expression of some but not all cone OS proteins.

3.4. Mislocalization of cone opsins and other OS proteins

To determine if the localization of cone opsin and other OS proteins was differentially affected by the *cpfl9* mutation, we stained dorsal/ventral-oriented sections with antibodies targeting OPN1SW, OPN1MW, and ARR3. At 12 weeks of age, while staining of rhodopsin was similar between mutant and controls (Supplementary Figure S4A), a pronounced mislocalization of cone opsins was observed in *cpfl9* mice

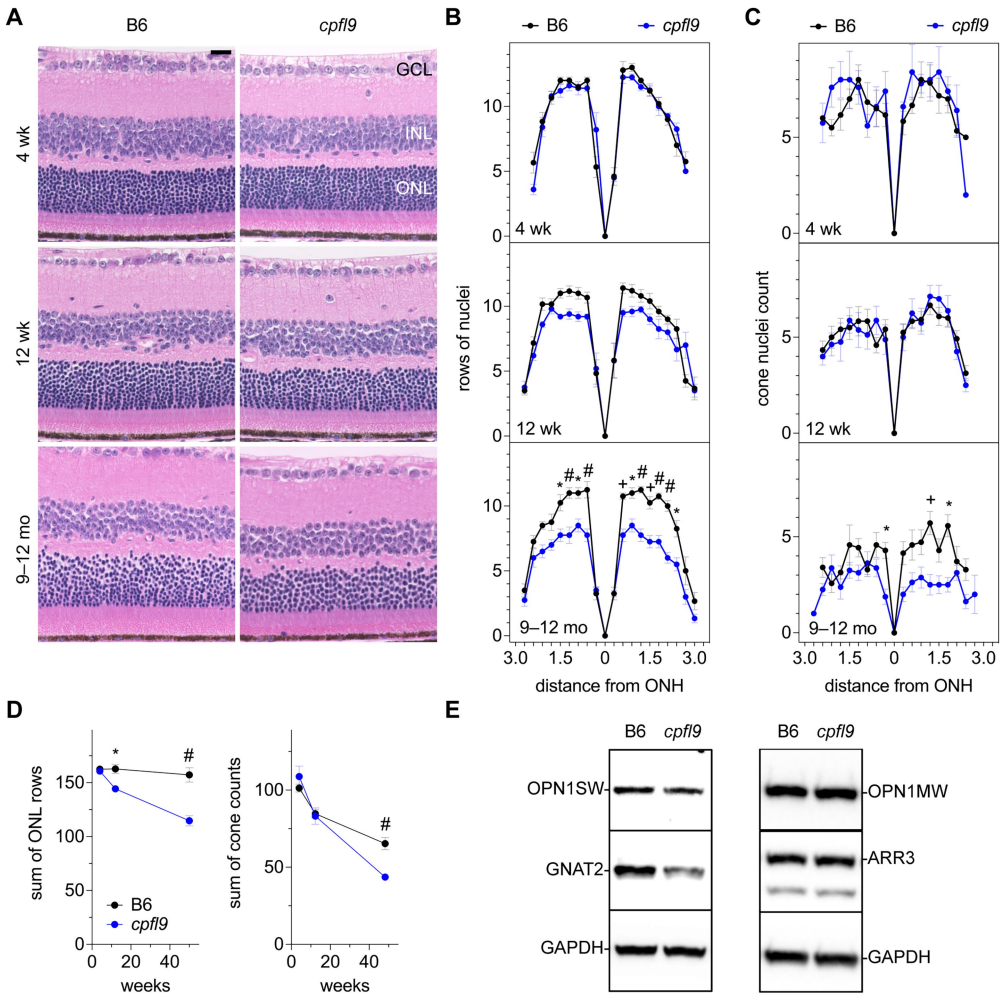

FIGURE 3
Effect of *cpfl9* mutation on retinal morphology and OS protein expression. **(A)** Retinal sections of *cpfl9* and B6 control eyes show similar hematoxylin-stained outer nuclear layer (ONL) thickness at 4 and 12weeks of age. In contrast, at 9–12months of age *cpfl9* mutants showed a thinned ONL compared to controls. GCL, ganglion cell layer; ONL, outer nuclear layer; INL, inner nuclear layer. Scale bar: 20μm. Images are representative of slide scans from n=4–8 *cpfl9* and n=4–12 B6 mice at all ages. **(B)** Longitudinal quantitation of the number rows of ONL nuclei within a 50-μm length of retina as a function of distance from the optic nerve head (ONH). B6 control mice, black circles; *cpfl9* mice, blue circles. Values represent mean±standard error of the mean (SEM); n=4–6. Statistically significant differences from *post hoc* multiple comparison testing of row counts between the strains are indicated by symbols: *, p<0.05; +, p<0.001; #, p<0.0001. **(C)** Longitudinal quantitation of cone photoreceptor nuclei within a 100-μm length of retina at regular intervals from the ONH. Values represent mean±SEM; n=4–12. Statistically significant differences from *post hoc* multiple comparison testing of cone counts between the strains are indicated by *, p<0.05; +, p<0.001. **(D)** Progressive change with age in the number of rows of ONL nuclei and cone nuclei counts summed over all retinal regions as measured in panels **B** and **C**. Values represent mean±SEM; n=4–12. *, p<0.05; +, p<0.001; #, p<0.0001. **(E)** Western analysis of retinal lysates probed with antibodies against cone-specific OS proteins: S opsin (OPN1SW), M opsin (OPN1MW), cone arrestin (ARR3) and G protein subunit alpha transducin-2 (GNAT2). GAPDH was used as a loading control. Western analysis indicated decreased expression of GNAT2 in *cpfl9* compared to B6 retinas at 12weeks of age. Images are representative of lysates from n=4 *cpfl9* and n=5 B6 mice analyzed in separate lanes of the same immunoblot.

(Figure 4A). In addition, staining of the OS protein, GNAT2 (Supplementary Figure S4B), was evident in the cone cell somata, pedicles, inner segment (ISs) and the distal OS of mutant retinas. ARR3 staining in the cone OS was similar between B6 and *cpfl9* mice at 4weeks of age, however at 12weeks, we detected intermittent regions of immune positivity in the distal OS adjacent to the RPE interface (Supplementary Figure S4C).

Examination of retinal flatmounts isolated from 12-week-old mice by confocal microscopy (Figure 4B) confirmed the immunohistochemical opsin results obtained from retinal sections. Approximate locations of areas used for quantifying cones are shown in Supplementary Figure S5. The expression of OPN1MW was decreased substantially in cone OSs of homozygous *cpfl9* mice compared to B6 mice, and the expression of OPN1SW in cone OSs of the ventral retina was also reduced, although to a lesser extent. Interestingly, although similar numbers of cone nuclei were observed between *cpfl9* mutants and B6 controls, PNA staining indicated a statistically significant reduction in the number of cone matrix sheaths in the ventral retina, as assessed by PNA staining (B6, 164 ± 15 cones, n = 4; *cpfl9*,

125 ± 6 cones, $n = 4$; unpaired two-tailed Student's *t*-test, $p = 0.008$; counts were made in an area of 0.01 mm^2; values represent mean ± SD). These results reveal a deficit in the accumulation of cone opsins in the OS of *cpfl9* mice and a loss of OS associated structures, indicating cone dystrophy.

3.5. Cone opsin mislocalization and cone dysmorphology

To understand the fate of cone opsins in the mutant mice, we further examined the stained retinal flatmounts by confocal microscopy at higher resolution (Figure 5). The OS as detected by cone opsin expression was uniformly shaped in both the dorsal (Figure 5A) and ventral (Figure 5B) regions of B6 retinas. By contrast, the accumulation of cone opsins in the OS of *cpfl9* mice was greatly diminished and the distribution of the protein within the OS was irregular. In some locations, opsins appeared to accumulate in round structures near the outer surface of the retina (Figures 5A, B, arrowheads). Thus, opsin is mislocalized, in part, to structures that are distinct from the OS and close to the subretinal space.

To assess the mislocalization of cone opsins further, we examined the retinal flatmount confocal data using Imaris display settings to visualize portions of the cone photoreceptor cells that were closer to the inner retina, including the cell body and synapse (Figure 6A). In B6 image datasets examined with these settings, a strong signal was observed in the OS region and no displacement of either OPN1MW or OPN1SW toward the inner retina was apparent. However, in *cpfl9* flatmount images, staining of these proteins was evident in the cell body (Figure 6A, white arrowheads) and in cellular processes directed toward the inner retina. OPN1SW staining appeared to include cone pedicles (Figure 6A). Thus, the cone opsins in homozygous *cpfl9* mice are also mislocalized to the cone cell bodies and pedicles.

As shown in Figure 4B, PNA staining was robust in homozygous *cpfl9* mice at 12 weeks of age, suggesting that cone matrix sheaths persist despite the decreased levels of cone opsins in the outer retinas of the mutant mice (compare *cpfl9* retinal flatmounts in 4B and 4C). To determine whether an alteration of cone sheath structure was correlated with the decreased opsin expression, we examined the high-resolution confocal datasets obtained from stained retinal flatmounts (Figure 6B). In both B6 and *cpfl9* retinas, cone sheaths as detected by PNA staining appear as elongated hollow structures in the outer retina. However, while OPN1MW and/or OPN1SW are present within the cone sheaths of B6 cone photoreceptors, these opsins are diminished in or absent from sheaths surrounding *cpfl9* cones. For example, only a small region of OPN1MW-positive staining is observed within the PNA envelope of the *cpfl9* cone shown in Figure 6B. These results suggest that cone sheaths are generated normally in *cpfl9* mice and are stable, while the contents of the associated OS changes with age.

Finally, to determine whether there were additional morphological defects in cone photoreceptors, we examined ultrathin retinal sections from homozygous *cpfl9* mutants ($n = 4$) and B6 controls ($n = 4$) at 6 weeks of age by transmission electron microscopy. The outer retina of B6 mice contained numerous OSs filled with disks in roughly perpendicular orientation to the OS axis (Figure 6C). In homozygous *cpfl9* mice, most OSs were similar to those in B6 mice. However, abnormal OS-like objects were also observed, which contained disorganized membranous structures appearing as vesicles and tubules, often adjacent to limited stacks of disks (Figures 6D–G). Long, electron dense lamellar stacks were sometimes observed to extended obliquely along the length of the OS-like objects (Figure 6E), which were found throughout the outer retina, including at the RPE (Figure 6F). Rarely, a disorganized OS was observed adjacent to an IS and/or soma of a cone cell (Figure 6G) suggesting that at least some OS-like objects derive from cone photoreceptors. The observation of disorganized vesicles and tubules in the OS-like objects of *cpfl9* mice is consistent with previous descriptions of *Gucy2e*^{tm1Gar} targeted knockout mice (Baehr et al., 2007).

4. Discussion

The *cpfl9* mouse model described in the current work shares many of the features of a previously described null mutation in *Gucy2e* mice, which has been characterized in several studies (Yang et al., 1999; Coleman et al., 2004; Baehr et al., 2007). However, our observations, which include older mice than in earlier studies, provide additional insights into the progression of disease associated with *Gucy2e* mutation in mice and provide a closer examination of the morphological changes of the cones, as these appear to be the most significantly affected cell type.

4.1. GUCY2E structure

Guanylate (also guanylyl or guanyl) cyclases (GCs) are homo- and heterodimeric enzymes that catalyze the conversion of GTP to cGMP. In current models of rGC function, ligand binding is thought to result in tilting of the transmembrane segments and rotation of the guanylate cyclase domain relative to other protein domains, thereby positioning polypeptide regions from each monomer to form a competent enzymatic active site (Kuhn, 2016; Sharma et al., 2016; Maruyama, 2017). Enzyme activation is also influenced by rGC binding partners in the cytosol, which interact with intracellular domains to regulate formation of the active site (Kuhn, 2016; Sharma et al., 2016; Maruyama, 2017).

Retinal guanylate cyclase 1 (GUCY2E; GUCY2D in humans) is a homodimeric enzyme belonging to the subfamily of receptor guanylate (also guanylyl or guanyl) cyclases (rGCs). These proteins localize to cellular membranes and possess extracellular, transmembrane, and intracellular domains that regulate the enzymatic activity of the guanylate cyclase domain (Maruyama, 2017). The structure of GUCY2E includes a processed N-terminal signal sequence and extracellular domain of unknown function

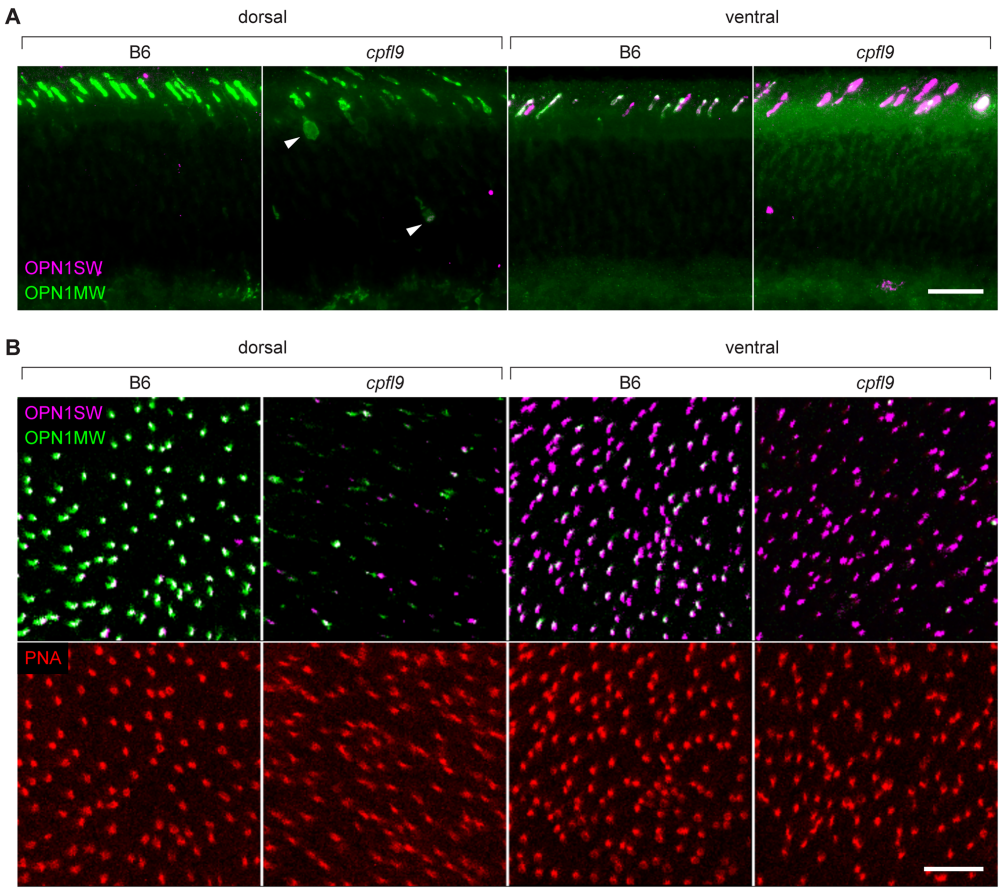

FIGURE 4
Immunostaining of cone opsins in *cpfl9* mutants and B6 controls at 12weeks of age. **(A)** Thin retinal sections stained with anti-OPN1MW (green) and anti-OPN1SW (magenta). In the dorsal retina, where expression of M cones is predominant, mislocalization of OPN1MW to the cone cell soma (arrowheads) and pedicles was observed. In the ventral retina, there was a significant reduction of OPN1MW expression in dual-expressing cones. **(B)** Stellaris confocal imaging of retinal flatmounts. Scale bars in **A** and **B**, 10μm. Images in **A** and **B** are representative of n=4 *cpfl9* and n=6 B6 mice.

and unknown ligand-binding capabilities, a single helical transmembrane domain, a kinase homology or pseudokinase domain, a linker segment of roughly 50 amino acids, and finally the guanylate cyclase catalytic domain (Figure 7). GUCY2E accumulates in the OS of rod and cone photoreceptor cells, where it plays an essential role in restoring cGMP levels in the dark following light excitation (Boye, 2014). A related protein, GUCY2F is unique to rod photoreceptor cells and contributes to cGMP production. In rods, rhodopsin excitation by light results in cGMP depletion by activating the heteromeric G protein transducin and consequently cGMP phosphodiesterase; decreased cGMP leads to closing of cGMP-gated cation channels. Recovery occurs in response to the ensuing decrease in intracellular calcium, as low calcium stimulates guanylate cyclase activating proteins (GCAPs) 1 and 2 to activate GUCY2E and GUCY2F. A similar recovery process occurs in cone photoreceptors in response to light excitation of cone pigments, activation of cone transducin and phosphodiesterase, and requires GUCY2E activation to restore cGMP and intracellular calcium levels (Karan et al., 2010).

In addition to its role in phototransduction, GUCY2E interacts with proteins of the phototransduction cascade and is implicated in the directional transport of some of these proteins to the OS, such as phosphodiesterase subunits and guanylate cyclase activating proteins (Karan et al., 2008, 2010). Additionally, GUCY2E has been shown to be modulated by bicarbonate (Duda et al., 2015, 2018; Makino et al., 2019), which may influence its activity in phototransduction and/or directional protein transport. Other roles for GUCY2E may yet be identified, by analogy with other rGCs that are activated or regulated by extracellular ligands, such as natriuretic factor, thrombin, guanylin and uroguanylin, or by the binding of calcium or chloride ion (Sharma et al., 2016; Maruyama, 2017).

Mutations in GUCY2D that lead to cone-rod dystrophy (CORD6; MIM#601777), choroidal dystrophy, central areolar (MIM#215500) and night blindness, congenital stationary, Type1I (CSNB1I; MIM#618555) are primarily found in the carboxyl terminal, dimer portion of the gene. However, mutations that lead to Leber congenital amaurosis 1 (LCA1; MIM#204000) are found throughout the gene, including the region encoding the

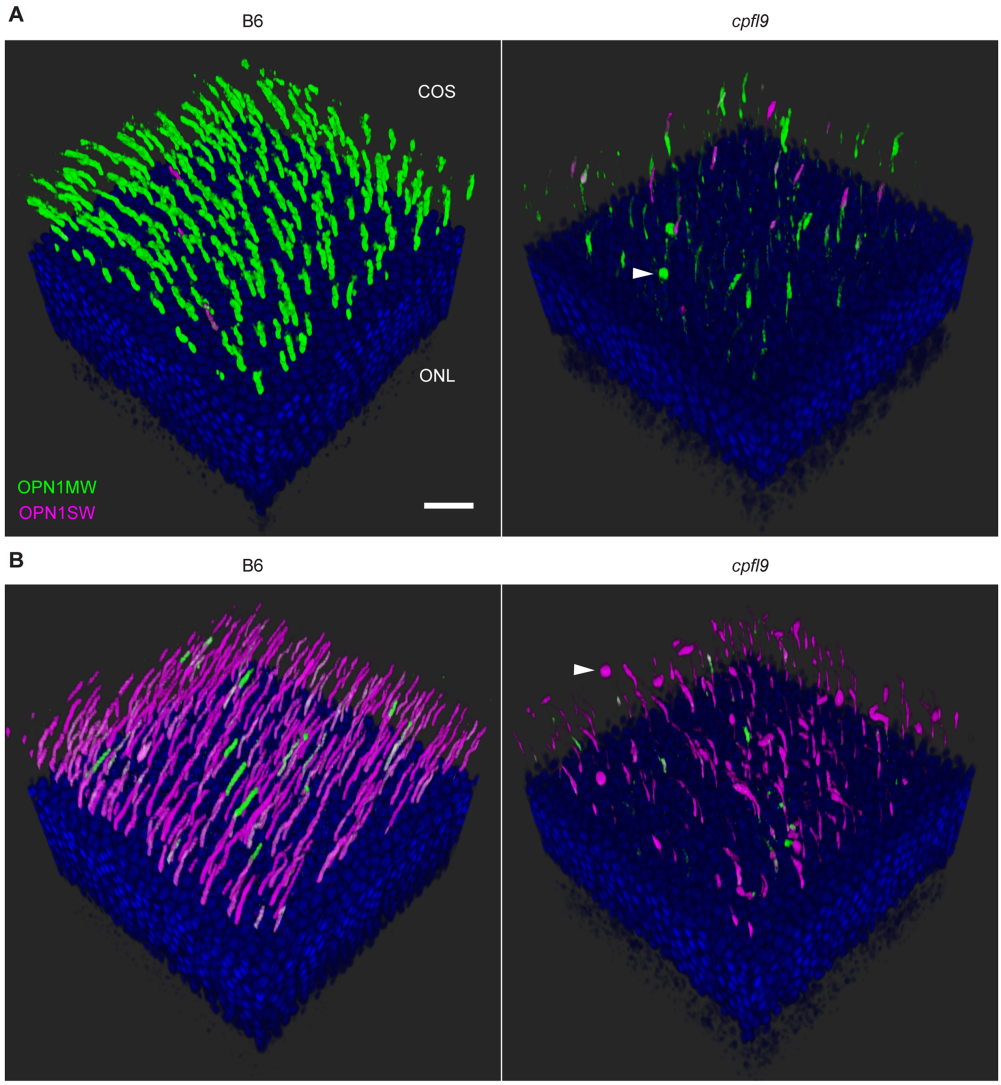

FIGURE 5
Confocal imaging of retinal flatmounts. B6 and *cpfl9* flatmount samples prepared at 12weeks of age were stained with cone opsin antibodies and PNA as in Figure 4. **(A)** Dorsal retina. Cone OS (COS) were OPN1MW-positive (green) except for a few OS that were partly or completely OPN1SW-positive (magenta). OPN1MW staining was substantially reduced in the *cpfl9* retina. Round OPN1MW-positive objects were occasionally noted in the outermost retina (arrowhead). The ONL was revealed by DAPI staining (blue). Scale bar, 20μm. **(B)** Ventral retina. OPN1SW-positive cones were observed in the ventral retina of B6 mice except for occasional cones that also were partly positive for OPN1MW. Reduced staining of both opsins was observed in the *cpfl9* ventral retina and round OPN1SW-positive objects were occasionally noted. Pseudocolors, symbols, and scale are the same as in panel **A**. Images are representative of n=4 *cpfl9* and n=5 B6 mice.

carboxy terminus of the protein (Figure 7). The mutation spectrum of human GUCY2D does not reveal a strong genotype–phenotype correlation, although most pathogenic missense mutations are found in the kinase homology and guanylate cyclase catalytic domains (Figure 7). A cluster of missense mutations leading to autosomal dominant cone-rod dystrophy is found in a helical region between the kinase homology and cyclase domains. Truncating mutations are found throughout the protein sequence. Interestingly, most of them are annotated in ClinVar as causing both LCA1 and CORD6. This may indicate the presence of modifier genes in the human population that affect disease onset and severity.

4.2. Phototransduction defects in *cpfl9* mice

Our functional analysis of the *cpfl9* model at 4 weeks of age revealed that the photopic ERG response was abolished and the scotopic ERG response was significantly reduced compared to that of control mice. However, at this age, retinal histology was normal and counts of ONL and cone nuclei did not reveal a statistically significant reduction in the number of photoreceptor cells compared to controls. Together, these findings suggest that the diminished ERG responses in young *cpfl9* mice are due to deficits in the cone and rod phototransduction pathways rather

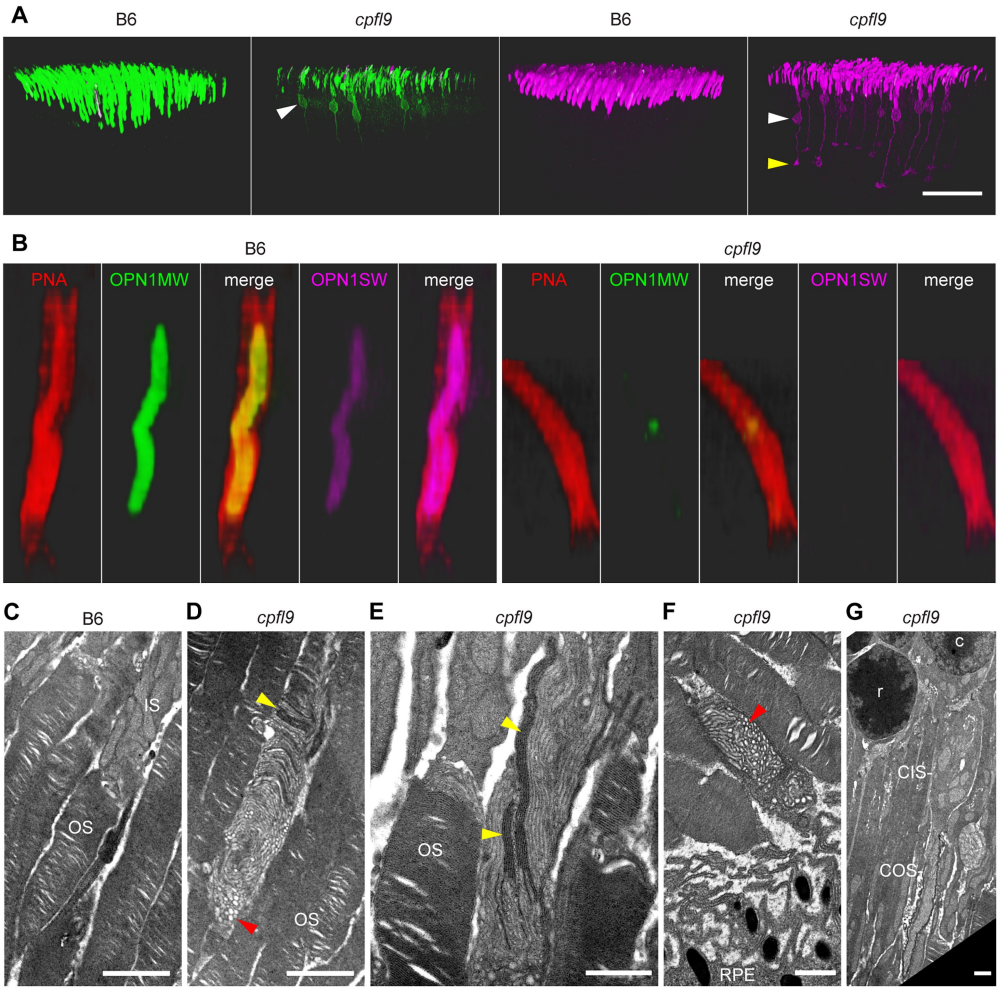

FIGURE 6
Opsin mislocalization and cone OS dysmorphology. **(A)** Confocal imaging of retinal flatmounts as described in Figure 5. In B6, OPN1MW (green) and OPN1SW (magenta) staining is observed only in the cone OS. By contrast, staining in *cpfl9* retinas is observed in cell bodies (white arrowheads) and structures toward the photoreceptor synapse. OPN1SW mislocalization reaches the cone pedicles (yellow arrowhead). Display settings were adjusted identically for all images in Imaris to emphasize opsin mislocalization. Scale bar, 50μm. **(B)** Opsin deficit within the cone matrix sheath. A single cone OS from the stained B6 and *cpfl9* flatmounts was viewed in Imaris. In B6 cones, often both OPN1MW and OPN1SW staining were associated with PNA staining (red). By contrast, most cone sheaths in *cpfl9* flatmounts exhibited little cone opsin staining. **(C–G)** Ultrastructure of the outer retina in mice at 6weeks of age by transmission electron microscopy. **(C)** Photoreceptor IS and OS in a B6 retina. Stacked disks were evident in the marked OS and in neighboring OSs. **(D)** An OS-like object in a homozygous *cpfl9* retina included disorganized membranes appearing as vesicles and tubules (red arrowhead). A few disks were stacked perpendicular to the OS axis as in B6 mice (yellow arrowhead). **(E)** Stacked membranes in OS-like objects of *cpfl9* mice were often much longer than in B6 mice and were oblique to the OS axis (yellow arrowheads). **(F)** OS-like objects exhibiting disorganized membranes (red arrowhead) were sometimes found in close proximity to RPE apical microvilli. **(G)** A *cpfl9* cone cell traced from its nucleus (c) included a disorganized OS containing oblique lamellar structures as in **E**. Images are representative of *n*=4 *cpfl9* and *n*=4 B6 controls. IS, inner segment; OS, outer segment; CIS, cone inner segment; COS, cone outer segment; RPE, retinal pigmented epithelium; c, cone cell nucleus; r, rod cell nucleus. Scale bars: C-G, 1 μm.

than a defect in photoreceptor development or rapid photoreceptor cell degeneration. In previous work, null mutations in the guanylate cyclase gene in the GUCY1*B chicken were found to decrease retinal cGMP production by 5- to 10-fold (Semple-Rowland et al., 1998) and abolish ERG responses in both rod and cone photoreceptor cells (Ulshafer et al., 1984). In mice, *Gucy2e* knockout abolished cone ERG responses; however, the presence GUCY2F in rod photoreceptors apparently allows a detectable but decreased rod ERG response (Yang et al., 1999; Baehr et al., 2007). A similar effect may explain the decreased rod response in young *cpfl9* mice.

4.3. Photoreceptor cell loss in *cpfl9* mice

The *cpfl9* model appears to result in a milder cone degenerative disease than other animal models of *GUCY2D* deficiency. In the GUCY1*B chicken, retinal morphology is normal at day 1 post-hatch, but loss of photoreceptor cell nuclei is observed starting at day

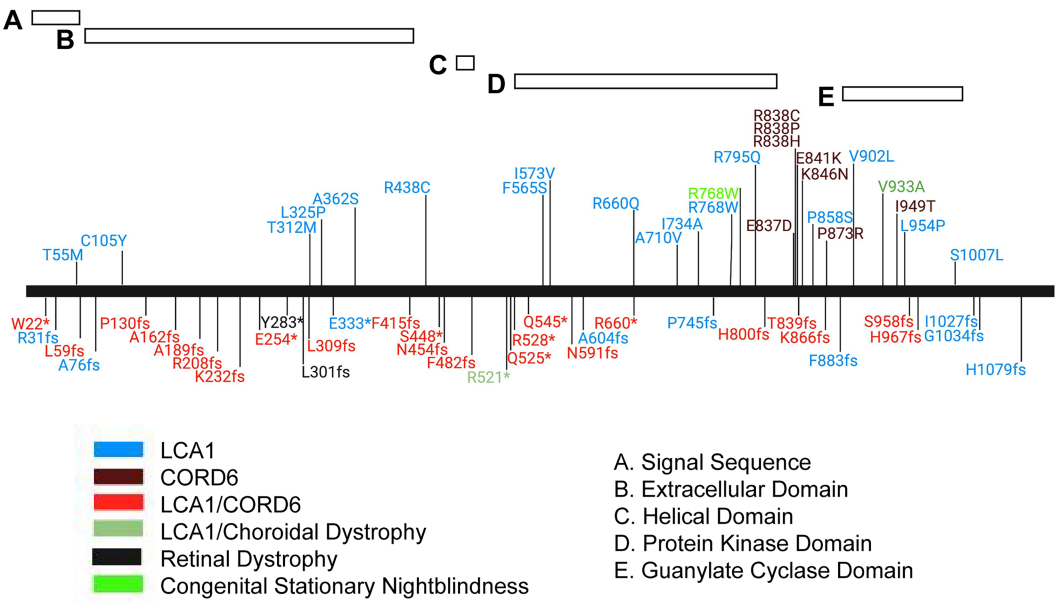

FIGURE 7
Mutation spectrum of the human GUCY2D protein. Schematic representation of the GUCY2D protein with relative position of protein domains. Alleles are localized by vertical lines and named. *, translation termination; fs, frameshift. Phenotype annotations are color coded in the allele symbol. LCA1, Leber congenital amaurosis 1, CORD6, cone-rod dystrophy 6.

21 post-hatch and is complete by ~3.5 months of age (Ulshafer et al., 1984). In this mutant, in-frame replacement of exons 4–7 with an 81 bp segment homologous to a portion of exon 9 leads to loss of the protein as assessed with antibodies directed to the intracellular domain (Semple-Rowland et al., 1998). Thus, the mutation is considered a null allele, which may explain the severe degenerative phenotype. In the *Gucy2e* knockout mouse, initial characterization indicated that cone cell nuclei were rapidly lost by five weeks of age (Yang et al., 1999). However, another study of mice bearing the same knockout allele indicated that cones survived for considerably longer periods, requiring six months for complete loss in the inferior retina and longer for the superior retina (Coleman et al., 2004). In the knockout allele, exon 5 is replaced with a *neo* cassette, resulting in premature termination of the protein. No polypeptide was detected in the knockout mice using a C-terminal antibody, indicating that the mutation was a null allele. By contrast, in *cpfl9* mice, cone cell nuclei numbers do not differ significantly from those in B6 control mice at 4 and 12 weeks of age. Even at 9–12 months of age, the sum of cone nuclei counts obtained at intervals throughout the *cpfl9* retina was 68% of that in B6. Thus, cone cell loss in *cpfl9* mice appears to progress less rapidly than in the GUCY1*B chicken and the *Gucy2e* knockout mouse.

The *cpfl9* model also exhibits rod cell loss, but its progression is intermediate between that of other animal models. In the GUCY1*B chicken, rod cell loss was first detected at about the same age as cone cell loss and was complete by 6–8 months of age (Ulshafer et al., 1984). In *Gucy2e* knockout mice, however, no rod cell loss was reported among the oldest mice examined at 6 months of age (Yang et al., 1999; Coleman et al., 2004). Our analysis of *cpfl9* mice revealed a small but statistically significant decrease in the number of rod cell nuclei across the retina at 12 weeks of age, and a further decrease at 9–12 months of age, compared to controls. This decline was accompanied by a decrease in rod cell function as measured by ERG. Thus, *cpfl9* mice model *GUCY2D*-associated cone-rod dystrophy. Interestingly, the difference in rod cell degeneration of *cpfl9* mutant and *Gucy2e* knockout mice parallels observations of LCA1 patients, in which abnormal cone function was accompanied by a range of rod dysfunction from near normal (<0.5 $\log_{10}$ unit rod loss) to severe (>3.5 $\log_{10}$ units rod loss) as determined by full-field sensitivity testing (Jacobson et al., 2017). Similarly, two studies that assessed nyctalopia among LCA1 patients, an indication of rod dysfunction, revealed that most patients were normal, with 14 and 38% reporting the condition (Bouzia et al., 2020; Hahn et al., 2022). These findings establish that the severity of rod dysfunction in LCA1 patients is highly variable, possibly due to *GUCY2D* allelic differences (Sharon et al., 2018; Bouzia et al., 2020) and/or interactions with background modifier gene variants (Jacobson et al., 2022). Comparison of a series of *Gucy2e* alleles, possibly including the knockout and *cpfl9* alleles, in mice of the same genetic background may be informative for understanding the molecular basis of such variation.

At the molecular level, our analysis of *cpfl9* genomic DNA revealed a homozygous 25 bp deletion in the *Gucy2e* gene, significant downregulation of *Gucy2e* mRNA in *cpfl9* mice compared to B6 controls, and undetectable full-length protein in western analysis using a carboxy-terminal antibody against GUCY2E. Residual expression of *Gucy2e* in *cpfl9* mutants suggests

partial escape of nonsense mediated decay (Supek et al., 2021), perhaps due to the presence of alternative splice isoforms or as a consequence of aberrant splicing resulting from the 25 bp deletion. However, since *Gucy2e* retinal transcripts were detected in *cpfl9* mutants, we cannot exclude the possibility that the 25 bp deletion results in a truncated form of the protein that retains partial GUCY2E function as conferred by the extracellular, transmembrane, and/or kinase homology domains. The truncated protein may lead to differences in the cone and rod degenerative phenotypes as compared to *Gucy2e* knockout mice, which may fail to express any protein, as described above. Further characterization of *Gucy2e* transcripts and/or amino-terminal GUCY2E polypeptides in the *cpfl9* mutant will be necessary to determine if the mutation results in complete loss of the GUCY2E protein.

4.4. Effect of the *cpfl9* allele on cone OS protein distribution

At 12 weeks of age, cone cell bodies of homozygous *cpfl9* seem to remain intact and there appears to be little effect of the *cpfl9* allele on cone opsin levels in retinal lysates. Nevertheless, OPN1MW and OPN1SW staining is greatly diminished in the cone OS and the proteins are mislocalized, both to objects near the outer retina and to the cone photoreceptor cell soma and synapse. The OPN1MW and OPN1SW objects detected by immunohistology in the outer retina may correspond to the abnormal membraneous particles containing intracellular vesicles, which were detected by TEM imaging and were found throughout the OS, extending as far as the subretinal space. Mislocalization of two other cone OS proteins, GNAT2 and ARR3, was also observed in *cpfl9* mice. The mislocalization of OS proteins in *cpfl9* mutants appears to be the result of an early defect of cone photopigments that are differentially expressed across the retina. The distribution of photopigments in cones that express OPN1MW is more profoundly affected; OPN1MW is observed in the cell soma and cone pedicles in the dorsal retina while a reduced expression is found in the ventral retina where there is a large population of cones expressing both pigments. These results strengthen similarities to the *Gucy2e* knockout mouse (Coleman et al., 2004; Coleman and Semple-Rowland, 2005; Baehr et al., 2007) and provide support for a model in which GUCY2E functions in the trafficking of membrane vesicles containing transmembrane and peripheral OS proteins from the endoplasmic reticulum and Golgi apparatus to the base of the photoreceptor cilium (Karan et al., 2010).

It is also possible that OS protein mislocalization in *cpfl9* mice results from defects in processes other than protein trafficking to the cilium. OS development and maintenance requires protein and lipid transport across the photoreceptor connecting cilium, followed by the formation and stacking of OS disks (Goldberg et al., 2016; Barnes et al., 2021). Disruption of the OS is expected to compromise the sequestration of OS proteins, which may subsequently become mislocalized to the IS, cell body, and synapse. In support of a defect in OS development and maintenance, ultrastructural analysis of *cpfl9* mice revealed cone OS defects, including the presence of overgrown, misaligned lamellae, accumulation of disorganized membrane vesicles and tubules, and displaced OS-like objects in the subretinal space. Ultrastructural defects in rod OSs were not detected; these may be rare due to the presence of functional GUCY2F in rods. A similar ultrastructural phenotype of misaligned OS disks combined with mislocalized OS proteins and progressive photoreceptor cell loss has been observed in several mouse retinal dystrophy models bearing mutations in genes involved in OS development and maintenance, including *Cngb1-Garp1-Garp2* (Zhang et al., 2009), *Kif3a* (Avasthi et al., 2009), *Prom1* (Zacchigna et al., 2009; Dellett et al., 2014), and *Rp1* (Gao et al., 2002; Liu et al., 2003; Song et al., 2014). As recently summarized (Goldberg et al., 2016), the proteins encoded by these genes are implicated in cargo transport across the connecting cilium (KIF3A), disk formation (CNGB1-GARP1-GARP2, PROM1, RP1), disk stacking (RP1), and disk stabilization (CNGB1-GARP1-GARP2). Of note, *Cngb3* knockout mice, which specifically target a homolog of *Cngb1* in cone photoreceptors, exhibit a similar combined phenotype (Carvalho et al., 2011; Xu et al., 2011), including defects in cone OS ultrastructure that are strikingly similar to those of *cpfl9* and *Gucy2e* knockout mice (Baehr et al., 2007). Thus, given the phenotypic similarities among these retinal dystrophy models and *Gucy2e* mutant mice, it is possible that GUCY2E functions in ciliary transport or disk formation, stacking and/or stabilization (Karan et al., 2008).

4.5. Cone matrix sheaths in the absence of cone opsins

At 12 weeks of age, cone matrix sheaths were abundant in *cpfl9* mice. However, based on our confocal analysis, the opsin content within the sheaths was low, and often no OPN1MW or OPN1SW staining was detected within the PNA-stained envelope. The persistence of cone sheaths over several months despite the absence of a cone opsin has been observed in *Opn1mw* knockout mice (Deng et al., 2018, 2019), although ultimately sheath loss is observed by PNA staining and is restored by delivery of a functional *Opn1mw* gene (Deng et al., 2019). These results, together with our findings, lead to the question, how do cone sheaths form when OPN1MW is absent, as in *Opn1mw* knockout mice, or mislocalized, as in *cpfl9* mice? A possible explanation relates to the developmental switch in cone OS opsin expression observed in mice and other vertebrates (Röhlich et al., 1994; Szél et al., 1994; Savelli et al., 2018). At early developmental stages, only short wavelength opsin accumulates in the OS, while at later stages both short and long wavelength opsins are present, often depending on topographic position within the retina (Szél et al., 1992; Applebury et al., 2000; Eldred et al., 2020). Mice express OPN1SW at early postnatal developmental stages but coexpress both OPN1SW and OPN1MW in a dorsal-ventral concentration gradient at later stages. For example, OPN1SW opsin but not OPN1MW opsin was observed in the OS of mouse cones at P7, while coexpression of both proteins were observed in cones at

P14 (Glaschke et al., 2010). Thus, in *Opn1mw* knockout and *cpfl9* mice it is possible that cone sheaths form in early development as OPN1SW is expressed and remain stable for months thereafter, despite deficits in OPN1MW synthesis or OS maintenance. This proposed mechanism raises the possibility that GUCY2E is not needed for early OS development and sheath formation in OPN1SW cones but is required as part of the subsequent developmental switch from exclusive OPN1SW expression to combined OPN1MW coexpression. Examination of cone opsin expression in *cpfl9* mice at early developmental stages may help to address this possibility.

4.6. Summary

This work provides a detailed characterization of cone dysmorphology and rod and cone photoreceptor loss in *cpfl9* mice, which carry a novel mutant allele of *Gucy2e*. The mild cone-rod dystrophy disease phenotype exhibited by this mouse model may make it attractive for testing therapeutic interventions designed to mitigate the human retinal diseases caused by *GUCY2D* mutations.

Data availability statement

The original contributions presented in the study are included in the article/Supplementary material, further inquiries can be directed to the corresponding author.

Ethics statement

The animal study was reviewed and approved by The Jackson Laboratory Institutional Animal Care and Use Committee.

Author contributions

GC, MK, and BC: conception and experimental design. AN, GC, JW, MK, and BC: execution of experiments. AN, GC, MK, and BC preparation of figures, manuscript. MK and BC: resources. All authors contributed to the article and approved the submitted version.

Funding

Research in this publication was supported by the National Eye Institute of the National Institutes of Health under award numbers R01EY019943 (to B.C.) and R01EY027305 (to Patsy M. Nishina and M.P.K). The authors also wish to acknowledge the National Cancer Institute of the National Institutes of Health under award number P30CA034196 for support of core services.

Acknowledgments

We acknowledge Bernie Fitzmaurice and Lisa Stone for their excellent assistance with animal husbandry and Melissa Berry for her critical review of this manuscript. We also gratefully acknowledge the contribution of Philipp Henrich and the Microscopy, Genome Technologies, and Histopathology Services at The Jackson Laboratory for expert assistance with the work described in this publication.

Conflict of interest

The authors declare that the research was conducted in the absence of any commercial or financial relationships that could be construed as a potential conflict of interest.

Publisher's note

Supplementary material

The Supplementary material for this article can be found online at: https://www.frontiersin.org/articles/10.3389/fnmol.2022.1080136/full#supplementary-material

References

Applebury, M. L., Antoch, M. P., Baxter, L. C., Chun, L. L., Falk, J. D., Farhangfar, F., et al. (2000). The murine cone photoreceptor: a single cone type expresses both S and M opsins with retinal spatial patterning. *Neuron* 27, 513–523. doi: 10.1016/s0896-6273(00)00062-3

Avasthi, P., Watt, C. B., Williams, D. S., Le, Y. Z., Li, S., Chen, C. K., et al. (2009). Trafficking of membrane proteins to cone but not rod outer segments is dependent on heterotrimeric kinesin-II. *J. Neurosci.* 29, 14287–14298. doi: 10.1523/JNEUROSCI.3976-09.2009

Baehr, W., Karan, S., Maeda, T., Luo, D. G., Li, S., Bronson, J. D., et al. (2007). The function of guanylate cyclase 1 and guanylate cyclase 2 in rod and cone photoreceptors. *J. Biol. Chem.* 282, 8837–8847. doi: 10.1074/jbc.M610369200

Baehr, W., and Palczewski, K. (2007). Guanylate cyclase-activating proteins and retina disease. *Subcell. Biochem.* 45, 71–91. doi: 10.1007/978-1-4020-6191-2_4

Barnes, C. L., Malhotra, H., and Calvert, P. D. (2021). Compartmentalization of photoreceptor sensory cilia. *Front. Cell Dev. Biol.* 9:636737. doi: 10.3389/fcell.2021.636737

Blake, J. A., Bult, C. J., Eppig, J. T., Kadin, J. A., and Richardson, J. E.Group, M.G.D (2009). The mouse genome database genotypes: phenotypes. *Nucleic Acids Res.* 37, D712–D719. doi: 10.1093/nar/gkn886

Bouzia, Z., Georgiou, M., Hull, S., Robson, A. G., Fujinami, K., Rotsos, T., et al. (2020). GUCY2D-associated Leber congenital amaurosis: a retrospective natural

history study in preparation for trials of novel therapies. *Am J. Ophthalmol.* 210, 59–70. doi: 10.1016/j.ajo.2019.10.019

Boye, S. E. (2014). Leber congenital amaurosis caused by mutations in GUCY2D. *Cold Spring Harb. Perspect. Med.* 5:a017350. doi: 10.1101/cshperspect.a017350

Carvalho, L. S., Xu, J., Pearson, R. A., Smith, A. J., Bainbridge, J. W., Morris, L. M., et al. (2011). Long-term and age-dependent restoration of visual function in a mouse model of CNGB3-associated achromatopsia following gene therapy. *Hum. Mol. Genet.* 20, 3161–3175. doi: 10.1093/hmg/ddr218

Chang, B., Hawes, N. L., Pardue, M. T., German, A. M., Hurd, R. E., Davisson, M. T., et al. (2007). Two mouse retinal degenerations caused by missense mutations in the beta-subunit of rod cGMP phosphodiesterase gene. *Vis. Res.* 47, 624–633. doi: 10.1016/j.visres.2006.11.020

Clarke, G., Collins, R. A., Leavitt, B. R., Andrews, D. F., Hayden, M. R., Lumsden, C. J., et al. (2000). A one-hit model of cell death in inherited neuronal degenerations. *Nature* 406, 195–199. doi: 10.1038/35018098

Coleman, J. E., and Semple-Rowland, S. L. (2005). GC1 deletion prevents light-dependent arrestin translocation in mouse cone photoreceptor cells. *Invest. Ophthalmol. Vis. Sci.* 46, 12–16. doi: 10.1167/iovs.04-0691

Coleman, J. E., Zhang, Y., Brown, G. A., and Semple-Rowland, S. L. (2004). Cone cell survival and downregulation of GCAP1 protein in the retinas of GC1 knockout mice. *Invest. Ophthalmol. Vis. Sci.* 45, 3397–3403. doi: 10.1167/iovs.04-0392

Collin, G. B., Gogna, N., Chang, B., Damkham, N., Pinkney, J., Hyde, L. F., et al. (2020). Mouse models of inherited retinal degeneration with photoreceptor cell loss. *Cells* 9:931. doi: 10.3390/cells9040931

Dellett, M., Sasai, N., Nishide, K., Becker, S., Papadaki, V., Limb, G. A., et al. (2014). Genetic background and light-dependent progression of photoreceptor cell degeneration in Prominin-1 knockout mice. *Invest. Ophthalmol. Vis. Sci.* 56, 164–176. doi: 10.1167/iovs.14-15479

Deng, W. T., Li, J., Zhu, P., Chiodo, V. A., Smith, W. C., Freedman, B., et al. (2018). Human L- and M-opsins restore M-cone function in a mouse model for human blue cone monochromacy. *Mol. Vis.* 24, 17–28.

Deng, W. T., Li, J., Zhu, P., Freedman, B., Smith, W. C., Baehr, W., et al. (2019). Rescue of M-cone function in aged Opn1mw$^{-/-}$ mice, a model for late-stage blue cone Monochromacy. *Invest. Ophthalmol. Vis. Sci.* 60, 3644–3651. doi: 10.1167/iovs.19-27079

Duda, T., Pertzev, A., and Sharma, R. K. (2018). CO_2/bicarbonate modulates cone photoreceptor ROS-GC1 and restores its CORD6-linked catalytic activity. *Mol. Cell. Biochem.* 448, 91–105. doi: 10.1007/s11010-018-3317-9

Duda, T., Wen, X. H., Isayama, T., Sharma, R. K., and Makino, C. L. (2015). Bicarbonate modulates photoreceptor guanylate cyclase (ROS-GC) catalytic activity. *J. Biol. Chem.* 290, 11052–11060. doi: 10.1074/jbc.M115.650408

Eldred, K. C., Avelis, C., Johnston, R. J., and Roberts, E. (2020). Modeling binary and graded cone cell fate patterning in the mouse retina. *PLoS Comput. Biol.* 16:e1007691. doi: 10.1371/journal.pcbi.1007691

Fairfield, H., Gilbert, G. J., Barter, M., Corrigan, R. R., Curtain, M., Ding, Y., et al. (2011). Mutation discovery in mice by whole exome sequencing. *Genome Biol.* 12:R86. doi: 10.1186/gb-2011-12-9-r86

Ferdous, S., Liao, K. L., Gefke, I. D., Summers, V. R., Wu, W., Donaldson, K. J., et al. (2021). Age-related retinal changes in wild-type C57BL/6J mice between 2 and 32 months. *Invest. Ophthalmol. Vis. Sci.* 62:9. doi: 10.1167/iovs.62.7.9

Fogerty, J., and Besharse, J. C. (2011). 174delG mutation in mouse MFRP causes photoreceptor degeneration and RPE atrophy. *Invest. Ophthalmol. Vis. Sci.* 52, 7256–7266. doi: 10.1167/iovs.11-8112

Gao, J., Cheon, K., Nusinowitz, S., Liu, Q., Bei, D., Atkins, K., et al. (2002). Progressive photoreceptor degeneration, outer segment dysplasia, and rhodopsin mislocalization in mice with targeted disruption of the retinitis pigmentosa-1 (Rp1) gene. *Proc. Natl. Acad. Sci. U. S. A.* 99, 5698–5703. doi: 10.1073/pnas.042122399

Glaschke, A., Glösmann, M., and Peichl, L. (2010). Developmental changes of cone opsin expression but not retinal morphology in the hypothyroid Pax8 knockout mouse. *Invest. Ophthalmol. Vis. Sci.* 51, 1719–1727. doi: 10.1167/iovs.09-3592

Goldberg, A. F., Moritz, O. L., and Williams, D. S. (2016). Molecular basis for photoreceptor outer segment architecture. *Prog. Retin. Eye Res.* 55, 52–81. doi: 10.1016/j.preteyeres.2016.05.003

Hahn, L. C., Georgiou, M., Almushattat, H., van Schooneveld, M. J., de Carvalho, E. R., Wesseling, N. L., et al. (2022). The natural history of Leber congenital amaurosis and cone-rod dystrophy associated with variants in the GUCY2D gene. *Ophthalmol Retina* 6, 711–722. doi: 10.1016/j.oret.2022.03.008

Jacobson, S. G., Cideciyan, A. V., Ho, A. C., Roman, A. J., Wu, V., Garafalo, A. V., et al. (2022). Night vision restored in days after decades of congenital blindness. *iScience* 25:105274. doi: 10.1016/j.isci.2022.105274

Jacobson, S. G., Cideciyan, A. V., Sumaroka, A., Roman, A. J., Charng, J., Lu, M., et al. (2017). Defining outcomes for clinical trials of Leber congenital amaurosis caused by GUCY2D mutations. *Am J. Ophthalmol.* 177, 44–57. doi: 10.1016/j.ajo.2017.02.003

Kameya, S., Hawes, N. L., Chang, B., Heckenlively, J. R., Naggert, J. K., and Nishina, P. M. (2002). Mfrp, a gene encoding a frizzled related protein, is mutated in the mouse retinal degeneration 6. *Hum. Mol. Genet.* 11, 1879–1886. doi: 10.1093/hmg/11.16.1879

Karan, S., Frederick, J. M., and Baehr, W. (2010). Novel functions of photoreceptor guanylate cyclases revealed by targeted deletion. *Mol. Cell. Biochem.* 334, 141–155. doi: 10.1007/s11010-009-0322-z

Karan, S., Zhang, H., Li, S., Frederick, J. M., and Baehr, W. (2008). A model for transport of membrane-associated phototransduction polypeptides in rod and cone photoreceptor inner segments. *Vis. Res.* 48, 442–452. doi: 10.1016/j.visres.2007.08.020

Kim, S. Y., Yang, H. J., Chang, Y. S., Kim, J. W., Brooks, M., Chew, E. Y., et al. (2014). Deletion of aryl hydrocarbon receptor AHR in mice leads to subretinal accumulation of microglia and RPE atrophy. *Invest. Ophthalmol. Vis. Sci.* 55, 6031–6040. doi: 10.1167/iovs.14-15091

Kuhn, M. (2016). Molecular physiology of membrane guanylyl cyclase receptors. *Physiol. Rev.* 96, 751–804. doi: 10.1152/physrev.00022.2015

Landrum, M. J., Lee, J. M., Benson, M., Brown, G. R., Chao, C., Chitipiralla, S., et al. (2018). ClinVar: improving access to variant interpretations and supporting evidence. *Nucleic Acids Res.* 46, D1062–D1067. doi: 10.1093/nar/gkx1153

Li, C., Cheng, M., Yang, H., Peachey, N. S., and Naash, M. I. (2001). Age-related changes in the mouse outer retina. *Optom. Vis. Sci.* 78, 425–430. doi: 10.1097/00006324-200106000-00015

Liu, Q., Lyubarsky, A., Skalet, J. H., Pugh, E. N. Jr., and Pierce, E. A. (2003). RP1 is required for the correct stacking of outer segment discs. *Invest. Ophthalmol. Vis. Sci.* 44, 4171–4183. doi: 10.1167/iovs.03-0410

Makino, C. L., Duda, T., Pertzev, A., Isayama, T., Geva, P., Sandberg, M. A., et al. (2019). Modes of accessing bicarbonate for the regulation of membrane guanylate cyclase (ROS-GC) in retinal rods and cones. *eNeuro* 6, ENEURO.0393–ENEU18.2019. doi: 10.1523/ENEURO.0393-18.2019

Maruyama, I. N. (2017). Receptor guanylyl Cyclases in sensory processing. *Front. Endocrinol. (Lausanne)* 7:173. doi: 10.3389/fendo.2016.00173

Pugh, E. N., Duda, T., Sitaramayya, A., and Sharma, R. K. (1997). Photoreceptor guanylate cyclases: a review. *Biosci. Rep.* 17, 429–473. doi: 10.1023/a:1027365520442

Rice, D. S., Calandria, J. M., Gordon, W. C., Jun, B., Zhou, Y., Gelfman, C. M., et al. (2015). Adiponectin receptor 1 conserves docosahexaenoic acid and promotes photoreceptor cell survival. *Nat. Commun.* 6:6228. doi: 10.1038/ncomms7228

Röhlich, P., van Veen, T., and Szél, Á. (1994). Two different visual pigments in one retinal cone cell. *Neuron* 13, 1159–1166. doi: 10.1016/0896-6273(94)90053-1

Savelli, I., Novales Flamarique, I., Iwanicki, T., and Taylor, J. S. (2018). Parallel opsin switches in multiple cone types of the starry flounder retina: tuning visual pigment composition for a demersal life style. *Sci. Rep.* 8:4763. doi: 10.1038/s41598-018-23008-y

Schindelin, J., Arganda-Carreras, I., Frise, E., Kaynig, V., Longair, M., Pietzsch, T., et al. (2012). Fiji: an open-source platform for biological-image analysis. *Nat. Methods* 9, 676–682. doi: 10.1038/nmeth.2019

Semple-Rowland, S. L., Lee, N. R., Van Hooser, J. P., Palczewski, K., and Baehr, W. (1998). A null mutation in the photoreceptor guanylate cyclase gene causes the retinal degeneration chicken phenotype. *Proc. Natl. Acad. Sci. U. S. A.* 95, 1271–1276. doi: 10.1073/pnas.95.3.1271

Sharma, R. K., Duda, T., and Makino, C. L. (2016). Integrative signaling networks of membrane guanylate cyclases: biochemistry and physiology. *Front. Mol. Neurosci.* 9:83. doi: 10.3389/fnmol.2016.00083

Sharon, D., Wimberg, H., Kinarty, Y., and Koch, K. W. (2018). Genotype-functional-phenotype correlations in photoreceptor guanylate cyclase (GC-E) encoded by GUCY2D. *Prog. Retin. Eye Res.* 63, 69–91. doi: 10.1016/j.preteyeres.2017.10.003

Song, D., Grieco, S., Li, Y., Hunter, A., Chu, S., Zhao, L., et al. (2014). A murine RP1 missense mutation causes protein mislocalization and slowly progressive photoreceptor degeneration. *Am. J. Pathol.* 184, 2721–2729. doi: 10.1016/j.ajpath.2014.06.010

Supek, F., Lehner, B., and Lindeboom, R. G. H. (2021). To NMD or not to NMD: nonsense-mediated mRNA decay in cancer and other genetic diseases. *Trends Genet.* 37, 657–668. doi: 10.1016/j.tig.2020.11.002

Szél, Á., Röhlich, P., Caffe, A. R., Juliusson, B., Aguirre, G., and Van Veen, T. (1992). Unique topographic separation of two spectral classes of cones in the mouse retina. *J. Comp. Neurol.* 325, 327–342. doi: 10.1002/cne.903250302

Szél, Á., van Veen, T., and Röhlich, P. (1994). Retinal cone differentiation. *Nature* 370:336. doi: 10.1038/370336a0

Tolone, A., Belhadj, S., Rentsch, A., Schwede, F., and Paquet-Durand, F. (2019). The cGMP pathway and inherited photoreceptor degeneration: targets, compounds, and biomarkers. *Genes (Basel)* 10:453. doi: 10.3390/genes10060453

Truett, G. E., Heeger, P., Mynatt, R. L., Truett, A. A., Walker, J. A., and Warman, M. L. (2000). Preparation of PCR-quality mouse genomic DNA with hot sodium hydroxide and Tris (HotSHOT). *BioTechniques* 29, 52–54. doi: 10.2144/00291bm09

Ulshafer, R. J., Allen, C., Dawson, W. W., and Wolf, E. D. (1984). Hereditary retinal degeneration in the Rhode Island red chicken. I. Histology and ERG. *Exp. Eye Res.* 39, 125–135. doi: 10.1016/0014-4835(84)90003-4

UniProt Consortium. (2021). UniProt: the universal protein knowledgebase in 2021. *Nucleic Acids Res.* 49, D480–D489. doi: 10.1093/nar/gkaa1100

Weatherly, S. M., Collin, G. B., Charette, J. R., Stone, L., Damkham, N., Hyde, L. F., et al. (2022). Identification of Arhgef12 and Prkci as genetic modifiers of retinal dysplasia in the Crb1rd8 mouse model. *PLoS Genet.* 18:e1009798. doi: 10.1371/journal.pgen.1009798

Xu, J., Morris, L., Fliesler, S. J., Sherry, D. M., and Ding, X. Q. (2011). Early-onset, slow progression of cone photoreceptor dysfunction and degeneration in CNG channel subunit CNGB3 deficiency. *Invest. Ophthalmol. Vis. Sci.* 52, 3557–3566. doi: 10.1167/iovs.10-6358

Yang, R. B., Robinson, S. W., Xiong, W. H., Yau, K. W., Birch, D. G., and Garbers, D. L. (1999). Disruption of a retinal guanylyl cyclase gene leads to cone-specific dystrophy and paradoxical rod behavior. *J. Neurosci.* 19, 5889–5897. doi: 10.1523/JNEUROSCI.19-14-05889.1999

Zacchigna, S., Oh, H., Wilsch-Brauninger, M., Missol-Kolka, E., Jaszai, J., Jansen, S., et al. (2009). Loss of the cholesterol-binding protein prominin-1/CD133 causes disk dysmorphogenesis and photoreceptor degeneration. *J. Neurosci.* 29, 2297–2308. doi: 10.1523/JNEUROSCI.2034-08.2009

Zhang, Y., Molday, L. L., Molday, R. S., Sarfare, S. S., Woodruff, M. L., Fain, G. L., et al. (2009). Knockout of GARPs and the beta-subunit of the rod cGMP-gated channel disrupts disk morphogenesis and rod outer segment structural integrity. *J. Cell Sci.* 122, 1192–1200. doi: 10.1242/jcs.042531

Zhu, Y., Aredo, B., Chen, B., Zhao, C. X., He, Y. G., and Ufret-Vincenty, R. L. (2019). Mice with a combined deficiency of superoxide dismutase 1 (Sod1), DJ-1 (Park7), and parkin (Prkn) develop spontaneous retinal degeneration with aging. *Invest. Ophthalmol. Vis. Sci.* 60, 3740–3751. doi: 10.1167/iovs.19-27212

frontiers | Frontiers in Molecular Neuroscience

TYPE Original Research
PUBLISHED 16 March 2023
DOI 10.3389/fnmol.2023.1131093

OPEN ACCESS

EDITED BY
Clint L. Makino,
Boston University,
United States

REVIEWED BY
Shai Berlin,
Technion Israel Institute of Technology,
Israel
David Lagman,
Uppsala University,
Sweden

*CORRESPONDENCE
Stephan C. F. Neuhauss
✉ stephan.neuhauss@uzh.ch

SPECIALTY SECTION
This article was submitted to Molecular Signalling and Pathways, a section of the journal Frontiers in Molecular Neuroscience

RECEIVED 24 December 2022
ACCEPTED 27 February 2023
PUBLISHED 16 March 2023

CITATION
Gesemann M and Neuhauss SCF (2023) Evolution of visual guanylyl cyclases and their activating proteins with respect to clade and species-specific visual system adaptation. *Front. Mol. Neurosci.* 16:1131093. doi: 10.3389/fnmol.2023.1131093

Evolution of visual guanylyl cyclases and their activating proteins with respect to clade and species-specific visual system adaptation

Matthias Gesemann and Stephan C. F. Neuhauss*

Department of Molecular Life Sciences, University of Zurich, Zurich, Switzerland

Membrane guanylyl cyclase receptors are important regulators of local cGMP production, critically influencing cell growth and differentiation as well as ion transport, blood pressure and calcium feedback of vertebrate phototransduction. Currently, seven different subtypes of membrane guanylyl cyclase receptors have been characterized. These receptors have tissue specific expression and are activated either by small extracellular ligands, changing CO_2 concentrations or, in the case of visual guanylyl cyclases, intracellularly interacting Ca^{2+}-dependent activating proteins. In this report, we focus on the visual guanylyl cyclase receptors (GCs) GC-E (*gucy2d/e*) and GC-F (*gucy2f*) and their activating proteins (GCAP1/2/3; *guca1a/b/c*). While *gucy2d/e* has been detected in all analyzed vertebrates, GC-F receptors are missing in several clades (reptiles, birds, and marsupials) and/or individual species. Interestingly, the absence of GC-F in highly visual sauropsida species with up to 4 different cone-opsins is compensated by an increased number of guanylyl cyclase activating proteins, whereas in nocturnal or visually impaired species with reduced spectral sensitivity it is consolidated by the parallel inactivation of these activators. In mammals, the presence of GC-E and GC-F is accompanied by the expression of one to three GCAPs, whereas in lizards and birds, up to five different GCAPs are regulating the activity of the single GC-E visual membrane receptor. In several nearly blind species, a single GC-E enzyme is often accompanied by a single variant of GCAP, suggesting that one cyclase and one activating protein are both sufficient and required for conferring the basic detection of light.

KEYWORDS

guanylyl cyclase activating protein (GCAP), evolution, opsin, blind, visual regression, photoreceptor, nocturnal, crepuscular

Introduction

Photoreceptors of the vertebrate retina use distinct sets of proteins to convert light stimulation into neurotransmitter mediated signals. While one set of proteins is involved in the light-induced activation of effector proteins (opsins, transducins, phosphodiesterases and cyclic nucleotide-gated channels), another set of proteins is responsible for shut-off reactions (GRKs, recoverins, arrestins, and RGS proteins) following light stimulation. Subsequently, visual guanylyl cyclase and their activating proteins play an essential role in the calcium feedback

system of vertebrate phototransduction (Lamb and Hunt, 2018; Gesemann and Neuhauss, 2020; Lamb, 2022) for resetting the detection cascade (Figures 1C,D).

Dim-light specialized rod and bright-light adapted cone photoreceptors often use a related, but slightly different set of phototransduction cascade proteins (Figure 1B; Lamb, 2013). The basis for this cell type specific specialization originates in two rounds of whole genome duplications (WGD) that shaped the vertebrate genome some 500 million years ago. In several reports Lamb and colleagues have demonstrated that most phototransduction genes originate from one ancestral region that is now represented in no more than five paralogous regions in extant vertebrates (Lamb, 2013, 2022). However, several genes have already experienced local duplications prior to WGD, suggesting that the origin of specialization of phototransduction predates the genome duplication events. As a result of these local and WGD duplications, a variable number of copies of ancestral phototransduction genes have adopted specialized or new functions and are expressed in a cell-type specific manner. This is particularly apparent for the different visual pigments, such as rhodopsin and the color sensitive red-, green-, blue- and UV-opsin based pigments that are found in the different types of photoreceptors. Furthermore, such a specialization can also be seen for transducin, PDE6 subunits, CNG channel subunits, arrestins, GRKs, recoverins and NCKX ion exchangers (Lamb, 2022). However, for some proteins of the phototransduction cascade, like guanylyl cyclases (GCs) and their activating proteins (GCAPs), an exclusive cell type specific expression has not been demonstrated and they are present in different types of photoreceptors (Figure 1).

In the tetrapod lineage two visual (GC-E and GC-F) and one phylogenetically closely related olfactory guanylyl cyclase receptor (GC-D) have been identified (Lamb and Hunt, 2018; Gesemann and Neuhauss, 2020). While GC-E is expressed in rods and cones (Dizhoor et al., 1994), GC-F is predominantly expressed in rods (Yang et al., 1995; Yang and Garbers, 1997). Moreover, GC-F expression is generally more restricted and severalfold lower than that observed for GC-E (Helten et al., 2007). These findings go hand in hand with the notion that disruption of *gucy2e* in mice causes severe cone dystrophy, while having little or no effect on rod morphology (Yang et al., 1999). In contrast, mice lacking both cyclases not only completely lack a light induced electrical response but also show a progressive degeneration of rod and cone photoreceptors (Baehr et al., 2007). Similar phenotypes are seen in human patients having mutations in *GUCY2E* (originally called *GUCY2D*), whereas no mutations in *GUCY2F* affecting phototransduction have been described so far (Perrault et al., 1996, 2000).

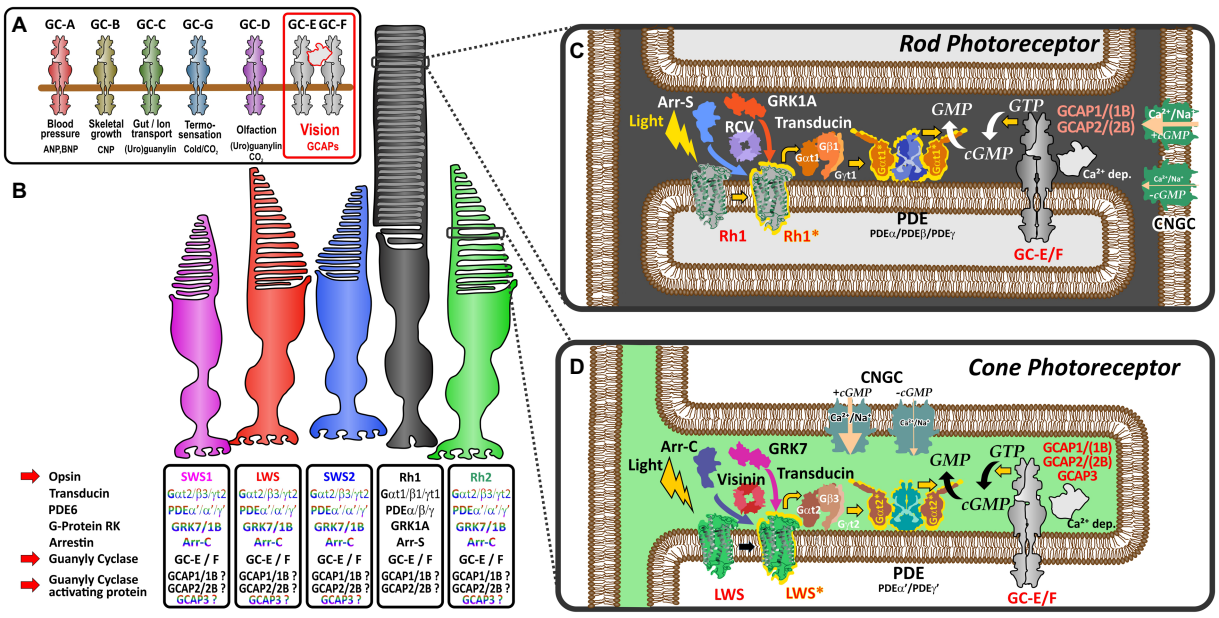

FIGURE 1
Schematic representation of vertebrate phototransduction and the role of receptor guanylyl cyclases and their activating proteins in vertebrate vision **(A)** Name, activators (ligands) and functions regulated by the different subtypes of membrane guanylyl cyclase receptors. Note that visual guanylyl cyclases have no external activators and are controlled by calcium sensitive intracellular guanylyl cyclase activating proteins (GCAPs). For more details on membrane guanylyl cyclase see Kuhn (2016). **(B)** Photoreceptor subtypes of the vertebrate retina. Four different single cone cell types (represented in color) and one rod cell type (represented in black) have been described in the vertebrate retina. Proteins involved in phototransduction in the different cell types are given in the boxes below the different photoreceptors. The font color indicates that these protein variants are cone specific whereas the black font indicates that cones and rods may use the same proteins to regulate phototransduction. Note that SWS2 and Rh2 expressing photoreceptors are absent in mammals. **(C,D)** Phototransduction cascade in rod **(C)** and cone **(D)** photoreceptors. Note that cones and rods use slightly different proteins in the phototransduction cascade (indicated by the different colors in the picture). Light triggers the activation of visual opsins (Rh1 in rods or SWS1, SWS2, Rh2, and LWS in cones), thereby activating transducin. The activated alpha subunit of transducin stimulates the phosphodiesterase PDE, which after activation increases the hydrolysis of cGMP, lowering the intracellular cGMP concentration. The decreased intracellular cGMP levels result in a closure of cyclic nucleotide gated ion channels (CNGCs). As the activity of the Na^+/Ca^{2+} K^+ exchanger NCKX (not depicted in this figure) is not affected by light, intracellular Ca^{2+} levels decrease due to the constant outward flow of Ca^{2+}. The decreased Ca^{2+} concentration leads to the activation of calcium dependent guanylyl cyclase activating proteins (GCAPs) which in turn stimulate GCs and the generation of cGMP increasing the intracellular concentration, subsequently reopening CNGCs bringing the Ca^{2+} levels back to the resting stage.

Neuronal calcium sensor proteins (NCS), which are highly conserved EF-hand superfamily proteins, tightly regulate the activity of GCs. More than 20 different members of the NCS family have been described, with some of them being species specific (Lim et al., 2014; Ames, 2018). Among these, six subfamilies fall into the category of guanylyl cyclase activating proteins (GCAPs), with teleost fish possessing additional 3R and 4R duplicates (Imanishi et al., 2004; Lamb, 2022). The most intensely studied members of this subfamily are *guca1a* (GCAP1) and *guca1b* (GCAP2), which have been shown to be expressed at different levels in rod and cone photoreceptors (Cuenca et al., 1998). While GCAP1 seems to be the predominant variant in cones, GCAP2 expression levels are higher in rods. Mutations in both proteins have been shown to cause retinal dystrophies, albeit with more severe phenotypes seen for *guca1a* (GCAP1) mutations (Sato et al., 2005; Behnen et al., 2010; Jiang and Baehr, 2010). Due to the often species-specific presence, far less is known about function and abundance of the other four members of the GCAP subfamily.

In a previous study we have analyzed the evolution of guanylyl cyclase following the two rounds of WGD (Gesemann and Neuhauss, 2020). Some clades and isolated species lack either GC-F, GC-D or both receptors relying on a single membrane linked cyclase to control the calcium feedback system of phototransduction. Interestingly, not only have species with reduced visual capabilities lost the second visual guanyly cyclase, but the same is true for some entire clades comprised of species with excellent vision, such as birds and lizards. We have therefore hypothesized that g*ucy-2f* gene loss occurring in ancestral or recent "bottleneck" species, which affects all extant downstream species, might be compensated by functional adaptation and/or duplication of other phototransduction cascade proteins. In contrast, gene loss in isolated lineages might be the result of adaption to specific habitats. In this report, we focus on the evolution of GCAPs in all major tetrapod clades following 1R and 2R and concentrate on a variety of highly adapted underground living species that have only limited visual capabilities. Our results show that while birds and lizards react to the sole presence of one GC with an increase in number of GCAPs, in visually impaired species the observed GC gene reduction is often mirrored by a similar reduction in GCAP gene content.

Materials and methods

Annotation of guanylyl cyclase activating sequences

As gene and cDNA sequence annotations created by computerized methods have been shown to contain frequent errors, cDNA sequences of guanylyl cyclase activating proteins (*guca's*), additional *gucy* genes and selected opsin genes used in this study were manually annotated. Sequences were identified and annotated using information from genome databases, nr/nt database, wgs contigs and expressed sequence tags (GeneBank,[1] last accessed February 8th, 2023; Ensembl,[2] last accessed December 8th, 2022). Mouse and human sequences were used as initial query [for more details on sequence annotation, see Gesemann et al. (2010)]. Nonsense as well as putative frame shift mutations within the manually annotated sequences were confirmed using whole genome shotgun (WGS) contigs and/or additional sequence information from expressed sequence tags. Only sequences with more than one inactivating or splice site mutation or with corresponding mutations in closely related species were considered relevant. Genome sequences with poor quality (multiple Ns in the extracted sequence or large sequence parts missing) were excluded from the analysis. Exon sizes as well as putative cDNA sequences from related species were used as additional references. Intron/Exon boundaries were identified using a combination of the genescan webpage[3] and manual inspection analyzing major as well as minor splice site consensus sequences (Patel and Steitz, 2003). A complete list of *guca* intron and exons sizes and putative inactivating mutations as well as the genomic region used is given in the Supplementary Table S1. Regions of annotated mammalian opsin sequences are given in Supplementary Table S2 and corresponding regions of sauropsida opsins are given in Supplementary Table S3.

Generation of phylogenetic trees

Phylogenetic trees were generated using the NGPhylogeny.fr platform[4] (last accessed February 17th, 2023) (Dereeper et al., 2008; Lemoine et al., 2019). 117 cDNA sequences of *guca1a* were aligned using MAFFT version 7 with default parameters (Katoh and Standley, 2013). The length of input sequences varied between 588 and 636 nucleotides. After alignment, ambiguous regions (i.e., containing gaps and/or being poorly aligned) were removed with BMGE (Block Mapping and Gathering with Entropy) (Criscuolo and Gribaldo, 2010) using default parameters: Sliding window size: 3; maximum entropy threshold: 0.5; gap rate cuttoff: 0.5; minimus block size: 5; matix: PAM250. Following curation 602 nucleotides (some sequences with gaps) were used for further analysis. Phylogenetic tree reconstructions were done using the FastTree method (Price et al., 2009). Graphical representations of the phylogenetic trees were obtained using iTol utility[5] and edited in Coral draw (CoralCorporation).

Synteny analysis

An initial rough synteny analysis was done using the synteny database[6] (last accessed November 14th, 2022) (Catchen et al., 2009). Synteny hits in the output files were further subjected to microsynteny analyses, where paralogous/orthologous genes of all the species of interest were analyzed in Ensembl (see Footnote 2) (last accessed December 20th, 2022) and confirmed by reciprocal tBLASTx searches. Final figures were edited using Coral draw (CoralCorporation).

1 http://www.ncbi.nlm.nih.gov
2 http://www.ensembl.org/index.html
3 http://hollywood.mit.edu/GENSCAN.html
4 https://ngphylogeny.fr
5 https://itol.embl.de
6 http://syntenydb.uoregon.edu/synteny_db/

Animal pictures

Animals pictures used in our figures were downloaded from the shutterstock photo repository[7] using a purchased license.

Results and discussion

Phylogeny and synteny analysis confirm absence of GC-F In sauropsids

In a previous study we have investigated the preservation, inactivation and possible functional adaptation of guanylyl cyclase genes across more than 300 different vertebrate species (Gesemann and Neuhauss, 2020). We have shown that eutherians commonly use two visual GCs, namely GC-E and GC-F. However, independent pseudogenization of the GC-F receptor occurred in some lineages, such as sauropsids and mustelidae (weasel-like) and some isolated, often non visual, species. A more recent report, however, suggested that sauropsids might still have two visual guanylyl cyclases (Gower et al., 2021), which is in contradiction to what we and Lamb and colleagues have reported. Therefore, we first reexamined our previously annotated sequences and compared them to the available sequences in the different databases and available information in the latest reports. In order to get a more conclusive overview, we used species that have both GC-F and GC-D variants and compared them to the putative *gucy2d/f* sequence of species of the sauropsida clade using phylogeny and synteny. Phylogeny as well as synteny analysis clearly indicated that the designated sauropsida GC-F variants group into the olfactory GC-D branch (Figure 2A). Remarkably, the relation between mammalian GC-D variants and the corresponding sauropsida ones is quite distant, as sequence conservation between these two clades is only in the range of 50%. Nevertheless, the sauropsida GC-D/F protein sequences are clearly more closely related to the GC-D sequences of anura (frogs) or coelacanth and holostei fish than that they are to their corresponding GC-F sequences. This view is further supported by the synteny of *gucy2f* (GC-F) and *gucy2d* (olf.) (GC-D) (Figures 2B,C). The gene alignment in the vicinity of mouse and Xenopus *gucy2d* (olf.) is evidently preserved in the eastern brown snake *Pseudonaja textilis* (Figure 2B). However, gene synteny in the region of mouse and Xenopus *gucy2f* clearly indicates that *gucy2f* is missing in the eastern brown snake. Taken together, we conclude that our previous analysis that sauropsids lack the second visual guanylyl cyclase GC-F holds true. This is further supported by the finding that none of the 13 lepidosauria eye transcriptomes detected a GC-F variant (Simões et al., 2018).

Loss of *gucy2f*/GC-F in sauropsids can be compensated by an increasing number of GCAPs

Having confirmed our previous findings on *gucy* gene evolution across species, we were then interested in the influence of *gucy* inactivation on the abundance of GCAPs, in particular in the context of the visual requirements of the analyzed species.

We initially assembled *guca* coding sequences of same species that we have previously used for our *gucy* analysis (Gesemann and Neuhauss, 2020). However, in the current study we omitted species, such as teleosts, whose genomes underwent an additional round of whole genome duplication, but included some additional species that have been shown to have either relatively poor eyesight or excellent visual capabilities. The coding sequences of all assembled *guca's* are spread over four exons which between paralogs are very similar in size but display slight, consistent variations that are typical for the different *guca* variants (Supplementary Table S1). Introns of *guca1c* are constantly larger (3 to 15 times) than the corresponding introns of *guca1a* and *guca1b* derived paralogs (Supplementary Table S1), suggesting that *guca1c* might be differently regulated than the other activating proteins.

Previous *in vitro* experiments have suggested that GCAP1 (encoded by *guca1a*) and GCAP2 (encoded by *guca1b*) are similarly active in stimulating GC-E and GC-F receptors (Koch and Stryer, 1988). However, more recent *in vivo* data from rod photoreceptors indicate that GC-E is predominantly regulated by GCAP1 (Olshevskaya et al., 2012). Therefore, we expected GCAP1 to be the dominant GCAP protein with GCAP2 and GCAP3 being under lower evolutionary pressure. In a first survey analysis, we selected one to two species per clade that are frequently used in scientific studies or represent key species for phylogenetic analysis. Among these analyzed species are 12 mammals; covering primates, rodents, carnivores, herbivores, bats, afrotherians and marsupials; 1 egg laying *prototheria*; five *sauropsida* species, including lizards, birds, turtles, crocodiles; two amphibians as well as 1 holostei fish species. As previously reported, all sauropsids and marsupials lack the second visual guanylyl cyclase (Lamb and Hunt, 2018; Gesemann and Neuhauss, 2020). This is also true for the mostly nocturnal monochromatic sloth *Choloepus hoffmanni*. As suggested in our previous report, sauropsids indeed compensate the loss of *gucy2f* with an increased number of *guca* genes (Figure 3). This is particularly striking for the lizard *Anolis caroliensis* in which we found five GCAPs, but also in chicken and turtles we detected four GCAP variants. Snakes only require one guanylyl cyclase and three guanylyl cyclase activating proteins. In general, visual requirements are reflected by the combinatorial possibilities of guanylyl cyclases and their activating proteins. Highly visual trichromats, such as humans, have six combinatorial possibilities (2×3), while dichromatic mammals such as elephants and cattle get by with four possibilities (2×2). Lizards on the other hand have five combinatorial possibilities, whereas birds and turtles have four and snakes still have three different possibilities. Interestingly, frogs and holeostei fish have the highest number of possibilities, as they possess both visual GCs in combination with five activating proteins.

Visual system adaptation in sauropsids is reflected in the number of active GCAPs

As visual performances among the different sauropsida and amphibian species can vary dependent on their ecological niches and lifestyle adaptation, we compared the integrity of *guca* genes in habitat extremists with more generalist species. In the snake (*serpents*) clade which includes the mainly nocturnal constricting snakes (pythons, boas

7 https://www.shutterstock.com

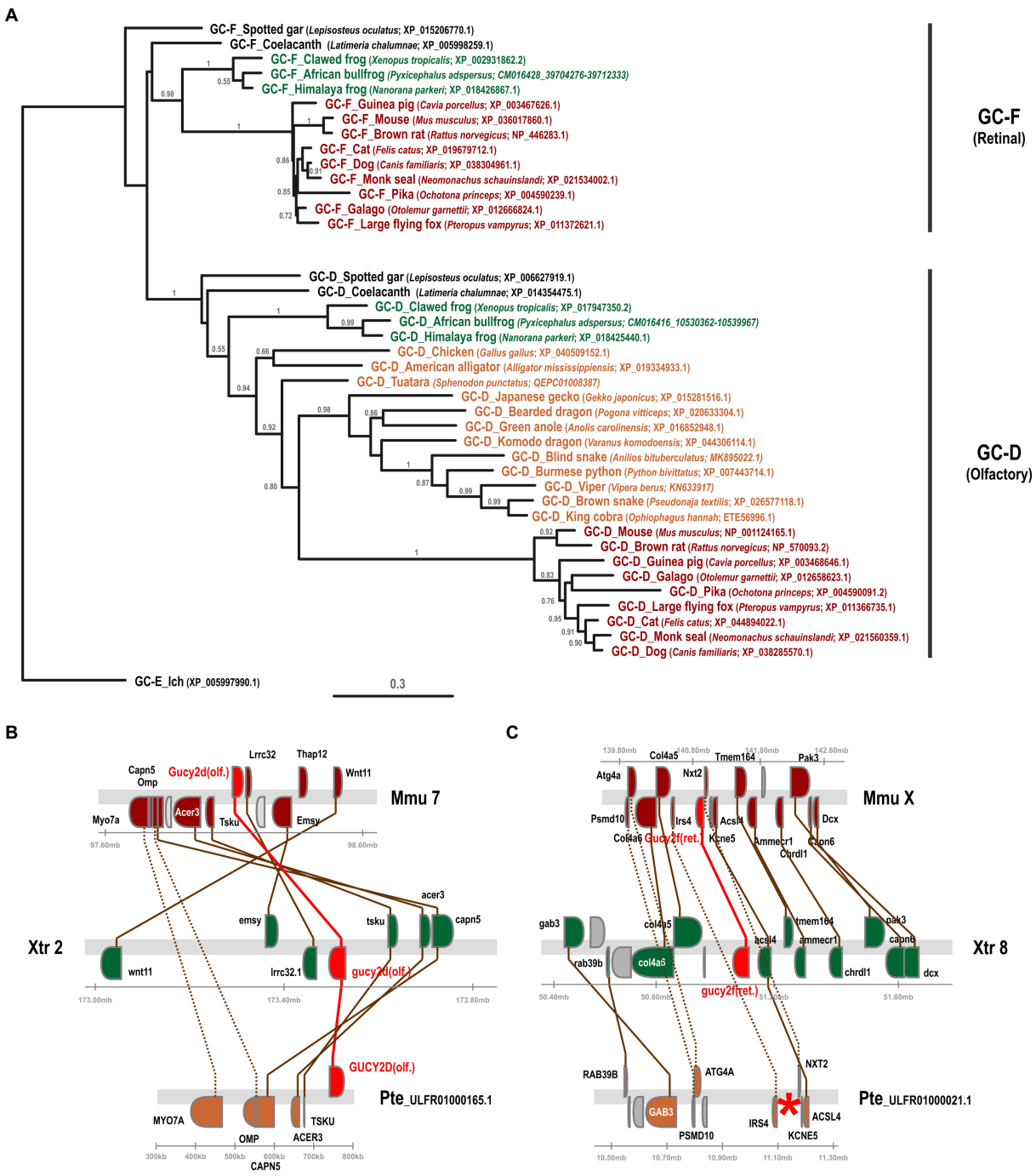

FIGURE 2
Phylogeny and synteny of *gucy2f*/GC-F (retinal) and *gucy2d*/GC-D (olfactory) confirm the absence of *gucy2f*/GC-F in sauropsids. **(A)** Phylogenetic tree of *gucy2f* and *gucy2d*. *gucy2f* as well as *gucy2d* (olf.) genes of selected mammalian (displayed in red) and amphibian (shown in green) species that have retained both genes were compared to the *gucy2f/d* genes described in sauropsids (depicted in orange). Common and scientific names for the species are given. The scale bar shows the percentage (0.3 equals 30%) of nucleotide substitutions required to generate the corresponding tree. Note that no *gucy2f* sequences are present in sauropsids. (B and C) Synteny of mouse (mmu), xenopus (xtr) and eastern brown snake (pte) *gucy2d* (olf.) **(B)** and *gucy2f* **(C)**. Genomic regions around the mouse, xenopus and eastern brown snake *gucy2d* **(B)** and *gucy2f* **(C)** are shown and the chromosomal location is indicated. The location of the *gucy* genes is highlighted in red and syntenic genes are given in colors. Orthologous genes are connected by colored lines, indicating that the vicinity of the *gucy2d* gene is conserved in all three species **(B)**, whereas, even if the vicinity of *gucy2f* is conserved between the species, the gene is absent in the eastern brown snake **(C)**. A red asterisk indicates the putative location of the missing gene.

and anacondas), crepuscular and diurnal vipers and the ground dwelling fossorial blind snakes, lifestyle has some effects on opsin (Gower et al., 2021) gene content. Compared to lizards which are generally tetrachromats, nocturnal and diurnal snakes are usually dichromatic and burrowing blind snakes are either rod or cone monochromats (Gower et al., 2021; Figure 4). The reduced number of

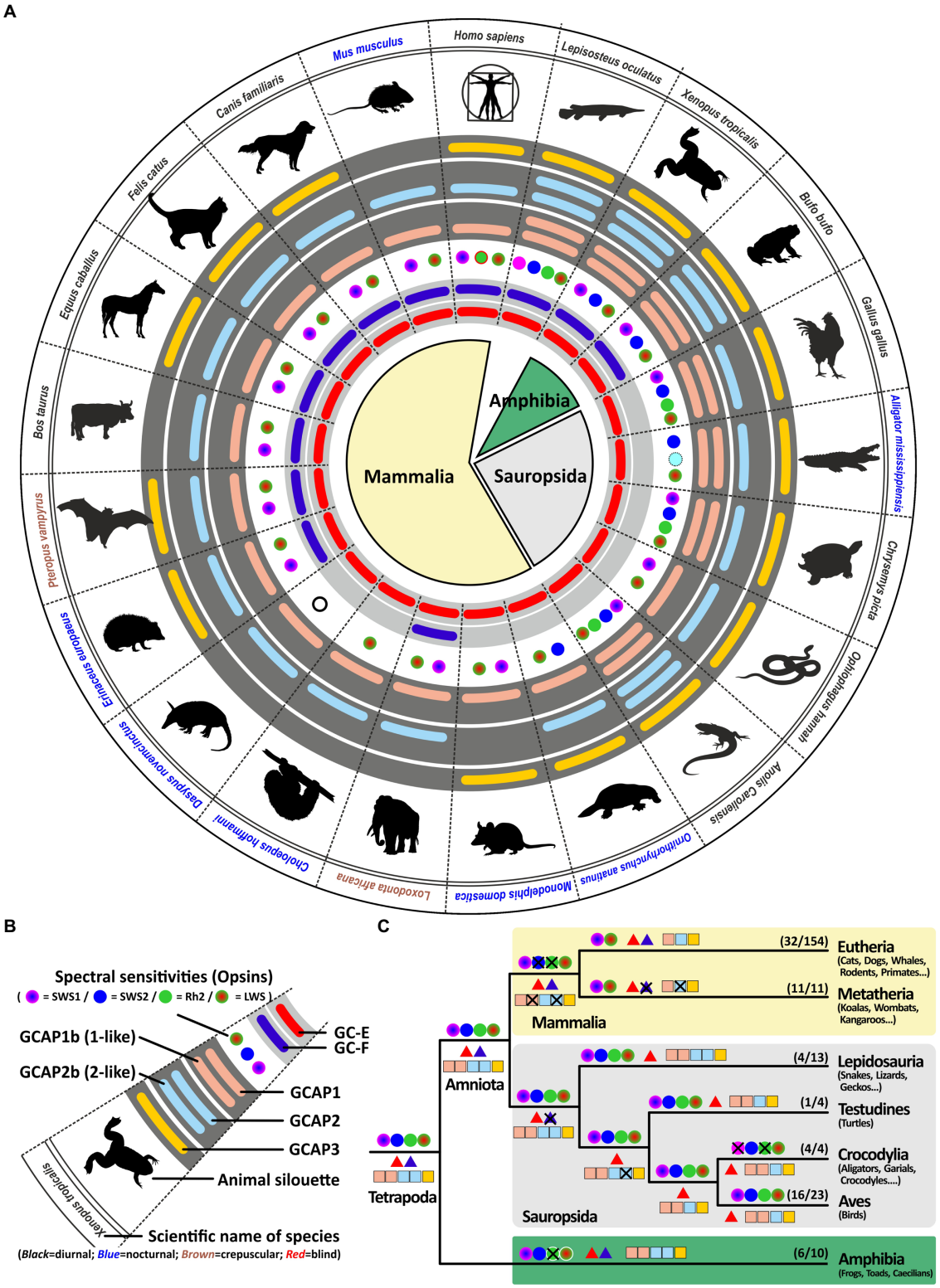

FIGURE 3
Reduction of visual GCs can be compensated by an increased number of GCAPs. **(A)** Expression of opsins, GCs and GCAPs in major vertebrate species. In the center, major vertebrate classes and clades are given. Mammals are depicted in light yellow, sauropsids in light gray and amphibians in green. **(B)** Explanation of symbols used in **(A)**. Pictograms for each chosen representative are shown and scientific names are given. Names of diurnal species are written in black, crepuscular species in brown and nocturnal species in blue. The presence of an open reading frame coding for GC-E is shown as a red bar in the innermost light gray circle and *gucy2f* genes without inactivating mutation are illustrated by a dark blue bar adjacent to it. The different types and color sensitivities of photoreceptor single cones are indicated by the colored dots and eventual rod monochromacy is shown by a white circle. Spectral sensitivities under debate are indicated by dotted lines. The presence or absence of intact ORFs for GCAPs are given by the colored bars

(Continued)

FIGURE 3 (Continued)
in the dark gray circles. *guca1aa* and *guca1ab* (from inside to outside) are given in light red, *guca1ba* and *guca1bb* are given in light blue and *guca1c* is shown in yellow. **(C)** Evolution of opsins, GCs and GCAPs in major vertebrate clades. Major vertebrate linages are shown. Opsins are given by circles, GCs by triangles and GCAPs by squares. The most likely ancestral situation at every major branch point is given. Numbers in parenthesis represent the species still displaying this gene content (first number) and the total number of species analyzed (second number). Note that sauropsids lack the second visual GC, but have often a higher number of intact GCAPs when compared to eutherians.

cone subtypes is reflected in the amount of functional GCAPs. Highly visual lizards combine their single visual guanylyl cyclase with up to five GCAPs, while neither analyzed serpent has more than three GCAPs and in the case of the blind snake *Anilios bituberculatus* this number is further reduced to only GCAP1 or GCAP2, respectively. However, some lizards and especially the more distantly related *gekkota* clade show with three or four GCAPs, also a reduced gene number. In the case of geckos this might be explained by their nocturnal lifestyle and the absence of rhodopsin and a fourth visual cone pigment (Pinto et al., 2019). However, not all diurnal lizards follow this pattern.

Tetrachromatic birds which represent a sister clade of the previously discussed Lepidosauria (scaled lizards), also have a maximum of 4 GCAPs. This suggests that all visual demands, even for highly visual tetrachromatic animals, can be covered by four GCAPs. Establishing a link between chromaticity and GCAPs in birds is however difficult as visual pigment genes in birds, with the exception of rh1 and rh2, are likely encoded on microchromosomes that often cause genomic sequencing problems (Waters et al., 2021). This might be the reason why tetrachromacy on the genomic level could not be confirmed in a variety of species (Borges et al., 2015). In the chicken case tetrachromacy is anatomically established (Kram et al., 2010) and could be confirmed by the identification of four visual pigment cDNA sequences (Enright et al., 2015; Yamagata et al., 2021), however, on a genomic level the *opsin1sw1* sequence is missing. This suggests that microchromosome sequence evasion is indeed a problem, even in species with high sequence coverage and broad scientific interest. Nevertheless, recent studies imply that owls lack the *opsin1sw1* gene (Hanna et al., 2017; Höglund et al., 2019), suggesting that a nocturnal or crepuscular lifestyle indeed influences vison in birds. Interestingly, we did not see a reduction of GCAPs, as all analyzed owl species still show four GCAPs (Supplementary Table S1).

While owls as nocturnal raptors have large eyes and excellent vison, another family of nocturnal birds, namely New Zealand kiwis, have greatly reduced eyes and in general poor vision (Corfield et al., 2015). Genome sequencing in kiwis indeed suggested that several opsins are either absent or have accumulated deleterious mutations (Le Duc et al., 2015). While the problem with sequencing GC-rich microchromosomes is acknowledged in this report, all expected opsin sequences could be identified. Several mutations in *opsin1sw1* and *rh2* (*opsin1mw*) seem to be present most likely rendering these chromophores non-functional (Le Duc et al., 2015). When we looked at kiwi opsin genes we could confirm alterations in the *rh2* sequences causing a frame shift in the 4th exon (Supplementary Table S1). However, we found no mutations in the partial *opsin1sw1* sequences of *Apteryx mantelli* and *Apteryx haastii*. Due to incompleteness of the *opsin1sw1* sequence in these species, the integrity of this gene remains unclear. In contrast to owls, the inactivation of opsins in kiwis is also reflected in accumulating mutations in the kiwi *guca1c* gene. As these mutations are present throughout the four analyzed kiwi genomes we are confident that this is indeed an occurring non-functionalization. We have also looked at a number of other nocturnal birds such as the kakapo, night heron, nightjar and others, but did not find obvious *guca* gene variation (Supplementary Table S1), suggesting that as for owls preserving four intact GCAPs might be beneficial for nocturnal as well as cathemeral species.

Two other sister clades of birds and reptiles are turtles and crocodiles. As land turtles are slow moving herbivores protected from predators by their stable shells, a good sense of vision seems not mandatory. Nevertheless, tetrachromatic vision still occurs in turtles (Emerling, 2017; Corredor et al., 2022) and we have confirmed the tetrachromacy of *Chrysemys picta* (Supplementary Table S3). A possible explanation may lie in the better ability of tetrachromats to distinguish color hues in fruits, part of the diets of turtles. In contrast to a previous report by Emerling and colleagues, we could only find open reading frames for three opsins in the aquatic turtle *Chelonia mydas* (*rh2*, *opsin1sw1* and *opsin1lw*) and the Pinta giant tortoise *Chelonoidis abingdonii (opsin1sw2, rh2 and opsin1lw)*. Interestingly, some of the previously published sequences have been removed, even if one of the removed sequences is clearly the *opsin1lw* sequence (XM_007052772.1). The other removed sequence (XM_007067421.1) is identical to a newer sequence (XM_037889438.1) both representing the *opsin1sw1* transcript. The transcript XM_007063507.2, which was and still is considered to be *opsin1sw2* is likely a *rh2* paralog (Supplementary Table S3). No *opsin1sw2* transcript or genomic sequence could be identified suggesting that *Chelonia mydas* is trichromatic rather than tetrachromatic. As suggested by Emerling and colleagues we also found the Chinese softshell turtle *Pelodiscus sinensis* to be most likely dichromatic, as *opsin1sw1* and *opsin1sw2* have accumulated various mutations, rendering the genes potentially non-functional (Supplementary Table S3). Interestingly, the amount of functional cone opsins has no immediate effect on the abundance of GCAP genes, as four of these proteins acting downstream in the rod and cone phototransduction pathway are present and most likely functional in all analyzed turtles (Supplementary Table S1).

The situation in the crocodile clade is somewhat different. The mainly nocturnal crocodiles have reduced their opsin gene content to two cone opsins (*opsin1sw2* and *opsin1lw*) and one regular rhodopsin (*rh1*) (Emerling, 2017). This is reflected by two morphological single cone types in caimans and alligators. However, in the case of the salt water crocodile *Crocodylus porosus*, the existence of a third single cone has been proposed (Emerling, 2017), in which the rod rh1 pigment is also used in cone photoreceptors, making these animals functional trichromats. Interestingly, dichromacy seems not to go hand in hand with a reduction of GCAPs as all crocodiles still have four GCAPs (Supplementary Table S1).

Amphibian visual spectra and number of GCs and GCAPs are highly variable

A previous study by Schott and colleges (Schott et al., 2022b) has shown that *Anura* (frogs and toads) are in general trichromats,

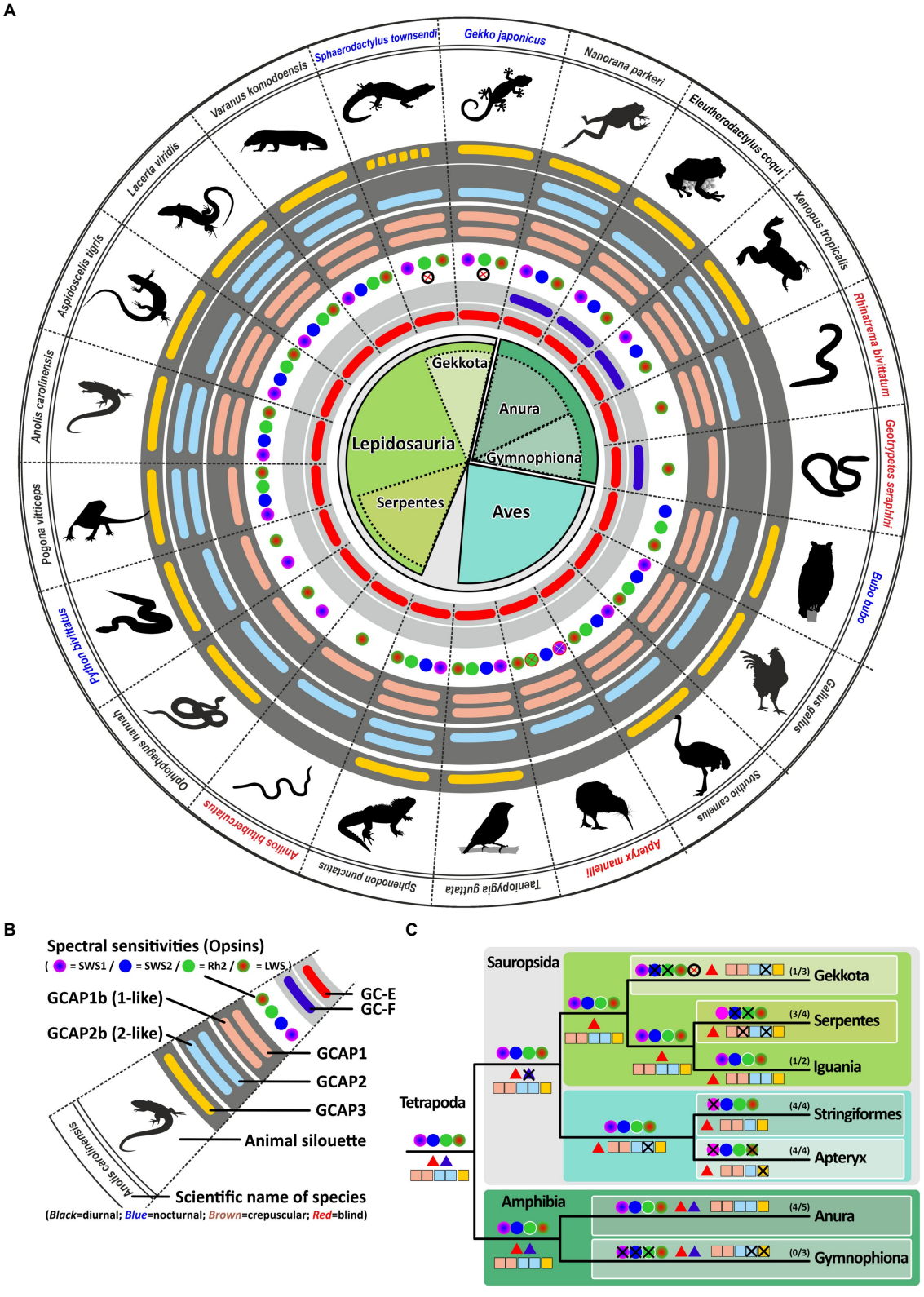

FIGURE 4
Reduction to one visual GC in sauropsids represents a bottleneck in the phototransduction calcium feedback system. **(A)** Expression of opsins, GCs and GCAPs in sauropsids and amphibians. In the center, major sauropside and amphibian classes, orders and suborders are given. Scaled lizard (*Lepidosauria*) are depicted in bright green, birds (*Aves*) in petrol, and amphibians in dark green. Suborders are indicated by a lighter shade. **(B)** Explanation of symbols used in **(A)**. Pictograms for each chosen representative are shown and scientific names are given. Names of diurnal species are written in black, nocturnal species in blue and blind or visually impaired species in red. The presence of an open reading frame encoding GC-E is shown as a red bar in innermost light gray circle and *gucy2f* genes without inactivating mutation are illustrated by a dark blue bar adjacent to it. The

(Continued)

FIGURE 4 (Continued)
different types and color sensitivities of photoreceptor single cones are indicated by the colored dots. In the case of geckos the crossed out white circle indicates the inactivation of the Rh1 gene. Crossed out circles in the kiwi case represent unverified losses. The presence or absence of intact ORFs for *guca* transcripts are given by the colored bars in the dark gray circles. *guca1aa* and *guca1ab* (from inside to outside) are given in light red, *guca1ba* and *guca1bb* are given in light blue and *guca1c* is shown in yellow. **(C)** Evolution of opsins, GCs and GCAPs in major sauropsid and amphibian clades. Major lineages are shown. Opsins are given by circles, GCs by triangles and GCAPs by squares. The most likely ancestral situation at every major branch point is given. Numbers in parenthesis represent the species still displaying this gene content (first number) and the total number of species analyzed (second number). Note that blind species have to the lowest number of combinatorial possibilities for *guca* and *gucy* genes, and that highly visual animals keep a higher number of combinations.

expressing *opsin1sw1*, *opsin1sw2* and *opsin1lw*. In contrast to sauropsida which have downstream of phototransduction only one guanylyl cyclase to regulated calcium feedback, amphibians have, similar to eutherians, two cyclases at their disposal (Gesemann and Neuhauss, 2020). In the case of eutherians (placental mammals), neither species expressing both visual cyclase genes has more than three guanylyl cyclase activating proteins, suggesting that all aspects of trichromatic vision, as observed in humans and old world monkeys, can be regulated by a 2/3 (2 guanylyl cyclases and 3 GCAPs) combination (Gesemann and Neuhauss, 2020). Surprisingly, frogs and toads seem to have preserved a more ancestral gene state as they have, similar to lizards and holostei (e.g., gars and bowfins), still five functional GCAPs (Figure 4) enabling 10 different combinatorial possibilities. While frog vision is well developed, there is at first glimpse no reason why frogs and toads should combine two visual guanylyl cyclases with five activating proteins. Frogs and toads in general go through two different developmental stages, hence the combination of two guanylyl cyclases with five activating proteins may very well be lifestyle related. They not only switch from an aquatic habitat to a more terrestrial lifestyle following metamorphosis from tadpoles to frogs, but they also show changes in the expression of opsins as well as other genes of the visual system during this transition (Schott et al., 2022a). This adaptive decoupling in the visual system might go hand in hand with anatomical changes observed in the tadpole versus frog retina. In the case of guanylyl cyclases and their activating proteins, adaptive decoupling might lead to differential expression of these genes during tadpole and adult stages. While some might be expressed in larval stages, other could be active in adults only. To test this hypothesis we analyzed the GCAP situation in the common coquí *Eleutherodactylus* coqui, a frog species that has no free swimming tadpoles (Townsend and Stewart, 1985; Westrick et al., 2022). Coquis lay eggs in palm trees and the larvae remain in the eggs until mature frogs emerge, thereby bypassing the tadpole stage. Indeed, *Eleutherodactylus coqui* was the only anuran species in which we identified only four CGAPs (Figure 4; Supplementary Table S1), suggesting that tadpoles and adult frogs may indeed rely on different GCAPs explaining their increased number in amphibians.

A sister clade to frogs, toads and salamanders are caecilians, blind, limbless worm-like amphibians. Caecilians mostly live underground and their vision is mainly limited to dark–light perception. Previous studies have shown that caecilians are rod monochmomats, lacking cone photoreceptors (Mohun et al., 2010; Mohun and Wilkinson, 2015). This adaptation to underground life is also reflected in the reduction of GCs and GCAPs. While in *Geotrypetes seraphini* the reduction is seen at the level of GCAPs, in *Rhinatrema bivittatum* the reduction occurs at the level of the cyclases (Figure 4) leaving them with either two or three combinatorial possibilities, respectively.

Lifestyle adaptations in rodents, rabbits and insectivores cause alteration in the calcium feedback system of phototransduction

Similar to caecilians, many animals of the rodent, rabbit and insectivore clade are underground living or at least nocturnal animals, with often reduced vision. In general, animals of the *glires* and *insectivore* clade are dichromatic. However, there are reports having shown that some underground specialists have reduced their active opsin complement (Peichl et al., 2000; Emerling and Springer, 2014). The blind mole rat *Nannospalax galili*, the naked mole rat *Heterocephalus glaber*, the cape golden mole *Chrysochloris asiatica* and the Eastern mole *Scalopus aquaticus* are either cone or rod monochromats (Emerling and Springer, 2014; Emerling, 2018); (Figure 5). We have previously shown that reduced visual capabilities are frequently reflected in a reduction of proteins involved in the calcium feedback system of phototransduction, namely guanylyl cyclases (Gesemann and Neuhauss, 2020). However, not all of these animals have completed the inactivation of the second visual GC, as the Eastern mole has still two intact visual GC sequences (Figure 5). There are nocturnal animals such as the porcupine *Hystrix cristata* and the European dormouse *Glis glis* that have both visual GCs but are cone monochomats. Interestingly, all the above mentioned visually impaired mole species rely also on only one GCAP, independent whether they poses one or two visual GCs. In contrast to this, dormice and porcupines have two GCAPs leaving them with four combinatorial possibilities. Remarkably, some visually impaired species such as the star nosed mole *Condylura cristata* and the common shrew *Sorex araneus* remain functional dichromats (Emerling, 2018). Nevertheless, they both only possess the *guca1a* gene and in the case of the shrew also only one *gucy* gene. While vision has in general little importance for rodents, rabbits and insectivores, there are some notable exceptions. Squirrels for instance have excellent vision (van Hooser and Nelson, 2006). Even if they have only one visual GC they possess as almost the only clade of this order three GCAPs. This is hardly surprising, as squirrels are diurnal animals that highly depend on visual input especially for tree-dwelling species.

Spectral sensitivity as well as nocturnality influences the calcium feedback system of phototransduction in carnivores and *Xenarthra*

With more than 280 different species, carnivores represent a large order within the mammalian class (van Valkenburgh and Wayne, 2010). Their members are very diverse including cat-like feliformes as well as dog-like caniformes in which dogs, bears, mustelids, raccoons and seals

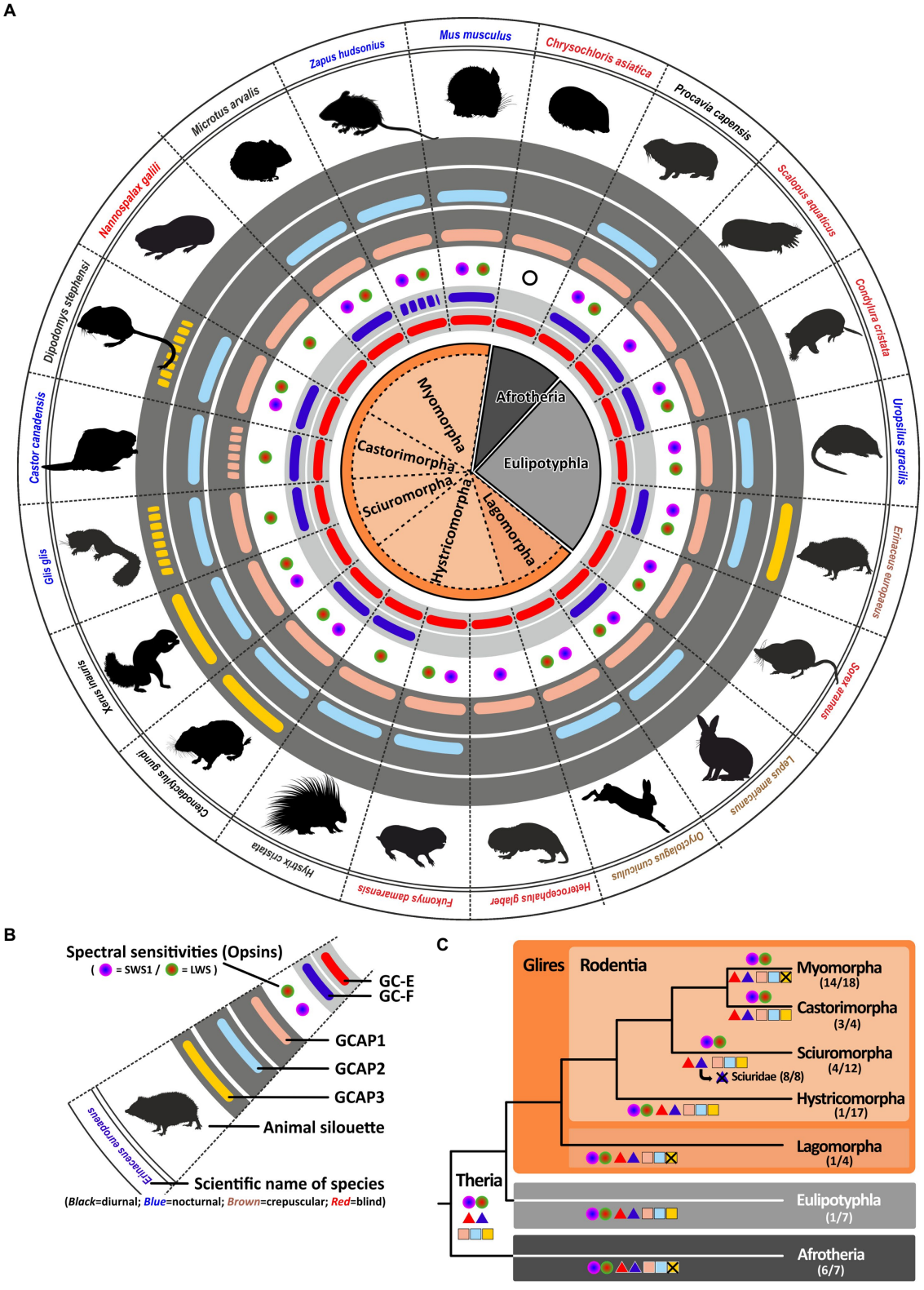

FIGURE 5
Regressive eye evolution in rodents and insectivores is reflected in the pseudogenization of *gucy* and *guca* genes. **(A)** Expression of opsins, GCs and GCAPs in glires, insectivores and afrotherians. In the center, major rodent and rabbit as well as insectivore and afrotherian orders and suborders are given. Glires are highlighted in brown, insectivores in gray and afrotherians in dark gray. Suborders (rodents and rabbits) are indicated by a lighter shade. **(B)** Explanation of symbols used in **(A)**. Pictograms for each chosen representative are shown and scientific names are given. Names of diurnal species are written in black, crepuscular species in brown, nocturnal in blue and blind or visually impaired species in red. The presence of an open reading frame encoding the GC-E protein is shown as a red bar in innermost light grey circle and *gucy2f* genes without inactivating mutation are illustrated by a dark blue bar adjacent to it. The different types and color sensitivities of photoreceptor single cones are indicated by the colored dots and rod

(Continued)

FIGURE 5 (Continued)
monochromacy is shown by a white circle. The presence or absence of intact ORFs for *guca* transcripts are given by the colored bars in the dark gray circles. *guca1aa* and *guca1ab* (from inside to outside) are given in light red, *guca1ba* and *guca1bb* are given in light blue and *guca1c* is shown in yellow. Sequences that have only a single mutation, that could be based on a sequencing error, are given by broken lines. **(C)** Evolution of opsins, GCs and GCAPs in major glires, insectivores and afrotherian orders. Major linages are shown. Opsins are given by circles, GCs by triangles and GCAPs by squares. The most likely ancestral situation at every major branch point is given. Numbers in parenthesis represent the species still displaying this gene content (first number) and the total number of species analyzed (second number). Note that for some nearly blind species the *gucy* and *guca* gene number has been reduced to one single copy each.

are combined. While dogs and cat-like species are true carnivores, most other members are rather omnivores having adapted to a broader range of diets (van Valkenburgh and Wayne, 2010). True carnivores are often diurnal, whereas many omnivores are rather nocturnal. All these lifestyle adaptations have also impacted the visual systems of these animals (Bowmaker and Hunt, 2006). In a previous study, we have shown that members of the weasel *(mustelidae)* family, which includes badgers, otters and martens, have lost their second visual guanylyl cyclase (Gesemann and Neuhauss, 2020). Interestingly, this also independently occurred in another carnivora family, namely the mongoose *(Herpestidae)* which combines more than 30 different species. However, while some *mustelidae* and *herpestidae* species are nocturnal and are less dependent on vision such as the honey badgers *Mellivora capensis*, others like the banded mongoose *Mungos mungo* or the meerkat *Suricata suricatta* are highly visual diurnal dichromatic animals (Wilson et al., 2009). Interestingly, this seems to influence the number of active GCAPs in these animals. While the honey badger has only persevered two GCAPs, the banded mongoose and also the sea otter have kept three GCAPs (Figure 6). Such a reduction in GCAPs can also observed in some nocturnal carnivores that have kept two GCs. While *Felidae* (cats) are often diurnal or crepuscular and display 3 GCAPs, members of the nocturnal hyena family lack an intact *guca1c* gene (Figure 6).

The most striking adaptions in phototransduction genes are observed in the *Procyonidae* family. It was reported that some *Procyonidae*, which includes raccoons and kinkajous, are highly specialized, nocturnal, monochromatic animals (Jacobs and Deegan, 1992). When we analyzed the opsin sequences of these species we found an intact open reading frame for the kinkajou *opsin1sw1* transcript (Supplementary Figure S2). The only abnormality that could be seen was at the 3′ splice site following exon3, where the regular splice site consensus at the exon/intron boundary was GC instead of GT. However, we found such a change quite frequently in our gene studies, suggesting that either splicing after GC can occur or that RNA editing can change the GC to a GT in these transcripts. Remarkably, the raccoon *Procyon lotor* as well as the kinkajou *Potos flavus* have reduced the guanylyl cyclase genes and their activating proteins to a minimum in preserving only one member each (Figure 6). This suggests that rod and cone monochromatic or dichromatic vision works well with only one protein of each subtype and that higher combinatorial possibilities are only beneficial for animals having a higher number of cone photoreceptors or are active under diurnal conditions.

We found such a striking reduction of *opsin*, *gucy* and *guca* genes also in the suborder of *Xenarthra.* Among xenarthrans are species like armadillos, sloths and anteaters, that have been shown to have only limited vision (Emerling and Springer, 2015). While armadillos are rod monochromats, sloths and anteaters are rod/cone monochromats. Interestingly, the diurnal anteater *Myrmecophaga tridactyla* shows the highest reduction rate in *gucy* and *guca* genes, leaving only one member of each protein family intact. While the rod monochromatic armadillo *Dasypus novemcinctus* might have inactivated all but one of the *gucy* and *guca* genes (for *guca1b* we however found only one slight modification), in the sloth *Choloepus hoffmanni* we still found an intact *guca1b* gene, suggesting that rods and cones might still use a separate activating protein.

Gucy and *guca* gene reduction can occur in visually impaired echolocating microbats

Bats are a surprisingly large and diverse mammalian order with more than 1,300 different species (Wilson and Reeder, 2005). With the exception of Antarctica, bats are present on all continents and even on isolated islands. Moreover, bats not only vary greatly in size, ranging from wingspans less than 15 cm in hog-nosed bats to more than 1.7 m in flying foxes, but also in their preferred diet being either frugivores, nectarivores, insectivores or in rare cases also praying on small mammals or using blood as their primary diet (Wilson and Reeder, 2005). In a previous report (Gesemann and Neuhauss, 2020) we have shown that megabats, which still strongly rely on their well-developed, rod dominated, visual system (Wang et al., 2004; Gutierrez et al., 2018), have conserved both visual GCs. In contrast to microbats, with often only rudimentary eyes, have often reduced their GC complement. This might be explained by the well-developed LDC (low duty cycle) or HDC (high duty cycle) echolocation system in microbats that compensates for the degeneration of the visual system (Simões et al., 2018). Such a system is absent in megabats, keeping visual input a viable requirement. The strongest reduction of phototransduction cascade calcium feedback genes is seen in the strictly nocturnal monochromatic ghost-faced bat *Mormoops blainvillei* (Lancaster and Kalko, 1996), which has reduced visual GCs and GCAPs to one variant each. Remarkably, the phylogenetically closely related Parnell's mustached bat *Pteronotus parnellii* still keeps an open reading frame for *guca1b* (Supplementary Table S1). This might be explained by the fact that in contrast to *Mormoops blainvillei, Pteronotus parnellii* has still dichromatic vision (Gutierrez et al., 2018). A similar situation is observed in the little tube-nosed bat *Murina aurata.* This dichromatic nocturnal species belongs to the family of *Vespertilionidae* (common bats) and has open reading frames for *guca1a* and *guca1b*. This is true for all analyzed *Vespertilionidae* species with the exception of the Natal long-fingered bat *Miniopterus natalensis*, in which the second active GCAP is *guca1c* instead of *guca1b*. The combination of *guca1a* and *guca1c* is not only observed in *Miniopterus natalensis* but also in the greater bulldog bat *Noctilio leporinus* that belongs to the family of *Noctilionidae.* Interestingly, independent of its phylogenetic relation, crepuscular bat species have the highest amount of combinatorial possibilities for guanylyl cyclases and their activating proteins, ranging from three (1×3) in the Mexican free-tailed bat *Tadarida brasiliensis*, to six (2×3) in the large flying fox *Pteropus vampyrus* and the Greater false vampire bat *Megaderma lyra*. While the monochromatic *Megaderma lyra*

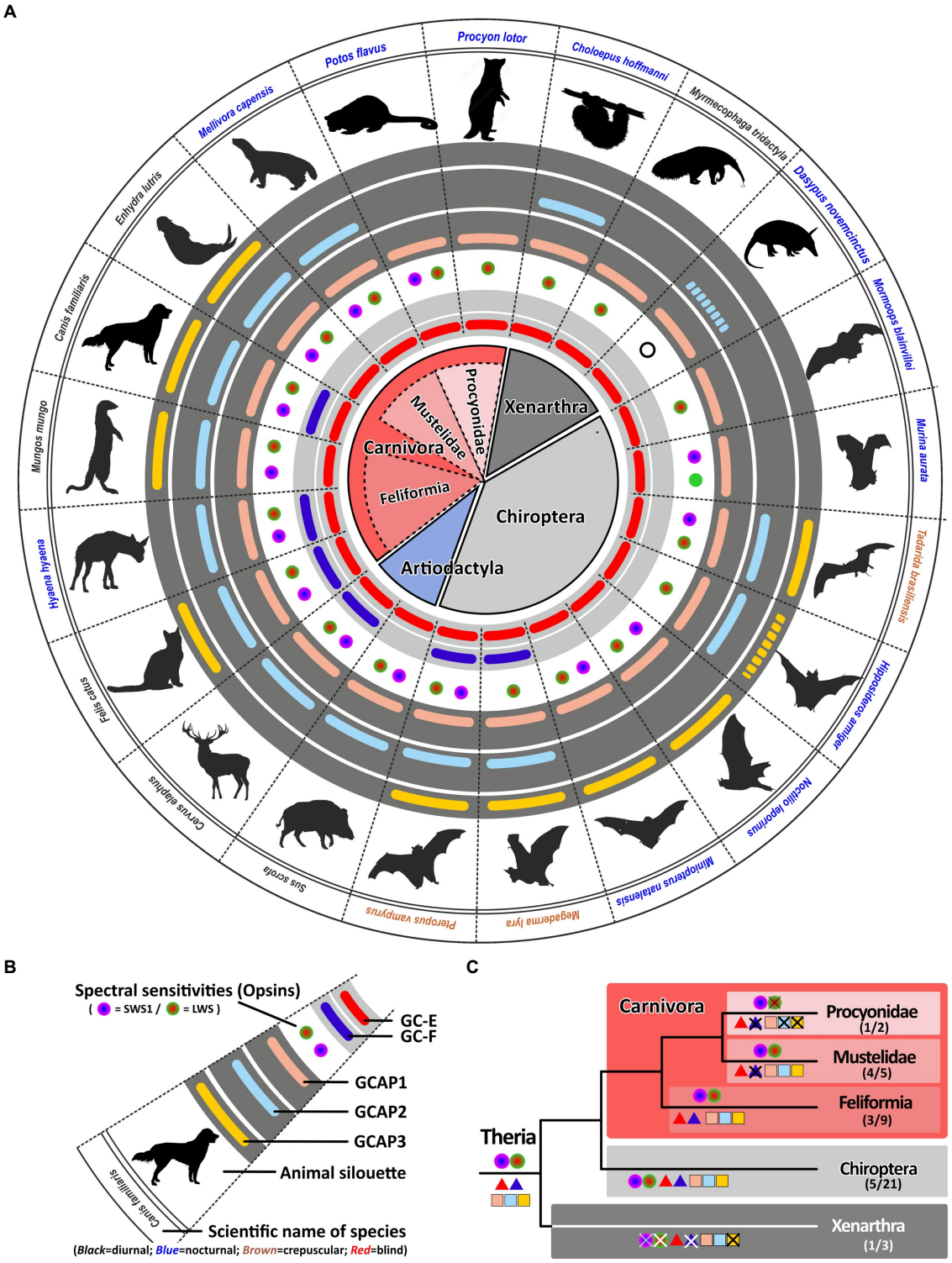

FIGURE 6
Monochromacy in carnivores, xenarthra and bats reduces the number of *gucy* and *guca* genes with intact ORFs. **(A)** Expression of opsins, GCs and GCAPs in carnivores, even toed ungulates, bats and xenarthras. In the center, major orders and suborders are given. Carnivores are highlighted in red, bats in gray and xenarthras in dark gray. Carnivore suborders are indicated by a lighter shade. **(B)** Explanation of symbols used in **(A)**. Pictograms for each chosen representative are shown and scientific names are given. Names of diurnal species are written in black, crepuscular species in brown and nocturnal species in blue. The presence of an open reading frame for *gucy2e* (*gucy2d* retinal) is shown as a red bar in the innermost light gray circle and *gucy2f* genes without inactivating mutation are illustrated by a dark blue bar adjacent to it. The different types and color sensitivities of photoreceptor single cones are indicated by the colored dots and rod monochromacy is shown by a white circle. The presence or absence of intact ORFs encoding GCAPs is given by the colored bars in the dark gray circles. *guca1a* is given in light red, *guca1b* in light blue and *guca1c* is shown in yellow. Sequences that have only a single mutation, which might be derived from sequencing errors, are given by broken lines. **(C)** Evolution of opsins, GCs and GCAPs in major carnivora, bat and xenarthra orders. Major linages are shown. Opsins are given by circles, GCs by triangles and GCAPs by squares. The most likely ancestral situation at every major branch point is given. Numbers in parenthesis represent the species still displaying this gene content (first number) and the total number of species analyzed (second number).

and dichromatic *Tadarida brasiliensis* use echolocation as well as visual input for hunting, the frugivorus and nectarivoros *Pteropus vampyrus* rely solely on their well developed eyesight for foraging (Figure 6). Overall we have analyzed the GCAP integrity in 21 different bat species and there seems to be a strong correlation between a well developed visual system and the preservation of GCAP genes (Supplementary Table S1), once again suggesting that a dual system of phototransduction offers benefits for highly visual animals.

Monochromatic aquatic mammals benefit from a redundant Set of *gucy* and *guca* genes

Our previous analysis has shown that regressive evolution of the visual system strongly influences the number of active phototransduction gene ohnologs. Many visually impaired, underground living species have not only reduced their spectral sensitivity but have also reduced ohnologous genes important in the calcium feedback system of phototransduction. Analogously, exclusively nocturnal animals have used a similar adaptation, even if their night vision might still be excellent. However, with one exception, the reduction to a minimal set of one *gucy* on one *guca* gene is only observed in monochromatic animals, either being rod or rod/cone monochromats. To test if monochromacy is indeed stimulating inactivation of GCs and their activating proteins we have analyzed the situation in aquatic mammals that have been shown to be primarily monochromatic (Levenson et al., 2006; Meredith et al., 2013).

Surprisingly, for all analyzed aquatic mammals we found open reading frames for both visual guanylyl cyclase genes (Figure 7), independent of them belonging to the order of whales or dolphins (*Cetaceans*), or to the clade of seals (*Pinnipeds*). Even more unexpectedly, neither species has less than two GCAPs. However, *guca1c*, seems to be under strong purifying selection being absent or pseudogenized in almost all analyzed species. The fact that aquatic mammals have kept two active GCAPs is particularly striking for deep diving whales such as the sperm whale *Physeter catodon*, the gray whale *Eschrichtius robustus* or the Sowerby's beaked whale *Mesoplodon bidens*, which are rod monochromats (Meredith et al., 2013). At first glimpse no obvious use for two independent sets of phototransduction genes exists. However, rod monochromatic bowhead whales (*Balaena mysticetus*) have preserved cone somata as well as cone bipolar cells, maintaining the possibility of an alternative photoreceptor signaling pathway (Schweikert et al., 2016). Therefore multichannel rod-based signaling enhancing dark-adapted vision could be possible in a variety of aquatic mammals and the fact that guanylyl cyclases and their activating proteins still exist in duplicates makes such a scenario quite likely.

While such adaptations have not been demonstrated in *pinnipeds*, other findings might explain the higher GC/GCAP preservation. Some studies have suggested that at least some seals still can discriminate colors (Oppermann et al., 2016). When we analyzed the opsin sequences of different *pinnipeds*, we surprisingly found an open reading frame for *opsin1sw* in the walrus *Odobenus rosmarus* (Supplementary Table S2; Supplementary Figure S3B). Also for the harbor seal *Phoca vitulina*, a nearly intact coding sequence was identified (Supplement Figure S3C), with only one bp deletion in exon 3. Whether this mutation is real or rather resulting from poor sequencing quality will certainly be determined by future database updates.

In contrast to *Cetaceans* and most *Pinnipeds*, the aquatic West Indian manatee *Trichechus manatus* is still dichromatic (Newman and Robinson, 2006). Remarkably, the same 2/2 combination of *gucy* and *guca* genes is present in sea cows, suggesting that the aquatic lifestyle somehow benefits from a dual system of phototransduction genes independent whether the species is a rod monochromat, a rod/cone monochromat or a dichromat. In contrast to whales, dolphins and seals, manatees are herbivores living in shallow coastal waters being exposed to a broad spectrum of light. Having dichromatic vision may help to locate appropriate food sources under photopic light conditions making the manatee visual system more comparable to that of terrestrial mammals. Therefore, the preservation of a dual system for phototransduction in the case of the manatee might be beneficial.

Convergent evolution of marsupials and eutherians is not directly reflected in *gucy* and *guca* gene inactivations

Marsupials and eutherians have split some 140 million years ago evolving independently on different continents. While the clade of eutherians consists of more than 6,000 different species, the marsupial clade comprises only around 330 extant species (Deakin and O'Neill, 2020). However, convergent evolution of these two clades has resulted in species displaying similar traits and occupying comparable ecological niches (Mitchell et al., 2014). There are for example, underground living marsupial moles and there was a now extinct dog-like Tasmanian wolf/tiger. Moreover, there are nocturnal as well as diurnal and crepuscular marsupials. As for eutherians it has been shown that marsupials are in general dichromatic, however, in contrast to eutherians which may have one or two active visual GCs, marsupials have only one (Gesemann and Neuhauss, 2020). We have now confirmed this in all sequenced marsupials, never being able to identify a second visual guanylyl cyclase (Figure 7). We found for all marsupials two GCAPs, but counterintuitively these are not *guca1a* and *guca1b,* but *guca1a* and *guca1c*, suggesting that *guca1b* was already lost in an early marsupial ancestor. Unfortunately, there is currently no genomic information for visually impaired marsupials, such as the marsupial mole, leaving the question unanswered whether regressive evolution also occurs for marsupial GCAPs. While we did always see the same opsin/*gucy*/*guca* situation in all marsupials independent of whether they are diurnal, nocturnal or crepuscular, neither of these species has impaired vision and all are still cone dichromats.

Conclusion

The visual system of extant tetrapods is a highly adaptive light sensing structure, working from detecting only light/dark differences in fossorial, subterranean living moles towards discriminating a wide range of colors in highly visual lizards, amphibians and primates. While dim light scotopic vision is mediated by rod photoreceptors, photopic color vision is based on different spectral sensitivities of up to four different types of single cones. Visually impaired species have often reduced their photoreceptor subtypes to either rod vision only or rod/cone monochromacy, whereas trichromatic or even tetrachromatic vision can be observed in primates and many sauropsida species. A reduction in spectral sensitivity is also apparent in many nocturnal terrestrial species or aquatic mammals (for summary see Figures 8, 9).

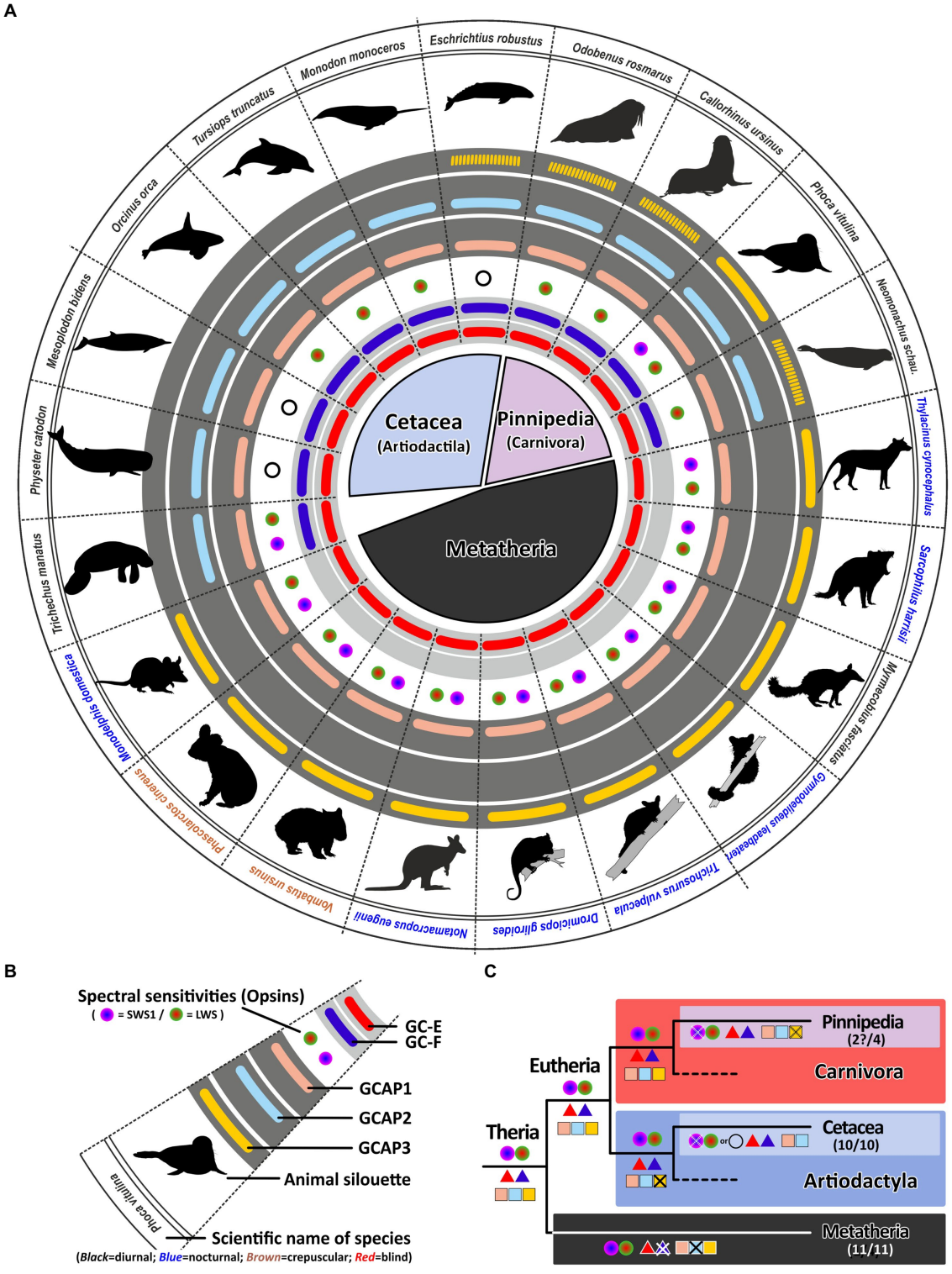

FIGURE 7
Monochromacy in aquatic mammals is not reflected in a reduction of genes involved in the calcium feedback system of phototransduction. **(A)** Expression of opsins, GCs and GCAPs in aquatic mammals and marsupials. In the center, major orders and suborders are given. *Cetaceans* (whale and dolphins) are highlighted in light blue, pinnipeds in pink and marsupials in black. **(B)** Explanation of symbols used in **(A)**. In the center, a GC-E cladogram of aquatic mammals such as seals (light blue and twilight blue) as well as marsupials (light gray) is given. Pictograms for each chosen representative are shown and scientific names are given. Names of diurnal species are written in black, crepuscular species in brown and nocturnal species in blue. The presence of an open reading frame for transcripts encoding GC-E are shown as a red bar in innermost light gray circle and *gucy2f* genes without inactivating mutation are illustrated by a dark blue bar adjacent to it. The different types and color sensitivities of photoreceptor single cones are indicated by the colored dots and rod monochromacy is shown by a white circle. The presence or absence of intact transcripts coding for GCAPs is given by the colored bars in the dark gray circles.
(Continued)

FIGURE 7 (Continued)
guca1a is given in light red, *guca1b* in light blue and *guca1c* is shown in yellow. Sequences that have only a single mutation, which might be derived from sequencing errors, are given by broken lines. **(C)** Evolution of opsins, GCs and GCAPs in major aquatic and metatherian orders. Major linages are shown. Opsins are given by circles, GCs by triangles and GCAPs by squares. The most likely ancestral situation at every major branch point is given. Numbers in parenthesis represent the species still displaying this gene content (first number) and the total number of species analyzed (second number). Note that rod monochromacy in aquatic mammals is not linked to a reduction of *gucy* and *guca* genes and marsupials have reduced their complement to one visual GC and two GCAPs.

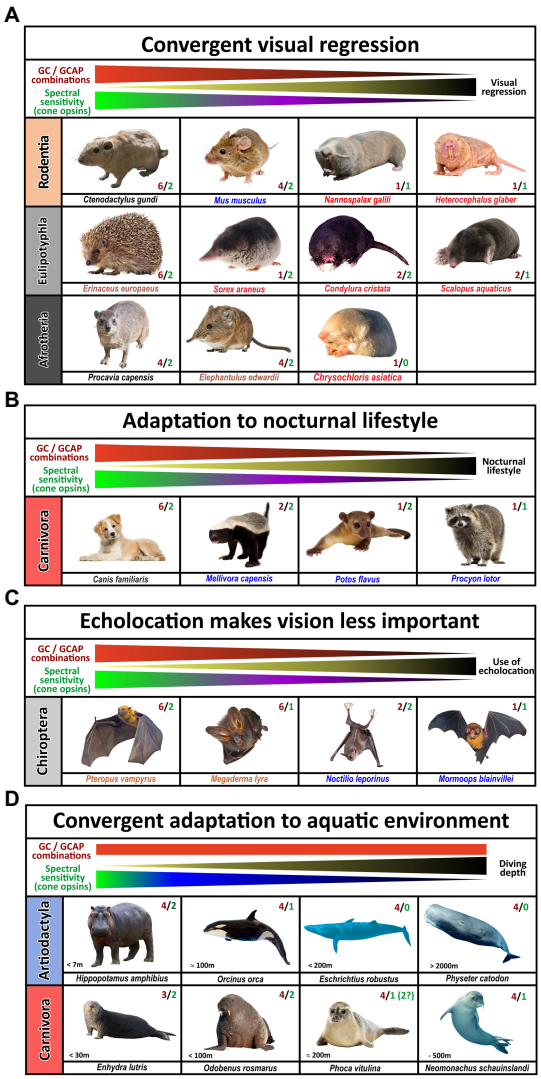

FIGURE 8
Influence of nocturnal and diurnal lifestyle and subterranean habitats on the evolution of guanylyl cyclase and guanylyl cyclase activating proteins in mammals. The name of the species listed is indicated. Red and green numbers specify the number of functional cone opsins (green) and GC/GCAP combinations (red). **(A)** Convergent visual regression. Visual regression occurred independently in animals of different orders. Species of the rodent, insectivore and afrotheria orders show animals that highly resemble each other and have evolved and adapted to underground life in similar but independent ways. While diurnal or crepuscular species still strongly depend on vision and are functional dichromats with multiple GCs and GCAPs, visually impaired or nearly blind species are often monochromatic and have a greatly reduced complement of GCs and GCAPs. **(B)** Adaptation to nocturnality in carnivores. Several nocturnal carnivores have reduced their opsin as well as their GC and GCAP gene content. While the honey badger *Mellivora capensis* still has dichromatic vision, members of the Procyonidae order are on their way to monochromatic vision. Moreover, Procyonidae have reduced their GC/GCAP content to one member each. **(C)** Echolocation makes vision less important. Nocturnality and echolocation have caused strong adaptation to the visual system of bats. While non-echolocating species such as the frugivorous *Pteropus vampyrus* still rely on vision for foraging, echolocating specialists such as the *Mormoops blainvillei* have greatly reduced their visual dependence. This goes hand in hand with a reduction of functional opsins as well as GCs and GCAP proteins. **(D)** Adaptation to aquatic environments. While aquatic animals often become either rod/cone or rod monochromats, they do not reduce the GC/GCAP complement accordingly. This might be due to the preservation of alternate phototransduction pathways that could enhance dim light vision (for whales and dolphins) or due to the fact that seals are not true monochromats.

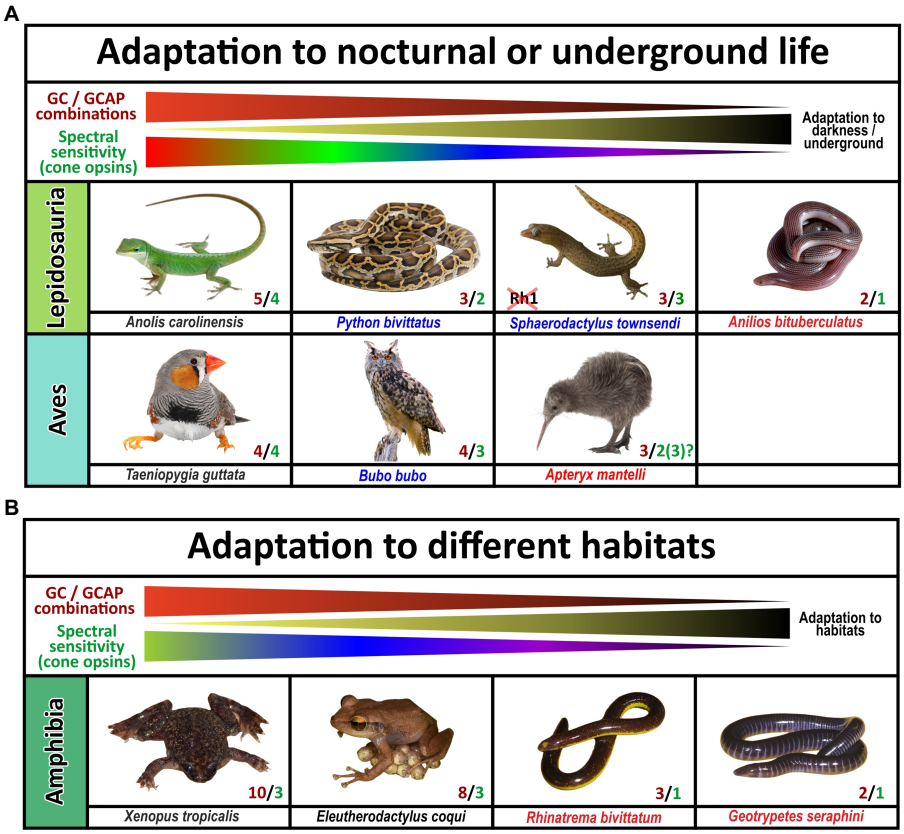

FIGURE 9
Influence of diurnal, nocturnal, subterranean or changing lifestyles on the evolution of guanylyl cyclase and guanylyl cyclase activating proteins in sauropsids and amphibians. The name of the species listed is indicated. Red and green numbers specify the number of functional cone opsins (green) and GC/GCAP combinations (red). **(A)** Adaptation to nocturnal or underground life in sauropsids. While burrowing, underground living snakes no longer depend on visual input and are cone monochromats, nocturnal predatory species are still di- or trichromatic and diurnal species are often tetrachromats. The reduction of functional visual pigments often correlates with a reduction in GC/GCAP gene content. Note that geckos have inactivated the Rh1 gene usually present in rods, but their cone photoreceptors rather show a rod-like morphology. Also noteworthy is the fact that kiwis as nocturnal birds with poor vision show the beginnings of a reduction of opsins and GCAPs, suggesting that kiwis rather rely on other senses than vision. **(B)** Adaptation to different habitats in amphibians. Frogs and toads show the highest numbers of combinatorial GC/GCAP possibilities, despite having only trichromatic vision. However, as frogs and toads often switch from a larval to an adult form that have different lifestyles and habitats; visual requirements during these phases might be different. These changes might explain the more complex GC/GCAP pattern. Species that do not switch between larval and adult stages or are mainly subterranean show a reduced opsin and GC/GCAP gene content. This is true for the common coqui *Eleutherodactylus coqui* whose offspring do not have a larval stage. Moreover, monochromatic caecilians, which do no longer rely on vision have few possible GC/GCAP combinations.

Signal propagation from activated rod or cone photopigments occurs *via* a dual system of phototransduction cascade proteins that differ slightly in rods and cones (Figure 1), with some components being shared, whereas others being exclusively rod or cone specific. In this study we have focused on visual GCs and GCAPs that control the calcium feedback system of phototransduction and are neither rod nor cone specifically expressed. While two *gucy* were active in eutherian and amphibian ancestors, the common ancestor of birds, turtles, crocodiles and lizards has pseudogenized the second visual guanylyl cyclase causing all extent sauropsida species to rely on only one *gucy* gene in cone as well as rod photoreceptors (Supplementary Figure S4). Interestingly, highly visual sauropsida species have compensated the loss of the second visual GC by preserving up to five GCAPs, whereas the mammalian ancestor has inactivated two of these. This leaves eutherians with six combinatorial possibilities (2 *gucy* and 3 *guca* genes) and sauropsids with five (1 *gucy* and 5 *guca* genes). In nearly blind species or species with reduced visual capabilities, we see a strong reduction of these combinatorial possibilities, in the most extreme cases to only one protein each. Such an event has occurred in several clades independently as we found such a situation in rodents, bats, *Procyonidae* (raccoons), *Xenarthra* (anteaters and armadillos) and insectivores (Figure 8). A strong reduction can also be seen in blind worm-like burrowing snakes and underground living limbless caecilians (an order of amphibians), even if the reduction of the gene complement is not or not yet complete (Figure 9). A strong reduction in phototransduction calcium feedback proteins is also seen in marsupials, independent on their lifestyle, where only one cyclase and two activating proteins are found. Interestingly, we found that aquatic mammals, which are almost exclusively rod or rod/cone monochromats, have kept two *gucy* and two *guca* genes. This finding together with the fact that some whales have retained cone somata and cone bipolar cells suggests that keeping an interacting

dual system of these enzymes intact might be beneficial to enhance the visual performance.

Data availability statement

The original contributions presented in the study are included in the article/Supplementary material, further inquiries can be directed to the corresponding author.

Author contributions

MG: conceptualization, assembled sequences, analysis, and writing. SN: conceptualization and editing. All authors contributed to the article and approved the submitted version.

Funding

This work was supported by the Swiss National Science Foundation (310030_204648).

Conflict of interest

The authors declare that the research was conducted in the absence of any commercial or financial relationships that could be construed as a potential conflict of interest.

Publisher's note

All claims expressed in this article are solely those of the authors and do not necessarily represent those of their affiliated organizations, or those of the publisher, the editors and the reviewers. Any product that may be evaluated in this article, or claim that may be made by its manufacturer, is not guaranteed or endorsed by the publisher.

Supplementary material

The Supplementary material for this article can be found online at: https://www.frontiersin.org/articles/10.3389/fnmol.2023.1131093/full#supplementary-material

References

Ames, J. B. (2018). Dimerization of neuronal calcium sensor proteins. *Front. Mol. Neurosci.* 11:397. doi: 10.3389/fnmol.2018.00397

Baehr, W., Karan, S., Maeda, T., Luo, D.-G., Li, S., Bronson, J. D., et al. (2007). The function of guanylate cyclase 1 and guanylate cyclase 2 in rod and cone photoreceptors. *J. Biol. Chem.* 282, 8837–8847. doi: 10.1074/jbc.M610369200

Behnen, P., Dell'Orco, D., and Koch, K.-W. (2010). Involvement of the calcium sensor GCAP1 in hereditary cone dystrophies. *Biol. Chem.* 391, 631–637. doi: 10.1515/BC.2010.063

Borges, R., Khan, I., Johnson, W. E., Gilbert, M. T. P., Zhang, G., Jarvis, E. D., et al. (2015). Gene loss, adaptive evolution and the co-evolution of plumage coloration genes with opsins in birds. *BMC Genomics* 16:751. doi: 10.1186/s12864-015-1924-3

Bowmaker, J. K., and Hunt, D. M. (2006). Evolution of vertebrate visual pigments. *Curr. Biol.* 16, R484–R489. doi: 10.1016/j.cub.2006.06.016

Catchen, J. M., Conery, J. S., and Postlethwait, J. H. (2009). Automated identification of conserved synteny after whole-genome duplication. *Genome Res.* 19, 1497–1505. doi: 10.1101/gr.090480.108

Corfield, J. R., Parsons, S., Harimoto, Y., and Acosta, M. L. (2015). Retinal anatomy of the New Zealand kiwi: structural traits consistent with their nocturnal behavior. *Anat Rec (Hoboken)* 298, 771–779. doi: 10.1002/ar.23080

Corredor, V. H., Hauzman, E., Gonçalves, A., and Ventura, D. F. (2022). Genetic characterization of the visual pigments of the red-eared turtle (Trachemys scripta elegans) and computational predictions of the spectral sensitivity. *J. Photochem. Photobiol.* 12:100141. doi: 10.1016/j.jpap.2022.100141

Criscuolo, A., and Gribaldo, S. (2010). BMGE (block mapping and gathering with entropy): a new software for selection of phylogenetic informative regions from multiple sequence alignments. *BMC Evol. Biol.* 10:210. doi: 10.1186/1471-2148-10-210

Cuenca, N., Lopez, S., Howes, K., and Kolb, H. (1998). The localization of guanylyl cyclase-activating proteins in the mammalian retina. *Invest. Ophthalmol. Vis. Sci.* 39, 1243–1250. PMID: 9620085

Deakin, J. E., and O'Neill, R. J. (2020). Evolution of marsupial genomes. *Annu Rev Anim Biosci* 8, 25–45. doi: 10.1146/annurev-animal-021419-083555

Dereeper, A., Guignon, V., Blanc, G., Audic, S., Buffet, S., Chevenet, F., et al. (2008). Phylogeny.fr: robust phylogenetic analysis for the non-specialist. *Nucleic Acids Res.* 36, W465–W469. doi: 10.1093/nar/gkn180

Dizhoor, A. M., Lowe, D. G., Olshevskaya, E. V., Laura, R. P., and Hurley, J. B. (1994). The human photoreceptor membrane guanylyl cyclase, RetGC, is present in outer segments and is regulated by calcium and a soluble activator. *Neuron* 12, 1345–1352. doi: 10.1016/0896-6273(94)90449-9

Emerling, C. A. (2017). Archelosaurian color vision, parietal eye loss, and the crocodylian nocturnal bottleneck. *Mol. Biol. Evol.* 34, 666–676. doi: 10.1093/molbev/msw265

Emerling, C. A. (2018). Regressed but not gone: patterns of vision gene loss and retention in subterranean mammals. *Integr. Comp. Biol.* 58, 441–451. doi: 10.1093/icb/icy004

Emerling, C. A., and Springer, M. S. (2014). Eyes underground: regression of visual protein networks in subterranean mammals. *Mol. Phylogenet. Evol.* 78, 260–270. doi: 10.1016/j.ympev.2014.05.016

Emerling, C. A., and Springer, M. S. (2015). Genomic evidence for rod monochromacy in sloths and armadillos suggests early subterranean history for Xenarthra. *Proc. Biol. Sci.* 282:20142192. doi: 10.1098/rspb.2014.2192

Enright, J. M., Lawrence, K. A., Hadzic, T., and Corbo, J. C. (2015). Transcriptome profiling of developing photoreceptor subtypes reveals candidate genes involved in avian photoreceptor diversification. *J. Comp. Neurol.* 523, 649–668. doi: 10.1002/cne.23702

Gesemann, M., Lesslauer, A., Maurer, C. M., Schönthaler, H. B., and Neuhauss, S. C. F. (2010). Phylogenetic analysis of the vertebrate excitatory/neutral amino acid transporter (SLC1/EAAT) family reveals lineage specific subfamilies. *BMC Evol. Biol.* 10:117. doi: 10.1186/1471-2148-10-117

Gesemann, M., and Neuhauss, S. C. F. (2020). Selective gene loss of visual and olfactory guanylyl cyclase genes following the two rounds of vertebrate-specific whole-genome duplications. *Genome Biol. Evol.* 12, 2153–2167. doi: 10.1093/gbe/evaa192

Gower, D. J., Fleming, J. F., Pisani, D., Vonk, F. J., Kerkkamp, H. M. I., Peichl, L., et al. (2021). Eye-transcriptome and genome-wide sequencing for Scolecophidia: implications for inferring the visual system of the ancestral snake. *Genome Biol. Evol.* 13:evab253. doi: 10.1093/gbe/evab253

Gutierrez, E., Schott, R. K., Preston, M. W., Loureiro, L. O., Lim, B. K., and Chang, B. S. W. (2018). The role of ecological factors in shaping bat cone opsin evolution. *Proc. Biol. Sci.* 285:20172835. doi: 10.1098/rspb.2017.2835

Hanna, Z. R., Henderson, J. B., Wall, J. D., Emerling, C. A., Fuchs, J., Runckel, C., et al. (2017). Northern spotted owl (Strix occidentalis caurina) genome: divergence with the barred owl (Strix varia) and characterization of light-associated genes. *Genome Biol. Evol.* 9, 2522–2545. doi: 10.1093/gbe/evx158

Helten, A., Säftel, W., and Koch, K.-W. (2007). Expression level and activity profile of membrane bound guanylate cyclase type 2 in rod outer segments. *J. Neurochem.* 103, 1439–1446. doi: 10.1111/j.1471-4159.2007.04923.x

Höglund, J., Mitkus, M., Olsson, P., Lind, O., Drews, A., Bloch, N. I., et al. (2019). Owls lack UV-sensitive cone opsin and red oil droplets, but see UV light at night: retinal transcriptomes and ocular media transmittance. *Vis. Res.* 158, 109–119. doi: 10.1016/j.visres.2019.02.005

Imanishi, Y., Yang, L., Sokal, I., Filipek, S., Palczewski, K., and Baehr, W. (2004). Diversity of guanylate cyclase-activating proteins (GCAPs) in teleost fish: characterization of three novel GCAPs (GCAP4, GCAP5, GCAP7) from zebrafish

(Danio rerio) and prediction of eight GCAPs (GCAP1-8) in pufferfish (Fugu rubripes). *J. Mol. Evol.* 59, 204–217. doi: 10.1007/s00239-004-2614-y

Jacobs, G. H., and Deegan, J. F. (1992). Cone photopigments in nocturnal and diurnal procyonids. *J. Comp. Physiol. A* 171, 351–358. doi: 10.1007/BF00223965

Jiang, L., and Baehr, W. (2010). GCAP1 mutations associated with autosomal dominant cone dystrophy. *Adv. Exp. Med. Biol.* 664, 273–282. doi: 10.1007/978-1-4419-1399-9_31

Katoh, K., and Standley, D. M. (2013). MAFFT multiple sequence alignment software version 7: improvements in performance and usability. *Mol. Biol. Evol.* 30, 772–780. doi: 10.1093/molbev/mst010

Koch, K. W., and Stryer, L. (1988). Highly cooperative feedback control of retinal rod guanylate cyclase by calcium ions. *Nature* 334, 64–66. doi: 10.1038/334064a0

Kram, Y. A., Mantey, S., and Corbo, J. C. (2010). Avian cone photoreceptors tile the retina as five independent, self-organizing mosaics. *PLoS One* 5:e8992. doi: 10.1371/journal.pone.0008992

Kuhn, M. (2016). Molecular physiology of membrane guanylyl cyclase receptors. *Physiol. Rev.* 96, 751–804. doi: 10.1152/physrev.00022.2015

Lamb, T. D. (2013). Evolution of phototransduction, vertebrate photoreceptors and retina. *Prog. Retin. Eye Res.* 36, 52–119. doi: 10.1016/j.preteyeres.2013.06.001

Lamb, T. D. (2022). Photoreceptor physiology and evolution: cellular and molecular basis of rod and cone phototransduction. *J. Physiol.* 600, 4585–4601. doi: 10.1113/JP282058

Lamb, T. D., and Hunt, D. M. (2018). Evolution of the calcium feedback steps of vertebrate phototransduction. *Open Biol.* 8:180119. doi: 10.1098/rsob.180119

Lancaster, W. C., and Kalko, E. K. V. (1996). Mormoops blainvillii. *Mamm. Species* 1:1. doi: 10.2307/3504228

Le Duc, D., Renaud, G., Krishnan, A., Almén, M. S., Huynen, L., Prohaska, S. J., et al. (2015). Kiwi genome provides insights into evolution of a nocturnal lifestyle. *Genome Biol.* 16:147. doi: 10.1186/s13059-015-0711-4

Lemoine, F., Correia, D., Lefort, V., Doppelt-Azeroual, O., Mareuil, F., Cohen-Boulakia, S., et al. (2019). NGPhylogeny.fr: new generation phylogenetic services for non-specialists. *Nucleic Acids Res.* 47, W260–W265. doi: 10.1093/nar/gkz303

Levenson, D. H., Ponganis, P. J., Crognale, M. A., Deegan, J. F., Dizon, A., and Jacobs, G. H. (2006). Visual pigments of marine carnivores: pinnipeds, polar bear, and sea otter. *J. Comp. Physiol. A Neuroethol. Sens. Neural Behav. Physiol.* 192, 833–843. doi: 10.1007/s00359-006-0121-x

Lim, S., Dizhoor, A. M., and Ames, J. B. (2014). Structural diversity of neuronal calcium sensor proteins and insights for activation of retinal guanylyl cyclase by GCAP1. *Front. Mol. Neurosci.* 7:19. doi: 10.3389/fnmol.2014.00019

Meredith, R. W., Gatesy, J., Emerling, C. A., York, V. M., and Springer, M. S. (2013). Rod monochromacy and the coevolution of cetacean retinal opsins. *PLoS Genet.* 9:e1003432. doi: 10.1371/journal.pgen.1003432

Mitchell, K. J., Pratt, R. C., Watson, L. N., Gibb, G. C., Llamas, B., Kasper, M., et al. (2014). Molecular phylogeny, biogeography, and habitat preference evolution of marsupials. *Mol. Biol. Evol.* 31, 2322–2330. doi: 10.1093/molbev/msu176

Mohun, S. M., Davies, W. L., Bowmaker, J. K., Pisani, D., Himstedt, W., Gower, D. J., et al. (2010). Identification and characterization of visual pigments in caecilians (Amphibia: Gymnophiona), an order of limbless vertebrates with rudimentary eyes. *J. Exp. Biol.* 213, 3586–3592. doi: 10.1242/jeb.045914

Mohun, S. M., and Wilkinson, M. (2015). The eye of the caecilian Rhinatrema bivittatum (Amphibia: Gymnophiona: Rhinatrematidae). *Acta Zool.* 96, 147–153. doi: 10.1111/azo.12061

Newman, L. A., and Robinson, P. R. (2006). The visual pigments of the west Indian manatee (Trichechus manatus). *Vis. Res.* 46, 3326–3330. doi: 10.1016/j.visres.2006.03.010

Olshevskaya, E. V., Peshenko, I. V., Savchenko, A. B., and Dizhoor, A. M. (2012). Retinal guanylyl cyclase isozyme 1 is the preferential in vivo target for constitutively active GCAP1 mutants causing congenital degeneration of photoreceptors. *J. Neurosci.* 32, 7208–7217. doi: 10.1523/JNEUROSCI.0976-12.2012

Oppermann, D., Schramme, J., and Neumeyer, C. (2016). Rod-cone based color vision in seals under photopic conditions. *Vis. Res.* 125, 30–40. doi: 10.1016/j.visres.2016.04.009

Patel, A. A., and Steitz, J. A. (2003). Splicing double: insights from the second spliceosome. *Nat. Rev. Mol. Cell Biol.* 4, 960–970. doi: 10.1038/nrm1259

Peichl, L., Künzle, H., and Vogel, P. (2000). Photoreceptor types and distributions in the retinae of insectivores. *Vis. Neurosci.* 17, 937–948. doi: 10.1017/s0952523800176138

Perrault, I., Rozet, J. M., Calvas, P., Gerber, S., Camuzat, A., Dollfus, H., et al. (1996). Retinal-specific guanylate cyclase gene mutations in Leber's congenital amaurosis. *Nat. Genet.* 14, 461–464. doi: 10.1038/ng1296-461

Perrault, I., Rozet, J. M., Gerber, S., Ghazi, I., Ducroq, D., Souied, E., et al. (2000). Spectrum of retGC1 mutations in Leber's congenital amaurosis. *Eur. J. Hum. Genet.* 8, 578–582. doi: 10.1038/sj.ejhg.5200503

Pinto, B. J., Nielsen, S. V., and Gamble, T. (2019). Transcriptomic data support a nocturnal bottleneck in the ancestor of gecko lizards. *Mol. Phylogenet. Evol.* 141:106639. doi: 10.1016/j.ympev.2019.106639

Price, M. N., Dehal, P. S., and Arkin, A. P. (2009). FastTree: computing large minimum evolution trees with profiles instead of a distance matrix. *Mol. Biol. Evol.* 26, 1641–1650. doi: 10.1093/molbev/msp077

Sato, M., Nakazawa, M., Usui, T., Tanimoto, N., Abe, H., and Ohguro, H. (2005). Mutations in the gene coding for guanylate cyclase-activating protein 2 (GUCA1B gene) in patients with autosomal dominant retinal dystrophies. *Graefes Arch. Clin. Exp. Ophthalmol.* 243, 235–242. doi: 10.1007/s00417-004-1015-7

Schott, R. K., Bell, R. C., Loew, E. R., Thomas, K. N., Gower, D. J., Streicher, J. W., et al. (2022a). Transcriptomic evidence for visual adaptation during the aquatic to terrestrial metamorphosis in leopard frogs. *BMC Biol.* 20:138. doi: 10.1186/s12915-022-01341-z

Schott, R. K., Perez, L., Kwiatkowski, M. A., Imhoff, V., and Gumm, J. M. (2022b). Evolutionary analyses of visual opsin genes in frogs and toads: diversity, duplication, and positive selection. *Ecol. Evol.* 12:e8595. doi: 10.1002/ece3.8595

Schweikert, L. E., Fasick, J. I., and Grace, M. S. (2016). Evolutionary loss of cone photoreception in balaenid whales reveals circuit stability in the mammalian retina. *J. Comp. Neurol.* 524, 2873–2885. doi: 10.1002/cne.23996

Simões, B. F., Foley, N. M., Hughes, G. M., Zhao, H., Zhang, S., Rossiter, S. J., et al. (2018). As blind as a bat? Opsin phylogenetics illuminates the evolution of color vision in bats. *Mol. Biol. Evol.* 36, 54–68. doi: 10.1093/molbev/msy192

Townsend, D. S., and Stewart, M. M. (1985). Direct development in Eleutherodactylus coqui (Anura: Leptodactylidae): a staging table. *Copeia* 1985:423. doi: 10.2307/1444854

van Hooser, S. D., and Nelson, S. B. (2006). The squirrel as a rodent model of the human visual system. *Vis. Neurosci.* 23, 765–778. doi: 10.1017/S0952523806230098

van Valkenburgh, B., and Wayne, R. K. (2010). Carnivores. *Curr. Biol.* 20, R915–R919. doi: 10.1016/j.cub.2010.09.013

Wang, D., Oakley, T., Mower, J., Shimmin, L. C., Yim, S., Honeycutt, R. L., et al. (2004). Molecular evolution of bat color vision genes. *Mol. Biol. Evol.* 21, 295–302. doi: 10.1093/molbev/msh015

Waters, P. D., Patel, H. R., Ruiz-Herrera, A., Álvarez-González, L., Lister, N. C., Simakov, O., et al. (2021). Microchromosomes are building blocks of bird, reptile, and mammal chromosomes. *Proc. Natl. Acad. Sci. U. S. A.* 118:e2112494118. doi: 10.1073/pnas.2112494118

Westrick, S. E., Laslo, M., and Fischer, E. K. (2022). The big potential of the small frog *Eleutherodactylus coqui*. *Elife* 11:e73401. doi: 10.7554/eLife.73401

Wilson, D. E., Mittermeier, R. A., and Cavallini, P. (2009). *Handbook of the mammals of the world*. Barcelona: Lynx.

Wilson, D. E., and Reeder, D. M. (2005) in *Mammal species of the world: a taxonomic and geographic reference*. eds. D. E. Wilson and D. A. M. Reeder (Baltimore, MD, London: Johns Hopkins University Press)

Yamagata, M., Yan, W., and Sanes, J. R. (2021). A cell atlas of the chick retina based on single-cell transcriptomics. *Elife* 10:e63907. doi: 10.7554/eLife.63907

Yang, R. B., Foster, D. C., Garbers, D. L., and Fülle, H. J. (1995). Two membrane forms of guanylyl cyclase found in the eye. *Proc. Natl. Acad. Sci. U. S. A.* 92, 602–606. doi: 10.1073/pnas.92.2.602

Yang, R. B., and Garbers, D. L. (1997). Two eye guanylyl cyclases are expressed in the same photoreceptor cells and form homomers in preference to heteromers. *J. Biol. Chem.* 272, 13738–13742. doi: 10.1074/jbc.272.21.13738

Yang, R. B., Robinson, S. W., Xiong, W. H., Yau, K. W., Birch, D. G., and Garbers, D. L. (1999). Disruption of a retinal guanylyl cyclase gene leads to cone-specific dystrophy and paradoxical rod behavior. *J. Neurosci.* 19, 5889–5897. doi: 10.1523/JNEUROSCI.19-14-05889.1999

frontiers | Frontiers in Molecular Neuroscience

TYPE Original Research
PUBLISHED 21 December 2022
DOI 10.3389/fnmol.2022.1076430

OPEN ACCESS

EDITED BY
Clint L. Makino,
Boston University,
United States

REVIEWED BY
Alexander Dizhoor,
Salus University,
United States
James Hurley,
University of Washington,
United States

*CORRESPONDENCE
Karl-Wilhelm Koch
karl.w.koch@uni-oldenburg.de

SPECIALTY SECTION
This article was submitted to Molecular Signalling and Pathways, a section of the journal Frontiers in Molecular Neuroscience

RECEIVED 21 October 2022
ACCEPTED 05 December 2022
PUBLISHED 21 December 2022

CITATION
Chen Y, Bräuer AU and Koch K-W (2022) Retinal degeneration protein 3 controls membrane guanylate cyclase activities in brain tissue.
Front. Mol. Neurosci. 15:1076430.
doi: 10.3389/fnmol.2022.1076430

Retinal degeneration protein 3 controls membrane guanylate cyclase activities in brain tissue

Yaoyu Chen[1,2], Anja U. Bräuer[2,3] and Karl-Wilhelm Koch[1,3]*

[1]Division of Biochemistry, Department of Neuroscience, Carl von Ossietzky University, Oldenburg, Germany, [2]Division of Anatomy, Department of Human Medicine, Carl von Ossietzky University, Oldenburg, Germany, [3]Research Center Neurosensory Science, Carl von Ossietzky University, Oldenburg, Germany

The retinal degeneration protein RD3 is involved in regulatory processes of photoreceptor cells. Among its main functions is the inhibition of photoreceptor specific membrane guanylate cyclases during trafficking from the inner segment to their final destination in the outer segment. However, any physiological role of RD3 in non-retinal tissue is unsolved at present and specific protein targets outside of retinal tissue have not been identified so far. The family of membrane bound guanylate cyclases share a high homology of their amino acid sequences in their cytoplasmic domains. Therefore, we reasoned that membrane guanylate cyclases that are activated by natriuretic peptides are also regulated by RD3. We analyzed transcript levels of the *rd3* gene and natriuretic peptide receptor genes *Npr1* and *Npr2* in the mouse retina, cerebellum, hippocampus, neocortex, and the olfactory bulb during development from the embryonic to the postnatal stage at P60. The *rd3* gene showed a lower expression level than *Npr1* and *Npr2* (encoding for GC-A and GC-B, respectively) in all tested brain tissues, but was at least one order of magnitude higher in the retina. RD3 and natriuretic peptide receptor GCs co-express in the retina and brain tissue leading to functional tests. We expressed GC-A and GC-B in HEK293T cells and measured the inhibition of GCs by RD3 after activation by natriuretic peptides yielding inhibitory constants around 25nM. Furthermore, endogenous GCs in astrocytes were inhibited by RD3 to a similar extent. We here show for the first time that RD3 can inhibit two hormone-stimulated GCs, namely GC-A and GC-B indicating a new regulatory feature of these hormone receptors.

KEYWORDS

natriuretic peptide, membrane bound guanylate cyclase, GC-A, GC-B, RD3 protein

Introduction

Membrane bound guanylate cyclases (GC) synthesize the second messenger guanosine 3′,5′-cyclic monophosphate (cGMP) that is involved in a variety of physiological functions including blood pressure, skeletal growth, kidney function, phototransduction, olfaction, and thermosensation (Sharma, 2010; Koch and Dell'Orco, 2015; Kuhn, 2016; Sharma et al.,

2016; Pandey, 2021). Extracellular ligands like natriuretic peptides (ANP, BNP, and CNP) bind to natriuretic peptide receptors at their extracellular ligand domains. These natriuretic peptide receptors are GCs switching to the active state, when binding natriuretic peptides. ANP and BNP activate GC-A expressed in the cardiovascular system and metabolic organs being involved in the regulation of blood pressure and metabolism. CNP activates GC-B and the CNP/GC-B signaling system is expressed in various organs, but also in cardiovascular cell types (Pandey, 2021). One of its main suggested physiological roles is to regulate skeletal growth (Kuhn, 2016). Expression of CNP and GC-B in different brain regions also indicate a functional role in neuronal tissue. For example, studies investigated a role in synaptic plasticity in the hippocampus (Decker et al., 2010; Barmashenko et al., 2014) and an involvement in the regulation of the circadian clock (Olcese et al., 2002). Natriuretic peptides and their receptors have also been identified in the retina (Rollín et al., 2004) and were linked to dopaminergic and cholinergic signaling in amacrine cells (Abdelalim et al., 2008), and to the modulation of GABA-receptor activity in bipolar cells (Yu et al., 2006). In addition to neuronal signaling, natriuretic peptides ANP and BNP exert protective effects in retinal neovascularization (Špiranec Spes et al., 2020).

A different activation process is found in membrane GCs expressed in sensory cells. For example, photoreceptor specific GC-E and GC-F form complexes with guanylate cyclase-activating proteins (GCAPs) on their intracellular site (Peshenko et al., 2011; Sulmann et al., 2017). GCAPs are calcium sensor proteins that respond to changes in cytoplasmic calcium concentration ($[Ca^{2+}]$) with a conformational change thereby switching the target GC-E or GC-F to the active state (Koch and Dell'Orco, 2015; Dizhoor and Peshenko, 2021).

Point mutations in the genes *GUCY2D* and *GUCA1A* coding for GC-E and GCAP1 cause forms of retinal degeneration like cone-rod dystrophies. Leber's congenital amaurosis (LCA) is a particularly severe form of retinal dysfunction leading to blindness after birth or in the first year of life. Patients suffering from LCA type 1 have point mutations in *GUCY2D* (Sharon et al., 2018) causing dysfunction of GC-E in alive photoreceptor cells opening routes for gene therapy (Jacobson et al., 2022). Mutations in the retinal degeneration protein 3 (RD3) of human patients correlate with the phenotypical characteristics of LCA12 (Friedman et al., 2006; Cideciyan 2010; Preising et al., 2012). In the physiologically normal state of a photoreceptor cell, RD3 binds to photoreceptor specific GCs and inhibits their GCAP-mediated activation at low cytoplasmic $[Ca^{2+}]$ (Peshenko et al., 2011, 2021). RD3 is further involved in GC-E trafficking from the endoplasmic reticulum to endosomal vesicles (Azadi et al., 2010; Molday et al., 2013; Zulliger et al., 2015). Correct trafficking and incorporation of GC-E in photoreceptor outer segments is essential for cell survival and interaction of RD3 with GC-E is a crucial requirement for these processes (Peshenko et al., 2016; Peshenko and Dizhoor, 2020; Plana-Bonamaisó et al., 2020). Wimberg et al. (2018a) observed in an *in vitro* study that purified RD3 evoked an increase in guanylate kinase (GUK) activity, an enzyme that is involved in the nucleotide cycle in photoreceptors catalyzing the 5'-GMP to GDP conversion. Both proteins directly interact and co-localize in photoreceptor inner segments and to a lesser extent in the outer plexiform layer in sections of the mouse retina. However, recent studies involving transgenic mice did not detect a regulatory impact of RD3 on GUK activity (Dizhoor et al., 2021).

Recent studies revealed that RD3 is also found in other tissue types such as epithelial cells and seems to be more ubiquitously expressed (Aravindan et al., 2017). Constitutive expression of RD3 was found in different mouse and human tissues including brain, kidney, liver, and spleen (Khan et al., 2015). The same authors further showed that RD3 loss in a mouse model correlates with aggressive neuroblastoma cancer. More recently, Somasundaram et al. (2019) found significant loss of RD3 expression on the transcript and protein level in patient derived tumor cells that survived intensive multi-modal clinical therapy. The authors conclude that transcriptional dysregulation might account for RD3 expression loss associated with advanced disease stage and low survival rate. However, these findings are in disagreement with a previous study showing that inactivation of both *rd3* alleles in LCA12 patients does not correlate with extraocular symptoms (Perrault et al., 2013).

The physiological role of RD3 in non-retinal tissue is unclear at present and basic issues related to its expression profile in brain tissue and the identity of its non-retinal targets are unsolved. A reasonable question in this context is, whether GCs activated by natriuretic peptide can be regulated by RD3. A necessary condition for such a regulation would be the expression of RD3 and GCs in the same tissue. We compared the expression levels of RD3, GC-A and GC-B in mouse retina and further determined their expression profiles in different brain regions during mouse brain development. We further compared gene expression in the retina with those in hippocampal neurons, astrocytes, and microglia. For functional studies, we expressed GC-A and GC-B in HEK293T cells and investigated the activity profiles in the presence and absence of added purified RD3.

Materials and methods

Heterologous expression of membrane GCs in HEK293T cell

HEK293T cells were grown in Dulbecco's Modified Eagle Medium (DMEM; Thermo Fisher Scientific) supplemented with 10% fetal bovine serum (FBS; PAN-Biotech, Aidenbach, Germany), 2 mM L-glutamine (Merck Millipore, Darmstadt, Germany), 100 units/ml Penicillin–Streptomycin (PAN-Biotech) in the incubator set at 5% (v/v) CO_2 and 37°C.

For cell transfection, the cDNA sequence of wildtype human GC-A and human GC-B was inserted into a pcDNA3.1 vector. The cDNA was amplified using the primers listed in the supplementary part (Supplementary Table S1). Cells were seeded for transfection in 100 mm petri dishes with 1.5×10^6 cells per dish. After 24 h, cells

were transfected with the pcDNA3.1 plasmids using the polyethylenimine (PEI) as transfection reagent. Stable cell lines expressing human GC-A or GC-B were created as described previously for GC-E (Wimberg et al., 2018a). The expression of GCs was confirmed *via* western blotting (see below) using commercial antibodies: polyclonal anti-GC-A (cat. Ab14357, Abcam) and polyclonal anti-GC-B (cat. Ab14356, Abcam). For the detection of photoreceptor GC-E we used a polyclonal antibody that was originally made against bovine GC-E, but showed crossreactivity to the human orthologue (Zägel et al., 2013). HA-tagged GC-A and GC-B were used in control experiments applying the pcDNA3.1 vector with HA-tag insertion.

Expression and purification of RD3

The RD3 protein was expressed in *E.coli* and purified following the method as described before Wimberg et al., 2018a. Briefly, *E.coli* BL21+ cells containing the pET-M11-RD3-His6-tag construct was grown overnight in LB-Medium at 37°C after induction by 1 mM isopropyl-thiogalactoside (IPTG). The cell pellets were harvested by centrifugation and suspended in 50 mM Tris/HCl pH 8.0. Cells were lysed by adding 100 mg/ml lysozyme and 5 U/ml DNase and incubation at 30°C for 30 min. The lysate was centrifuged for 1.5 h at 50,000 × *g* at 4°C after adding 1 mM DTT and 0.1 mM phenylmethyl-sulfonylfluoride (PMSF). The RD3 containing pellet was homogenized in buffer 1 (20 mM phosphate buffer pH 7.4, 8 M urea, 10 mM imidazole, 500 mM NaCl, 5 mM β-mercaptoethanol (β-ME), 1 mM PMSF), and kept overnight at 4°C. The suspension was centrifuged for 1 h at 50,000 × *g* and 4°C, the supernatant was collected for Ni-NTA column-based purification. After sample loading onto the column, buffer 1 was applied for washing and was then gradually replaced by buffer 2 (20 mM phosphate buffer pH 7.4, 10 mM imidazole, 500 mM NaCl, 5 mM β-ME, 1 mM PMSF, 1 mM histidine, 10% glycerol) to facilitate protein refolding. Buffer 3 (20 mM phosphate buffer pH 7.4, 500 mM imidazole, 20 mM histidine, 500 mM NaCl, 5 mM β-ME, 1 mM PMSF) eluted RD3 containing fractions that were collected in volumes of 1 ml and analyzed *via* sodium dodecyl sulfate polyacrylamide gel electrophoresis (SDS-PAGE). Purified RD3 was tested for biological activity, namely inhibiting GCAP activated human GC-E present in HEK-293T cells that stably expressed GC-E (Wimberg et al., 2018a).

Gel electrophoresis and immunoblotting

HEK-293T cells were harvested and the membrane protein fractions were collected as previously described Wimberg et al., 2018a. The protein fractions were incubated with 5 × Laemmli buffer containing 1% (v/v) β-ME at 95°C for 5 min and analyzed by SDS-PAGE having either 12% or 7.5% acrylamide. Immunoblotting was performed using a 0.45 µm nitrocellulose (NC) membrane, and a tank or semi-dry blotting system. RD3 was analyzed by SDS-PAGE on a 12% acrylamide gel and a semi-dry blotting procedure of 200 mA for 30 min. For GC-A and GC-B we used a 7.5% acrylamide gel and the tank blotting procedure (100 V for 70 min at 4°C). Afterwards, the blotted membrane was incubated with blocking solution [either 5% (w/v)] bovine serum albumin (BSA; Carl Roth, Karlsruhe, Germany, or 2.5–5% milk powder (Carl Roth)) in TBST at room temperature (RT) for 1 h. Primary anti-GC antibodies were incubated overnight at 4°C in blocking solution at a dilution of 1:5,000. The blot membranes were washed three-times with TBST at RT. Afterwards, the blot membranes were incubated for 1 h at RT with horseradish peroxidase-conjugated secondary antibodies (GE Healthcare, Boston, MA, United States) at a dilution of 1:10,000 in blocking solution. Membranes were again washed three times at RT with TBST, and immunoreaction was detected with Clarity or Clarity Max ECL substrate (Bio-Rad Laboratories, Hercules, CA, United States) according to the manufacturer's protocol.

Guanylate cyclase activity assay

The guanylate cyclase stimulator human atrial natriuretic factor (1–28; ANP, cat. H-2095) and the human c-type natriuretic peptide (1–53; CNP, cat. H-8420) were purchased from Bachem AG (Switzerland). Ten microliter of HEK-293T membranes expressing GC-A or GC-B were incubated with 2 µM ANP or CNP, or various concentrations RD3 in a final volume of 30 µl for 5 min at RT. The guanylate cyclase reaction was started by adding 20 µl GC buffer (75 mM Mops/KOH pH 7.2, 150 mM KCl, 10 mM NaCl, 2.5 mM DTT, 8.75 mM $MgCl_2$, 4 mM GTP, 0.75 mM ATP, 0.4 mM Zaprinast). After incubation for 5 min at 30°C, the reaction was stopped by adding 50 µl 0.1 M EDTA and short incubation (5 min) at 95°C. After centrifugation at 13,000 × *g* for 10 min, the supernatant was harvested and analyzed for cGMP content as previously described (Wimberg et al., 2018a). Assays were pursued in three independent groups, each with 3 replicates ($N = 9$). Test series were performed to find the optimal assay conditions including a concentration dependence of GTP and a time series.

RNA extraction, cDNA synthesis and qRT-PCR

The mRNA from mouse cerebellum, neocortex, hippocampus, and olfactory bulbs of the developmental stages of embryonic days (E) E14, E16, E19, and of postnatal days (P) P0, P5, P10, P15, P20, P30, P42, P60 was collected as described in Gross et al. (2022) and stored at-80°C until use. Briefly, the tissues were dissociated from sacrificed mice, at embryonic stages, one litter of all embryos (7–10 embryos; $N = 21–30$, sex not specified) were pooled. At postnatal stages, tissues from six mice of both sexes were pooled, for all stages with three independent replicates ($n = 3$). The retinas were obtained from the mice at P10, P20, P30 of both sexes with

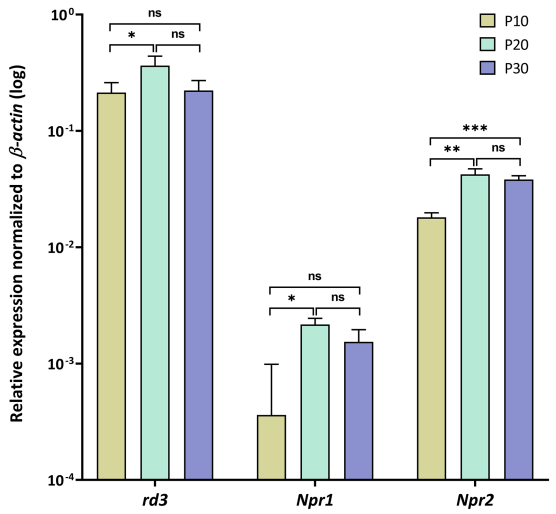

FIGURE 1
Gene expression profiles in mouse retina analyzed by quantitative RT-PCR. Relative transcript levels of *rd3, Npr1* and *Npr2* were determined in retina tissue at P10, P20 and P30 and normalized to β–*actin* expression. Analysis of statistics were based on one-way ANOVA followed by Bonferroni's multiple comparisons test. Data are shown as mean±SD. Specific numbers of *p*-values are shown in Supplementary Table S2 (Supplementary material).

3 replicates. Primary hippocampal neurons, astrocytes and microglia cells were obtained as described (Gross et al., 2022). The TRIzol™ reagent (Thermo Fisher Scientific, Waltham, MA, United States) was applied for RNA extraction from homogenized cells and tissues following the protocol from the manufacturer. RNA concentrations were determined by UV/Vis spectroscopy using the BioSpectrometer basic (Eppendorf, Hamburg, Germany). The cDNA was obtained according to the protocol of the high-capacity cDNA reverse transcription kit from Thermo Fisher Scientific.

Quantitative-RT-PCR was performed using the TaqMan™ Fast Universal PCR Master Mix, No AmpErase™ UNG (Thermo Fisher Scientific) on hard-shell 96-Well PCR plates from Bio-Rad Laboratories (Hercules, CA, United States), and TaqMan probes. Reactions were prepared according to the manufacturer's protocols and detected by the CFX96 real-time PCR detection system (Bio-Rad Laboratories) using the following cycling parameters: 95°C for 20 s, 95°C for 1 s and 60°C for 20 s, for 45 cycles. Expression data of three independent preparations with duplicates of each reaction were calculated using the ΔCt method, with normalization to *Gapdh* and *Actb* as housekeeping genes.

Culturing of astrocytes and GC activities in astrocytes

The astrocytes were cultured and collected according to Gross et al. (2022). Membranes containing membrane proteins were harvested after 10–12 days *in vitro* for endogenous guanylate cyclase activity tests. Guanylate cyclase activities in astrocyte membranes were stimulated by adding ANP or CNP. Inhibitory effects of RD3 were measured adding increasing amounts of purified RD3. The enzyme reaction started by adding 4 mM GTP. After 30 min incubation at 30°C, the reaction stopped by adding 0.1 M EDTA and incubation at 95°C for 5 min. The GC activities were measured using a cGMP ELISA Kit™ from Enzo Life Sciences according to the protocol of the manufacturer, three independent groups with two replicates each ($N=6$). A cGMP standard curve was created between 0.01 and 500 pmol × mL^{-1} being maximally sensitive between 1 and 100 pmol × mL^{-1}.

Statistical analysis

The qRT-PCR data of developmental stages in retina (Figure 1), in different brain areas (Figure 2) and primary cell cultures (Figure 3A) was processed using a one-way analysis of variance (ANOVA) followed by a Bonferroni's multiple comparisons test. Developmental stages of E14, P0, P20, and P60 were included into gene expression difference analysis of embryonic, birth, adult and elder. Evaluation of cyclase activities regulated by ANP (Figure 4B), CNP, or RD3 (Figures 5A,B) was performed by using the dose response simulation or the inhibition algorithm under nonlinear regression provided by GraphPad Prism 7 (GraphPad Software, San Diego, CA, United States). For the analysis of the functional test of purified RD3 (Figures 3B, 5C) we employed One-Way ANOVA Calculator and Tukey HSD[1].

Results

Expression of natriuretic peptide receptor GCs and RD3 in mouse neuronal tissue

First, we analyzed *rd3*, *Npr1* and *Npr2* transcript levels in the mouse retina at developmental stages P10, P20 and P30 and found high expression levels for *rd3*, but 10-100-fold lower levels for *Npr2* and *Npr1*, respectively (Figure 1). Next, we compared the expression in the retina with those in certain brain regions and observed that *rd3* transcript levels were several orders of magnitude higher in the retina than in brain tissue (compare Figures 1, 2A). For example, the expression of *rd3* in the retina was between 10^{-1} and 10^{0} relative to the β-*actin* expression, but only 10^{-4} to 10^{-3} in the cerebellum, hippocampus, neocortex and the olfactory bulb. These findings confirm the retina being the prominent neuronal tissue of *rd3* localization, but they also showed significant levels of *rd3* transcripts in several brain regions. We tested gene expression pattern of *rd3*, *Npr1* and *Npr2* during development in different mouse brain parts starting from E14 up

1 https://www.statskingdom.com/180Anova1way.html

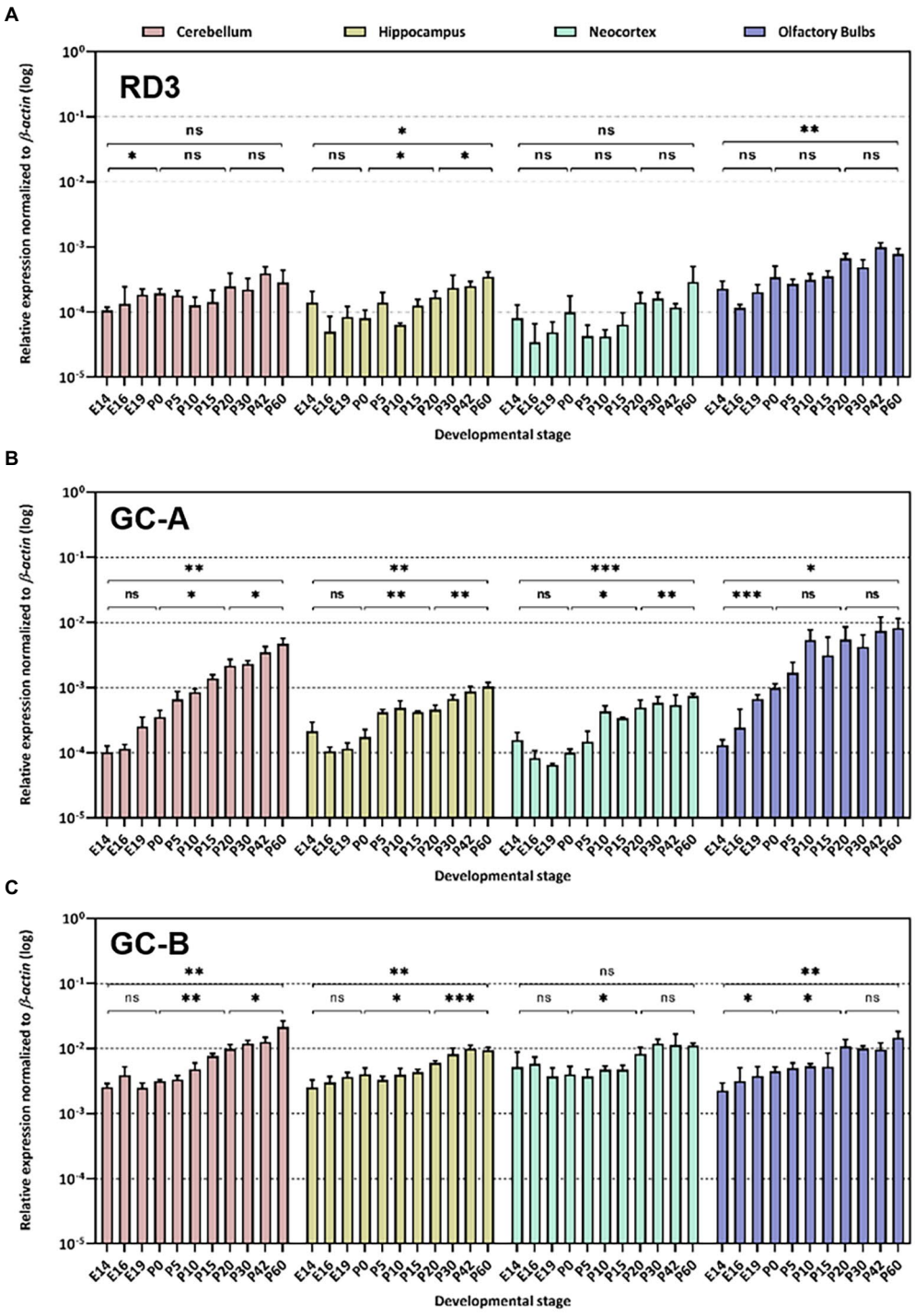

FIGURE 2
Quantitative RT-PCR. Gene expression pattern of *rd3* **(A)**, *Npr1* encoding GC-A **(B)** and *Npr2* encoding GC-B **(C)** was analyzed in different neuronal tissues as indicated. The relative expression was normalized to β–*actin* expression. Analysis of statistics were based on one-way ANOVA followed by Bonferroni's multiple comparisons test. Data are shown as mean±SD and were considered significant for $p \leq 0.05$ ($p \leq 0.05$=*; $p \leq 0.01$=**; $p \leq 0.001$=***; ns=not significant). Specific numbers of *p*-values are shown in Supplementary Table S3 (Supplementary material).

to P60 (Figure 2). The analysis performed by qRT-PCR included tissue from cerebellum, hippocampus, neocortex, and olfactory bulb. In general, *rd3* showed a lower expression level than *Npr1* and *Npr2* (Figure 2A compared to Figures 2B,C) and reached the highest steady-state expression level in the olfactory bulb between P20 and P60. However, the level was at least one order of magnitude lower than that for *Npr2* in all tested brain tissues (Figure 2C), which reached the highest values between P20 and

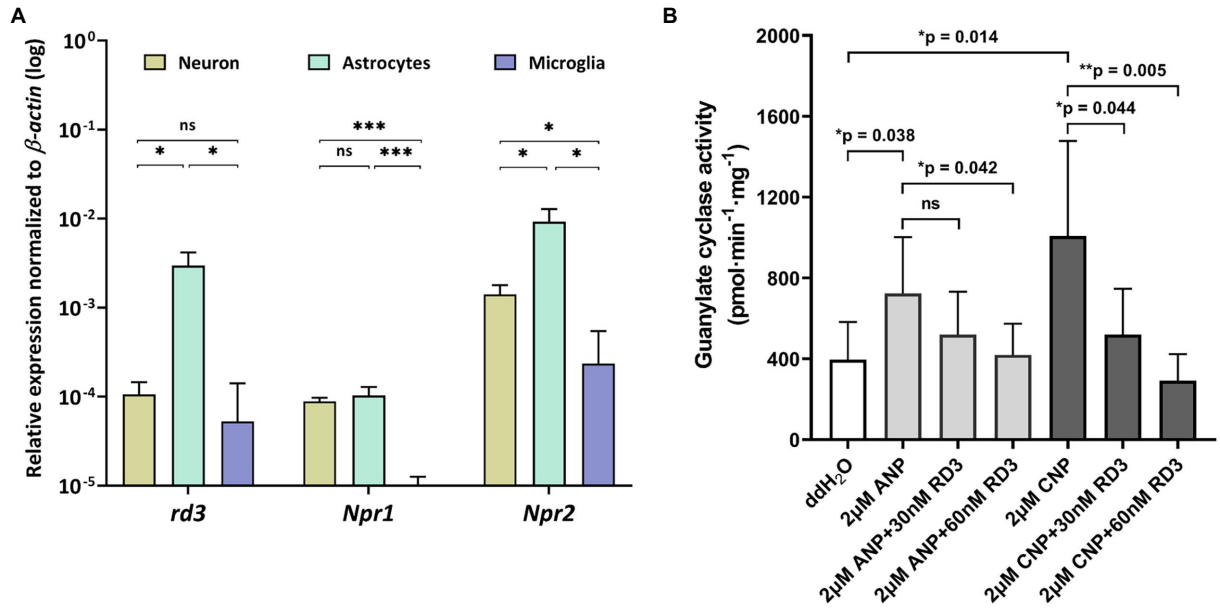

FIGURE 3
Expression and activity profiles of *rd3*, *Npr1* and *Npr2* in astrocytes. **(A)** Relative transcript levels of *rd3*, *Npr1* and *Npr2* in neurons, astrocytes, and microglia. Analysis of statistics were based on one-way ANOVA followed by Bonferroni's multiple comparisons test. Data are shown as mean±SD and were considered significant for $p \leq 0.05$ ($p \leq 0.05$=*; $p \leq 0.01$=**; $p \leq 0.001$=***; ns=not significant). Specific numbers of p-values are shown in Supplementary Table S4 (Supplementary material). **(B)** Inhibition of GC-A and GC-B in astrocytes by RD3.

P60. *Npr1* showed the highest expression at P60 in cerebellum and from P10 onwards in the olfactory bulb. Gene expression of *Npr1* was more dynamic exhibiting a steeper progressive increase in expression levels than *Npr2* and *rd3*. This was particularly visible for patterns observed in cerebellum and olfactory bulb (Figure 2B). Both *Npr* genes types showed lower expression levels in the retina than *rd3*. However, *Npr2* reached normalized expression levels in the retina that were close to those observed in cerebellum and olfactory bulb at P60 (compare Figures 1, 2C).

RD3 can inhibit hormone activated GC-A and GC-B

Coexpression of *rd3* and natriuretic peptide receptor GC genes in brain tissue led to the next question whether RD3 can regulate the enzymatic activities of membrane bound GC-A and GC-B. The high sequence homology of photoreceptor GCs and natriuretic peptide receptor GCs in the cytoplasmic domains (Goraczniak et al., 1994; Lange et al., 1999) could indicate that membrane bound GCs share similar regulatory features. RD3 is supposed to interact with regions in the cytoplasmic part of photoreceptor GC-E (Peshenko et al., 2011), although the exact binding site has not been determined. To test for any influence of RD3 on GC-A or GC-B activity we tested the impact of purified RD3 on GC activities in a cell culture system. Transient expression of GC-A and GC-B in HEK 293T cells was confirmed by immunoblotting using GC specific antibodies that recognized a single band around 120 kDa (Figure 4A), in agreement with the expectation and the documented molecular masses of membrane bound GCs (Kuhn, 2016). Non-transfected cells (HEK 293T control) or cells transfected with the empty pcDNA3.1 vector showed no GC bands (Figure 4A). HA-tagged variants of GC-A and GC-B were used in positive control transfections. Polyclonal antibodies directed against GC-A or GC-B recognized specifically the HA-tagged GC bands. To our surprise, the tagged variant of GC-A gave a stronger response to the antibody than the non-tagged variant. We have no explanation for this result.

Functional expression of both GCs was tested by monitoring a ligand dependent increase in GC activities. We incubated HEK293T cell membranes containing GC-A or GC-B with increasing concentrations of natriuretic peptides. Both peptides stimulated cGMP production about 10-fold reaching saturation above 4 μM of ANP (activating GC-A) or CNP (activating GC-B; Figures 4B,C). Further controls and test incubations to optimize our assay system included measurements upon GTP dependent cGMP synthesis (Supplementary Figure S1) and a time series resulting in a robust assay system (Materials and Methods) suitable for further studies. Activity tests in the presence and absence of DTT showed no or very negligible differences (Supplementary Figure S1C).

For testing the regulatory impact of RD3 on GC-A or GC-B, we purified RD3 to homogeneity (Supplementary Figure S2) and verified its identity by immunoblotting using two different anti-RD3 antibodies (Supplementary Figure S3). We activated GC-A and GC-B with 2 μM ANP and CNP, respectively, and

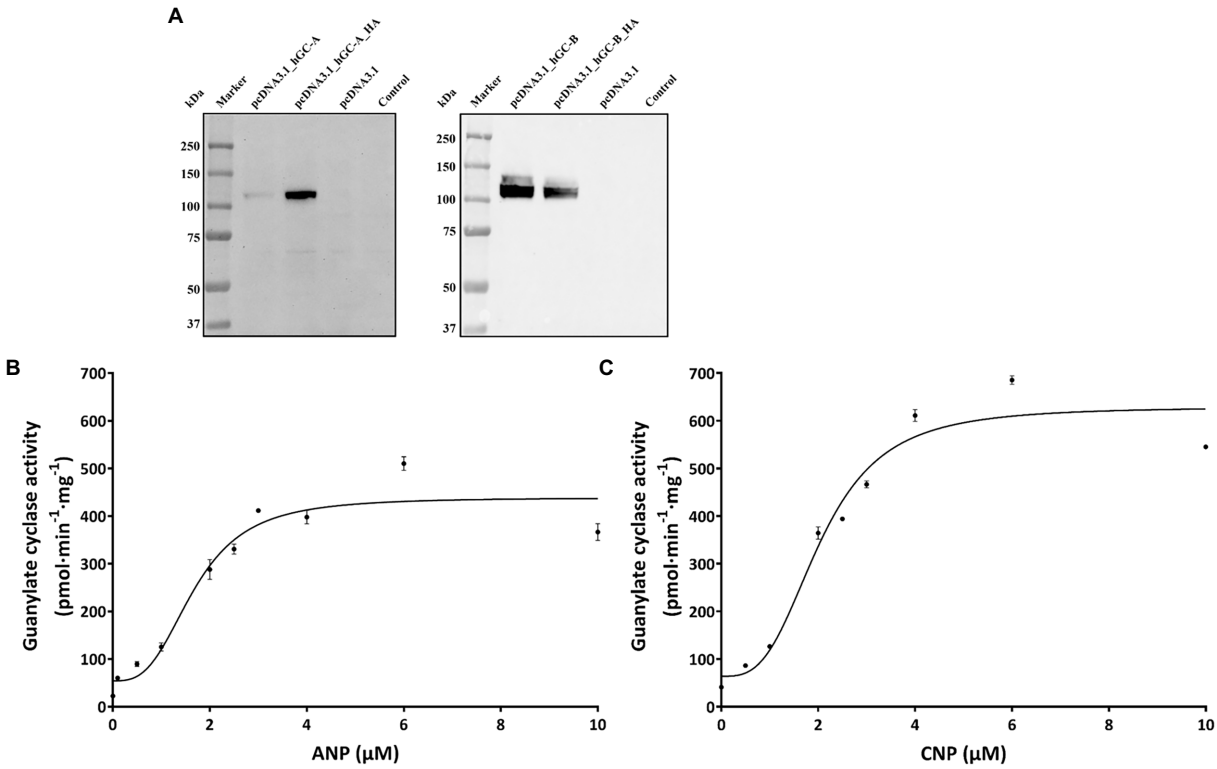

FIGURE 4
Heterologous expression GC-A and GC-B in HEK 293T cells. **(A)** Immunoblotting of HEK 293 T cell membrane suspension. Primary antibodies were directed against GC-A (left panel) or GC-B (right panel) at a dilution of 1:1000 in both cases. The antibodies detected also the HA-tagged variants. In case of GC-A, the HA-tagged variant was even stronger detected by the polyclonal anti-GC-A antibody. Transfection with the empty vector (pcDNA3.1) or non-transfected HEK293T cells did not react with the antibodies. Ligand dependent increase in GC-activities. **(B)** Regulation of GC-A by ANP and of GC-B **(C)** by CNP.

reconstituted the GC containing HEK 293T cell membranes with increasing concentrations of purified RD3. Inhibition of GC-A was significant, and several replicates ($N = 9$) showed reproducible results yielding a mean IC_{50} value (± SD) of 24 ± 13 nM RD3. A summarizing graph of the experiments is shown in Figure 5A. RD3 had a similar effect upon GC-B activity. The IC_{50} value for half-maximal inhibition was 29 ± 21 nM RD3 ($N = 9$) and a summarizing graph is shown in Figure 5B. However, inhibition was not complete for both GCs (Figures 5A,B) as higher concentrations between 0.5 and 1 μM RD3 did not reach a complete inhibition. Instead, the activity of GC-A and GC-B remained at a constant level (Figures 5A,B). We can exclude by immunoblotting any presence of photoreceptor GC-E in HEK293T cell membranes expressing either GC-A or GC-B (Supplementary Figure S4). This inhibitory feature differed significantly from the effect of RD3 upon photoreceptor specific GC-E (Figure 5C; Peshenko et al., 2011; Wimberg et al., 2018b). Since RD3 is a notoriously unstable protein, we controlled the functional activity of purified RD3 in a well-established assay system. HEK293T cell membranes that stably expressed photoreceptor GC-E were activated in the presence of 5 μM GCAP1. Addition of RD3 inhibited GCAP1 stimulated GC-E activity to a similar extent as reported in the literature (Peshenko et al., 2011; Wimberg et al., 2018b; Figure 5C). This confirmed that RD3 was active and controlled the activity of GC-A and GC-B in a similar, but not identical manner to GC-E.

Regulation of GC-A and GC-B by RD3 in astrocytes

Extending our analysis to cultured neurons, astrocytes, and microglia, revealed highest expression of *Npr2* in neurons and astrocytes, but also quite high expression of *rd3* in astrocytes (Figure 3A). The relative high transcript levels of *Npr2* and *rd3* in astrocytes led us investigate and compare regulatory features of GC-A and GC-B in primary cultures of astrocytes. Endogenous levels of GC activities around 400 pmol × min^{-1} × mg^{-1} resulted mainly from both GC-A and GC-B as seen in Figure 3 under conditions where no exogenous natriuretic peptides were added (ddH_2O). Adding natriuretic peptides (ANP and CNP) increased the activities at least twofold. The presence of 30 or 60 nM exogenously added RD3 inhibited the ANP or CNP stimulated GC activity leaving only a basal GC activity level as in the non-stimulated

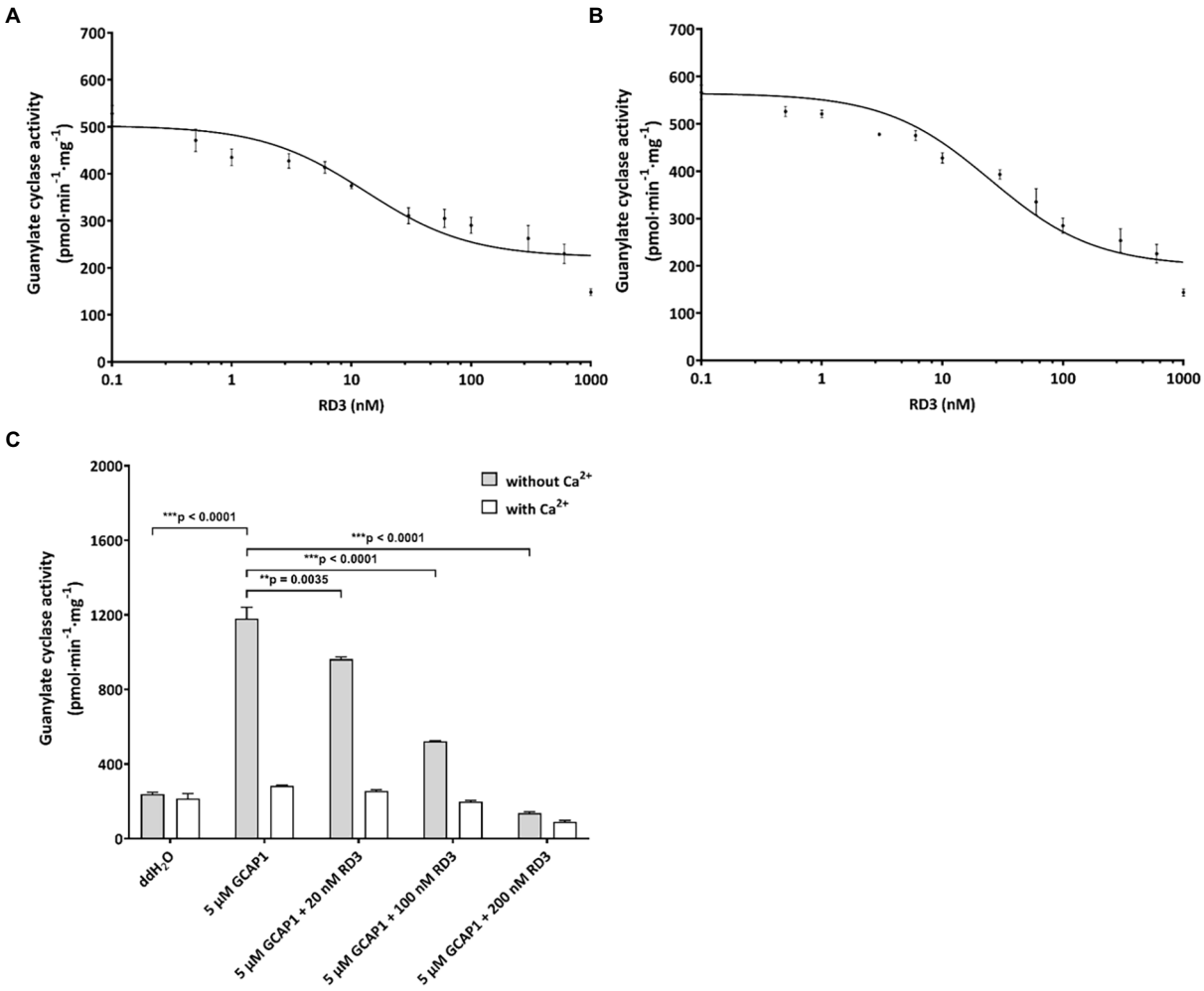

FIGURE 5
Inhibition of GC variants by RD3. **(A)** GC-A was activated by 2µM ANP and inhibited by increasing concentrations of RD3. The graph summarizes nine sets of incubations (see Results section). **(B)** GC-B was activated by 2µM CNP and inhibited by increasing concentrations of RD3 as indicated. The graph summarizes nine sets of incubations. **(C)** Control incubations with photoreceptor GC-E expressed in HEK293T cells that was activated by 5µM GCAP1 in the absence of Ca^{2+}. Adding RD3 at three different concentrations (20nM, 100nM, and 200nM) resulted in decrease in activity being complete between 100 (***p=0.00004511) and 200nM (***p=0.000007409), N=3. Adding double-distilled water (ddH_2O) to GC-E in HEK293T cell membranes showed no activation. Analysis of statistics were based on one-way ANOVA followed by Bonferroni's multiple comparisons test. Data are shown as mean±SD.

case (Figure 3B). These results showed that endogenously expressed GC-A and GC-B in primary astrocyte cell culture are sensitive to RD3 confirming our results with recombinant GC constructs and pointing to a potential physiologically relevant regulation of natriuretic peptide activated GCs by RD3.

Discussion

The presence of RD3 in non-retinal tissue seems enigmatic because we lack essential information about its cellular target(s) for defining possible physiological roles. On the other hand, the primary expression site of *rd3* in the mammalian retina (Azadi et al., 2010; Wimberg et al., 2018a; Dizhoor et al., 2019; Plana-Bonamaisó et al., 2020; Figure 1 in this study) well supports several functional roles of RD3 in the retina. For example, RD3 inhibits the activated form of photoreceptor GC-E and GC-F, it is involved in trafficking processes from photoreceptor inner to outer segments and might regulate the nucleotide cycle in photoreceptor cells. In the present work, we investigated the expression pattern of *rd3* in brain tissue and analyzed the enzymatic features of possible target enzymes. The central finding of our study is that RD3 can inhibit two hormone-stimulated GCs, namely GC-A and GC-B indicating a new regulatory feature of these hormone receptors.

Earlier work identified natriuretic peptides and their receptors GC-A and GC-B (or natriuretic peptide receptors) in mammalian retinae using expression and cloning studies (Fernandez-Durango et al., 1989; Kutty et al., 1992; Duda et al., 1993). Subsequent

studies performed in various vertebrate species showed the expression of natriuretic peptides and/or their receptors in retinal bipolar, retinal Müller cells, amacrine and ganglion cells (Spreca et al., 1999; Blute et al., 2000; Yu et al., 2006; Cao and Yang, 2007; Abdelalim et al., 2008; Xu et al., 2010). Thus, there is evidence for *Npr1* and *Npr2* expression in retina tissue, but it was unclear so far how the expression level relates to protein levels with a critical function in retinal physiology. In the present study, we compared the transcript levels of *rd3* with those of *Npr1* and *Npr2* and found a relatively high expression level of *Npr2* in the retina. The level is about one order of magnitude higher than that of *Npr1*, but about one order of magnitude lower than that of *rd3*.

Natriuretic peptides and their receptors are involved in various physiological processes in the retina. For example, natriuretic peptides are involved in dopaminergic and cholinergic signaling in amacrine cells (Abdelalim et al., 2008), and Yu et al. (2006) reported that they modulate GABA-receptor activity in bipolar cells and strong immunolabeling of GC-A and GC-B in the outer plexiform layer (OPL). RD3 mainly localizes in inner segments of photoreceptor cells, but in addition expresses in the OPL (Azadi et al., 2010; Wimberg et al., 2018a; Dizhoor et al., 2019). Natriuretic peptide signaling *via* GC-A or GC-B leads to an increase in cGMP targeting, for example cyclic nucleotide-gated ion channels or cGMP dependent protein kinase (PKG). The latter had been discussed as part of a signaling pathway mediating the suppression of GABA-receptor current by BNP (Yu et al., 2006). Thus, RD3 could be involved in balancing the cGMP concentration by inhibiting GC-A or GC-B in the OPL, but high resolution immunohistochemistry of GC-A, GC-B and RD3 to support such a physiological role is missing so far.

Recent studies reported expression of RD3 on the transcript and protein level in several organs and tissues including brain (Khan et al., 2015; Aravindan et al., 2017), but the expression levels appear significantly lower than in the retina. We found that expression of *rd3* is more than 100-fold higher in the retina than in different brain parts (compare Figures 1, 2), which was in broad agreement with the report by Aravindan et al. (2017), who reported significant, but modest or low expression in human cerebellum and olfactory bulb in comparison to retinal expression. When we determined the relative expression levels of *rd3*, *Npr1* and *Npr2* during mice development, it became apparent that the expression of *Npr2* is stronger in all analyzed brain parts than those of *rd3* and *Npr1*. Our findings are consistent with reports showing *Npr2* mRNA expressing cell populations in neocortex, hippocampus, and olfactory bulb (Herman et al., 1996). GC-B has a critical role in the bifurcation of axons during development (Schmidt et al., 2018) extending previous observations that the natriuretic peptide systems play roles in regulating neural development (DiCicco-Bloom et al., 2004; Müller et al., 2009). Collectively, these findings support the notion that CNP is a prominent regulatory factor in the nervous system (Kuhn, 2016; Regan et al., 2021).

Therefore, inhibition of GC-A or GC-B by RD3 in brain tissue might be a critical regulatory feature. We observed stimulation of GC activities by ANP and CNP in astrocytes (Figure 3B) that was broadly consistent with a previous investigation that correlates ligand binding to cGMP accumulation by ANP and CNP (Deschepper and Picard, 1994). We here show that RD3 inhibited both GCs in astrocytes demonstrating that RD3 can exert its effects in a primary cell culture. Although this combination of *in situ* and *in vitro* studies provides only circumstantial evidence for RD3 regulating GC-A and GC-B activities, it might already indicate an impact on the development of retinopathies. In astrocytes, the ANP/GC-A/cGMP signaling counteracts neovascularization in proliferative retinopathies (Burtenshaw and Cahill, 2020; Špiranec Spes et al., 2020). Any inhibitory effect of RD3 would therefore reinforce the development of angiogenic dependent retinopathies indicating how critical the expression level of RD3 is.

Trigger events that up-or downregulate RD3 levels apparently facilitate protein or cell dysfunction. For example, previous work showed that RD3 is downregulated or lost in neuroblastoma cells that remained resistant to multi-modal clinical therapy (Somasundaram et al., 2019). Furthermore, a previous study on the gene expression pattern in the *rd3* mouse, an animal model of congenital blindness with low or no *rd3* expression, reported that more than 1,000 genes are differentially regulated (Cheng and Molday, 2013). An annotation of these genes indicated the involvement of different biochemical pathways including phototransduction, metabolism and a variety of signaling processes. These studies collectively showed that a loss of RD3 is a critical factor in different pathophysiological contexts. It could have an effect on the expression pattern of other proteins in signaling pathways and thereby facilitate tumor development.

In summary, RD3 seems to control the activities of GC-A and GC-B in retinal and non-retinal tissue. These features could be critical for transport processes from the ER to the plasma membrane, but might be involved in different cellular scenarios, where a tight control of intracellular cGMP levels is essential for cell function and survival.

Data availability statement

The original contributions presented in the study are included in the article/Supplementary material, further inquiries can be directed to the corresponding author.

Ethics statement

All protocols were in accordance with the German Animal Protection Law and were approved by the local ethics body of Mecklenburg-Western Pomerania (LALLF) and Lower Saxony (LAVES).

Author contributions

YC, AB, and K-WK designed the study and analyzed the data. YC performed the experiments. K-WK wrote the first draft of the manuscript. YC and AB contributed to writing of the manuscript. All authors contributed to the article and approved the submitted version.

Funding

This work was supported by a grant from the Deutsche Forschungsgemeinschaft to K-WK (GRK 1885/2) and an intramural research funding of the Faculty VI, School of Medicine and Health Sciences at the University of Oldenburg to AB and K-WK.

Acknowledgments

We thank Maike Möller, Jennifer Sevecke-Rave, Beate Bous, and Uwe Maschmann for technical assistance.

Conflict of interest

The authors declare that the research was conducted in the absence of any commercial or financial relationships that could be construed as a potential conflict of interest.

Publisher's note

Supplementary material

The Supplementary material for this article can be found online at: https://www.frontiersin.org/articles/10.3389/fnmol.2022.1076430/full#supplementary-material

References

Abdelalim, E. M., Masuda, C., and Tooyama, I. (2008). Expression of natriuretic peptide-activated guanylate cyclases by cholinergic and dopaminergic amacrine cells of the rat retina. *Peptides* 29, 622–628. doi: 10.1016/j.peptides.2007.11.021

Aravindan, S., Somasundaram, D. B., Kam, K. L., Subramanian, K., Yu, Z., Herman, T. S., et al. (2017). Retinal degeneration protein 3 (RD3) in normal human tissues: novel insights. *Sci. Rep.* 7:13154. doi: 10.1038/s41598-017-13337-9

Azadi, S., Molday, L. L., and Molday, R. S. (2010). RD3, the protein associated with Leber congenital amaurosis type 12, is required for guanylate cyclase trafficking in photoreceptor cells. *Proc. Natl. Acad. Sci. U. S. A.* 107, 21158–21163. doi: 10.1073/pnas.1010460107

Barmashenko, G., Buttgereit, J., Herring, N., Bader, M., Ozcelik, C., Manahan-Vaughan, D., et al. (2014). Regulation of hippocampal synaptic plasticity thresholds and changes in exploratory and learning behavior in dominant negative NPR-B mutant rats. *Front. Mol. Neurosci.* 7:95. doi: 10.3389/fnmol.2014.00095

Blute, T. A., Lee, H. K., Huffmaster, T., Haverkamp, S., and Eldred, W. D. (2000). Localization of natriuretic peptides and their activation of particulate guanylate cyclase and nitric oxide synthase in the retina. *J. Comp. Neurol.* 424, 689–700. PMID: 10931490

Burtenshaw, D., and Cahill, P. A. (2020). Natriuretic peptides and the regulation of retinal neovascularization. *Arterioscler. Thromb. Vasc. Biol.* 40, 7–10. doi: 10.1161/ATVBAHA.119.313566

Cao, L. H., and Yang, X. L. (2007). Natriuretic peptide receptor-a is functionally expressed on bullfrog retinal Müller cells. *Brain Res. Bull.* 71, 410–415. doi: 10.1016/j.brainresbull.2006.10.010

Cheng, C. L., and Molday, R. S. (2013). Changes in gene expression associated with retinal degeneration in the rd3 mouse. *Mol. Vis.* 19, 955–969. PMID: 23687432

Cideciyan, A. V. (2010). Leber congenital amaurosis due to RPE65 mutations and its treatment with gene therapy. *Prog. Retin. Eye Res.* 29, 398–427. doi: 10.1016/j.preteyeres

Decker, J. M., Wójtowicz, A. M., Bartsch, J. C., Liotta, A., Braunewell, K. H., Heinemann, U., et al. (2010). C-type natriuretic peptide modulates bidirectional plasticity in hippocampal area CA1 in vitro. *Neuroscience* 169, 8–22. doi: 10.1016/j.neuroscience.2010.04.064

Deschepper, C. F., and Picard, S. (1994). Effects of C-type natriuretic peptide on rat astrocytes: regional differences and characterization of receptors. *J. Neurochem.* 62, 1974–1982. doi: 10.1046/j.1471-4159.1994.62051974.x

DiCicco-Bloom, E., Lelièvre, V., Zhou, X., Rodriguez, W., Tam, J., and Waschek, J. A. (2004). Embryonic expression and multifunctional actions of the natriuretic peptides and receptors in the developing nervous system. *Dev. Biol.* 271, 161–175. doi: 10.1016/j.ydbio.2004.03.028

Dizhoor, A. M., Olshevskaya, E. V., and Peshenko, I. V. (2019). Retinal guanylyl cyclase activation by calcium sensor proteins mediates photoreceptor degeneration in an rd3 mouse model of congenital human blindness. *J. Biol. Chem.* 294, 13729–13739. doi: 10.1074/jbc.RA119.009948

Dizhoor, A. M., Olshevskaya, E. V., and Peshenko, I. V. (2021). Retinal degeneration-3 protein promotes photoreceptor survival by suppressing activation of guanylyl cyclase rather than accelerating GMP recycling. *J. Biol. Chem.* 296:100362. doi: 10.1016/j.jbc.2021.100362

Dizhoor, A. M., and Peshenko, I. V. (2021). Regulation of retinal membrane guanylyl cyclase (RetGC) by negative calcium feedback and RD3 protein. *Pflugers Arch.* 473, 1393–1410. doi: 10.1007/s00424-021-02523-4

Duda, T., Goraczniak, R. M., Sitaramayya, A., and Sharma, R. K. (1993). Cloning and expression of an ATP-regulated human retina C-type natriuretic factor receptor guanylate cyclase. *Biochemistry* 32, 1391–1395. doi: 10.1021/bi00057a001

Fernandez-Durango, R., Sanchez, D., Gutkowska, J., Carrier, F., and Fernandez-Cruz, A. (1989). Identification and characterization of atrial natriuretic factor receptors in the rat retina. *Life Sci.* 44, 1837–1846. doi: 10.1016/0024-3205(89)90301-9

Friedman, J. S., Chang, B., Kannabiran, C., Chakarova, C., Singh, H. P., Jalali, S., et al. (2006). Premature truncation of a novel protein, RD3, exhibiting subnuclear localization is associated with retinal degeneration. *Am. J. Hum. Genet.* 79, 1059–1070. doi: 10.1086/510021

Goraczniak, R. M., Duda, T., Sitaramayya, A., and Sharma, R. K. (1994). Structural and functional characterization of the rod outer segment membrane guanylate cyclase. *Biochem. J.* 302, 455–461. doi: 10.1042/bj3020455

Gross, I., Tschigor, T., Salman, A. L., Yang, F., Luo, J., Vonk, D., et al. (2022). Systematic expression analysis of plasticity-related genes in mouse brain development brings PRG4 into play. *Dev. Dyn.* 251, 714–728. doi: 10.1002/dvdy.428

Herman, J. P., Dolgas, C. M., Rucker, D., and Langub, M. C. (1996). Localization of natriuretic peptide-activated guanylate cyclase mRNAs in the rat brain. *J. Comp. Neurol.* 369, 165–187. doi: 10.1002/(SICI)1096-9861(19960527)369

Jacobson, S. G., Cideciyan, A. V., Ho, A. C., Roman, A. J., Wu, V., Garafalo, A. V., et al. (2022). Night vision restored in days after decades of congenital blindness. *iScience* 25:105274. doi: 10.1016/j.isci.2022.105274

Khan, F. H., Pandian, V., Ramraj, S. K., Aravindan, S., Natarajan, M., Azadi, S., et al. (2015). RD3 loss dictates high-risk aggressive neuroblastoma and poor clinical outcomes. *Oncotarget* 6, 36522–36534. doi: 10.18632/oncotarget.5204

Koch, K.-W., and Dell'Orco, D. (2015). Protein and signaling networks in vertebrate photoreceptor cells. *Front. Mol. Neurosci.* 8:67. doi: 10.3389/fnmol.2015.00067

Kuhn, M. (2016). Molecular physiology of membrane guanylyl cyclase receptors. *Physiol. Rev.* 96, 751–804. doi: 10.1152/physrev.00022.2015

Kutty, R. K., Fletcher, R. T., Chader, G. J., and Krishna, G. (1992). Expression of guanylate cyclase-a mRNA in the rat retina: detection using polymerase chain reaction. *Biochem. Biophys. Res. Commun.* 182, 851–857. doi: 10.1016/0006-291x(92)91810-d

Lange, C., Duda, T., Beyermann, M., Sharma, and R. K., Koch, K. W. (1999). Regions in vertebrate photoreceptor guanylyl cyclase ROS-GC1 involved in Ca(2+)-dependent regulation by guanylyl cyclase-activating protein GCAP-1. *FEBS Lett.* 460, 27–31. doi: 10.1016/s0014-5793(99)01312-5.

Molday, L. L., Djajadi, H., Yan, P., Szczygiel, L., Boye, S. L., Chiodo, V. A., et al. (2013). RD3 gene delivery restores guanylate cyclase localization and rescues photoreceptors in the Rd3 mouse model of Leber congenital amaurosis 12. *Hum. Mol. Genet.* 22, 3894–3905. doi: 10.1093/hmg/ddt244

Müller, D., Hida, B., Guidone, G., Speth, R. C., Michurina, T. V., Enikolopov, G., et al. (2009). Expression of guanylyl cyclase (GC)-a and GC-B during brain development: evidence for a role of GC-B in perinatal neurogenesis. *Endocrinology* 150, 5520–5529. doi: 10.1210/en.2009-0490

Olcese, J., Majora, C., Stephan, A., and Müller, D. (2002). Nocturnal accumulation of cyclic 3′,5′-guanosine monophosphate (cGMP) in the chick pineal organ is dependent on activation of guanylyl cyclase-B. *J. Neuroendocrinol.* 14, 14–18. doi: 10.1046/j.0007-1331.2001.00732.x

Pandey, K. N. (2021). Molecular signaling mechanisms and function of natriuretic peptide receptor-a in the pathophysiology of cardiovascular homeostasis. *Front. Physiol.* 12:693099. doi: 10.3389/fphys.2021.693099

Perrault, I., Estrada-Cuzcano, A., Lopez, I., Kohl, S., Li, S., Testa, F., et al. (2013). Union makes strength: a worldwide collaborative genetic and clinical study to provide a comprehensive survey of RD3 mutations and delineate the associated phenotype. *PLoS One* 8:e51622. doi: 10.1371/journal.pone.0051622

Peshenko, I. V., and Dizhoor, A. M. (2020). Two clusters of surface-exposed amino acid residues enable high-affinity binding of retinal degeneration-3 (RD3) protein to retinal guanylyl cyclase. *J. Biol. Chem.* 295, 10781–10793. doi: 10.1074/jbc.RA120.013789

Peshenko, I. V., Olshevskaya, E. V., and Dizhoor, A. M. (2016). Functional study and mapping sites for interaction with the target enzyme in retinal degeneration 3 (RD3) protein. *J. Biol. Chem.* 291, 19713–19723. doi: 10.1074/jbc.M116.742288

Peshenko, I. V., Olshevskaya, E. V., and Dizhoor, A. M. (2021). Retinal degeneration-3 protein attenuates photoreceptor degeneration in transgenic mice expressing dominant mutation of human retinal guanylyl cyclase. *J. Biol. Chem.* 297:101201. doi: 10.1016/j.jbc.2021.101201

Peshenko, I. V., Olshevskaya, E. V., Savchenko, A. B., Karan, S., Palczewski, K., Baehr, W., et al. (2011). Enzymatic properties and regulation of the native isozymes of retinal membrane guanylyl cyclase (RetGC) from mouse photoreceptors. *Biochemistry* 50, 5590–5600. doi: 10.1021/bi200491b

Plana-Bonamaisó, A., López-Begines, S., Andilla, J., Fidalgo, M. J., Loza-Alvarez, P., Estanyol, J. M., et al. (2020). GCAP neuronal calcium sensor proteins mediate photoreceptor cell death in the rd3 mouse model of LCA12 congenital blindness by involving endoplasmic reticulum stress. *Cell Death Dis.* 11:62. doi: 10.1038/s41419-020-2255-0

Preising, M. N., Hausotter-Will, N., Solbach, M. C., Friedburg, C., Rüschendorf, F., and Lorenz, B. (2012). Mutations in RD3 are associated with an extremely rare and severe form of early onset retinal dystrophy. *Invest. Ophthalmol. Vis. Sci.* 53, 3463–3472. doi: 10.1167/iovs.12-9519

Regan, J. T., Mirczuk, S. M., Scudder, C. J., Stacey, E., Khan, S., Worwood, M., et al. (2021). Sensitivity of the natriuretic peptide/cGMP system to hyperammonaemia in rat C6 glioma cells and GPNT brain endothelial cells. *Cells* 10:398. doi: 10.3390/cells10020398

Rollín, R., Mediero, A., Roldán-Pallarés, M., Fernández-Cruz, A., and Fernández-Durango, R. (2004). Natriuretic peptide system in the human retina. *Mol. Vis.* 10, 15–22. PMID: 14737067

Schmidt, H., Dickey, D. M., Dumoulin, A., Octave, M., Robinson, J. W., Kühn, R., et al. (2018). Regulation of the natriuretic peptide receptor 2 (Npr2) by phosphorylation of juxtamembrane serine and threonine residues is essential for bifurcation of sensory axons. *J. Neurosci.* 38, 9768–9780. doi: 10.1523/JNEUROSCI.0495-18.2018

Sharma, R. K. (2010). Membrane guanylate cyclase is a beautiful signal transduction machine: overview. *Mol. Cell. Biochem.* 334, 3–36. doi: 10.1007/s11010-009-0336-6

Sharma, R. K., Duda, T., and Makino, C. L. (2016). Integrative signaling networks of membrane guanylate cyclases: biochemistry and physiology. *Front. Mol. Neurosci.* 9:83. doi: 10.3389/fnmol.2016.00083

Sharon, D., Wimberg, H., Kinarty, Y., and Koch, K.-W. (2018). Genotype-functional-phenotype correlations in photoreceptor guanylate cyclase (GC-E) encoded by GUCY2D. *Prog. Retin. Eye Res.* 63, 69–91. doi: 10.1016/j.preteyeres.2017.10.003

Somasundaram, D. B., Subramanian, K., Aravindan, S., Yu, Z., Natarajan, M., Herman, T., et al. (2019). De novo regulation of RD3 synthesis in residual neuroblastoma cells after intensive multi-modal clinical therapy harmonizes disease evolution. *Sci. Rep.* 9:11766. doi: 10.1038/s41598-019-48034-2

Špiranec Spes, K., Hupp, S., Werner, F., Koch, F., Völker, K., Krebes, L., et al. (2020). Natriuretic peptides attenuate retinal pathological neovascularization via cyclic guanosine monophosphate signaling in pericytes and astrocytes. *Arterioscler. Thromb. Vasc. Biol.* 40, 159–174. doi: 10.1161/ATVBAHA.119.313400

Spreca, A., Giambanco, I., and Rambotti, M. G. (1999). Ultracytochemical study of guanylate cyclases a and B in light-and dark-adapted retinas. *Histochem. J.* 31, 477–483. doi: 10.1023/a:1003712110751

Sulmann, S., Kussrow, A., Bornhop, D. J., and Koch, K.-W. (2017). Label-free quantification of calcium-sensor targeting to photoreceptor guanylate cyclase and rhodopsin kinase by backscattering interferometry. *Sci. Rep.* 7:45515. doi: 10.1038/srep45515

Wimberg, H., Janssen-Bienhold, U., and Koch, K.-W. (2018a). Control of the nucleotide cycle in photoreceptor cell extracts by retinal degeneration protein 3. *Front. Mol. Neurosci.* 11:52. doi: 10.3389/fnmol.2018.00052

Wimberg, H., Lev, D., Yosovich, K., Namburi, P., Banin, E., Sharon, D., et al. (2018b). Photoreceptor guanylate cyclase (GUCY2D) mutations cause retinal dystrophies by severe malfunction of Ca2+−dependent cyclic GMP synthesis. *Front. Mol. Neurosci.* 11:348. doi: 10.3389/fnmol.2018.00348

Xu, G. Z., Tian, J., Zhong, Y. M., and Yang, X. L. (2010). Natriuretic peptide receptors are expressed in rat retinal ganglion cells. *Brain Res. Bull.* 82, 188–192. doi: 10.1016/j.brainresbull.2010.03.004

Yu, Y. C., Cao, L. H., and Yang, X. L. (2006). Modulation by brain natriuretic peptide of GABA receptors on rat retinal ON-type bipolar cells. *J. Neurosci.* 26, 696–707. doi: 10.1523/JNEUROSCI.3653-05.2006

Zägel, P., Dell'Orco, D., and Koch, K.-W. (2013). The dimerization domain in outer segment guanylate cyclase is a Ca2+−sensitive control switch module. *Biochemistry* 52, 5065–5074. doi: 10.1021/bi400288p

Zulliger, R., Naash, M. I., Rajala, R. V., Molday, R. S., and Azadi, S. (2015). Impaired association of retinal degeneration-3 with guanylate cyclase-1 and guanylate cyclase-activating protein-1 leads to leber congenital amaurosis-1. *J. Biol. Chem.* 290, 3488–3499. doi: 10.1074/jbc.M114.616656

Frontiers in
Molecular Neuroscience

Leading research into the brain's molecular structure, design and function

Part of the most cited neuroscience series, this journal explores and identifies key molecules underlying the structure, design and function of the brain across all levels.

Discover the latest Research Topics

See more →

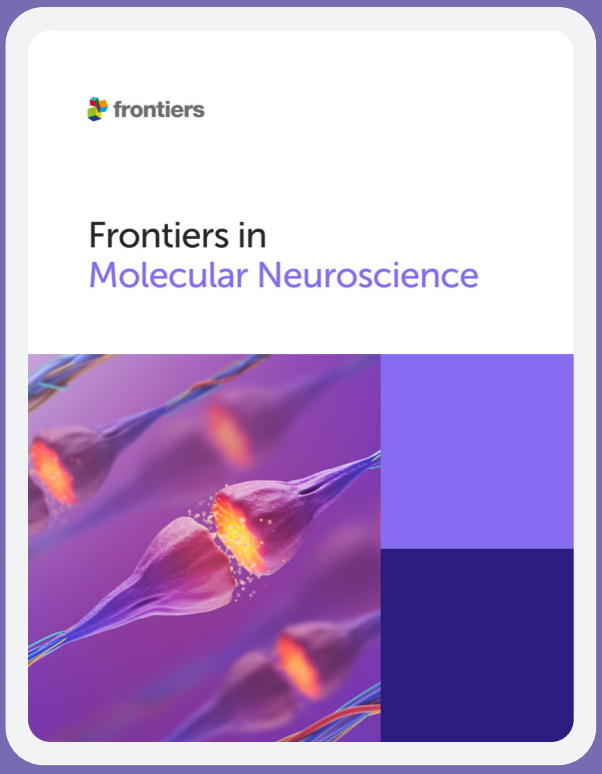

Frontiers

Avenue du Tribunal-Fédéral 34
1005 Lausanne, Switzerland
frontiersin.org

Contact us

+41 (0)21 510 17 00
frontiersin.org/about/contact